The Resistance of Functionalised PET Samples to Hydrolytic Degradation

By

Kimberley Miller

A thesis submitted to the department of Pure and Applied Chemistry, University of Strathclyde, in part fulfillment of the regulations for the degree of Doctor of Philosophy.

'I certify that the thesis has been written by me. Any help I have received in my research work and the preparation of the thesis itself has been acknowledged. In addition, I certify that all information sources and literature used are indicated in the thesis.'

Signed - Date –

Acknowledgements

I would like to express my appreciation to my supervisor, Dr John Liggat for giving me the opportunity to work in his group and for his continual help and support.

A special thank you goes to Bill Brennan, Simon Mortlock and Kirstin Forstyh for allowing me to participate in this project and for their continual input that helped to move the project forward.

I would like to thank Pat Keating for her advice regarding the GCMS. I would also like to thank Craig Irving and Professor Parkinson for teaching me how to use the NMR instruments and for all of their advice throughout the years.

I would also like to thank all the students (past and present) in TG521 for the welcoming and friendly atmosphere throughout the years, as well as all the support and advice they have given.

I would also like to thank my boyfriend, Des, for always being there for me and keeping me sane (well trying at least).

Well, it looks like I won Eve and got my thesis sorted before you got your book finished, Thanks for all the laughs pal!

Lastly, I would like to thank my Mum for everything, but I still don't care if you are stuck at your games!

Dedicated to the loving memory

of

James Miller

“Hope you’re proud Da”

Abstract

It is well documented in the literature that poly(ethylene terephthalate) (PET) undergoes hydrolysis. PET has been previously used in short lifetime applications such as food packaging and textile fibers. The condition that PET is exposed to when used in these applications allows hydrolysis to occur very slowly, and so does not cause any concern. In recent years PET has been considered for more long term outdoor applications such as use in solar cells. In these applications, it is a concern that PET is a hydrolysis sensitive polymer.

One of the tried and tested ways to reduce the impact of hydrolytic degradation is to involve lowering the carboxyl end group concentration. An esterification reaction between PET and epoxides will successfully lower the carboxyl end group concentration. Three epoxides were investigated, namely; Cardura, Heloxy and Vikolox.

Reliable titration and nuclear magnetic resonance (NMR) methods were utilised during this PhD to detect the esterification reaction and how quickly it was occurring. All three epoxides were shown to be subjected to the esterification reaction with the model compounds benzoic acid and poly(ethylene isophthalate) (PEI). Cardura, however, was shown to have a greater extent of reaction with carboxyl end groups than the other epoxides. The NMR data obtained for the 3 epoxides clearly show that a higher level of esterification reaction is occurring in Cardura when compared to Heloxy and Vikolox (after 1 minute at 150 ^{o}C, all epoxide groups were reacted in the Cardura samples, whereas no reaction was detected in the other 2 epoxide samples).

DuPont Teijin Films (DTF) requires the additive they will use to be capable of being manufactured in a reactive extrusion process. Their current processing lines could be easily modified to include a liquid feed, preventing the substantial capital costs that would otherwise be required to manufacture the new product. A small scale system was established to determine if the selected additives could be added in this way; all three epoxides could successfully be added in this manner. Though all three epoxides could be added, the carboxylic end group concentration of the PET samples containing Cardura was reduced the most. With

the addition of 6% Cardura the carboxylic acid was reduced from 41.54 to 7.56 equivalence per 10^6 grams, but was only reduced to 17.28 and 18.02 equivalents per 10^6 grams for samples of PET containing 6% Heloxy and 6% Vikolox respectively. The fact that the carboxyl end group concentration of the samples containing Cardura is significantly lower allows Cardura to be added in a lower concentration, which is desired in order to minimise raw material costs.

For Cardura to be a suitable additive, it must display extrusion stability when exposed to various conditions. Additionally, the chosen additive must not have any adverse effects on the polymer samples properties such as clarity, molecular weight, crystallinity and melting point. Cardura was shown to have good extrusion stability and no adverse effect on the polymer sample.

Cardura was shown to increase the resistance to hydrolytic degradation but to not have any adverse effects on the thermal or thermal-oxidative degradation of the polymer samples. The data gathered in this thesis indicates that Cardura could be utilised to increase the resistance of PET to hydrolytic degradation in long term outdoor applications such as solar cells.

Abbreviations

List of the abbreviations used are:

2,6-NDA – 2,6-naphthalenedicarboxylic acid

2,6-NDC-2,6-naphthalatedicarboxylate

ATR – Attenuated total reflectance

BHET – Bishydroxyethyl terephthalate

DCl_3 – Deuterated chloroform

DEG – Diethylene glycol

DMSO – Dimethyl sulfoxide

DMT – Dimethyl terephthalate

DSC – Differential scanning calorimetry

DTF – DuPont Teijin Films

EG – Ethylene glycol

EVA – Ethylene vinyl acetate

FID – Free induction decay

FT – Fourier transform

GC-MS – Gas chromatography – mass spectrometry

HFIP – Hexafluoroisopropanol

ICI = Imperial Chemical Industries

ICTAC – International Confederation for Thermal Analysis and Calorimetry

IR – Infrared

IV – Intrinsic viscosity

NMR – Nuclear magnetic resonance

PBT – Poly(butadiene terephthalate)

PDGET – Poly(diethylene glycol) terephthalate

PEI – Poly(ethylene isophthalate)

PEN – Poly(ethylene naphthalate)

PET – Poly(ethylene terephthalate)

PMDA – Pyromellitic dianhydride

PV – Photovoltaic

PVF – Poly(vinyl fluoride)

SATVA – Sub ambient thermal volatilisation analysis

SSP – Solid-state polymerisation

TAI – Trichloroacetyl isocyanate

TCE – Tetrachloroethane

TFA – Trifluoroacetic acid

TFT – Triflurotoluene

Tg – Glass transition temperature

TGA – Thermogravimetric analysis

Tm – Melting point

TPA – Terephthalic acid

TVA – Thermal volatilisation analysis

UV – Ultraviolet

Contents

1.0 Introduction

1.1 Photovoltaic Devices

1.1.1 Brief History of Solar Cells

The word photovoltaic (PV) comes from a combination of the Greek word *photo* meaning light and *Volta,* the name of the Italian physician who discovered the electrical battery. [1] PV devices convert sunlight directly into an electrical current to create electricity. They are also known as solar cells and they were first made in the 1950s for use in space satellites. [2-3] It was in the 1970s that they became more commercially available and found applications in street lights, emergency telephones, watches and cameras.

There are many reasons for the increase in popularity, including their reduced cost, it is a renewable energy, no greenhouse gases are emitted, they are made from mostly recyclable materials, the way they are manufactured minimises toxic waste and they are reliable. [1]

1.1.2 Construction of a Solar Cell

PV devices must have specific optical and electrical properties in order to convert light into electricity. [1-2] There are two groups of materials that have the properties required to be used in PV devices. These groups are solid crystalline material and thin films. [3] Thin films such as cadmium telluride and copper indium selenide are often used in solar cells. Solid crystalline material includes amorphous silica and gallium arsenic. Crystalline silica will be discussed later in more detail as it is the most commonly used material in PV devices since the technology has been most developed. [4]

Silica, like the other materials used in PV cells, is a semiconductor, which means at low temperatures it acts as an insulator, but as a conductor when energy/heat is available. [4] Two models are used to explain the electrical properties of semiconductors, namely the bond and band models.

The band model uses the covalent bonds present in the materials to explain semiconductor behaviour. [4] Silicon can form four covalent bonds with neighbouring atoms, providing each silicon atom with its full complement of electrons. This gives a very stable structure and, at low temperature, silicon acts as an insulator as the bonds are intact. At higher temperatures the covalent bonds break, and conduction can occur as electrons from broken bonds are free to move, and electrons from neighbouring bonds can move into the hole that is created from the broken bond. This allows the hole to move as if it has a positive charge. Figure 1.1 shows this diagrammatically. [5]

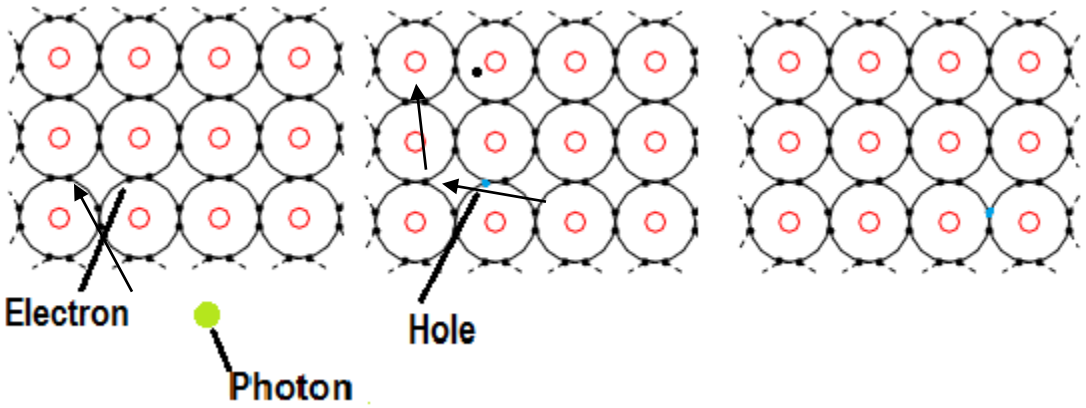

Figure 1.1 – Diagram showing the movement of electrons and holes in a semiconducting material. The arrows show the transfer of energy from the photon to the core electron and then the movement of electrons and holes in a semiconducting material. [After 5]

The breaking of the covalent bond mentioned in the bond model compliments the band model which is also used to describe semiconductor behaviour. [4] The band model describes semiconductor behaviour in terms of the energy levels between valence and conduction bands. When a covalent bond breaks, the electrons can enter the conduction band where it is free and can conduct. The holes remaining then conduct in the opposite direction.

The generation of electrons and holes can be enhanced by doping the silicon lattice. [1-4] In a crystalline silicon semiconductor, one half of the material is doped with phosphorous which has

five electrons. Only four electrons are required to bind with the silicon so this gives a supply of electrons. This is called an n-type semiconductor. The other half are doped by boron or aluminum which have three electrons, and as four electrons are needed to produce bonds with the silicon, positive holes are generated. This type of semiconductor is known as a p-type. When the p-type and n-type materials are joined together the excess holes in the p-type material flow by diffusion to the n-type material and vice versa. This movement causes a depleted electron region to occur.

When sunlight shines on a semiconductor material, two essential steps occur. [6] The first is that, when photons have energy (E_{ph}) greater than the energy corresponding to the gap between the valence and conduction bands (E_g), it will interact with the electrons in covalent bonds. [4] This causes the photon to use up its energy, breaking the covalent bonds and creating an electron-hole pair. The electron and holes cause exposed charges to occur on dopant atom sites, creating an electric field (Ê) to build up in the depleted region. When Ê is reduced the electrons and holes can flow producing a current. To reduce Ê a voltage can be applied. If the photons energy (E_{ph}) is less than the bandgap energy (E_g) it reacts weakly with the semiconductor material with no notable effect. The second essential step is to collect the current that is generated. [6] Electrodes are deposited onto the semiconductor material to collect the generated current. [1-2] The negative electrode is normally a metal grid which is deposited onto the front of the semiconductor. A solderable metal (positive electrode) is deposited onto the back of the semiconductor thus producing a PV cell.

Connecting the PV cells is achieved by using silver as it is a solderable material. [1] They are fit together using two strips of metal which connect the negative electrode of one PV cell to the positive electrode of the next PV cell. This process is delicate as the PV cells are very fragile. Collections of the cells are known as a string, and a series of strings are known as a module.

The module must be protected from the environment as many semiconductors will degrade in the presence of moisture, and hail stones could fracture the cells. [7] Another reason why the cells must be encased is to protect the consumer, as the cells become an electrical hazard when they are irradiated with sunlight. The module is embedded in an encapsulant, normally

ethylene vinyl acetate (EVA). The EVA is added to both sides of the cell as a solid. It is then heated to approximately 120 ^{o}C to liquefy the resin before pressure is applied to remove any air bubbles and ensure adhesion. A glass panel is normally added to the front of the cell as well as a backsheet, which can be glass or polymeric. The polymer normally used as a backsheet is poly (vinyl fluoride) (PVF). A frame and junction box is added to allow the module to be fitted to buildings. Figure 1.2 shows a diagram of a completed solar cell.

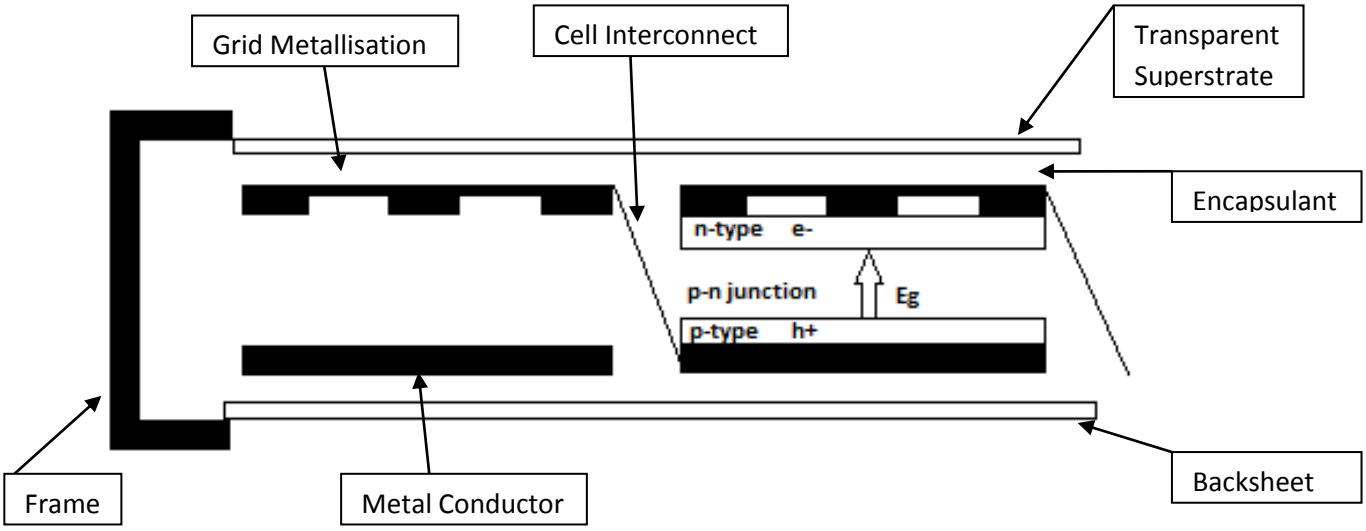

Figure 1.2 - Diagram of a solar cell. [7]

1.1.3 Polymers in Solar Cells

Polymers have been used as packaging in the electrical, pharmaceutical and food industries because of their excellent balance of properties. [7] It is no surprise that they appear in the PV industry as packaging for the module. Polymers are now widely used in the PV industry as encapsulants, substrates, backsheets, adhesives, frames and junction boxes to contain the wires.

Backsheets are a primary barrier to the environment, so, like the substrate, must be impermeable to moisture and oxygen. [7] The backsheets were originally made from glass, but

moisture and oxygen were able to penetrate at the laminated edges. Glass is also fragile and can be damaged during installation or in storms. Lightweight polymeric materials are now frequently used as the backsheet to replace glass. PVF is the material that is frequently used as the backsheet of PV devices.

1.2 Poly(ethylene terephthalate)

1.2.1 Introduction

Poly(ethylene terephthalate) (PET) is a semi-crystalline thermoplastic that was first synthesised in the 1930s by W. Carothers. [8] It was in 1941 that two British scientists, J. Whinfield and J. Dickson, patented the synthesis of PET, and, in 1950, Imperial Chemical Industries (ICI) first manufactured PET under the trade name Terylene. DuPont obtained the exclusive rights to produce PET in the United States, and released it as several branded products, for example Dacron and Mylar to name but a few. PET is known as a polyester because it has ester groups in the polymer backbone. [9] The repeat unit is shown in figure 1.3. PET is currently one of the most widely produced polymers in the market. It has found numerous applications, including in the pharmaceutical, textile and food industries.

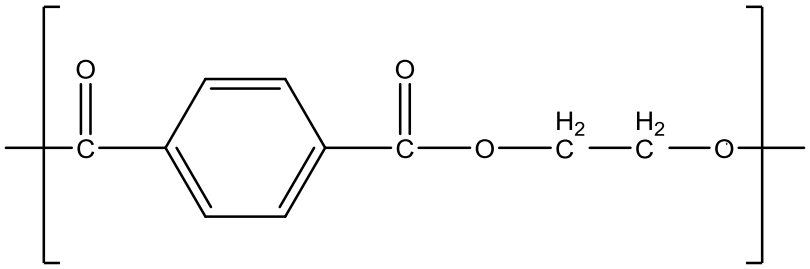

Figure 1.3 – PET repeat unit. [9]

1.2.2 Direct Esterification

PET can be formed by a two stage step-growth polymerisation of ethylene glycol (EG) and terephthalic acid (TPA). [10] The first stage of the reaction involves the esterification of TPA with EG to form the pre-polymer bishydroxyethyl terephthalate (BHET). The reaction is shown in figure 1.4. Esterification is a moderately endothermic process that produces water as a by-product.

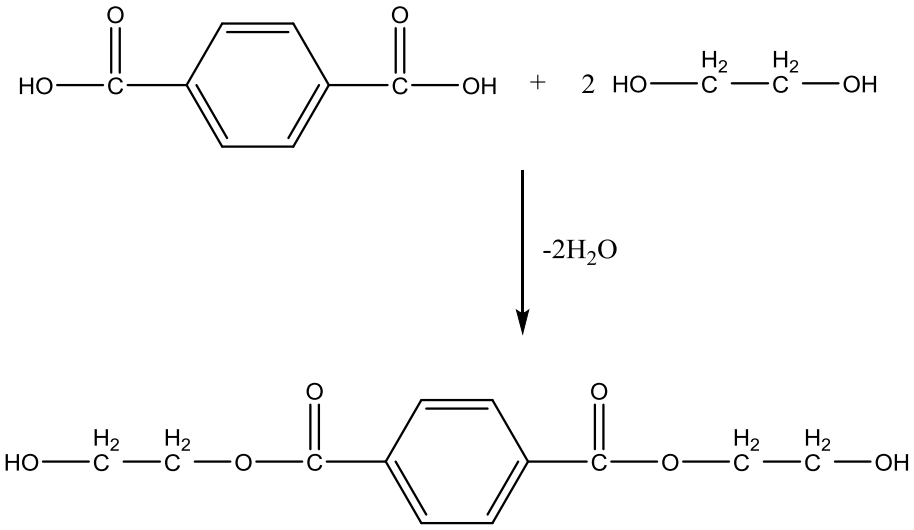

Figure 1.4 – Production of BHET by esterification of TPA and EG. [After 10]

The second stage is known as polycondensation and involves a transesterification reaction of BHET. [10] The process is shown in figure 1.5. The by-product of this reaction is EG and can be removed from the system with a high vacuum. The reaction is exothermic. The reverse reaction is known as glycolysis.

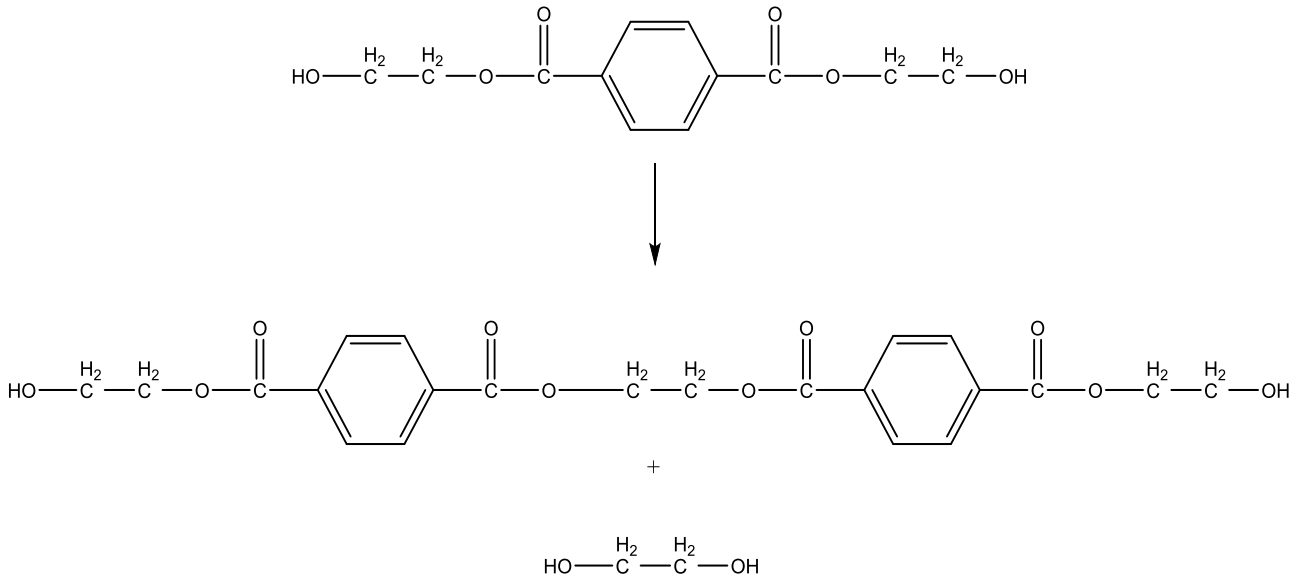

Figure 1.5 – Polycondensation reaction of BHET to produce PET. [10]

The formation of BHET is carried out at a temperature between 200 and 250 ^{o}C to achieve acceptable reaction rates. [10] The reaction is always carried out under pressure to keep the EG as a liquid in the system.

1.2.3 Transesterification

PET can also be formed by the transesterification of dimethyl terephthalate (DMT) with EG to produce the pre-polymer BHET; this reaction is shown in figure 1.6. [10] The by-product of this reaction is methanol. Highly pure DMT can be produced by distillation for the reaction and is often dissolved in EG for a liquid phase transesterification reaction to occur. The BHET produced will undergo a polycondensation reaction to produce PET, just like during the esterification reaction of TPA and EG.

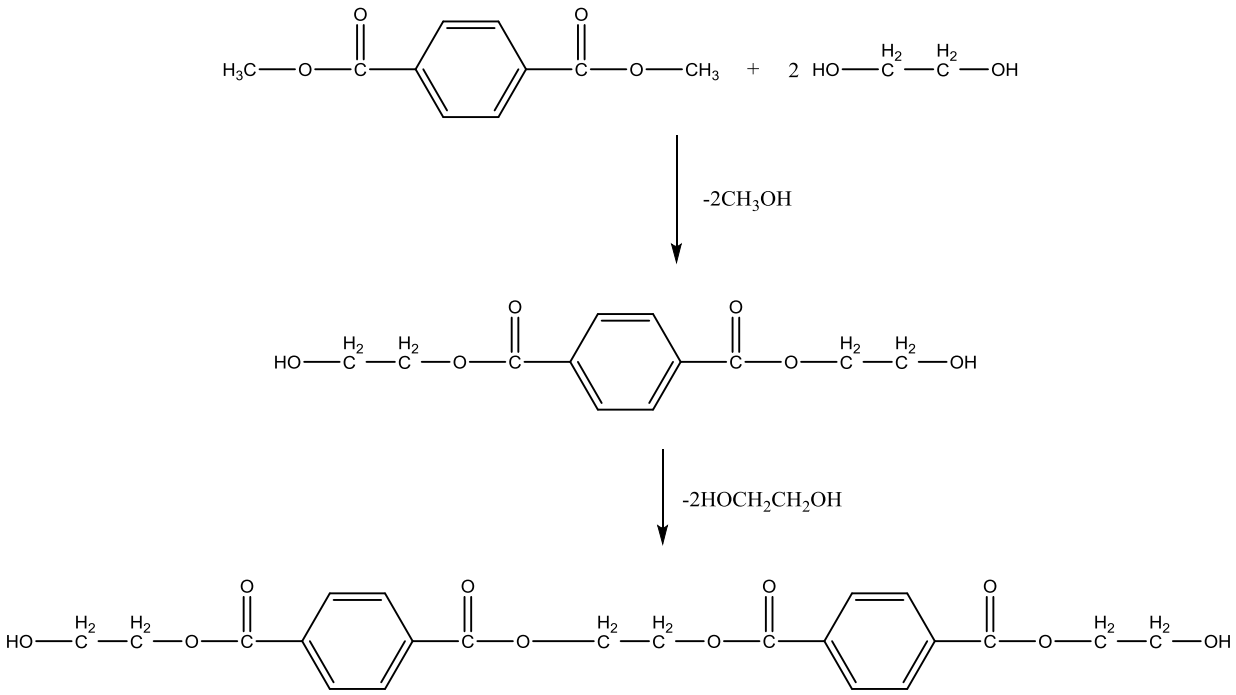

Figure 1.6 – Formation of PET from DMT and EG. [After 7]

1.2.4 Catalysts

Catalysts are often required when producing PET to obtain suitable reaction rates. [10-15] The esterification and transesterification processes are both catalysed by carboxylic acid groups. [10-11] The concentration of carboxyl end groups is normally sufficient in the esterification and transesterification reactions so that another catalyst is not required. However, catalysts tend to be required during the polycondensation reaction as the concentration of carboxyl end groups is considerably lower during this process. Otton *et. al*. used a series of small model compounds such as benzoic acid, 2,6-dimethyl benzoic acid and terephthalic acid to propose a mechanism for carboxylic acid groups being used as a catalyst. [11] The mechanism proposed is that the carboxylic acid groups form an ion pair which undergo nucleophilic attack by the alcohol. This mechanism is shown in figure 1.7.

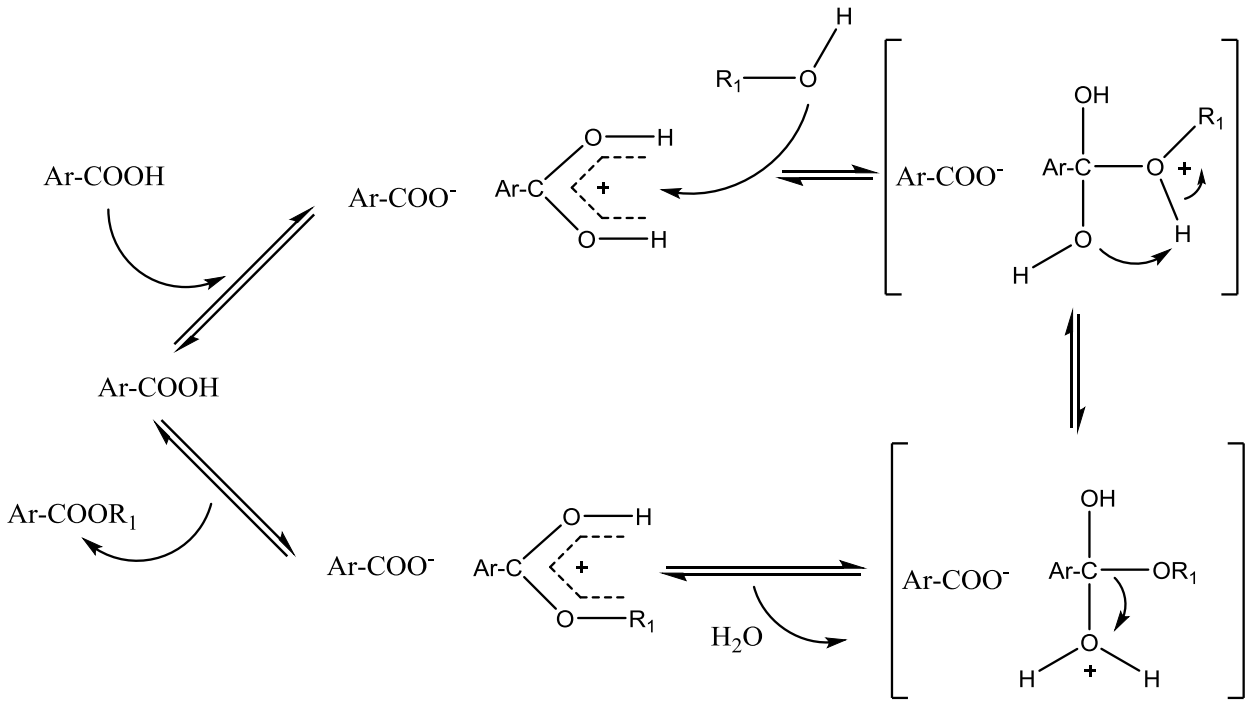

Figure 1.7 - Mechanism for the carboxylic acid-catalysed esterification reaction. [After 11]

Various metal compounds have been used for the esterification and transesterification reactions. The metals investigated include lithium, sodium, potassium, zinc, cobalt, manganese and titanium. [10-15] Research has shown that titanium compounds are the most active catalyst type. On the other hand, zinc compounds have been reported to be the one of the least active catalysts for the production of PET since they are easily poisoned by traces of acidic groups. Antimony is very rarely used because it is poisonous. The mechanism for the catalysed esterification reaction with the metal compounds containing lithium, sodium, potassium, zinc, cobalt and manganese involves the dissolution of the metal compound, which leads to an ion pair and the solvation of M^+ occurs. [15]An acid-base reaction is the next step, followed by either reaction with the carboxylic acid group, or it undergoes the concerted mechanism. Finally the metal compound is regenerated.

Titanium compounds will always undergo ligand exchange with the solvent first. [10 and 15] Two mechanisms are then proposed for the titanium catalysed esterification reaction. The first is a concerted mechanism which brings in a closed approach around the metal, acid, and alcohol, and the second is that the titanium atoms act as a Lewis acid by coordinating the acid through the carbonyl group.

1.2.5 Solid-state Polymerisation

The molar masses of PET achieved by direct esterification/ polycondensation and transesterification/polycondensation processes are typically between 16000 and 19000 g mol^{-1}. [7] The molar mass of PET can be increased up to 27000 and 38000 g mol^{-1} in the solid state.

Solid-state polymerisation (SSP) involves the end groups of the polymer chains coming together and reacting to form water and EG. [7] The rate of reaction is affected by the mobility of the end groups and the diffusion of the by-product through the semi-crystalline solid, followed by removal to the gas phase.

There are many factors that influence the reaction rate of SSP including temperature, time, particle size, end group concentration, crystallisation, catalyst and molar mass. [7] The catalysts that can be used to improve the SSP process include antimony, titanium and manganese. Crystallisation is extremely important in the SSP process because it reduces the chain mobility and increases the diffusion path length of the by-products. It was shown that, as the polymer starts to crystallise, the rate of increase of molar mass will decrease. The crystallisation process will be discussed in more detail in section 1.4.2.

Some of the notable advantages of increasing the molar mass in the solid state are that there is no need to stir viscous melts, degradation/side reactions are limited due to the lower processing temperatures used, and there are lower investments /running costs of a continuous solid state polymerisation process as high temperatures/vacuums are not required. [7]

1.2.6 Industrial Preparation of PET

In industry PET can be produced as a continuous or batch process. [7] Continuous processes can produce up to 600 tons per day in a single processing line. The batch process is normally used for specialised products and can produce around 60 tons per day.

A typical industrial batch set up will consist of two reactors. [7] The first of these is for the esterification reaction and the second is for the polycondensation reaction. The monomers are mixed together before they are added to the esterification reactor. The monomers will usually be added in a ratio between 1:1 and 1:3 (EG: TPA or DMT). The by-product, water, is removed from the system via a column process. The bottom product of the column will be EG, which can be fed back into the esterification process. The temperature at which the esterification reaction occurs is between 235 and 265 ^{o}C. The absolute pressure is normally kept at ambient pressure or around 0.1-0.4 MPa. The temperature of the esterification vessel, and pressure, is reduced at the end of the esterification reaction to evaporate any excess EG. The pre-polymer is then transferred into a polycondensation reaction. The reaction temperature of the polycondensation reaction is between 270 to 295 ^{o}C, and the pressure is reduced with time. The PET produced is then cooled by water or air before being cut into the desired size.

In a continuous process, the ratio is normally between 1:1.05 and 1:1.15 (EG: TPA or DMT) [7] This is prepared in a slurry preparation vessel before being fed into a reactor. In normal industrial continuous processes, there can be between three and six reaction vessels in series. There are normally one or two esterification reactors, one or two polycondensation reactors and one or two finisher reactors. The final polymer from the finisher is cooled and cut to the desired size.

Once prepared by either a batch or continuous process, the initial polymer can be processed further for different applications, such as being extruded into films or blow moulded for plastic bottles. [7] For application in solar cells the polymer is produced as a film. [16-17] The initial polymer is dried at temperatures between 140 to 160 ^{o}C. The dried polymer is then melted in an extruder. The molten material from the extruder is forced from the dye and dropped onto a chilled casting drum. The film is sent through a series of rollers and heaters which pull the film

in one direction - this is to align all the polymer chains in the same direction. The film is then fed into a Stenter Oven which heats the film and draws it sideways. This causes all of the remaining polymer chains to align in this direction. The film is known as biaxial orientated film. The film is then cooled and then cut to the desired size.

1.2.7 Production Issues and Side Reactions

Imperfections or agglomerations in the polymer melt can cause several problems in the film manufacturing process. [10 and 16] Some of the problems that can occur include issues with obtaining the desired optical behaviour, avoiding haze and avoiding streaks.

To obtain the desired optical properties in the polymer, it depends on crystallinity, content of contaminations and the presence of solid particles. [10 and 16] To prevent contamination, the starting materials must be highly pure. Care has to be taken when using titanium or tin catalysts as the derivatives of these compounds can give the final polymer a yellowish tint. Haze is caused by inhomogenities in crystalline polymers scattering light from the visible region.

Differences in the intrinsic viscosities of the polymer can result in streaks forming during extrusion. [10 and 16] Factors that affect differences in the intrinsic viscosities include non-uniform intrinsic viscosities in the polymer chips, non-uniform heating conditions during extrusion, inadequate regulation of residence times or temperatures, and variable water content of the dried polymer chips.

Streaks can also be formed by additives aggregating and separating during quenching. [10 and 16] Another way streaks can be formed is by a process known as pinning which involves the molten polymer being pressed against a chill roller by electrostatic forces to improve quenching. High levels of oligomers in the polymer result in a loss of efficiency in the quenching process as it causes a non-uniform cooling in the film. This leads to differences in the crystallinity which cause the appearance of streaks on the polymer.

Droplets on the die caused by degradation products can also cause the presence of streaks. [10 and 16] Polyesters can undergo several types of degradation including thermal, thermal-oxidative

and photo-degradation. The different degradation products will be discussed in more detail in section 1.5.

1.2.8 Side Reaction of PET

Side reactions affect the quality of PET that is produced. One of the most important side reactions in PET synthesis is the formation of diethylene glycol (DEG) units in the polymer backbone. [10] DEG units are formed during the early stages of the polycondensation reaction. There are different mechanisms proposed for the formation of DEG units. One way that has been proposed for the formation of DEG units is by the esterification of two hydroxyl groups. [10] It has been suggested that there is an intermolecular assistance provided by the carbonyl oxygen from the ester group which will accelerate S_N2 type nucleophilic substitution reactions. Another mechanism that has been proposed for the formation of DEG units is from the reaction of intermediate molecules that are produced during thermal degradation. Thermal degradation of PET is discussed in more detail in section 1.5.2. The presence of DEG units will decrease the melting point and thermal stability of the polymer. [10] For some applications 1.5-2.5% of DEG is added to PET to improve its extrusion properties.

It has been shown that DEG groups can form dioxanes. [10] Hovenkamp and Munting proposed an intermolecular mechanism for the formation of dioxane from terminal DEG groups; the reaction is shown in figure 1.8. [19]

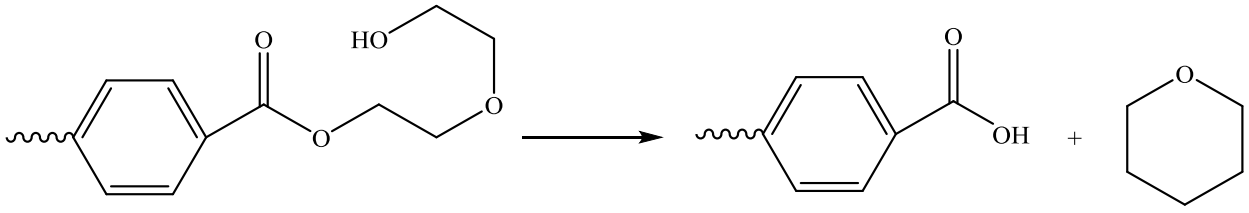

Figure 1.8 – Reaction showing the formation of dioxane. [After 19]

PET also contains 2-3% of short chain oligomers. [10] These oligomers can be linear or cyclic. They have been found to form at temperatures exceeding 270 ^{o}C. Peebles *et al*. discovered that their formation increases as molecular weight of the PET decreases. [20] A back biting mechanism was proposed for the formation of cyclic oligomers (figure 1.9). [10]

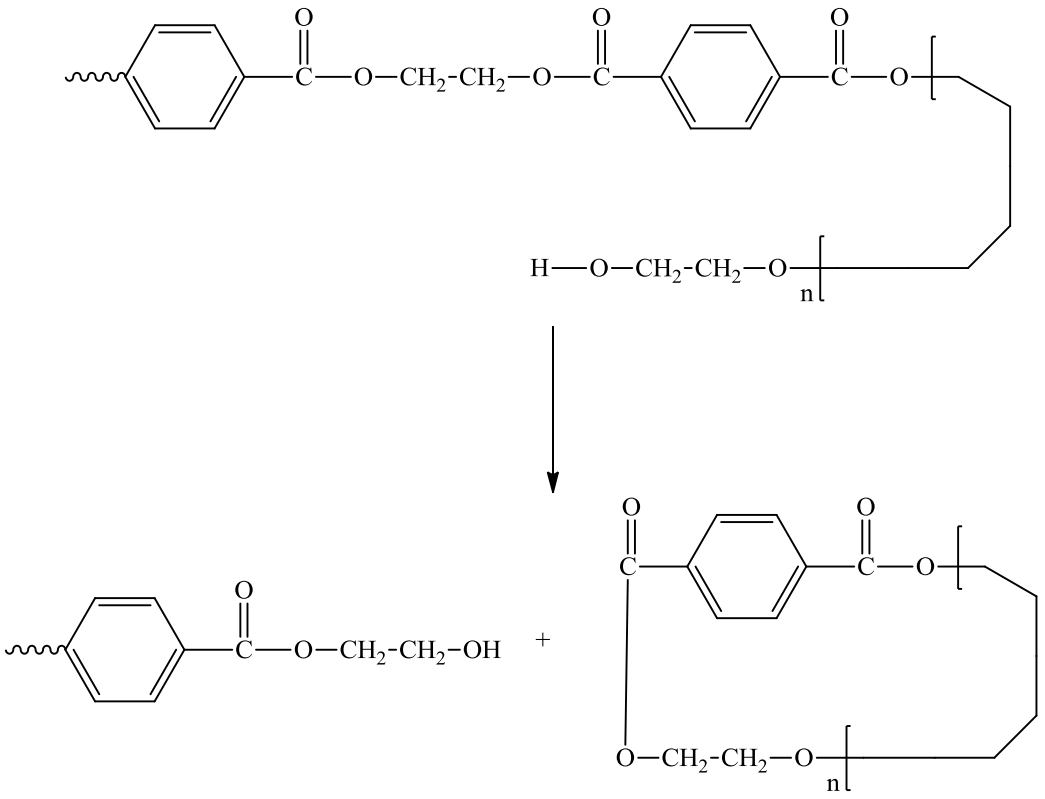

Figure 1.9- Back-biting reaction for the formation of cyclic oligomers. [After 10]

1.3 Other Polyesters

There are several other polyesters available with different properties. [21-34] With the exception of PET, the main polyesters available commercially, and used extensively in research, are poly(diethylene glycol) terephthalate (PDGET), poly(butadiene terephthalate) (PBT), poly(ethylene isophthalate) (PEI) and poly(ethylene naphthalate) (PEN).

1.3.1 Poly(diethylene glycol) terephthalate

PDGET is derived from terephthalic acid and diethylene glycol at temperatures exceeding 220 ^{o}C. [21] The polymer produced is a complex mixture of oligomers and possibly some cyclic compounds. Figures 1.10 and 1.11 show the oligomers produced and the cyclic compounds that can be formed respectively. The cyclic polyesters produced are an undesirable by-product as they don't have hydroxyl function. PDGET is referred to as a polyester polyol created using an aromatic acid. The aromatic acids are widely used since they provide mechanical strength, a high thermal stability and a resistance to solvents. [21-24]

It is often used as a copolymer with PET with 1-3% w/w of PDGET being added. [22] It is added as a processing aid for the purpose of reducing hazing observed in blow-moulded objects such as beverage bottles. [23] The other main purpose of adding PDEGT to PET is to enhance the ability of PET fibres to be dyed. [21-23] It is used as a model polymer to study the effect of DEG units in PET. [23-24] Lecomte *et al.* used PDGET to study the influence of DEG units on the thermal degradation of PET. A new mechanism consisting of two distinct steps is proposed. The first step initiates some 100 K below the normal degradation temperature of PET. It has been suggested that random ester groups along the backbone can back bite and form cyclic oligomers. The second step is similar to the degradation of PET.

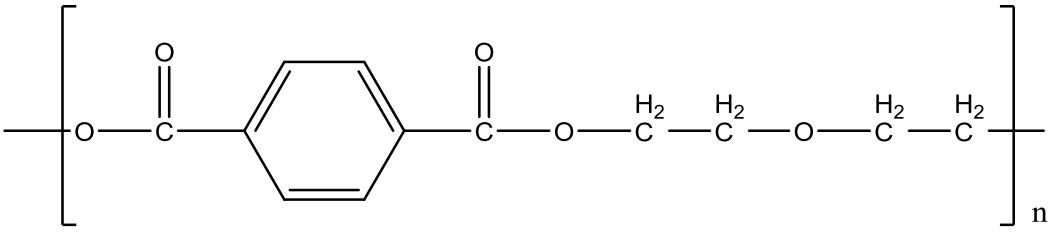

Figure 1.10- Repeat unit of PDGET. [After 21]

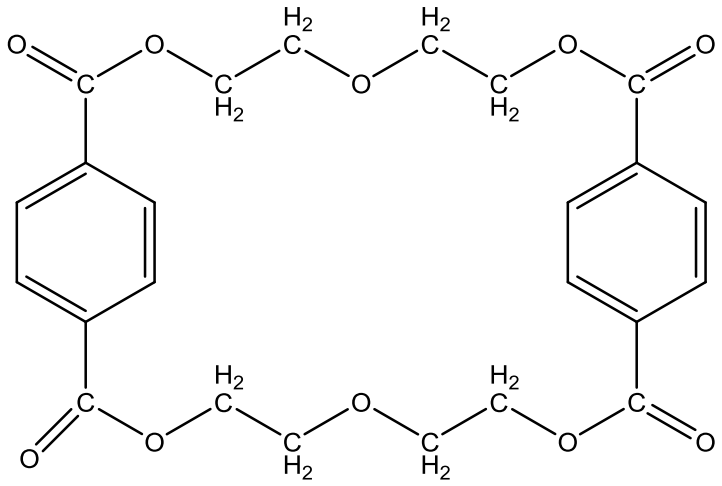

Figure 1.11- Cyclic components produced when manufacturing PDGET. [After 21]

1.3.2 Poly(ethylene isophthalate)

Poly(ethylene isophthalate) (PEI) is made by condensation polymerisation of isophthalic acid and ethylene glycol. [25-29] The isophthalic acid is slightly more expensive than terephthalic acid. The catalysts used for the polymerisation reaction are metallic compounds, normally germanium, zinc and antimony. The monomer of PEI is shown in figure 1.12. [25-26] The polymer is a structural isomer of PET.

Research shows that PEI has the potential to replace PET as a packaging material because gas sorption tests show that PEI film has a much lower carbon dioxide diffusion coefficient than PET. [25-29] The other main use of PEI is as a copolymer with PET to prevent haziness forming in the polymer produced and to lower the acetaldehyde content.

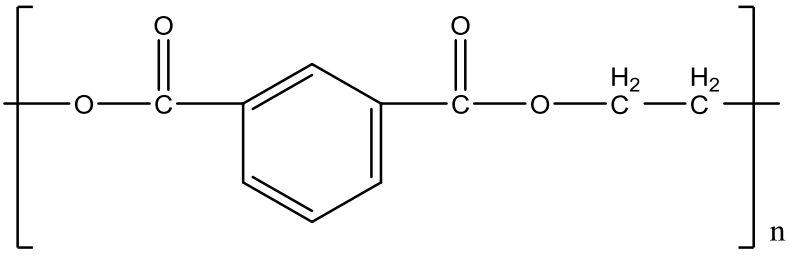

Figure 1.12- Repeat unit of PEI. [After 25-26]

1.3.3 Poly(butylene terephthalate)

Poly(butylene terephthalate) (PBT) is prepared from the reaction between 1,4 butylene glycol and terephthalic acid.[30-31] It can also be made by reaction dimethyl terephthalate and 1,4 butylene glycol. The repeat unit for PBT is shown in figure 1.13. [30]

PBT has many advantages including a high electrical insulation, it blocks ultraviolet radiation, it has high strength, it is resistant to staining, and it has a better impact resistance than PET. [30-31] The list of advantages means it has found applications in a number of industries, particularly in the electrical and automotive industries. Some examples of the items manufactured from PBT include switches, sockets and brake cable liners. The disadvantages of PBT are that it has a lower strength and rigidity than PET. It also does not have satisfactory resistance to acids, bases and hydrocarbons.

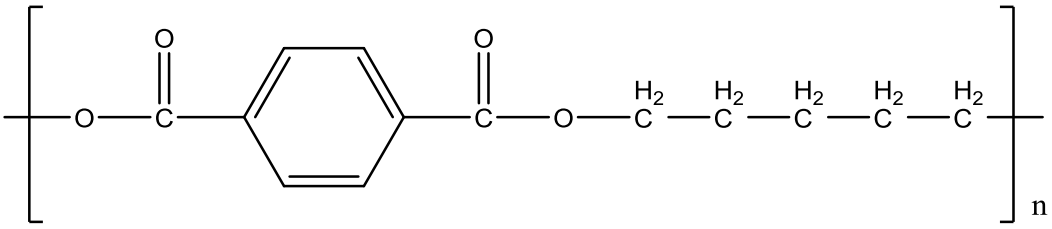

Figure 1.13- Repeat unit of PBT. [After 30]

1.3.4 Poly(ethylene naphthalate)

Poly(ethylene naphthalate) (PEN) was first synthesised in 1945 but only became commercially available in 1990. Until then the polymer intermediates 2, 6-naphthalenedicarboxylic acid (2, 6-NDA) and dimethyl-2, 6-naphthalenedicarboxylate (2, 6-NDC) could only be prepared in semi-commercial quantities at a very high price. [32-33] The first large scale commercial plant set up by BP Amoco to manufacture the intermediates involved a multi step process shown in figure 1.14. [33] The intermediates 2, 6-NDA and 2, 6-NDC could then be reacted with EG to produce PEN. [32-33] The repeat unit for PEN is shown in figure 1.15.

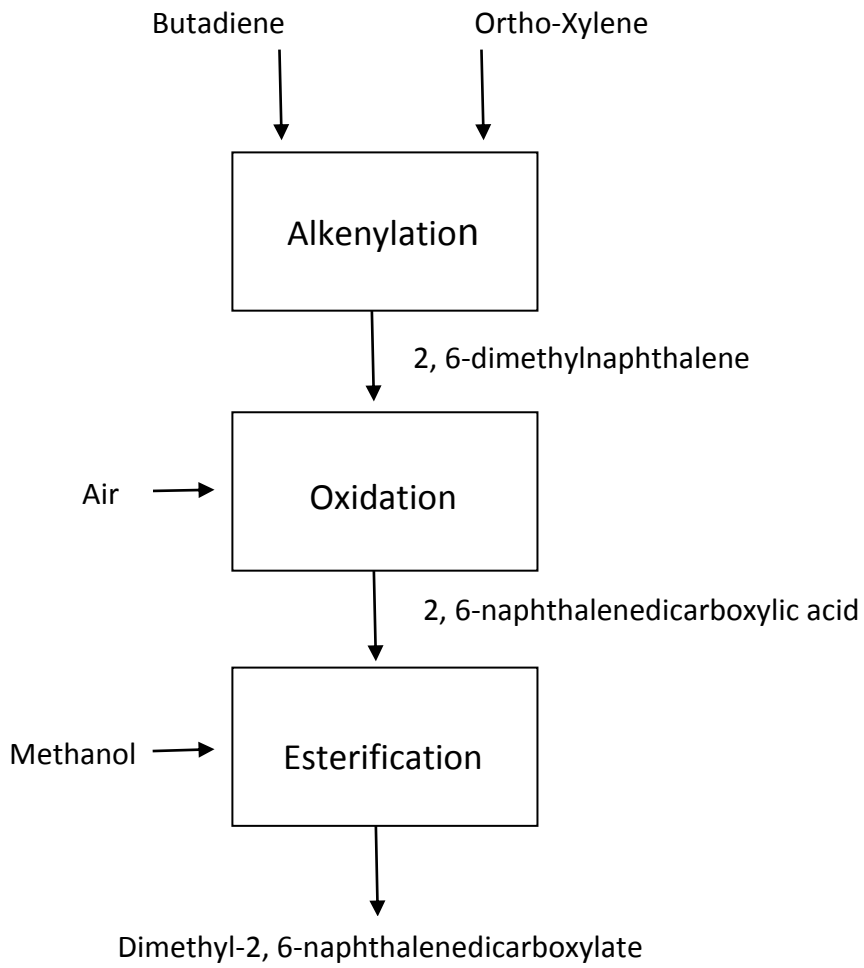

Figure 1.14 – Process of the first large scale plant for manufacturing the intermediates of PEN. [After 33]

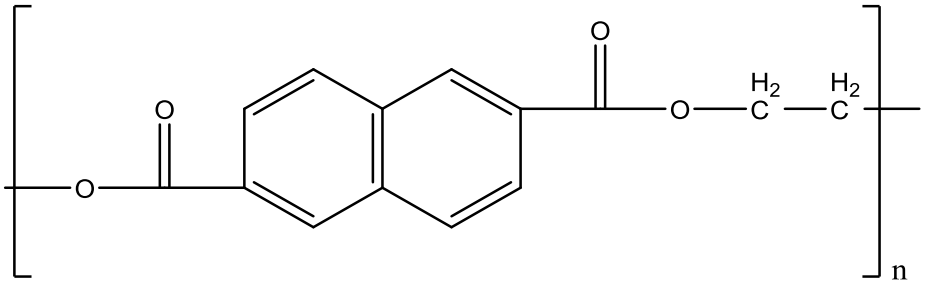

Figure 1.15- Repeat unit of PEN. [After 32-33]

The first commercial PEN polymer was manufactured by DuPont Teijin Films (DTF) and is known as Teonex. [16 and 34] PEN has superior properties over PET in the areas of strength, heat resistance and anti-hydrolysis properties. The tensile strength of PEN film was 550 MPa and comparable PET film had a tensile strength of 460 Mpa. PEN was also shown to have a better resistance to hydrolysis. In an autoclave, PET survived for 50 hours, but PEN lasted 200 hours. It is also shown that the thermal shrinkage for PEN is lower than PET; the percentage is 0.4% for PEN and 1.5% for PET.

Despite PEN being more expensive than PET it has found a number of applications in areas such as capacitors, electrical insulation, battery casings, medical product containers and cosmetic containers. [32-34] It is also used to make high performance sail cloths because it is resistant to ultraviolet radiation. PEN resin is frequently added in tyres to add rigidity and to reduce road noise. The polymer has better barrier properties than PET which makes it suitable for packaging beverages, especially beer. Like PEI, copolymers with PET are often made with PEN to improve the properties of the resulting polymer.

1.4 Properties of Polyesters

1.4.1 Glass Transition Temperature

An important property of polymers is the glass transition temperature (T_g). [9 and 35] This is the temperature at which high molecular weight polymers have enough energy to transform from a hard glass like state to a more rubbery state. The atoms in the polymer chain are not rigid and inflexible; the motion of the chain provides the energy required for the change of state to occur. [35] There are two types of motion that occur in a polymer. The first is known as β-segmental motion, or localised vibrations, which is the rotation of atoms or side groups of a polymer chain with the rest of the molecule being fixed in space. The other type of motion involves short segments of the polymer backbone, known as α-segmental motion. It is the α-segmental motion that occurs at the glass transition. The glass transition is a property that occurs in the amorphous state.

1.4.2 Amorphous and Crystalline States

Polymers have two morphologies in the solid state; crystalline and amorphous. [36-39] The polymer chains are randomly orientated and entangled in the amorphous region. The chains are often compared to a bowl of spaghetti. [9] A schematic of the amorphous region is shown in figure 1.16.

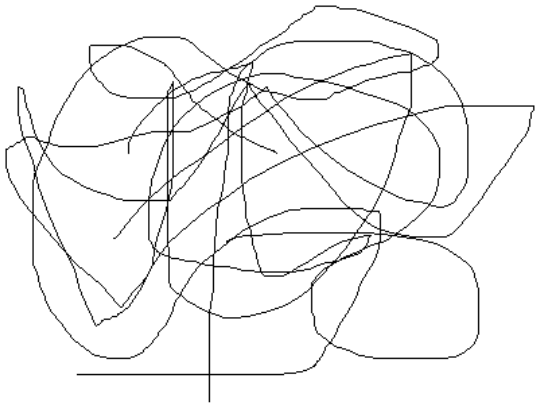

Figure 1.16 - Diagram showing the amorphous morphology of polymers. [After 9]

The crystallisation of the polymers do not form ordered reticula with repetitive units like metals, inorganic oxides or salts. [38] Polymers can crystallise in three ways - during polymerisation, induced by orientation and under quiescent conditions.

Monomer units can sometimes join, forming a crystal during polymerisation. [37] Macroscopic polymer crystals can be created when these monomers forming crystals join up into long chains during solid state polymerisation. This process can be seen in the schematic in figure 1.17. The crystal is obtained from reactions at the gas/solid or liquid/solid interface. This is different from normal crystallisation processes as it is obtained due to a change in physical state. When crystallisation is occurring during polymerisation the monomer can be gaseous.

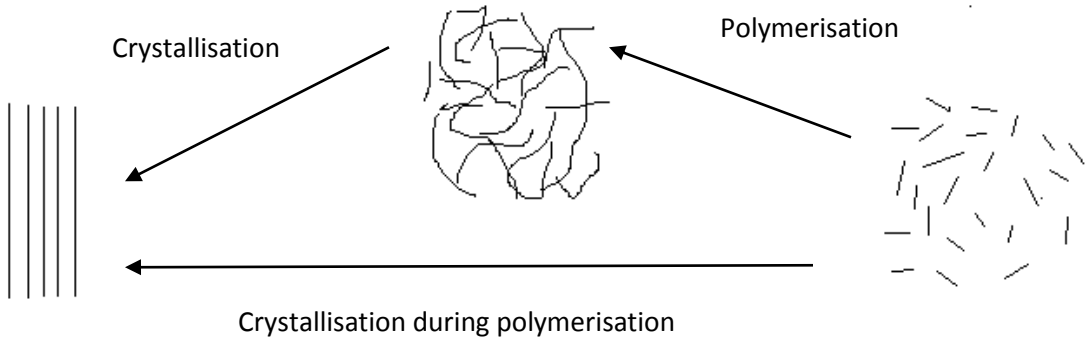

Figure 1.17 - Diagram showing the crystallisation of polymer chains during polymerisation. [After 37]

Some polymers are known as semi-crystalline polymers, which means that they have both amorphous and crystalline sections. [9] PET is an example of a semi-crystalline polymer. There have been various models released to explain how these two phases co-exist; broadly classified as the fringed micelle model and the lamellar type morphology. [35-39]

The fringed micelle model was first proposed in 1930 and involves the crystalline regions being dispersed in the amorphous regions. [36] The molecules in the crystalline region are parallel to one another, allowing them to pack closely together. [26-39] The crystalline and amorphous regions are completely entangled in one another. The fringes are the regions of the chains travelling from the crystalline region into the amorphous region. [37] Figure 1.18 shows a diagram of how this model would look. [9]

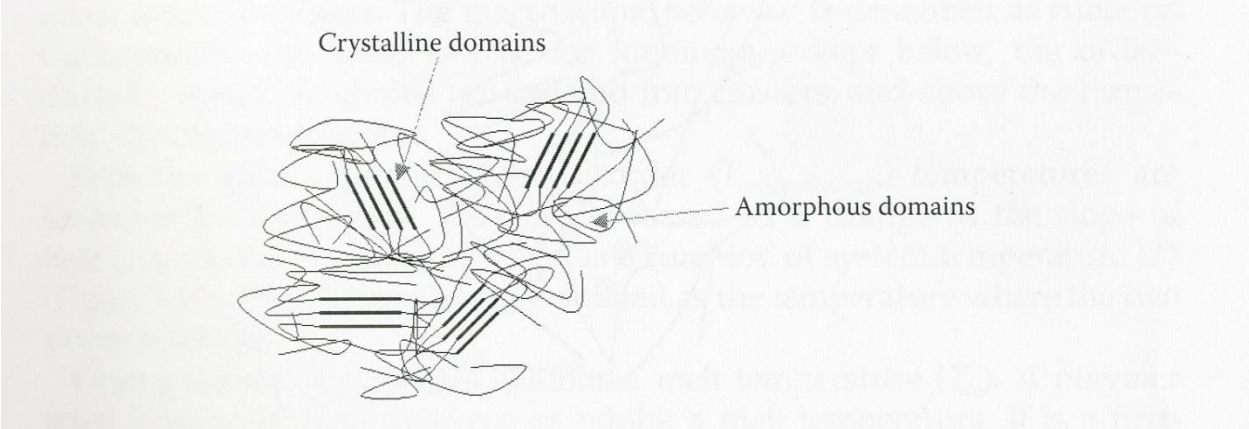

Figure 1.18 - Diagram of the fringed micelle model. [9]

The fringed micelle model is believed to be inaccurate for describing quiescent crystallisation as it does not explain the occurrence of large symmetrical crystalline superstructures, which are referred to as spherulites. [36-37] It was in 1957 that Fischer *et al*. showed, with the use of an electron microscope, that the spherulites in PE were more likely to be lamellar than fibrous in nature. [36] The model is useful at describing special occurrences in polymers such as thermoreversible gels. [37]

The lamellar model arises from the discovery that thin crystals of poly(ethylene) can grow from dilute solutions, producing crystals that are thin platelets or lamellae. [39] This was found to occur in other polymers and not just poly(ethylene). The polymer chains will fold back on themselves, re-entering the crystalline region (lamellae). [36-38] There are several models proposed for the reentry of the chains back into the lamellae. [37] The first is the random reentry, or the switchboard model, where the chains randomly fold back into the same lamellae or even participate in adjoining lamellae. The smooth surface adjacent reentry chain folded model involves reentry to the adjacent neighbours, with only a few exceptions due to multiple nucleation and chain end defects. This is an idealised visualisation of the process. The rough surface adjacent reentry chain folded model still involves reentry of the chain to local neighbours, but variation in the fold length may exist on a local scale. A schematic of polymer lamellar is shown in figure 1.19. [41]

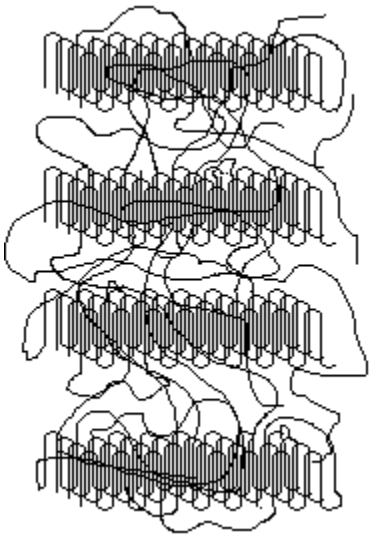

Figure 1.19 – Schematic of polymer lamellar. [41]

In quiescent conditions, the chain-folded lamellar radiate from a centre point, causing spherical structures known as spherulites to be created. [38] A diagram showing the spherulites can be seen in figure 1.20. [40] The centre of the spherulites is known as the nuclei. [37] Two types of nuclei exist. The first is referred to as homogeneous nucleation, where the origin arises from the polymer itself, and the second is referred to as heterogeneous nucleation, where the origin occurs from a particle different from the polymer, such as dust, catalyst or filler particles.

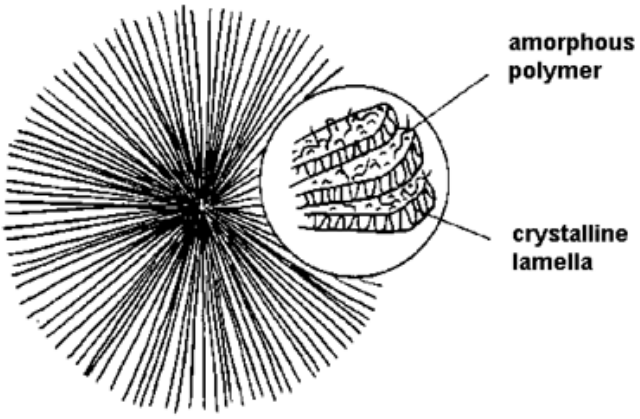

Figure 1.20 - Diagram of spherulites. [40]

Pennings *et al*. noticed a different morphology from the spherulites, and that the crystallisation takes place 20 ^{o}C higher than expected when polymer solutions where not stirred. [37-38] This process can be described as the long polymer chains being stretched out to form fibrous crystals. The resulting morphology is long bars of solid polymers with disks of chain folded lamellae growing longitudinally. This causes it to take on an almost shish-kebab shape. This process is shown in figure 1.21.

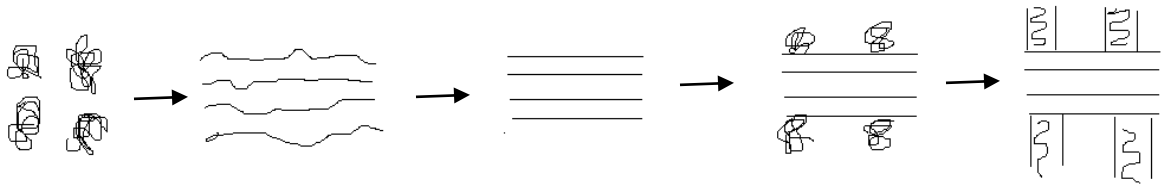

Figure 1.21 – Schematic showing the production of shish-kebab morphology in crystallisation induced by orientation. [37-38]

Crystallisation occurs best if there are no bulky side groups, such as aromatic rings, which can possibly affect the way the chains pack together. There are three ways bulky side groups can be arranged around the polymer backbone. [9 and 35] These three arrangements are atactic, isotactic and syndiotactic, and are shown diagrammatically in figure 1.22. [35] Atactic polymers have the

bulky side groups randomly arranged along the polymer backbone, whereas Isotactic polymers have the bulky groups positioned on the same side of the chain. Syndiotactic polymers have the bulky groups at alternating positions along the chain. Branched polymers and copolymers tend to decrease the crystallinity of the polymer because they do not fit into the most suitable conditions for crystallisation to occur, i.e. when the chain is symmetrical and linear.

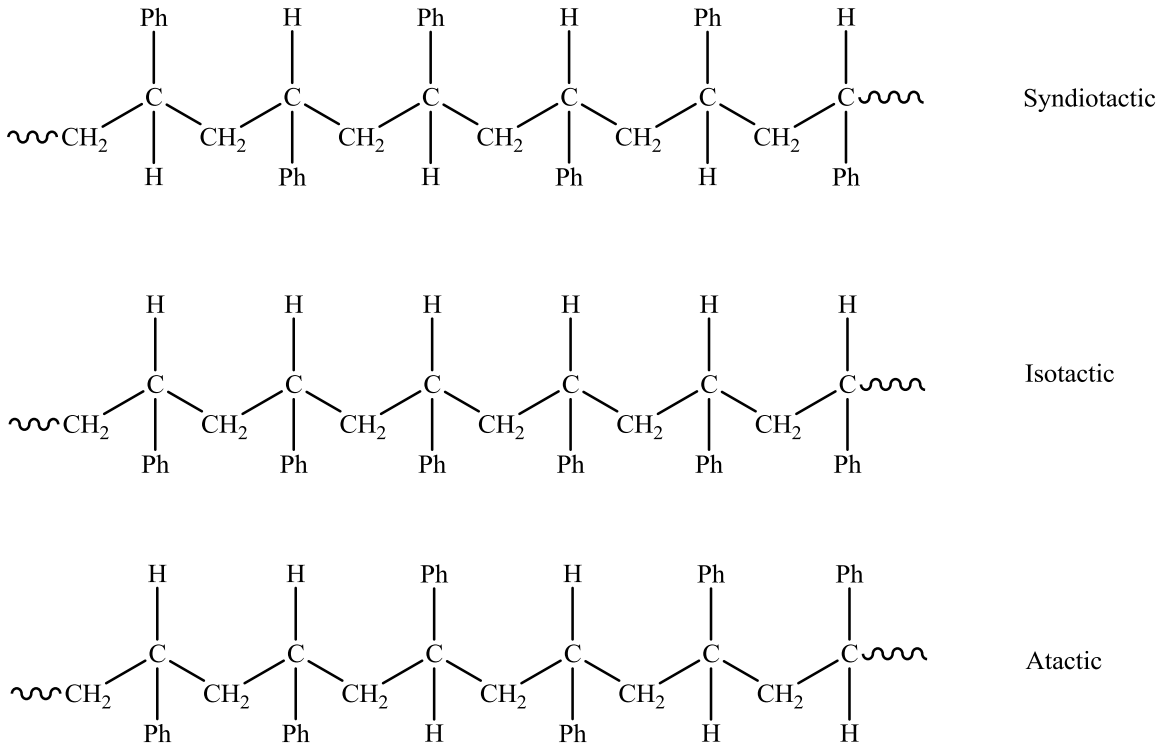

Figure 1.22 - Diagram showing atactic, isotactic and syndiotactic polymers. [After 35]

1.4.3 Melting Point

The transition from a crystalline solid to a liquid polymer is known as the melting point (Tm). [9] This means that amorphous polymers such as polycarbonate do not exhibit a melting point. Semicrystalline polymers like PET will have a melting point.

1.5 Degradation of Polyesters

1.5.1 Hydrolytic Degradation

There is concern that PET would not be suitable for long term outdoors applications such as solar cells due to hydrolytic degradation occurring. PET is quite resistant to attack by water, it shows resistance because of its aromatic nature and the fact that the chains are tightly packed. [10 and 42] At temperatures higher than the T_g, significant hydrolytic degradation occurs. Hydrolytic degradation produces carboxyl and hydroxyl end groups. [43-45] These end groups are produced by the chain scission reactions at ester linkages. One water molecule will break down one ester link therefore small amounts of water can have dramatic effects on average molar mass. The reaction showing the hydrolytic degradation of PET is shown in figure 1.23. [44]

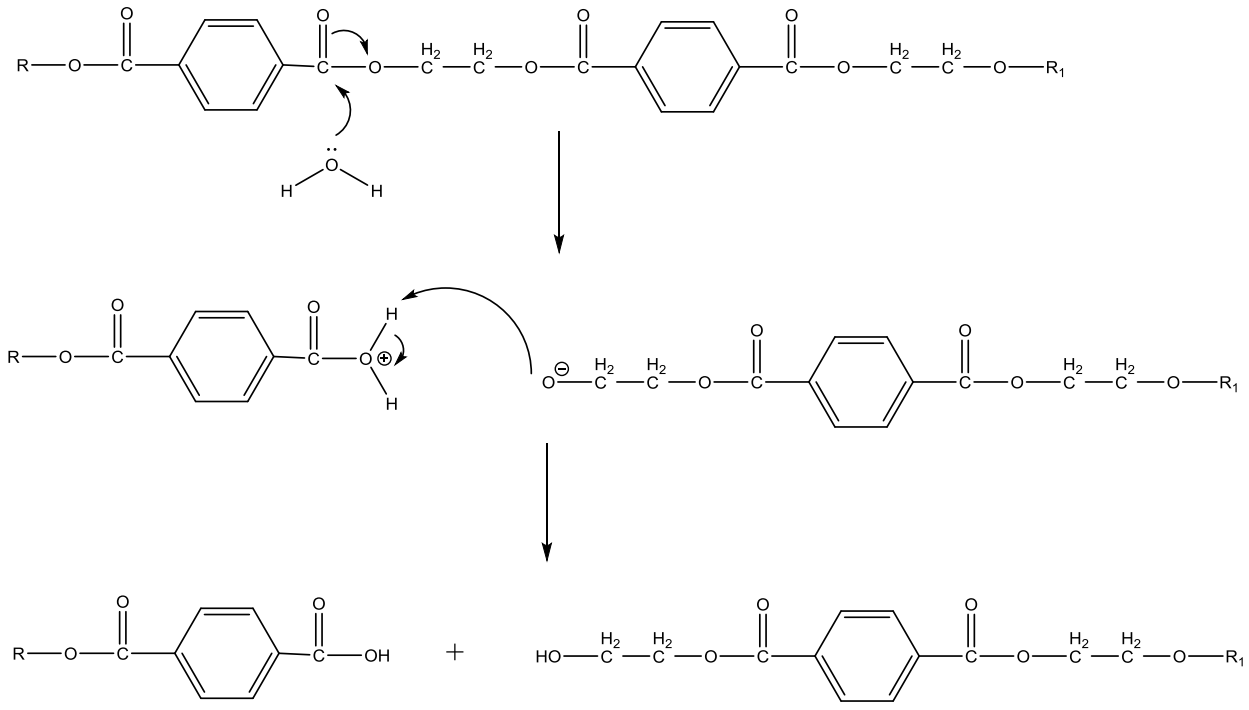

Figure 1.23 - Mechanism for hydrolytic degradation of PET. [After 44]

PET absorbs moisture rapidly. [10] The volume of water absorbed by PET will depend on the time exposed to moisture, particle size, crystallinity and relative humidity. PET is a semi-crystalline

polymer. The crystalline fraction will not take part in hydrolysis because it acts as a barrier to water. [44-47] The water molecules can diffuse into the amorphous regions of PET, where the chain scission reaction can occur. This causes a phenomenon known as chemi-crystallisation to occur. This is where the chain scission process causes small chains to mobilise and align to form crystalline regions. Therefore the crystallinity will increase as hydrolytic degradation occurs. Hydrolytic degradation has been proven to occur at the crystalline edges as well as the amorphous regions.

Hydrolysis is a very rapid reaction, but it does not reach completion. [46] It is suggested that as the number of end groups increase during degradation, there will be an increase in hydrophilicity and more water will penetrate into the system, giving the conditions for an autocatalytic reaction i.e. water and carboxylic acid end groups. [44] As water molecules are being used up in the reaction, it reduces the volume of water in the system, causing a reduction in the hydrolysis process and preventing the reaction from reaching completion. The rate of hydrolysis also increases in alkaline conditions. In alkaline conditions, the hydroxide will attack the carboxyl oxygen of the ester group to produce carboxyl and hydroxyl end groups. The reaction is shown in figure 1.24.

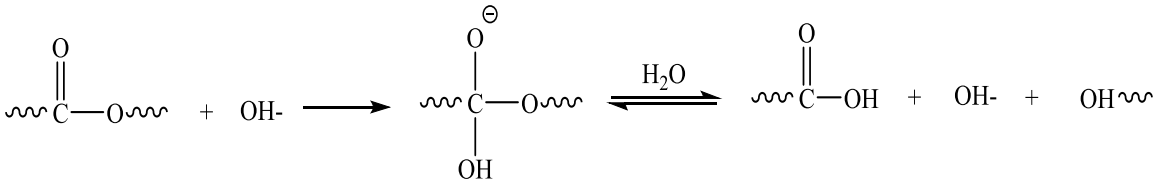

Figure 1.24 –Alkaline conditions for hydrolytic degradation. [After 46]

1.5.2 Thermal Degradation

Thermal degradation always occurs to some degree during synthesis and processing of PET. [10] It tends to occur at temperatures above the melting point, especially at temperatures higher than 400 ^{o}C.

The first stage of thermal degradation is the scission of the polymer chain at an ester link. [42 and 49-51] Ester groups degrade by a *β*-hydrogen transition to give olefins and acids. The decomposition tends to be achieved through a cyclic transition state. [42 and 49] This method has been proven by using the model compound ethylene dibenzoate. [42] The mechanism for the degradation of ester groups by a cyclic transition state is shown in figure 1.25.

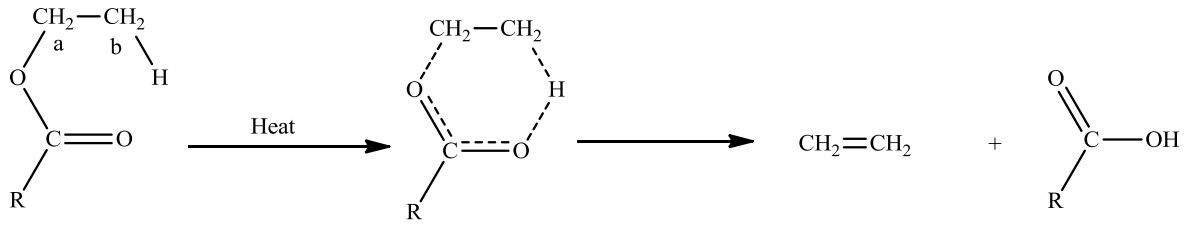

Figure 1.25 – Process for the degradation of ester groups by a cyclic transition state. [After 42]

The olefinic group produced during thermal degradation can be a terminal vinyl group from the scission of a bound ester group. [10] If the concentration of hydroxyl groups is low, then carboxyl end groups can add to the olefinic double bond. This will produce an acylal group which will decompose to give an anhydride, which can react with hydroxyl groups, producing more carboxyl end groups. [10 and 50] Acetaldehyde will also be produced during this stage. The reaction is summarised in figure 1.26 [10] Normally, the main product from thermal degradation will be acetaldehyde and will generate carboxyl end groups in the polymer. The process for this is shown in figure 1.27. [50]

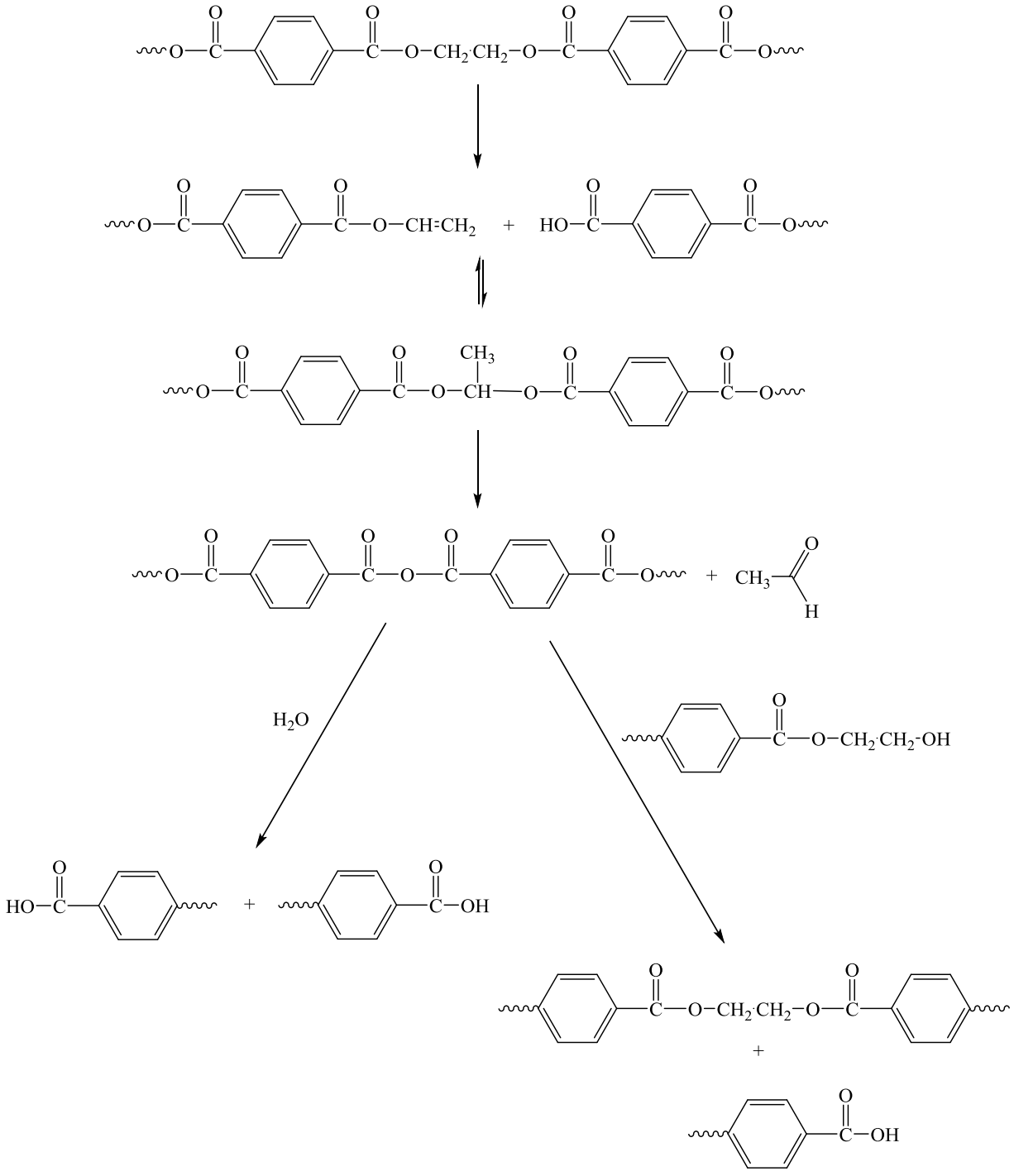

Figure 1.26 - Thermal degradation pathway that occurs if carboxyl end group concentration is low. [After 10]

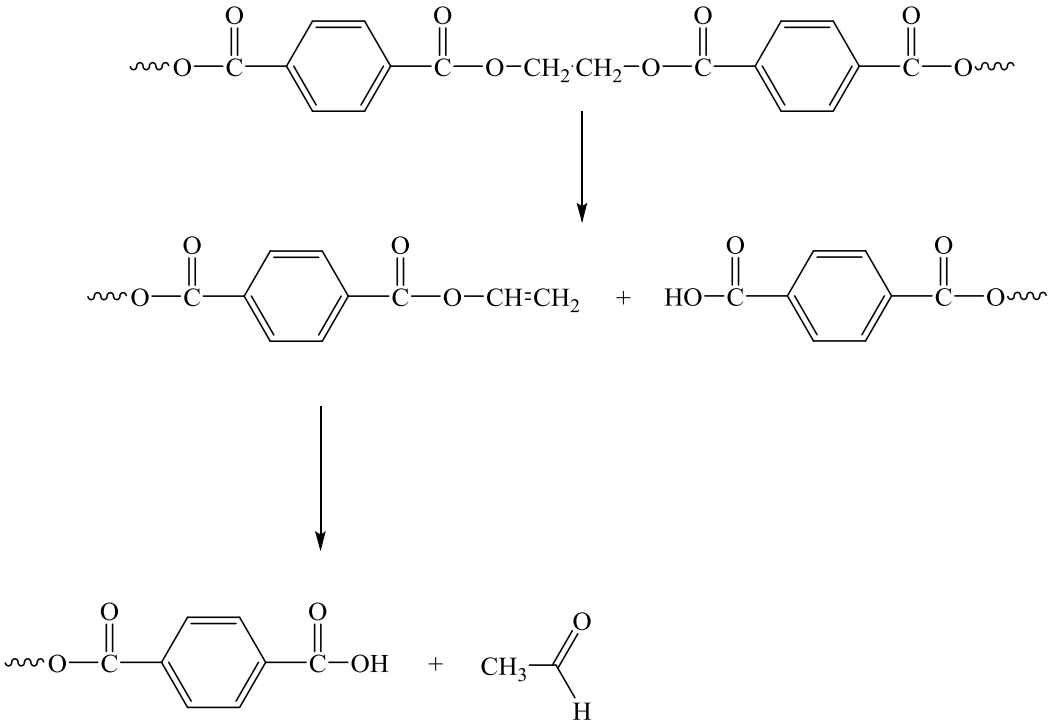

Figure 1.27 – Most common thermal degradation reaction of PET. [After 10 and 50]

If 2-hydroxyethyl end groups are present in the polymer, then the reaction shown in figure 1.28 can occur, again producing carboxyl end groups and acetaldehyde. [9 and 50]

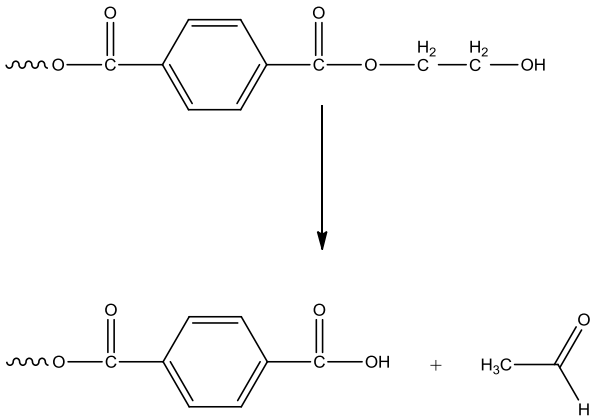

Figure 1.28 – Reaction of 2-hydroxyethyl groups during thermal degradation. [10 and 50]

As can be seen from the above mechanisms, one of the major components of thermal degradation of PET is acetaldehyde. [49-52] This is a major problem in polymer manufacture as acetaldehyde can migrate into the food or drink, causing flavour issues. [10] Other gaseous products include carbon monoxide, water, ethene, methane and benzene. [51-52]

As well as the gaseous products that are produced, solid products are also produced in the thermal degradation of PET. [10 and 53] Solid products include derivatives of benzoic acids, TPA and short chain oligomers. It has also been proven that cross-linked structures, known as gels, can be produced during thermal degradation. Holland *et al*. proposed reaction mechanisms for the thermal degradation of PET that could result in the formation of gels. [49] The reactions proposed by Holland *et al*. are shown in figure 1.29.

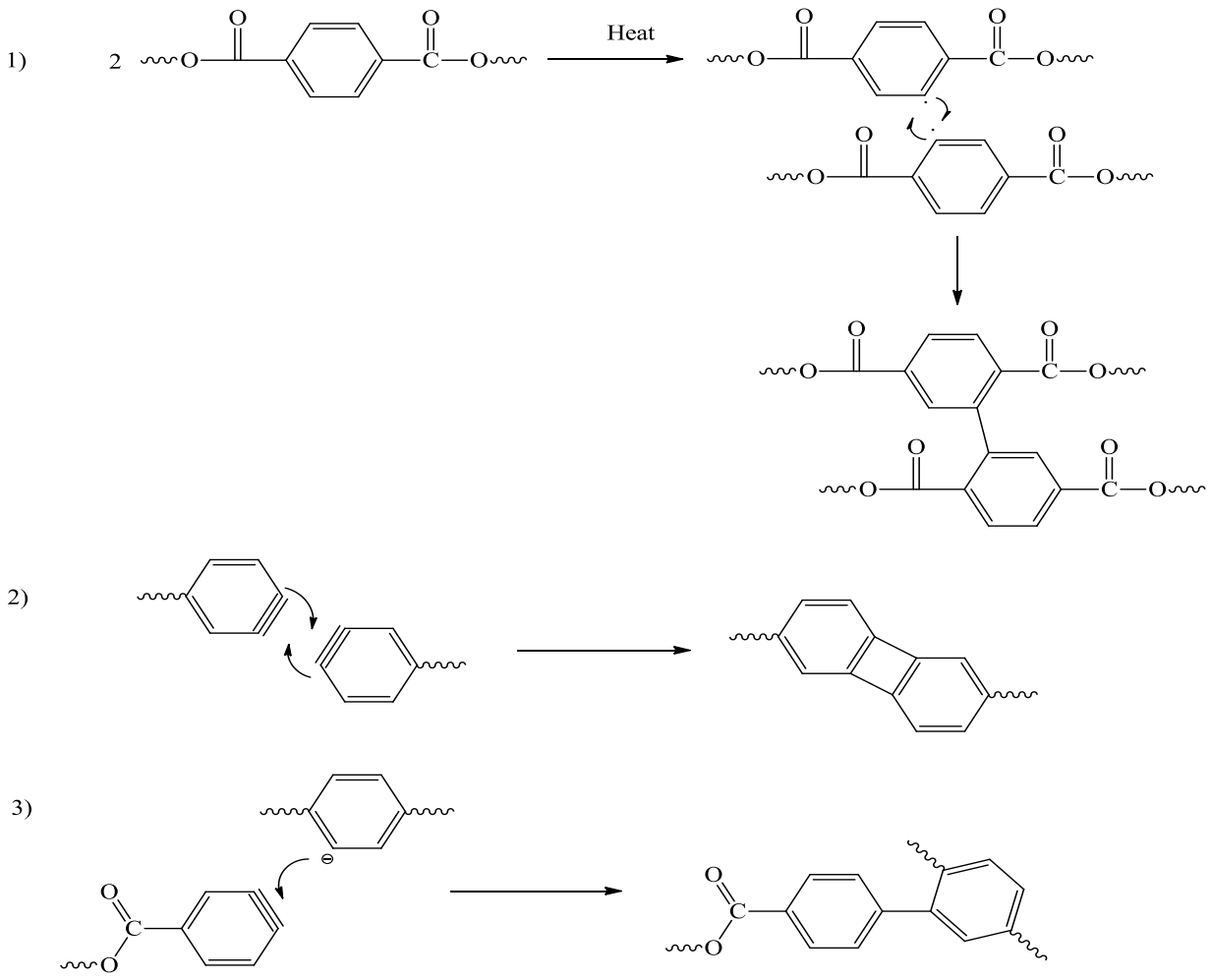

Figure 1.29 – Cross-linking reactions that can occur during thermal degradation of PET. [After 49]

Thermal degradation of PET can be influenced by metal catalysts. [10] The most active catalysts are zinc, cobalt, cadmium and nickel. The thermal degradation of polymers can be reduced by using triaryphosphites or triarylphosphates, which can block the metal ions in the polymer to reduce thermal degradation of PET. One of the simplest methods to reduce thermal degradation in PET is to reduce the process temperature.

1.5.3 Thermo-oxidative Degradation

When oxygen is present, a process known as thermo-oxidative degradation occurs instead of the thermal degradation behaviour discussed later in chapter 7. [10] Thermo-oxidative

degradation occurs much faster than thermal degradation. Radical mechanisms have been proposed for this type of degradation. The reaction is shown in figure 1.30.

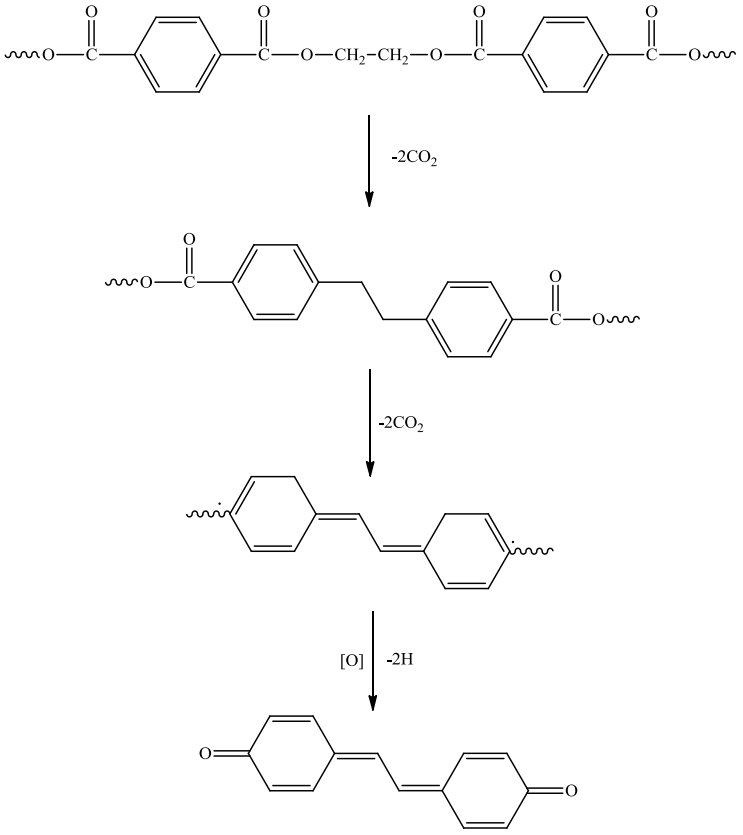

Figure 1.30 –The radical mechanism for thermo-oxidative degradation. [After 10]It has been well documented that thermal and thermal-oxidative degradation causes yellowing of the polymer. [10 and 51] The yellowing of polymers can be caused by the aldol condensation of acetaldehyde to produce polyaldehyde. [7] The production of polyaldehyde is shown in figure 1.31 [After 10]

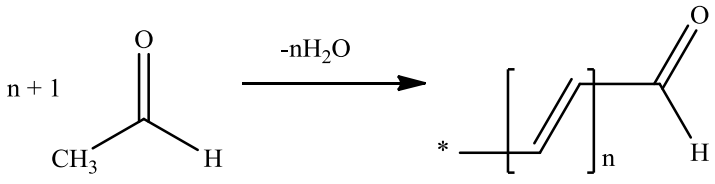

Figure 1.31 - Aldol condensation of acetaldehyde to produce polyaldehyde. [After 10]

Chromophores can also be produced from the formation of polyenes from vinyl acid end groups. [10] This process occurs in two steps. The first is the polymerisation of vinyl end groups to form polyvinyl esters. Carboxylic acids are then eliminated to form polyenes. The reaction showing the formation of polyenes is shown in figure 1.32.

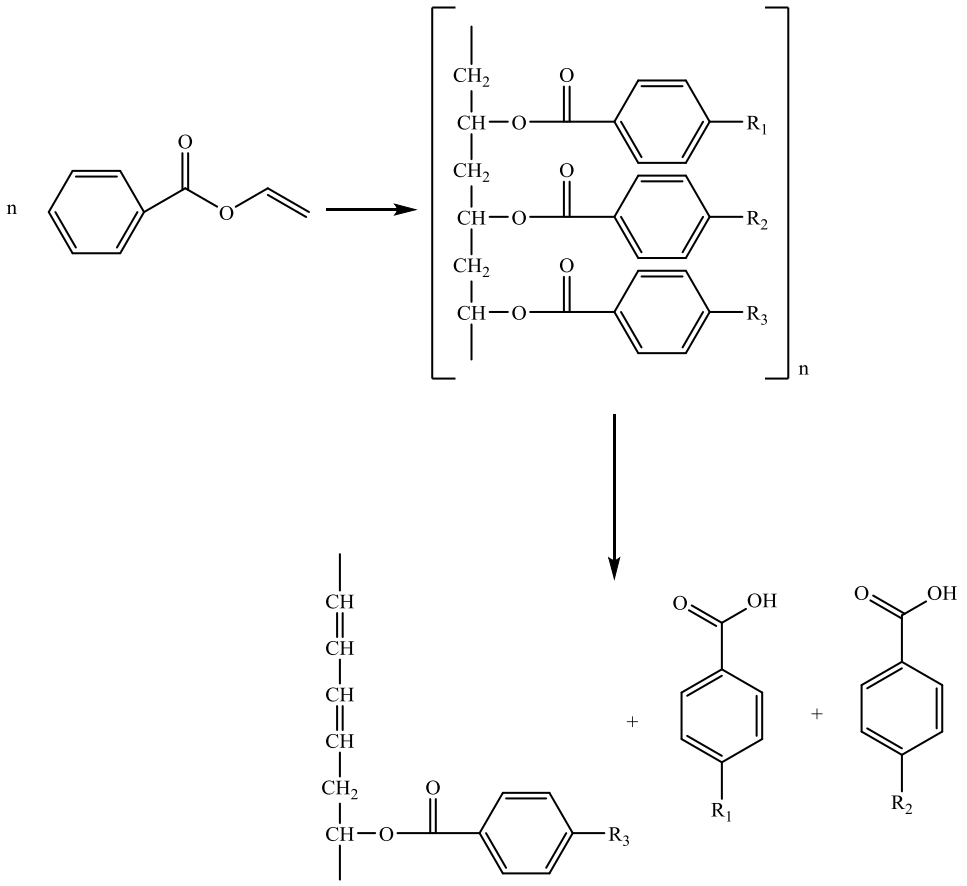

Figure 1.32- Reaction showing the formation of polyenes. [After 10]

Edge *et al*. investigated PET samples degrading at melt temperatures in both air and nitrogen. It was shown that the yellowing occurred faster in the presence of oxygen. [51] It was shown that, for short residence times, the formation of polyenes were not the cause of the yellowing. It was proposed that the yellowing was caused by the formation of quinone structures. [10 and 51] The mechanisms proposed for the formation of these quinone species are shown in figure 1.33.

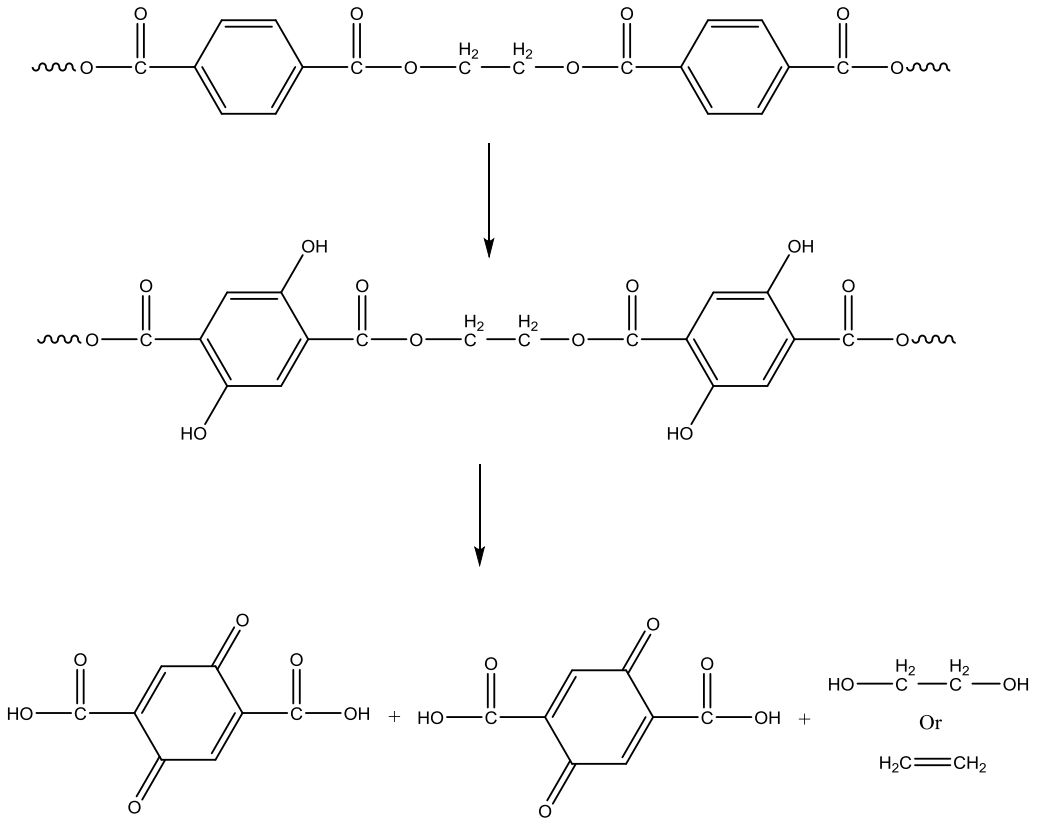

Figure 1.33 - Thermo-oxidative degradation showing the formation of quinones. [10 and 51]

1.5.4 Photolysis

PET is normally considered to be quite stable when exposed to ultraviolet (UV) light. [42] However degradation of PET occurs under different exposure conditions. It has been reported that photolysis is caused by light with wavelengths in the range 290 – 420 nm. [42 and 54-56] There have been reports that the wavelength of 390 nm in particular causes degradation to occur. The light is absorbed by the ester carbonyl groups that are present in the polymer backbone. The absorption of light causes the molar mass of the polymer to reduce significantly, and affects the physical properties of the polymer. It affects properties such as tensile strength and surface crazing occurs. Yellowing of the polymer can also occur.

The degradation has been shown to occur mainly at the surface because of strong surface absorptions. [54-59] Work has been carried out by several different groups and has shown that the chemical composition of the film on the surface is different from the bulk. One of the most useful techniques for studying this is the attenuated total reflectance (ATR) spectroscopy. Day *et al*. demonstrates, using ATR, that the concentration of carboxyl end groups was higher on the surface of the polymer compared to the bulk material. [54] They showed that the buildup of carboxyl end groups was not only on the side facing the light source, there was also a buildup of carboxyl end groups on the other side of the polymer sample. It was also shown that the mechanical properties of the damaged surface are very different from those of the bulk. [54-56]

There have been reports that the photo-degradation process occurs in two stages, a very rapid initial step followed by a slower step. [60] The very fast initial step is the main chain scission of the PET chain followed by subsequent reactions. The volatile products that have been widely reported to occur when PET is irradiated with UV light includes carbon monoxide, carbon dioxide, hydrogen, methane, ethane, water, methanol, butanone, acetic acid, formaldehyde, benzene and toluene. [10, 54 and 61-62] Other products reported include the formation of carbonyls, carboxylic acids, quinones, diquinones, hydroperoxides and vinyl species. [10, 54 and 63] There are three processes that can occur when a polymer is exposed to UV light; photo-degradation, photo-hydrolysis and photo-oxidation. [10]

It is assumed that these processes occur in the amorphous region or at the edges of the crystalline regions. [10] The degradation products produced are smaller polymer molecules. These molecules may regroup and result in structural modification of the surface of the polymer. This has been confirmed as an increase in the crystalline region has been noticed. This is because the smaller degradation products will realign into a crystalline region. This effect is known as chemi-crystallisation. [10 and 64] When the polymer is being irradiated no reordering or reconstruction can take place when stress is applied, the applied load is distributed throughout the degraded areas. [10 and 54-58] This results in cracks in the surface layer. These cracks that are

responsible for the initiation of fractures which travel through the bulk of the polymer; it is this that causes tensile failure.

1. Photo-degradation

Photo-degradation occurs when no oxygen is present as UV light degrades the polymer. [10] The polymer is seen to yellow as well as have a reduction in the molar mass. [10 and 54-58] There is also a large increase in the carboxyl end group concentration. There have been several different mechanisms proposed. [10 and 62] It is well known that PET, when irradiated with UV radiation, can degrade by the Norrish type 2 reactions shown in figure 1.34. [62] The vinyl products that are produced during photo-degradation are expected to contribute to the yellowing of the polymers. This reaction however does not explain the production of carbon monoxide and carbon dioxide. The productions of these volatile gases suggest a Norrish type 1 degradation reaction of ester functionality. [10 and 62] There are three possibilities that occur for Norrish type 1 reactions, which are shown in figure 1.35. [10]

Day *et al*. suggested that for the reaction shown in figure 1.35 part C to occur, it would require a wavelength of 281 nm. [54-56] this would be unlikely to be the mechanism for photo-degradation as terrestrial sunlight cuts off around 295 nm. Work has been carried out in vacuum systems by Day *et al*. to show that the formation of carbon monoxide and carboxyl end groups are present in much higher yields than carbon dioxide. This suggests that the mechanism shown in figure 1.35 part B is the most favorable mechanism, and that carbon dioxide is produced by another reaction, because this reaction does give some of the products that are produced such as formic acid and *β*-hydroxyethoxybenzoic acid, which have been reported in the literature. All of the reactions that occur produce products that have been reported over the years.

The yellowing of the polymer in UV light can be explained by the production of cross-linked species. [10 and 54-56]

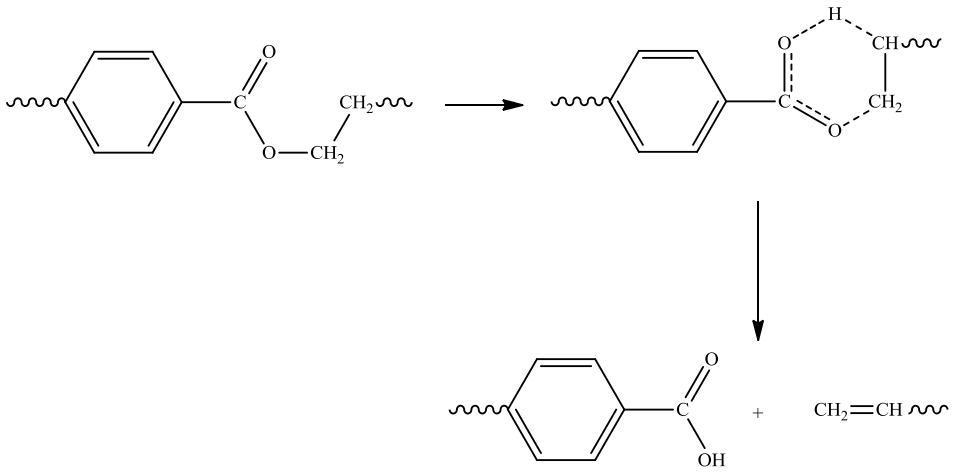

Figure 1.34 - Norrish type 2 reaction. [After 62]

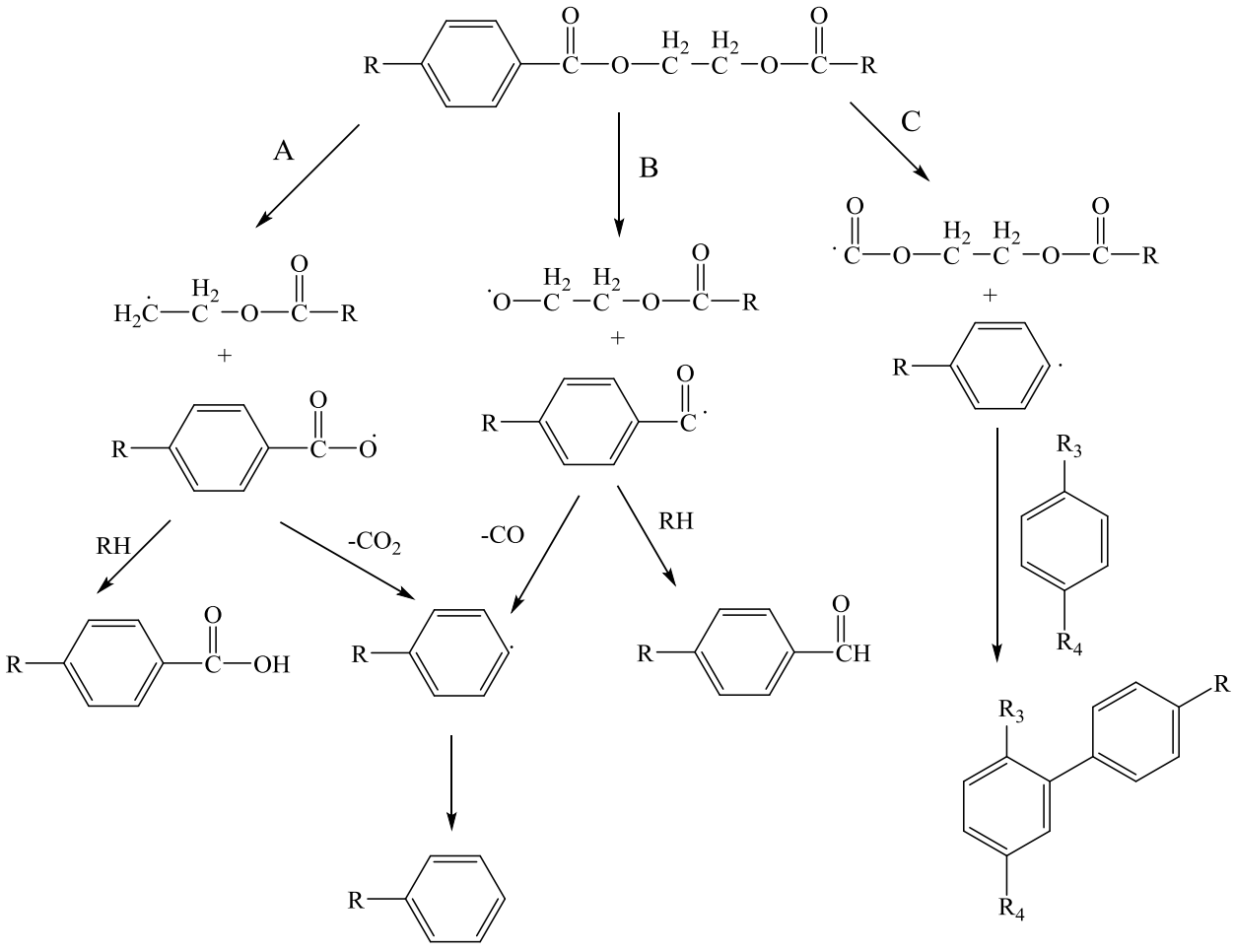

Figure 1.35 - Three possible Norrish type 1 reactions. [After 10 and 62]

2. Photo-hydrolysis

The presence of hydroxyl groups suggest that hydrolysis can also occur in the presence of UV light. [12] This reaction is known as photo-hydrolysis, and the reaction is shown in figure 1.36.

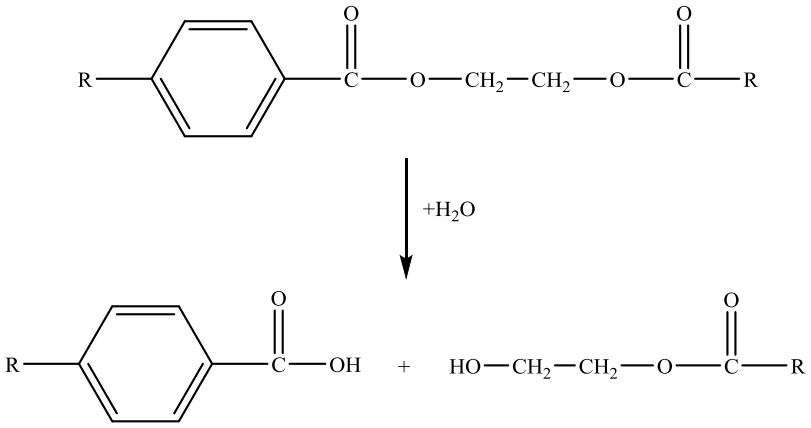

Figure 1.36 – The photo-hydrolysis reaction. [After 10]

3. Photo-oxidation

When oxygen is present in the system the reaction that occurs with UV light is known as photo-oxidation. [10 and 54-65] In photo-oxidation it has been reported that the polymer does not yellow in colour, but there is evidence of an increase in the production of carbon dioxide. Work by Day *et al*. shows that cross-linking does not occur during photo-oxidation, which is why the polymer does not yellow when oxygen is present. [54-56] It was shown that only a small presence of air inhibits cross-linking. It has been suggested that there is a completely different mechanism for photo-oxidative degradation.

Two mechanisms are proposed for the photo-oxidation of PET. [10] The first mechanism explains the increase in carbon dioxide production noticed when air is present compared to the reaction under vacuum. This reaction involves the formation of a hydroperoxy radical that is

subsequently followed by hydrogen abstraction to form a hydroperoxide (figure 1.37). [10 and 54-57] This will produce two radical species; an alkoxy radical and a hydroxy radical. The hydroxy radical can diffuse easily through the polymer matrix because it is not attached to the bulk polymer chain ends, which makes it more destructive.

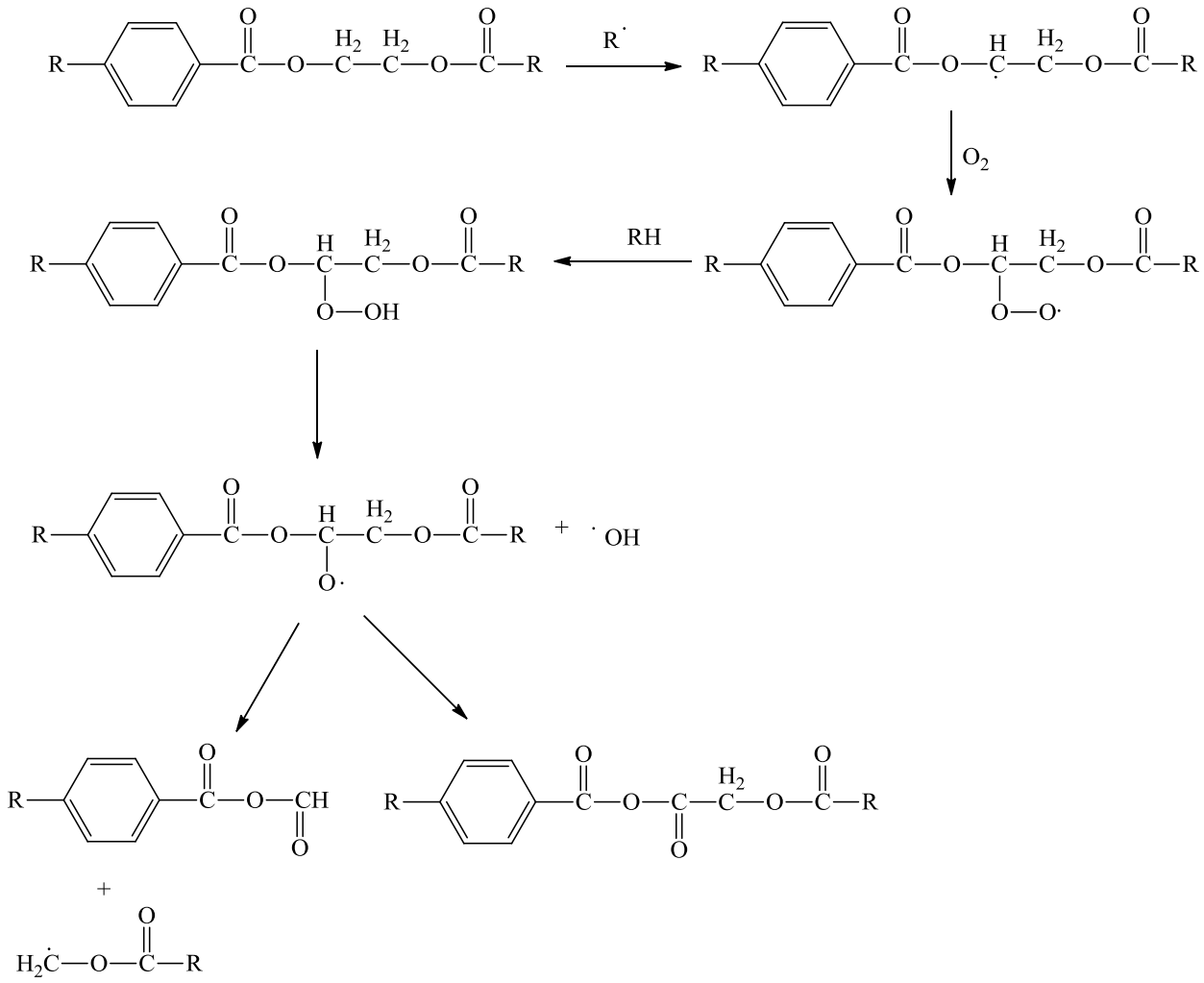

Figure 1.37 – First possible reaction for photo-oxidative degradation. [After 10 and 54-57]

The other reaction proposed for the photo-oxidation is shown in figure 1.38 and involves a ring oxidation reaction. [10 and 54-57]] The production of the dihydroxy species is expected to be responsible for the fluorescent species that are observed in photo-oxidised PET. The ease of oxidation of hydroquinone results in the formation of quinones.

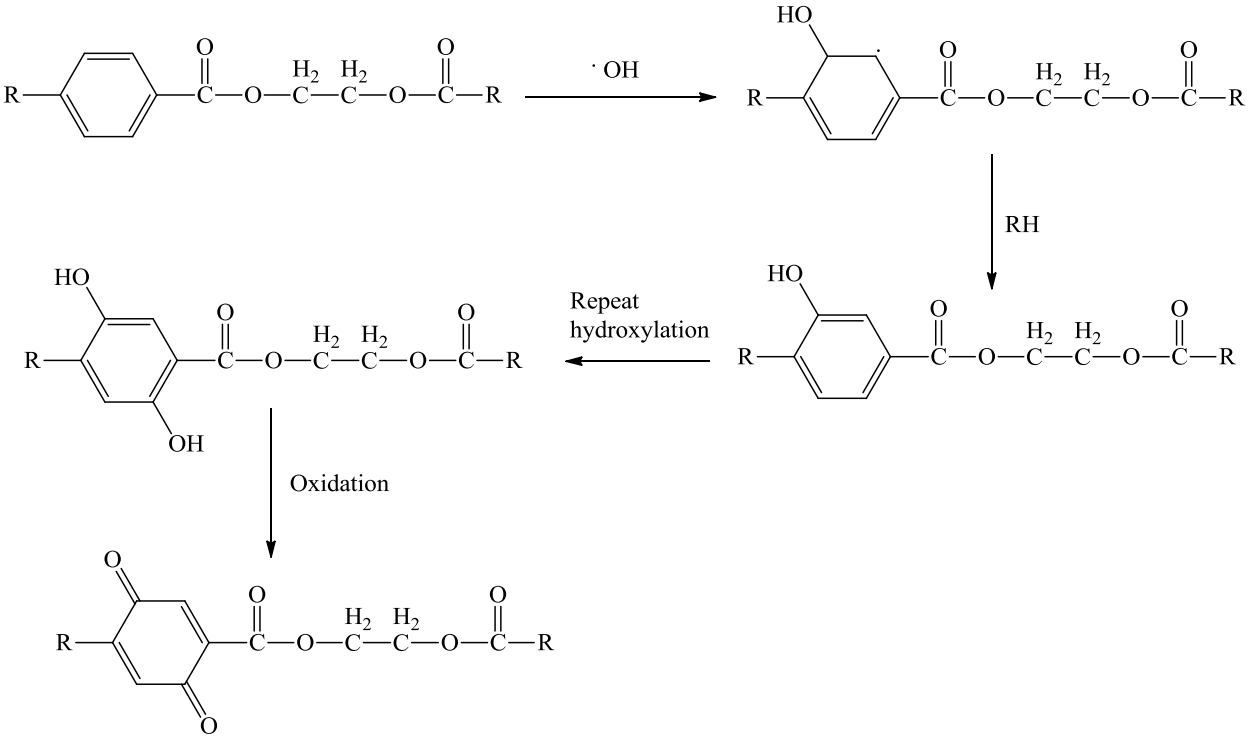

Figure 1.38 – Second possible reaction for photo-oxidative degradation. [After 10 and 54-57]

1.6 Additives for PET

PET's resistance to hydrolytic degradation can be improved by using anti-hydrolysis additives, carboxylic acid scavengers and chain extenders. [10] Anti-hydrolysis additives will react with any moisture that is present, preventing the hydrolysis of PET. Carbodiimides, polycarbodiimides and calcium oxide are some of the anti-hydrolysis reagents. These types of additive do not

provide a long term solution, but are useful to maintain the molecular weight of the polymer during melt processing. Polycarbodiimides and phenylenebisoxazoline are used as carboxyl acid scavengers because they can react with the carboxyl end groups of PET, reducing the carboxyl end group concentration, which has been shown to influence the hydrolysis resistance of the polymer. These compounds can be monofunctionalised and can behave similarly to chain extenders.

Chain extenders have been widely researched with PET because they can increase the molecular weight after hydrolysis. [10] These are multifunctional compounds that react quickly with the end groups of PET. This process can increase the molecular weight of the polymer produced with melt polymerisation without the need for the PET to go through solid-state polymerisation afterwards. This is an advantage because it is more flexible, it does not require extra investments, it has a faster reaction rate and a lower system cost. The reaction of mixing chain extenders with PET is normally carried out in the melt state using an extruder; this process is called reactive extrusion. [66-67] The chain extenders must be easily prepared, thermally stable, non-volatile at PET processing temperatures and not react to give volatile products. [10] The most common chain extenders that are used with PET include diepoxides, diisocyanates, dianhydrides, bis-oxazolines and triphenyl phosphate. [66-74] The structure of some of the compounds that are used as chain extenders are shown in figure 1.39.

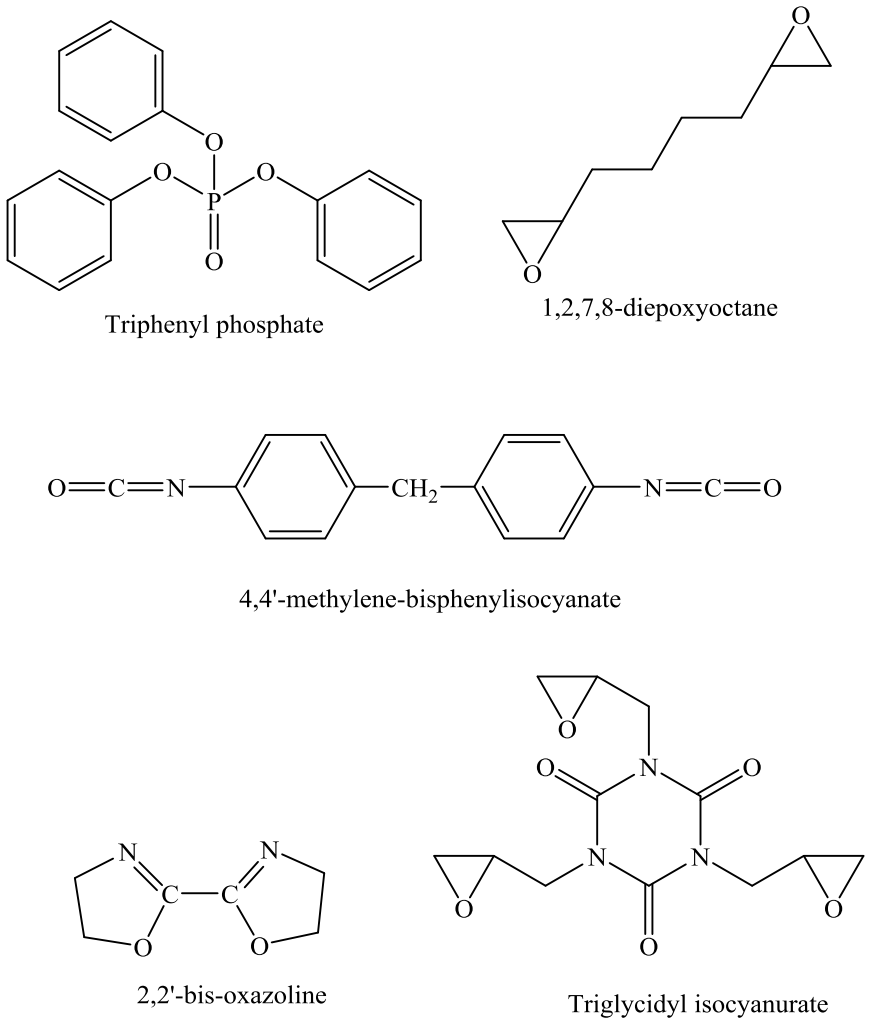

Figure 1.39 - Structures of possible chain extenders. [66-74]

One of the most common types of chain extenders used are dianhydrides. [66-67] The most common dianhydride used for chain extension is pyromellitic dianhydride (PMDA). PMDA has been used in reactive extrusion of PET with great effect. It was added at levels between 0.50 and 0.75% to industrial scraps of PET and successfully produced a polymer that was suitable for blow moulding processes. [75] It has also been added to increase the IV of PET with clay nanocomposites during extrusion as it has been shown to have little influence on the clay's exfoliation in PET/clay nanocomposites. [76] The reaction of PMDA with PET chains is shown in figure 1.40. [20] As with all chain extenders, the concentration of PMDA has to be carefully controlled as cross-linking will occur if the chain extender is used in excess of theoretical

amounts. [67] Unlike dianhydride compounds, bis-oxazolines have been shown to react with the carboxyl end groups of PET. [68 and 72] The reaction between bis-oxazoline and carboxyl end groups produce a stable ester amine linkage [68] Several research groups have shown that the reaction between bis-oxazoline and carboxyl end groups of PET occurs better at high temperatures. [68, 72]

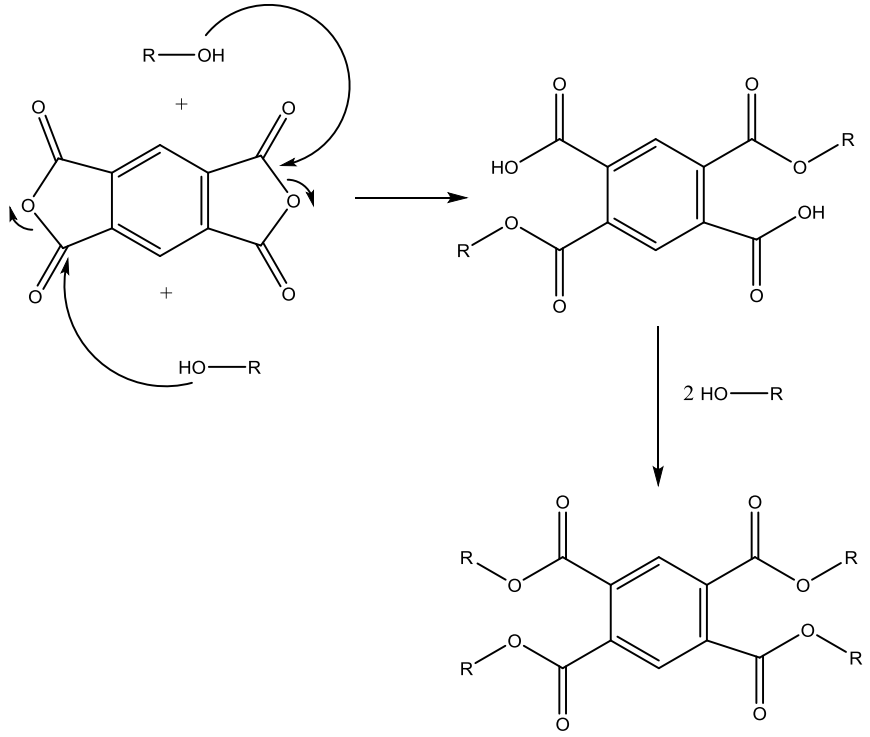

Figure 1.40 - Mechanism for the chain extension of PET with PDMA. [After 66]

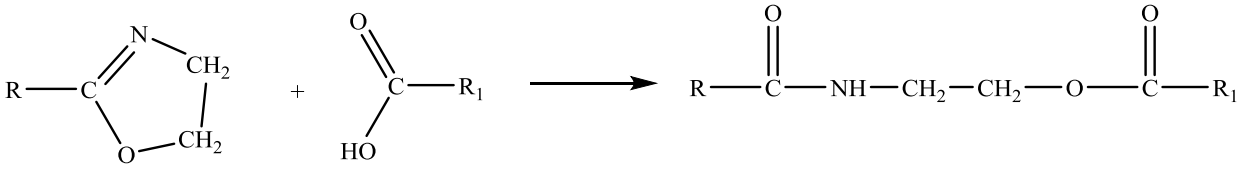

Figure 1.41 – Reaction of the chain extension of PET with bis-oxazoline. [After 68]

Diisocyanates are able to react with both carboxyl and hydroxyl end groups of PET. [68, 70 and 77] However, they react preferentially with the hydroxyl end groups of PET. The reaction between hydroxyl end groups and diisocyanates gives a urethane group. [68 and 77] This reaction is shown in figure 1.42 part A. An amide is formed from the reaction between the diisocyanate and a carboxyl end group; this reaction is shown in figure 1.42 part B.

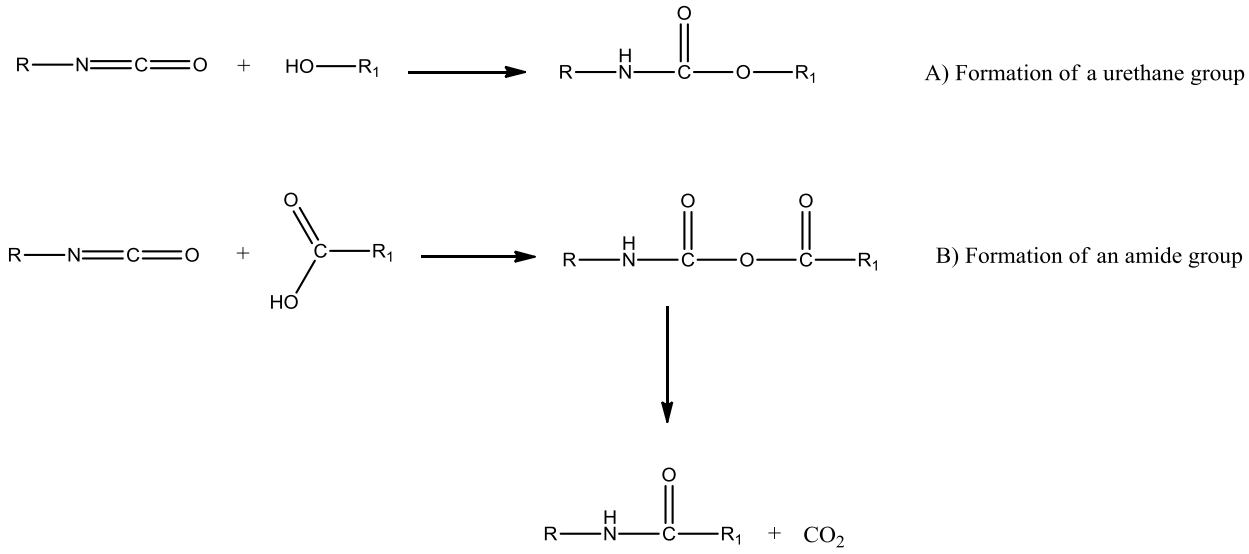

Figure 1.42 – Reaction of diisocyanates with hydroxyl and carboxyl end groups of PET. [After 68 and 77]

Torres *et al*. studied diisocyanates, bis-oxazolines and diepoxides. [68] The work carried out showed that the diisocyanates were the most reactive towards the end groups of PET. There is evidence to state that aromatic diisocyanates are more reactive than aliphatic diisocyanates. An issue with diisocyanates was shown by Raffa *et al*., where it can react with water that is present in the system. The reaction that can potentially occur is shown in figure 1.43. [77]

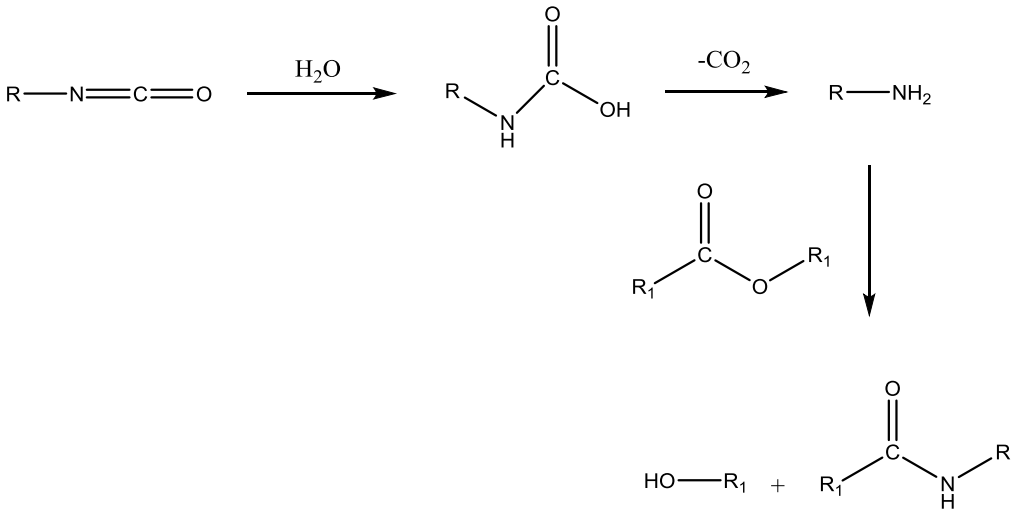

Figure 1.43 – Reaction of diisocyanates with water. [After 77]

Many research groups have worked with diepoxide chain-extenders of PET. [68 and 78-81] Like diisocyanates, the diepoxides can react with both hydroxyl and carboxyl end groups. The epoxide groups can also react with amine and imides groups. [73] However, they react with carboxyl end groups preferentially. [68] Japon *et al*. carried out experimental work to show that the esterification reaction is the most preferred during reactive extrusion. [81] This is because they are more reactive and the reaction time is short in the extruder. The reaction time is normally less than two minutes. Etherification is the reaction that occurs between the hydroxyl end groups of PET and diepoxides. [68, 78 and 82-83] It is called an etherification reaction because an ether group is formed during the reaction. The reaction is shown in figure 1.44 part A. The reaction between diepoxides and carboxyl end groups is known as an addition esterification reaction as an ester group is formed during the reaction. The esterification reaction between diepoxides and PET is shown in figure 1.44 part B. The addition esterification reaction has been widely reported to produce a secondary alcohol. It is possible that a primary alcohol can also be produced in the reaction between epoxides and carboxyl end groups. The products of esterification are shown in figure 1.44. The formation of the primary alcohol is less favoured due to steric hindrance of the epoxide group.

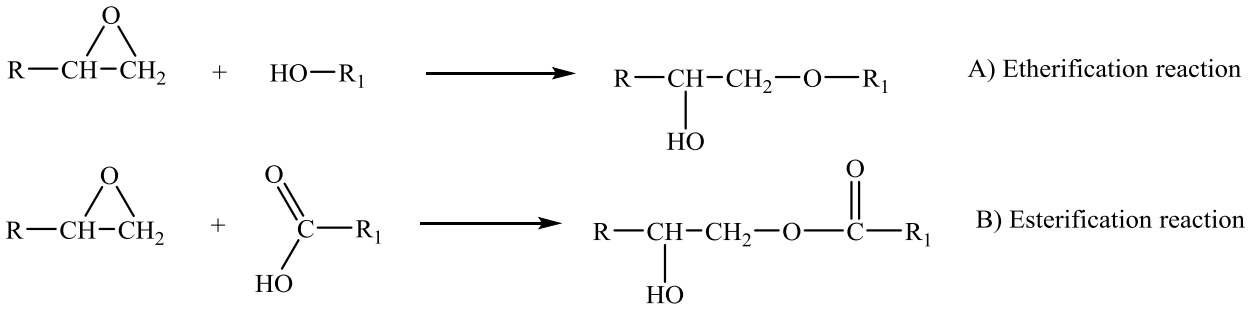

Figure 1.44 – Reaction showing the etherification and esterification reactions of hydroxyl and carboxyl end groups of PET with epoxides. [68, 78 and 82-83]

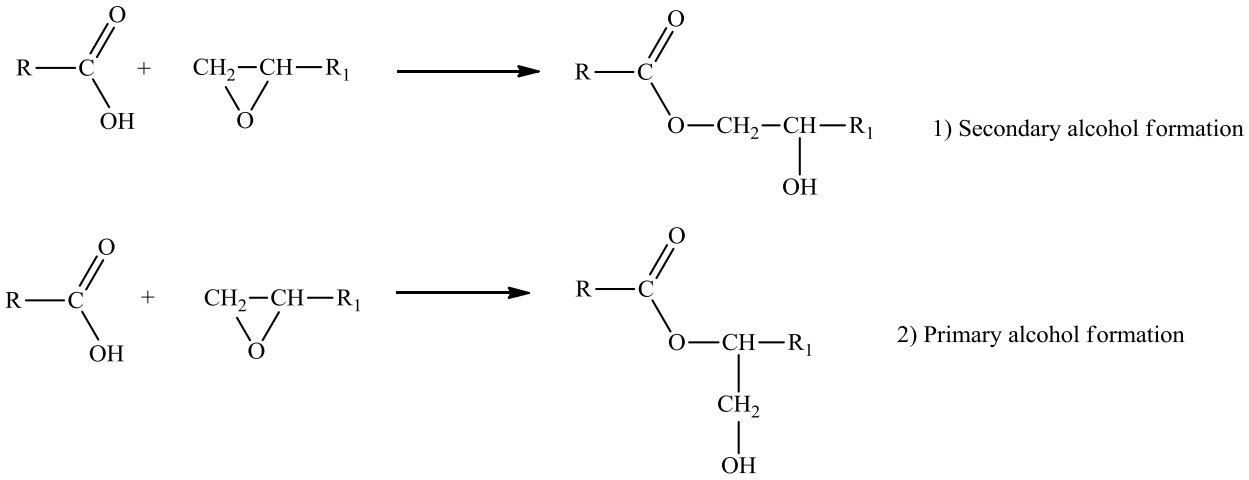

Figure 1.45 – Reaction showing the formation of primary and secondary alcohols from the esterification reaction of an epoxide and carboxyl end groups of PET. [68, 78 and 82-83]

The alcohol groups produced can further react with epoxide groups (etherification reaction) or with an acid (condensation esterification). [82] The condensation reaction can occur at the high temperatures used in the reactions, normally between 230 to 280 ^{o}C. Water is produced during

a condensation esterification reaction. The reaction scheme is shown in figure 1.46, and branching and cross-linking of the polymer results from this reaction. The rate that branching occurs is slow due to steric hindrance. If the concentration of the chain extender is low then the reaction with the secondary alcohol is negligible. [68, 78 and 82-83] Cross-linking can be a problem as it occurs uncontrollably, so care has to be taken to control the level of chain extender in the reaction. In film production the presence of branching/cross-linking is undesirable. However, for other applications, such as extrusion blow moulding, producing highly viscous cross-linked samples is beneficial. [84-85] In these cases where cross-linking is useful it is beneficial to use tri-functionalised or higher functionalised epoxides. Japon carried out an experiment reacting epoxides with different functionalities with PET. [81] The results showed different rates of reaction depending on the epoxide. The work showed the importance of selecting an epoxide that will react to the desired level inside an extruder. Dhavalikav reported that excessive branching occurred with small concentrations of epoxides. [84-85]

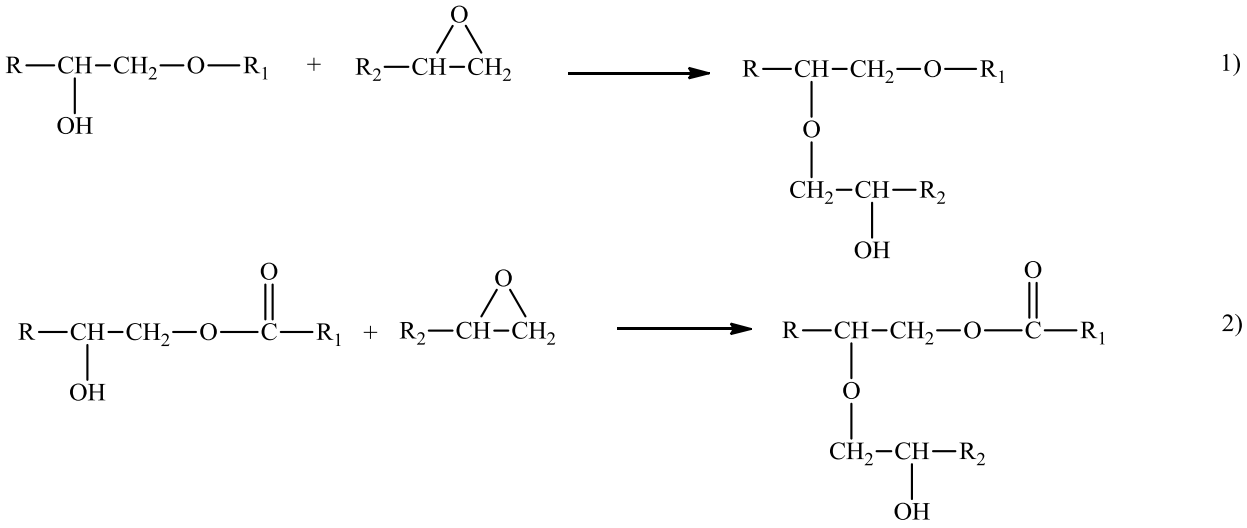

Figure 1.46 - The condensation esterification reaction between the secondary alcohols and epoxide groups. [After 82]

The polymer can be monitored easily for branching because a linear chain-extending reaction would produce polymers that have a low carboxyl end group concentration and high viscosity.

[9] Branched chain extension reactions would give polymer samples that have a low carboxyl end group concentration with an intermediate viscosity.

1.7 End Group Determination Methods

The importance of the carboxyl end groups concentration has been discussed as it affects the crystallisation of the polymer, reduces the polymer's stabilisation against degradation and allows for further reactions to occur. Over the years, there have been numerous ways that the carboxyl end group concentration of PET can be measured. [86-93] These include titration and spectrometric techniques, such as infrared (IR) spectroscopy and nuclear magnetic resonance (NMR).

One of the oldest methods for determining the concentration of carboxyl end group concentrations in PET is titration. For carboxyl end groups, the most commonly used method is the titration outlined by Pohl in 1954. [86] This method involves between 0.1 to 0.2 g of PET being dissolved in 5 ml of benzyl alcohol that has been heated up to 215 ^{o}C. The polymer is stirred continually for the 110 seconds that the polymer is heated. The test tube containing the dissolved polymer is quenched in cold water for 6 seconds before being emptied into a beaker containing 10 ml of chloroform. Chloroform is added as a liquefier to prevent too thick a gel from forming. A rinsing of 5 ml of benzyl alcohol is then added to the test tube. This is allowed to heat up for 60 seconds before being added to the beaker. Two drops of phenol red indicator are added to the beaker and the mixture is titrated with a 0.1N sodium hydroxide solution in benzyl alcohol or ethyl alcohol. This method was shown by Pohl to be reliable by comparing results with another titration method - both methods agreed within experimental error.

The advantage of this method is that the hot benzyl alcohol used in the Pohl titration dissolved a wide range of PET samples. [86] One of the most important considerations that has to be taken into account with this method is that the high temperature used to dissolve the polymer could potentially cause thermal degradation to occur in the sample. Pohl calculated the rate of

degradation that occurred in the polymer at the conditions used. It was proposed that 1.6 equivalence per 10^6 grams should be subtracted from the carboxyl end group concentration obtained to compensate for the degradation that occurs.

Some of the other titration methods used for the calculation of carboxyl end group concentration in PET include dissolving the polymer in freshly distilled aniline at 140 ^oC, adding phenolphthalein and titrating with sodium hydroxide, or dissolving the polymer in a mixture of *o*-cresol and chloroform (70 + 30 g) and then potentiometrically titrating with 0.1N ethanolic potassium hydroxide solution. [87-88] The latter method was reported to produce considerably higher values than expected, despite several modifications that were tried. It has been reported that acidic solvents could potentially cause inaccurate end group concentrations to be obtained; this is why Pohl used benzyl alcohol. [88] The potentiometric method has the advantage that a correction value for thermal degradation does not need to be applied because the dissolution of the polymer occurs at 90 ^oC. [87] The reaction does take considerably longer however, as the PET normally takes about 30 minutes to dissolve. Maurice and Huizinga provided evidence to show that the Pohl titration and potentiometric titration provide similar carboxyl end group concentration values. [88] The advantage of all of the titration methods is that there is no requirement for expensive spectrometers and they are simple to carry out.

Ward worked on a method in 1957 for determining the carboxyl end group concentration of PET using IR spectroscopy. [90] The PET pellets were first pressed into films that were 0.012 inches thick. The polymer sample was then repeatedly immersed in pure D_2O and the polymer was then dried and burned. The water from the combustion was collected and the deuterium content of this water was determined by IR spectroscopy. This measurement allowed the total number of –OH and – COOH groups to be determined.

Other methods of obtaining the carboxyl end group concentration by IR spectra are based on the principles outlined by Ward. Al-Abdulrazzak *et al*. placed film samples in a vacuum cell that was specially designed to fit in the path of the IR beam of the spectrometer. [94] A plot of percentage transmittance against frequency in the range 4000 cm^{-1} to 2380 cm^{-1} was obtained.

This method shown by Al-Abdulrazzak was reproducible and produced similar carboxyl end group concentrations obtained from other methods.

Much research has been done on determining a reliable method for the determination of carboxyl end groups of PET by nuclear magnetic resonance (NMR). This research has been carried out in order to reduce the errors and disadvantages of the other methods, which include the endpoint of titrations being subjective, broad peaks being produced in the IR spectra that are difficult to interpret and large amounts of sample can be required for titrations. [86-91]

One of the main issues with using NMR for analysis of PET is that it will only dissolve in dimethyl sulfoxide (DMSO) and tetrachloroethane (TCE) at high temperatures. [92-95] The high temperatures used will promote thermal degradation to occur, especially if there are trace levels of water present. This means that, for a long time, NMR was only used for PET samples with a low molecular weight. Mixtures of fluorinated solvents such as hexafluoroisopropanol (HFIP)/deuterated chloroform ($CDCl_3$) and trifluoroacetic acid (TFA)/$CDCl_3$ will dissolve PET at room temperature for analysis by NMR.

Fox *et al*. suggested that TFA was not useful as a solvent because it was not reliable at determining the end group concentration of PET, as the signals overlapped with that of the end groups. [93] They did, however, suggest that it is useful for determining the presence of co-monomers. Deuterated acids have been reported to give large lock peaks that cause signal overlap to occur. A combination of HFIP and $CDCl_3$ has been reported to be a good solvent system for NMR analysis of PET.

Ma *et al*. provided a method for the determination of the end groups of PET. This method is based on the carbodiimide-mediated room temperature esterification of carboxyl end groups of polyesters with HFIP. [96] Figure 1.47 shows the reaction that is taking place. The ester that is formed is compared with the external reference, triflurotoluene (TFT). Both ^{1}H and ^{19}F NMR

spectra are obtained for this reaction. The main advantage of this method is that the reaction occurs at room temperature, so degradation is not a concern.

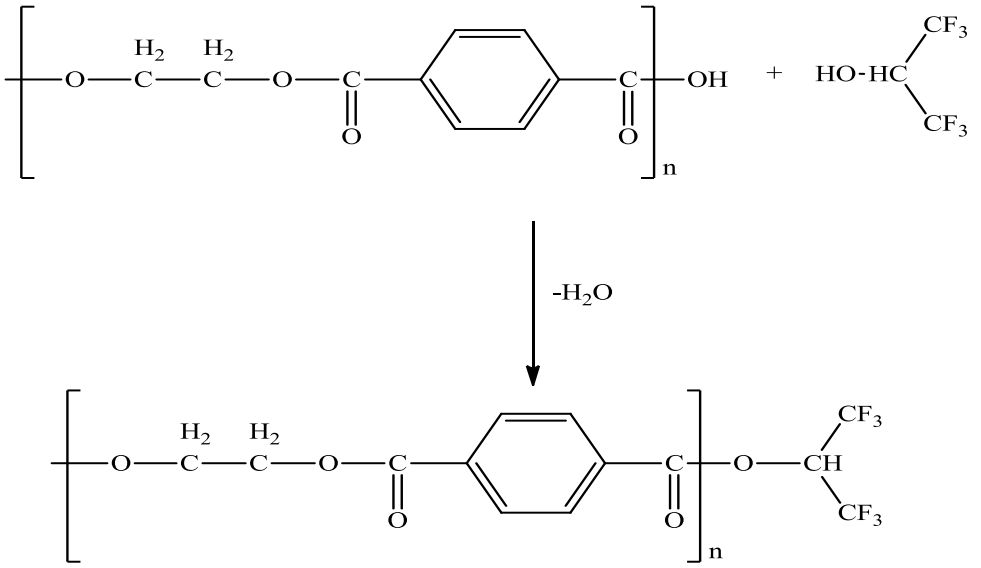

Figure 1.47 – Reaction showing the carbodiimide-mediated room temperature esterification of carboxyl end groups of polyesters with HFIP. [After 96]

One of the most commonly used methods for analysing the end groups of PET is to react trichloroacetyl isocyanate (TAI) with PET to give end group derivatives that are commonly analysed by ^{1}H NMR. [97] TAI will react rapidly and quantitatively with both carboxyl end groups and hydroxyl end groups to give derivatives that can be analysed by NMR. Figure 1.48 shows the reactions that can take place. The integrals of the derivatives produced are compared with the integral of the signal produced by the hydrogens from the polymer backbone. Donovan showed that this method allowed for both quantitative and qualitative analysis of carboxyl end groups of PET. Disadvantages of this method include that the polymer is required to be quenched before it will dissolve, it requires the sample to be dissolved at 140 ^{o}C which potentially causes degradation reactions to occur, and long scan times are required.

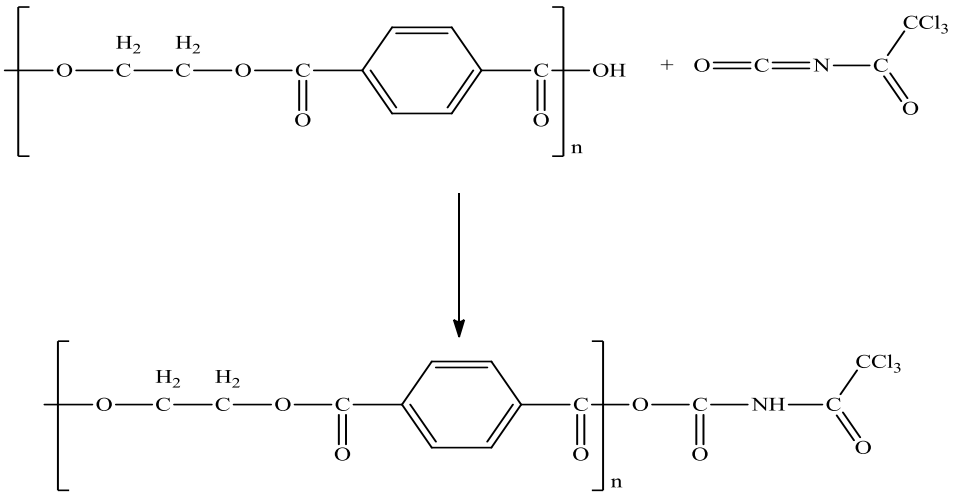

Figure 1.48 – Reaction of TAI with the carboxyl end groups of PET. [After 97]

1.8 Aims

The overall aim of this study was to investigate if the polymer PET could be end capped so as to prevent hydrolytic degradation in long term outdoor applications, such as in the protective backsheet on a solar cell. A previous screening study at Strathclyde University, carried out on behalf of Dupont Teijin Films (DTF), had shown that 3 epoxides in particular could achieve this: the mono-functional epoxide Cardura (Neodecanoic acid glycidyl ester), Heloxy (p-tert-butylphenyl glycidyl ether) and Vikolox (1, 2-epoxyhexadecane).[16]

DTF therefore had great interest in looking further into the possibility of manufacturing a backsheet with Cardura, Heloxy or Vikolox in order to further improve the hydrolytic degradation, as in their current formulations of polymers there are significant problems with yellowing when exposed to many outdoor environmental conditions.

The first aim throughout this study was to prove that the 3 epoxides would undergo an esterification reaction in order to reduce the carboxylic end group concentration. This is believed to protect against hydrolytic degradation and was therefore one of the first necessary steps in evaluating the epoxides. Part of the evaluation of the epoxides was to use benzoic acid instead of a polymer system as a model compound. The model compound was studied because

the esterification reaction has been shown in the literature to be difficult to follow due to various problems encountered when studying reactions with PET. The outcome of this is seen in Chapter 4.

Once this data had been adequately evaluated the next aim was to carry out the esterification reaction between the epoxides and a simple polymer system, as previously only model compounds were used in order to obtain the necessary data to progress to the next stage of the study. This simple system was used to develop a reliable titration method for evaluating esterification reactions in polymer systems as seen in Chapter 5. This was necessary in order to evaluate if the epoxides could reduce the carboxylic end group efficiently enough to impact the resistance to hydrolytic degradation before progressing to a more advanced PET system.

Once the simple polymer system had been found to be successful, the next aim was to move to a PET system in place of the PEI used previously. An extrusion line capable of adding the liquid additives was necessary, both to manufacture the samples and to show DTF the capability and limitations of the formulations. Chapter 6 discusses this in detail. One essential aim, as discussed in Chapter 7, was to show that these new PET formulations had gained increased resistance to hydrolytic degradation.

Once this had been proven to be effective, further studies were undertaken to investigate the thermal and thermo-oxidative degradations of the formulations in order to highlight potential issues in the manufacturing stage of the backsheets produced by DTF. These were the primary aims of the work discussed in Chapters 8 and 9.

2.0 Instrumental Theory

2.1 Nuclear Magnetic Resonance Spectroscopy

An electron is considered to be a particle spinning on its axis which results in it having spin angular momentum. [98-100] Two spin states are possible and will degenerate in the absence of an external magnetic field. As the spinning particle is charged, it also has a magnetic moment (μ). A diagrammatic representation of the behaviour of an electron in a magnetic field B_o is shown in figure 2.1. [98]

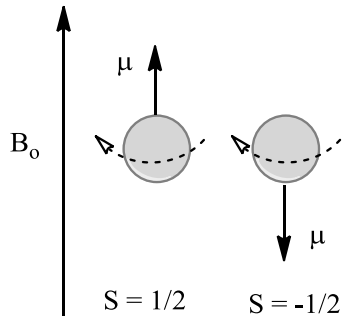

Figure 2.1 – Diagrammatic representation showing the spinning electrons with magnetic moment when experiencing the magnetic field B_o. [After 98]

Protons are also charged particles so will behave similarly to electrons. They have a nuclear spin quantum number (m) which can determine its nuclear spin (I). Small particles such as protons and electrons have two magnetic spin orientations; +½ or -½. [98] More complex nuclei will have more than two spin orientations, and the possible number of spin orientations can be calculated from equation 2.1. [98-101]

$$\text{Multiplicity}=2I+1 \qquad \textbf{Equation 2.1}$$

where Multiplicity stands for the number of possible spin orientations and I is the nuclear spin.

The different nuclear spins will separate in the presence of a magnetic field. [98-99] The energy can be calculated using equation 2.2.

$$E_i=m_l \, \gamma h B_o/_{2\pi} \qquad \textbf{Equation 2.2}$$

where E_i is the energy of the ith spin state, m_I is the nuclear spin quantum number, γ is the magnetogyric ratio, h is Planck's constant and B_o is the applied magnetic field.

The magnetic moments are required to remain at a certain angle to B_o which causes them to process. [98-100] The procession occurs with a characteristic frequency known as the Larmor frequency (ω), and is calculated from the equation shown in equation 2.3. This can be transferred into a linear frequency (v) using equation 2.4. The precession will cause the tip of the magnetic moment to trace out a circular path as shown in figure 2.2.

$$\omega=\gamma B_o \qquad \textbf{Equation 2.3}$$

Where ω is the Larmor frequency, γ is the magnetogyric ration and B_o is the applied magnetic field.

$$\nu= \omega/_{2\pi} \qquad \textbf{Equation 2.4}$$

where v is the linear frequency and ω is the Larmor frequency.

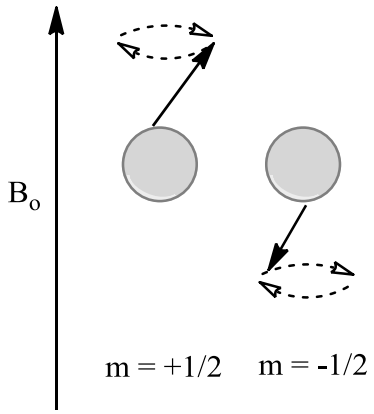

Figure 2.2 – Diagrammatic representation of the movement of the magnetic moments of the two possible spin states in a nucleus with I = ½ caused by the external magnetic field B_o. [After 98]

The vector sum of all of the individual nuclei magnetic moments is known as the net nuclei magnetation (M). [98 and 102] The magnetism is determined by the excess of up spins over down spins. The vector M has no processional motion. If a magnetic field (B_1) is supplied perpendicular to B_o, this new field will process in the XY plane which oscillates at the same frequency as the nuclei's magnetic moments. The individual nuclear magnetic moments will become phase coherent, meaning they will track the new magnetic field and move as one processing bundle (Figure 2.3). When the phase coherence occurs, M will move away from the Z axis and will process in the XY plane with its usual Larmor frequency. M has a new component in the XY plane which is given by equation 2.5. When B_1 is removed, the individual nuclear magnetic moments begin to lose their phase coherence, meaning M will return to the Z axis. This is called spin-spin relaxation. [98]

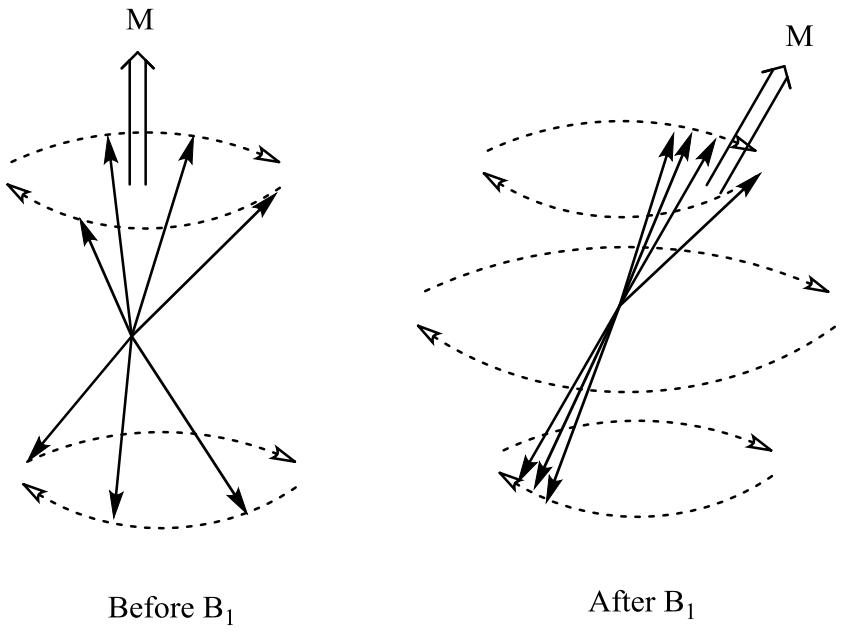

Figure 2.3 - Diagram showing the precession of a collection of I = 1/2 nuclei caused by an external magnetic field such as B_o before irradiation with B_1 and after. [After 98]

$$M_{xy}=M \sin \alpha \qquad \textbf{Equation 2.5}$$

where M_{xy} is the net nuclear magnetisation of the xy plane after irradiation with B_1, M is the net magnetisation before irradiation with B_1 and α is the flip angle. The flip angle is determined by the power and duration of the irradiation by B_1.

An NMR instrument involves 6 main components, including a magnet, radiofrequency (RF) transmitter, a probe, an RF receiver with an amplifier, an analogue to digital converter and a computer. [98-99] The magnet is used to create the Zeeman effect in nuclei. [98-102] The three most important characteristics of the magnet are the strength, stability and homogeneity of its magnetic field. The magnetic field stability is monitored by a technique known as locking. [98] The solvent is often used as the lock signal and is referred to as an internal lock. The frequency of the lock signal is continually monitored and electronically compared to a fixed reference frequency. The field can be controlled by passing a small current through a series of shimming

coils that are located around the probe. The small magnetic fields that are generated can be adjusted to improve the homogeneity of the magnetic field.

The sample is normally placed in a specially constructed glass tube. [98-102] The sample holder is placed in the probe. [102-103] An air stream turns a plastic turbine which is attached to the top of the tube, causing the tube to spin. The spinning will help to smooth any inhomogenities in the magnetic field that are present in the sample region. A coil of wire is attached around the probe. [98] This coil is referred to as the receiver coil and is where the NMR signal is generated. A coil is used because of a phenomenon known as Faraday Induction, which is where a current is induced in the wire by the movement of a magnetic field near the wire. Any time there is a component of M in the XY plane, a current of the same frequency will be induced in the coils.

A second loop of wire (transmitting coil) is positioned perpendicular to B_o and the axis of the receiver coil. [98] When an alternating RF current is passed through a transmitter coil it will generate circular rotating magnetic fields. Modern instruments are operated in pulse mode where the magnetic field, B_o, and RF frequency are kept constant. [98] The RF radiation is supplied by a controlled pulse of current through the transmitter coil. The pulse will only last a few microseconds and will cover a wide range of frequencies. The pulse has to be powerful enough to cause all nuclei processing at frequencies within the spectral boundaries to become phase coherent, resulting in the M_{xy} component which is measured.

The induced AC signal in the receiver coil will be monitored as a function of time; the computer will measure the voltage present in the receiver coil at regular intervals. [98] The receiver coil must be sampled regularly enough to make a recognised pattern. The intensity of the signal will decay with time; this is a result of spin-spin relaxation. The output produced is called the modulated free induction decay (FID). The computer will perform a Fourier transform (FT) on the FID data. The FT displays the FID in the frequency domain, which is how NMR is normally presented. It is from the FT that the computer can determine the frequency and intensity of each component.

When the data is expressed as frequency the result will vary if the operating frequency is different. [98-102] The signals are therefore often referred to as chemical shift which is independent of operating conditions. The chemical shift can be calculated using equation 2.6.

$$\delta_x = {(\nu_x - \nu_{TMS})}/{\nu_o} \qquad \textbf{Equation 2.6}$$

where δ_x is the chemical shift, ν_x is the frequency of the signal, ν_{TMS} is the frequency of TMS used as the reference and ν_o is the operating frequency.

The NMR signals are electronically integrated. [52] The integration value provides the number of nuclei that cause the signal. This enables NMR spectroscopy to provide both quantitative and qualitative information.

2.2 Extrusion

There are several applications for extruders such as compounding, melt blending, degassing or drying, filtration, blow moulding or reactive extrusion. [103] One of the most common uses of extrusion is compounding, which involves the mixing of stabilisers, antioxidants, fillers, plasticisers, lubricants, pigments and other additives into the polymer melt. A significant amount of work is being carried out on reactive extrusion. This involves the use of an extruder to cause a chemical reaction to cause a change in the structure of the polymer. This has been used in both cross-linking and end group modification reactions. [103-104] Some advantages of reactive extrusion are that there is no need for solvents, the process is highly flexible and saves money and time because it combines a multiple step process into one stage.

A typical screw extruder set up is shown in figure 2.4. It consists of three main sections - the hopper, the barrel/screw and the die.

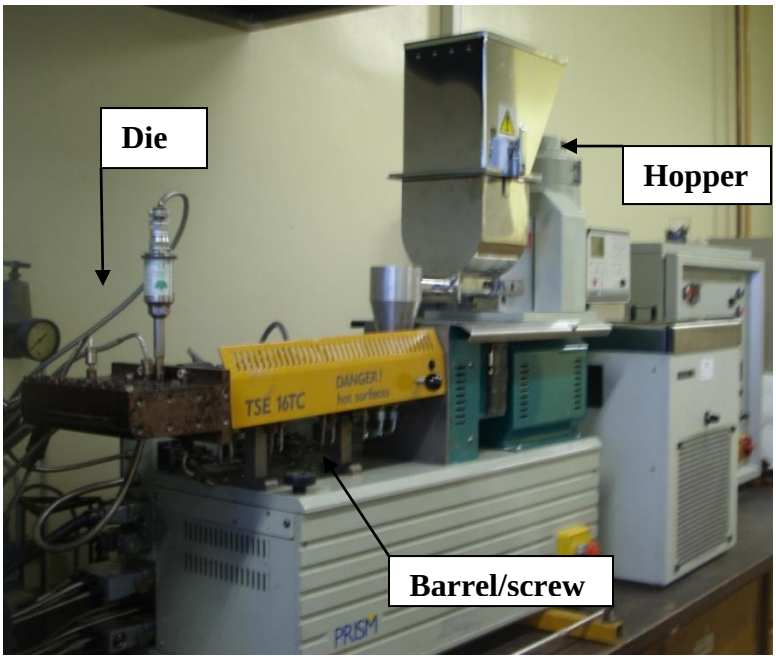

Figure 2.4 - Picture of a twin screw extruder. Hopper, barrel/screw and die are labelled on the picture.

Twin screw extruders were designed to produce a more homogenised sample. The screws are designed so that different sections of the screw can be removed and replaced with different parts depending on the application. The two screws in a twin screw extruder can be either counter-rotating or co-rotating. [105] The way the polymer melt travels down the barrel is very similar in both co-rotating and counter-rotating screws; it is the degree of mixing that is different. [103 and 106] In co-rotating screws there is a shear on the melt in the space between the two screws. This allows the breakdown of agglomerates and promotes homogeneity, which makes them useful for compounding applications. In extruders with counter-rotating screws the melt is transferred from top to bottom to give a much gentler mixing. Figure 2.5 shows a diagram of the screw movement. [103] The two screws can be intermeshing or non-intermeshing. Figure 2.6 shows a representation of the intermeshing and non-intermeshing screws. When the screws are non-intermeshing the separation between the screw axis is at least the diameter of the screw. Intermeshing screws are more commonly used because they provide a more positive pumping action as the polymer is trapped in 'packets' and then gets pushed along the barrel by the rotation of the screws.

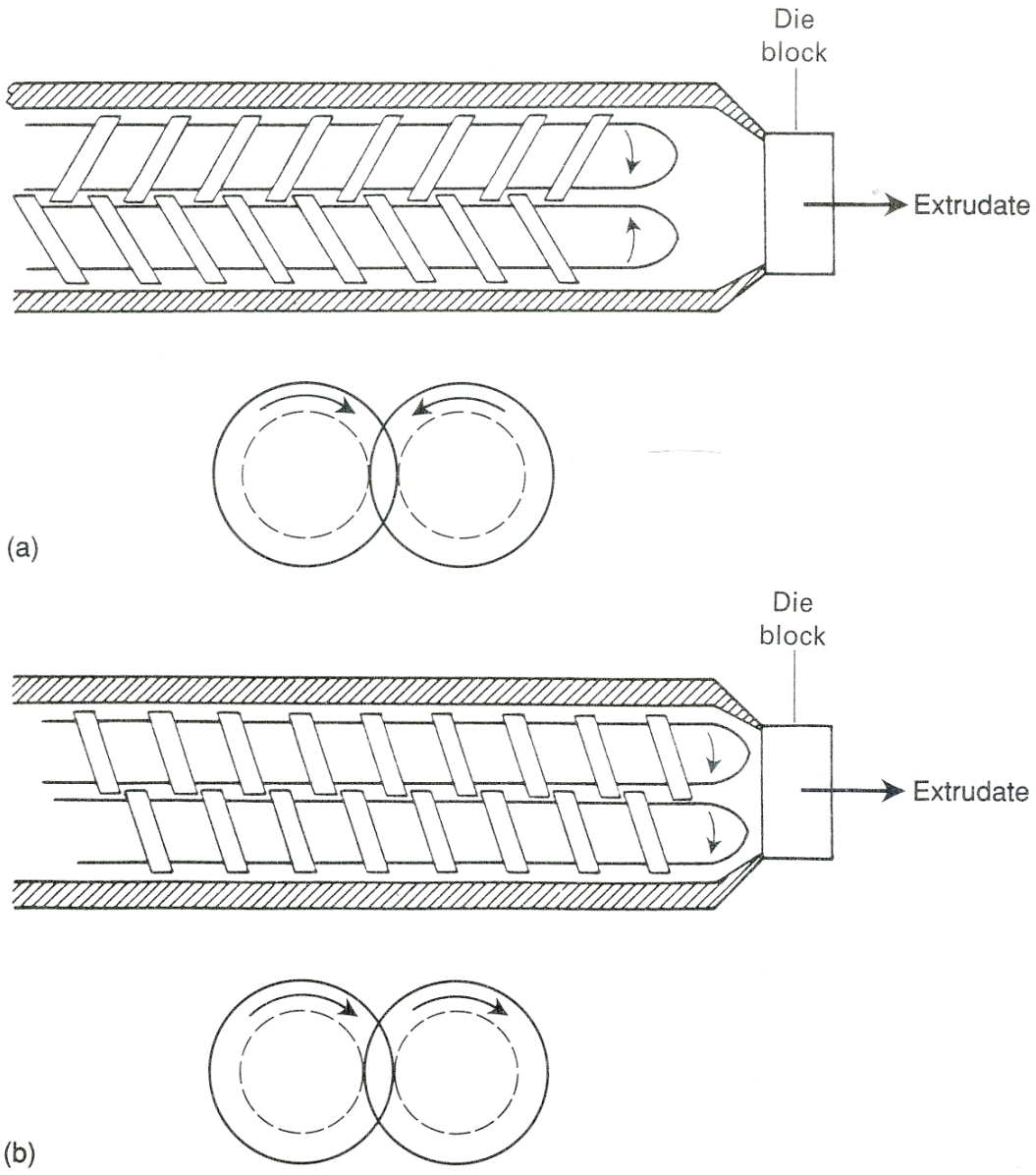

Figure 2.5 – Diagram of the type of screws movement in a twin screw extruder. A) counter-rotating and B) co-rotating. [103]

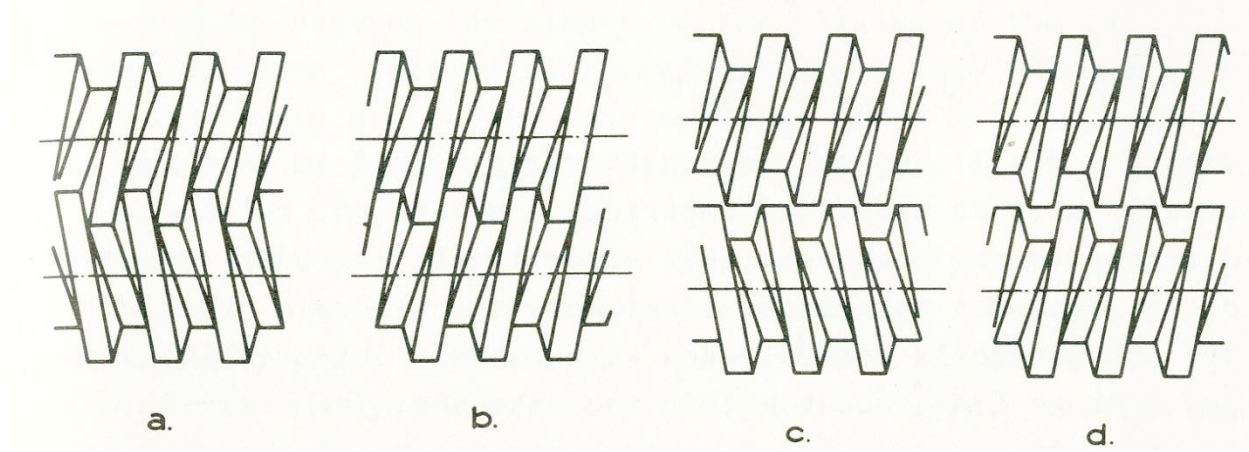

2.6 – Diagram representing the possible screw combinations in a twin screw extruder. A) counter-rotating intermeshing, B) co-rotating intermeshing, C) counter-rotating non-intermeshing and D) co-rotating non-intermeshing. [103]

The screw/barrel section of an extruder is responsible for mixing and melting the polymer. [106] In order to make the process more effective the screw/barrel section of an extruder is considered as three separate sections; the feed zone, compression zone and melt zone. The feed zone collects the granules from the hopper and transports them up the screw chamber. The granules heat up and will begin to compound. The heat in the barrel is supplied by heaters and friction from the process. It is important to control the temperature as, if it is too hot, degradation of the polymer may occur or the melt may become too fluid. If the temperature is too low, the polymer will not melt properly. It has been shown that the most efficient heating program for extrusion is to heat the barrel and screw chamber with a steady gradient which increases from the feed to the die. The temperature used depends on the polymer used. To prevent overheating the barrel tends to be cooled by water or air through channels that are drilled through the barrel. Thermocouples are often used to monitor the temperature and can be connected to a controller to increase or decrease the temperature as required.

The compression zone allows the polymer to melt and mix sufficiently. [106] Two types of mixing occur - dispersive and distributive. The latter dispersive mixing involves any particles that are present reducing in size. An example of this is that when preparing a coloured master batch, all

of the pigment particles will be reduced in size and wetted with polymer. This type of mixing is important as polymers tend to have a lower surface energy than most additives which causes the additives to aggregate. To improve the mixing, a side feeder can be used to add solid additives directly into the polymer melt which can overcome the problem of the additives aggregating. A liquid injection can also be used to feed in liquid or waxy additives directly into the polymer melt. This prevents issues with volatile materials escaping and issues of mixing between two separate phases.

The final section is the melt zone which is required to bring the melt up to the correct consistency and pressure required for extrusion. [106] Twin screw extruders push the melt down the barrel using positive displacement unlike single screw extruders, which rely entirely on frictional forces caused by the melts interaction with the forces exerted on it by the surfaces of the screw and barrel.

The shape of the product from the extruder (extrudate) is determined by the die. The product from the extruder can be in the form of solid sections (rods and strips), hollow sections (pipes), wire covering, fibres, flat sheets (thickness normally less than 0.025 cm) and films. The output of the extruder depends on the screw dimensions, die dimensions and screw speed.

The polymer is molten and extremely hot as it emerges from the die, and is cooled by air, water baths or chill rollers. [106] Air cooling tends to be insufficient for certain polymers that flow very easily in their molten state, such as PET. These polymers will distort if they are not cooled quickly - this is achieved by the use of water baths and chilled rollers.

2.3 Differential Scanning Calorimetry

The main parts in differential scanning calorimetry (DSC) include a cell where the sample and reference are placed, temperature sensors and a method of heating the sample and reference. [102 and 107] There are two different types of DSC - power compensation and heat flux. The most commonly used DSCs are heat flux DSCs, which have the sample and reference pans positioned in the same furnace, but have separate temperature sensors. The instrumental signal is produced from the temperature difference between the sample and reference. The

temperature difference is measured by thermocouples. Figure 2.7 shows a diagram for a heat flux DSC.

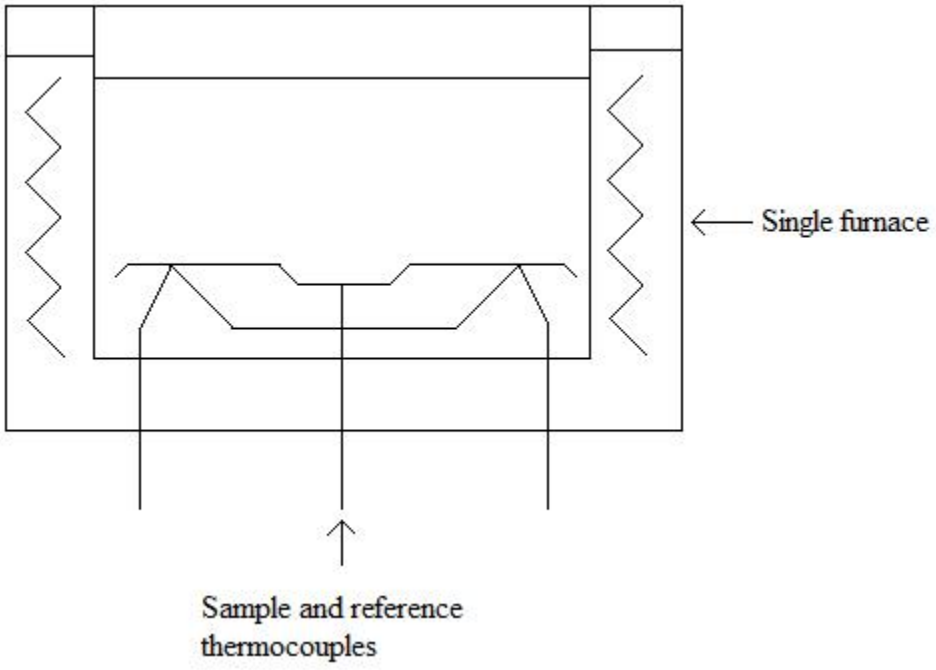

Figure 2.7 – Diagram of a heat flux DSC. [After 107]

An expression for the instrument signal in response to the heat evolved from a sample has been derived. [107] This is represented as dh/dt. The expression involves three components, namely the instrument signal, a heat capacity displacement and a third term which corresponds to thermal lag. The expression is shown in equation 2.7.

$$\frac{dh}{dt} = -\frac{dq}{dt} + (Cs - Cr)\frac{dTp}{dt} - RCs\frac{d^2q}{dt^2} \qquad \textbf{Equation 2.7}$$

The instrument measures dq/dt, which is the heat flow between the thermal energy source and the sample. [107] It is assumed that there is a source of thermal energy of temperature Tp. The

heating rate is represented by dTp/dt. The reference crucible has a heat capacity Cr. The sample and crucible are considered to have a total heat capacity Cs. The R term is for thermal impedance between the sample and the source of thermal energy, and between the reference and the source of thermal energy. The third term highlights the importance of reducing the thermal lag in the experiment. Several methods can be used to reduce the thermal lag including smaller sample sizes, slower heating/cooling rates and better contact between the sample/crucible.

To reduce the thermal lag, only a few milligrams of the samples are required for analysis. [107] The samples are normally placed into crucibles, which must be clean and free from contamination. The crucibles can be made from a variety of different materials such as silver, gold, quartz, aluminium and graphite. Different shapes of crucibles are available such as hermetic and standard. The reference used can be either an inert reference or simply an empty crucible.

The normal temperature program that is used is a linear temperature change with time. More complex temperature programs are possible with various heating/cooling rates and isothermal periods. DSC allows samples to be studied at temperatures ranging from -150 ^{o}C to about 1600 ^{o}C.

Computer software is responsible for the operation of the instrument and analysis of the results. The results are displayed as a thermal analysis curve, where the instrument signal is normally plotted against temperature or time. [108] Curves using temperature are called thermograms and are the most commonly seen. Figure 2.8 shows a thermogram and the types of information that can be obtained. It is important to state which way the exotherms and endotherms are appearing on the thermogram to prevent confusion.

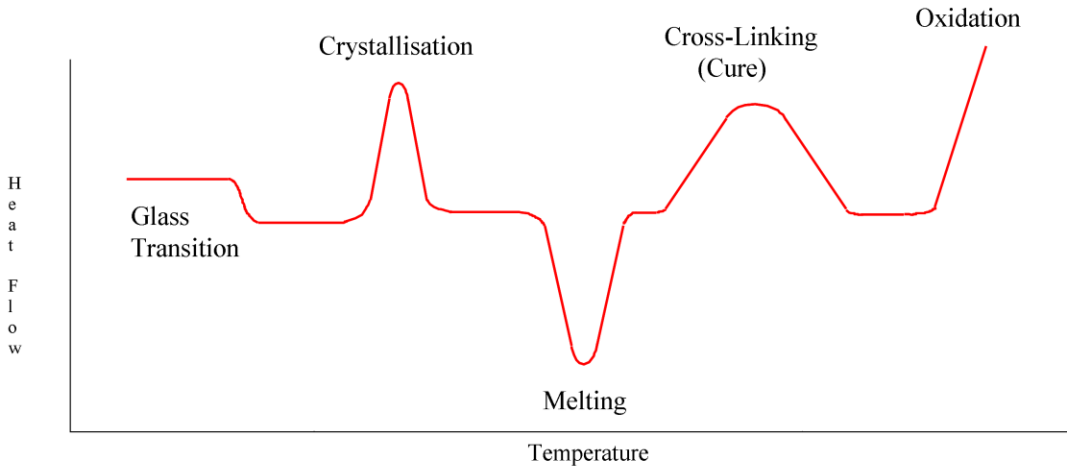

Figure 2.8 – Example of a DSC thermogram. [108]

2.4 Thermogravimetric Analysis

The International Confederation for Thermal Analysis and Calorimetry (ICTAC) describes thermogravimetric analysis (TGA) as a technique that analyses a sample mass as a function of temperature. [107] Mass losses are seen if volatile components are released from the sample. These mass losses can occur from volatiles such as water being absorbed onto the samples surface or degradation of the sample occurring.

The large sample masses are used in TGA, which have the advantage that there is plenty of residual material left for analysis. [107-108] Most modern instruments can handle sample masses as low as 1 mg. The samples are placed in an inert crucible, which can be made of various materials such as platinum, nickel, alumina, silica or ceramic. Platinum is the best choice because it is inert to most gases and molten materials. It will not melt until it reaches 1769 ^{o}C and can be cleaned by strong acids. The platinum crucible must be very thin to keep the mass low and prevent thermal lag. There are several issues with platinum crucibles as they are easy to distort and are very expensive.

The crucible is attached to a microbalance which has a surrounding furnace. [107-108] The combination of a balance and furnace is referred to as a thermobalance. A computer system is used to control the furnace and retrieve the data. Software packages can also be used to further analyse the data. The results from TGA are normally plotted as mass versus temperature or time.

The temperature during a TGA experiment is normally raised at a constant rate. For kinetic studies another type of heating profile is used, where the temperature is held constant and the mass loss of the sample is monitored over time. There are some issues with carrying out this type of experiment as it takes time to reach the desired temperature and some unwanted reaction may occur in getting the sample to this temperature.

The instrument can be flushed with a gas to carefully control the atmosphere that the sample is exposed to; this can be a reactive or an inert gas. Most modern instruments are even able to operate under vacuum if the joints are sufficiently sealed.

2.5 Infrared Spectroscopy

2.5.1 Infrared Theory

Infrared (IR) spectroscopy involves IR radiation being passed through a sample. [109] Some of the light is absorbed or transmitted, and detecting the IR radiation from this allows parts of the sample to be identified. It is frequently used to identify unknown materials, determine the quality or consistency of a sample and determine the amount of a component in a mixture.

The infrared spectrum has three regions; far infrared (0 – 400 cm^{-1}), mid infrared (400-4000 cm^{-1}) and near infrared (4000 – 14285 cm^{-1}). [109] Most infrared applications use the range 650 – 4000 cm^{-1}. The technique works due to certain molecules absorbing discrete frequencies. The frequencies absorbed are easily calculated as the energy involved can be carefully measured.

$$\Delta E = h\nu \qquad \textbf{Equation 2.8}$$

where h is Planck's constant and v is frequency.

The energy is absorbed because molecules have both vibrational and rotational energy. [109-111] Radiation of the appropriate energy raises the molecule from one vibrational energy state to the next. Some modes of vibration are associated with individual bonds or functional groups and others with the whole molecule. Localised vibrations can be stretching, bending, rocking, twisting or wagging. The vibrational energies that are possible can be calculated from equation 2.9. The possible rotational energies are calculated from equation 2.10.

$$E_{vib} = \left(V + \frac{1}{2}\right) h\nu_o \qquad \textbf{Equation 2.9}$$

where V is a quantum number and v_o is the fundamental energy.

$$E_{rot} = \frac{h^2 J(J+1)}{8\pi^2 I} \qquad \textbf{Equation 2.10}$$

where h is Planck's constant (6.626 X 10^{-34} Js), J is a quantum number and I is the moment of inertia.

The equation for calculating the moment of inertia is shown in equation 2.11.

$$I = \frac{m_1 m_2}{(m_1 + m_2)} R_o^2 \qquad \textbf{Equation 2.11}$$

where m_1 and m_2 are the mass of each atom and Ro is the bond length.

Only certain vibrational and rotational energies are allowed, meaning the quantum numbers V and J are governed by selection rules. These selection rules are $\Delta V + 1$ and $\Delta J = \pm 1$. Once the

frequency absorbed is calculated, this can be converted into wavelength using the equation shown below.

$$C = \lambda\nu \qquad \textbf{Equation 2.12}$$

where C is the velocity of light, λ is wavelength and ν is frequency.

Wavenumber (cm^{-1}) is the unit commonly used, and is the number of electromagnetic waves in a length of one centimeter. It is given by the following relationship. [109-111]

$$\bar{\upsilon} = \frac{1}{\lambda} \qquad \textbf{Equation 2.13}$$

2.5.2 Fourier Transform Infrared Spectroscopy

Modern Fourier transform infrared (FTIR) spectroscopy consists of the following set of components; a source of infrared radiation, interferometer, sample holder, detector and data processor. [109-111]

There are two types of infrared sources; thermal unpolarised IR sources and bright pulsed micro IR sources. [109-111] Thermal unpolarised IR sources consist of a solid material heated to incidence by an electric current. One of the most popular solids used is Nernst Glower, which consists mainly of oxides of rare earths such as zirconium and yttrium. Another popular choice is a Globar which is a silicon carbide rod. Bright, pulsed, micro-IR sources produce infrared radiation by accelerating charged particles (e.g. electrons) in a magnetic field or by laser sources that emit IR beams. The radiation normally passes through an aperture which controls the amount of energy presented to the sample (and, ultimately, to the detector).

The Interferometer will divide the light emitting from the IR source into two beams using a beam splitter, change the optical path of one beam using a moveable mirror, recombine the

two beams to create optical interference and then pass the IR light through the sample. [109-111] The beam enters the sample where it either is transmitted or reflected off of the sample and the beam is then passed to the detector. Usually a number of scans are taken and averaged by the computer which reduces the noise. FT of the interference pattern using a computer converts it to a plot of absorbance versus wavelength. When using FTIR plotting data in absorbance is preferred since data manipulation, such as spectral subtraction, is possible.

There are two types of detector used; thermal detectors and selective detectors. [109-111] Thermal detectors measure the heating effects of radiation and respond equally well to all wavelengths. Examples of thermal detectors include thermocouple, bolometer and pyroelectric devices. Selective detectors change radiation into electrical energy which can be processed to generate a spectrum. The most important selective detector is the photoconductor cell. Modern instruments tend to use thermopile detectors, which work on the principle that if two dissimilar metal wires are joined head to tail, the difference in temperature between them causes a current to flow. This current will be proportional to the intensity of radiation falling on the thermopile.

The main advantage of FTIR is that it can acquire the whole spectra in just a few seconds. Other advantages include that it is good for small samples, it allows easy subtraction of components in mixtures, high resolution spectra are possible, detailed information is produced and it is an inexpensive process. The instrument is mechanically simple which helps to prevent breakdowns. IR spectroscopy can easily identify samples since they give rise to a uniquely characteristic set of absorption bands. This band pattern occurs from 900 to 1400 cm^{-1} and is referred to as the fingerprint region. The disadvantages are that small changes in large molecules show very little change and, to be truly identical, the sample would have to be analysed on the same instrument under identical conditions.

2.5.3 Attenuated Total Reflectance Infrared Spectroscopy

Attenuated total reflectance (ATR) infrared spectroscopy involves infrared light passing through a prism at an angle exceeding the critical angle for internal reflection. [102] This creates an evanescent wave at the crystal. The sample is then mounted onto the crystal, and the distortion

of the evanescent wave by the sample is measured. Important things to consider in ATR are path length and crystal type. [102 and 112] The type of crystal that is chosen affects the wavenumber range analysed. The contact between the sample and crystal is also extremely important; good contact can be achieved by casting a film over the crystal, or by using a physical clamping device. The clamping pressure and thickness of the film cast are experimental parameters which can affect the spectra produced.

The advantages of ATR are that it has been designed to have good temperature control and is easy to clean. The main disadvantage is that quantitative analysis is very complicated with ATR due to wavelength dependence and dispersion effects. Wavelength dependence in the spectra is where the absorption bands at longer wavelengths are relatively more intense than those of shorter wavelengths. Dispersion effects are noticed in samples where the reflective index changes with wavelength.

2.6 Intrinsic Viscosity

Intrinsic viscosity (IV) measurements are a simple and inexpensive way to obtain an estimate of the molecular weight of a polymer sample. [102] It is noted that the molecular weight obtained is solvent dependent and often less accurate than other methods used to determine the molecular weight of a polymer. The IV measurement can be obtained for all polymers that can be fully dissolved in a solvent where no chemical reaction or degradation of the polymer occurs.

The sample is dissolved in a suitable solvent such as chloroform, phenol, cyclohexane and trichloroethane. [102 and 113] Dilute samples are used to ensure that the interactions occurring are kept to a minimum. The ideal condition is where the solution is dilute enough that the polymer molecules only interact with solvent. In this state the polymer molecules take on a coil conformation, which is the statistically favored option.

The dissolved sample and viscometer are placed on a water bath that is kept at a constant temperature. [102 and 113] After being left in this bath to reach thermal equilibrium, the solution is

then brought up above the upper gradation mark of the viscometer. The time that the solution takes to travel to the lower graduation mark is recorded.

The flow time is proportional to the viscosity of the solvent or solution and is inversely proportional to the density. [113] This is shown in equation 2.14.

$$t_{solution} = \frac{\eta_{solution}}{\rho_{solution}} \qquad \textbf{Equation 2.14}$$

The relative velocity (η_{rel}) is a simple ratio of the viscosity of the solution to the viscosity of the solvent, shown in equation 2.15. [113-114]

$$\eta_{rel} = \frac{\eta_{solution}}{\eta_{solvent}} \qquad \textbf{Equation 2.15}$$

The reduced viscosity is not totally independent of concentration as there are still small polymer interactions that decrease as the concentration gets weaker. [113-114] The specific velocity (η_{SP}) is also frequently calculated which is the fractional change in viscosity when the polymer is added.

$$\eta_{SP} = \frac{\eta_{solution} - \eta_{solvent}}{\eta_{solvent}} \qquad \textbf{Equation 2.16}$$

Einstein assumed, and was later proven correct, that the coils formed by the polymer in a dilute solvent behave like hard spheres, giving the relationship shown in equation 2.17. [113-114].

$$\eta_{SP} = 2.5\phi \qquad \textbf{Equation 2.17}$$

$$\text{where, } \phi = \frac{V_{polymer}}{V_{Solution}} = \frac{(\frac{M_{Polymer}}{\rho_{equ}})}{V_{Solution}} = \frac{C}{\rho_{equ}} \qquad \textbf{Equation 2.18}$$

The reduced and specific viscosities are both dependant on the concentration, so the "intrinsic" properties of the polymer must be extrapolated. [113-114] This is achieved by plotting either $C^{-1}\ln(\eta_{rel})$ versus C or by plotting ηsp/C versus C. The value at C = 0 is referred to as the intrinsic viscosity. Since the intrinsic viscosity of the polymer is independent of concentration the true viscosity is calculated by equation 2.19. Assuming that Vη is proportional to root-mean squared radius cubed ($\sqrt{(r^2)^3}$ and Q is the proportionality constant, the term $V\eta = Q\sqrt{(r^2)^3}$ is obtained. When this is placed into the equation, the outcome is equation 2.20.

$$[\eta] = 2.5L\frac{V_\eta}{M} \qquad \textbf{Equation 2.19}$$

$$[\eta] = 2.5LQ\ \frac{(r^2)^{\frac{3}{2}}}{M} \qquad \textbf{Equation 2.20}$$

The root- mean-squared end to end distance can be rewritten in Equation 2.21 using an expansion coefficient and the unperturbed end to end distance. [113-114] This means replacing the term with (r^2) with $\alpha^2(r^2)_0$.

$$[\eta] = 2.5LQ \frac{(r^2)_0}{M} M^{\frac{1}{2}} \alpha^3 \qquad \textbf{Equation 2.21}$$

When a theta solvent is used the expansion factor (α) is equal to 1. The $(r^2)_0$ and M are proportional to the number of bonds so $(r^2)_0$ / M is a constant which simplifies equation 2.21 to the following equation. [113-114]

$$[\eta] = KM^{\frac{1}{2}} \qquad \textbf{Equation 2.22}$$

For solvents that are non-theta the α term is no longer 1. In this type of solvent there will also be no square root dependency of [η] on M. This gives the equation shown in equation 2.23. [113-114]

$$[\eta] = KM^{\frac{1}{2}} \alpha^3 \qquad \textbf{Equation 2.23}$$

In this case the α term depends on the polymers molecular weight which allows them to be combined in the equation. [113-114] The equation is shown in equation 2.24. The α term is normally in the range between 0.5 and 0.8.

$$[\eta] = KM^{\alpha} \qquad \textbf{Equation 2.24}$$

2.7 Thermal Volatilisation Analysis

The technique of thermal volatilisation analysis (TVA) was developed by I. C. McNeill in the 1960s at the University of Glasgow. [115] It is believed that inspiration for this technique came from his mentor, Norman Grassie, and the vacuum fractioning manifolds that were developed by A. Stock. [116] McNeil developed the technique for the characterisation of polymers and the study of polymer degradation. [117-119] The technique has been modernised by researchers at Strathclyde University for a number of applications, including the study of polymer degradation.

The method for TVA has largely remained the same from when McNeill developed the technique in the 1960's. [120] Figure 2.9 shows a diagram of the current TVA line:

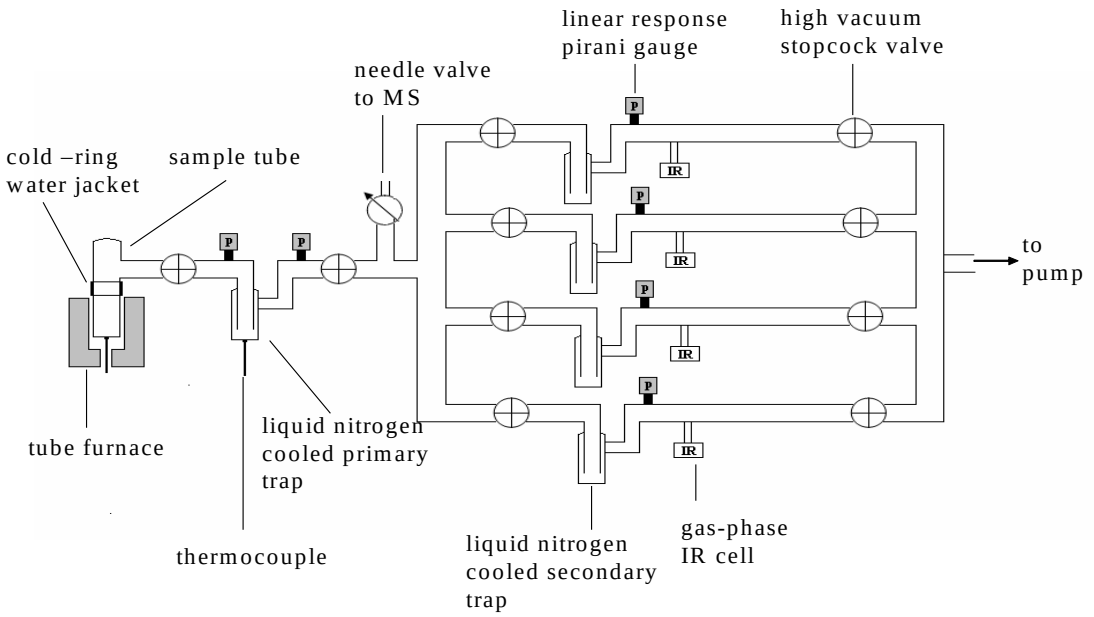

Figure 2.9 - Diagram of the TVA line. [120]

The TVA line is continually pumped to a pressure of approximately 10^{-5} Torr using a two stage pump consisting of an EO50/60 air-cooled diffusion pump backed by a RV3 rotary pump. [120] The diffusion and rotary pumps used for the system are supplied by Edwards.

Sample sizes used are normally between 20 – 100 mg. [120] The nature of the sample can vary, but the most commonly used samples are powders or thin films. Thin films are often cast along the bottom of the tube to minimise temperature gradients. The samples are placed in flat-bottomed borosilicate tubes which have an outer diameter of 33 mm. Quartz glass tubes are used for temperatures higher than 550 ^{o}C. All of the tubes are fitted with a B40 ground glass Quickfit^{TM} cone so that it can be added to the TVA tube head.

The TVA tube head is connected to the sample tube. It has a stopcock valve to allow air or moisture sensitive samples to be loaded into the TVA tube in a glove box before being fitted to the rest of the TVA line. [120] A K type thermocouple is inserted through the TVA tube head to allow direct sample temperatures to be measured. This is easier than calibrating every tube that is being used on the TVA line.

The sample is placed inside a Carbolite vertical tube furnace which can heat to 1000 ^{o}C. [120] A brass block is placed inside the oven to reduce the thermal gradient across the tube which occurs due to the tube's large size. The sample tube is heated either isothermally or, more commonly, under a controlled heating profile.

When the sample is heated, volatiles are released from the sample and travel through the TVA line where many of the volatiles will condense in the primary trap. [120] The primary trap consists of a u-tube trap that was experimentally determined at Strathclyde University to be the preferred shape. The u-trap is surrounded by a metal tin that contains glass beads to insulate the trap and prevent it from warming up too quickly. This is surrounded by a Dewar flask containing liquid nitrogen. An N-type thermocouple measures the temperature of the primary trap.

Pirani gauges are positioned before and after the primary trap to monitor the volatile gases going past. [120] Volatiles being released from the sample that condense at liquid nitrogen temperatures will give a signal on the Pirani gauge before the trap but not on the second gauge. This fraction is referred to as the condensable volatiles. Any gases that do not condense at

liquid nitrogen temperatures will pass through the primary trap, registering on both Pirani gauges. These gases are referred to as non-condensable. The resulting thermogram will be in the form of pressure versus temperature.

Pirani gauges are used because they are cheap, robust and capable of working over 7 decades of pressure (10^{-4} – 10^{3} mbar), which is the entire working of range of the TVA line. [120] The Pirani gauges used on the TVA line at Strathclyde University are from Edwards. To maximise the TVA signal, the Pirani gauges are positioned as close as possible to the out section of the cold trap. The side arms for the Pirani gauges are kept to 3 cm long to ensure a quick response time.

The volatile components (condensable and non-condensable) are not the only fraction produced. [120] Two other fractions are also obtained, namely involatile and residue fractions. The residue is normally removed from the tube for further analysis. A water-cooled jacket is placed around the section of tube where it leaves the oven; this is referred to as a cold ring. This is placed around the sample tube to obtain the products which are volatile at higher temperatures, but not at room temperature. The cold ring prevents contamination of the apparatus by isolating these products in one place and prevents the grease softening. The cold ring can be scraped off with a spatula or swabbing with a suitable solvent.

The next stage of the TVA process is to separate the condensable products, which is commonly referred to as sub ambient thermal volatilisation analysis (SATVA). [120] This involves the Stopcock valves between the furnace and sub-ambient trap being closed and the liquid nitrogen being removed from the primary trap. As the primary trap is heated to ambient temperature the products will distil off one-by-one, and travel into the liquid nitrogen cooled limbs. There are four liquid nitrogen cooled secondary limbs which can be isolated by the closing the stopcock valves. As volatiles leave the primary trap this will cause the pressure to rise and be detected by the Pirani gauge at the exit of the primary trap. The primary trap is normally externally heated to provide a linear response to room temperature. The SATVA thermogram produced will be in the form of pressure versus cold trap temperature and gives a fingerprint of the products. Caution has to be employed when using the SATVA trace as a fingerprint since the peaks are very broad and can shift with the quantity of volatiles.

Special cells have been made to attach to the TVA line to analyse the volatile components by IR and GC-MS. [120] On-line mass spectrometry can identify the non-condensable gases such as hydrogen, methane, oxygen and carbon monoxide. A Hiden HP20 quadruple mass spectrometer is used on the TVA line at Strathclyde University. The volatiles can also be collected for analysis off-line. Gardner and McNeill collected the evolved hydrochloric acid from TVA experiments and quantified it using titration. [121] IR and NMR Spectroscopy are commonly used to analyse the cold ring fraction. [120] The insoluble residue is routinely analysed by solid state NMR.

2.8 CATLAB

The Hiden CATLAB system is a bench top instrument that was designed to identify catalysts and to study the evolution of gases from reactions. [122] It allows the gases being released from reactions to be studied in real time. Hiden designed this system to make the analysis of catalysts simple and quick. The system is modular and involves two components; a microreactor and a mass spectrometer. The two components are standalone instruments and can be used separately, or can be connected to other components such as a TGA. A computer system is used for data acquisition and control of the instruments.

A picture of the microreactor is shown in figure 2.10. [122] The sample is placed in a quartz glass tube that is opened at both ends. One end is plugged with quartz wool to prevent the sample falling out and the tube is then fitted into the microreactor. The tube is placed directly into the furnace which is designed to be a tight fit to ensure consistent heating. The sample and tube are then sealed in the microreactor using Swagelok fittings. The furnace used can be heated up to 1000 ^{o}C. The temperature of the system is monitored using k-type thermocouples. Another thermocouple is positioned inside the tube containing the sample. Positioning of the thermocouple a few mm above the sample allows the temperature of the sample to be accurately monitored. The microreactor can cope with reactions being carried out at high pressures and using different gases. The microreactor comes with a sensitive mass flow control that has 4 separate channels for analysing the different gases. The gas stream then travels

through a heated capillary to the second component which is a mass spectrometer. The inlets to the mass spectrometer are kept as close as possible to the sample.

Figure 2.10 - Picture of the CATLAB microreactor. [122]

Mass spectrometry is a technique that is used for determining the elemental composition of a sample. [110 and 123] All mass spectrometers can perform three functions, which are:

- Creating gas phase ions from sample
- Sorting ions according to the mass: charge ratio
- Measuring the abundance of each ion

The instrument can be programmed to either continually sweep the entire mass range, measure only certain m/z values that the analyst can select or monitor a single m/z ratio. [110] The typical components in a mass spectrometer are an inlet system, ion source, mass analyser and ion detector.

The mass spectrometer is required to be at vacuum so that ions are not deflected by collisions with air molecules. [110 and 123] A sample inlet system is a small independent vacuum system that is used to introduce samples. The sample inlet system is required so that the rest of the

instrument stays under vacuum. To ensure that only a small proportion of the sample is going through the instrument, molecular leaks are used. A molecular leak is a pinhole restriction in a thin gold foil. The restriction will cause the pressure to drop, keeping the instrument safe from high pressure.

Ion sources have two functions - to convert the sample to gas phase ions, and to accelerate the ions into the mass analyser. [123] There are many different types of ion source. The two that are most commonly used are electron impact and chemical ionisation. Electron impact involves the molecules being ionised by collision with a beam of energetic electrons. This can be seen in figure 2.11. Chemical ionisation involves a reagent gas such as methane or ammonium being passed into an ion chamber where it is ionised by electrons from a hot filament.

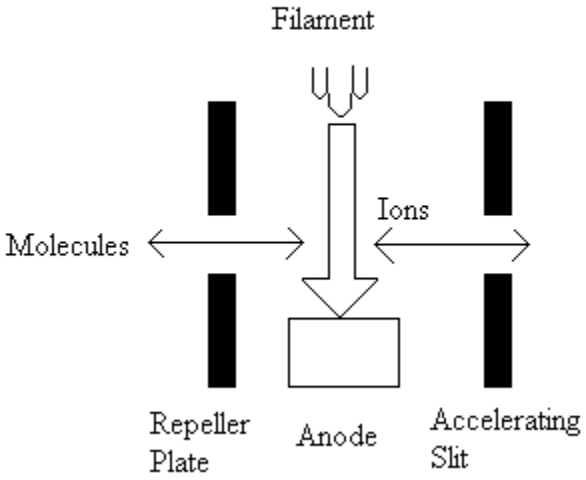

Figure 2.11 – Diagram of the electron impact ionisation system. [After 110]

There are several types of mass analyser, such as magnetic-sector, time-of-flight and quadrupole mass spectrometer. [110 and 123] The most common type of mass analyser is the quadrupole. The quadrupole mass analyser involves the ions being separated under the influence of both DC and RF fields. These are applied between four conducting parallel rods, and the ions are injected between these rods. They undergo motion at right angles to the

direction of flight, which results in the ions following spiral pathways down the cavity between the rods. Only ions with the correct m/z ratio will pass through. The other ions will escape the cavity, or hit the rods, and will be neutralised.

Normally mass spectrometers have two detectors to collect the ions and measure their volumes. [123] The two detectors that are most often used are the Faraday cup and the channel electron multiplier. The Faraday cup consists of a single ion collecting cup that is surrounded by electrodes and is used for the most abundant ions. This is because it is less sensitive and the larger volumes of ions are unlikely to damage the detector. The detector is slower than the channel electron multiplier, which involves an ion striking a conversion plate to emit an electron into a multiplication channel. The walls are covered in a material that can easily emit electrons. There are a series of ring shaped electrodes positioned around the channel resulting in the electrode current being multiplied.

The main advantage of the mass spectrometer is its sensitivity. It also provides both quantitative and qualitative information. The main disadvantages are that the technique is destructive and the instruments are expensive.

3.0 Experimental

3.1 Materials

The three monofunctionolised epoxides investigated were provided by DTF. These epoxides are neodecanoic acid glycidyl ester (Cardura), 1,2-epoxyhexadecane (Vikolox) and *p*-tert-butylphenyl glycidyl ether (Heloxy). The structures are shown in figures 3.1 to 3.3.

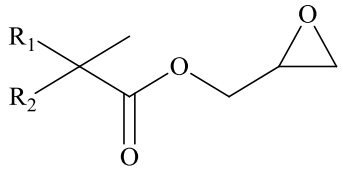

Figure 3.1 - Structure of Cardura. R_1 and R_2 are alkyl groups with a total of 7 carbons.

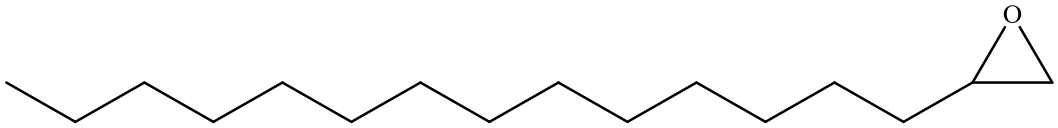

Figure 3.2 - Structure of Vikolox.

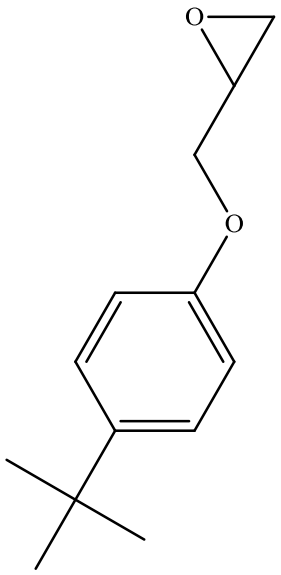

Figure 3.3 - Structure of Heloxy.

The model compounds, benzoic acid and PEI Chip were supplied from Sigma Aldrich and DuPont Teijin Films, respectively. The PEI is labeled E354 and has a molar mass of 54363 g mol^{-1}.

Three different grades of PET were supplied by DTF for use in this work. The three types are labeled E187, E239 and E240. E187 is a clear polyester chip containing an additive which promotes the reaction between the carboxyl end groups of PET and the epoxide. The intrinsic viscosity (IV) of the E187 chip is 0.57. The E239 and E240 have been solid state polymerised, giving them a higher molecular weight and a lower end group concentration than E187. The IV for both E239 and E240 is 0.79. The solid state polymerised chip samples both have the additive added to promote esterification. The E239 also contains 0.6% w/w titanium dioxide.

3.2 Infrared Spectroscopy

Small drops of the liquid epoxides were placed between two sodium chloride disks. The samples were analysed on a Perkin Elmer, spectrum 100, FTIR spectrum using the following parameters. The range covered 4000 cm^{-1} to 45 cm^{-1}, resolution was set to 8 cm^{-1} and the number of accumulations was set to 16 scans. The data was analysed using Specview software.

100 mg of PEI chip was weighed into a sample bottle and 2 ml of spectrophotometric grade chloroform was added. This sample was then left overnight to dissolve. The spectrophotometric grade chloroform was purchased from Sigma-Aldrich. The solution was then spotted onto a sodium chloride disc and the chloroform was allowed to evaporate before being analysed using a Perkin Elmer, spectrum 100, FTIR spectrum using the same parameters as described above for the epoxides.

An Agilent Technologies, 5550 series, attenuated total reflectance infrared (ATR-IR) spectrometer was used to analyse all of the solid samples except the PEI. The spectrometer was fitted with the most common type of interface used in ATR-IR spectroscopy, which is the diamond interface. The resolution was set to 8 cm^{-1} and the number of accumulations was set to 64 scans. The data was analysed using KnowItAll software.

3.3 Nuclear Magnetic Resonance Spectroscopy

100 mg of the samples to be analysed were dissolved in 2 ml of 80% $CDCl_3$ and 20% hexafluoroisopropanol (HFIP) for PET samples and 2 ml of deuterated chloroform ($CDCl_3$) for all other samples. The $CDCl_3$ used was purchased from Sigma-Aldrich and the HFIP used was purchased from Apollo scientific. The samples were shaken vigorously and then left overnight to fully dissolve. The solutions were then transferred to clean, dry NMR tubes. The samples were analysed on a Bruker AV500 NMR spectrometer using the parameters outlined below. The ^{1}H NMR and ^{13}C NMR spectra were obtained for each sample. The data was analysed using Bruker Topspin 2.1 software.

The parameters used to obtain the ^{1}H NMR spectrum include the number of scans being set to 64. A 1D sequence was used with a 30 degree flip angle.

The parameters for the ^{13}C NMR spectrum include the number of scans being set to 1024. A 1D sequence with power-gated decoupling was used with a 30 degree flip angle.

3.4 Thermogravimetric Analysis

12.0 g ± 1.5 mg of the samples were placed in a platinum crucible and analysed using a Perkin-Elmer TGA 7 thermogravimetric analyser. Starting material samples were heated from 50 – 500 ^{o}C under helium with a flow rate of 10 ^{o}C min^{-1}. Samples used to study the degradation behaviour were heated from 50 – 600 ^{o}C under both helium and air with a flow rate of 10 ^{o}C min^{-1}. The data was analysed using Microsoft Excel.

3.5 Differential Scanning Calorimetry

The DSC scans of all the samples were obtained using a TA Q1000 differential scanning calorimeter attached to a RC90 refrigerated cooling system. 10 mg of the samples were placed in a hermetic shaped aluminium pan and a hole was placed in the lid. The programs used to obtain the DSC scans are shown below. The data produced was analysed using TA's Universal Analysis software.

The program used to study the samples melting and crystallisation behaviour is shown below:

- Select gas and mass flow: Nitrogen at 20.0 mL min^{-1}
- Equilibrate at 25.0°C and Isothermal for 1.0 min
- Ramp 10.00°C min^{-1} to 320.0°C
- Isothermal for 2.0 min
- Ramp 10.00°C min^{-1} to 25.0°C
- Isothermal for 1.0 min
- Ramp 10.0°C min^{-1} to 320.0°C

Each sample was analysed three times and the average melting points, enthalpy of crystallisations and crystallisation temperatures were quoted.

The following program was used to study the samples degradation behaviour:

- Select gas and mass flow: Nitrogen or air at 60.0 mL min^{-1}
- Equilibrate at 30.0°C
- Isothermal for 15.0 min
- Ramp 20.0°C min^{-1} to 550.0°C

3.6 Gas Chromatography – Mass Spectrometry

A sample of Cardura was submitted for analysis by gas chromatography – mass spectrometry (GCMS). The sample was analysed using an Agilent Technologies 7890A GC system that has an Agilent Technologies 7693 auto sampler connected. The detector used was an Agilent Technologies 5975C. The samples were analysed using helium gas. The data was analysed by the software Excalibur.

3.7 Epoxide Reactions

0.5 g of the epoxide samples were carefully weighted into 5 ml round bottom flasks which were specially designed for the six position Radleys reaction carousel (Figure 3.4).

Figure 3.4 – Picture of the 6 position Radleys reaction carousel.

The reaction carousel was placed on an IKA Werke, RCT basic hotplate which is capable of both heating and stirring. The hotplate can reach temperatures up to 360 ^{o}C. The hotplate and reaction carousel were calibrated for each temperature. The hotplate was pre-heated to the desired temperature before use. The temperatures used were 90 ^{o}C, 110 ^{o}C, 130 ^{o}C and 150 ^{o}C.

The Radleys reaction carousel allows samples to be analysed under different environments. All of the epoxide samples were analysed under both air and nitrogen. The gases were allowed to continually flow at a rate of 60 ml min^{-1}. The rate of gas used was carefully controlled by a flow meter. The gases used were dried before they entered the reaction carousel. The samples were allowed to purge under the desired gas for 1 minute before they were added to the pre-heated reaction carousel.

The water was switched on so that the condensers attached to the flask could cool any vapours that were released from the sample. The hotplate was set to stir the samples at a speed of 50 rpm.

The samples were left for the desired lengths of time, which were 1, 2, 5, 10, 15 and 30 minutes before the flasks were carefully removed. They were allowed to cool before their contents were dissolved in 3ml of deuterated chloroform and transferred carefully into a labeled sample bottle. Two 1 ml rinsings of the Radleys flask were taken with deuterated chloroform and added to the sample bottle.

1 ml of this solution was transferred to a clean dry NMR tube. The ^{1}H and ^{13}C NMR spectra were obtained for all the samples using the same method as mentioned above for the starting material.

3.8 Reaction of Benzoic Acid and Epoxides

The Radleys reaction carousel was used to study the reactions occurring between benzoic acid and the epoxides. The same conditions for the hotplate were used as mentioned above for studying the epoxide reactions. The reactions were only studied under nitrogen with a continuous flow rate of 60 ml min^{-1}. Three different ratios of epoxides to benzoic acid were studied; namely (1:2), (1:1) and (2:1).

Each ratio was studied at 4 different temperatures which were 90 ^{o}C, 110 ^{o}C, 130 ^{o}C and 150 ^{o}C. A sample was obtained at each temperature after 1, 2, 5, 10, 15 and 30 minutes. Once the flask had cooled to room temperature, the sample was dissolved in 3ml of deuterated chloroform and transferred carefully into a labelled sample bottle. Two 1 ml rinsings of the Radleys flask were taken with deuterated chloroform and added to the sample bottle. All of the samples generated were homogeneously mixed.

1 ml of this solution was transferred to a clean dry NMR tube. The ^{1}H and ^{13}C NMR spectra were obtained for all the samples using the same method as mentioned above for the starting material.

3.9 Carboxyl End Group Concentration

Two methods were developed for calculating the carboxyl end group concentration - the Pohl titration method and the Ma *et al*. NMR method.

3.9.1 Pohl Titration Method

This method was developed in 1954 by Pohl. [86] A solution of 0.1 M sodium hydroxide in benzyl alcohol solution was made and standardised with 1 M hydrochloric acid. The standardisation

was carried out at least 48 hours before the sodium hydroxide in benzyl alcohol solution was used for the carboxyl end group titrations. The sodium hydroxide was purchased from FSA laboratory supplies and the hydrochloric acid was purchased from Sigma-Aldrich. Normally the benzyl alcohol used was the reagent plus >=99% purchased from Sigma-Aldrich. One bottle of pure benzyl alcohol was also purchased from Fisher Scientific.

Type 4 molecular sieves (purchased from Sigma Aldrich) were activated at 250 ^{o}C for 30 minutes in a fan assisted oven. A suitable ratio of the benzyl alcohol was poured over the molecular sieves and left for 24 hours for the solvent to dry.

0.10 ± 0.01 g of the dried polymer samples were placed in sample bottles. The polymer was dried in a pre-heated Vulcan oven at 160 ^{o}C for 4 hours under vacuum. The samples were cooled enough to allow them to be safely transferred to the vacuum desiccator. The samples were allowed to pump down for at least 30 minutes before being sealed under vacuum until they were required for analysis.

The polymer samples were then placed into a test tube containing 5 ml of benzyl alcohol that was preheated to 215 ^{o}C. The solution was allowed to heat for 110 seconds, with constant stirring using a glass rod to ensure the polymer fully dissolved. The test tube was then carefully removed and placed in cold water for 6 seconds to allow the sample to quench. The sample was then poured into a small conical flask containing 10 ml of chloroform. The chloroform was added to prevent too thick a gel from forming. The chloroform used was purchased from Sigma-Aldrich. A rinsing of 5 ml benzyl alcohol was added to the test tube and allowed to heat at 215 ^{o}C for 60 seconds, before being added to the conical flask. The hot plate that was used to dissolve the polyester was calibrated to ensure the sample reached 215 ^{o}C, and a thermocouple was used to ensure the temperature was consistent for all the samples that were analysed, as the high temperature used to dissolve the polymer could potentially cause thermal degradation to occur. Pohl suggests that 1.6 equivalents per 10^{6} grams should be removed from the entire carboxyl end group concentration values obtained by this method to compensate for the thermal degradation occurring at the conditions used. It is important as a result to keep the time that the polymer spends in the hot benzyl alcohol constant for all samples.

A micropipette was used to add 150 µl of phenyl red indicator to the dissolved polymer sample. This ensured that a similar starting colour was obtained each time and that the phenol red indicator did not interfere with the end group concentration. The phenol red was purchased from Sigma-Aldrich and dissolved in ethanol (purchased from Sigma-Aldrich). This turned the solution a pale yellow colour.

The sample was then titrated with the standardised 0.1 M sodium hydroxide in benzyl alcohol solution until a pale pink colour appeared. The solution was stirred using a magnetic stirrer bar at this stage. All of the samples were analysed in triplicate and an average obtained.

The titration process was carried out without polymer to obtain a blank titre value. The average blank titre is normally in the range 17 ± 10 equivalents per 10^6 grams. This is important as the reagents give the colour change from yellow to pink as well. The value for the blank is incorporated into the calculation. All of the carboxyl end group concentrations obtained are shown in the appendices. A sample of the calculation used to achieve the carboxyl end group concentration is shown below for a PET sample.

Carboxyl end group concentration = [[75.60 – 26.40] x 10^{-6} x 0.11308] / 0.1052 g

= 5.5635 / 0.1052 g

= 52.90 equivalents per 10^6 grams (Uncorrected)

= 51.30 equivalents per 10^6 grams (Corrected)

where 75.60 equivalents per 10^6 grams is the value obtained from the titration, 26.40 equivalents per 10^6 grams is the value obtained from the blank titration, 0.11308 moles per litre is the molarity of the sodium hydroxide in benzyl alcohol solution and 0.1052 g is the weight of PET used.

Despite the steps mentioned above to minimise the errors associated with this method, titration methods have been reported in literature to have a very high error value compared with some other methods of carboxyl end group determination. Several experiments were carried out to study the error associated with this method. The first experiment involved a sample of PET E187 being analysed 10 times in order to allow an average of error to be calculated. The standard deviation obtained was 1.17 equivalents per 10^6 grams. The main sources of error are expected to be from weighing, loss of polymer in the test tube and the fact that the colour change is subjective. The average carboxyl end group concentration of 31.00 equivalents per 10^6 grams obtained for the 10 repeats is in good agreement with the carboxyl end group concentration of 36.01 equivalents per 10^6 grams obtained from DTF. This shows the Pohl titration method is reliable and has an acceptable error within a batch. The values obtained for each individual titration are shown in the appendices (A3.1.1 - A3.1.16).

Four batches of the same polymer were analysed to obtain an idea of the error that is present between different batches; figure 3.5 shows a bar chart of this data. The error was considerably higher than that produced within batches. The value for the error was 5 equivalents per 10^6 grams. The high error value was expected for titration methods and is one of the main reasons that the NMR methods were also investigated for determining the carboxyl end group concentration of polyesters. These experiments not only give an indication of the error value for the titration method, but also highlight that it is not a suitable method for very low carboxyl end group concentrations. The SJ3 film sample has a carboxyl end group concentration of 3.4 equivalents per 10^6 grams, and with the titration method could be as high as 10 equivalents per 10^6 grams.

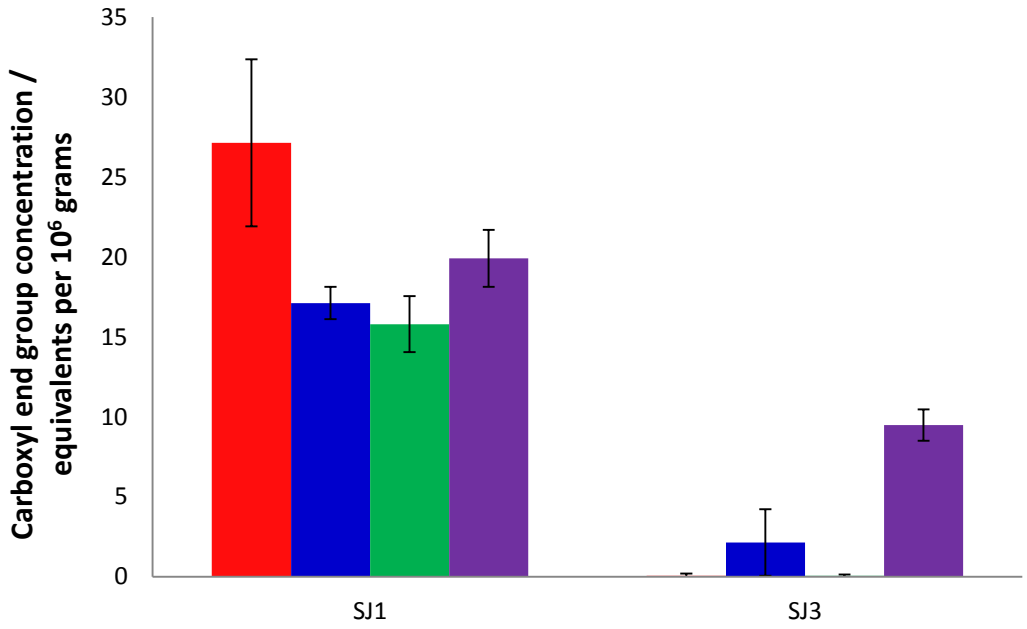

Figure 3.5 - Bar chart showing the carboxyl end group concentration for different grades of PET. Each grade of PETwas analysed four times and the values quoted are the average of three repeats for each set. The error bar shows the standard deviation calculated for each sample set.

After the method was optimised, it was tested using eight different grades of PET and compared with the carboxyl end group concentration value obtained from DTF. Figures 3.6 and 3.7 show the bar charts of the carboxyl end group concentration of the different PET samples and compare them with the value obtained from DTF, which was obtained using an NMR method. The values produced from the titration method are in reasonable agreement with the values obtained from DTF. The error value is very high, but the method overall does provide an indication of the carboxyl end group concentration and was used to analyse further samples as it is inexpensive and time efficient.

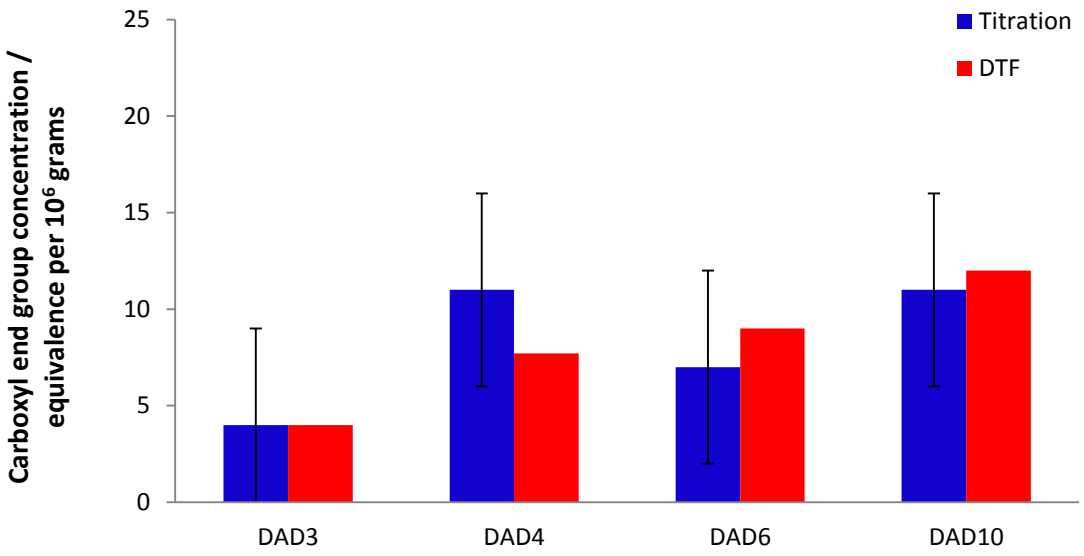

Figure 3.6 – Bar chart showing the carboxyl end group concentration for some PET film samples. The titration values quoted are the average of three repeats while the value provided by DTF was obtained from a single NMR measurement. Error bars are the 5 equivalents per 10^6 grams that were calculated as error in the titration method.

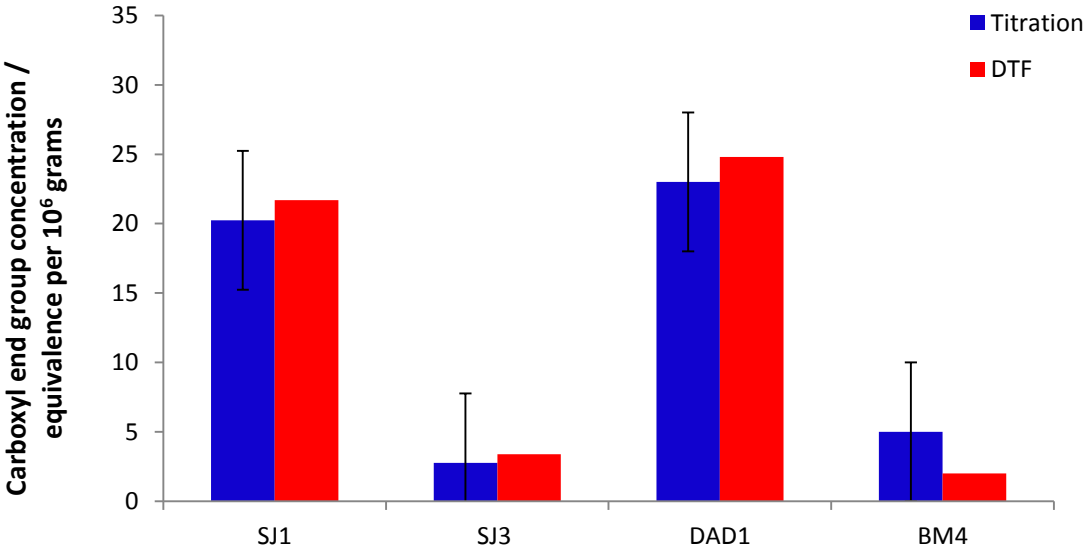

Figure 3.7 - Bar chart showing the carboxyl end group concentration for some PET film samples. The titration values quoted are the average of three repeats while the value provided by DTF was obtained from a single NMR measurement. Error bars are the 5 equivalents per 10^6 grams that were calculated as error in the titration method.

3.9.2 Ma et al. NMR Method

This method is based on the carbodiimide-mediated room temperature esterification of carboxyl end groups of polyesters with HFIP. [96] The reaction that is taking place is shown in figure 1.47.

The sample preparation was carried out at room temperature. Hydrolytic degradation was not considered to be an issue as the polymer was not being heated, so the polymer samples were not dried.

The polymer was dissolved in a mixture of $CDCl_3$ (1.00500g ± 0.00500g) and HFIP (0.22g ± 0.02g). The samples were left overnight to dissolve fully.

The following solutions were prepared:

- 0.00280g ± 0.00080g of 4-pyrrolidinopyridine was dissolved in 2.0450g ± 0.0200g of CDCl3. The 4-pyrrolidinopyridine was purchased from Sigma-Aldrich.

- 0.01550g ± 0.00100g of dicycohexylcarbodiimide (DCC) was dissolved in 3.0150g ± 0.0050g of CDCl3. The DCC was purchased from Sigma-Aldrich.

- 0.02059g ± 0.00500g of TFT was dissolved in 4.15043g ± 0.01000g of CDCl3. The TFT was purchased from Sigma-Aldrich.

Firstly 0.11000g ± 0.01000g of solution 1 was added to the dissolved polymer. Then 0.32500g ± 0.02000g of solution 2 was added. The mixture was left to stand for 10 minutes before 0.11000g ± 0.01000g of solution 3 was added.

The mixture was then carefully transferred to a clean dry NMR tube using a Pasteur pipette. The samples were then analysed on the Bruker AV400 NMR spectrometer with the parameters outlined in section 3.3. The number of scans was changed to 1024 and the data was analysed using Bruker Topspin 2.1 software. A sample of the full ^1H NMR spectra is shown in figure 3.8;

this is before the spectrum is zoomed in. The most dominant peaks correspond to the peaks of PET and the solvents used. The multiplet corresponding to the hexafluoroisopropyl ester, which is produced from derivitisation of the carboxyl end groups of the polyester, produces a peak at 6.02 ppm.

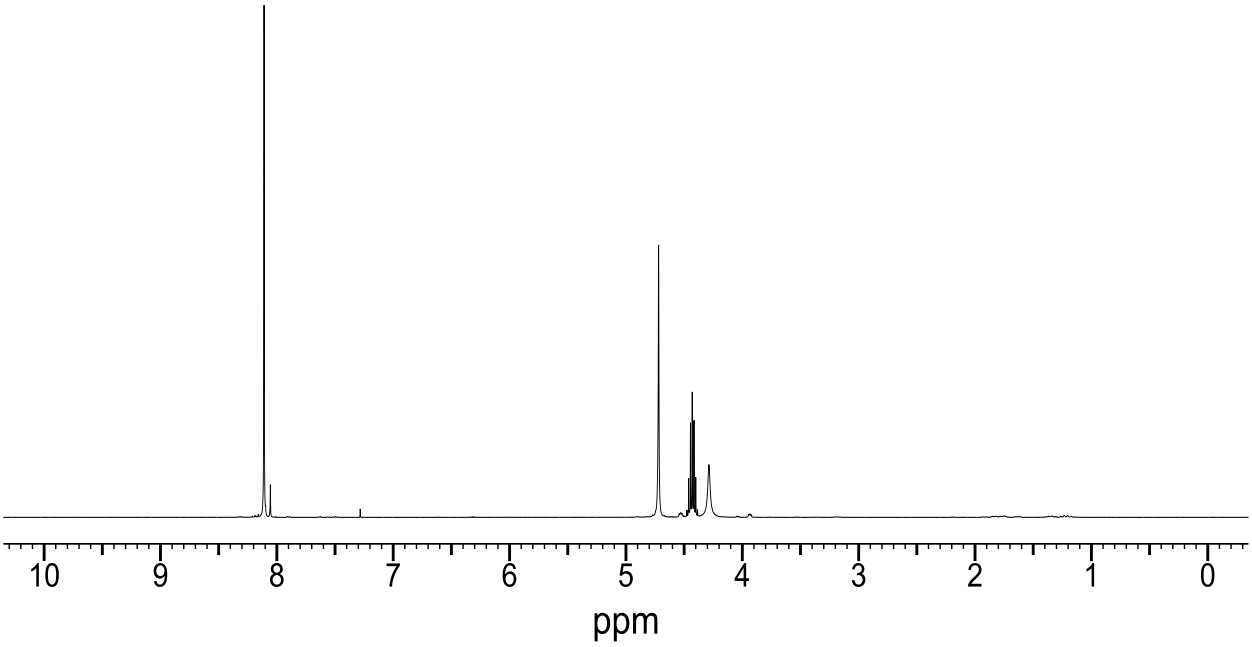

Figure 3.8 - ^{1}H NMR spectra of an E187 PET sample being analysed by Ma *et al.* NMR method.

The baseline was badly out of phase as the HFIP used was not deuterated. This meant that the best approach was to trim the spectrum to the area of interest, only between 5.8 ppm and 7.8 ppm. A sample of the area of interest is shown in figure 3.9. This allowed the automatic phase correction and baseline correction to be carried out. The spectra were then calibrated to the solvent peak at 7.27 ppm. The multiplet at 6.25 ppm is for the adduct that is formed from the reaction between DCC and HFIP. Figure 3.10 shows the structure of the adduct.

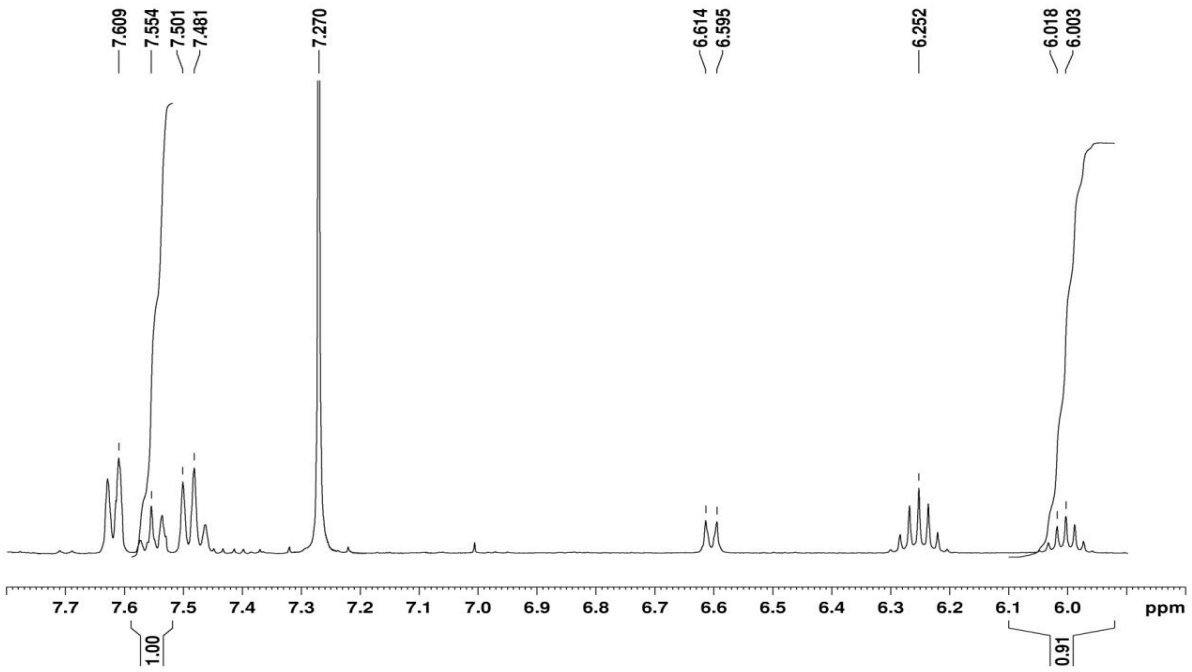

Figure 3.9 – ^{1}H NMR spectrum of the area of interest for one of the E187 PET sample being analysed by Ma *et al.* titration method.

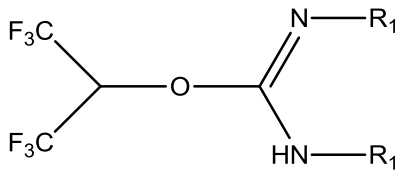

Figure 3.10 – Structure of the adduct formed from the reaction between DCC and HFIP. $R_1 = C_6H_{11}$.

All of the integral values from the ^{1}H NMR spectra obtained for chapter 3 are shown in the appendices (A3.1.5, A3.1.7, A3.1.9, A3.1.11 and A3.1.14). The individual carboxyl end group concentrations obtained as a comparison to those obtained by the NMR method are also shown in the appendices (A3.1.13).

A sample calculation is shown below for a sample of PET E187 chip samples:

A solution was prepared that contained 0.02050g of TFT in 4.15043g of chloroform, which gives 0.000530277g of TFT in 0.10736g of chloroform

As a result, there is 0.000530277g of TFT in NMR tube

1 mole of TFT is 146.1105g; therefore there is 0.000003629 moles of TFT in the NMR tube

There are 0.91 moles of end groups for every one mole of TFT (Value obtained from the ratio of the two peaks in the NMR spectra (Figure 3.10)

0.000003012 moles of end groups in 0.09541g

Therefore there are 34.61 equivalents per 10^6 grams

The error in the Ma et al. method was determined by performing 10 repeats of the same polymer type. The error value obtained for this experiment is 1.91 equivalents per 10^6 grams, which is a significant reduction from the 5 equivalents per 10^6 grams value obtained from the titration method. This allows a significant improvement when studying small effects that occur because of the addition of different additives to polyesters. The errors were expected to be caused by weighing. There was also some concern, however, that the error could be due to interpretation of the spectra. To rule this out as a possibility three experiments were obtained on the single sample. The error value was 0.28 equivalents per 10^6 grams, which is much smaller than the variation between the samples. This means that the error in the Ma *et al*. NMR method was indeed mostly due to weighing.

With the conditions optimised, and errors determined for the ^{1}H NMR spectra, several different polymer types were investigated to confirm that it produced a similar response to the value obtained by DTF. The bar chart in figure 3.11 shows the carboxyl end group concentration for 5 samples compared with the values obtained from DTF's NMR method. Normally, the value

obtained using this method matches closely with the value obtained from DTF. The polymer film samples with low carboxyl end group concentration give a better match to the carboxyl end group concentration obtained from DTF.

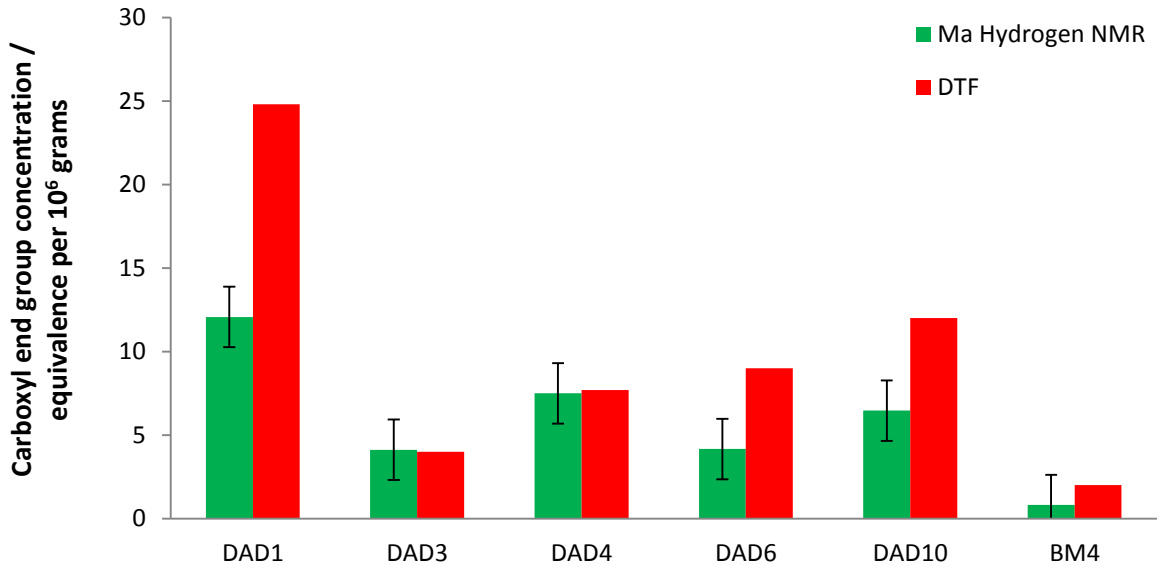

Figure 3.11 – Bar chart showing the carboxyl end group concentration of different types of PET film. Both methods used a single NMR measurement to obtain carboxyl end group value. Errors bars are 1.91 equivalents per 10^6 grams which is the calculated error within the Ma *et al*. NMR method

3.9.3 Comparison of Titration and NMR Methods

The two methods investigated were proven to be sufficient in determining the carboxyl end group concentration of polyesters. Figures 3.12 and 3.13 compare the carboxyl end group concentrations obtained from the titration and the hydrogen Ma *et al*. ^{1}H NMR method with the value supplied by DTF; this was to ensure that all three methods were in good agreement with each other. The Ma *et al*. NMR method showed that the titration method produces reliable results. The Pohl titration method was preferred because it was quicker and did not require the use of expensive solvents; as a result the titration method was selected as the method of choice for examining the carboxyl end group concentration for future samples. The Ma *et al*. method can be used to check samples if required, and to randomly check the performance of the Pohl titration method. All of the data can be seen in the appendices.

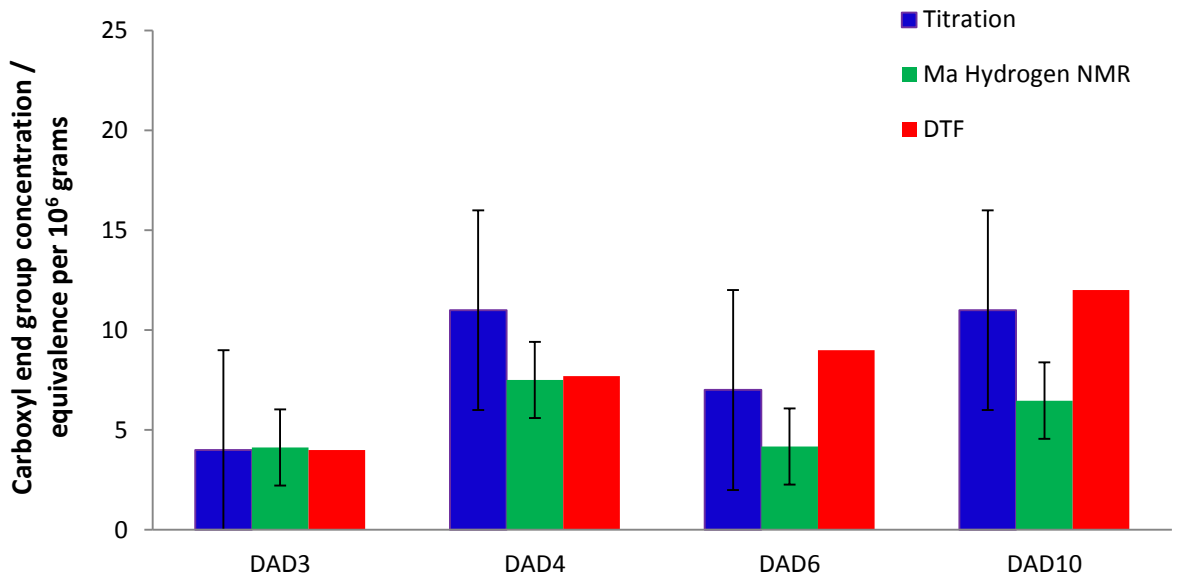

Figure 3.12 – Bar chart comparing the carboxyl end group concentrations obtained by titration (N=3), Ma *et al*. NMR method (N=1) and the value supplied by DTF (obtained using an NMR method) for a range of PET films. Error bars are 5 equivalence per 10^6 grams and 1.91 equivalents per 10^6 grams for the titration method and Ma et al. NMR titration method, respectively.

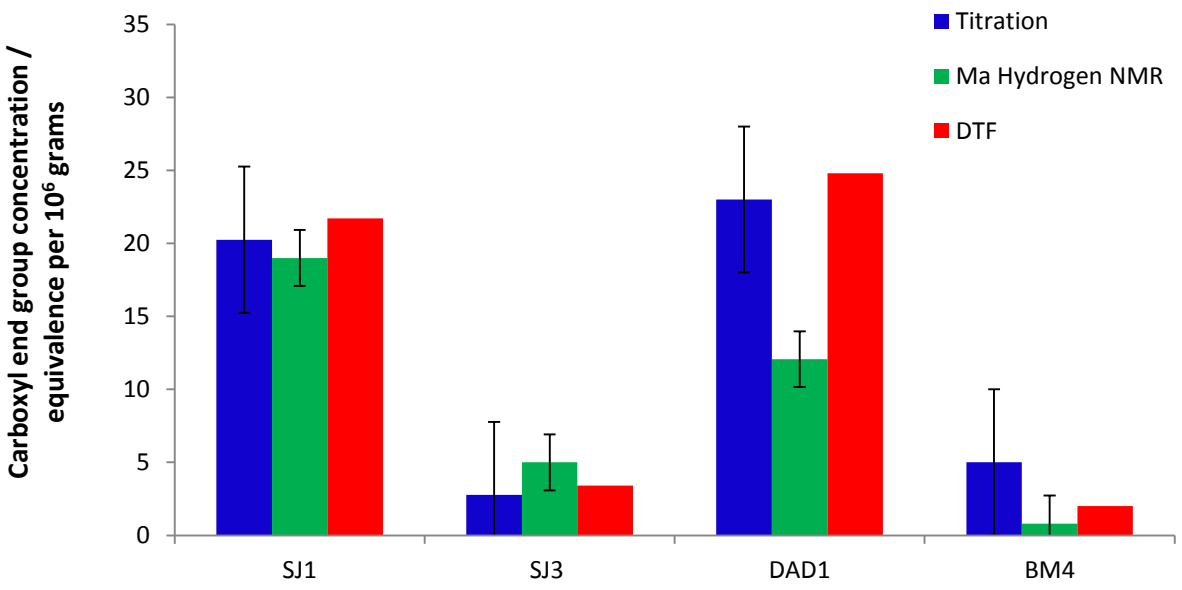

Figure 3.13 – Bar chart comparing the carboxyl end group concentrations obtained by titration (N=3), , Ma *et al*. NMR method (N=1) and the value supplied by DTF (obtained using an NMR method) for a range of PET films. Error bars are 5 equivalence per 10^6 grams and 1.91 equivalents per 10^6 grams for the titration method and Ma et al. NMR titration method, respectively.

3.10 Reaction of PEI and Epoxides

18.75 ± 0.01 g of PEI E354 chips were dissolved in 200 ml of chloroform. The chloroform was of reagent grade that was purchased from Sigma Aldrich. The solution was transferred to a 250 ml standard flask. A rinsing of 20 ml was taken from the beaker and added to the standard flask. This was repeated and the flask was made up to the mark with chloroform.

Samples were also prepared with the desired ratio by weight of the epoxides. Samples were prepared with 1% Cardura, 6% Cardura, 1% Vikolox, 6% Vikolox, 1% Heloxy and 6% Heloxy. The weight of the epoxide required was added to the beaker and mixed well.

10 ml of the solutions were pipetted into test tubes that had suitable connectors for the rig used. The solvent was left for 48 hours to evaporate which allowed the sample to coat the glass of the test tube walls evenly. The residual mix in the test tubes was heated in a grant BT50 hotplate was calibrated to be used at 90 ^{o}C, 110 ^{o}C, 130 ^{o}C and 150 ^{o}C. The rig used allowed an individual stream of dry nitrogen to be continually supplied to each of the test tubes. The test tubes were all connected and purged with nitrogen for 1 minute before the samples were put onto the pre-heated hotplate. The samples were left for the desired lengths of time which were 1, 2, 5, 10, 15 and 30 minutes. The tubes were then removed and allowed to cool to room temperature. 15 ml of chloroform was added and allowed to fully dissolve. The solution was transferred to an aluminium tray before a rinsing of 5 ml was taken from the tray and also added. The solution was allowed to evaporate before the film produced was used for further analysis.

3.11 Extrusion

The best method for carrying out reactive extrusion was thoroughly investigated as part of this study. A PRISM – TSE 16TC twin screw extruder was used for all of the experiments as this counter-rotating twin screw offered better mixing capabilities than the other available extruder. The single screw is larger and would have wasted considerably larger volumes of the polymer samples compared to the twin screw extruder. The instrument used is pictured in figure 2.4.

The extruder die was set up to produce a thin strand of PET, with a typical diameter of 0.9 mm, which would be pulled through a Rondol water bath to cool. The strands of PET produced from the extruder were then cut to the desired size for further analysis.

Several different temperature profiles of the barrel were investigated. The temperature profile selected was considerably higher than what would have been expected to ensure that the sample was molten by the time it reached the open port in order to allow the addition of the epoxides. There are 5 different temperature zones on the extruder and these are set to the following program:

- Zone 1 – 240 ^{o}C
- Zone 2 – 270 ^{o}C
- Zone 3 – 280 ^{o}C
- Zone 4 – 280 ^{o}C
- Zone 5 – 285 ^{o}C

The residence times of the polymer in the extruder were investigated to understand how long the polymer spends under processing temperatures. This is important as thermal degradation can occur if the polymer is held at processing temperatures too long, and indicates how long the polymer has to react with the epoxides. To calculate the residence time of the polymer in the extruder, a stopwatch was started when the first polymer chip was fed into the barrel of the extruder, and stopped when the polymer came out of the die of the extruder. This was repeated three times for each set of conditions to obtain an average and a standard deviation. The residence time was calculated to be 75 seconds for the standard method. The screw speed of the extruder was always set at 100 rpm unless otherwise stated.

The PET chips were dried in an oven at 140 ^{o}C for 24 hours before they were extruded. 500 g of the chip was placed in the hopper each time to ensure that a known polymer mass was fed into the extruder barrel. It was found that 500 g of polymer chip in the hopper provided enough material for samples of PET to be collected before running out. The feed rate of the hopper was investigated to ensure that the mass of polymer being added to the extruder barrel per second

was known. The polymer that was fed out of the hopper was caught in a weighed glass sample bottle. This was recorded every minute for 20 minutes. This process was repeated in triplicate. The first two minutes were not included in the calculation as it took time for the polymer to be fed through the screw. The calculation was determined for each of the individual experiments and the average obtained. Two different hopper screw sizes were investigated to see which would produce the lowest standard deviation. The two screws had the following dimensions:

- Larger screw had an inner diameter of 1.0 cm and an outer diameter of 1.8 cm
- Smaller screw had an inner diameter of 0.90 cm and an outer diameter of 1.4 cm

Figure 3.14 shows a bar chart to highlight the differences between the two hopper screws used. It can be clearly seen that the smaller screw produces a more acceptable error than the larger screw. This gives a more accurate mass of polymer being added to the extruder barrel per minute, and therefore allows the desired volume of epoxide being added using the liquid feed to be more accurate. The smaller screw was selected as the default method of preparing the samples used for all further work.

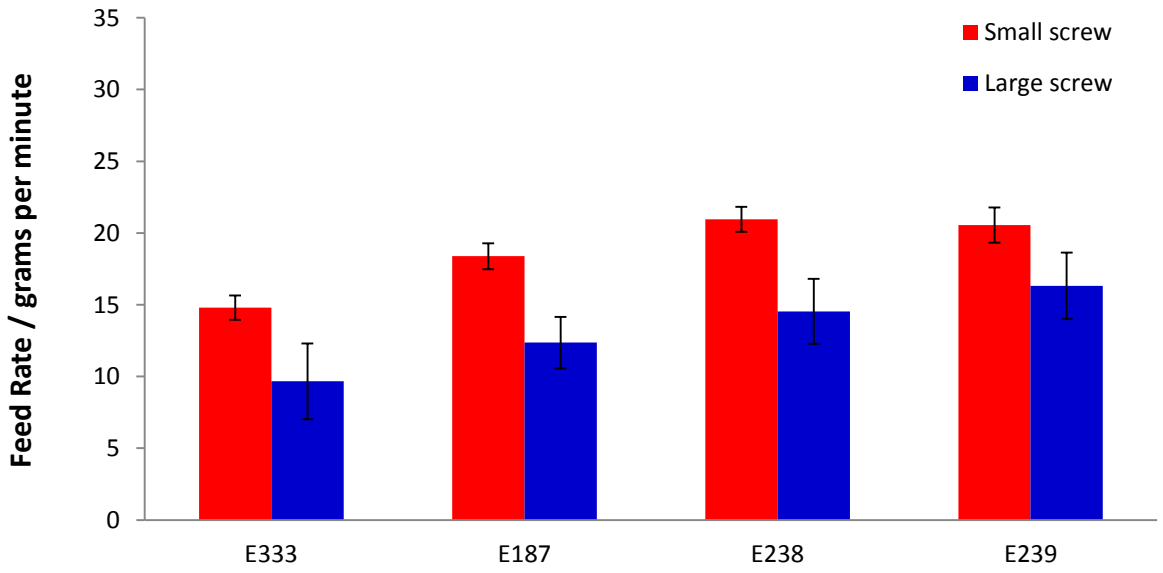

Figure 3.14 - Bar chart comparing the average feed rate of the two screws. The error bars represent the standard deviation of three repeats of the experiments.

The extruder that was set up at DTF to carry out trials on end capping PET with monofunctionalised epoxide groups involved a home built liquid feed that was put together using an electric motor and a syringe. The syringe used was calibrated for Cardura, Heloxy and Vikolox. The first port of the extruder was removed and the liquid feed was positioned over the port so that the liquid feed would drip the liquid epoxides into the open port at a controlled rate. The liquid feeder was set to the desired setting before being switched on. The liquid feeder was allowed to operate for a few minutes before a sample was obtained. The average carboxyl end group concentration of the initial samples can be seen in figures 3.15. The initial results indicated that the epoxide was reacting with the acid end groups of PET as there was a noticeable reduction in the carboxyl end group concentrations of the samples that contain the epoxide compared with the samples without.

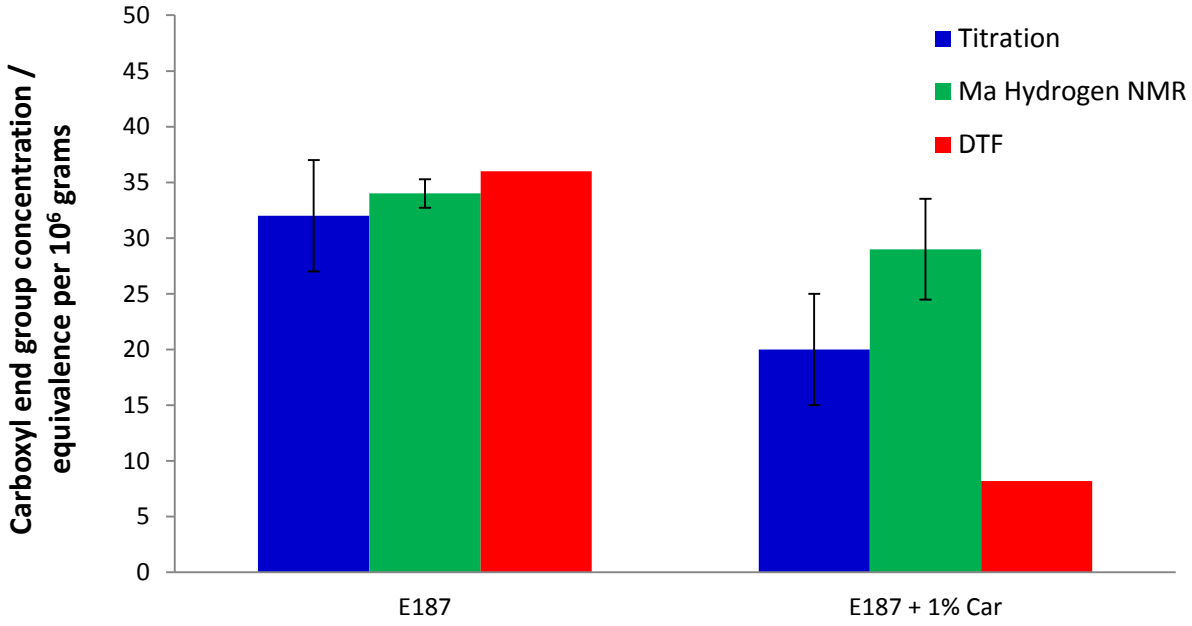

Figure 3.15 - Bar chart showing the carboxyl end group concentration of the E187 and E187 +1% Cardura samples obtained by the liquid feed. N=3 for the titration method,n=1 for both the Ma *et al*. NMR method and the value obtained by DTF.. Error bars are 5 equivalence per 10^6 grams and 1.91 equivalents per 10^6 grams for the titration method and Ma et al. NMR titration method, respectively.

The levels of Cardura were determined in the liquid feed samples to ensure that the desired volume was being added. The results of the samples tested are shown in table 3.1. The levels were slightly lower than desired, especially the 1% Cardura and E239 sample, because the levels of inorganic filler were not taken into account. The lower values for the E187 + 1% Cardura were expected to be a result of Cardura evaporating. The volume of Cardura was increased slightly to compensate for the values being lower than desired. The liquid feed has proven to be a suitable method for the addition of Cardura to the extruder.

Table 3.1 – Calculated percentage of Cardura that was present in the samples prepared using the liquid feed system.

Sample	% Cardura calculated at DTF
E239 + 1% Cardura	0.72
E187 + 1% Cardura	0.91

The method of mixing PET and the epoxide was checked to ensure that the method was adding a similar level of epoxide all the time. Samples of E239 + 1% Cardura and E239 + 6% Cardura were prepared for 20 minutes, and samples were collected for further analysis. The collected samples were analysed by the Pohl titration method and the results are shown in figures 3.16 and 3.17. The results of the experiments show that the end group concentration is not very consistent which is due to the high error value of the titration method. Despite the high error value it was decided that the information provided showed that this reactive extrusion method was an efficient way to carry out the esterification reaction between the epoxides and the carboxyl end groups of poly(ethylene terephthalate).

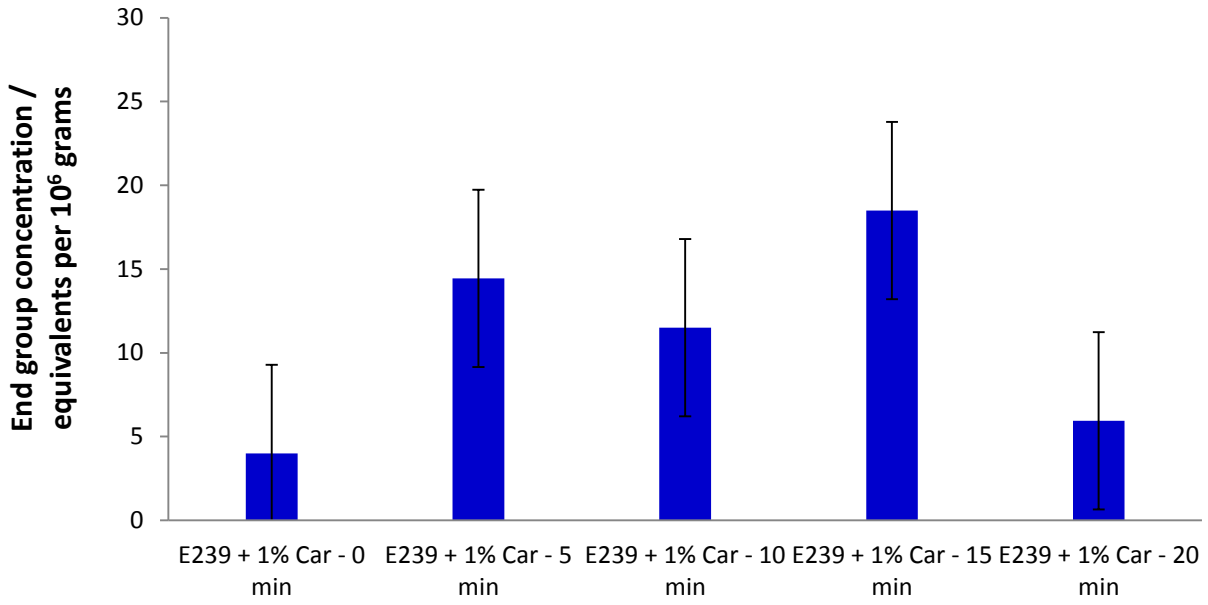

Figure 3.16 - Bar chart showing the carboxyl end group concentration of the E239 + 1% Cardura samples obtained by the liquid feed over time. Titrations were performed in triplicate and error bars are 5 equivalence per 10^6 grams.

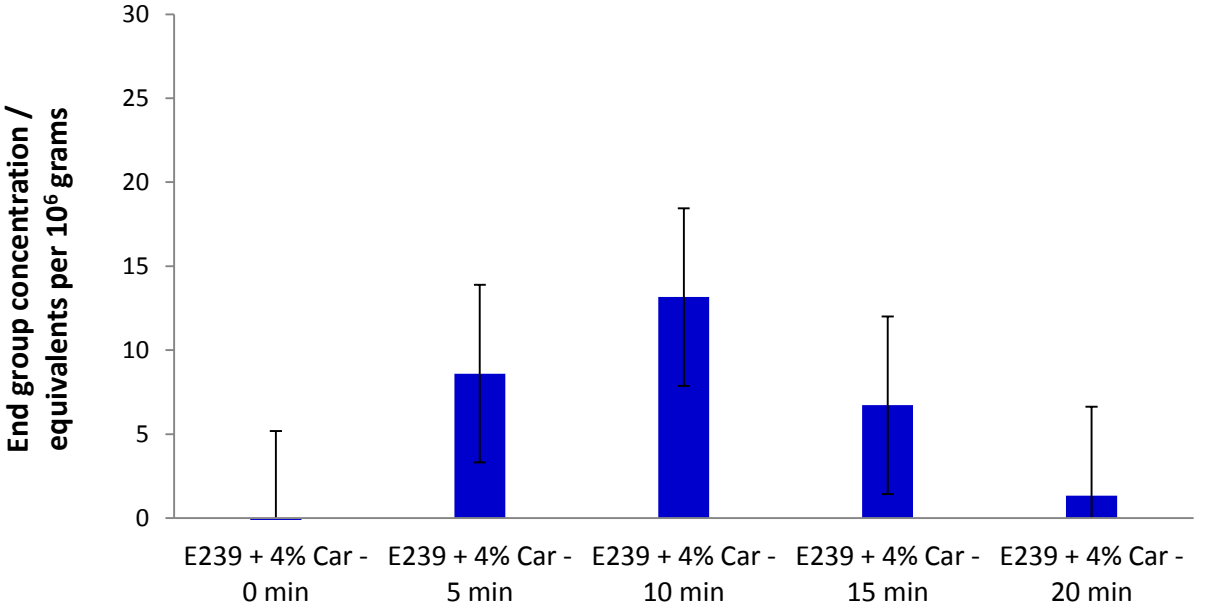

Figure 3.17 - Bar chart showing the carboxyl end group concentration of the E239 + 4% Cardura samples obtained by the liquid feed over time.] Titrations were performed in triplicate and error bars are 5 equivalence per 10^6 grams.

3.12 Intrinsic Viscosity

The IV of the E187 starting material was measured in orthochlorophenol using a Viscotex 430 viscometer. The IV of the E239 and E240 starting materials was obtained by melt viscosity using an Instron compression model melt rheometer. The sample was dried under vacuum for 36 hours at 135 ^{o}C before being analysed. The barrel temperature was 290 ^{o}C, and the shear rate was 100 S^{-1}. The IV measurement for all of the hydrolysed samples was measured using the same procedure as the E187 starting material.

3.13 Gel Content

100 mg samples were dissolved in a mixture of 50% chloroform and 50% HFIP. The samples were left for 24 hours to ensure that the samples were fully dissolved. Fisherbrand FB59011, qualitative filter paper purchased from Fisher Scientific was used and dried in the vacuum oven at 90 ^{o}C for 4 hours. It had a range quoted as QL100 and the size was 42.5 mm. The filter paper was then weighed as soon as it came out of the oven. The paper was used in a Büchner filtration apparatus to remove all of the solvent from the samples, leaving behind the gel. The samples were then placed in the vacuum oven at 90 ^{o}C for several hours and the samples were weighed to a constant mass.

The percentage of gel in the samples was calculated based on the original mass before volatilisation (Equation 3.1) and the mass of the residual material after ageing (Equation 3.2). W_o is the initial mass of the sample before ageing, W_r is the initial mass of the residual material used in the gel content experiment and W_g is the mass of the gel produced during the experiment.

$$\% \text{ Gel Content (Original)} = \frac{W_g}{W_o} \text{ X } 100 \qquad \textbf{Equation 3.1}$$

$$\% \text{ Gel Content (Residual)} = \frac{W_g}{W_r} \text{ X } 100 \qquad \textbf{Equation 3.2}$$

Blanks of the filter paper were analysed to ensure that the temperature used to dry the paper did not cause degradation. Samples were also prepared and filtered with just the solvent system used to ensure that this solvent had no effect on the filter paper.

3.14 Cardura Content

The Cardura samples were sent to DuPont Teijin Films in order to determine their concentration.. The Cardura concentration was determined by examination using the ^{1}H NMR spectrum. The samples were dissolved in deuterated tetrachloroethane and analysed using an Eclipse +500 instrument at 80 ^{o}C.

3.15 Hydrolysis of samples

3.15.1 Hydrolysis at Room Temperature

0.5 g of the polymer samples were placed in a glass sample bottle with 10 ml of distilled water. The lids were loosely placed on the samples to prevent contamination. The samples were left for the desired length of time; they were exposed to these conditions for 3, 7, 10 and 14 days before removing and drying.

Samples were also created using the methods described above, but in this instance the water in the experiment was changed every 2 days to maintain the pH value of the water. It has been discussed in the literature that small components are able to break off the polymer during degradation which would affect the pH value.

3.15.2 Hydrolysis at 50 ^{o}C

0.5 g of the polymer samples were placed in a glass sample bottle with 10 ml of distilled water. The lids were loosely placed on the samples before they were placed into the drilled aluminium blocks present in the pre-heated Grant hot plate. The samples were covered in aluminium foil to ensure the temperature of the water was maintained at 50 ^{o}C. The samples were exposed to these conditions for 3, 7, 10 and 14 days before removing and drying.

Samples were also created using the methods described above, but in this instance the water in the experiment was changed every 2 days.

3.15.3 Hydrolysis at 100 ^{o}C

5 g of extruded polymer sample was placed in a round bottom flask with 100 ml of distilled water. A Graham condenser was fitted to the flask, and the water was allowed to reflux for the desired length of time. A calibrated three place heating mantle was used for the reflux experiments. The times that the polymer samples were exposed to the conditions to encourage hydrolytic degradation to occur were 3, 7, 10, 14 and 28 days. The samples were then allowed to cool before being removed and dried.

Samples were also created using the methods described above, but in this instance, the water in the experiment was changed every 2 days

3.16 Hydrolysis Kinetics

The hydrolysis reaction of PET is considered to be a single-step process due to the ester linkages (EL) in the polymer chain simply being broken down into carboxyl (COOH) and hydroxyl (OH) end groups. [10, 43-47 and 124]

$$\mathrm{EL} + \mathrm{H_2O} \rightarrow \mathrm{COOH} + \mathrm{OH} \qquad \textbf{Equation 3.3}$$

It has been reported that the reverse reaction can be ignored when water is greatly in excess. [125-127] The rate of the reaction can be monitored using either the ester linkage concentration or the carboxyl/hydroxyl end group concentration. [10 and 43-47]

$$\text{Rate} = -\frac{\Delta[\text{EL}]}{\Delta t} = \frac{\Delta[\text{COOH}]}{\Delta t} = \frac{\Delta[\text{OH}]}{\Delta t} \qquad \textbf{Equation 3.4}$$

$$\text{Rate} = \frac{[\text{COOH}]x \text{ days} - [\text{COOH}]0 \text{ days}}{x \text{ days}} \qquad \textbf{Equation 3.5}$$

The hydrolytic degradation has been reported in the literature to be a pseudo first order reaction when water is greatly in excess. [44 and 128] If water is not in excess the reaction is second order. [124] Several other research groups have reported a half order reaction with respect to the carboxyl end group concentration because the acid end groups produce an auto-catalytic effect on the reaction rate which is shown in the equation below: [45 and 128]

$$\frac{\Delta[\text{COOH}]}{\Delta t} = k[\text{EL}][\text{H}_2\text{O}][\text{COOH}]^{0.5} \qquad \textbf{Equation 3.6}$$

Zhang and Ward proposed a half order reaction rate with the carboxyl end group concentration acting as a catalyst. [129] They also considered the effects of the polyester's initial crystallinity, as hydrolytic degradation has been widely reported to only occur in the amorphous regions. Crystallinity will therefore have an effect on the number of ester linkages available for hydrolysis, the water concentration that can penetrate into the amorphous region, and the carboxyl end group concentration that is present. The rate of the reaction when in terms of the carboxyl end group concentration becomes:

$$\frac{\Delta[\mathrm{COOH}]}{\Delta t} = \frac{k}{(1-\mathrm{crystallinity})^{0.5}}[\mathrm{EL}][\mathrm{H_2O}][\mathrm{COOH}]^{0.5} = K[\mathrm{COOH}]^{0.5} \qquad \textbf{Equation 3.7}$$

$$K = \frac{k}{(1-\mathrm{crystallinity})^{0.5}}[\mathrm{EL}][\mathrm{H_2O}] \qquad \textbf{Equation 3.8}$$

In the above equations, k is referred to as the true reaction rate constant and K is the apparent reaction rate constant. When the above equation was integrated with time, it provides the following expression:

$$[\mathrm{COOH}]_t^{0.5} - [\mathrm{COOH}]_0^{0.5} = \frac{K}{2}t \qquad \textbf{Equation 3.9}$$

Where $[COOH]_t$ is the concentration of the carboxyl end group concentration at time, t and $[COOH]_0$ is the initial concentration. A plot of $[COOH]_t^{0.5}$ – $[COOH]_0^{0.5}$ against time produces a straight line where the gradient produced is the apparent reaction rate constant divided by 2.

3.17 TVA

The TVA line is continually pumped to a pressure of approximately 10^{-5} torr.

20 mg of the polymer samples were dissolved in a mixture of 50% HFIP and 50% chloroform. This solution was cast into a thin film on the bottom of a flat-bottomed borosilicate tube which has an outer diameter of 33 mm. The tube had a B40 ground glass Quickfit™ cone fitted, so it could be added to the TVA tube head. The solvents were allowed to dry before they were connected to the TVA line.

The sample was allowed to pump down for 24 hours before being analysed. All of the samples analysed were heated to 550 ^{o}C at a rate of 10 ^{o}C min^{-1}and held at 550 ^{o}C for 30 minutes.

The condensable volatiles were separated into four limbs. Limb one contained the volatiles from -196 ^{o}C to -140 ^{o}C, limb two contained the volatiles from -140 ^{o}C to -80 ^{o}C, limb three contained the volatiles from -80 ^{o}C to -29 ^{o}C and limb four contained the volatiles from -29 ^{o}C to 25 ^{o}C.

Special cells were attached to the TVA line so that IR spectra and GC chromatograms could be obtained for each of the fractions. The gas phase IR spectra of the four limbs were obtained using a Perkin Elmer, spectrum 100, FTIR spectrum using the following parameters: The range covered 4000 cm^{-1} to 45 cm^{-1}, resolution was set to 8 cm^{-1} and the number of accumulations was set to 16 scans. The data was analysed using Spec Viewer software. Analysis by GC-MS was carried out on fraction 4 using a ThermoQuest Polaris Q instrument with an integrated trace GC ion trap. The program used involved a temperature ramp from 20-320 ^{o}C with a helium carrier gas used at a flow rate of 1 ml min^{-1}. The mass spectrometer scanned the range of 50-650 m/z. The data obtained, both gas chromatogram and mass spectra, were analysed using Xcalibur software.

The cold ring and cold finger were also analysed by GC-MS. The cold ring was removed with spectroscopy grade chloroform and analysed using the same instrument and parameters as described above.

3.18 Ageing Rig

Louise Turnbull designed a system that could examine the degradation of polyester samples under a variety of different conditions for her PhD thesis. [130] The sample preparation for the system involved the samples being dried sufficiently before analysis. The polymer samples to be analysed were chopped into rods that were 2 to 3 mm in length. They were then dried in a pre-heated Vulcan oven at 160 ^{o}C for 4 hours under vacuum. The samples were cooled enough to allow them to be safely transferred to a desiccator until they were required for analysis.

The sample was then spread evenly onto a circular aluminium foil base. 1 g of sample was used to reduce errors when dealing with small samples, and to provide enough material to analyse the samples after ageing, such as in gel-content analysis. The sample and aluminium foil were carefully weighed to allow the percentage volatilisation to be accurately calculated.

The sample and aluminium foil were placed into the ageing rig sample chamber, which was made from circular quartz glass. This sample chamber was able to repeatedly withstand the high temperatures used in the experiment. The lid of the chamber was stainless steel, with Swagelok unions for the gas inlet and outlet tube. To ensure that the sample chamber was air tight, metal clips were used.

The nitrogen gas used to provide the environment in which to study the thermal degradation of the samples was dried by being passed through a silica gel desiccant before flowing through a flow meter. The gas then entered a stainless steel coil which was inside the Lenton ARF 7/22 recirculation air furnace used. The coil allowed the gas to be pre-heated before it entered the sample chamber. It was found that to prevent cooling of the sample, and to maximise the extent of volatilisation, that a gas flow rate of 400 ml min^{-1} should be used. This rate was therefore used for all experiments. The samples were connected and allowed to purge for 15 minutes before being heated to ensure that all the air had evacuated the chamber.

The temperature of the sample was monitored throughout the ageing experiment by a thermocouple which was positioned 2 cm above the sample. In the application for solar cell panels the highest temperatures that the sample will ever experience will occur during processing or re-processing for recycling. This resulted in processing temperatures being used to investigate the effects of thermal degradation on the samples containing the epoxides. The temperatures studied were 290 ^{o}C, 305 ^{o}C and 320 ^{o}C. All of the experiments carried out were heated at a rate of 10 ^{o}C min^{-1}.

The samples were held for 5 minutes, 60 minutes and 300 minutes once they had reached the desired temperature. Once the sample was aged they were allowed to cool and placed back into a desiccator for 24 hours. The sample was then reweighed. The percentage volatilisation

was then calculated using the following equation, where W_o is the samples initial mass and W_a is the mass of sample after ageing:

$$\% \text{ Volatilisation} = \frac{(W_o - W_a)}{W_o} \text{ X } 100 \qquad \textbf{Equation 3.10}$$

3.19 CATLAB

All of the samples used in the Hiden CATLAB microreactor system were dried in the vacuum oven before being placed inside a quartz sample tube which was specially designed for the ageing rig. Approximately 12 mg of the sample was used per experiment. These sample tubes are opened at both ends to allow the gas to flow through the sample. Quartz wool was added to a depth of 2 cm at the bottom of the tube to prevent the sample from contaminating the instrument. This also ensured that the sample was placed at the same position in the oven each time, in turn ensuring consistent heating between experiments. The sample tube was sealed tight inside the oven using Swagelok fittings.

The helium and air gases used to create the atmospheres had flow rates of 40 ml min^{-1} which was controlled using an electronic mass flow unit. The samples were allowed to purge for 15 minutes before being heated to ensure that the system was purged out. The samples were heated up to 550 ^oC with flow rates of 5 ^oC min^{-1}, 10 ^oC min^{-1} and 20 ^oC min^{-1}. The temperature of the sample was monitored using a k-type thermocouple positioned inside the quartz sample tube at a height of 1 cm above the sample.

The volatile gases being released during the thermal degradation process were transferred to a Hiden HP20 quadruple mass spectrometer using a heated capillary. The mass spectrometer was operated in scanning mode, searching from 5 to 200 amu in a helium atmosphere, and 35 to 200 amu in air.

4.0 Reactions of Benzoic Acid and Epoxides

4.1 Introduction

Chain extenders have been extensively researched with PET as they can increase both the molecular weight of a polymer sample and the samples resistance to hydrolytic degradation. [66-85] The most commonly used chain extenders for PET are the diepoxides which can react with the two main end groups of PET, namely hydroxyl and carboxyl end groups.

The three epoxides, Cardura, Vikolox and Heloxy are monofunctionalised epoxides and were chosen because extensive cross linking was undesirable. Cross linking in the PET film samples could affect the requirements needed (for example, the clarity of the polymer) for the sample to be used as a polymeric backsheet in photovoltaic devices.

The three epoxides of interest supplied by DTF were fully characterised before the end capping reaction was studied. It is well documented in the literature that epoxides can undergo ring opening. Weak nucleophiles, such as water, can react with epoxides in the presence of acid catalysts. [131] The mechanism for this occurring is shown in figure 4.1. After the three epoxides were characterised they were investigated to ensure that this phenomenon was not occurring at the conditions investigated.

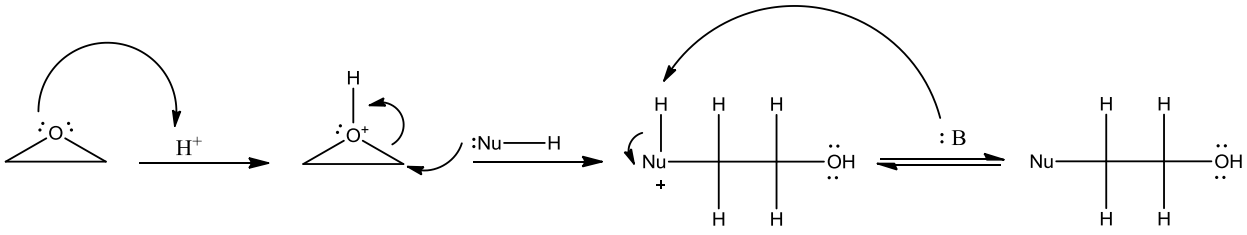

Figure 4.1 – Mechanism for the ring opening of epoxides in the presence of weak nucleophiles. [After 131]

The esterification reaction of the individual epoxides was studied to determine which epoxide would be most effective at end capping the polymer chains. The effectiveness of each epoxide was based on the concentration of epoxide required, to minimise the cost for DTF, and the time for the esterification reaction to occur. The reaction time of the esterification reaction is important to DTF to ensure the production time is minimised, and the aim would be to be able to add the epoxide to their current film processing line. [16]

Several research groups have shown that diepoxides can react with the carboxyl end groups of PET in the melt state, which is referred to as reactive extrusion. [80-81] Dhavalikar studied the reaction of poly(ethylene terephthalate) in the melt phase with the following epoxies; diglycidyl ether of bisphenol A, N, N' – bis [3(carbo-2'3' epoxypropoxy) phenyl] pyromellimide, triglycidyl glycerol and triglycidyl isocyanurate. He concluded that triglycidyl glycerol was shown to be the most effective modifier and can successfully react with a high molecular weight PET inside an extruder. [135]

Reactive extrusion requires a suitable laboratory scale extruder which can use large quantities of starting material, which is a disadvantage when the starting material is valuable. The carboxyl end group concentration of the polymers produced from reactive extrusion can also be difficult to obtain as the levels are often very low. The above reasons are why many research groups use model compounds to study the reaction of polymers including PET. [42, 49 and 132-134] The model compounds used to study PET's reactions included benzoic acid, ethylene dibenzoate, 2-hydroethyl benzoate and diethyleneglycol dibenzoate. For example, Botelho *et. al*. used the model compound diethyleneglycol dibenzoate to study the thermo-oxidative degradation mechanisms in a copolymer of poly(butylene terephthalate) and polyethylene oxide. [132] The model compound, hyroxyethyl benzoate, was used to study new catalyst mechanisms for PET. [133]

In this chapter the model compound benzoic acid was studied with the chosen three monofunctionalised epoxides; Cardura, Vikolox and Heloxy. Three different ratios of the epoxides to benzoic acid samples were studied; namely (1:2), (1:1) and (2:1). Several ratios were studied so that any possible side reactions could be investigated, as well as the main

esterification reaction. The side reactions that are possible include the etherification reaction discussed in chapter 1. The production of side reactions can affect the properties, such as clarity of the polymer, and can alter the process temperatures of the polymer being manufactured.

4.2 Results and Discussion

4.2.1 Starting Materials

4.2.1.1 Cardura

The IR spectrum for Cardura is consistent with a glycidyl ester (Figure 4.2). The CH_2 groups rocking movement is shown by the peak at 793 cm^{-1}. The peaks consistent with the epoxide group are clearly shown at 850, 911, 996, 1087 and 1254 cm^{-1}. The peaks at 1343 and 1384 cm^{-1} are for CH_3 groups undergoing symmetrical deformations, and the peak at 1466 cm^{-1} is for the CH group undergoing deformations. The carbonyl group for the saturated ester is shown at 1732 cm^{-1}. The CH groups undergoing stretching are shown in the peaks 2875 and 2962 cm^{-1}. The peak at 3057 cm^{-1} is the CH stretching band for the epoxide group. There are small peaks at 3445 and 3536 cm^{-1} which are for hydroxyl groups; these were determined to be either ring opening of the epoxide or from moisture on the sodium chloride discs.

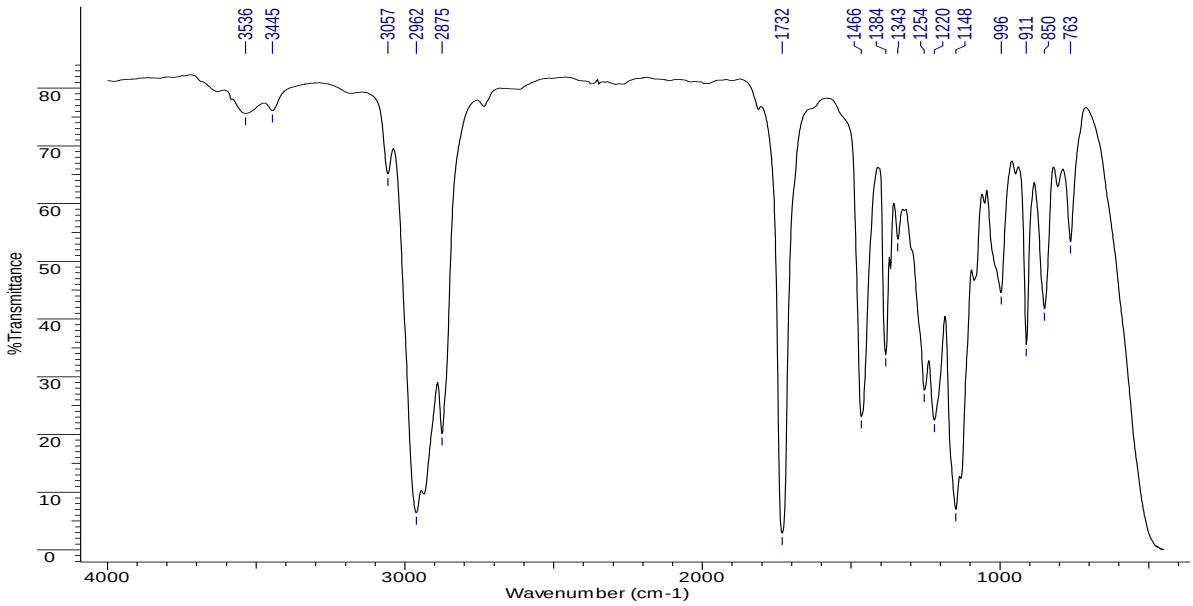

Figure 4.2 - IR spectrum of Cardura.

The ^{1}H NMR spectrum (Figure 4.3) and ^{13}C NMR spectrum (Figure 4.4) of Cardura are both very complex and indicate that Cardura is possibly a mixture of different isomers. The peaks in both spectra are consistent with aliphatic, epoxide and ester groups. The multiple peaks between 0.60 and 2.40 ppm in the ^{1}H NMR spectrum are consistent with the Cardura having different isomers. The peaks at 2.65, 2.82 and 3.20 ppm are for the epoxide group. The same findings are seen in the ^{13}C NMR spectrum, including the large volumes of aliphatic peaks between 12 and 50 ppm, suggesting a mixture of isomers. The peaks for the epoxide group are clearly seen in the ^{13}C NMR spectrum at 44.6 and 49.4 ppm. Figure 4.5 shows a diagrammatic representation of the peak values and the part of the epoxide they relate to. To confirm that Cardura was a mixture of isomers, a gas chromatogram of the epoxide was obtained. Figure 4.6 shows the gas chromatogram for the Cardura sample. It can be seen from the gas chromatogram that there are many peaks eluting between 11.99 and 12.34 minutes, suggesting that the sample of Cardura is made up of more than one molecular structure. The mass spectra produced are all very similar, with the parent ion being at 269 m/z, confirming that Cardura consists of seven isomers. An example of the mass spectra can be seen in the appendices (Figure A4.1.1) and all other mass spectra can be seen on the attached disc in the folder *Chapter 4* under *Starting Materials*.

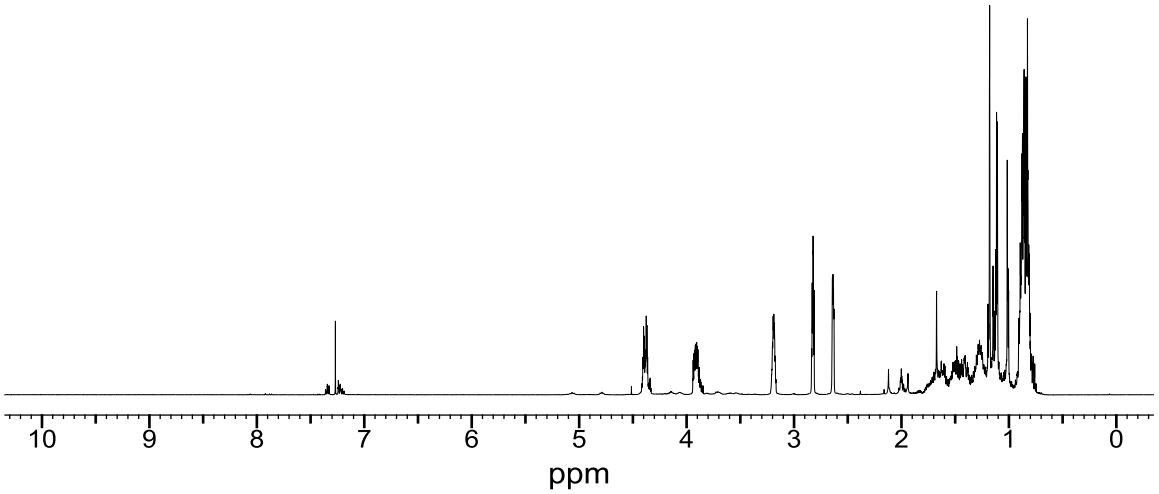

Figure 4.3 – ^{1}H NMR spectrum of Cardura, dissolved in chloroform.

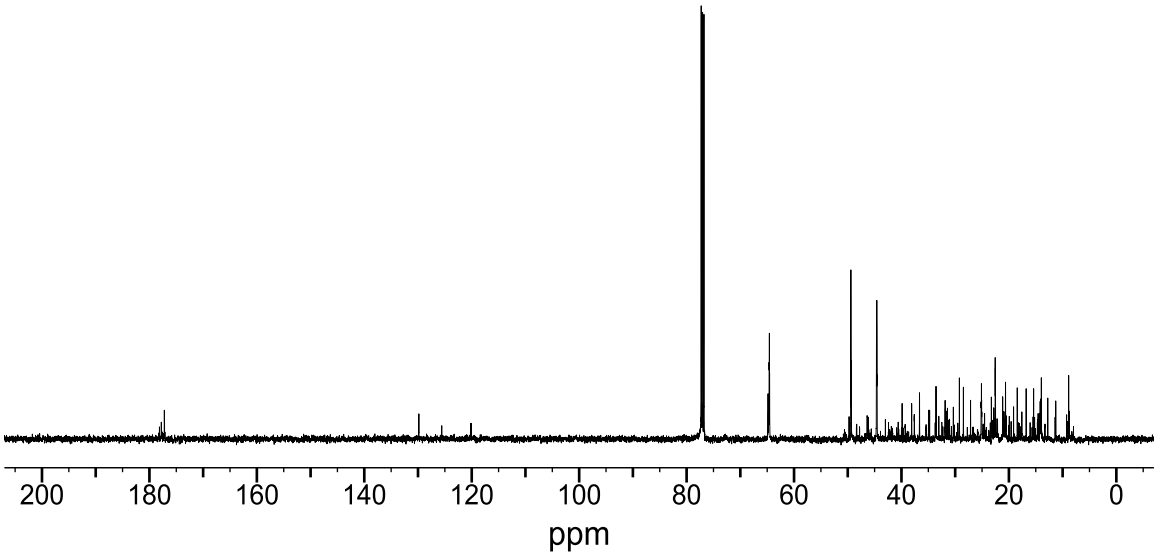

Figure 4.4 – ^{13}C NMR spectrum of Cardura, dissolved in chloroform.

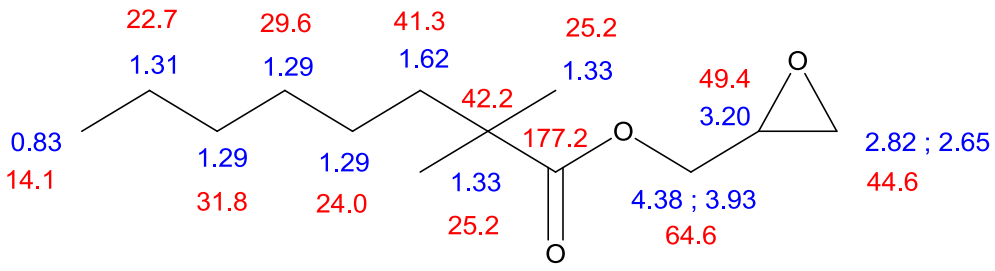

Figure 4.5 –Theoretical ^{1}H NMR (Blue) and ^{13}C NMR (Red) peak assignments for Cardura. The chemical shift values for both the ^{1}H NMR and ^{13}C NMR data are in ppm.

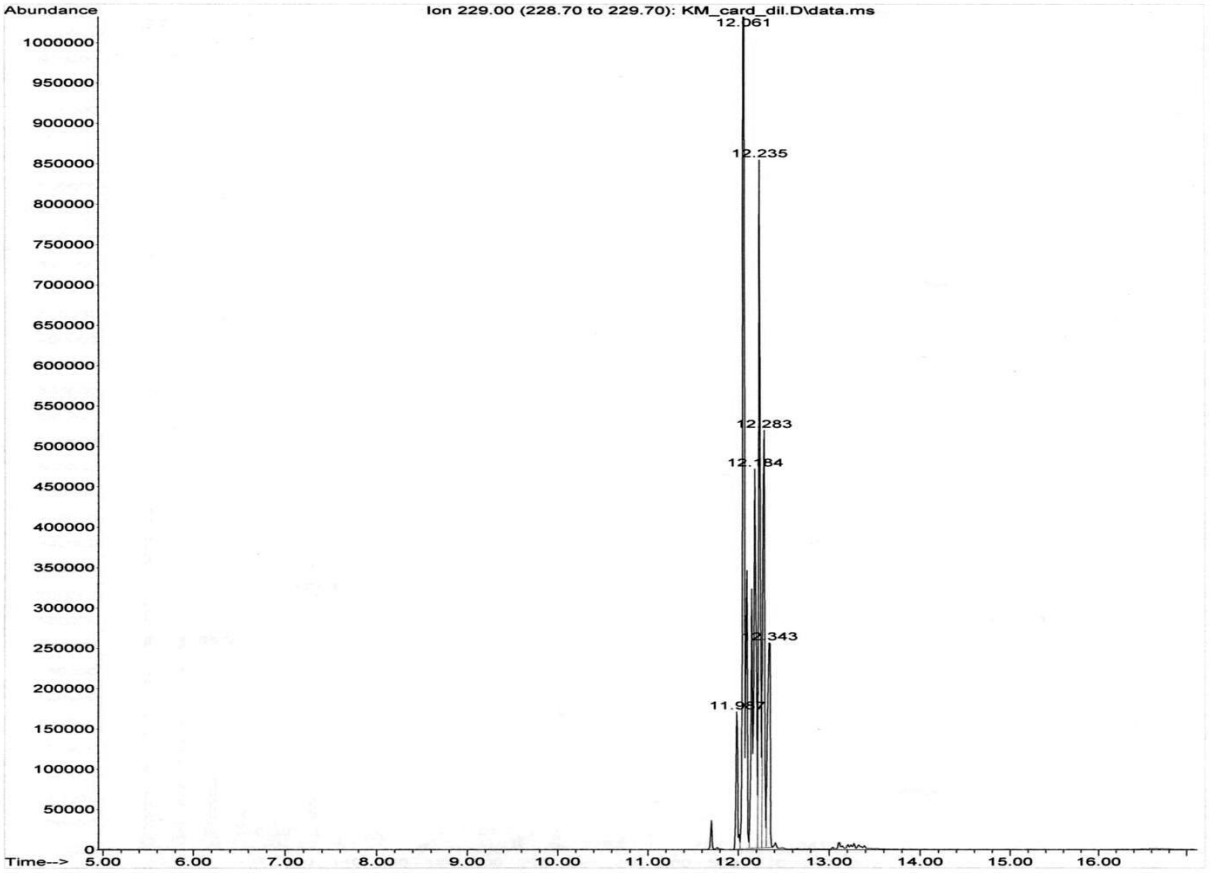

Figure 4.6 – Gas chromatogram of the Cardura sample.

The thermal properties of Cardura were investigated by DSC and TGA. The DSC scan (Figure 4.7) shows two endothermic events. There was some concern that, despite the pan being sealed, the endotherms are a result of the sample volatilising. A TGA thermogram (Figure 4.8) was obtained and the mass loss did occur at similar onset temperatures. The ease at which Cardura volatilised was taken into account when planning experiments.

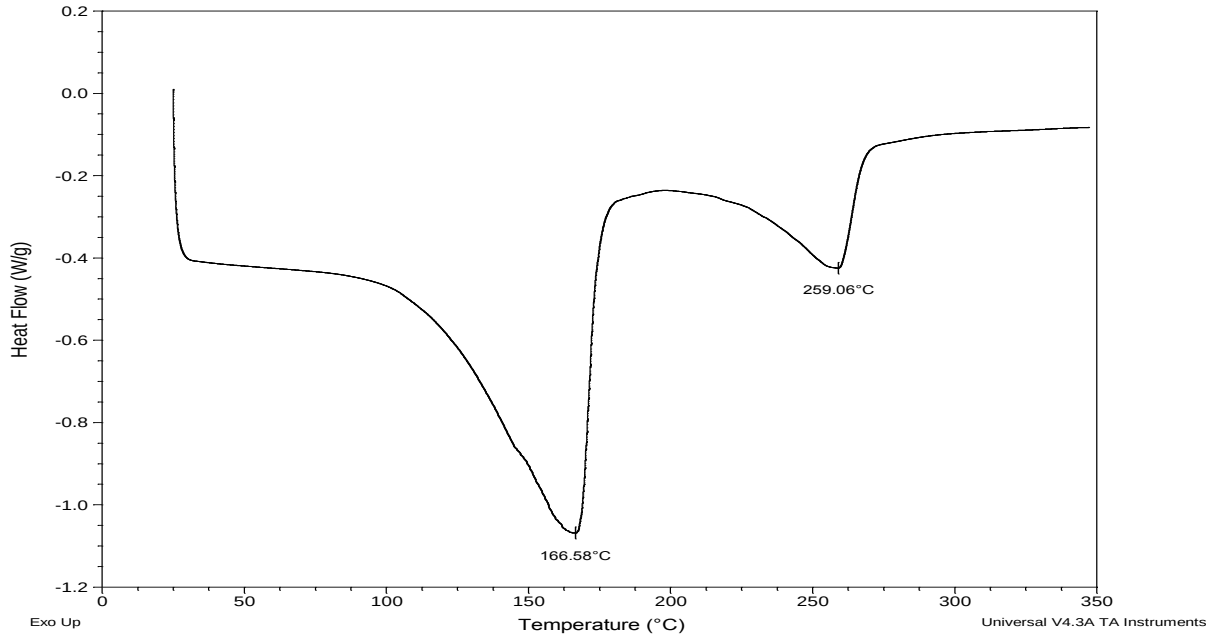

Figure 4.7 – DSC scan of Cardura heated under nitrogen at 10 °C min^{-1}.

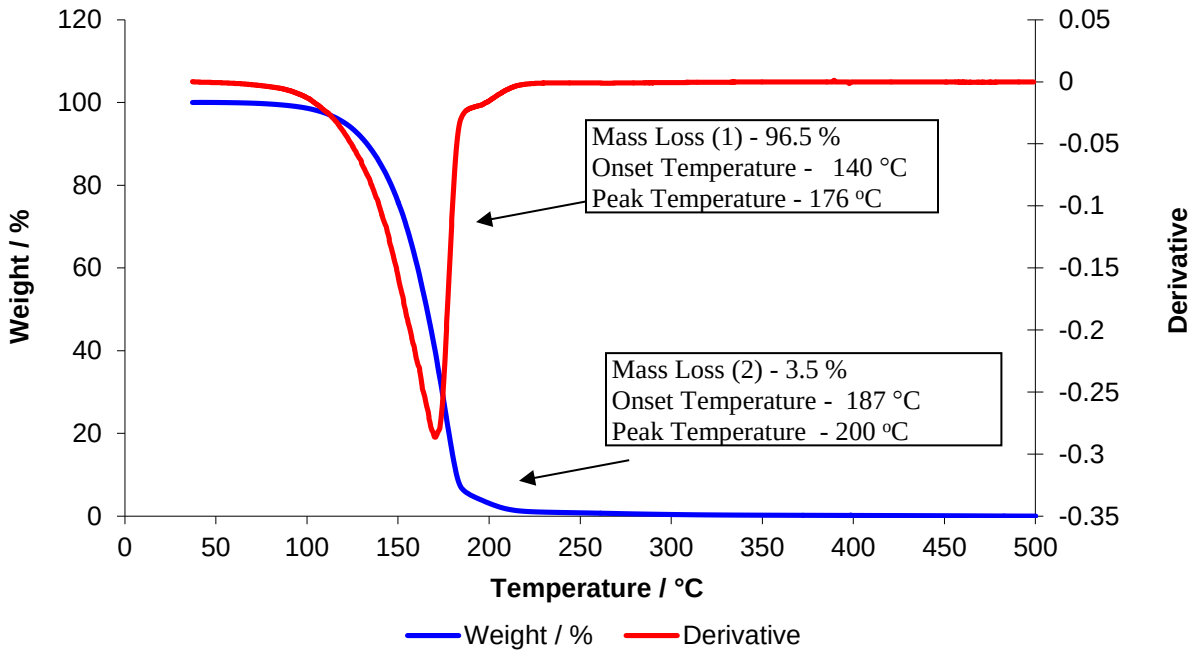

Figure 4.8 – TGA thermogram of Cardura heated under helium at 10 °C min^{-1}.

4.2.1.2 Vikolox

The dominant peaks in the IR spectrum obtained for Vikolox are consistent with an aliphatic epoxide. The CH_2 groups rocking movement is shown by the peak at 722 cm^{-1}. The peaks consistent with the epoxide group are clearly shown at 836, 917, 996, 1129 and 1259 cm-1. The peak at 1378 cm^{-1} is for CH_3 groups undergoing symmetrical deformations, and the peaks at 1410 and 1466 cm^{-1} are for the CH group undergoing deformations. The CH groups undergoing stretching are shown in the peaks 2874 and 2925 cm^{-1}. The peak at 3042 cm^{-1} is the CH stretching band for the epoxide group. The IR spectrum for Vikolox can be seen in the appendices (Figure A4.1.2).

The ^{1}H NMR and ^{13}C NMR spectra of Vikolox have peaks that are expected for an aliphatic epoxide. Figure 4.9 shows the assignments for both spectra. The ^{1}H NMR and ^{13}C NMR spectra of Vikolox are shown in the appendices, figures A4.1.3 and A4.1.4 respectively. The peaks for the epoxide group are clearly shown in the ^{1}H NMR spectrum at 2.46, 2.74 and 2.90 ppm. The epoxide groups are seen in the ^{13}C NMR spectrum at 47.1 and 52.6 ppm.

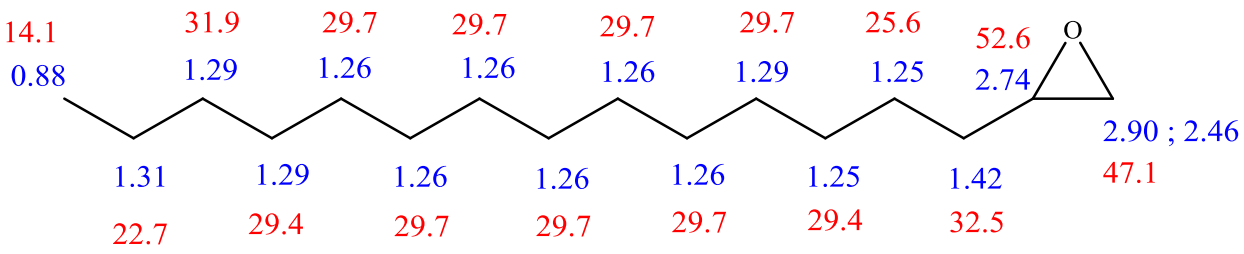

Figure 4.9 –Theoretical ^{1}H NMR (Blue) and ^{13}C NMR (Red) peak assignments for Vikolox. The chemical shift values for both the ^{1}H NMR and ^{13}C NMR data are in ppm.

The thermal properties of Vikolox were studied by both DSC and TGA. The DSC scan of Vikolox produced two endotherm peaks. This could be a result of the sample volatilising or degrading. It

is expected that the main endotherm at 208 ^{o}C is a result of the sample volatilising and the smaller peak at 324 ^{o}C is due to the remaining Vikolox degrading. TGA supports the theory that the Vikolox is evaporating as it has two mass loss peaks. The main peak in the TGA thermogram is at 217 ^{o}C, which is similar to the main peak in the DSC scan at 208 ^{o}C. The second peak is much higher in the DSC scan. This may be because the pan is sealed slightly and results in the gases taking longer to escape. The DSC scan and TGA thermogram for Vikolox are shown in figures A4.1.5 and A4.1.6 in the appendices section.

4.2.1.3 Heloxy

The IR spectrum of Heloxy is shown in the appendices (Figure A4.1.7). The peaks for this spectrum are much sharper than those seen in the IR spectra of Cardura and Vikolox. The IR spectrum of Heloxy has several more peaks than the other epoxides, which is expected as Heloxy has aromatic groups present, as well as the peaks corresponding to the aliphatic groups and epoxide groups. CH_2 groups rocking movement and para-disubstituted benzene rings produce a peak around 768 cm^{-1}. The peaks consistent with the epoxide group are clearly shown at 830, 917, 1039, 1118, 1246 and 1294 cm^{-1}. The CO stretching from the ether group is shown in the peak at 1186 cm^{-1}. The peak at 1364 cm^{-1} is for the CH_3 groups undergoing symmetrical deformations, and the peak at 1459 cm^{-1} is for the CH group undergoing deformations. The peaks at 1514 and 1609 cm^{-1} are due to carbon – carbon stretching vibrations in the aromatic group. The CH groups undergoing stretching are shown in the peaks 2869 and 2962 cm^{-1}. The peak at 3042 cm^{-1} is the CH stretching band for the epoxide group and the peak at 3101 cm^{-1} is for CH absorption of an aromatic ring.

The ^{1}H and ^{13}C NMR spectra of Heloxy are consistent with the structure for Heloxy. Figure 4.10 shows all assignments for the NMR spectra and both spectra can be seen in the appendices (Figures A4.1.8 and A4.1.9). The peaks for the epoxide group are present in the ^{1}H NMR spectrum at 2.8, 2.9 and 3.4 ppm. In the ^{13}C NMR spectrum, the important epoxide peaks that will be involved in the esterification reaction are present at 44.8 and 50.3 ppm.

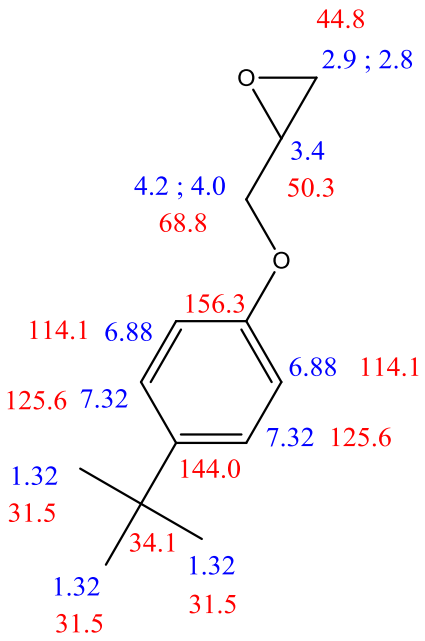

Figure 4.10 – Theoretical ^{1}H NMR (Blue) and ^{13}C NMR (Red) peak assignments for Heloxy. The chemical shift values for both the ^{1}H NMR and ^{13}C NMR data are in ppm.

The thermal properties of Heloxy were studied by obtaining a DSC scan and a TGA thermogram. The DSC scan for Heloxy can be seen in figure A4.1.10 in the appendices section. As with Cardura and Vikolox, two endothermic peaks are present in the DSC scan for Heloxy. This was expected to be as a result of volatilisation or degradation. A TGA thermogram was obtained to confirm these findings. The TGA thermogram is shown in the appendices (Figure A4.1.11) and consists of two mass loss events. The main mass loss event occurs at 197 ^{o}C and is consistent with the first endotherm event in the DSC scan at 191 ^{o}C. The temperatures of the second mass loss event and the second endotherm differ, which is expected as the DSC pan was sealed.

4.2.1.4 Benzoic Acid

The IR spectrum for the solid benzoic acid is shown in the appendices (Figure A4.1.12). The peaks for the aromatic and carboxylic acid groups are clearly visible in the spectra. The aromatic groups are shown in the spectrum, including the peak at 690.0 cm^{-1}, confirming the mono-substituted pattern of the benzene ring. The other bands at 931.6, 1583.7 and 1602.35 cm^{-1}

indicate that benzoic acid is a 6-membered aromatic ring. The carboxylic acid group of the acid is shown clearly at 1680.6 cm^{-1}. The C-O stretching band is seen between 1028 and 1181 cm^{-1}. The OH bending bands are seen at 1289 – 1326 cm^{-1} and the OH stretching bands are seen between 1420 cm^{-1} and 2828 cm^{-1}. The very broad band in the region 2556 – 3074 cm^{-1} is a result of intermolecular hydrogen bonding.

The ^{1}H and ^{13}C NMR spectra of benzoic acid are consistent with the expected structure. Figure 4.11 shows all assignments for both the ^{1}H and ^{13}C NMR spectra. The peaks for the carboxylic acid group are present in the ^{1}H NMR spectrum at 12.48 ppm. In the ^{13}C NMR spectrum, the important carboxylic acid groups that will be involved in the esterification reaction are shown at 172.54 ppm. The ^{1}H and ^{13}C NMR spectra for benzoic acid can be seen in the appendices (Figures A4.1.13 and A4.1.14).

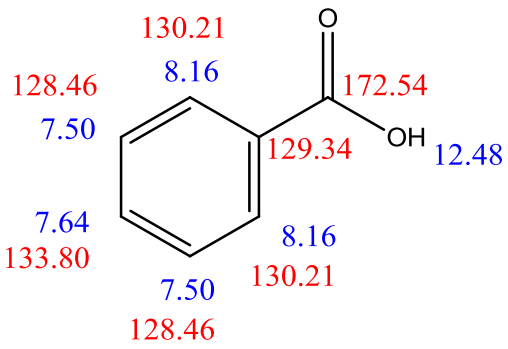

Figure 4.11 – Theoretical ^{1}H NMR (Blue) and ^{13}C NMR (Red) peak assignments for benzoic acid. The chemical shift values for both the ^{1}H NMR and ^{13}C NMR data are in ppm.

The thermal properties of benzoic acid were studied by obtaining a DSC scan and a TGA thermogram. The DSC scan for benzoic acid produces a sharp melting peak at 124.26 ^{o}C. This is the melting point expected for benzoic acid. The DSC scan produced for benzoic acid can be seen in the appendices (Figure A4.1.15). A TGA thermogram was obtained to identify the maximum exposure temperatures. The TGA thermogram is shown in the appendices (Figure A4.1.16) and highlights that the onset of mass loss is at 163 ^{o}C. This is expected to be the benzoic acid boiling off and, as a result, all experiments were kept below 160 ^{o}C.

4.2.2 Epoxide Reactions

4.2.2.1 Cardura

It was necessary to demonstrate that Cardura did not auto-polymerise through ring opening at the conditions chosen to study the reactions between Cardura and benzoic acid. Samples of Cardura were heated at temperatures of 90 – 150 ^{o}C for periods of up to 30 minutes under nitrogen and air. The ^{1}H and ^{13}C NMR spectra generated for all of the samples post-heating are identical to those produced for the Cardura starting material. This suggests that at the conditions investigated ring opening of Cardura was not occurring. Examples of the ^{1}H and ^{13}C NMR spectra for the Cardura sample heated at 90 ^{o}C in nitrogen for 30 minutes can be seen in figures 4.12 and 4.13. All other ^{1}H and ^{13}C NMR spectra generated can be seen in the attached disc in the folder *Chapter 4* under *Epoxide Reactions*.

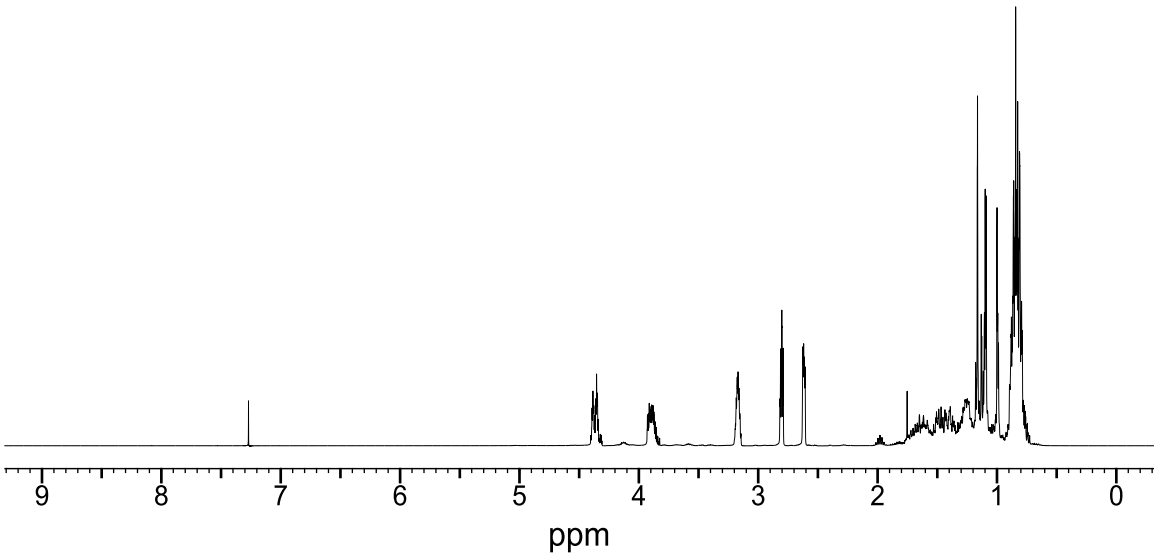

Figure 4.12 – ^{1}H NMR spectrum of a Cardura sample heated under nitrogen at 90 ^{o}C for 30 minutes.

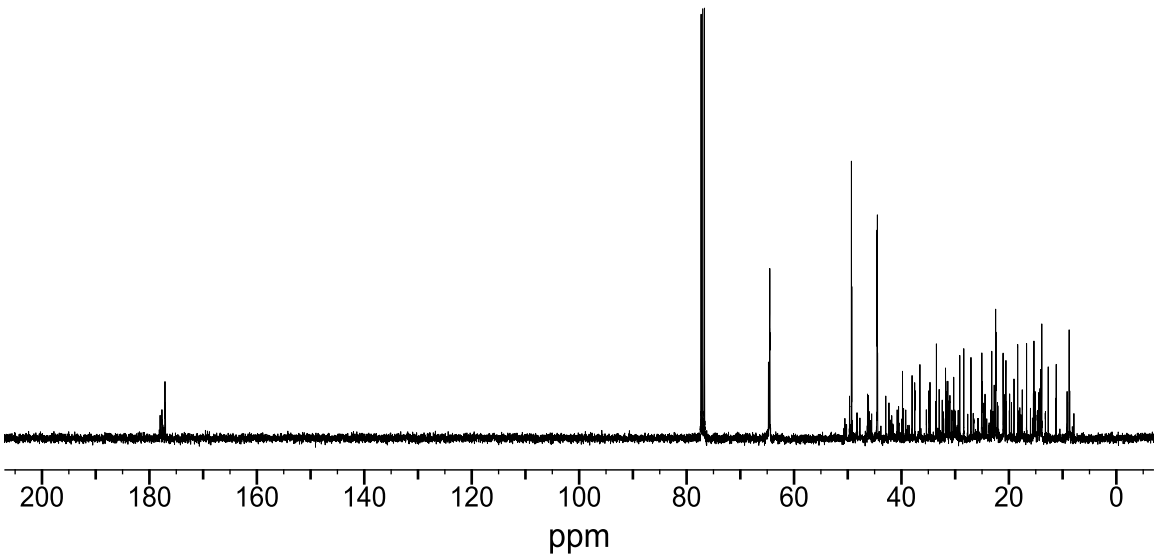

Figure 4.13 – ^{13}C NMR spectrum of a Cardura sample heated under nitrogen at 90 ^{o}C for 30 minutes.

If ring opening of Cardura was occurring at the conditions investigated, then the peaks in the ^{1}H NMR spectra at 2.65, 2.82 and 3.20 ppm, which correspond to the epoxide group, would disappear. Alcohol groups are produced during the ring opening of an epoxide group. These new groups would produce peaks in the ^{1}H NMR spectra at approximately 3.56, 3.58, 3.65, 3.81 and 3.90 ppm. In the ^{13}C NMR spectra the peaks at 44.6 and 49.4 ppm which correspond to the epoxide group would reduce in size. New peaks would appear in the ^{13}C NMR spectra at 63.7 and 70.9 ppm which would be the new hydroxyl peaks forming during ring opening of the epoxide.

To confirm that there was no ring opening of the epoxide group occurring in any of the samples of Cardura prepared, further analysis was carried out on the ^{1}H NMR spectra. The peaks at 2.62, 2.80 and 3.17 ppm were integrated to look for small changes in the intensity of these peaks. The regions integrated were 2.56 - 2.66, 2.75 - 2.86 and 3.10 - 3.25. Figure 4.14 shows an example of the scatter plot of the integrals obtained for the Cardura samples heated at 150 ^{o}C under nitrogen. All other scatter plots created for the other conditions are shown in the appendices section between figures A4.2.1 to A4.2.7. These plots confirm that no ring opening of Cardura is occurring at the conditions investigated

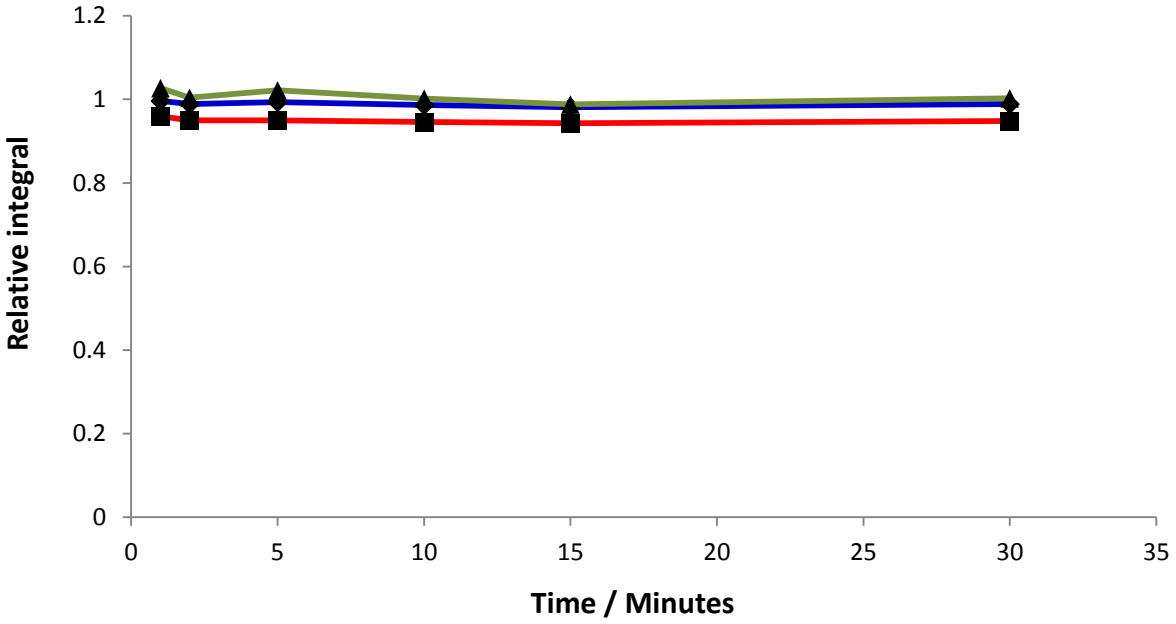

Figure 4.14 –Relative integrals from the ^{1}H NMR spectra of the Cardura samples heated under nitrogen at 150 ^{o}C. The blue line represents the peak at 2.62 ppm, the red line is for the peak at 2.80 ppm and the green line is for the peak at 3.17 ppm.

4.2.2.2 Vikolox

Vikolox was also investigated to ensure that ring opening of the epoxide group does not occur. The temperatures investigated were 90 ^{o}C, 110 ^{o}C, 130 ^{o}C and 150 ^{o}C. Vikolox samples were prepared under both nitrogen and air for 1, 2, 5, 10, 15 and 30 minutes. All ^{1}H and ^{13}C NMR spectra generated for the samples that were heated under air and nitrogen were similar to the NMR spectra of the Vikolox starting material, which suggests that ring opening of Vikolox was not occurring at the conditions investigated. All ^{1}H and ^{13}C NMR spectra can be seen on the attached disc in the folder *Chapter 4* under *Epoxide Reactions*. If ring opening of Vikolox was occurring, the epoxide group at 2.46, 2.74 and 2.90 ppm in the ^{1}H NMR spectra and 47.1 and 52.6 ppm in the ^{13}C NMR spectra would disappear. New peaks would also appear at 3.56, 3.58, 3.65, 3.81 and 3.30 ppm in the ^{1}H NMR spectra because of the formation of alcohol groups during ring opening. The peaks corresponding to the formation of alcohol groups would appear at 66.5 and 72.0 ppm in the ^{13}C NMR spectra.

The integrals were also obtained of the peaks corresponding to the epoxide groups in all of the ^{1}H NMR spectra of the Vikolox samples. The regions integrated were 2.30 - 2.50, 2.65 - 2.80 and 2.80 – 2.96 ppm. The scatter plots obtained for other temperatures investigated in both air and nitrogen can be seen in the appendices (Figures A4.2.8 to A4.2.15). All scatter plots show that ring opening of the epoxide group is not occurring at any of the conditions investigated.

4.2.2.3 Heloxy

Samples of Heloxy were prepared using the same conditions as those used to prepare the samples of Cardura and Vikolox. All ^{1}H NMR spectra generated for the samples were similar to the spectra of the starting material. This suggests that ring opening of Heloxy was not occurring at the conditions investigated. If ring opening of the epoxide group had occurred, the peaks at 2.80, 2.90 and 3.40 ppm would disappear. Alcohol groups are produced during the ring opening of an epoxide group. These new groups would produce peaks in the ^{1}H NMR spectra at approximately 3.56, 3.58, 3.65 and 3.81 ppm. All ^{13}C NMR spectra of the Heloxy samples support the conclusion that ring opening of the epoxide groups is not occurring. If ring opening of the epoxide group was occurring the peaks at 44.8 and 50.3 ppm would disappear. New peaks corresponding to the formation of alcohol groups would appear at 63.8 and 71.6 ppm. All ^{1}H and ^{13}C NMR spectra for the Heloxy samples can be seen on the attached disc in the folder *Chapter 4* under *Epoxide Reactions*.

To confirm that ring opening of the epoxide was not taking place at any of the conditions investigated the peaks corresponding to the epoxide groups were integrated. The regions integrated were 2.70 - 2.85, 2.85 – 3.00 and 3.30 - 3.50 ppm. The data shows that no ring opening of the epoxide group is occurring at these temperatures. The scatter plots can be seen in the appendices (Figures A4.2.16 to A4.2.22).

4.2.3 Benzoic Acid and Epoxide Reactions

4.2.3.1 Benzoic Acid

Samples were also prepared of the benzoic acid to ensure that the changes in the acid end group concentration could be monitored and also to ensure that no side reactions were occurring at the conditions used. Samples were prepared at 90, 110, 130 and 150 ^{o}C under nitrogen. At each temperature samples were held for 1, 2, 5, 10, 15 and 30 minutes similarly to the epoxides. All peaks were clearly identified, including the peak at 11.99 ppm for the carboxylic acid proton. No changes were noticed in any of the ^{1}H and ^{13}C NMR spectra obtained for any of the samples. All ^{1}H and ^{13}C NMR spectra can be seen on the attached disc in the folder *Chapter 4* under *Benzoic Acid and Epoxide Reactions*. To confirm that no side reaction was occurring in the benzoic acid samples, the broad singlet at 11.99 ppm was integrated. The region integrated was for the peak corresponding to the carboxylic acid proton between 10.00 to 14.50 ppm. No changes were noticed in any of the sample sets, confirming that no side reactions were occurring. All other scatter plots can be seen in the appendices (Figures A4.3.1 to A4.3.4).

4.2.3.2 Benzoic Acid and Cardura Reactions

Unheated Benzoic Acid and Cardura (1:1) Samples

The peaks present in the ^{1}H and ^{13}C NMR spectra for the unheated sample of Cardura and benzoic acid with a ratio of 1:1 are mostly consistent with the starting materials that have not reacted. In the ^{1}H NMR spectra there are small extra peaks at 3.82 ppm, 4.51 ppm, 5.56 ppm, 5.88 ppm and 8.02 ppm. There are also very small peaks between 4.0 and 4.5 ppm, which are difficult to positively identify as they are very small and overlap with the other peaks present. The extra peaks identified are consistent with the changes expected for the ring opening of the epoxide group into a secondary alcohol which occurs during the esterification reaction between Cardura and benzoic acid.

The aromatic region in the ^{1}H NMR spectra supports that an esterification reaction is occurring. The peaks at 8.02 and 8.11 ppm are doublets which are consistent with what is expected for the ortho position of the aromatic ring in the esterification product (Figure 4.15) and benzoic acid

starting material respectively. The peaks at 7.45 and 7.57 ppm are multiplets but would be expected to be triplets in both the esterification product and benzoic acid. The complex multiplets produced are expected to be mixtures of the main esterification product and benzoic acid. Figure 4.16 shows the ^{1}H NMR spectrum for a sample with a 1:1 ratio of benzoic acid and Cardura that was not heated.

The ^{13}C NMR spectra of the Cardura and benzoic acid samples support the conclusion that the esterification reaction is occurring. Figure 4.17 shows the ^{13}C NMR spectrum for the Cardura and benzoic acid sample (1:1) that was unheated. The peaks for the starting material are seen in the spectrum, but there are other peaks in the ^{13}C NMR spectrum that are consistent with the formation of a secondary alcohol from the esterification between Cardura and benzoic acid, such as peaks at 133.13 and 166.5 ppm. There are also several peaks between 60 and 75 ppm that correspond to the presence of the secondary alcohol.

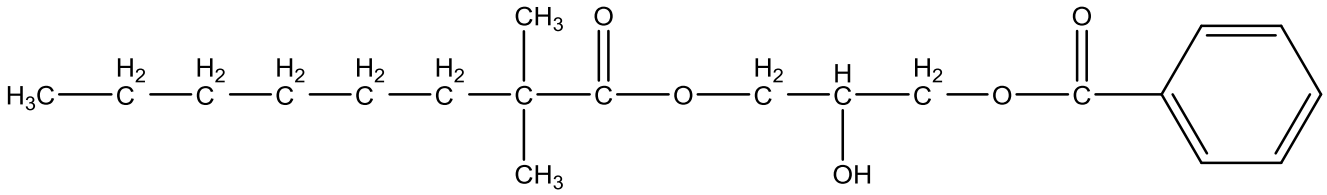

Figure 4.15 – A possible structure of the secondary alcohol produced in the esterification reaction between Cardura and benzoic acid.

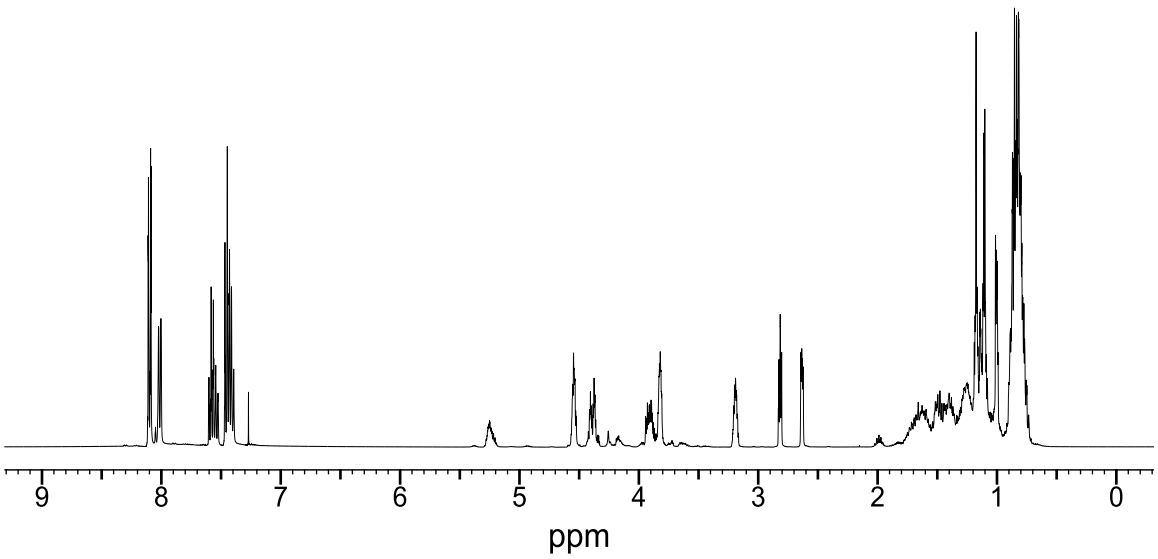

Figure 4.16 – ^{1}H NMR spectrum of the benzoic acid and Cardura sample (1:1) with no heating.

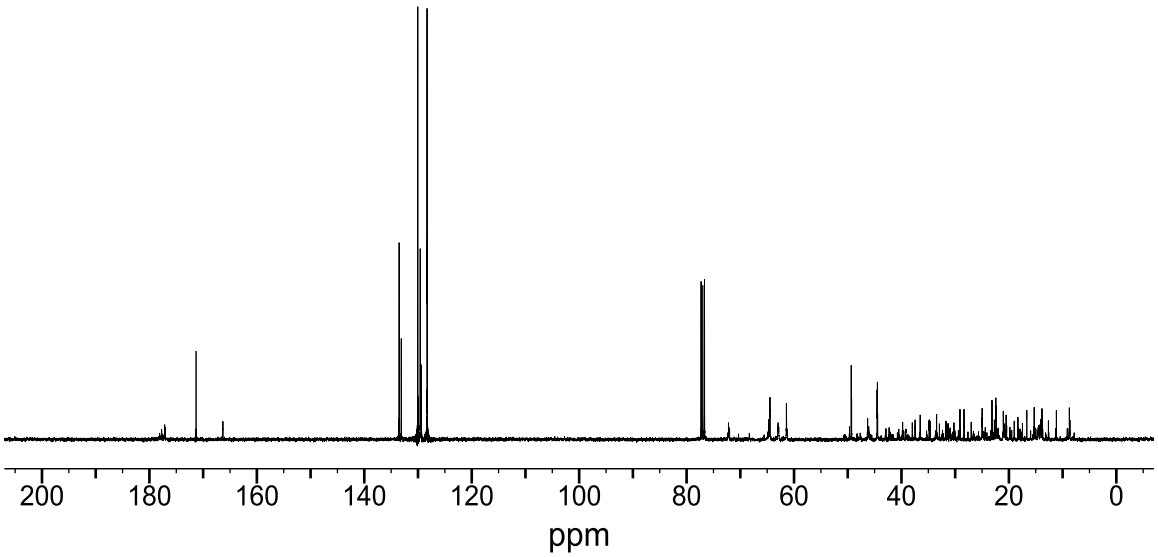

Figure 4.17– ^{13}C NMR spectrum of the benzoic acid and Cardura sample (1:1) with no heating.

The ^{1}H and ^{13}C NMR spectra for the unheated samples of Cardura and benzoic acid (1:2) and Cardura and benzoic acid (2:1) also contain peaks that are mostly from the starting material. The very small extra peaks mentioned above were also present in the NMR spectra, suggesting that the esterification reaction was occurring. All spectra can be seen on the accompanying disc in the folder *Chapter 4* under *Benzoic Acid and Epoxide Reactions*.

Heated Benzoic Acid and Cardura (1:1) Samples

The ^{1}H NMR spectra for the Cardura and benzoic acid samples heated to 90, 110 and 130 ^{o}C have the main peaks that correspond to the Cardura and benzoic acid starting material. The spectra have the seven small peaks between 3.5 and 5.0 ppm that indicate the presence of the secondary alcohol produced during the esterification reaction. These peaks increase in size and become easier to identify in the ^{1}H NMR spectra of samples of Cardura and benzoic acid prepared at higher temperatures and/or longer reaction times. The spectra for the ^{1}H NMR spectra for the samples prepared at 90 ^{o}C for 1 minute and 30 minutes are shown in figures 4.18 and 4.19 respectively. All other spectra can be seen on the attached disc in the folder *Chapter 4* under *Benzoic Acid and Epoxide Reactions*.

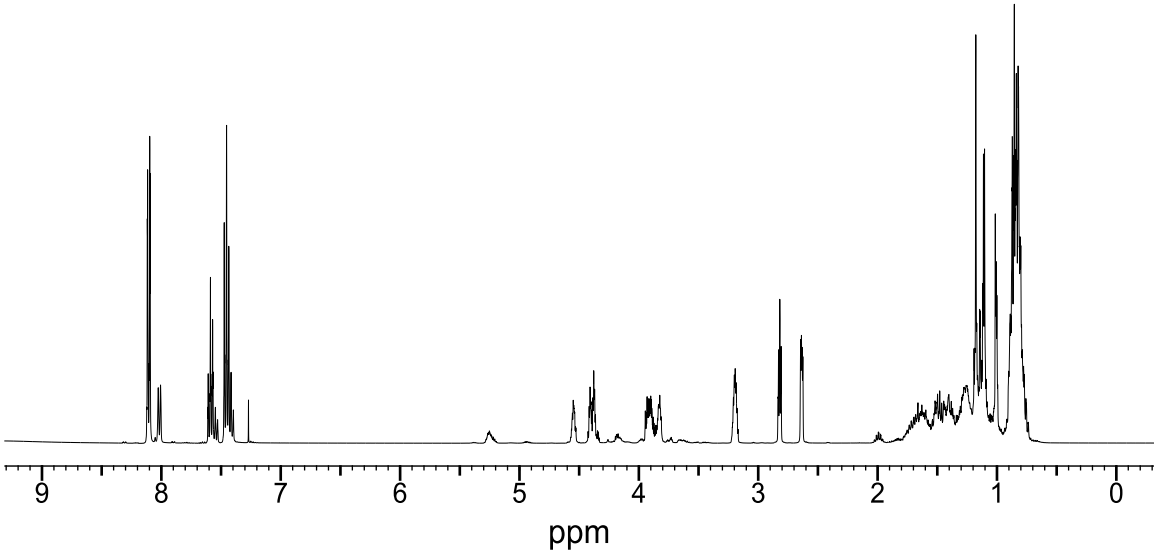

Figure 4.18 – ^{1}H NMR spectrum of the benzoic acid and Cardura sample (1:1) heated at 90 ^{o}C for 1 minute.

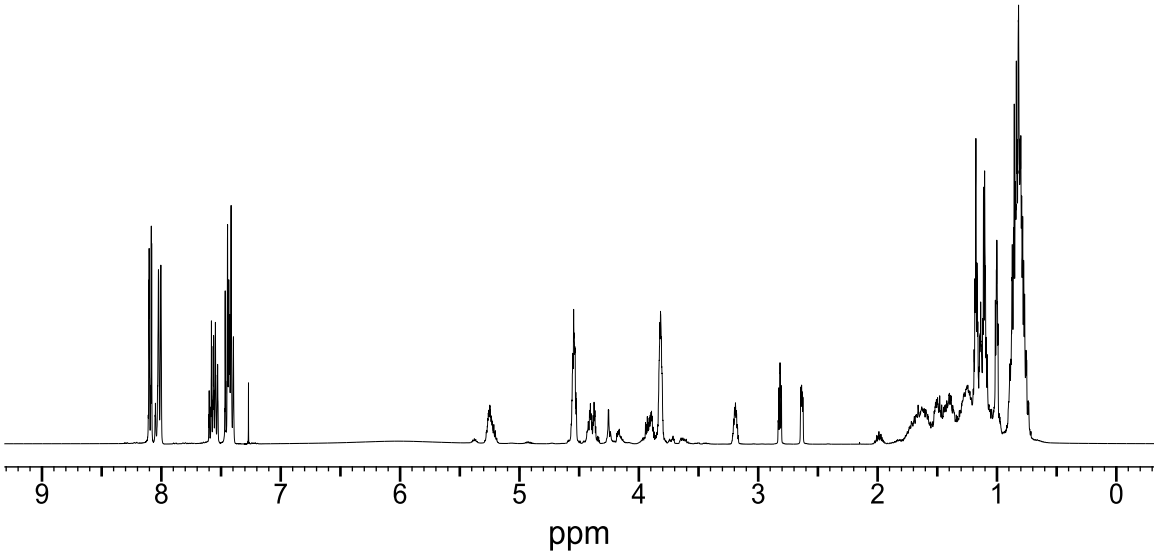

Figure 4.19 – ^{1}H NMR spectrum of the benzoic acid and Cardura sample (1:1) heated at 90 ^{o}C for 30 minutes.

In the ^{1}H NMR spectrum for the benzoic acid and Cardura samples, it was noticed that the three peaks at 2.66, 2.83 and 3.22 ppm, which correspond to the hydrogen atoms present in the epoxide ring, visibly reduced in intensity going from the samples prepared at 1 minute to 30 minutes. In some cases, the peaks for the epoxide group even disappear completely. The three peaks at 2.62, 2.80 and 3.17 ppm for the epoxide group were integrated to study the rate of the esterification reaction between Cardura and benzoic acid. A peak in the aromatic region was also integrated to be the internal standard as this peak does not change throughout the reaction. Figure 4.20 shows the scatter plots for the average integrals obtained for all of the samples prepared at 90, 110 and 130 ^{o}C. The plot shows that the epoxide group is reacting, confirming that the esterification reaction is occurring and that the reaction is occurring quicker at the higher temperatures.

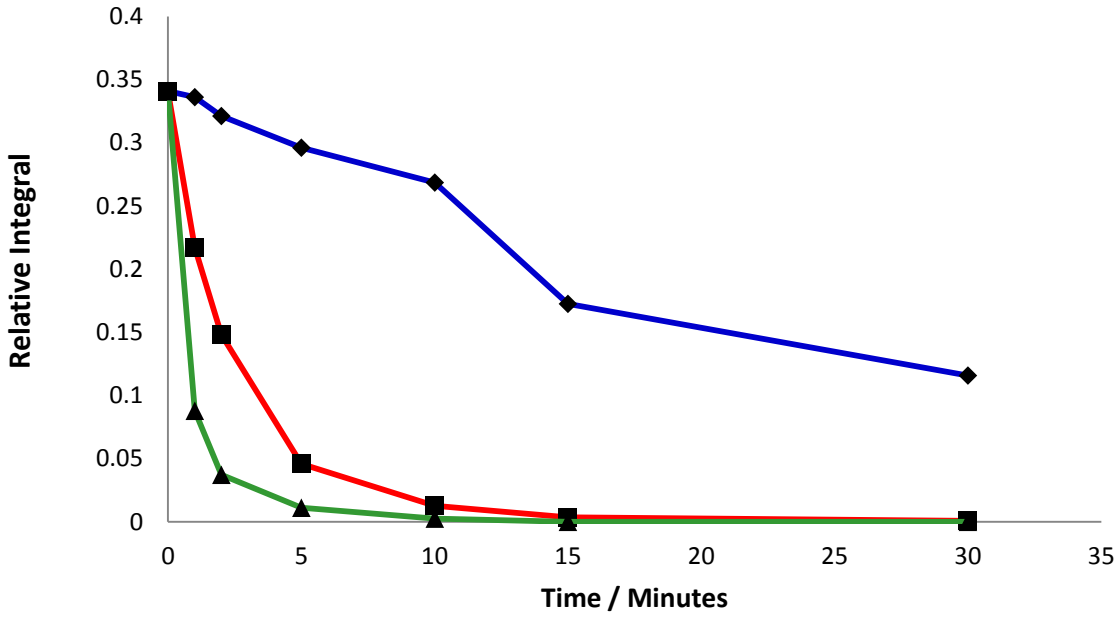

Figure 4.20 – Relative integrals for the epoxide group from the ^{1}H NMR spectra of the benzoic acid and Cardura samples (1:1) heated at 90, 110 and 130 °C. The blue line is the data for the samples heated at 90 °C, the red line is the data for the samples heated at 110 °C and the green line is the data for the samples heated at 130 °C. The peak that was integrated was for the epoxide group at 2.62 ppm.

Figures 4.21 and 4.22 show the ^{13}C NMR spectra of the Cardura and benzoic acid sample heated to 90 °C for 1 minute and 30 minutes respectively. The extra peaks at 61.46, 62.96 and 64.49 ppm are from the secondary alcohol produced during the esterification reaction. These peaks are growing as the reaction time increases from 1 to 30 minutes. This is similar to the findings from the ^{1}H NMR spectra. The same conclusions were also shown for the samples prepared at 110 and 130 °C. The ^{13}C NMR spectra for the samples prepared at 110 and 130 °C are shown on the attached disc in the folder *Chapter 4* under *Benzoic Acid and Epoxide Reactions*.

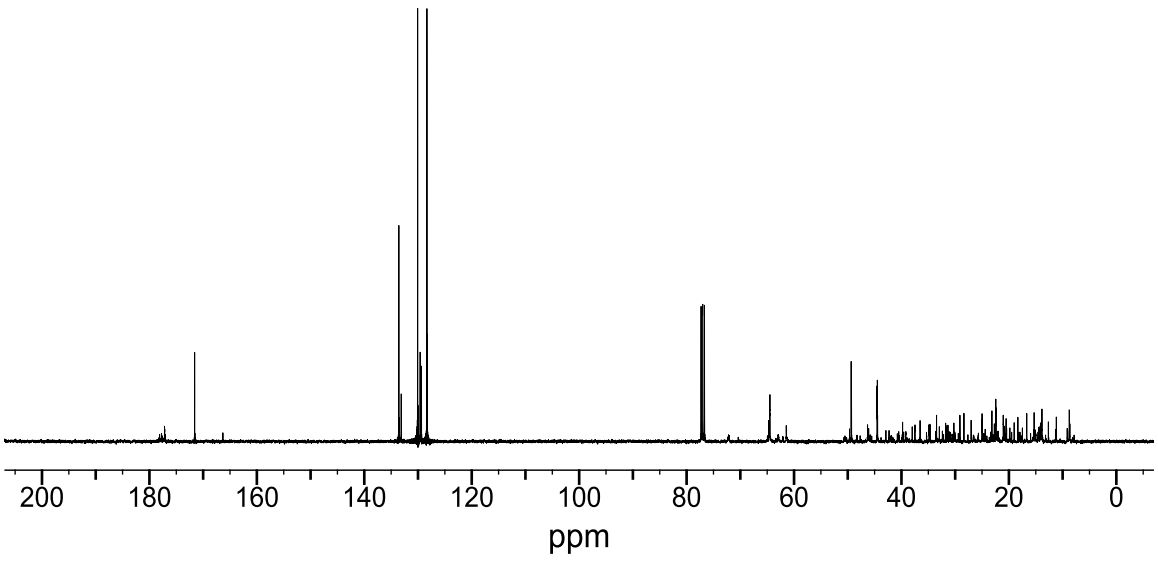

Figure 4.21 – ^{13}C NMR spectrum of the benzoic acid and Cardura sample (1:1) heated at 90 ^{o}C for 1 minute.

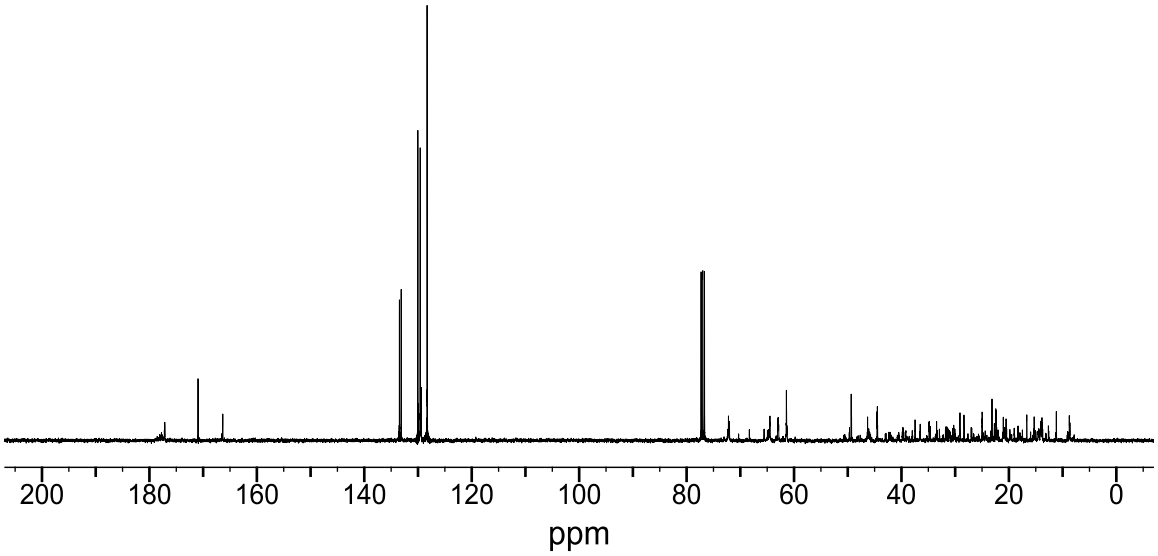

Figure 4.22 – ^{13}C NMR spectrum of the benzoic acid and Cardura sample (1:1) heated at 90 ^{o}C for 30 minutes.

The ^{1}H NMR spectrum for the sample heated to 150 ^{o}C for 1 minute has nine peaks between 3.5 and 5.0 ppm. These include the seven peaks noticed in the sample heated at 90, 110 and 130 ^{o}C, indicating the formation of the esterification product and two extra peaks. The two extra peaks are present at 3.61 and 4.94 ppm, suggesting side reactions are occurring. The position of

the peaks between 3.5 and 4.0 ppm also appear at a slightly lower range than witnessed in the other sample sets. This is expected to be a result of the chemical environment changing. The changes in the spectra indicate that side reactions are occurring. These side reactions are expected to be the esterification reaction forming the primary alcohol and the etherification reaction. The products expected from these reactions can be seen in figures 4.23 and 4.24. The number and location of the peaks suggest that both of these side reactions are occurring, but due to the similar spectra produced and the peaks overlapping, it was not possible to confirm. The ^{1}H NMR spectra show the intensity of these peaks increasing as the reaction time increases. Examples of the ^{1}H NMR spectra heated to 150 ^{o}C for 1 minute and 30 minutes are shown in figure 4.25. The other ^{1}H NMR spectra for the samples prepared at 150 ^{o}C can be seen on the accompanying disc in the folder *Chapter 4* under *Benzoic Acid and Epoxide Reactions*.

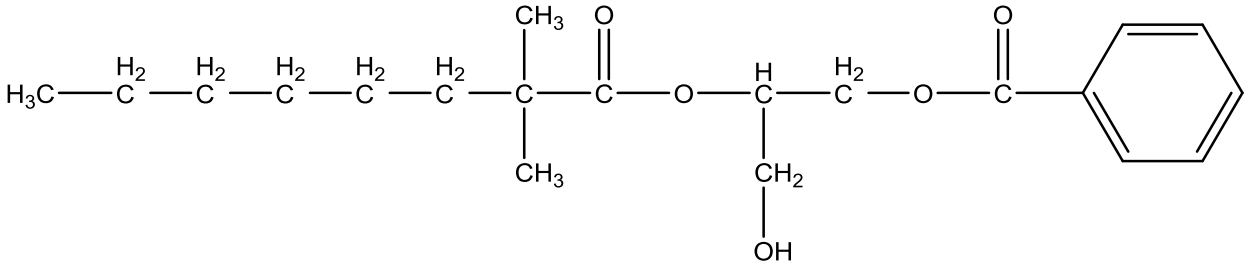

Figure 4.23 – Diagram showing a possible structure for the primary alcohol produced in the esterification reaction between Cardura and benzoic acid.

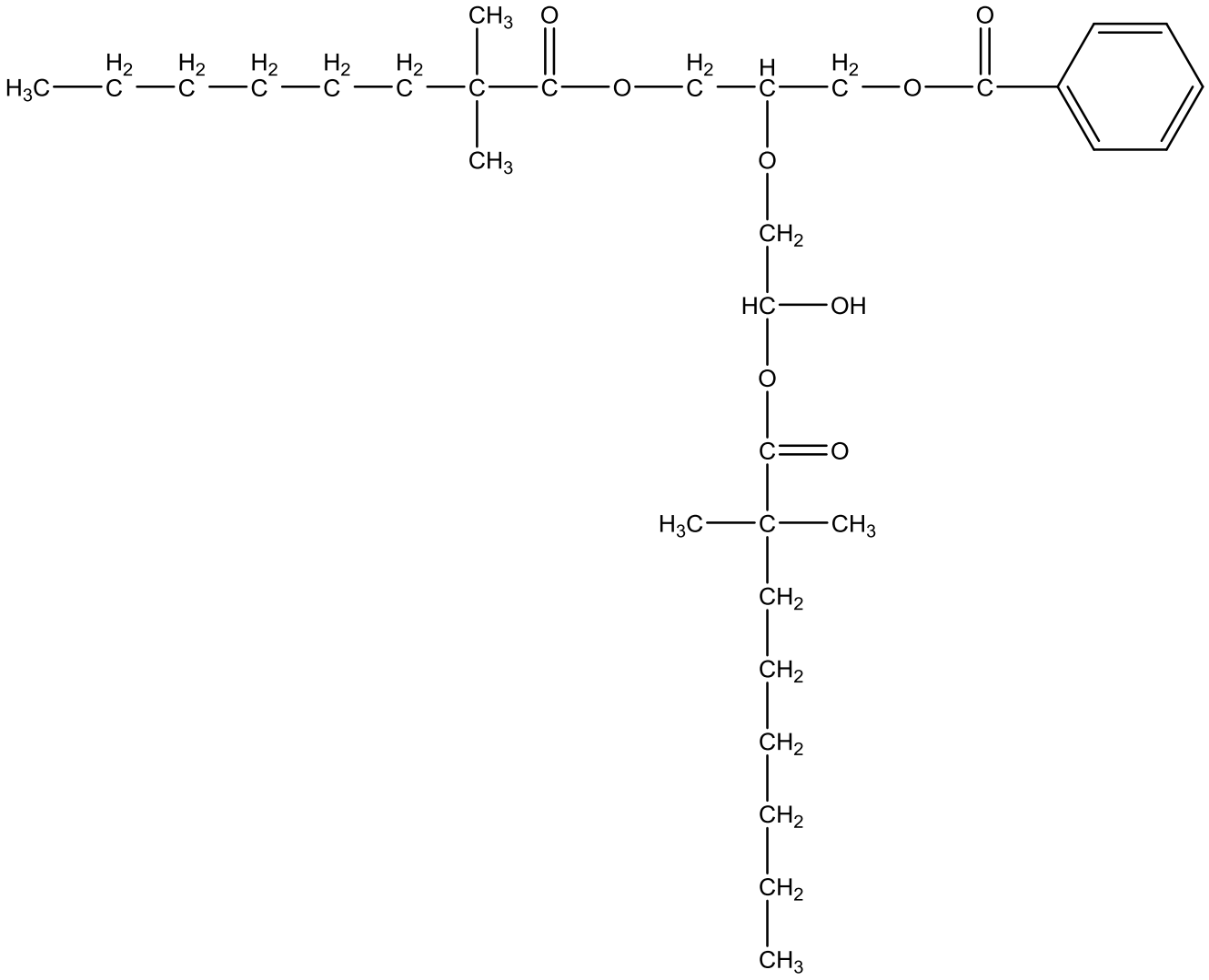

Figure 4.24 – Diagram of the etherification product possibly forming between the main esterification product and Cardura.

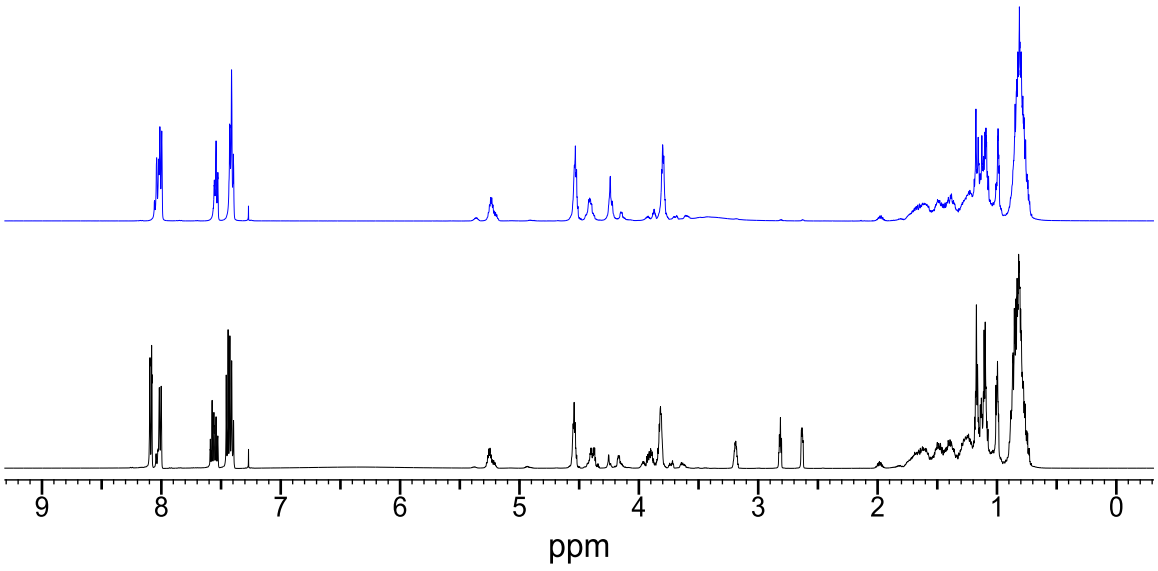

Figure 4.25- Comparison of ^{1}H NMR spectra of the benzoic acid and Cardura sample (1:1) heated at 150 ^{o}C for 1 minute (Black spectrum) and the benzoic acid and Cardura sample (1:1) heated at 150 ^{o}C for 30 minutes (Blue Spectrum).

Similar to the samples prepared at a lower temperature, the peaks at 2.66, 2.83 and 3.22 ppm for the epoxide group disappear. The esterification reaction is occurring quicker at 150 ^{o}C than that in the samples prepared at lower temperatures. After only 5 minutes, the peaks for the epoxide group had disappeared, indicating that the Cardura had fully reacted with the benzoic acid. The scatter plot showing the integrals obtained for the samples prepared at 150 ^{o}C is shown in figure 4.26.

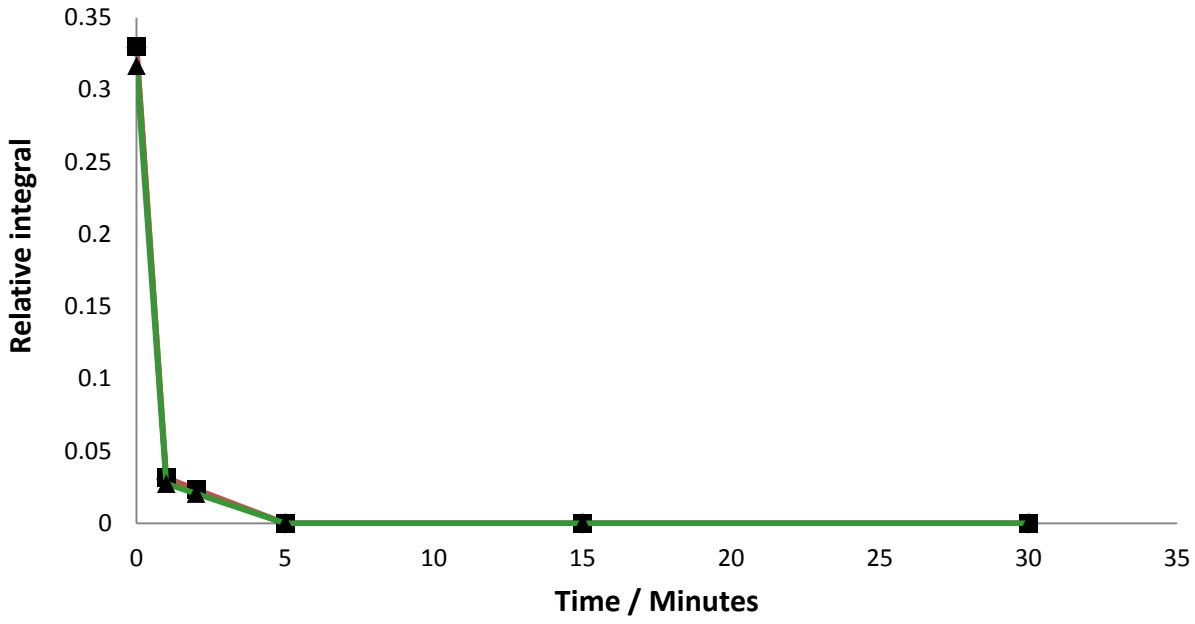

Figure 4.26 – Relative integrals for the epoxide group from the ^{1}H NMR spectrum of the benzoic acid and Cardura samples (1:1) heated at 150 ^{o}C. The blue line is for the peak at 2.62 ppm, the red line is for the peak at 2.80 ppm and the green line is for the peak at 3.17 ppm. The peak that was integrated was for the epoxide group at 2.62 ppm.

The possibility of side reactions occurring in the samples heated at 150 ^{o}C is supported by the ^{13}C NMR spectrum obtained. The Cardura and benzoic acid sample heated to 150 ^{o}C for 5 minutes shows slight differences in the ^{13}C NMR spectrum compared to that for the sample prepared at lower temperatures. These changes include the peak at 129.59 ppm increasing in height considerably and becoming much broader. This peak continues to grow throughout the remainder of the set. Another change that is identified is the peak at 133.28 ppm reducing in size throughout the sample set. Examples of the ^{13}C NMR spectra generated for samples of Cardura and benzoic acid prepared at 150 ^{o}C for 1 and 30 minutes are shown in figure 4.27. All other ^{13}C NMR spectra for the Cardura and benzoic acid aged samples can be seen on the accompanying disc in the folder *Chapter 4* under *Benzoic Acid and Epoxide Reactions*.

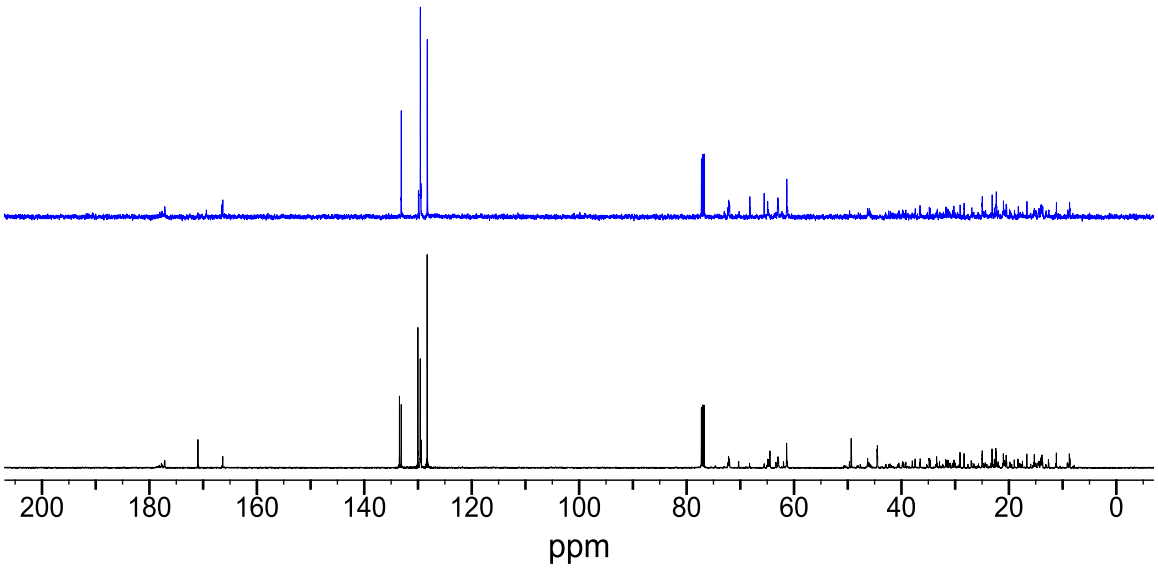

Figure 4.27 – Comparison of ^{1}H NMR spectra of the benzoic acid and Cardura sample (1:1) heated at 150 ^{o}C for 1 minute (Black spectrum) and the benzoic acid and Cardura sample (1:1) heated at 150 ^{o}C for 30 minutes (Blue Spectrum).

Heated Benzoic Acid and Cardura (2:1) Samples

The esterification reaction between benzoic acid and Cardura was also seen in the sample prepared with a higher ratio of benzoic acid to Cardura. The ^{1}H NMR spectra of the benzoic acid and Cardura (2:1) samples heated at 110 and 130 ^{o}C have 7 small peaks between 3.5 to 5.0 ppm, which indicate the presence of the secondary alcohol formed during the esterification reaction. These peaks grow with increasing residence time. The three peaks at 2.62, 2.80 and 3.17 ppm for the epoxide group were also integrated in the ^{1}H NMR spectra generated for the sample of benzoic acid and Cardura (2:1) heated to 110 and 130 ^{o}C. Figure 4.28 shows the scatter plot for the integrals obtained for all of the samples prepared at 110 and 130 ^{o}C. The scatter plots show that the reaction is occurring quicker at the higher temperatures, similar to the samples of Cardura and benzoic acid (1:1).

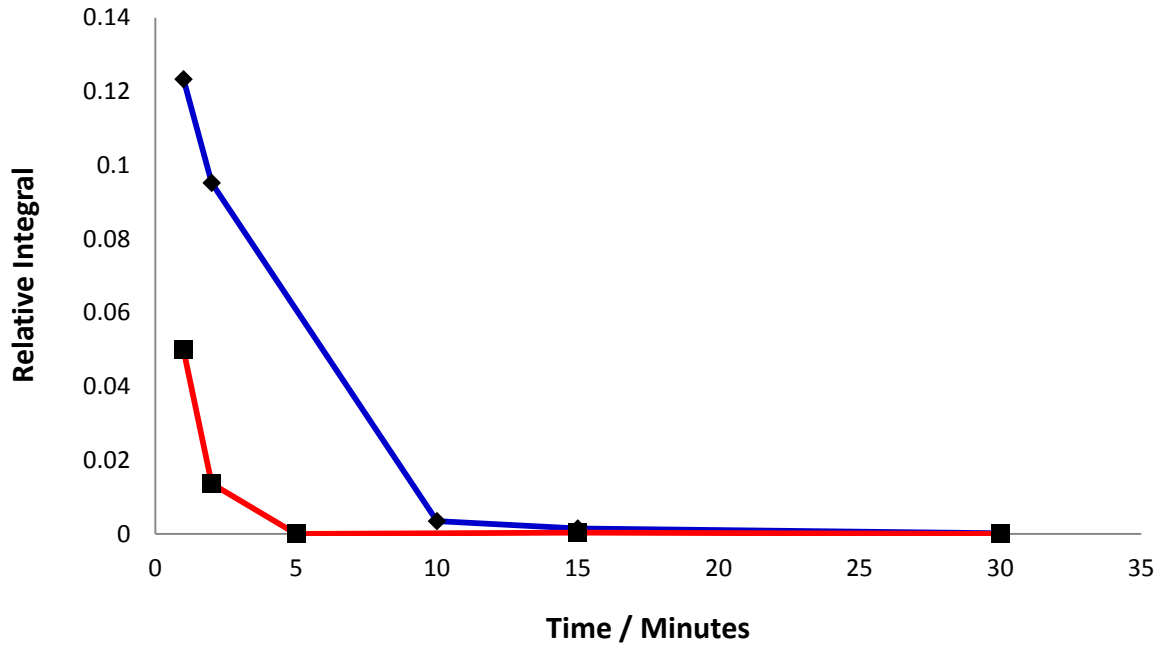

Figure 4.28 – Relative integrals for the epoxide group from the ^{1}H NMR spectrum of the benzoic acid and Cardura samples (2:1) heated at 110 and 130 ^{o}C. The blue line is the data for the samples heated at 110 ^{o}C and the red line is the data for the samples heated at 130 ^{o}C. The peak that was integrated was for the epoxide group at 2.62 ppm.

The ^{13}C NMR spectra obtained for the benzoic acid and Cardura (2:1) samples prepared at 110 ^{o}C and 130 ^{o}C are shown on the disc attached in the folder *Chapter 4* under *Benzoic Acid and Epoxide Reactions*. The spectra show similar findings to those for the benzoic acid and Cardura (1:1) samples. The ^{13}C NMR spectra are noisier, and the peaks generated are less intense, which makes them difficult to interpret. The main peaks for the Cardura and benzoic starting materials are present in all of the spectra generated. There are several peaks including 62.12, 63.44, 65.66, 68.50, 70.46 and 166.20 ppm in many samples which confirm that the esterification reaction is occurring.

Heated Benzoic Acid and Cardura (1:2) Samples

The ^{1}H NMR spectra of the benzoic acid and Cardura (1:2) samples that were heated to 90, 110, 130 and 150 ^{o}C all contain the peaks mentioned in the other sample sets that indicate the formation of the secondary alcohol. These peaks are also seen to be growing slightly with increased reaction time. The aromatic region becomes more complicated as the samples are

heated for a longer period of time, especially for samples heated to 130 and 150 ^{o}C. The complex nature of the aromatic region, and the number of the peaks, suggest that side reactions are occurring. It is not possible to obtain more information about the side reactions as the peaks are all very close together. The Cardura was added at a higher level than the benzoic acid to confirm if any side reactions were occurring. The side reactions arise because there is not enough benzoic acid to react with all of the epoxide groups. The indication of these extra peaks highlights the importance of not adding excess Cardura to the polymer as unwanted products could form altering the properties. All spectra generated can be seen on the accompanying disc in the folder *Chapter 4* under *Benzoic Acid and Epoxide Reactions*.

The peaks at 2.62, 2.80 and 3.17 ppm for the epoxide group in the ^{1}H NMR spectra were integrated to study the rate of the esterification reaction between benzoic acid and Cardura (1:2). Figure 4.29 shows the scatter plot for the integrals obtained for all of the samples prepared at 90, 110, 130 and 150 ^{o}C. All scatter plots show the epoxide group is reacting and occurring faster at higher temperatures.

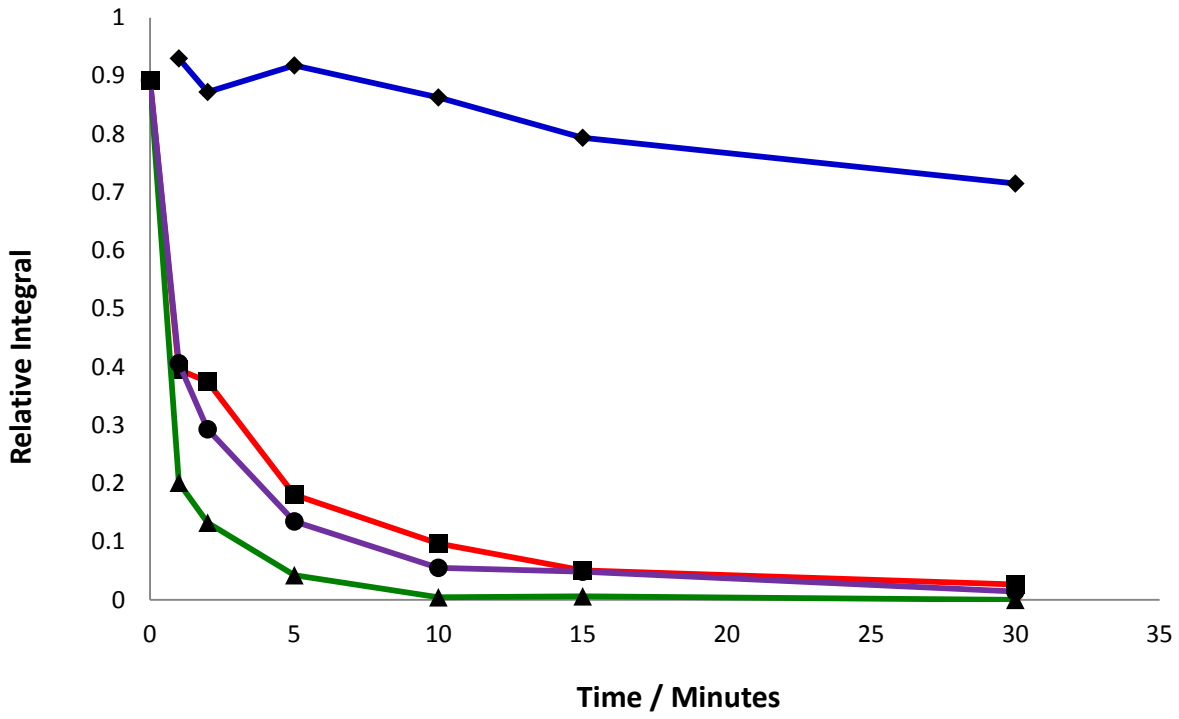

Figure 4.29 – Relative integrals for the epoxide group from the ^{1}H NMR spectrum of the benzoic acid and Cardura samples (1:2) heated at 90, 110, 130 and 150 °C. The blue line is the data for the samples heated at 90 °C, the red line is the data for the samples heated at 110 °C, the green line is the data for the samples heated at 130 °C and the purple line is the data heated at 150 °C. The peak that was integrated was for the epoxide group at 2.62 ppm.

The ^{13}C NMR spectra were also obtained for the benzoic acid and Cardura (1:2) samples and the peaks corresponding to the esterification reaction can be clearly seen in the spectra. The peaks at 61.44, 62.97, 64.50, 64.81, 65.56, 68.37, 70.34, 72.18 and 64.50 ppm in the ^{13}C NMR spectra are consistent with the formation of a secondary alcohol from the esterification reaction between Cardura and benzoic acid. In the aromatic region of the spectra, there are also extra peaks between 128 to 134 ppm, which are also consistent with the formation of a secondary alcohol during the esterification reaction. The peaks that correspond to the secondary alcohol are shown to be growing in the ^{13}C NMR spectra as the reaction time increases. All ^{13}C NMR spectra generated can be seen on the attached disc in the folder *Chapter 4* under *Benzoic Acid and Epoxide Reactions*.

The manufacturer's recommended temperature for Cardura is 130 ^{o}C, but the temperature of 130 ^{o}C is below the melting point of PET so a higher temperature would need to be used. [16] Higher temperatures have been shown to decrease the reaction time required for the film to be prepared using a reactive extrusion process. Care has to be taken to ensure that no undesirable side products are produced when Cardura is used at higher temperatures.

4.2.3.3 Benzoic Acid and Vikolox Reactions

Unheated Benzoic Acid and Vikolox (1:1) Samples

The peaks present in the ^{1}H and ^{13}C NMR spectra for the unheated sample of Vikolox and benzoic acid are mostly consistent with the starting materials. Figure 4.30 shows the ^{1}H NMR spectra for a sample with a 1:1 ratio of benzoic acid and Vikolox that was not heated. The peaks between 0.91 to 2.95 ppm are for the Vikolox starting material. The benzoic acid that has not reacted is seen in the peaks at 7.49, 7.62, 8.14 and 11.50 ppm. The ^{1}H NMR spectrum also has a number of very small extra peaks between 3 to 6 ppm, which suggests that the esterification reaction could be occurring. The secondary alcohol that is formed is shown in figure 4.31. The alcohol formed would produce 4 peaks between 3.5 to 5.0 ppm, and the aromatic region would alter slightly. The peaks at 7.49, 7.62 and 8.15 ppm would decrease in intensity as the starting materials are being used up during the esterification reaction. New peaks would appear in the ^{1}H NMR spectra at approximately 7.46, 7.60 and 8.08 ppm.

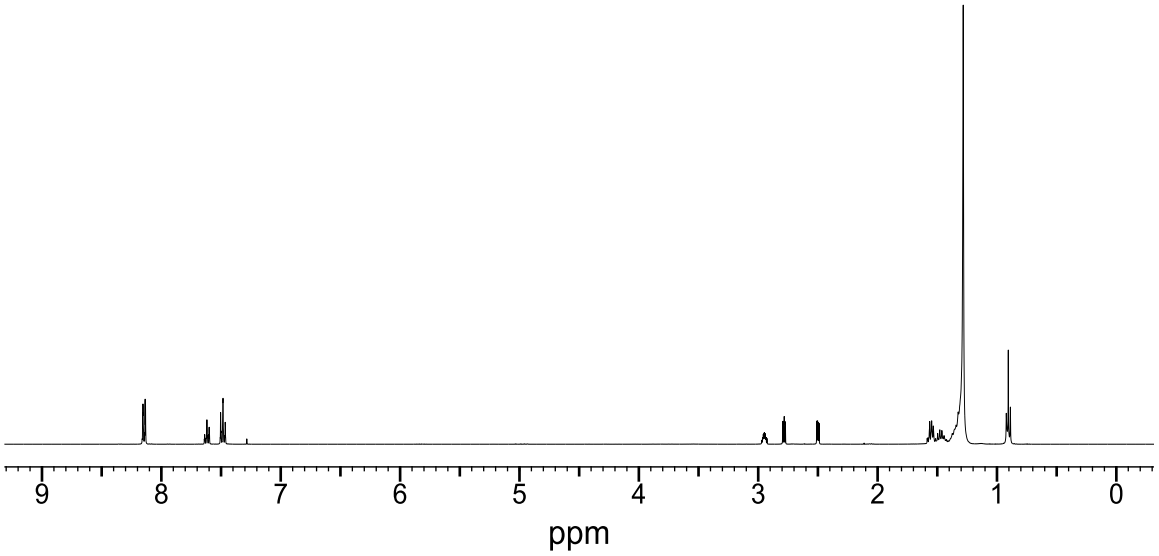

Figure 4.30 – ^{1}H NMR spectrum of the Vikolox and benzoic acid (1:1) with no heating.

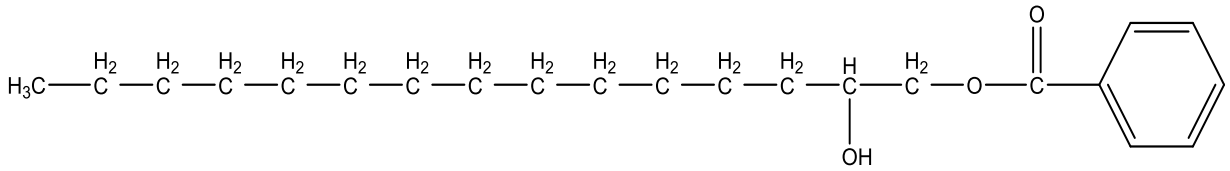

Figure 4.31 – Diagram of the secondary alcohol produced in the esterification reaction between Vikolox and benzoic acid.

The ^{13}C NMR spectrum for the Vikolox and benzoic acid sample (1:1) that was unheated is shown in figure 4.32. The peaks for the starting material are seen in the spectrum. There are peaks at 14.12, 22.69, 25.89, 29.57, 31.92, 32.47, 47.19 and 52.81 ppm which are consistent with the main peaks for the Vikolox starting material. The benzoic acid starting material produces peaks at 128.46, 129.34, 130.22, 133.65 and 172.30 ppm. There are no other peaks noticed in the ^{13}C NMR spectrum.

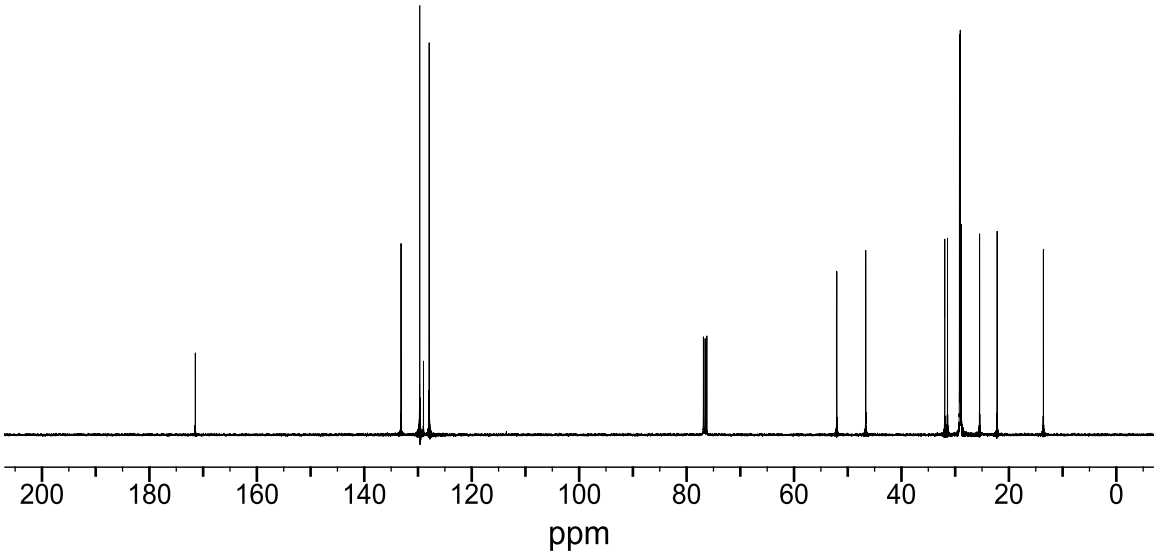

Figure 4.32 – ^{13}C NMR spectrum of the Vikolox and benzoic acid (1:1) with no heating.

Heated Benzoic Acid and Vikolox (1:1) Samples

The ^{1}H NMR spectra of the benzoic acid and Vikolox samples (1:1) prepared at 90 ^{o}C are all very similar to the spectrum that was obtained for the unheated sample. There are several very small peaks between 3 and 6 ppm. It is difficult to confirm the exact number of small peaks that are present as the peaks are complex and overlap. These extra peaks are consistent with the possibility that the secondary alcohol is being formed during the esterification reaction. There is very little change in the aromatic region of the 90 ^{o}C samples, except that the peak at 8.10 ppm is growing with increased reaction time.

The ^{1}H NMR spectra obtained for the samples of benzoic acid and Vikolox (1:1) that are heated to 110, 130 and 150 ^{o}C are similar to those for the samples prepared at 90 ^{o}C. The peak at 8.10 ppm appears in the sample prepared at 5 minutes and grows throughout the sample set. The main peaks in the aromatic region are also shifted to a slightly lower region. These main peaks appear at 7.42, 7.55 and 8.10 ppm, with small extra peaks appearing at 7.40 and 7.55 ppm. The extra peaks in the region 7.35 to 7.60 ppm are difficult to confirm as they occur at such a similar range to the main peaks. The extra peaks between 3 to 6 ppm are seen in the ^{1}H NMR spectra of the samples, confirming the esterification reaction is occurring. The three peaks for the

epoxide group at 2.51, 2.79 and 2.95 ppm remain dominant in all of the spectra, unlike those generated for the samples of benzoic acid and Cardura. All spectra of benzoic acid and Vikolox can be seen on the attached disc in the folder *Chapter 4* under *Benzoic Acid and Epoxide Reactions*.

The peaks for the epoxide groups were integrated to study the rate of the esterification reaction between benzoic acid and Vikolox. A peak in the aromatic region was also integrated to be the internal standard as this peak does not change throughout the reaction. The regions integrated were 2.40 to 2.60 ppm, 2.70 to 2.85 ppm, 2.85 to 3.05 ppm and 7.4 to 7.55 ppm. Figure 4.33 shows the scatter plot for the integrals obtained from all of the samples prepared at 90, 110, 130 and 150 ^{o}C. The plots show that the esterification reaction is occurring, but it is significantly slower than the esterification reaction between benzoic acid and Cardura at the same reaction conditions.

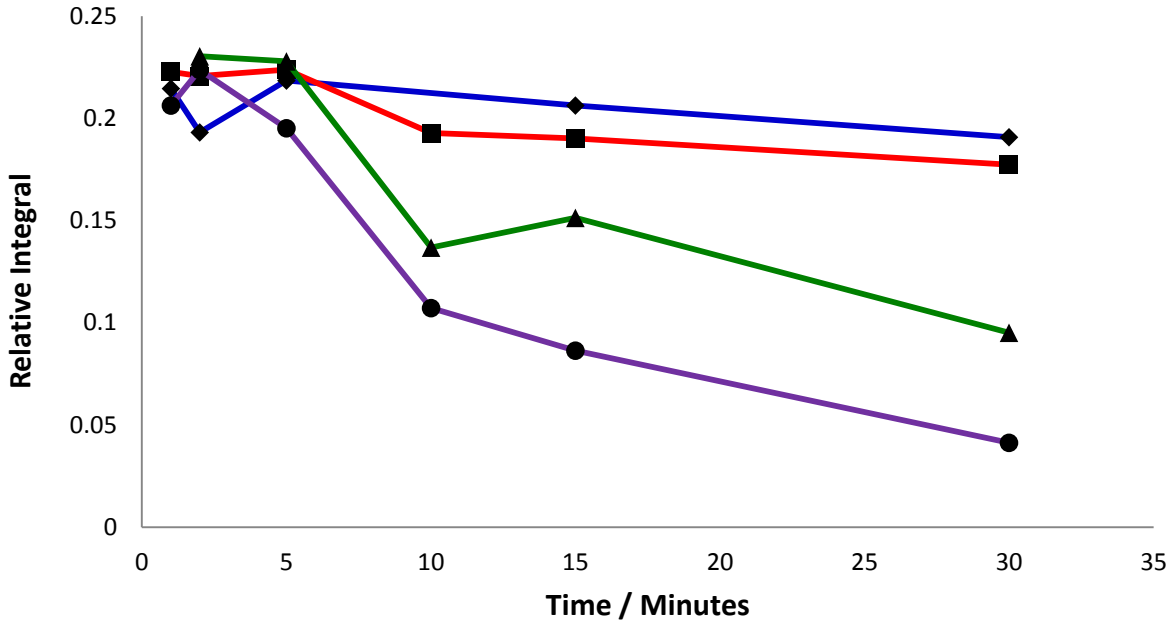

Figure 4.33 – Relative integrals for the epoxide group from the ^{1}H NMR spectrum of the benzoic acid and Vikolox samples (1:1) heated at 90, 110, 130 and 150 ^{o}C. The blue line is the data for the samples heated at 90 ^{o}C, the red line is the data for the samples heated at 110 ^{o}C, the green line is the data for the samples heated at 130 ^{o}C and the purple line is the data heated at 150 ^{o}C. The peak that was integrated was for the epoxide group at 2.62 ppm.

The ^{13}C NMR spectra obtained for the benzoic acid and Vikolox (1:1) samples prepared at 90 ^{o}C look similar to that for the starting material. An extra peak at 70.20 ppm is noticed in the sample prepared at 90 ^{o}C for 30 minutes. The extra peak is very small and difficult to determine from the noisy baseline. A peak at 70.20 ppm would indicate the product of the esterification reaction is being produced. The samples prepared at 110 and 130 ^{o}C have the same dominant peaks as the unheated sample. There are some very small peaks noticed in the samples with increased reaction time such as 33.78, 70.15, 114.10 and 138.80 ppm. These peaks can be seen growing in the spectra of samples with increased reaction time. The ^{13}C NMR spectra for the sample of benzoic acid and Vikolox prepared at 150 ^{o}C follow a similar trend to the other sample sets. The product for the esterification reaction can be clearly seen in the ^{13}C NMR spectra for the samples prepared at 150 ^{o}C for 5 minutes. The ^{13}C NMR spectra can be viewed on the attached disc in the folder *Chapter 4* under *Benzoic Acid and Epoxide Reactions*.

Heated Benzoic Acid and Vikolox (2:1) Samples

Samples of benzoic acid and Vikolox (2:1) were also prepared to study the esterification reaction. The formation of the secondary alcohol can be seen to occur at some of the conditions investigated using a lower ratio of Vikolox to benzoic acid. The ^{1}H NMR spectra of the benzoic acid and Vikolox (2:1) samples, heated at 110 ^{o}C for 1 and 2 minutes, contain peaks that correspond to the starting material. There are no extra peaks corresponding to the esterification reaction noticed in these samples. Very small peaks are appearing in the samples prepared at 5 minutes and they grow throughout the remainder of the sample set. These peaks include 3.96, 4.47, 5.27 and 8.09 ppm, and indicate that the esterification reaction is occurring. These extra peaks are also present in all of the ^{1}H NMR spectra for samples prepared with a lower ratio of Vikolox to benzoic acid at 130 ^{o}C. The peaks that correspond to the esterification reaction are growing as the reaction time increases. All ^{1}H NMR spectra generated for the samples prepared at a lower ratio are shown on the disc in the folder *Chapter 4* under *Benzoic Acid and Epoxide Reactions*.

The peaks at 2.52, 2.81 and 2.98 ppm remain dominant in the ^{1}H MR spectra for all of the samples, unlike the sample prepared with Cardura. The three peaks in the ^{1}H NMR spectra were

integrated. The scatter plot in figure 4.34 shows the relative integral for the samples heated at 110 and 130 ^{o}C. This plot confirms that the esterification reaction is occurring and at a similar rate as the samples generated using a 1:1 ratio of benzoic acid and Vikolox. The results also highlight that the epoxide, Vikolox, is less reactive than Cardura.

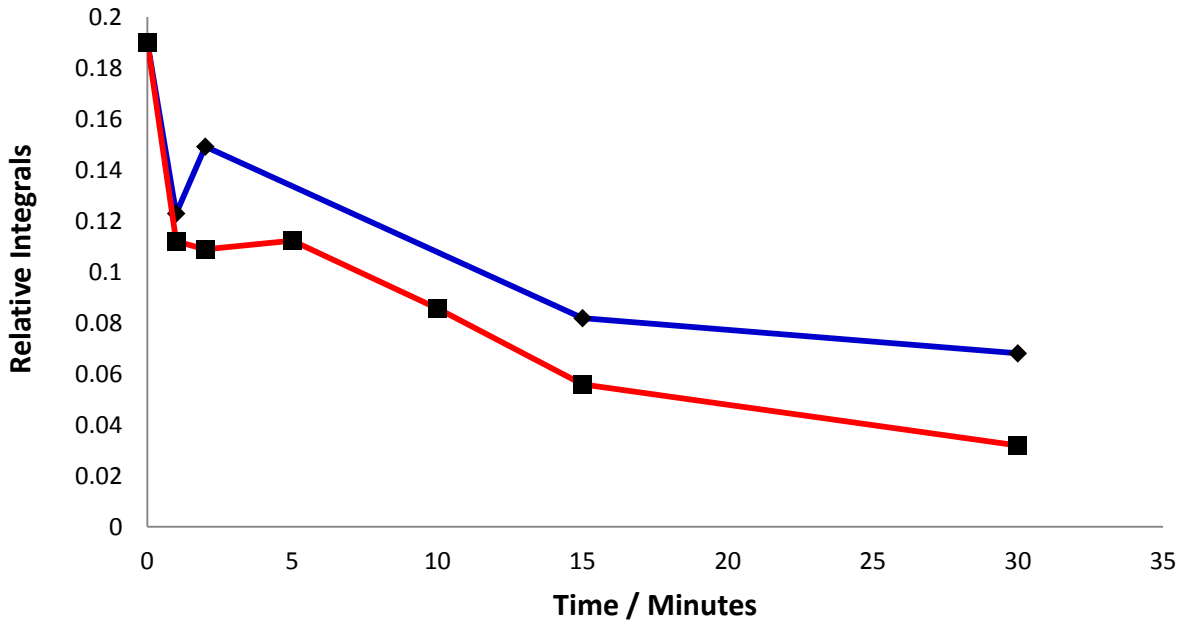

Figure 4.34 – Relative integrals for the epoxide group from the ^{1}H NMR spectrum of the benzoic acid and Vikolox samples (2:1) heated at 110 and 130 ^{o}C. The blue line is the data for the samples heated at 110 ^{o}C and the red line is the data for the samples heated at 130 ^{o}C. The peak that was integrated was for the epoxide group at 2.62 ppm.

The ^{13}C NMR spectra obtained for the benzoic acid and Vikolox (2:1) samples prepared at 110 and 130 ^{o}C are shown on the disc in the folder *Chapter 4* under *Benzoic Acid and Epoxide Reactions*. The ^{13}C NMR spectra obtained for the benzoic acid and Vikolox (2:1) samples, prepared at 110 and 130 ^{o}C, look similar to the starting material. The ^{13}C NMR spectra are noisier than the ^{1}H NMR spectra, and the peaks generated are less intense, which makes it difficult to identify the presence of small peaks. A peak at 70.20 ppm is noticed in the sample

prepared at 110 ^{o}C for 5 minutes. The peak at 70.20 ppm indicates the presence of the secondary alcohol produced from the esterification reaction. This peak becomes more dominant in samples prepared with a higher reaction time. Other peaks at 33.78, 70.15, 114.10 and 138.80 ppm are positively identified from the baseline at higher temperatures as well. The samples prepared at 130 ^{o}C produce spectra that are similar to the sample set prepared at 110 ^{o}C. The peaks that correspond to the esterification reaction are noticeably growing as the samples are heated for a longer period of time.

Heated Benzoic Acid and Vikolox (1:2) Samples

Samples were also studied with a lower concentration of benzoic acid to Vikolox (1:2). The ^{1}H NMR spectra for all samples can be seen on the disc attached. The ^{1}H NMR spectra for samples heated for a short period of time at 90,110, 130 and 150 ^{o}C are dominated by peaks that correspond to the Vikolox and benzoic acid starting materials. There are several small extra peaks corresponding to the esterification reaction that can be seen at 3.89, 4.05, 4.28, 4.42, 4.45, 5.22, 7.46, 7.60 and 8.08 ppm. These peaks become more dominant as the reaction time is increased.

The three peaks at 2.52, 2.81 and 2.97 ppm for the epoxide group were integrated in the ^{1}H NMR spectra obtained for the sample of benzoic acid and Vikolox (1:2) heated to 90, 110, 130 and 150 ^{o}C. The scatter plot generated can be seen in figure 4.35. These plots confirm that the esterification reaction is occurring and that it occurs slightly faster at higher temperatures. The data indicates that the Vikolox peaks do not change as much as with the other ratios as the Vikolox is in excess and doesn't have sufficient carboxyl groups to react with.

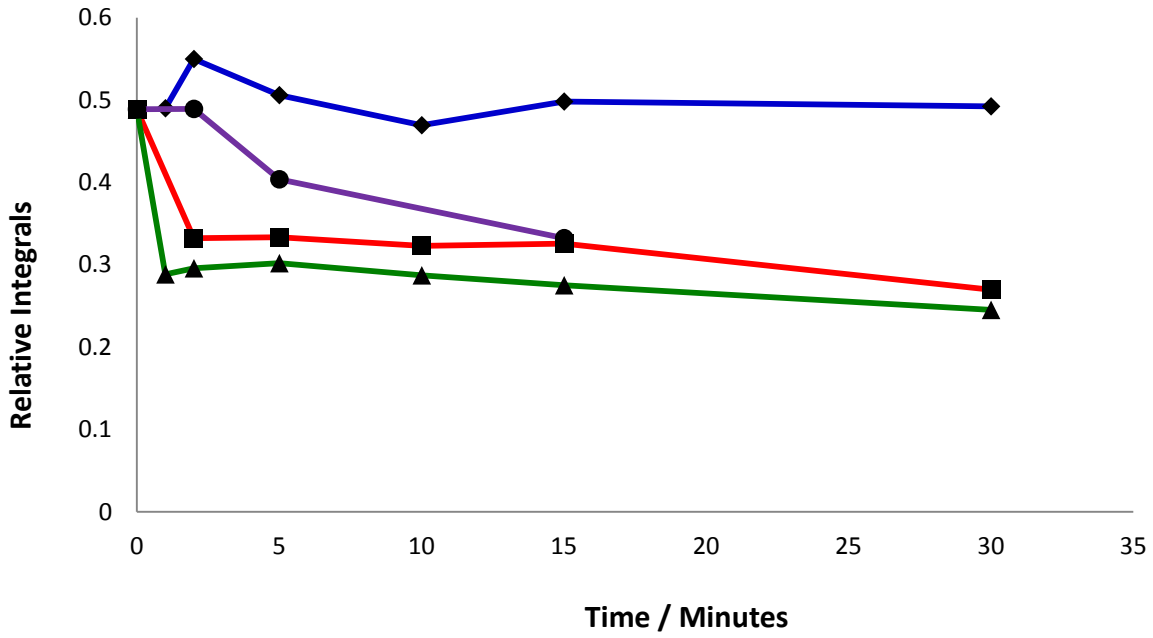

Figure 4.35 – Relative integrals for the epoxide group from the ^{1}H NMR spectrum of the benzoic acid and Vikolox samples (2:1) heated at 90, 110, 130 and 150 °C. The blue line is the data for the samples heated at 90 °C, the red line is the data for the samples heated at 110 °C, the green line is the data for the samples heated at 130 °C and the purple line is the data for the samples heated at 150 °C. The peak that was integrated was for the epoxide group at 2.62 ppm.

4.2.3.4 Benzoic Acid and Heloxy Reactions

Unheated Benzoic Acid and Heloxy (1:1) Samples

The peaks present in the ^{1}H and ^{13}C NMR spectra for the unheated sample of benzoic acid and Heloxy are mostly consistent with the starting materials. All ^{1}H and ^{13}C NMR spectra for the unheated samples with a 1:1 ratio of benzoic acid and Heloxy can be seen on the attached disc. The ^{1}H NMR spectra of benzoic acid and Heloxy (1:1) have a considerable number of very small peaks present due to impurities in the Heloxy and/or satellite peaks. There are small peaks at 3.78 and 4.44 ppm which suggest the formation of an alcohol from the esterification reaction. The secondary and primary alcohols that can be produced through the esterification reaction between benzoic acid and Heloxy can be seen in figures 4.36 and 4.37 respectively. The secondary alcohol is the most likely to be produced due to steric hindrance. The peaks for the starting material are also seen in the ^{13}C NMR spectra of the unheated benzoic acid and Heloxy

samples. The peaks for the Heloxy starting material are seen at 31.36, 33.91, 44.57, 50.16, 68.61, 114.02, 126.13, 143.76 and 156.13 ppm. The benzoic acid starting material produces peaks at 128.33, 129.34, 130.05, 133.60 and 171.92 ppm. There are no other peaks noticed in the ^{13}C NMR spectra to suggest the formation of esterification products.

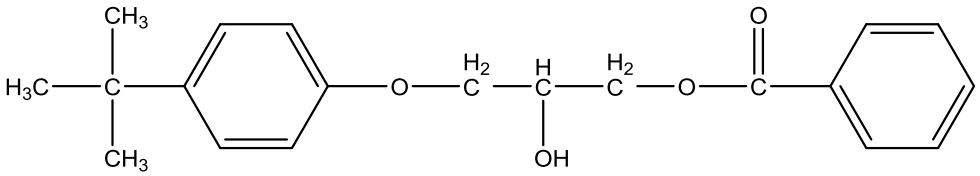

Figure 4.36 – Diagram of the secondary alcohol produced in the esterification reaction between Heloxy and benzoic acid.

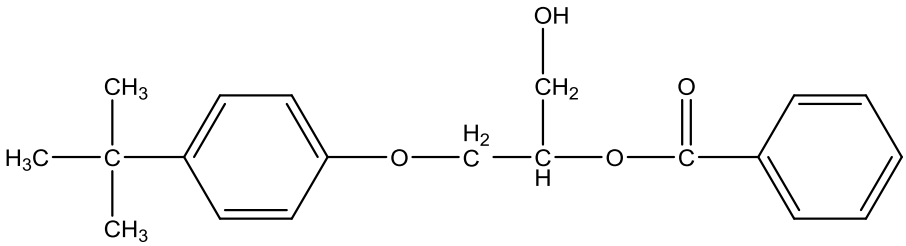

Figure 4.37 – Diagram of the primary alcohol produced in the esterification reaction between Heloxy and benzoic acid.

Heated Benzoic Acid and Heloxy (1:1) Samples

The main peaks for the Heloxy and benzoic acid starting material are also the dominant peaks in the ^{1}H NMR spectra for the Cardura and benzoic acid samples heated to 90, 110, 130 and 150 ^{o}C. There are small peaks that highlight the possibility that the esterification reaction is occurring, and these extra peaks get more dominant at higher temperatures and higher reaction times. This includes the peaks forming at 4.63, 5.58, 5.68, 6.94, 7.37, 7.52 and 8.15 ppm. All ^{1}H NMR spectra for the benzoic acid and Heloxy can be seen on the attached disc in the folder *Chapter 4* under *Benzoic Acid and Epoxide Reactions*.

The peaks for the epoxide group were integrated to study the rate of the esterification reaction between Heloxy and benzoic acid. A peak in the aromatic region was also integrated to be the internal standard as this peak does not change throughout the reaction. The regions integrated were 2.70 to 2.85 ppm, 2.85 to 3.00 ppm, 3.30 to 3.50 ppm and 6.80 to 7.00 ppm. Figure 4.38 shows the scatter plot for the integrals obtained for all of the samples prepared at 90, 110, 130 and 150 ^{o}C. The plots show the esterification reaction is occurring, and that the reaction is occurring quicker at the higher temperatures. Like with Vikolox, the esterification reaction between Heloxy and benzoic acid appears to occur significantly slower than the esterification reaction between Cardura and benzoic acid.

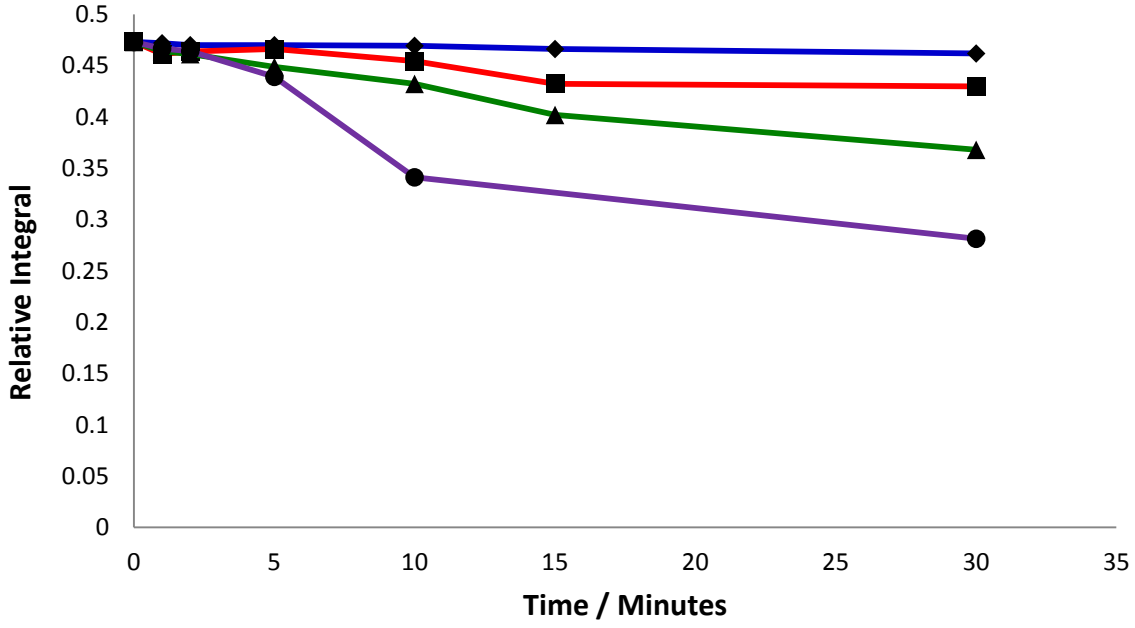

Figure 4.38 – Relative integrals for the epoxide group from the ^{1}H NMR spectrum of the benzoic acid and Heloxy samples (1:1) heated at 90, 110, 130 and 150 ^{o}C. The blue line is the data for the samples heated at 90 ^{o}C, the red line is the data for the samples heated at 110 ^{o}C, the green line is the data for the samples heated at 130 ^{o}C and the purple line is the data for the samples heated at 150 ^{o}C. The peak that was integrated was for the epoxide group at 2.62 ppm.

The ^{13}C NMR spectra for all samples of benzoic acid and Heloxy (1:1) prepared at 90, 110 and 130 ^{o}C look similar to the ^{13}C NMR spectra obtained for the unheated sample. It is difficult to determine if there are any extra small peaks present as the baseline is very noisy. If the esterification reaction is occurring, then new peaks would be expected at approximately 65.85

ppm, 166.80 ppm, and between 180 and 190 ppm. Some very small extra peaks were positively identified in the ^{13}C NMR spectrum for the sample prepared at 130 ^{o}C for 30 minutes. The extra peaks noticed were at 65.85, 129.27, 129.71, 133.20 and 166.80 ppm, which are all consistent with the main product of esterification being produced. The samples prepared at 150 ^{o}C with a lower reaction time look similar to the samples that were not heated. The small peaks mentioned above that correspond to the secondary alcohol being formed are seen in the samples heated for a longer period of time. The peaks are also shown to be growing as the reaction time is increased. All other ^{13}C NMR spectra generated can be seen on the attached disc in the folder *Chapter 4* under *Benzoic Acid and Epoxide Reactions*.

Heated Benzoic Acid and Heloxy (2:1) Samples

The secondary alcohol produced during the esterification reaction between Heloxy and benzoic acid is also seen in samples prepared with a lower ratio of Heloxy to benzoic acid. The ^{1}H NMR spectra of the benzoic acid and Heloxy (2:1) samples heated at 110 and 130 ^{o}C have the main peaks present for both of the starting materials. There is no peak positively identified in any of the ^{1}H NMR spectra that indicates the presence of the secondary alcohol being formed, except for the sample prepared at 130 ^{o}C for 30 minutes. This spectrum has small peaks at 4.63, 5.58, 5.68 and 8.12 ppm which indicate the presence of the esterification product. The three peaks at 2.81, 2.95 and 3.41 ppm for the epoxide group were also integrated in the ^{1}H NMR spectra. The scatter plot generated for the integrals obtained for the three peaks in the ^{1}H NMR spectra are shown in figure 4.39. The scatter plots generated show that the esterification reaction is occurring slowly. The esterification reaction between benzoic acid and Heloxy is actually occurring more slowly than the reactions between benzoic acid and the other epoxides (Cardura and Vikolox). All ^{1}H NMR spectra generated for the samples prepared at a lower ratio are shown on the accompanying disc in the folder *Chapter 4* under *Benzoic Acid and Epoxide Reactions*.

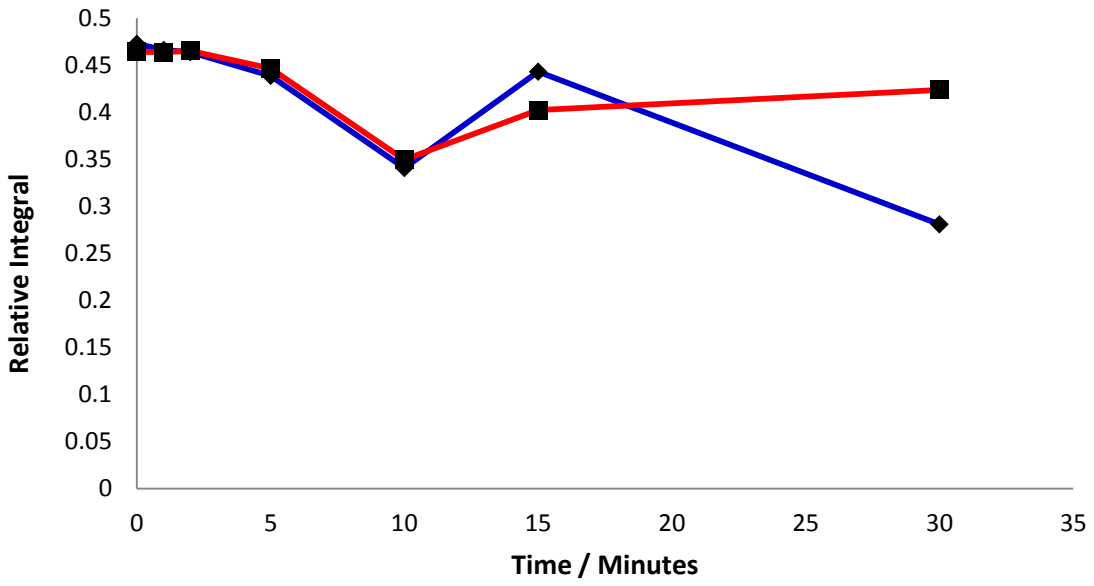

Figure 4.39 – Relative integrals for the epoxide group from the ^{1}H NMR spectrum of the benzoic acid and Heloxy samples (2:1) heated at 110 and 130 °C. The blue line is the data for the samples heated at 110 °C and the red line is the data for the samples heated at 130 °C. The peak that was integrated was for the epoxide group at 2.62 ppm.

The ^{13}C NMR spectra generated for the benzoic acid and Heloxy (2:1) samples prepared at 110 and 130 °C are shown on the disc attached in the folder *Chapter 4* under *Benzoic Acid and Epoxide Reactions*. Most of the spectra produced for the samples heated to 110 and 130 °C are identical to those for the unheated sample, where the only peaks identified were due to the starting material. At higher reaction times, a few small extra peaks are noticed at 65.80, 129.71 and 166.70 ppm, confirming that the esterification reaction is occurring at these conditions.

Heated Benzoic Acid and Heloxy (1:2) Samples

The ^{1}H and ^{13}C NMR spectra were obtained for samples with a higher ratio of Heloxy to benzoic acid. The NMR spectra generated can be seen on the disc attached in the folder *Chapter 4* under *Benzoic Acid and Epoxide Reactions*. The dominant peaks in the spectra generated for the samples prepared at 90, 110, 130 and 150 °C are for the starting material. As the reaction time increases, very small extra peaks are witnessed at 4.63, 5.58, 5.68 and 8.12 ppm. These peaks confirm the esterification reaction is occurring at these conditions. These peaks are shown to increase in intensity the longer the samples are heated. The three peaks at 2.81, 2.94 and 3.40

ppm for the epoxide group were also integrated in the ^{1}H NMR spectra generated for the sample of benzoic acid and Heloxy (1:2) heated to 90, 110, 130 and 150 ^{o}C. The scatter plot generated can be seen in figure 4.40. This plot confirms that the esterification reaction is occurring, but the reaction is slower when compared with the epoxides, Cardura and Vikolox.

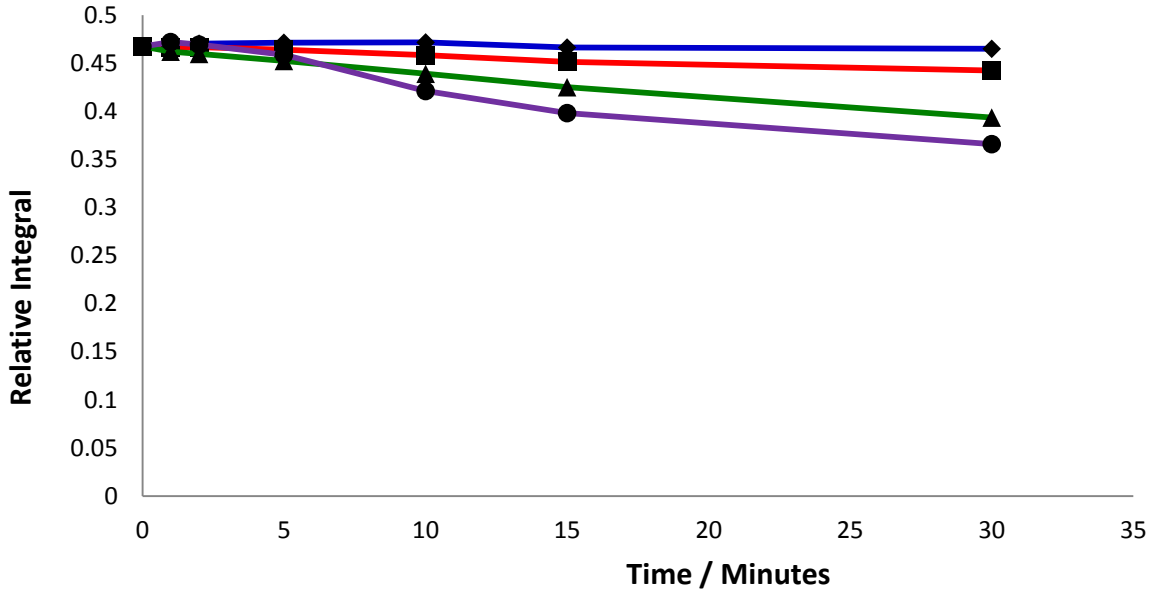

Figure 4.40 – Relative integrals for the epoxide group from the ^{1}H NMR spectrum of the benzoic acid and Heloxy samples (1:2) heated at 90, 110, 130 and 150 ^{o}C. The blue line is the data for the samples heated at 90 ^{o}C, the red line is the data for the samples heated at 110 ^{o}C, the green line is the data for the samples heated at 130 ^{o}C and the purple line is the data for the samples heated at 150 ^{o}C. The peak that was integrated was for the epoxide group at 2.62 ppm.

All ^{13}C NMR spectra obtained for the benzoic acid and Heloxy (1:2) samples prepared at 90, 110, 130 and 150 ^{o}C are shown on the disc attached in the folder *Chapter 4* under *Benzoic Acid and Epoxide Reactions*. The ^{13}C NMR spectra generated for the samples have the dominant peaks corresponding to the Heloxy and benzoic acid starting materials. The ^{13}C NMR spectra of the samples containing more Heloxy are very noisy, making it difficult to identify the presence of small peaks. The spectra produced for the samples prepared at 90, 110, 130 and 150 ^{o}C contain only peaks that correspond to the starting material, with the exception of the samples prepared at 130 ^{o}C for 30 minutes, 150 ^{o}C for 15 minutes and 150 ^{o}C for 30 minutes where there are

some extra peaks corresponding to the esterification reaction at 65.90, 129.60, 132.90 and 166.40 ppm. This set of spectra again highlights the slower rate of the esterification reaction compared with the epoxides Cardura and Vikolox.

4.2.4 Comparison of Epoxides

The integral values for the epoxide group were used to obtain the values for I_t/I_o, so a detailed comparison could be made between the different conditions and epoxides. The I_t value is the integral value (of the epoxide peak at 2.62 ppm) at a specific time and I_o is the initial integral value.

4.2.4.1 Comparing I_t/I_o as temperature changes

The I_t/I_o values obtained for the samples with different epoxides prepared at different temperatures are shown in tables 4.1 to 4.3. The I_t/I_o values for the samples containing Heloxy and Vikolox prepared at 90 and 110 ^oC show no significant changes over the reaction time studied. At 130 ^oC the I_t/I_o values drop significantly at longer reaction times for samples containing Heloxy and Vikolox. The I_t/I_o values were lower for the sample containing Vikolox than Heloxy. The I_t/I_o value was 0.78 for the sample containing Heloxy reacted for 30 minutes at 130 ^oC, but was 0.50 for the sample containing Vikolox reacted for 30 minutes. The I_t/I_o values decrease even further at 150 ^oC. The Vikolox sample is again lower than the Heloxy samples. The I_t/I_o values corresponding to Cardura follow the same trend as Heloxy and Vikolox, in that as the temperature at which the samples were prepared increases, the I_t/I_o value decreases.

Table 4.1 – I_t/I_o values for the epoxide group of the benzoic acid and Cardura samples prepared at different temperatures. The peak integrated was at 2.62 ppm

	90 °C	110 °C	130 °C	150 °C
1 minute	0.99	0.63	0.26	0.09
2 minutes	0.94	0.43	0.11	0.07
5 minutes	0.87	0.13	0.03	0.00
10 minutes	0.79	0.04	0.01	0.00
15 minutes	0.51	0.01	0.00	0.00
30 minutes	0.34	0.00	0.00	0.00

Table 4.2 – I_t/I_o values for the epoxide group of the benzoic acid and Heloxy samples prepared at different temperatures. The peak integrated was at 2.62 ppm

	90 °C	110 °C	130 °C	150 °C
1 minute	1	0.98	0.98	0.99
2 minutes	0.99	0.98	0.97	0.98
5 minutes	0.99	0.99	0.95	0.93
10 minutes	0.99	0.96	0.91	0.72
15 minutes	0.99	0.91	0.85	0.94
30 minutes	0.98	0.91	0.78	0.59

Table 4.3 – I_t/I_o values for the epoxide group of the benzoic acid and Vikolox samples prepared at different temperatures. The peak integrated was at 2.62 ppm

	90 °C	110 °C	130 °C	150 °C
1 minute	1.10	1.18	1.18	1.09
2 minutes	1.02	1.17	1.23	1.19
5 minutes	1.16	1.19	1.12	1.03
10 minutes	1.62	1.03	0.72	0.57
15 minutes	1.09	1.00	0.80	0.43
30 minutes	1.01	0.92	0.50	0.17

4.2.4.2 Comparing I_t/I_o as epoxide changes

As the epoxides change, the I_t/I_o value changes drastically. The epoxide, Heloxy, has already been shown to be less reactive than Vikolox at higher temperatures in the section above. This conclusion is shown in tables 4.4 and 4.5, which also clearly show the dramatically different effect that Cardura has on the I_t/I_o value. The I_t/I_o value starts to drop at a reaction time of 2 minutes at 90 ^oC. The I_t/I_o value for the Cardura sample prepared at 150 ^oC for only one minute was 0.09. This highlights that the most reactive epoxide to be used for solar cell panels would be Cardura, as it could successfully react in the short residence time of an extruder barrel. The Heloxy is slowest at reacting, and would be the least desirable choice for DTF to use in the production of backsheets for solar cell panels.

Table 4.4 – I_t/I_o values for the epoxide group of the benzoic acid and epoxide samples prepared at 90 ^oC. The peak integrated was at 2.62 ppm

	Cardura	Heloxy	Vikolox
1 minute	0.99	1.00	1.10
2 minutes	0.94	0.99	1.02
5 minutes	0.87	0.99	1.16
10 minutes	0.79	0.99	1.62
15 minutes	0.51	0.99	1.09
30 minutes	0.34	0.98	1.01

Table 4.5 – I_t/I_o values for the epoxide group of the benzoic acid and epoxide samples prepared at 150 ^oC. The peak integrated was at 2.62 ppm

	Cardura	Heloxy	Vikolox
1 minute	0.09	0.99	1.09
2 minutes	0.07	0.98	1.19
5 minutes	0.00	0.93	1.03
10 minutes	0.00	0.72	0.57
15 minutes	0.00	0.94	0.43
30 minutes	0.00	0.59	0.17

4.2.4.3 Comparing I_t/I_o with changing ratios of epoxide to benzoic acid

The I_t/I_o values do not change significantly with the different ratios investigated. Tables 4.6 to 4.8 show the values produced at the different conditions. The I_t/I_o values are similar for the samples containing Cardura and Heloxy. There are some higher values for the lower reaction times but the later samples are again all the same. The reactivity of the epoxides was not impacted with the change in ratio. Care has to always be taken regarding side reactions and too much starting material being present in the final product.

Table 4.6 – I_t/I_o values for the epoxide group of the samples of benzoic acid and Cardura prepared at 130 °C with different ratios (benzoic acid: Cardura). The peak integrated was at 2.62 ppm

	1:1	2:1	1:2
2 minutes	0.11	0.14	0.15
5 minutes	0.03	0.04	0.05
10 minutes	0.01	0.00	0.00
15 minutes	0.00	0.00	0.01
30 minutes	0.00	0.00	0.00

Table 4.7 – I_t/I_o values for the epoxide group of the samples of benzoic acid and Heloxy prepared at 130 °C with different ratios (benzoic acid: Heloxy). The peak integrated was at 2.62 ppm

	1:1	2:1	1:2
2 minutes	0.97	1.00	1.00
5 minutes	0.95	0.96	0.98
10 minutes	0.91	0.75	0.95
15 minutes	0.85	0.87	0.92
30 minutes	0.78	0.92	0.85

Table 4.8– I_t/I_o values for the epoxide group of the samples of benzoic acid and Vikolox prepared at 130 °C with different ratios (benzoic acid: Vikolox). The peak integrated was at 2.62 ppm

	1:1	2:1	1:2
2 minutes	1.23	0.68	0.61
5 minutes	1.12	0.66	0.62
10 minutes	0.72	0.61	0.59
15 minutes	0.80	0.55	0.56
30 minutes	0.50	0.68	0.50

4.2.4.4 Kinetics

The integral values were used to obtain graphs of $\ln(I_t/I_o)$ versus time and $1/I_t$ versus time to determine the order of the reaction. The data fits the first order model, as confirmed by many research groups including Parker *et al*. [136] Figure 4.41 shows an example of the graph obtained for the benzoic acid and Cardura sample heated at 90 °C. All other graphs generated can be seen on the disc attached in the folder *Chapter 4* under *Benzoic Acid and Epoxide Reactions*.

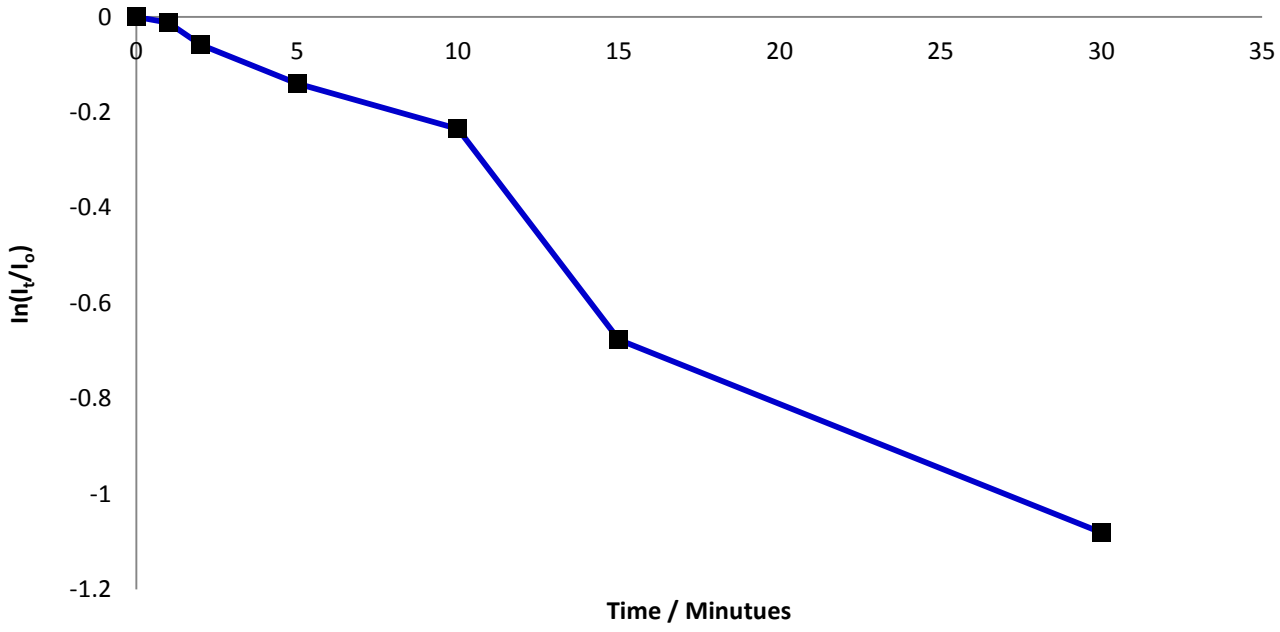

Figure 4.41 – Graph of ln(It/Io) versus time for the benzoic acid and Cardura sample heated at 90 °C. The peak integrated was at 2.62 ppm.

The rate constant, given from the slopes of the $\ln(I_t/I_o)$ versus time graphs were used to prepare Arrhenius plots. Figure 4.42 shows the Arrhenius plots obtained for the samples with the different epoxides. All of the data produced straight line trends. The activation energy was calculated for each of the esterification reactions involving the different epoxides. Table 4.9 shows the activation energy of the esterification reaction when the different epoxides were involved. The activation energies produced for the different epoxides were very similar.

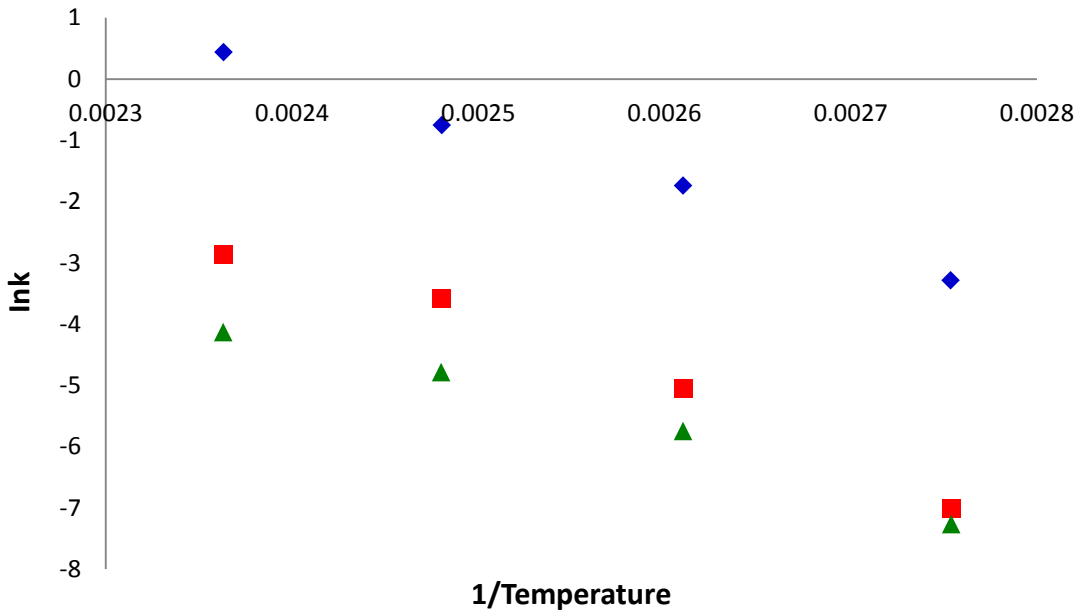

Figure 4.42 - Graph of lnk versus time for the benzoic acid and epoxide samples. The blue data is for Cardura, the red data is for Vikolox and the green data is for Heloxy.

Table 4.9– Activation energies for the benzoic acid and epoxide reactions.

Sample	Activation Energy / J mol^{-1}
Benzoic Acid and Cardura	1035
Benzoic Acid and Heloxy	980
Benzoic Acid and Vikolox	1363

4.3 Conclusions

Ring opening of Cardura was investigated at 110, 130 and 150 ^{o}C under both air and nitrogen. There were no changes witnessed when the NMR spectra of any of the Cardura samples prepared were compared to the starting material. The integrals from the ^{1}H NMR specta for the peaks at 2.62, 2.80 and 3.17ppm remain the same from the sample prepared at 1 minute to 30 minutes. The results highlight that none of the epoxides undergo ring opening at any of the conditions investigated.

The benzoic acid samples were also prepared at 90, 110, 130 and 150 ^{o}C under nitrogen to monitor any reactions that were occurring at the conditions investigated. No changes were noticed in the spectra obtained, indicating that no reactions, such as degradation, are occurring.

The esterification reaction was shown to occur for all three epoxides. The data gathered shows the esterification reaction is more dominant when carried out at longer reaction times. The analysis of the ^{1}H NMR spectra, and the more detailed kinetic samples, also show that the higher the reaction temperature, the faster the esterification reaction occurs.

It was shown that the most reactive monofunctionalised epoxide was Cardura followed by Vikolox, with Heloxy being the least reactive. Cardura is therefore the most likely choice to undergo reactive extrusion with PET to improve the sample's resistance to hydrolytic degradation for the use in solar cell panels. The esterification reaction was shown to be nearly complete after only one minute, which would be similar to the residence time of the extruder barrel.

The data shows the possibility of side reactions occurring, resulting in the samples being extensively tested in later chapters.

5.0 Reactions of Poly(ethylene isophthalate) and Epoxides

5.1 Introduction

Small compounds, such as benzoic acid, ethylene dibenzoate, 2-hydroethyl benzoate and diethyleneglycol dibenzoate are frequently used as model compounds for PET. [14 and 80-83] These compounds are used because any changes that occur are easily detected by infrared spectroscopy or nuclear magnetic resonance spectroscopy. It is more difficult for changes to be detected in polymer samples that have a high molecular weight like PET. The challenges in monitoring changes in polymer samples arise because the samples are often difficult to dissolve for analysis, and the changes occurring are very small. The end group concentrations of polymers are often monitored because several reactions, such as degradation, alter the concentration of the end groups. [40-47] There have been a number of methods over the years for measuring end group concentrations of PET. These include titration and spectrometric techniques, such as infrared (IR) spectroscopy and nuclear magnetic resonance (NMR).

The esterification reaction was detected between the epoxides (Cardura, Vikolox and Heloxy) and the model compound benzoic acid; this is shown in Chapter 4. The next stage was to develop a suitable method to monitor the esterification reaction in polymer samples. Dupont Teijin Films sought an inexpensive and simple method that could detect changes in the carboxyl end group concentration of polymer samples. The Pohl *et al*. titration method was selected and optimised at Strathclyde University to allow the carboxyl end group concentration of the polymers to be studied. Section 3.9 shows all of the details for this method.

The titration method developed was then tested with the polymer PEI. The PEI is chemically similar to PET, but dissolves more easily than samples of PET. Samples of PEI will dissolve at room temperature in chloroform, but samples of PET will not dissolve in chloroform. The PEI dissolves more easily that PET because it has lower crystallinity. This is due to the ester groups that are attached to the aromatic ring in the ortho relationship, which reduces the ability of the

chains to tightly pack compared to PET, where the ester groups are attached to the para positions on the aromatic ring.

Once the method had been developed, samples were prepared with the epoxides and PEI in order to be investigated. This was to determine if the epoxides could successfully end cap polymer chains. The effectiveness of each of the epoxides was determined by reaction time and concentration required. These are two key parameters for DTF to keep production costs to a minimum and allow the samples to be prepared in their current film processing line. [16]

5.2 Results and Discussion

5.2.1 Starting Material

The IR spectrum that was obtained for the PEI E354 is shown in figure 5.1. The presence of the aromatic groups is clearly identified by the peaks at 1588, 1609, 3024 and 3079 cm^{-1}. The di-substituted pattern of the aromatic region is shown by the peaks at 655, 728 and 756 cm^{-1}. The peaks at 1372, 1438, 2890 and 2960 cm^{-1} correspond to aliphatic groups. The ester groups are shown at 1236 and 1297 cm^{-1}. The ester group is also seen in the large peak at 1726 cm^{-1}. The carboxyl end groups would also produce a small peak around 1750 cm^{-1}. The carboxyl and hydroxyl end groups are also responsible for the peak at 3430 cm^{-1}.

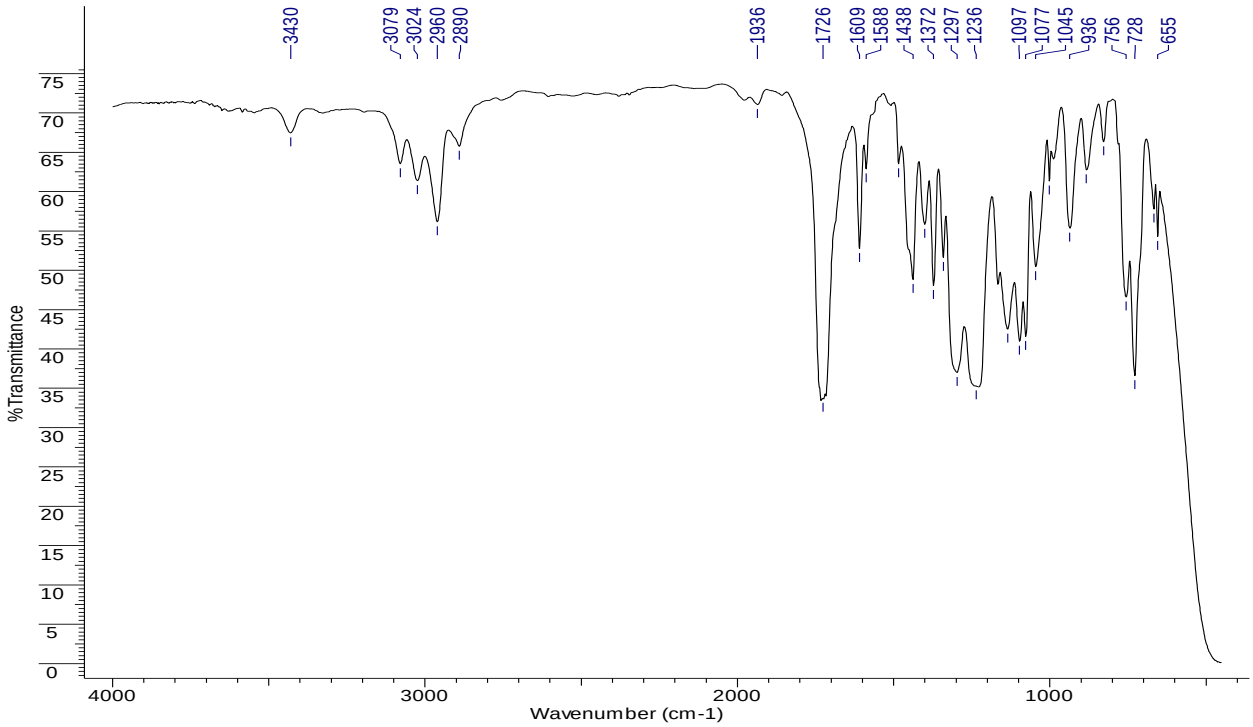

Figure 5.1 – IR spectrum of PEI.

The ^{1}H and ^{13}C NMR spectra are shown in figures 5.2 and 5.3 respectively, and both spectra generated show all of the dominant peaks expected for PEI. In the ^{1}H NMR spectrum the dominant peaks appear at 4.69, 7.51, 7.64, 8.32, 8.33 and 8.70 ppm. The peak at 4.69 ppm corresponds to the CH_2 groups on the polymer backbone. The peaks at 7.51 and 7.64 ppm correspond to the hydrogens at the para position of the aromatic rings. The hydrogens at the meta position of the aromatic rings can be seen in the peaks at 8.32 and 8.33 ppm. The peak at 8.70 ppm corresponds to the iso positions of the aromatic rings. There are also several other peaks which are noticed in this spectrum, suspected to come from the isophthalic starting material and diethylene glycol units in the PEI backbone.

The ^{13}C spectrum also has many extra peaks at 64.00, 70.00, 128.56, 129.21 and 133.58 ppm. All of these peaks are consistent with diethylene glycol units. The dominant peaks are at 62.46, 128.27, 129.81, 130.49, 134.05 and 164.89 ppm. The peak at 129.81 ppm corresponds to the carbons at the iso position of the aromatic rings, 134.05 ppm corresponds to the carbons at the ortho position of the aromatic rings, the carbons at the meta positions of the aromatic ring are

shown at 130.49 ppm, and the peak at 128.27 ppm corresponds to the carbons at the para position. The other peaks at 62.46 ppm show the presence of the CH_2 aliphatic groups in the polymer backbone, and the peak at 164.89 ppm corresponds to a carbonyl group, which is expected from an ester.

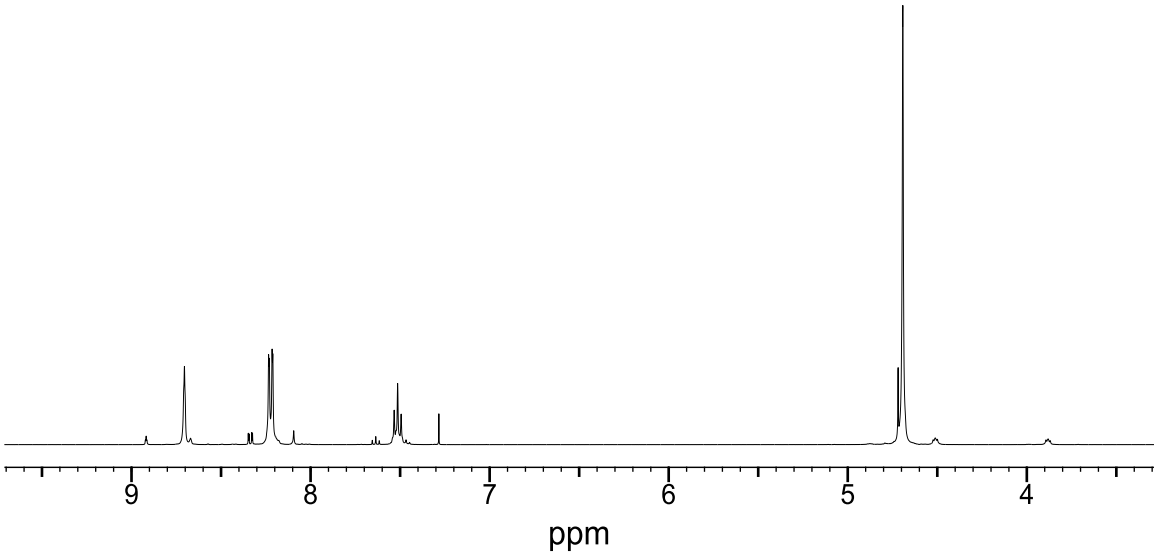

Figure 5.2 - ^{1}H NMR spectrum of the PEI.

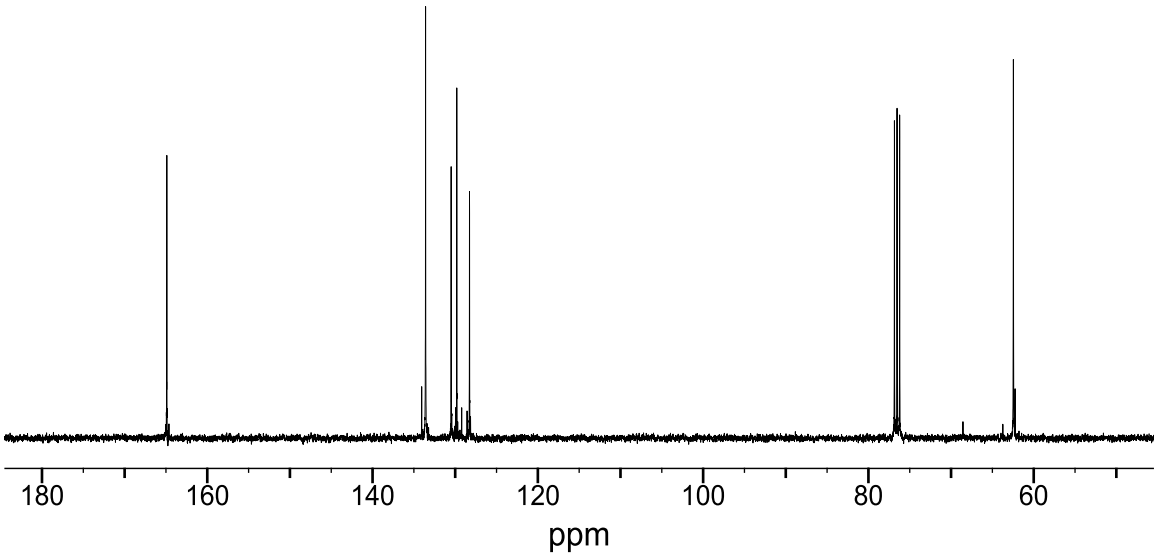

Figure 5.3 – ^{13}C NMR spectrum of the PEI.

The thermal properties of the PEI were investigated by obtaining a DSC scan (Figure 5.4) and a TGA thermogram (Figure 5.5). The DSC scan shows four transitions, namely the glass transition (T_g), crystallisation temperature, melting point and degradation for PEI. Table 5.1 summarises the information obtained from the DSC scan. The T_g obtained for PEI is 61 ^oC and the value quoted in the literature for PEI is 55 – 60 ^oC. [9-10] The melting point was determined by DSC to be 232 ^oC. The peak that corresponds to the melting point of PEI is very small because the sample has low crystallinity. The onset of degradation occurs at approximately 366 ^oC from the DSC scan and 373 ^oC from the TGA thermogram. The values obtained from the DSC and TGA experiments are in close agreement with the values for degradation. The peak temperature obtained from the derivative of the data in the TGA thermogram was 444 ^oC. This was obtained as the derivative peak temperature is more reliable than the onset temperatures. The degradation peak in the DSC scan gave a similar value as the TGA thermogram at 437 ^oC.

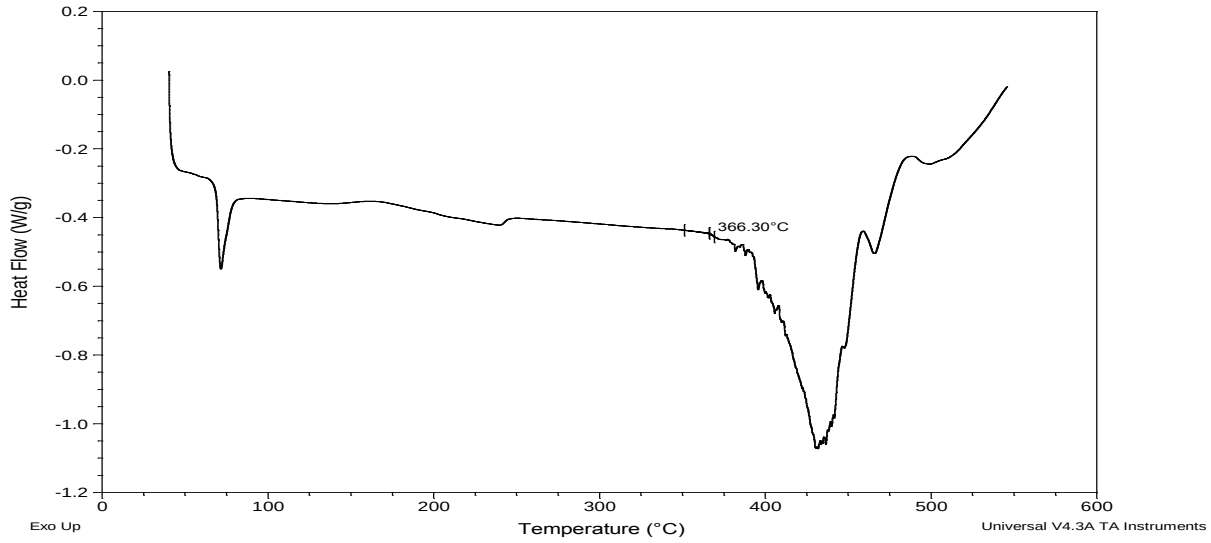

Figure 5.4– DSC scan of PEI.

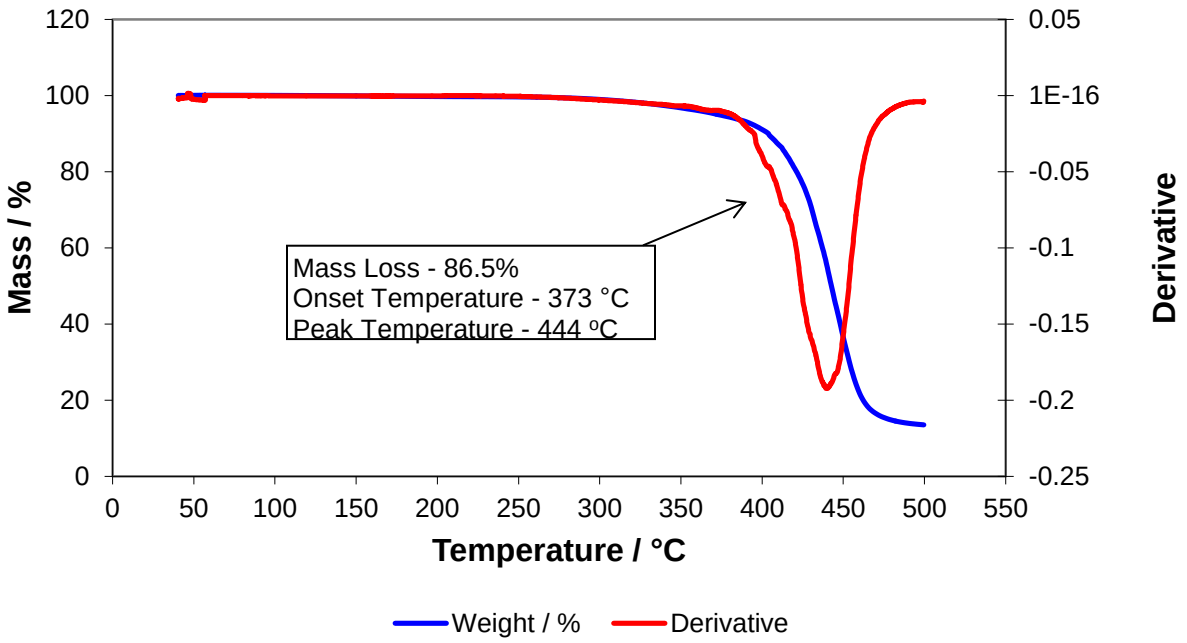

Figure 5.5 - TGA thermogram of PEI.

Table 5.1 – Summary of the transitions present in the DSC scan for PEI

Transition	**Temperature °C**	**ΔH J/g**
Glass Transition	61	N/A
Crystallisation Temperature	162	0.80
Melting Point	232	7.27
Onset of Degradation	366	N/A
Degradation	437	287

5.2.2 PEI and Epoxide Blends

5.2.2.1 Unheated Blends

The carboxyl end group concentrations of the unheated PEI and Cardura blends are shown in figure 5.6. The end group concentration is clearly reducing as more Cardura is added to the PEI. The PEI film has an end group concentration of 57.45 equivalents per 10^6 grams. The sample with the addition of 1% Cardura has a similar end group concentration of 59.49 equivalents per 10^6 grams. The reason for this is that 1% of Cardura is not sufficient to react with all of the carboxyl end groups that are present in the polymer. The film samples of PEI and 6% Cardura give an end group concentration of 23.54 equivalents per 10^6 grams, which is considerably less than the blank samples of PEI. This shows that the esterification reaction between the epoxide group and carboxyl end group of the polyester is occurring, as the amount of end groups in the polymer sample is reducing. These samples also show that the reaction can be detected and monitored in polymer samples even for reactions at room temperature.

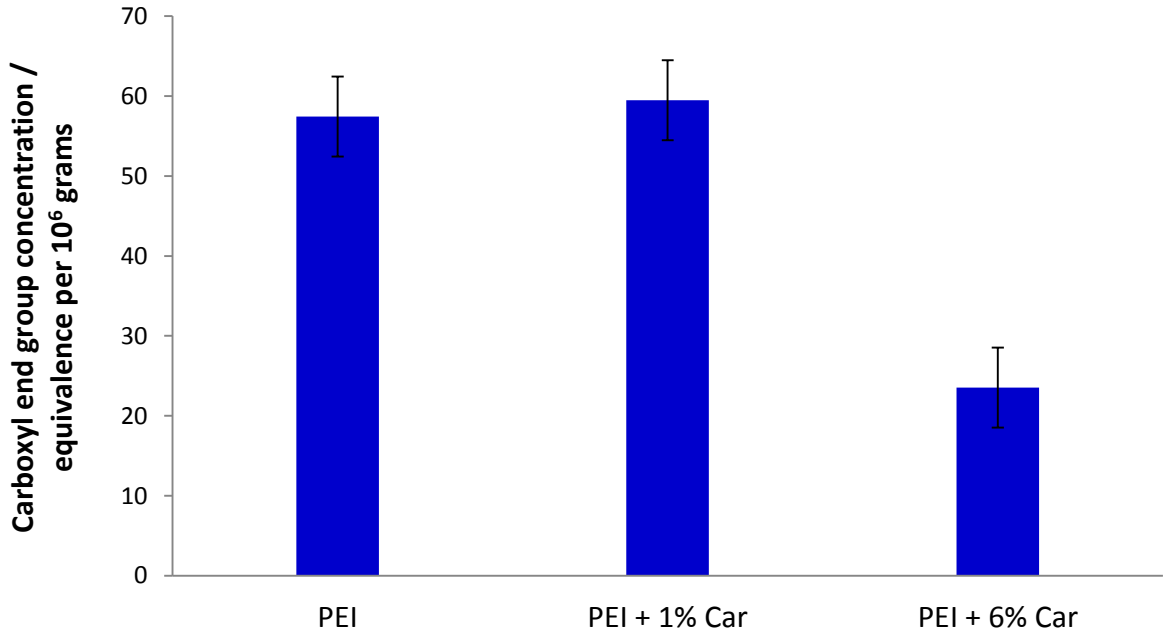

Figure 5.6 – Bar chart showing the carboxyl end group concentration of blends of PEI and Cardura with no heating. N=3. The error bar is 5 equivalents per 10^6 grams which is the calculated error in the method.

Titrations were also carried out on the samples prepared with Heloxy and Vikolox. Figure 5.7 shows a bar chart of the carboxyl end group concentration of the PEI and Heloxy samples. The carboxyl end group concentration of the sample with 6% Heloxy is 46.36 equivalence per 10^6 grams, and the blank PEI has an end group concentration of 57.45 equivalents per 10^6 grams. The reduction of the sample is very low, and with the large errors in the experiment, it suggests that the esterification reaction between PEI and Heloxy is occurring much slower than the reaction with PEI and Cardura.

The bar chart showing the carboxyl end group concentration of the PEI and Vikolox samples is shown in figure 5.8. The results appear to be increasing significantly with the addition of Vikolox. This is expected to be a result of further thermal degradation occurring during the titration process in some of the film samples than is compensated for by the Pohl titration method. The titration method was optimised for small PET rods rather than film samples with potentially variable thicknesses, resulting in the possibility of more degradation occurring in these samples. Given more time these samples would be repeated to ensure a constant thickness and a study carried out to compensate for the thermal degradation that occurred in the thin film samples. The information gathered was sufficient for DTF to show that the esterification reaction was occurring, and that it was occurring quicker when Cardura was used compared with the other epoxides. Chapter 4 supports that the Heloxy and Vikolox epoxides reacted with carboxyl groups more slowly than Cardura.

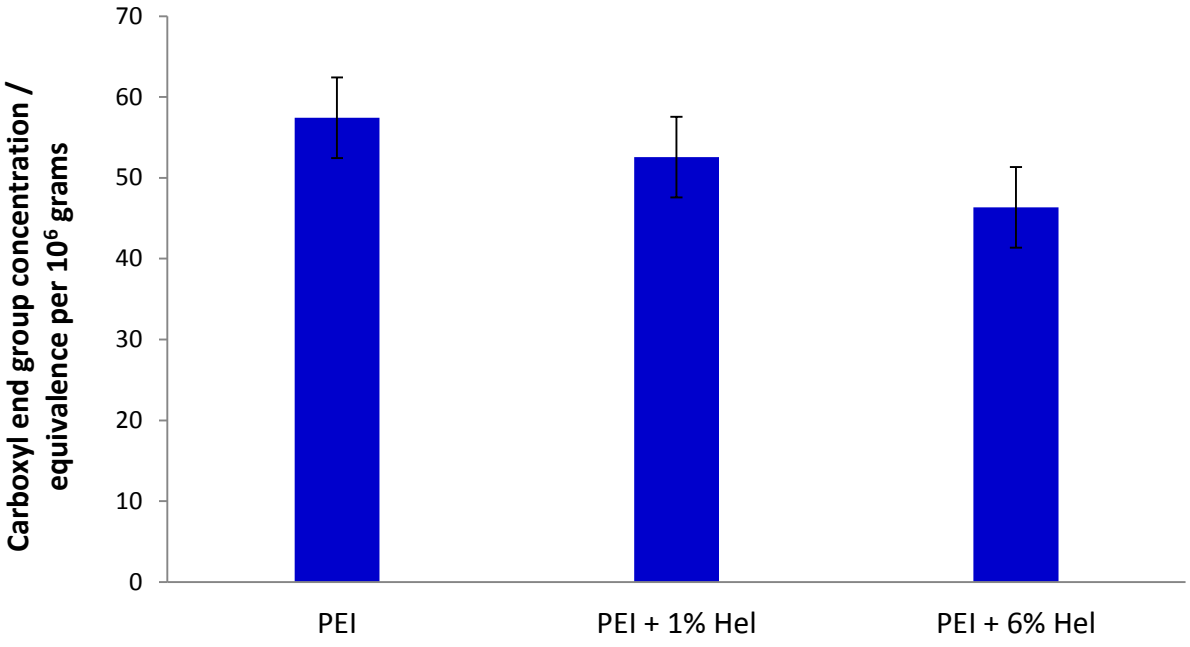

Figure 5.7 – Bar chart showing the carboxyl end group concentration of blends of PEI and Heloxy with no heating. N=3. The error bar is 5 equivalents per 10^6 grams which is the calculated error in the method.

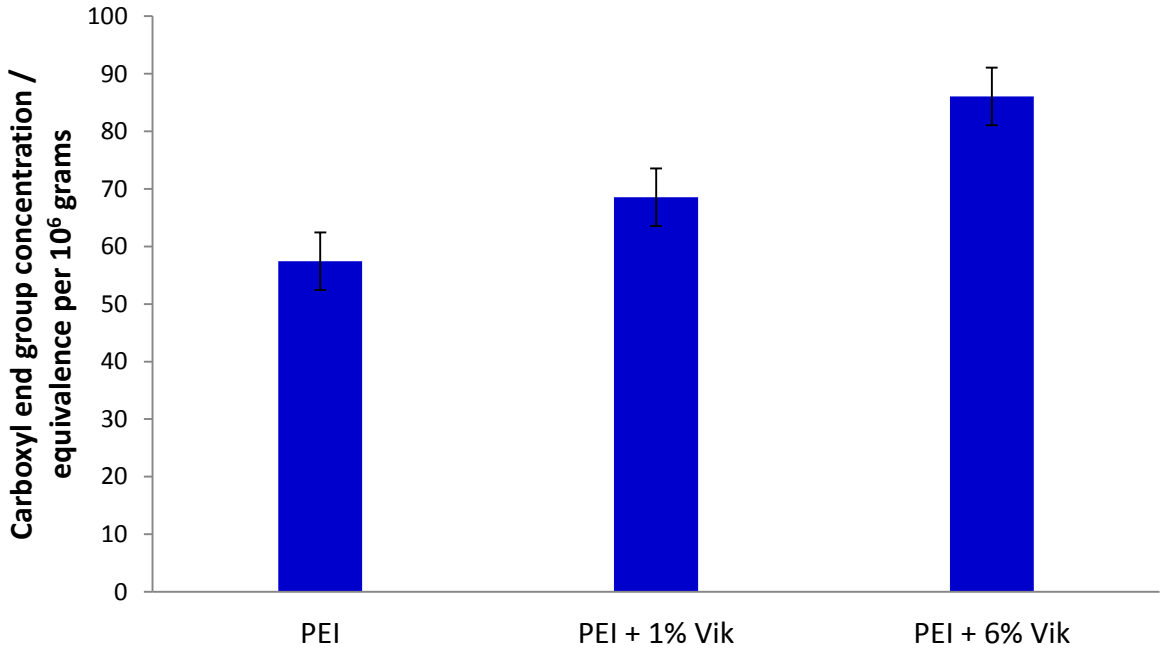

Figure 5.8 – Bar chart showing the carboxyl end group concentration of blends of PEI and Vikolox with no heating. N=3. The error bar is 5 equivalents per 10^6 grams which is the calculated error in the method.

5.2.2.2 Heated PEI Samples

The end group concentrations of the PEI samples heated in the absence of epoxide to 110 °C did not change with time. Similar results are shown with the samples heated to 130 °C, 150 °C and 200 °C. Figure 5.9 shows a scatter plot of the end group concentrations for the samples heated to 110, 130, 150 and 200 °C. When the high error of the titration method is considered, there is no significant change at any temperature investigated. This shows that there was no significant thermal degradation occurring at any of the conditions investigated.

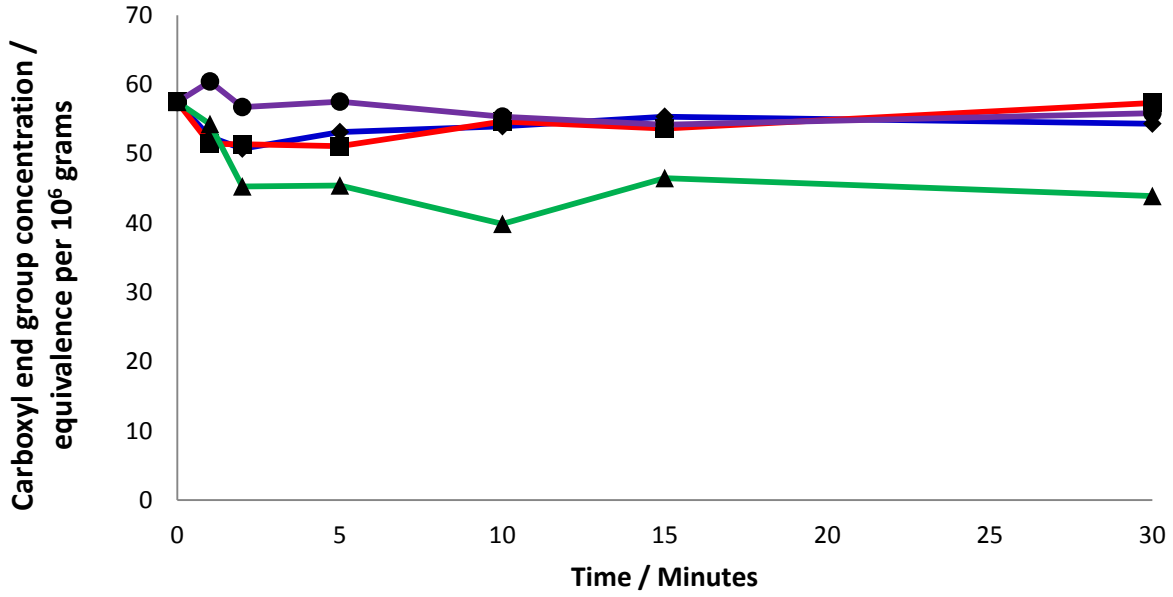

Figure 5.9 – End group concentration of PEI samples heated to 110 °C (Blue), 130 °C (Red), 150 °C (Green) and 200 °C (Purple). N=3.

5.2.2.3 Heated PEI and Epoxide Samples

PEI + 1% Cardura

The end group concentrations of samples prepared with 1% Cardura at 110 °C were noticed to reduce in the sample set. The carboxyl end group concentration reduced from 59.49 equivalents per 10^6 grams to 43.88 equivalents per 10^6 grams going from the unheated sample to the sample heated to 110 °C for 30 minutes. The reduction in the end group concentration is expected since the epoxide group is reacting with the carboxyl end groups forming alcohol

groups. There are some out-lying points on the scatter plot which was expected to be a result of thermal degradation occurring during the titration process in the films created containing various thicknesses. The samples heated at 130 °C, 150 °C and 200 °C also show the general trend of the end group concentration decreasing with time. There are no significant changes between the samples heated at a higher temperature, which was expected to be a result of the high error value, and that 1% w/w of the epoxide is not enough to react with all of the carboxyl end groups present in the PEI sample. The results of the titration for the samples of PEI and 1% Cardura heated to 110 °C are shown in figure 5.10.

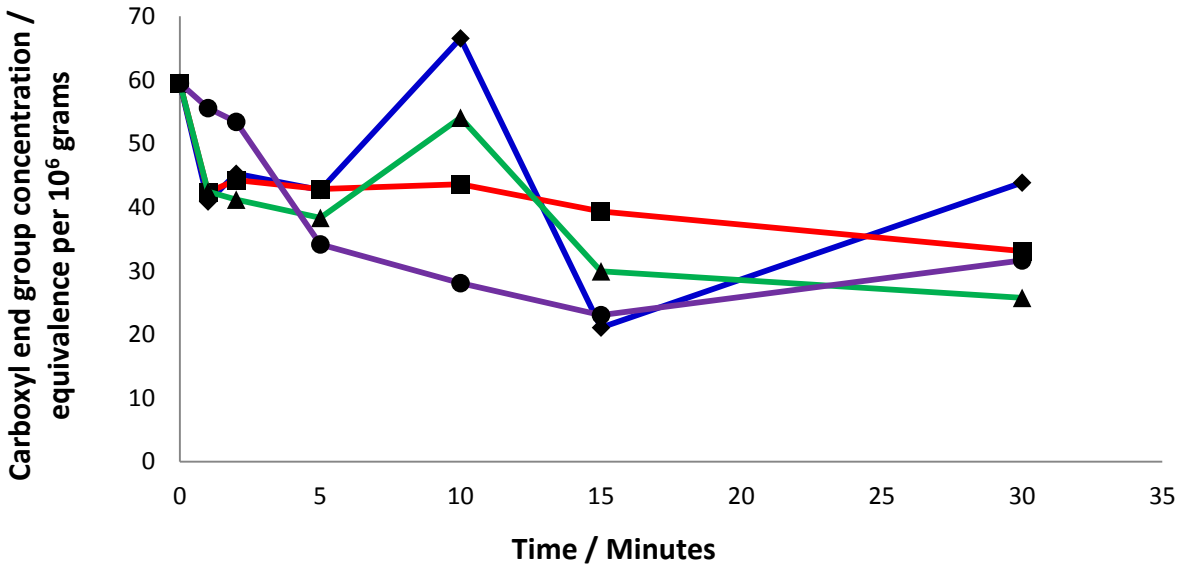

Figure 5.10 – End group concentration of PEI + 1% Cardura samples heated to 110 °C (Blue), 130 °C (Red), 150 °C (Green) and 200 °C (Purple). N=3

PEI + 6% Cardura

Samples were also investigated with a higher Cardura concentration. The carboxyl end group concentrations of samples prepared with 6% Cardura at 110 °C were observed to reduce the longer the samples were heated. The carboxyl end group concentration reduced from 23.54 equivalents per 10^6 grams to 15.34 equivalents per 10^6 grams going from the unheated sample to the sample heated to 110 °C for 30 minutes. The reduction confirmed that the esterification reaction was occurring. There are some samples prepared with 6% Cardura that did not follow

the trend as expected, which is believed to be as a result of experimental error due to thermal degradation occurring in thinner film samples. The scatter plots generated of end group concentration versus time for the samples of PEI and 6% Cardura heated at 130, 150 and 200 °C also show the general trend of the end group concentration decreasing as reaction time increases. The samples heated to 130 °C and higher had a significantly lower end group concentration; for example the carboxyl end group concentration reduced from 23.54 equivalents per 10^6 grams to being undetectable going from the unheated sample to the sample heated to 200 °C for 30 minutes. Figure 5.11 shows the scatter of the end group concentration versus time of the PEI and 6% Cardura samples heated at 110, 130, 150 and 200 °C.

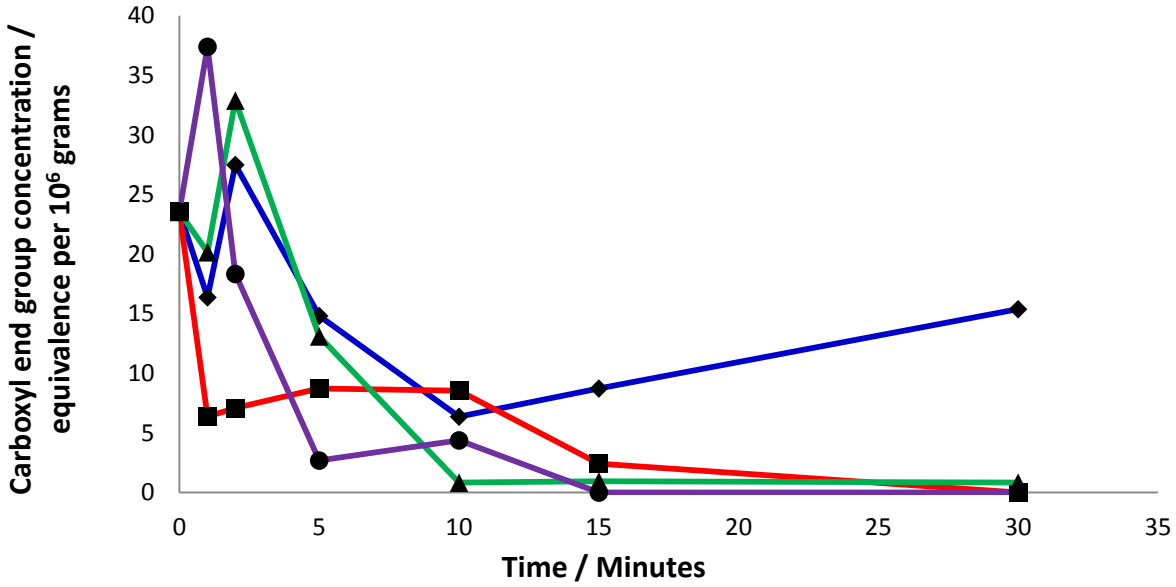

Figure 5.11 – End group concentration of the PEI and 6% Cardura samples heated to 110 °C (Blue), 130 °C (Red), 150 °C (Green) and 200 °C (Purple). N=3.

The data collected clearly shows that the esterification reaction was being detected in the samples. This means that Cardura could be a possibility for DTF to use with PET in order to make an end capped polymer to be used as a backsheet for photovoltaic cells. The esterification reaction was more significantly noted in samples with higher concentrations of Cardura, which supports the conclusions identified in Chapter 4.

PEI + 1% Heloxy

Samples of PEI and 1% Heloxy were also prepared at 110, 130, 150 and 200 °C. The graphs of the end group concentration versus time for the PEI and 1% Heloxy samples prepared at 110, 130, 150 and 200 °C can be seen in figures 5.12. There are no significant changes in the end group concentration between the PEI samples and the PEI with 1% Heloxy samples. The carboxyl end group concentration for the unheated PEI sample is 57.45 equivalents per 10^6 grams and the unheated PEI + 1% Heloxy sample is 52.57 equivalents per 10^6 grams. There was no significant reduction noticed in the end group concentration at any of the conditions investigated. The results indicate that the esterification reaction was not occurring in the samples. The data in Chapter 4 indicates that Heloxy is less reactive than Cardura at the conditions investigated.

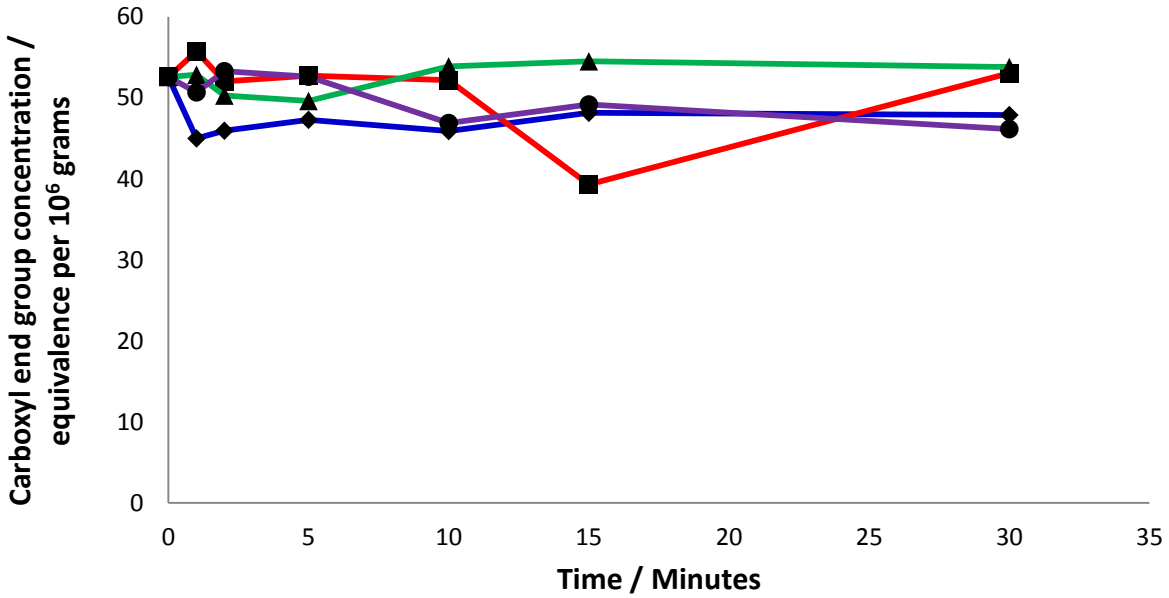

Figure 5.12 – End group concentration of the PEI + 1% Heloxy samples heated to 110 °C (Blue), 130 °C (Red), 150 °C (Green) and 200 °C (Purple). N=3.

PEI + 6% Heloxy

There was a slight reduction noticed in the samples prepared with higher concentrations of Heloxy. There is also a slight reduction in the carboxyl end group concentration noticed in the unheated PEI + 6% Heloxy blends compared with the unheated PEI sample. The carboxyl end

group concentration reduced from 57.45 equivalents per 10^6 grams in the unheated PEI sample to 46.36 equivalents per 10^6 grams in the unheated PEI and 6% Heloxy sample. The samples heated to 110, 130 and 150 ^oC showed no significant differences in the end group concentration; this suggests that the esterification reaction was not occurring. The esterification reaction was noticed in the PEI and 6% Heloxy samples that were heated to 200 ^oC, as the carboxyl end group concentration reduced significantly. The unheated PEI + 6% Heloxy sample had an average carboxyl end group concentration of 46.36 equivalents per 10^6 grams, which was reduced to 23.86 equivalents per 10^6 grams for the sample heated to 200 ^oC for 30 minutes. The scatter plot for the PEI and 6% Heloxy samples heated to 110, 130, 150 and 200 ^oC is shown in figure 5.13.

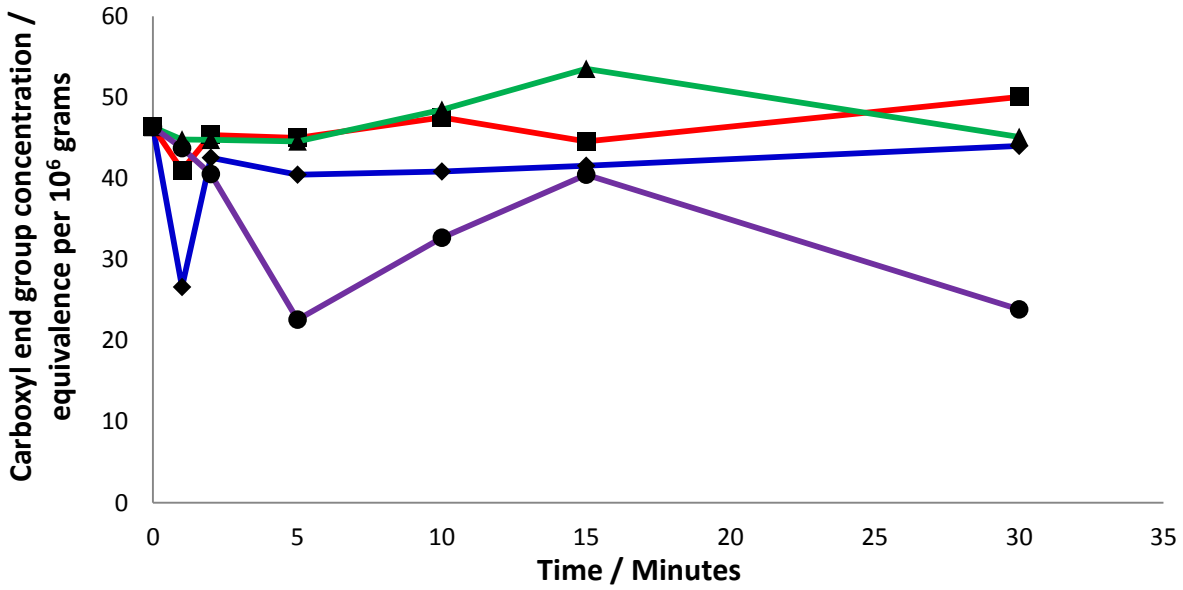

Figure 5.13 – End group concentration of the PEI + 6% Heloxy samples heated to 110 ^oC (Blue), 130 ^oC (Red), 150 ^oC (Green) and 200 ^oC (Purple). N=3.

PEI + 1% Vikolox

There was a slight increase in the end group concentrations of the unheated sample of PEI and 1% Vikolox compared with the unheated PEI sample. The carboxyl end group concentration was

68.53 equivalents per 10^6 grams for the unheated PEI and 1% Vikolox sample compared to 57.45 equivalents per 10^6 grams for the unheated PEI sample. This apparent increase was due to the high error obtained when determining the carboxyl end group concentration by the Pohl titration method. There are no significant changes in the carboxyl end group concentration for any of the conditions investigated. Figure 5.14 shows the graphs of the end group concentration versus time for the PEI and 1% Vikolox samples heated to 110, 130, 150 and 200 ^oC.

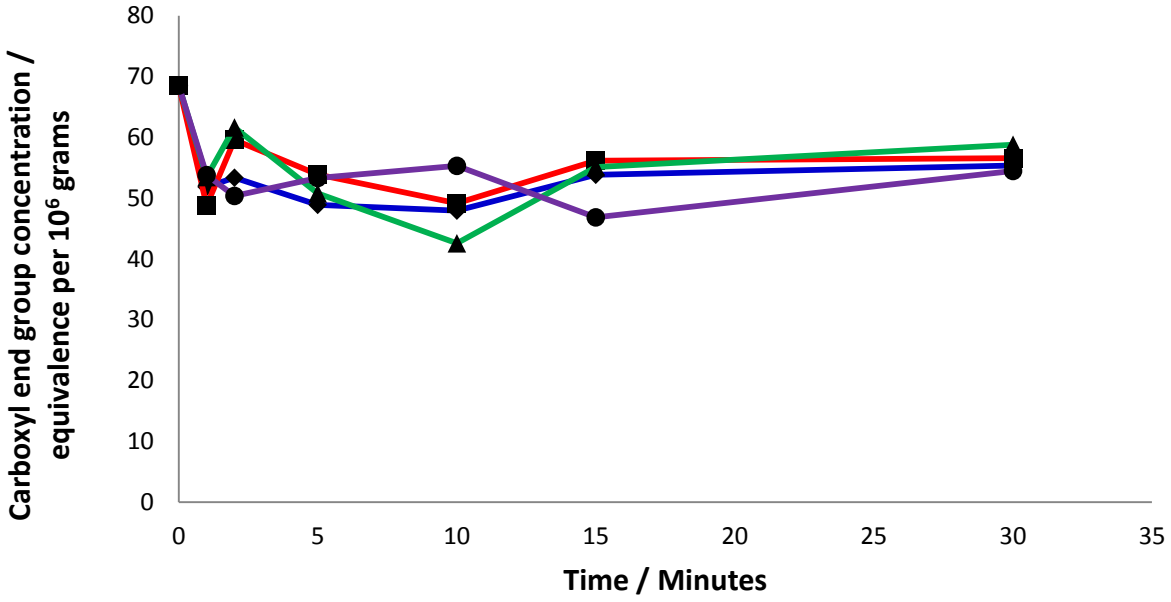

Figure 5.14 – End group concentration of the PEI + 1% Vikolox samples heated to 110 ^oC (Blue), 130 ^oC (Red), 150 ^oC (Green) and 200 ^oC (Purple). N=3.

PEI + 6% Vikolox

Blends of PEI + 6% Vikolox were prepared to see if the esterification reactions could be determined. There was an increase in the end group concentration of unheated PEI and 6% Vikolox samples compared with the unheated PEI samples. The carboxyl end group concentration increased from 57.45 equivalents per 10^6 grams in the unheated PEI sample to 86.08 equivalents per 10^6 grams in the unheated PEI and 6% Vikolox sample. This increase was expected to be a result of thermal degradation occurring in the thin film samples during the

titration process. There is a slight reduction noticed in the end group concentrations of the PEI + 6% Vikolox samples heated to 110, 130 and 150 °C, for example, the carboxyl end group concentration reduced from 86.08 equivalents per 10^6 grams in the unheated PEI + 6% Vikolox sample to 61.87 equivalents per 10^6 grams in the PEI and 6% Vikolox sample heated at 110 °C for 30 minutes. This suggests that the esterification reaction was occurring, but very slowly. This supports the conclusions that were identified in Chapter 4 that the Vikolox reaction with carboxyl groups occurs much slower than Cardura reacting with the carboxyl end group. An increase is noticed in the PEI + 6% Vikolox sample heated to 150 °C for 30 minutes and for the PEI and 6% Vikolox samples heated to 200 °C. This was expected to be a result of thermal degradation occurring in the thin films during the titration process. It was decided that this data completed the objectives set out for this piece of work, and that no further effort should be spent on it at this time. A scatter plot of the end group concentration versus time for the PEI and 6% Vikolox samples heated to 110, 130, 150 and 200 °C are shown in figure 5.15.

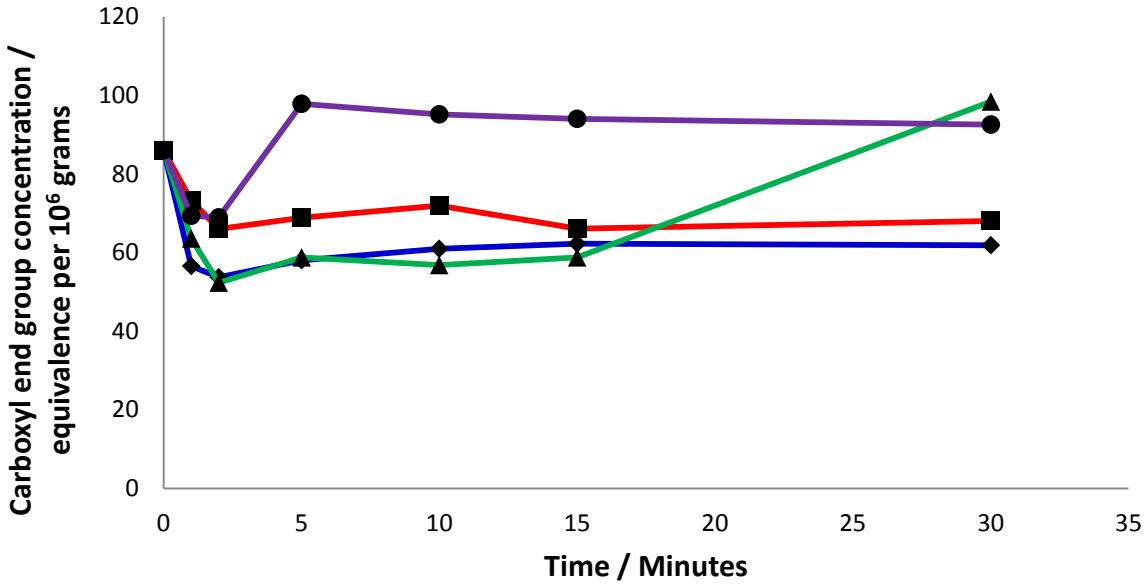

Figure 5.15 – End group concentration of the PEI +6% Vikolox samples heated to 110 °C (Blue), 130 °C (Red), 150 °C (Green) and 200 °C (Purple). N=3.

5.3 Conclusions

The carboxyl end group concentrations of the PEI samples were similar for all of the temperatures investigated, which indicated that no side reactions or degradation was occurring. The Pohl titration method outlined in section 3 has been shown to provide a simple and inexpensive method for detecting the carboxyl end group concentration. This method was used for further work at Strathclyde University and was also carried out for other projects at DTF sites.

The end group concentrations of the PEI and 1% Cardura samples that were prepared at 110 ^{o}C reduced the longer the samples were heated. This is the same for the samples prepared at 130, 150 and 200 ^{o}C. The PEI and 6% Cardura samples also followed this trend for all of the samples prepared. It was also noticed that the rate of the esterification reaction seemed to quicken with the higher temperature used for the samples prepared with 6% Cardura. The esterification reaction was not detected in the PEI and 1% Vikolox or the 6% Vikolox samples. When using the epoxide Heloxy the reaction was only noticed in the PEI + 6% Heloxy samples that were prepared at 200 ^{o}C.

This study with the model polymer PEI suggests that Cardura is the most effective epoxide for the end capping of polyesters. This supports the conclusion obtained from Chapter 4 that Cardura is the most effective of the three epoxides evaluated in terms of reactivity with PEI end groups and benzoic acid.

6.0 Reactions of Poly(ethylene terephthalate) and Epoxides

6.1 Introduction

The reaction of mixing chain extenders with PET is normally carried out in an extruder, where the polymer is in the melt state. [20 – 21, 83 – 89 and 137- 140] This process is called reactive extrusion. The chain extenders used in this process must be easily prepared, thermally stable, non-volatile at PET processing temperatures, and must not react to create volatile products. [7] The most common chain extenders that are used with PET include diepoxides and diisocyanates. [20 – 27] Reactive extrusion has several advantages; it is low cost, and preparation is simple as the process can be carried out using standard industrial extruders operating under normal conditions. [20 – 21]

Reactive extrusion was selected by DTF as the method for adding the chosen epoxide to PET because it could be carried out on their current processing lines without the need for large capital investment.

A lab scale PRISM – TSE 16TC twin screw extruder was used at Strathclyde University for all of the development work. This extruder was successfully shown in Chapter 3 to allow the epoxides (Cardura, Heloxy and Vikolox) to react with the carboxyl end groups in PET inside the extrusion barrel.

Using the optimised extruder process gives information that can be applied to the processing lines at DTF regarding the performance parameters of the different epoxides. These parameters include the effectiveness of end capping, the extrusion stability and to have minimal influence on the polymers properties (for example, crystallisation temperature and degradation behaviour).

6.2 Results and Discussions

6.2.1 Starting Material

The IR spectra for the three grades of PET used in this work are extremely similar. The IR spectrum of PET E187 is shown in figure 6.1, and all other spectra are shown in the appendices (A6.1.1 and A6.1.2). The peaks in the IR spectra were identified, for example, the aliphatic groups can be clearly seen at 1373, 1410, 2892 and 2962 cm^{-1}. The presence of the aromatic groups is clearly identified by the peaks at 1455, 1505, 1579 and 3068 cm^{-1}. The di-substituted pattern of the aromatic region is shown by the peaks at 686, 728 and 840 cm^{-1}.The ester groups are shown at 1183 and 1264 cm^{-1}. The ester group is also evidenced by the large peak at 1730 cm^{-1}. The carboxyl and hydroxyl end groups are also responsible for the peak at 3430 cm^{-1}.

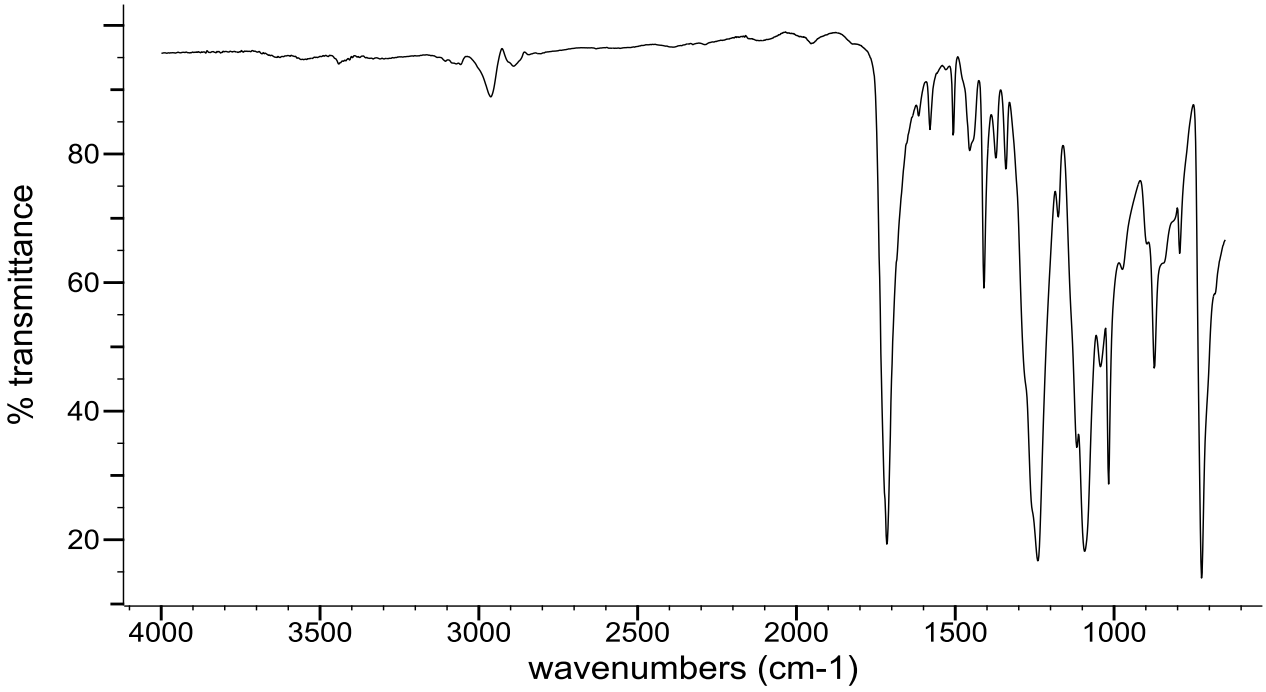

Figure 6.1 – IR spectrum of PET E187.

As all of the IR spectra of the different grades of PET were similar, ^{1}H and ^{13}C NMR spectra were also obtained for the E187 and E239 PET samples. NMR is a more sensitive technique which should show more subtle changes between different samples. The ^{1}H and ^{13}C NMR spectra for the samples of PET show no differences. A sample of the ^{1}H and ^{13}C NMR spectra for PET E187 are shown in figures 6.2 and 6.3. The ^{1}H and ^{13}C NMR spectra for the E239 PET samples are shown in the appendices (A6.1.3 and A6.1.4).

In the ^{1}H NMR spectra the dominant peaks appear at 4.40, 4.46, 4.69, 4.73, 7.28 and 8.12 ppm. The peaks at 4.69 and 4.73 ppm correspond to the CH_2 groups on the polymer backbone. The peak at 8.12 ppm corresponds to the hydrogens on the aromatic ring. When zoomed in on the ^{1}H NMR spectra, satellite peaks are noticed coming from the large peak at 8.12 ppm. The peaks at 4.40, 4.46 and 7.28 ppm are from the solvents hexafluoroisopropanol (HFIP) and $CDCl_3$. There are also several other peaks in the spectra, which are believed to be from terephthalic acid, diethylene glycol units and water present in the PET sample.

In the ^{13}C NMR spectra, the peaks for the solvents are shown at 68.88 ppm, 76.40 ppm and between 116 and 126 ppm. The dominant peaks are at 62.79, 129, 133 and 166 ppm. The peak at 129.32 ppm corresponds to the ortho and meta position of the aromatic rings, and the peak at 132.94 ppm corresponds to the carbons at the iso and para position of the aromatic rings. The other peak at 62.79 ppm shows the presence of the CH_2 aliphatic groups in the polymer backbone, and the peak at 166.32 ppm corresponds to a carbonyl group.

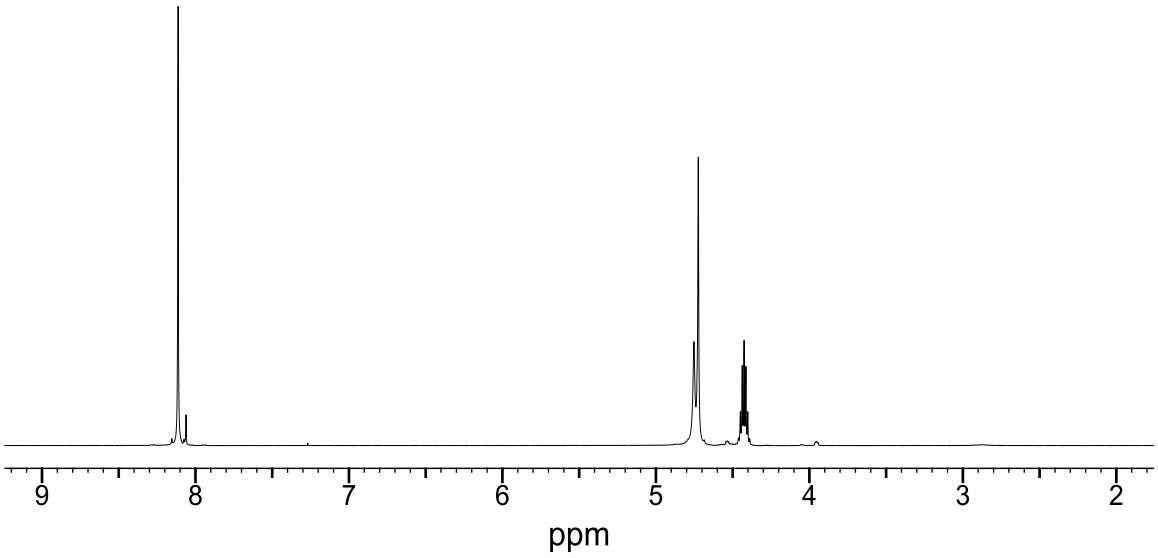

Figure 6.2 – ^{1}H NMR spectrum of E187.

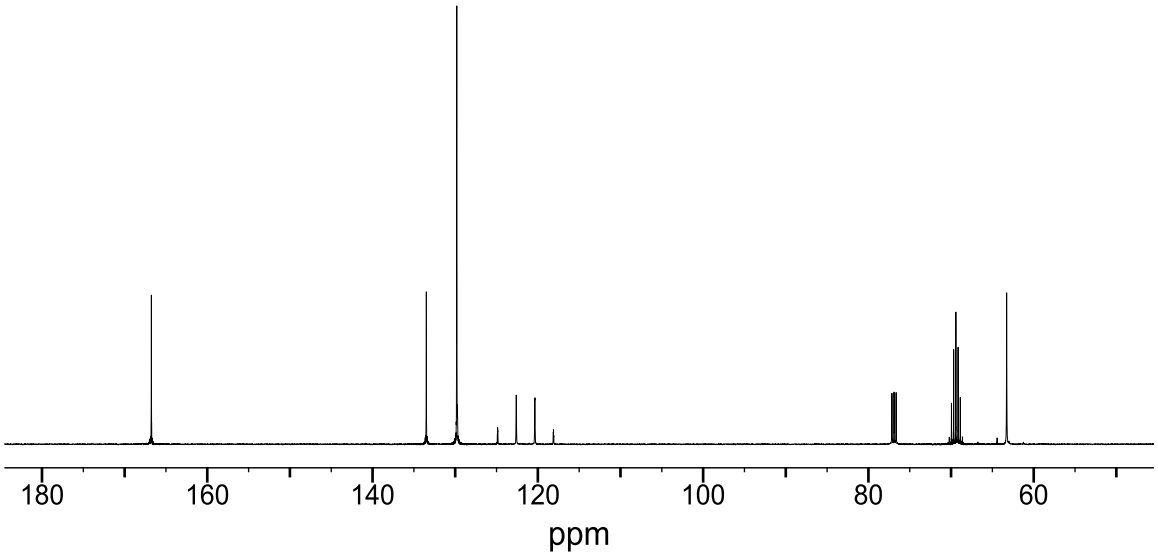

Figure 6.3 – ^{13}C NMR spectrum of E187.

The thermal behaviour of the three types of PET was investigated by DSC and TGA. A sample of the DSC scans showing the T_g, crystallisation peak, melting point and degradation peak is shown in figure 6.4 for PET E187. Table 6.1 shows the information obtained from all of the DSC scans.

All DSC scans for the other grades of PET are shown in the appendices (A6.1.5 to A6.1.7). The reheat scan from the heat-cool-reheat cycle was used to obtain the T_g and the melting point. The literature states the T_g of PET to be 70 ^oC and the melting point to be 265 ^oC. [7] PET E187 has a T_g of 78 ^oC and a melting point of 253 ^oC, which are fairly close to the values stated in the literature. The values of the three polymers used in this study have very similar thermal properties. This allowed the optimal extrusion parameters outlined in Chapter 3 to be used for all of the polymer grades, which makes comparisons between different conditions possible.

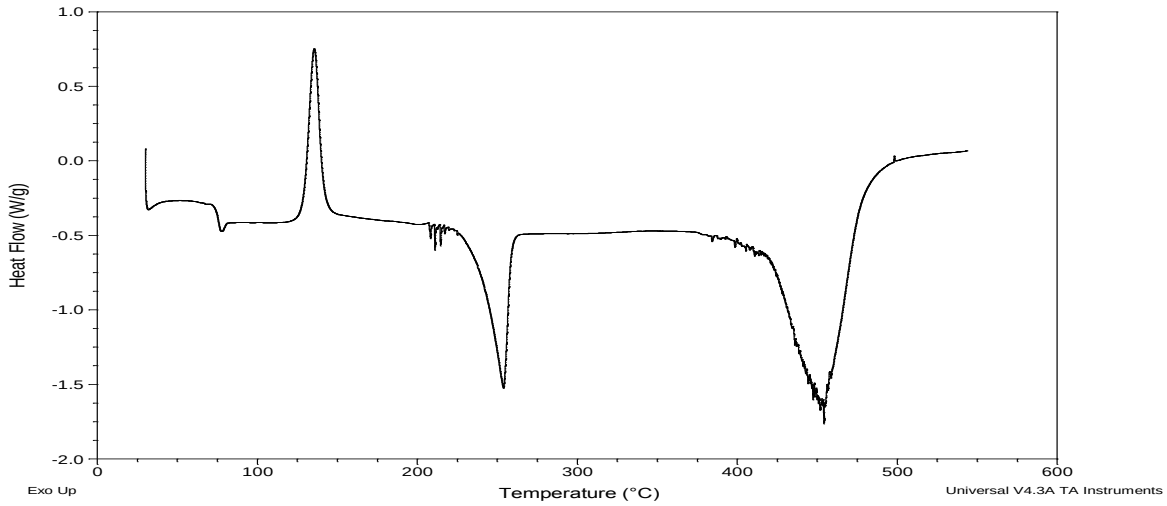

Figure 6.4 – DSC scan showing the transitions of E187.

Table 6.1 – Data from the DSC scans of PET.

	E187	E239	E240
Glass Transition / ^oC	74	74	75
Crystallisation Temperature / ^oC	130	127	136
Enthalpy of Crystallisation / J/g	30	26	31
Melting Point / ^oC	257	256	253
Enthalpy of Fusion / J/g	45	39	43
Onset of Degradation / ^oC	400	403	N/A
Degradation Peak / ^oC	445	441	N/A

Like the DSC scans, all of the TGA thermograms for the different PET samples are very similar. A sample of the TGA thermogram obtained is shown in figure 6.5. All other TGA thermograms can be seen in the appendices section (A6.1.8 to A6.1.9). The mass loss, onset of degradation and the peak temperature for degradation are all similar and can be seen in table 6.2 for all PET samples. The onset of thermal degradation temperature of the PET samples obtained from the TGA thermograms are very similar to the values obtained from the DSC. What is noticed from the TGA results is that the E239 sample has a slightly lower mass loss than E187 and E240 which is a result of the presence of TiO_2.

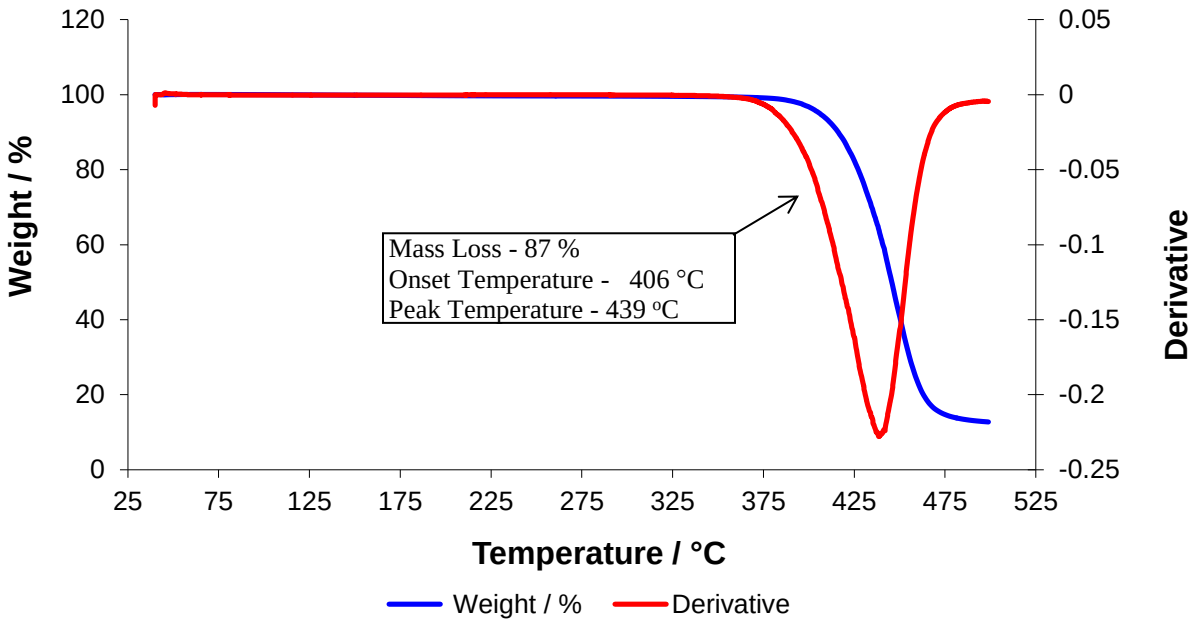

Figure 6.5 –TGA thermogram of PET E187.

Table 6.2 – Data from the TGA thermograms of PET.

Sample	Mass Loss %	Onset of Degradation °C	Degradation Peak Temperature °C
E187	87	406	439
E239	80	403	431
E240	84	408	489

6.2.2 Epoxide Concentration

One of the important factors to consider is the concentration of epoxide that is added into the extruder. The concentration is important because a sufficient amount needs to be added to successfully lower the number of carboxyl end groups of the PET. Excess should not be added as this increases the cost for raw materials, may impact the properties of the polymer such as molecular weight, and it has been suggested in the literature that chain extenders can increase the gel content produced in the samples. [10, 79 - 85 and 138]

The desired level of epoxide to add to the molten PET was determined based on both the feed rates that were calibrated and the rate the different epoxides fed out of the motorised liquid feed. Samples were prepared with E239 and epoxide concentrations of 0.5%, 1%, 2%, 4% and 6% by weight. The samples were prepared using the parameters outlined for the extruder in Chapter 3, and the carboxyl end group concentration of the samples were obtained using the Pohl titration method. Figure 6.6 shows the concentration of carboxyl end groups in PET samples prepared with different levels of Cardura. The carboxyl end group concentration decreases as the concentration of Cardura increases. The average end group concentration of the E239 samples is 17.63 equivalents per 10^6 grams, but the E239 + 6% Cardura has an end group concentration of 2.42 equivalents per 10^6 grams. There was no significant difference noticed in the end group concentration with additions of Cardura over 1%, since all of the end groups of the PET have been reacted. This confirms that the epoxide Cardura has a quick

enough reaction time when reacting with the carboxyl end groups of PET to occur in the extruder at DTF with the addition of a reasonable concentration.

Samples were also prepared using E187 and E240 with different levels of Cardura. Table 6.3 shows the end group concentrations for the PET samples prepared with Cardura. The same trend is noticed, where the carboxyl end group concentration reduces as the concentration of Cardura used increases. No significant difference was noticed in the end group concentration with the E187 samples after 2% of Cardura was added. The E239 samples did not change after 1%. This is due to the fact that this polymer has a lower initial carboxyl end group concentration compared to E187. The E240 sample required 1% w/w addition of Cardura to react with all of the carboxyl end groups that are present in the polymer sample, which is similar to the E239 polymer grade. This data indicates that the esterification reaction can be successfully carried out with a range of different PET grades at DTF.

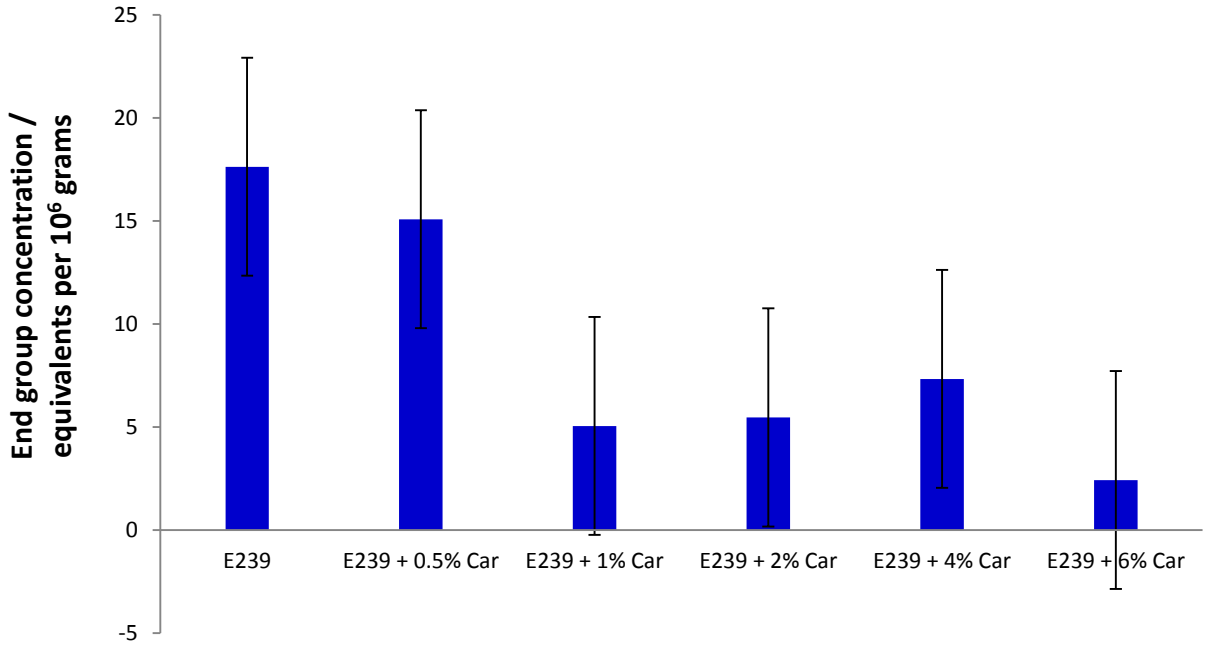

Figure 6.6 - Bar chart showing the average carboxyl end group concentration of the E239 samples obtained with the different Cardura concentrations. The error bar is the standard deviation of three repeats. N=3. The error bar is 5 equivalents per 10^6 grams which is the calculated error in the method.

Table 6.3 - Table showing the carboxyl end group concentration of the E187, E239 and E240 samples obtained with the different Cardura concentrations. The carboxyl end group concentration is the average of three repeats.

Cardura Concentration %	**E187** Equivalents per 10^6 grams	**E239** Equivalents per 10^6 grams	**E240** Equivalents per 10^6 grams
0.0	41.54	17.63	19.30
0.5	19.82	15.08	9.33
1.0	21.44	5.05	5.81
2.0	8.22	5.46	1.58
4.0	6.97	7.33	0.61
6.0	7.56	2.42	Not Detectable

The epoxide Heloxy was also prepared with the polymers E187, E239 and E240. All of the polymers were prepared with 1% and 6% by weight of the additive. E239 samples were also prepared with concentrations of 0.5%, 2% and 4%. The bar chart showing the end group concentration of the E239 samples with the different concentrations of Heloxy samples is

shown in figure 6.7. Table 6.4 shows the carboxyl end group concentrations for all of the polymer samples containing Heloxy.

Two of the sample sets show a decrease in the carboxyl end group concentration as the concentration of Heloxy increases. The average end group concentration of the E239 samples is 17.63 equivalents per 10^6 grams, but the E239 + 6% Heloxy has an end group concentration of 5.85 equivalents per 10^6 grams. This shows that the esterification reaction is occurring in the extruder, but less efficiently than Cardura. The samples prepared with E240 showed no significant reduction, which is expected to be a result of Heloxy not being as efficient as Cardura at end capping the polymer chains inside the extruder barrel. The data gathered from Chapters 4 and 5 supports the statement that Heloxy is not as reactive as Cardura. It is suggested as this epoxide is less reactive and is producing less consistent results it would be an undesirable choice for DTF to use in the manufacture of polymeric backsheets for solar cell panels.

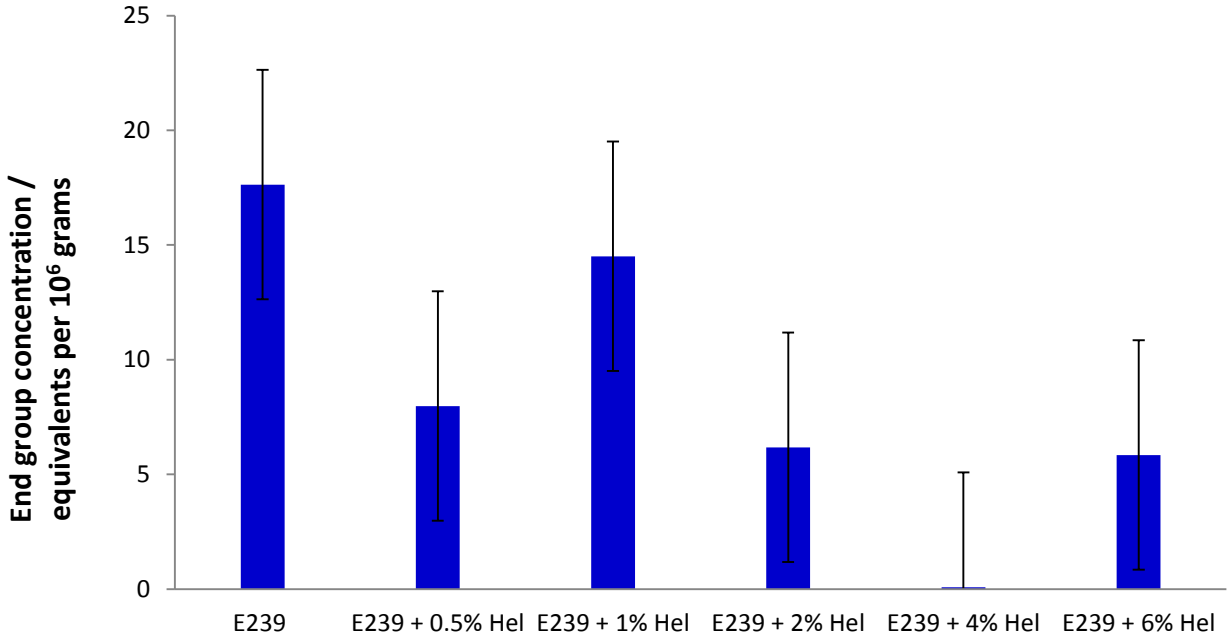

Figure 6.7 - Bar chart showing the average carboxyl end group concentration of the E239 samples obtained with the different levels of Heloxy. . N=3. The error bar is 5 equivalents per 10^6 grams which is the calculated error in the method.

Table 6.4 – Table showing the average carboxyl end group concentration of the E187, E239 and E240 samples obtained with the different levels of Heloxy. The carboxyl end group concentration is the average of three repeats.

Heloxy Concentration %	**E187** Equivalents per 10^6 grams	**E239** Equivalents per 10^6 grams	**E240** Equivalents per 10^6 grams
0.0	41.54	17.63	19.30
1.0	26.25	14.50	22.17
6.0	17.28	5.85	19.29

E187, E239 and E240 were also prepared with 1% and 6% Vikolox, and the E239 samples were also prepared with concentrations of 0.5%, 2% and 4%. A reduction in the carboxyl end group concentration was noticed in the E187 samples. The average end group concentration of the E187 samples was 41.54 equivalents per 10^6 grams, but the E187 + 6% Vikolox had an end group concentration of 18.02 equivalents per 10^6 grams. This reduction in the carboxyl end group concentration shows that the esterification reaction is occurring in the extruder. The E239 and E240 samples show no significant difference in the carboxyl end group concentration

due to the high error value. This epoxide was shown to be less reactive in Chapters 4 and 5. The bar chart showing the end group concentration of the E239 samples with the different concentrations of Heloxy is shown in figure 6.8. Table 6.5 shows the carboxyl end group concentrations for the E187 and E240 samples with Vikolox. The insignificant change noticed makes this an unsuitable choice for DTF to use in the manufacture of backsheets for solar cell panels.

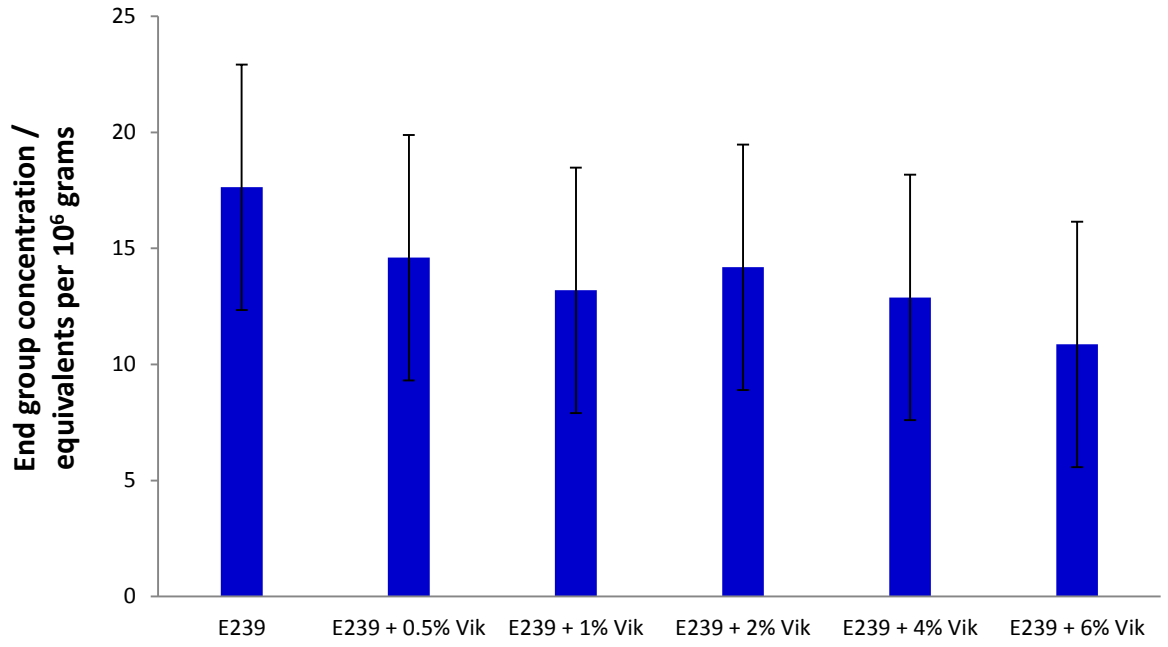

Figure 6.8 - Bar chart showing the average carboxyl end group concentration of the E239 samples obtained with the different levels of Vikolox. N=3. The error bar is 5 equivalents per 10^6 grams which is the calculated error in the method.

Table 6.5 – Table showing the average carboxyl end group concentration of the E187, E239 and E240 samples obtained with the different levels of Vikolox. The carboxyl end group concentration is the average of three repeats.

Vikolox Concentration %	**E187** Equivalents per 10^6 grams	**E239** Equivalents per 10^6 grams	**E240** Equivalents per 10^6 grams
0.0	41.54	17.63	19.30
1.0	23.71	13.19	22.96
6.0	18.02	10.87	20.02

All of the above trends were confirmed by analysing several of the above samples by the Ma *et. al.* NMR method. The values obtained were shown to be similar to the carboxyl end group concentrations obtained by the Pohl titration method. The carboxyl end group concentrations obtained using the Ma *et. al* NMR method can be seen on the accompanying disc in the folder *Chapter 6* under *Epoxide Concentration*.

The esterification reaction between PET and the three epoxides has been shown to occur in the extruder. Cardura was the most effective at end capping PET so was deemed a suitable candidate for DTF to use as an end capping additive for PET in solar cell applications. The fact that Cardura was the most effective end capping agent is based on the low concentrations required to end cap PET and the fast reaction time. Several research groups have studied various epoxides to determine the most reactive epoxides to participate in reactive extrusion. [66-75] For example Xanthos *et. al* examined the reactive extrusion process with different modifiers including N, N'-bis[3(carbo-2',3'-epoxypropoxy) phenyl] pyromellitimide, triglycidyl isocyanurate and tetraglycidyl diamine diphenyl methane. [66] The research group found that the tri functional and tetra functional epoxides were more reactive. The difference in reactivity is due to how strained the epoxide rings are and how stable the intermediates formed are. The work by other research groups focuses on multi functionalised epoxides instead of mono functionalised epoxides like Cardura, Heloxy and Vikolox. [66-75]

For an additive such as Cardura to be successfully used by DTF it should not have deleterious effects on the polymer's molecular weight and the gel content produced. The IV of some samples was also obtained to investigate changes in the molecular weight. Table 6.6 shows the IV data obtained for the different polymer samples with Cardura. There is little effect on the IV with the addition of 1% but a significant reduction is noticed with the 6% w/w addition of Cardura. The reduction with the 6% w/w sample is due to the liquid epoxide diluting the polymer. The epoxide would be used by DTF at levels around 1% w/w, as it has been shown above that any higher concentration would be an excess.

Table 6.6 – Table showing the IV data for the E187 E239 and E240 samples obtained with the different levels of Cardura. A single sample was analysed.

Cardura Concentration %	**E187 IV** dl/gm	**E239 IV** dl/gm	**E240 IV** dl/gm
0.0	0.58	0.72	0.76
1.0	0.57	0.73	0.70
6.0	0.49	0.59	0.61

It has been reported in the literature that epoxides added can cause extensive cross linking to occur in polymer samples. [10, 79 - 85 and 138] The percentage of gel content in the E239 samples with different concentrations of Cardura was determined using the method described in Chapter 3. The percentage gel content in the samples is shown in the bar chart in figure 6.9. The results obtained show no significant changes in the gel content produced for samples containing up to 4% Cardura. The error in the experiment was very high but does allow for large changes in the gel content to be determined. An increase in the percentage gel content is noticed in the E239 + 6% Cardura sample, which is due to the Cardura causing cross linking to occur by reacting with hydroxyl groups that are present in the polymer chain. There were no

significant changes noticed in the E187 samples containing Cardura as the E187 samples have a higher carboxyl end group concentration, meaning there is less excess epoxide available for other possible reactions, such as etherification. The experiment has a high error value and may not be sensitive enough to detect very small changes in the gel content produced. The gel contents produced for the E187 and E239 samples are shown in table 6.7.

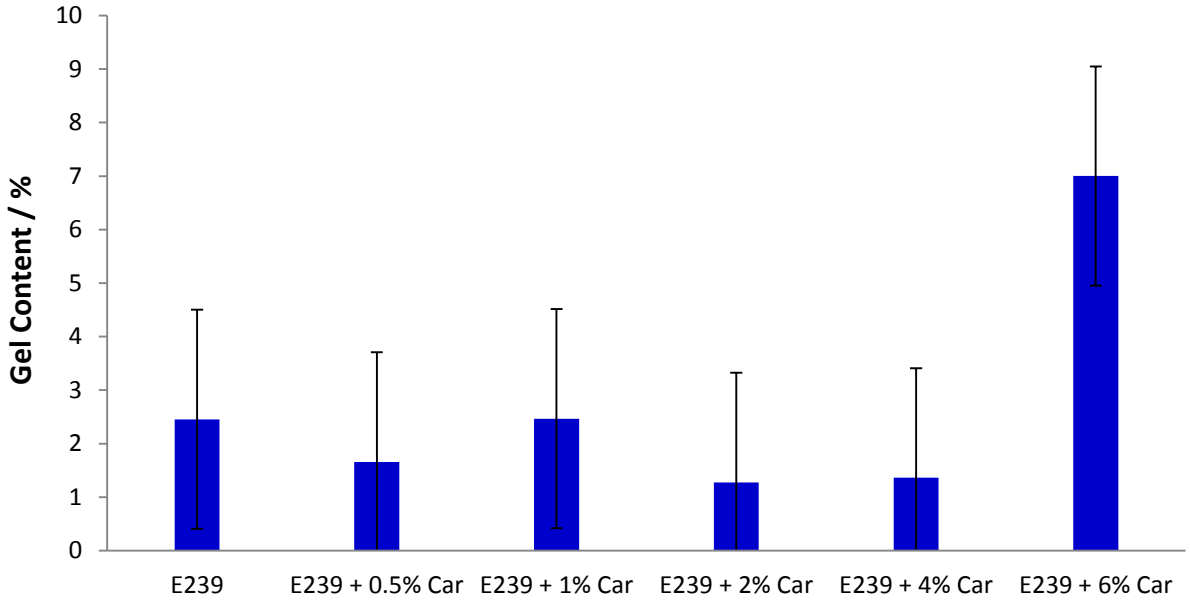

Figure 6.9 - Bar chart showing the average percentage gel content for the E239 samples obtained with the different levels of Cardura. N=3. The error bar is 1.81% which is the calculated error in the method.

Table 6.7 – Table showing the average percentage gel content for the E239 samples obtained with the different levels of Cardura. The percentage gel is the average of three repeats.

Cardura Concentration %	**E187 Gel Content** %	**E239 Gel Content** %
0.0	1.21	2.46
0.5	1.52	1.66
1.0	1.36	2.47
2.0	1.24	1.28
4.0	1.23	1.36
6.0	1.18	7.00

The percentage gel content in the E187, E239 and E240 samples containing different concentrations of Vikolox and Heloxy were also investigated. Tables 6.8 and 6.9 show the percentage gel content for the polymer samples containing Heloxy and Vikolox for the E239 and E187 polymers respectively. No significant changes were noticed in the percentage gel for any of the samples.

Table 6.8 - Table showing the average percentage gel content for the E239 samples obtained with the different levels of epoxides. The percentage gel is the average of three repeats.

Epoxide Concentration %	**E239 + Cardura Gel Content** %	**E239 + Heloxy Gel Content** %	**E239 + Vikolox Gel Content** %
0.0	2.46	2.46	2.46
0.5	1.66	1.60	1.04
1.0	2.47	0.81	1.06
2.0	1.28	1.50	1.11
4.0	1.36	1.76	2.95
6.0	7.00	0.92	4.63

Table 6.9 - Table showing the percentage gel content for the E187 samples obtained with the different levels of epoxides. The percentage gel is the average of three repeats.

Epoxide Concentration %	**E187 + Cardura Gel Content** %	**E187 + Heloxy Gel Content** %	**E187 + Vikolox Gel Content** %
0.0	1.21	1.21	1.21
1.0	1.36	0.00	0.85
6.0	1.18	0.21	1.39

The melting points of the E239 samples with different Cardura concentrations were calculated to see if any trends were noticed. DTF do not want any changes in the melting points or crystallisation behaviour as this could affect the processing conditions of the samples. Tables

6.10 to 6.12 show the average melting points obtained using both the initial and reheat scans of the DSC program, crystallisation temperature and enthalpy of fusion. The initial melting points for all of the polymer types are higher than the melting points obtained from the reheat scans. This is because the thermal history is lost and after crystallisation the melting point is sharper.

There are no changes in the melting point for any of the samples that were obtained for the samples with the increasing Cardura concentration. There is a slight reduction noticed in the reheat scan for the E187 and E240 polymers that have different levels of Cardura, but too small a change to suggest that it is significant. No changes were noticed in the crystallisation temperature or the enthalpy of fusion, which confirms that the epoxide Cardura is having no significant effect on the melting point and crystallisation behaviour. This is important as the additive used in the manufacture of backsheets for solar cell panels cannot affect the other parameters, as this could affect the manufacture of the polymer and also the properties in it's final applications.

Table 6.10 - Table summarising the data from the DSC scans for the E239 + Cardura samples. A single sample was analysed.

Epoxide Concentration %	Initial		Cooling		Reheat		
	Tm / ^oC	ΔH / Jg^{-1}	Tc / ^oC	ΔH / Jg^{-1}	Tg / ^oC	Tm / ^oC	ΔH / Jg^{-1}
0.0	255	40	190	39	78	253	34
0.5	254	38	184	41	78	251	33
1.0	254	40	184	35	76	250	34
2.0	254	41	184	43	79	251	34
4.0	253	39	183	41	77	250	35
6.0	247	42	194	47	71	246	34

Table 6.11 - Table summarising the data from the DSC scans for the E187 + Cardura samples. A single sample was analysed.

Epoxide Concentration %	Initial		Cooling		Reheat		
	Tm / °C	ΔH / Jg^{-1}	Tc / °C	ΔH / Jg^{-1}	Tg / °C	Tm / °C	ΔH / Jg^{-1}
0.0	258	40	193	38	77	253	34
0.5	254	42	181	42	75	252	36
1.0	256	43	191	41	76	252	34
2.0	253	40	185	37	74	249	33
4.0	253	43	184	41	73	248	34
6.0	253	42	183	39	72	247	33

Table 6.12 - Table summarising the data from the DSC scans for the E240 + Cardura samples. A single sample was analysed.

Epoxide Concentration %	Initial		Cooling		Reheat		
	Tm / °C	ΔH / Jg^{-1}	Tc / °C	ΔH / Jg^{-1}	Tg / °C	Tm / °C	ΔH / Jg^{-1}
0.0	253	41	183	41	79	251	36
1.0	251	42	175	49	80	249	37
6.0	251	43	182	42	70	247	36

6.2.3 Extrusion Stability

Processing temperature is extremely important in extrusion, particularly in reactive extrusion as it has been shown that significant degradation can occur to PET during the process. [10, 16 and 141] It was therefore essential that DTF was aware if the additives promote thermal and/or mechanical degradation inside the extruder barrel. This was investigated in three ways - by increasing the barrel temperature, increasing the samples residence time of the samples and increasing the shear rate.

6.2.3.1 Increasing the Extruder Temperature

The optimal barrel temperature profile discussed in Chapter 3 is referred to as T1 in table 6.13. T1 is the lowest temperature profile that allowed the polymer to be fully molten by the time it reached the open port / liquid feed for the epoxide additive. Samples were prepared using

higher barrel temperature profiles to investigate if the additives were adversely affected by different temperature profiles. The temperature profiles investigated are shown in table 6.13.

Table 6.13– Table showing the extrusion temperature profiles used.

Heating Zone	T1 / °C	T2 / °C	T3 / °C	T4 / °C
1	240	250	260	270
2	270	280	290	300
3	280	290	300	310
4	280	290	300	310
5	285	295	305	315

A slight increase is noticed in the concentration of carboxyl end groups in the E239 samples that were prepared with higher temperatures. The high error associated with calculating the carboxyl end group concentration using a titration method makes this increase insignificant. The bar chart showing the E239 samples extruded at different temperatures is shown in figure 6.10. The same trend was noticed for the E240 samples heated with the different temperatures, and the data is shown in table 6.14. Finally the E187 samples were prepared using the different temperature profiles outlined in table 6.13. The carboxyl end group concentrations of the E187 samples prepared at different temperatures are shown in table 6.15. This sample set shows a significant increase in the carboxyl end group concentrations for samples that were prepared at a higher temperature profile. The carboxyl end group concentration rose from 42 equivalents per 10^6 grams when prepared using temperature profile T1, but increased to 70.18 equivalents per 10^6 grams with temperature profile T4. The E187 has a lower molecular weight than the others, resulting in the initial carboxyl end group concentrations of this polymer being higher than the E239 and E240 polymers. When polymer samples with higher carboxyl end group concentrations are extruded at considerably higher temperatures the high carboxyl end group concentration acts like a catalyst to further increase the carboxyl end group concentration. [10, 42-43 and 50-53] Investigation shows that even with a short residence time of approximately 75 seconds, significant thermal degradation is occurring at higher processing temperatures. This is why temperature profile 1 was used as the standard

temperature profile - to ensure the temperature is high enough to melt the polymer by the time it reached the open port, but as low as possible to minimise the thermal degradation.

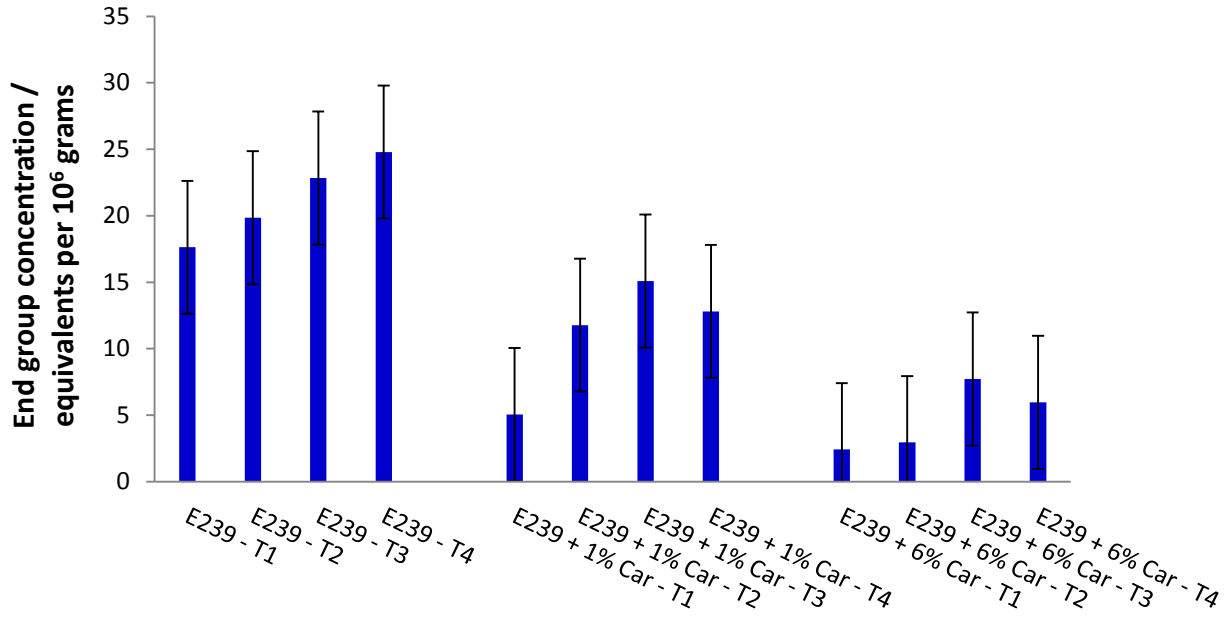

Figure 6.10 - Bar chart showing the average end group concentration of the E239 samples obtained at different temperature profiles. T1 – T4 refers to the temperature profile in table 6.13 used to prepare the samples. N=3. The error bar is 5 equivalents per 10^6 grams which is the calculated error in the method.

Table 6.14 – Table showing the average end group concentration of the E240 samples obtained at different temperature profiles. T1 – T4 refers to the temperature profile in table 6.13 used to prepare the samples. The carboxyl end group concentration is the average of three repeats.

Temperature Profile	**E240** Equivalents per 10^6 grams	**E240 + 1% Cardura** Equivalents per 10^6 grams
T1	19.30	5.81
T2	14.18	3.01
T3	24.25	3.91
T4	22.43	9.33

Table 6.15 – Table showing the average end group concentration of the E187 samples obtained at different temperature profiles. T1 – T4 refers to the temperature profile in table 6.12 used to prepare the samples. The carboxyl end group concentration is the average of three repeats.

Temperature Profile	E187 Equivalents per 10^6 grams	E187 + 1% Cardura Equivalents per 10^6 grams
T1	41.54	4.18
T2	47.67	28.26
T3	46.60	28.70
T4	70.18	52.56

The E239 + 1% Cardura, E239 + 6% Cardura and E240 + 1% Cardura samples that have been prepared at different temperatures show no significant changes in the carboxyl end group concentrations. The E187 + 1% Cardura samples prepared at different temperatures have a more noticeable difference in the carboxyl end group concentration as the temperature profile increases. Like the E187 samples prepared at different temperatures a significant increase was noticed with the E187 + 1% Cardura sample heated with different temperature profiles. This increase is due to the higher initial carboxyl end group concentration acting as a catalyst to promote degradation as discussed in Chapter 1. [10, 42-43 and 50-53]

The IV measurement of some of the polymer samples prepared at different temperature profiles were obtained to see if the data indicated any significant changes. Tables 6.16 to 6.18 show the IV data for the E239, E187 and E240 samples. There is a slight reduction noticed in the IV when going from samples prepared at T1 to T4. This is due to thermal degradation occurring inside the extruder as the samples are prepared. This has been noticed to occur significantly in the literature. No significant differences were noticed in the samples with and without Cardura, suggesting that Cardura is not having adverse effects on the degradation process, making it a possibly useful additive to be used in the manufacture of solar cell backsheets. The IV for the E187 and E240 samples follow a similar trend. There are some samples, such as the E240 sample prepared using temperature profile 2 that gave an IV of 0.929 dl/gm, which were higher than expected. Some further work would be beneficial to obtain more samples to support the data obtained. The results for the IV measurements overall support the conclusions from the

carboxyl end group concentration data that the presence of Cardura is having no adverse effects on the processing parameters of PET.

Table 6.16– Table showing the IV data for the E239 samples, T1 – T4 refers to the temperature profile in table 6.12 used to prepare the samples. A single sample was analysed.

Temperature Profile	E239 IV dl/gm	E239 + 1% Cardura IV dl/gm
T1	0.720	0.731
T2	0.719	0.718
T3	0.703	0.707
T4	0.660	0.665

Table 6.17 – Table showing the IV data for the E187 samples, T1 – T4 refers to the temperature profile in table 6.12 used to prepare the samples. A single sample was analysed.

Temperature Profile	E187 IV dl/gm	E187 + 1% Cardura IV dl/gm
T1	0.578	0.572
T2	0.623	0.567
T3	0.629	0.547
T4	0.575	0.573

Table 6.18 – Table showing the IV data for the E240 samples, T1 – T4 refers to the temperature profile in table 6.12 used to prepare the samples. A single sample was analysed.

Temperature Profile	E240 IV dl/gm	E240 + 1% Cardura IV dl/gm
T1	0.762	0.698
T2	0.929	0.725
T3	0.735	0.622
T4	0.689	0.737

The percentage of gel content in the E239 samples prepared at different temperature profiles was calculated using the method described in Chapter 3. The percentage gel content in the E239 samples is shown in the bar chart in figure 6.11. The samples of E239 prepared using the different temperature profiles in table 6.13 show no significant changes. There were also no changes noticed in the percentage of gel content for the E239 samples containing Cardura. The epoxide Cardura is the most reactive and would be expected to cause cross linking to occur by the formation of secondary reactions. The lack of changes suggests that no significant secondary reactions are occurring that would cause production issues and contamination.

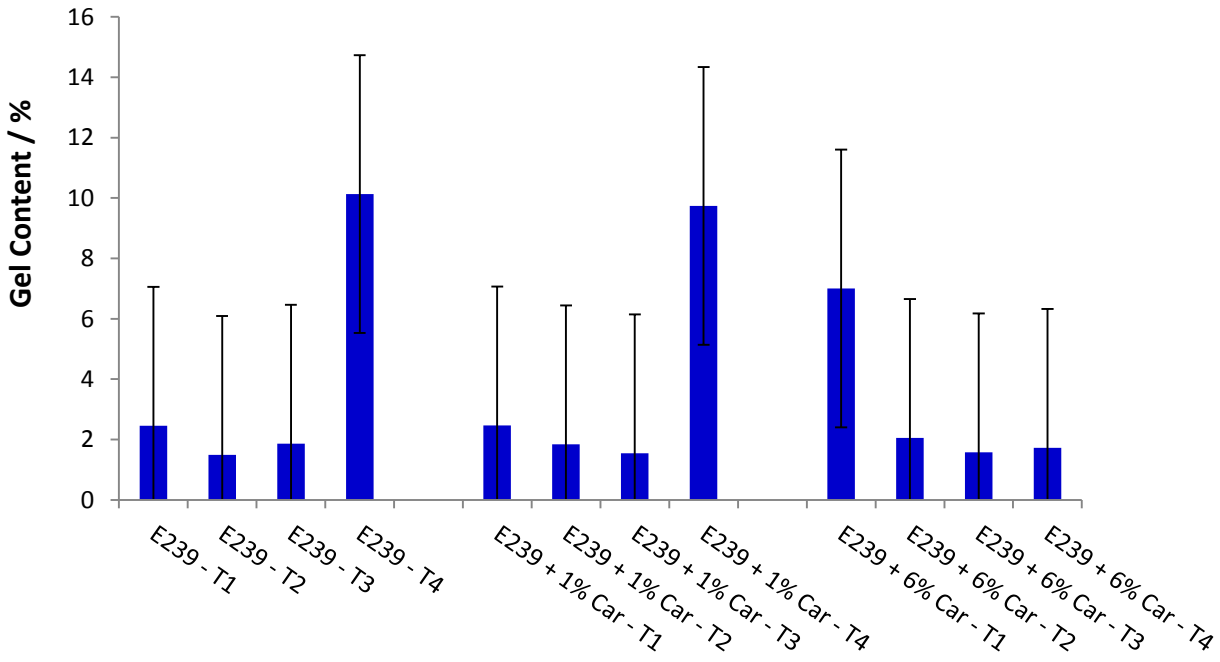

Figure 6.11 - Bar chart showing the average end group concentration of the E239 samples obtained at different temperature profiles, T1 – T4 refers to the temperature profile in table 6.12 used to prepare the samples. N=3. The error bar is 1.81% which is the calculated error in the method.

The average melting points of the E239 samples that were prepared using a different temperature profile can be seen in tables 6.19 and 6.20. The initial melting points for the samples are again higher than the melting points obtained for the reheat scans due to the thermal history being lost in the initial heating, which is due to the crystallisation peak being sharper during the reheat scan.

There are no changes in the melting point for any of the E187 and E239 samples prepared using a different temperature profile. For example, the E239 sample prepared using temperature profile 4 has a melting point of 252 ^{o}C and the E239 + 1% Cardura prepared at the same conditions has a melting point of 251 ^{o}C. All of the samples prepared with different temperature profiles were also analysed by DSC to obtain the crystallisation temperature. The crystallisation temperature was monitored to see if there is a change in crystallisation behaviour as a result of chain scission or cross-linking. No changes were noticed in the crystallisation temperature in the samples prepared at different process temperatures, indicating that there is no significant thermal degradation occurring. This suggests that the additive Cardura is not promoting degradation in the extruder barrel during processing, therefore it meets the requirements mentioned by DTF. The thermal degradation of the samples containing Cardura will be studied in more detail during Chapter 8.

Table 6.19 – Table showing the melting points (initial and reheat), crystallisation temperature and enthalpy of fusion for the E239 samples, T1 – T4 refers to the temperature profile in table 6.12 used to prepare the samples. A single sample was analysed.

Epoxide Concentration %	Initial		Cooling		Reheat		
	Tm / ^{o}C	ΔH / Jg^{-1}	Tc / ^{o}C	ΔH / Jg^{-1}	Tg / ^{o}C	Tm / ^{o}C	ΔH / Jg^{-1}
E239 /T1	255	40	189	39	78	253	34
E239 /T2	254	37	185	43	79	252	30
E239 /T3	255	35	186	43	79	251	33
E239 /T4	255	39	186	42	80	251	32
E239 + 1% Car / T1	254	40	184	35	76	250	34
E239 + 1% Car / T2	254	42	183	41	80	251	32
E239 + 1% Car / T3	255	39	184	42	80	251	33
E239 + 1% Car / T4	254	40	186	42	78	251	35

Table 6.20 – Table showing the melting points (initial and reheat), Crystallisation temperature and enthalpy of fusion for the E187 samples, T1 – T4 refers to the temperature profile in table 6.12 used to prepare the samples. A single sample was analysed.

Epoxide Concentration %	Initial		Cooling		Reheat		
	Tm / °C	ΔH / Jg^{-1}	Tc / °C	ΔH / Jg^{-1}	Tg / °C	Tm / °C	ΔH / Jg^{-1}
E187 /T1	258	40	193	38	77	253	34
E187 /T2	255	42	185	42	78	252	35
E187 /T3	255	43	184	44	82	252	35
E187 /T4	255	45	183	44	78	252	36
E187 + 1% Car / T1	256	43	191	41	76	252	34
E187 + 1% Car / T2	253	45	178	41	77	250	35
E187 + 1% Car / T3	254	42	179	41	77	251	36
E187 + 1% Car / T4	254	43	178	40	77	251	35

6.2.3.2 Increasing the Residence Time

The extruder residence time is approximately 75 seconds for the standard experiment. To increase the residence time on the PRISM – TSE 16TC twin screw extruder significantly, the barrel is filled with polymer and the screws are then stopped. The samples were left in the barrel for the desired length of time. The chosen residence times that were investigated were 5, 10, 20 and 40 minutes. The screws were started up again and the first 15 seconds of extrudate were collected.

There were no significant changes in the carboxyl end group concentrations of the E239 samples which had been prepared with the longer residence times using the standard temperature profile,T1. Figure 6.12 shows the data for the E239 samples. The same trend can be seen in the E187 and E240 samples prepared with different residence times. The data is shown in tables 6.21 to 6.22 respectively. The E239 sample held in the barrel for 5 minutes gave an average carboxyl end group concentration of 14.68 equivalents per 10^6 grams, but the sample held in the barrel for 40 minutes gave an average carboxyl end group concentration of 29.30 equivalents per 10^6 grams. There were no significant changes noticed for the E239 samples that were prepared using temperature profile 2. There was a slight increase due to thermal degradation occurring in the E239 samples that were prepared using temperature

profile 3. This is shown due to a significant increase in the carboxyl end group concentration for these samples compared to the carboxyl end group concentration of the samples prepared using temperature profiles 1 and 2. The E240 samples follow a similar trend as higher residence times and higher temperatures start causing significant changes in the carboxyl end group concentration due to thermal degradation. There is the occasional data point that does not follow the trend, such as the sample prepared with a 20 minute residence time with temperature profile 3, which has a higher carboxyl end group concentration than the sample prepared with a residence time of 40 minutes. Some further repeats would be beneficial to strengthen the data gathered. The carboxyl end group concentrations obtained for the E187 samples show a similar trend as there is no significant difference in most of the samples prepared with temperature profiles 2 and 3 except for the two samples with a residence time of 40 minutes. The increase is due to thermal degradation occurring more significantly than in the solid state polymerised samples due to the higher initial carboxyl end group concentration acting as a catalyst for the degradation as discussed in Chapter 1.

Most of the E239 samples prepared at temperature profile 4 with various residence times have a similar end group concentration to the samples prepared using temperature profile 3. The carboxyl end group concentration obtained for the E239 sample prepared using temperature profile 4 with a residence time of 40 minutes inside the barrel is 133.54 equivalents per 10^6 grams, which is almost double the carboxyl end group value for the samples prepared with a lower residence time. The same trend was noticed with the E187 and E240 samples. The data is shown in tables 6.21 and 6.22 respectively.

The presence of Cardura lowered the carboxyl end group concentration in all samples prepared at the different conditions. The trends noticed for the samples containing 1% and 6% Cardura are still the same, for example there was no significant difference in any of the different residence times at any of the temperature profiles noticed for the E239 + 1% Cardura samples except the sample prepared at temperature profile 4 with a residence time of 40 minutes. The lack of a noticeable increase in the carboxyl end group concentration shows that the Cardura is

not promoting thermal degradation inside the extruder barrel. This is an important factor as any chosen additive by DTF cannot have any significant effect on the manufacturing of the polymer.

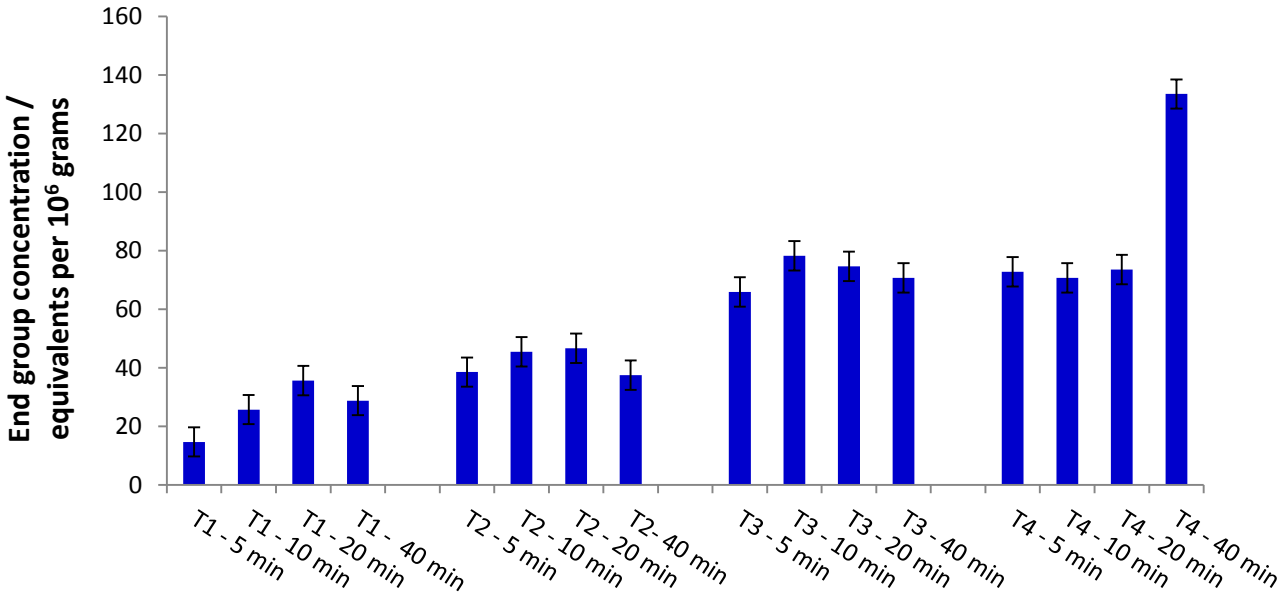

Figure 6.12 - Bar chart showing the average end group concentration of the E239 samples obtained at different residence times, T1 – T4 refers to the temperature profile in table 6.12 used to prepare the samples. N=3. The error bar is 5 equivalents per 10^6 grams which is the calculated error in the method.

Table 6.21– Table showing the end group concentrations for the E187 samples, T1 – T4 refers to the temperature profile in table 6.12 used to prepare the samples. The carboxyl end group concentration is the average of three repeats.

Sample	E187 Equivalents per 10^6 grams	E187 + 1% Cardura Equivalents per 10^6 grams
T1 – 05 min	38.62	21.58
T1 – 10 min	42.15	29.89
T1 – 20 min	32.74	73.64
T1 – 40 min	39.33	22.61
T2 – 05 min	20.24	15.48
T2 – 10 min	35.31	17.89
T2 – 20 min	32.20	26.71
T2 – 40 min	54.61	43.79
T3 – 05 min	30.22	24.19
T3 – 10 min	26.87	37.38
T3 – 20 min	65.42	N/A
T3 – 40 min	89.25	85.05
T4 – 05 min	51.75	39.64
T4 – 10 min	50.71	65.50
T4 – 20 min	39.22	72.14
T4 – 40 min	151.37	156.86

Table 6.22– Table showing the end group concentrations for the E240 samples, T1 – T4 refers to the temperature profile in table 6.12 used to prepare the samples. The carboxyl end group concentration is the average of three repeats.

Sample	E240 Equivalents per 10^6 grams	E240 + 1% Cardura Equivalents per 10^6 grams
T1 – 05 min	17.74	6.18
T1 – 10 min	25.27	7.05
T1 – 20 min	27.78	4.61
T1 – 40 min	33.64	27.81
T2 – 05 min	29.49	40.45
T2 – 10 min	35.70	16.57
T2 – 20 min	60.75	16.26
T2 – 40 min	52.06	44.37
T3 – 05 min	63.48	16.70
T3 – 10 min	64.74	34.83
T3 – 20 min	106.18	26.95
T3 – 40 min	63.71	53.05
T4 – 05 min	45.94	58.26
T4 – 10 min	133.45	65.98
T4 – 20 min	25.94	73.34
T4 – 40 min	160.69	33.72

The IV data for the E239, E239 + 1% Cardura and E239 + 6% Cardura samples that had a residence time of 40 minutes inside the extruder barrel which were heated using temperature profile 1 are shown in table 6.23. The IVs for E239 and E239 + 1% Cardura are significantly lower than the optimal processing conditions outlined in Chapter 3, suggesting that thermal degradation is occurring. The sample of E239 + 6% Cardura has an even lower IV, which is due to the excess Cardura diluting the polymer sample. Care would have to be taken by DTF to ensure that the additive was not in excess to ensure this behaviour on the viscosity of the polymer was prevented.

Table 6.23 – Table showing the IV data for the E239, E239 + 1% Cardura and E239 + 6% Cardura samples held for 40 minutes inside the extruder barrel, T1 refers to the temperature profile in table 6.13 used to prepare the samples. A single sample was analysed.

Sample	IV dl/gm
E239 – T1 – 40 min	0.662
E239 + 1% Cardura – T1 – 40 min	0.659
E239 + 6% Cardura – T1 – 40 min	0.484

.

The percentage of gel content in the E239 samples prepared with different residence times are shown in the bar chart in figure 6.13. There is a slight increase in the percentage gel content for the E239 and E239 + 1% Cardura prepared with different residence times but the E239 + 6% Cardura samples do not increase, suggesting that the presence of Cardura may inhibit gel formation. No significant changes were noticed for the E240 samples prepared with different residence times, even when increasing the temperature profile. The percentage gel content of the E240 samples can be seen in table 6.24. This again highlighted that the epoxide Cardura would be a suitable choice for end capping the PET chains to improve the polymer's resistance to hydrolytic degradation, because if issues arise during the extrusion process resulting in it being stopped the residence time can increase quickly. Gel particles have been shown to be very difficult to remove from the extruder, and this data shows Cardura is not promoting the

formation of these particles. [16] It was expected that when Cardura was in excess, because it is so reactive, that etherification reactions could occur and build up more complex structures than desired. It was highlighted that side reactions were possibly occurring at temperatures lower than the processing temperatures of PET in Chapter 4.

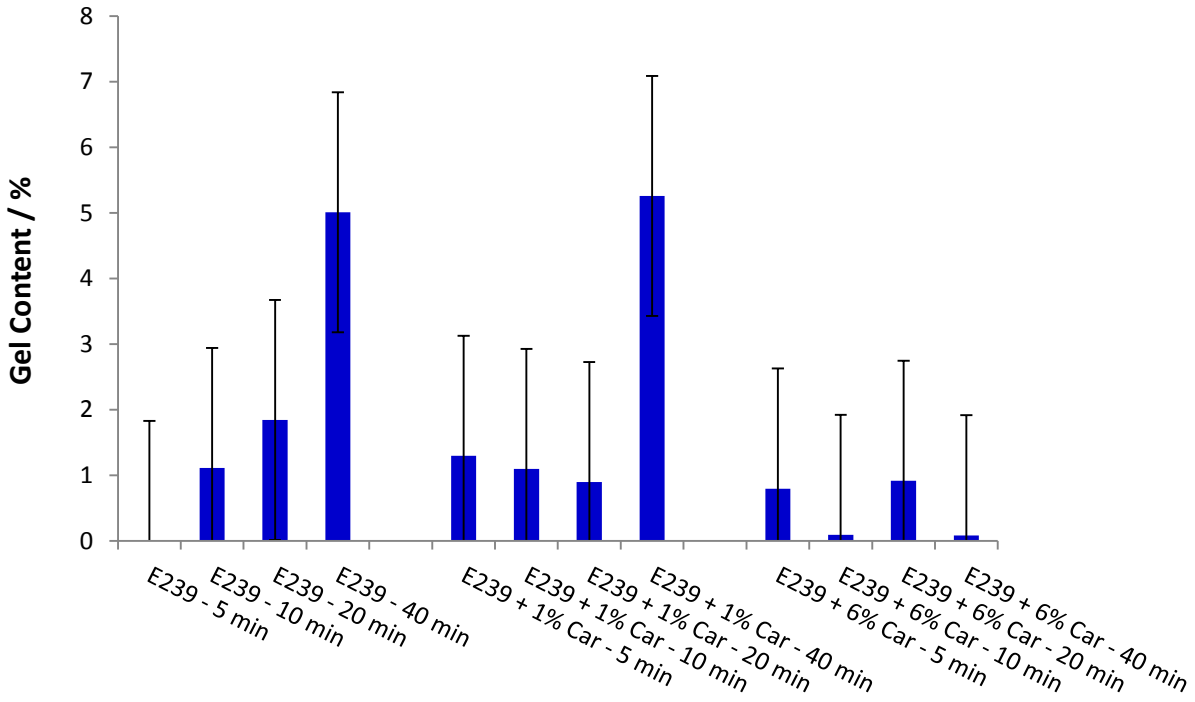

Figure 6.13 - Bar chart showing the average percentage gel content of the E239, E239 + 1% Cardura and E239 + 6% Cardura samples prepared with different residence times. N=3. The error bar is 1.81% which is the calculated error in the method.

Table 6.24 – Table showing the average gel content of the E240 samples. T1- T4 refers to the temperature profile in table 6.12 used to prepare the samples. The gel content is the average of three repeats.

Sample	E240 Gel Content %	E240 + 1% Cardura Gel Content %
T1 – 05 min	0.74	0.78
T1 – 10 min	1.25	0.37
T1 – 20 min	0.61	0.72
T1 – 40 min	0.48	1.19
T2 – 05 min	0.00	0.51
T2 – 10 min	0.65	0.37
T2 – 20 min	0.49	0.84
T2 – 40 min	0.61	0.56
T3 – 05 min	0.75	0.00
T3 – 10 min	2.70	0.29
T3 – 20 min	1.00	0.74
T3 – 40 min	1.04	0.37
T4 – 05 min	0.91	0.64
T4 – 10 min	2.46	1.24
T4 – 20 min	1.30	1.26
T4 – 40 min	0.91	0.84

There were no changes in the melting points of the E187 and E239 samples prepared with different residence times. Tables 6.25 and 6.26 show the average melting points obtained using both the initial and reheat scans of the DSC program. As with all of the other samples, the initial melting points are higher than the melting points obtained from the reheat scans. There were no significant changes noticed in the crystallisation and melting points, confirming that no degradation was occurring inside the extruder barrel when the samples were being processed.

The data obtained from the DSC scans of the E187 and E239 samples that contain 1% w/w of Cardura indicated that no thermal degradation is occurring in the samples. There was no significant difference between the samples with and without 1% Cardura at the residence times studied. If degradation was occurring there would be changes in the melting point, enthalpy of

fusion and crystallisation temperature. There were no significant changes noticed in the enthalpy of fusion and crystallisation temperature of the E239 + 6% Cardura samples. There was a slight decrease in the melting point, which dropped from 252 ^{o}C for the E239 sample held in the barrel for 5 minutes using temperature profile T1, to 246 ^{o}C for the E239 + 6% Cardura sample prepared at the same temperature. Further work would have to be carried out to confirm as the change is very subtle. The fact that very few changes are occurring, even in the samples where Cardura is significantly in excess, results in the additive being considered a highly attractive option to be added to PET to improve the hydrolytic degradation of the samples for external use.

Table 6.25 –Table showing the melting points (initial and reheat), crystallisation temperature and enthalpy of fusion for the E239 samples. All samples were processed using temperature profile T1. A single sample was analysed.

Epoxide Concentration %	Initial		Cooling		Reheat		
	Tm / ^{o}C	ΔH / Jg^{-1}	Tc / ^{o}C	ΔH / Jg^{-1}	Tg / ^{o}C	Tm / ^{o}C	ΔH / Jg^{-1}
E239 – 05 min	254	39	186	41	80	252	33
E239 – 10 min	255	38	186	41	80	252	31
E239 – 20 min	255	38	187	43	79	252	32
E239 – 40 min	254	40	188	42	79	252	32
E239 + 1% Cardura – 05 min	254	38	185	41	79	251	32
E239 + 1% Cardura – 10 min	254	40	183	41	77	250	32
E239 + 1% Cardura – 20 min	254	38	186	44	78	251	32
E239 + 1% Cardura – 40 min	253	38	186	44	78	251	31
E239 + 6% Cardura – 05 min	249	52	185	46	73	246	38
E239 + 6% Cardura – 10 min	250	45	156	45	73	246	38
E239 + 6% Cardura – 20 min	249	46	184	45	73	246	36
E239 + 6% Cardura – 40 min	248	46	187	46	70	246	38

Table 6.26 – Table showing the melting points (initial and reheat), crystallisation temperature and enthalpy of fusion for the E187 samples. All samples were processed using temperature profile T1. A single sample was analysed.

Epoxide Concentration %	Initial		Cooling		Reheat		
	Tm / °C	ΔH / Jg^{-1}	Tc / °C	ΔH / Jg^{-1}	Tg / °C	Tm / °C	ΔH / Jg^{-1}
E187 – 05 min	255	42	184	44	79	252	35
E187 – 10 min	256	43	188	43	79	252	33
E187 – 20 min	256	43	186	43	79	252	35
E187 – 40 min	256	45	191	45	79	253	36
E187 + 1% Cardura – 05 min	254	43	183	40	77	251	34
E187 + 1% Cardura – 10 min	254	41	179	39	76	250	35
E187 + 1% Cardura – 20 min	254	43	183	43	79	250	35
E187 + 1% Cardura – 40 min	254	44	184	43	79	251	35

6.2.3.3 Increasing the Shear

Inside the extruder barrel there is a gap between the barrel wall and the flights of the screw. It has been shown in the literature that as the gap decreases the temperature of the melt goes up due to shear heating. It was decided that the best way to alter this parameter was by increasing the screw speed as it increases the volume of material inside the barrel that is being forced through this narrow gap, altering the shear that the samples will be exposed to. [10 and 141] The speed of the screws on the PRISM – TSE 16TC twin screw extruder was changed to alter the shear occurring inside the extruder. The speeds of the screws that were selected included 75, 100, 150 and 200 rpm. The E187 samples were also prepared at 50 rpm but the two solid state polymerised samples were rising out of the open port too much for the additive to be added due to the increased volume of material inside the barrel. It is noted that the residence time decreases as the screw speed increases.

The bar chart in figure 6.14 and table 6.27 shows the carboxyl end group concentration for the samples that have been prepared with increased levels of shear at each of the different temperature profiles. The data shows that there is no significant change in the carboxyl end

group concentration of the E239 samples that were prepared with different levels of shear at temperature profile 1. For example, the E239 sample prepared at a speed of 75 rpm gave an average carboxyl end group concentration of 13.11 equivalents per 10^6 grams, and the sample prepared with a speed of 200 rpm gave an average carboxyl end group concentrations of 11.43 equivalents per 10^6 grams. The same trend was seen with the E187 and E240 sample sets.

The samples of E239 prepared with different screw speeds at temperature profiles 2 and 3 showed no significant changes in the carboxyl end group concentration compared with the samples prepared at temperature profile 1. For example, the carboxyl end group concentration for the E239 sample prepared using temperature profile 1with a screw speed of 200 rpm was 11.43 equivalents per 10^6 grams, and the carboxyl end group concentration for the E239 sample prepared with the same screw speed at temperature profile 3 was 18.41 equivalents per 10^6 grams. There was also no significant difference noticed in the E187 and E240 sample sets, which can be seen in tables 6.28 and 6.29, respectively.

The samples prepared with temperature profile 4 have a significant change in the carboxyl concentration for higher screw speeds. The E239 sample prepared with temperature profile 1 at a speed of 200 rpm gave an average carboxyl end group concentration of 11.43 equivalents per 10^6 grams, and the sample prepared with a speed of 200 rpm using temperature profile 4 gave an average carboxyl end group concentration of 49.38 equivalents per 10^6 grams. This shows that increased shear causes significant thermal degradation to occur at higher temperatures despite the faster screw speed reducing the residence times inside the extruder barrel.

There was no significant change in the carboxyl end group concentration for all of the samples prepared with 1% or 6% Cardura with different screw speeds and different temperature profiles. For example, the E239 + 6% Cardura sample prepared at a speed of 75 rpm with temperature profile 1 gave an average carboxyl end group concentration of 9.56 equivalents per 10^6 grams, and the E239 +6% Cardura sample prepared at a speed of 200 rpm using temperature profile 4 gave an average carboxyl end group concentration of 19.28 equivalents

per 10^6 grams. The lower initial carboxyl end group concentration in the samples with Cardura protected the samples from thermal degradation when processed with high temperatures and high shear. The mechanism for thermal degradation is discussed in Chapter 1.

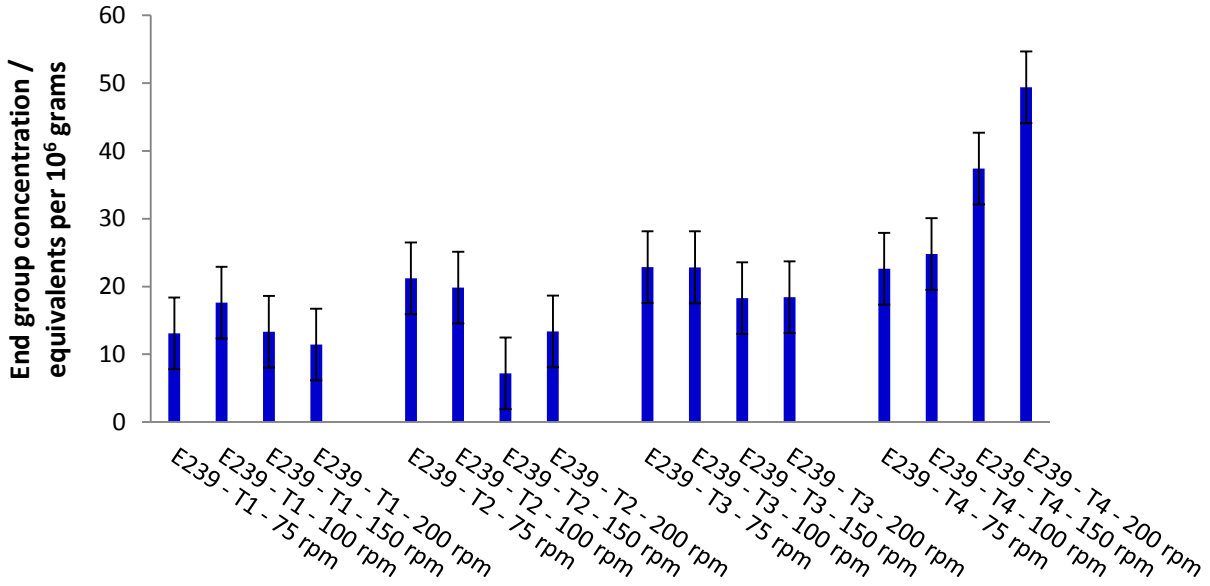

Figure 6.14 - Bar chart showing the average end group concentration of the E239 samples obtained with higher levels of shear carried out at different temperature profile. N=3. The error bar is 5 equivalents per 10^6 grams which is the calculated error in the method.

Table 6.27 – Table showing the average carboxyl end group concentration for the E239 samples at different temperature profiles. The carboxyl end group concentration is the average of three repeats.

Sample	E239 Equivalents per 10^6 grams	E239 + 1% Cardura Equivalents per 10^6 grams	E239 + 6% Cardura Equivalents per 10^6 grams
T1 – 075 rpm	13.11	28.32	9.56
T1 – 100 rpm	17.63	5.05	2.42
T1 – 150 rpm	13.33	16.00	2.47
T1 – 200 rpm	11.43	18.82	Not Detectable
T2 – 075 rpm	21.21	18.86	1.04
T2 – 100 rpm	19.85	11.78	2.95
T2 – 150 rpm	7.17	4.87	4.30
T2 – 200 rpm	13.36	4.43	3.42
T3 – 075 rpm	22.86	5.26	3.38
T3 – 100 rpm	22.84	15.09	7.73
T3 – 150 rpm	18.29	5.37	Not Detectable
T3 – 200 rpm	18.41	6.02	3.49
T4 – 075 rpm	22.64	7.95	5.01
T4 – 100 rpm	24.80	12.81	5.97
T4 – 150 rpm	37.41	9.26	16.03
T4 – 200 rpm	49.38	9.81	19.28

Table 6.28 – Table showing the average carboxyl end group concentration for the E187 samples at different temperature profiles. The carboxyl end group concentration is the average of three repeats.

Sample	**E187** Equivalents per 10^6 grams	**E187+ 1% Cardura** Equivalents per 10^6 grams
T1 – 050 rpm	29.15	2.96
T1 – 075 rpm	33.78	Not Detectable
T1 – 100 rpm	41.54	4.18
T1 – 150 rpm	30.86	6.79
T1 – 200 rpm	29.75	6.11
T2 – 050 rpm	32.70	13.46
T2 – 075 rpm	30.15	7.38
T2 – 100 rpm	47.67	28.26
T2 – 150 rpm	28.31	5.14
T2 – 200 rpm	26.87	10.13
T3 – 050 rpm	25.90	21.61
T3 – 075 rpm	27.87	10.63
T3 – 100 rpm	46.60	28.70
T3 – 150 rpm	36.27	10.33
T3 – 200 rpm	21.73	14.92
T4 – 050 rpm	30.65	17.05
T4 – 075 rpm	30.90	15.04
T4 – 100 rpm	70.18	52.56
T4 – 150 rpm	37.07	10.84
T4 – 200 rpm	31.19	19.47

.

Table 6.29 – Table showing the average carboxyl end group concentration for the E240 samples at different temperature profiles. The carboxyl end group concentration is the average of three repeats.

Sample	E240 Equivalents per 10^6 grams	E240+ 1% Cardura Equivalents per 10^6 grams
T1 – 075 rpm	15.21	4.43
T1 – 100 rpm	19.30	5.81
T1 – 150 rpm	15.22	4.08
T1 – 200 rpm	16.62	5.34
T2 – 075 rpm	16.62	Not detectable
T2 – 100 rpm	14.18	3.01
T2 – 150 rpm	23.10	3.75
T2 – 200 rpm	22.04	6.01
T3 – 075 rpm	21.17	9.59
T3 – 100 rpm	24.25	3.91
T3 – 150 rpm	20.77	5.80
T3 – 200 rpm	13.82	16.22
T4 – 075 rpm	26.05	5.38
T4 – 100 rpm	22.43	9.33
T4 – 150 rpm	20.11	14.68
T4 – 200 rpm	22.47	8.67

IV measurements were performed on samples of E239, E187 and E240 prepared using temperature profile 1 with varying screw speeds. The results of this are shown in tables 6.30 to 6.32. The IV data obtained shows that there are no significant differences occurring between the samples by varying the level of shear. For example, the sample of E239 prepared with a screw speed of 75 rpm had an IV of 0.722 dl/gm, and the sample prepared at 200 rpm gave an IV of 0.721 dl/gm.

There was no significant change in the IV data obtained for the samples with 1% Cardura compared with the blank polymer. For example, the sample of E239 prepared using temperature profile 1 with a screw speed of 200 rpm gave an IV of 0.721 dl/gm and the sample with 1% Cardura prepared at the same conditions gave an IV of 0.714 dl/gm. The IV data for the

6% Cardura sample was significantly lower. As mentioned above this is due to the sample being diluted with the liquid additive.

Table 6.30 – Table showing the IV data for the E239 samples, T1 refers to the temperature profile in table 6.12 used to prepare the samples. A single sample was analysed.

Sample	E239 IV dl/gm	E239 + 1% Cardura IV dl/gm	E239 + 6% Cardura IV dl/gm
T1 – 075 rpm	0.722	0.700	0.575
T1 – 100 rpm	0.720	0.731	0.588
T1 – 150 rpm	0.709	0.739	0.593
T1 – 200 rpm	0.721	0.714	0.618

Table 6.31 – Table showing the IV data for the E187 samples, T1 refers to the temperature profile in table 6.12 used to prepare the samples. A single sample was analysed.

Sample	E187 IV dl/gm	E187 + 1% Cardura IV dl/gm
T1 – 075 rpm	0.581	0.545
T1 – 100 rpm	0.591	0.541
T1 – 150 rpm	0.590	0.541
T1 – 200 rpm	0.586	0.540

Table 6.32 – Table showing the IV data for the E240 samples, T1 refers to the temperature profile in table 6.12 used to prepare the samples. A single sample was analysed.

Sample	E240 IV dl/gm	E240 + 1% Cardura IV dl/gm
T1 – 075 rpm	0.761	0.750
T1 – 100 rpm	0.762	0.698
T1 – 150 rpm	0.768	0.762
T1 – 200 rpm	0.765	0.761

The gel content level was also measured for the E239 samples prepared at different temperature profiles with varying screw speeds. The percentage gel content in the samples is shown in the bar chart in figure 6.15 and table 6.33. There was only one sample which produced a significant difference, which was the sample of E239 processed using temperature profile 4 with a screw speed of 100 rpm. It was concluded that this was simply due to a higher error than normal. The same trend was noticed with samples that were prepared at the same conditions with 1% and 6% Cardura. This confirms that no adverse effects should occur using Cardura during various extrusion scenarios, making it an attractive option for DTF to use in the manufacture of backsheets for solar cell panels.

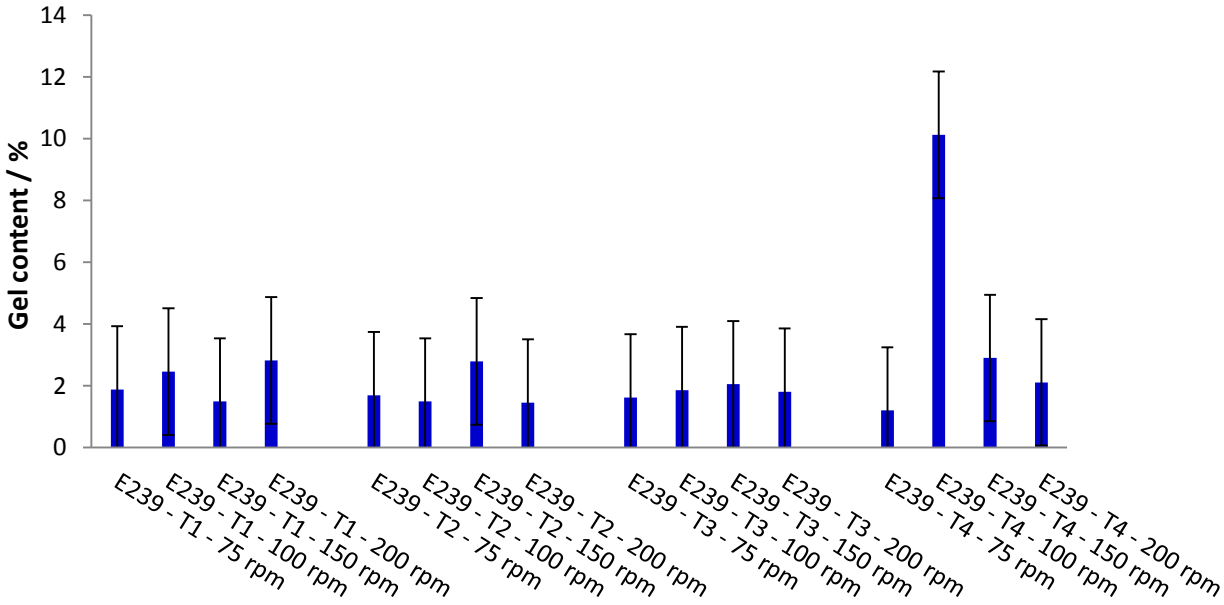

Figure 6.15 - Bar chart showing the average percentage gel content of the E239 samples obtained with different shear levels, T1 – T4 refers to the temperature profile in table 6.13 used to prepare the samples. N=3. The error bar is 1.81% which is the calculated error in the method

Table 6.33 – Table showing the average gel content for the E240 samples, T1 refers to the temperature profile in table 6.12 used to prepare the samples. The gel content is the average of three repeats.

Sample	E239 Gel Content %	E239 + 1% Cardura Gel Content %	E239 + 6% Cardura Gel Content %
T1 – 075 rpm	1.88	1.15	0.98
T1 – 100 rpm	2.46	2.47	7.00
T1 – 150 rpm	1.49	1.09	1.50
T1 – 200 rpm	2.82	0.84	0.72
T2 – 075 rpm	1.69	0.76	0.60
T2 – 100 rpm	1.49	1.84	2.05
T2 – 150 rpm	2.79	1.16	0.26
T2 – 200 rpm	1.45	0.00	0.86
T3 – 075 rpm	1.62	0.00	0.73
T3 – 100 rpm	1.86	1.54	1.58
T3 – 150 rpm	2.05	0.49	1.38
T3 – 200 rpm	1.81	0.08	1.82
T4 – 075 rpm	1.20	0.00	0.98
T4 – 100 rpm	10.13	9.77	1.72
T4 – 150 rpm	2.90	0.00	0.53
T4 – 200 rpm	2.11	0.00	0.47

6.3 Conclusions

The data collected above provides the conclusion that the epoxide Cardura can successfully be utilised in a reactive extrusion process as the reaction occurs sufficiently in the extruder with a residence time of only 78 seconds. To make the production of chain extended PET for solar cell panels commercially viable the additive must be manufactured on DTF's current processing lines, which can be set up cheaply for liquid addition to carry out the reactive extrusion process.

Cardura was shown to be the optimal epoxide to use because the esterification reaction is occurring significantly enough to lower the carboxyl end group concentration, reducing the impact of hydrolytic degradation on the polymer. No further reaction occurred with an increase in concentration of 2% of Cardura with E187 and only 1% additive with the solid state polymerised polymer samples. This low addition requirement means that the raw material

costs are kept at a minimum and the excess epoxide could not create complications, such as the epoxide leaching out of the polymer.

No significant differences were detected in the carboxyl end group concentration for the samples containing Cardura that were prepared at different temperature profiles, increased residence times and exposed to an increase in shear. This provides DTF with the confidence that the material will not cause adverse effects if the extrusion process is interrupted to troubleshoot any production problems arising.

One of the other requirements put forth by DTF was to ensure that the additive did not have any adverse effects on the polymer's properties, for example the molecular weight, molecular weight or crystallinity. The experiments carried out show that the Cardura is having no significant effect on the polymer. The gel content was not shown to increase; this could affect clarity, which is an important property in the manufacture of films. The IV was shown to decrease with the addition of 6% Cardura, which was described as being due to dilution effects. At 6% the epoxide is in excess and would not be used at this concentration in the manufacture of films for solar cell panels.

The esterification reaction occurring inside the extruder was less efficient with the epoxides Vikolox and Heloxy because they are less reactive. These two additives were deemed unsuitable due to them not reacting as well as Cardura at the temperature and residence times required by DTF to successfully manufacture the PET film.

7.0 Characterisation of the Degradation Behaviour of Extruded Materials - Hydrolytic Degradation

7.1 Introduction

PET has been shown in the literature to be quite resistant to attack by water, acids and bases under certain conditions. [7 and 14] It has this resistance due to its partial aromatic nature and the fact that the chains are tightly packed. At temperatures higher than the T_g hydrolytic degradation occurs. As with all types of degradation of PET, hydrolytic degradation produces carboxyl end groups. [15 - 17]

It has been suggested that as the number of carboxyl end groups increases during degradation there will be an increase in hydrophilicity and more water will penetrate into the system, giving the conditions for an autocatalytic reaction i.e. water and carboxylic acid end groups.

Chain extenders are the most commonly used additive with PET to increase the resistance to hydrolytic degradation by reacting with carboxylic acid end groups. Chain extenders that are used with PET include diisocyanates, dianhydrides and bis-oxazolines, but the most commonly used are the diepoxides. [22 and 32 - 35] The diepoxides can react with both the hydroxyl and carboxyl end groups of PET. However, they react with carboxyl end groups preferentially. [22] Japon *et al*. carried out experimental work to show that the esterification reaction is the most preferred as the reaction occurs quickly inside the extruder which is essential as the residence time in the extruder is short. [35] A significant amount of research has shown the importance of selecting an epoxide that will react to the desired level inside an extruder. [38 - 39].

The epoxides; Cardura, Heloxy and Vikolox were investigated for the end capping of PET in order to reduce the impact of hydrolytic degradation on the films used as backsheets in solar cells. A series of conditions were investigated with a range of samples. The range of samples also allowed the effect of solid state polymerisation on hydrolysis to be investigated.

7.2 Results and Discussion

7.2.1 Hydrolysis at room temperature

The polymers that were investigated had both a high initial carboxyl end group concentration (E187) and low initial carboxyl end group concentrations (E239 and E240). The E187 samples have an initial carboxylic end group concentration of 42 equivalents per 10^6 grams. The solid state polymerised samples E239 and E240 have carboxylic end group concentrations of 18 and 19 equivalents per 10^6 grams respectively. The polymers were also studied with different concentrations of the epoxides; Cardura, Heloxy and Vikolox. The concentrations of the epoxides investigated were 1% and 6%.

It is well known in the literature that acidic conditions can catalyse the hydrolytic degradation of the PET. [14 and 42] There was a concern that acidic degradation products from the polymer chain can cause the pH of the water to decrease. The pH of the water was monitored to ensure that this was not the case. This was achieved by placing 5 g of the extruded polymer samples into a round bottom flask with 100 ml of distilled water. The samples tested were E187, E187 + 1% Cardura, E239 and E239 + 1% Cardura. A Graham condenser was fitted to the flask and the water was allowed to reflux for the desired length of time. Samples were prepared for 1, 2, 3 and 4 days. The pH of the water was monitored. Figure 7.1 shows a scatter plot for the pH versus hydrolysis time. There was a significant reduction in the pH of water for all samples tested. It was decided that the water would be changed every two days to prevent it becoming acidic and catalysing the degradation reaction.

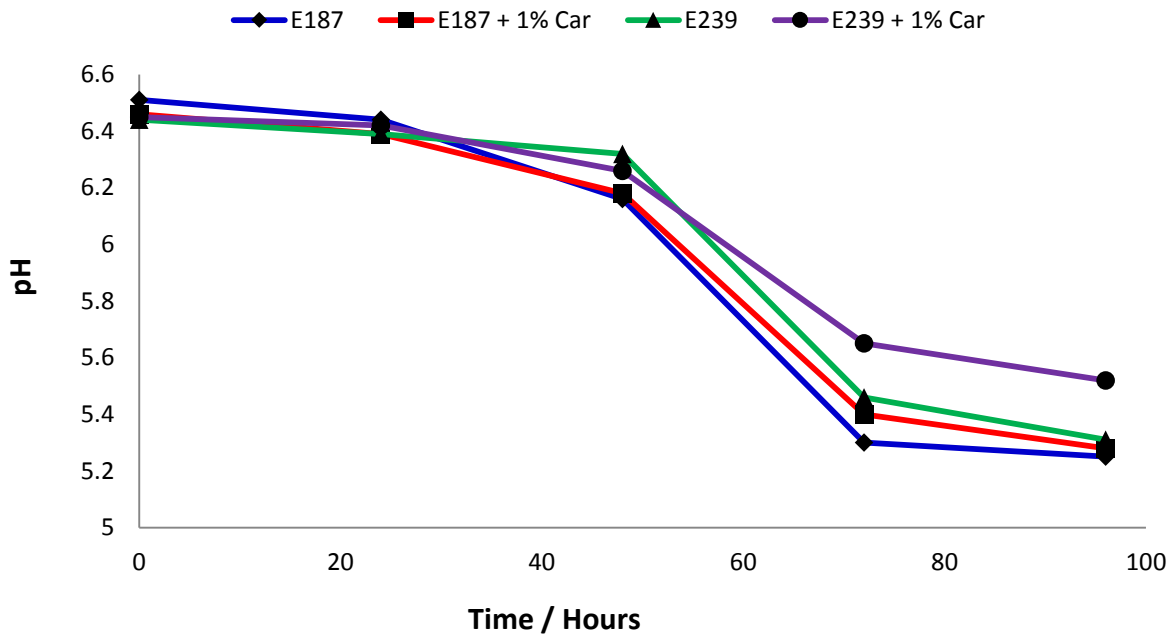

Figure 7.1 - Scatter plot for the pH versus hydrolysis time.

Figure 7.2 shows a scatter plot of the carboxyl end group concentration versus the time that samples were exposed to the conditions in order to promote hydrolysis. There was a significant reduction noticed in the carboxyl end group concentration of E187 samples that had been aged up to 14 days. The initial sample had a carboxyl end group concentration of 41.54 equivalents per 10^6 grams, and after being exposed to the conditions for hydrolysis for 3 days the carboxyl end group concentration was 25.44 equivalents per 10^6 grams. This reduction in carboxyl end group is expected to have been caused by low molecular weight oligomers, present from the polymerisation process, that are soluble in water. This would lower the pH as is seen in figure 7.1.

There was no additional significant change in the carboxyl end group concentration of the aged samples. This shows that hydrolytic degradation was not occurring in the sample under these ageing conditions. The same trend is noticed for the samples of E187 + 1% Cardura and E187 + 6% Cardura. The polymers E239 and E240 were also analysed with and without Cardura, and

similar trends were identified. The scatter plots for the E239 and E240 samples are shown in figures 7.3 and 7.4.

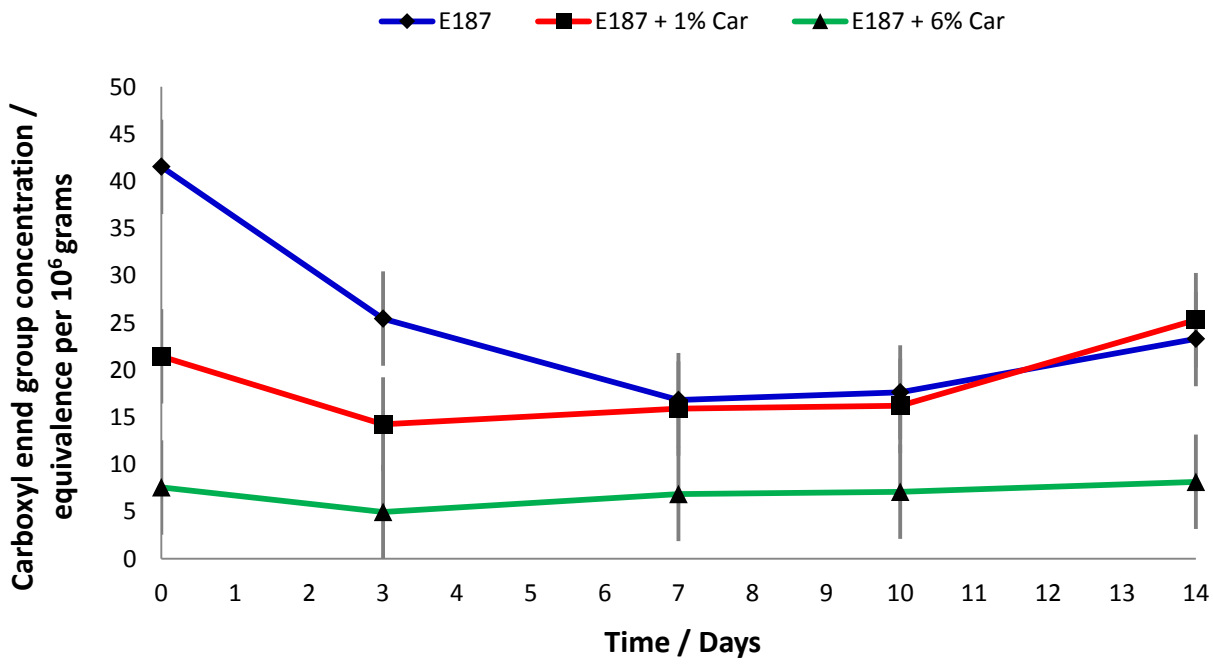

Figure 7.2 - Scatter plot for the average carboxyl end group concentration versus hydrolysis time for the E187 samples with Cardura aged at room temperature. N=3. The error bar is 5 equivalents per 10^6 grams which is the calculated error in the method.

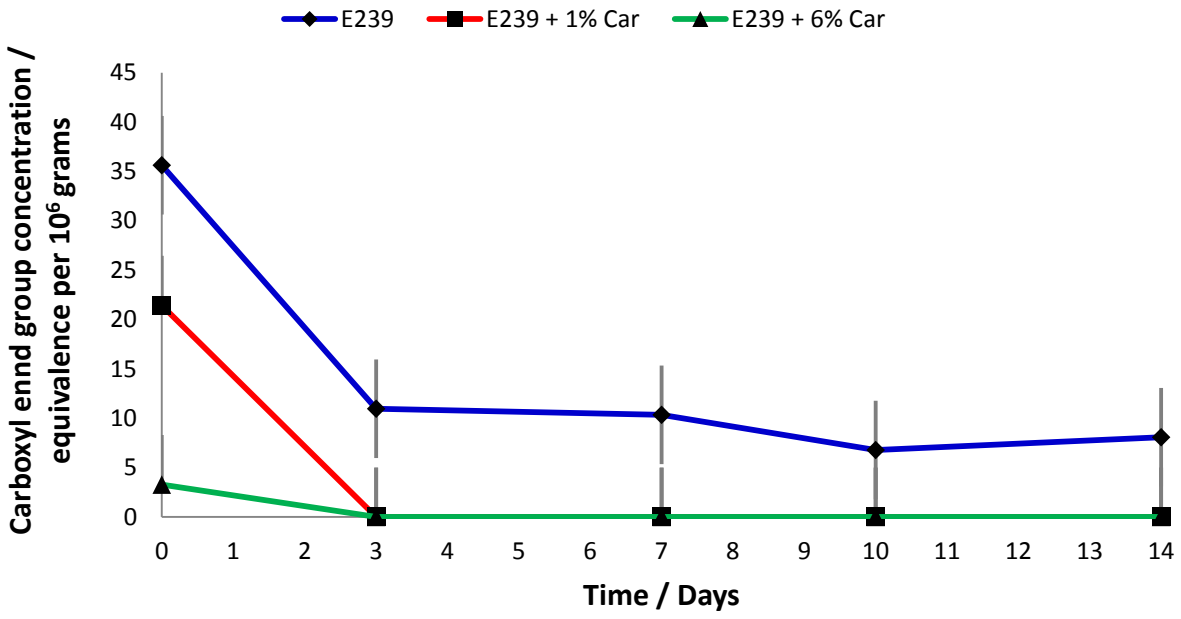

Figure 7.3 - Scatter plot for the average carboxyl end group concentration versus hydrolysis time for the E239 samples with Cardura aged at room temperature. N=3. The error bar is 5 equivalents per 10^6 grams which is the calculated error in the method.

.

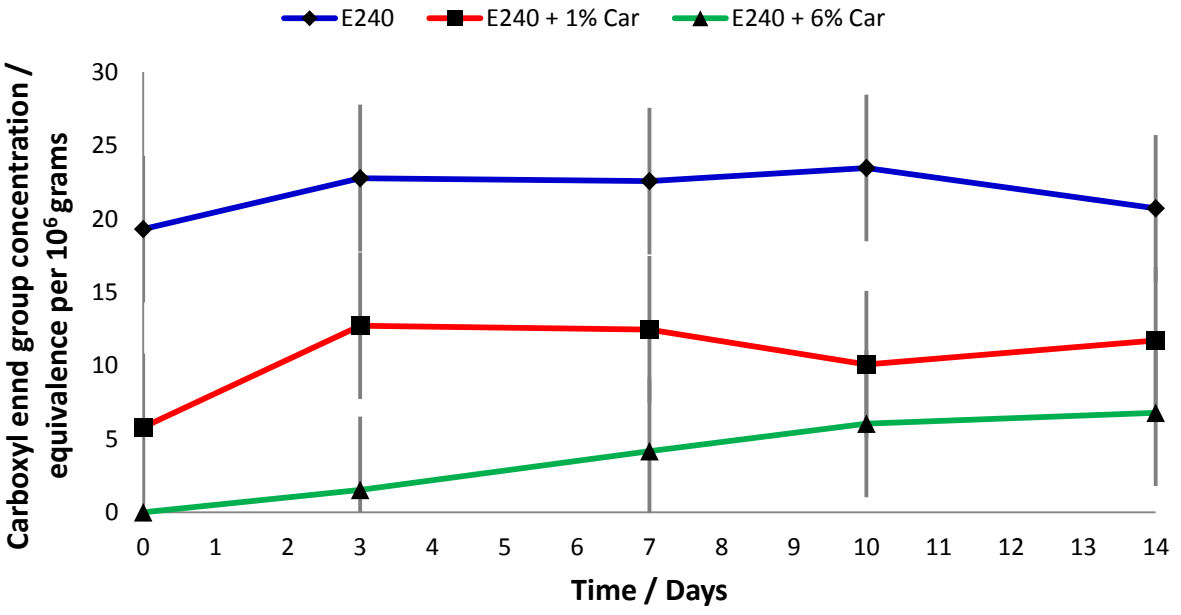

Figure 7.4– Scatter plot for the average carboxyl end group concentration versus hydrolysis time for the E240 samples with Cardura aged at room temperature. N=3. The error bar is 5 equivalents per 10^6 grams which is the calculated error in the method.

The polymers E187 and E240 were also investigated with the epoxides Vikolox and Heloxy. There were no significant changes in the E187 + 1% Vikolox and E187 + 6% Vikolox samples that had been aged up to 10 days. The initial sample of the E187 + 6% Vikolox had a carboxyl end group concentration of 18.02 equivalents per 10^6 grams, and after being exposed to the conditions for hydrolysis the carboxyl end group concentration was 17.14 equivalents per 10^6 grams. The same trend was also noticed for the E240 samples. There were no significant changes witnessed in the carboxyl end group concentration in any of the polymer samples that were prepared with 1% and 6% Heloxy samples. Scatter plots are shown in figures 7.5 and 7.6 for the E187 samples containing Vikolox and Heloxy respectively. Figures 7.7 and 7.8 are the scatter plots for the E240 samples containing Vikolox and Heloxy respectively.

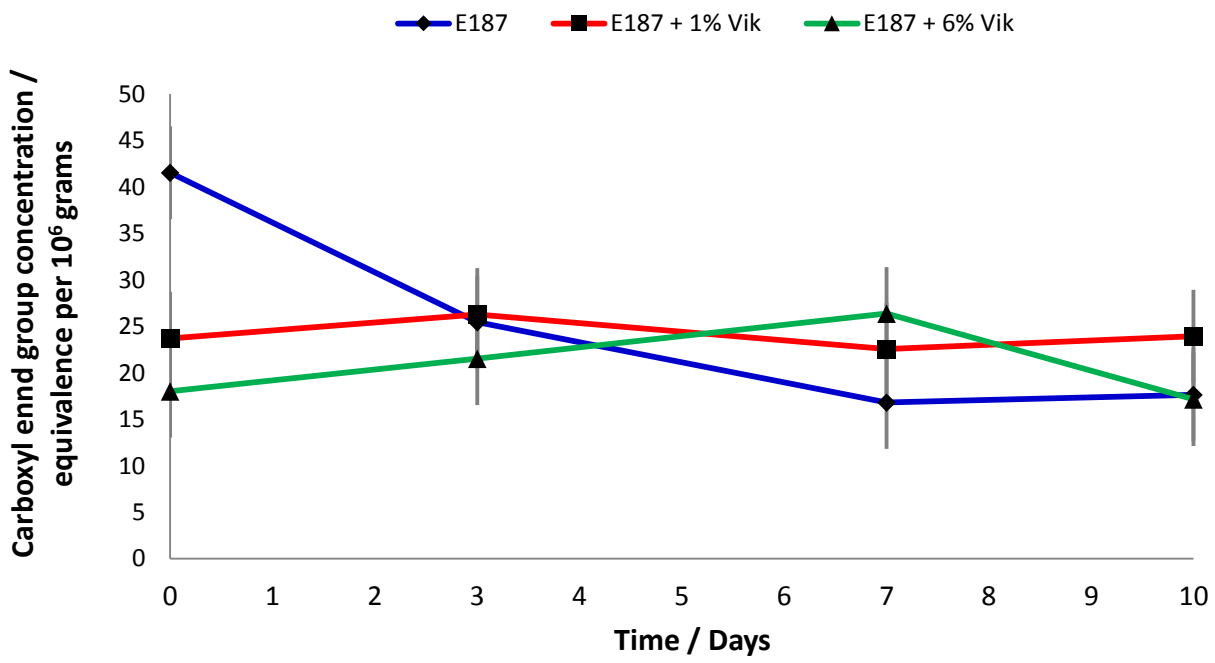

Figure 7.5 - Scatter plot for the average carboxyl end group concentration versus hydrolysis time for the E187 samples with Vikolox aged at room temperature. N=3. The error bar is 5 equivalents per 10^6 grams which is the calculated error in the method.

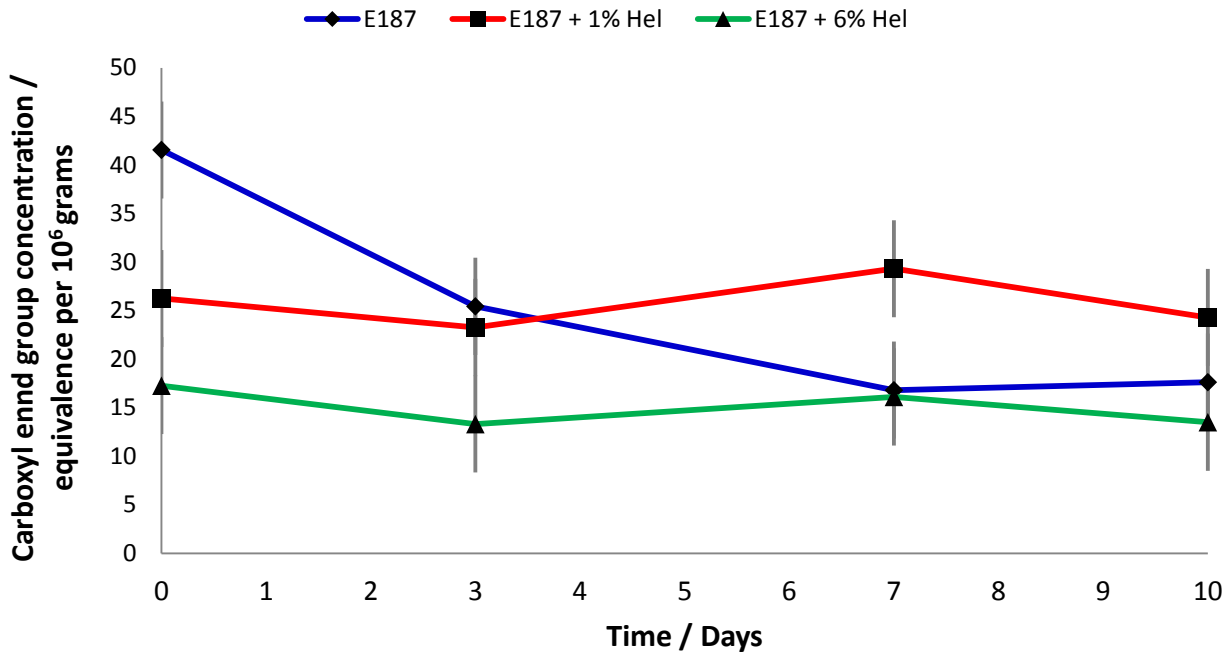

Figure 7.6 - Scatter plot for the average carboxyl end group concentration versus hydrolysis time for the E187 samples with Heloxy aged at room temperature. N=3. The error bar is 5 equivalents per 10^6 grams which is the calculated error in the method.

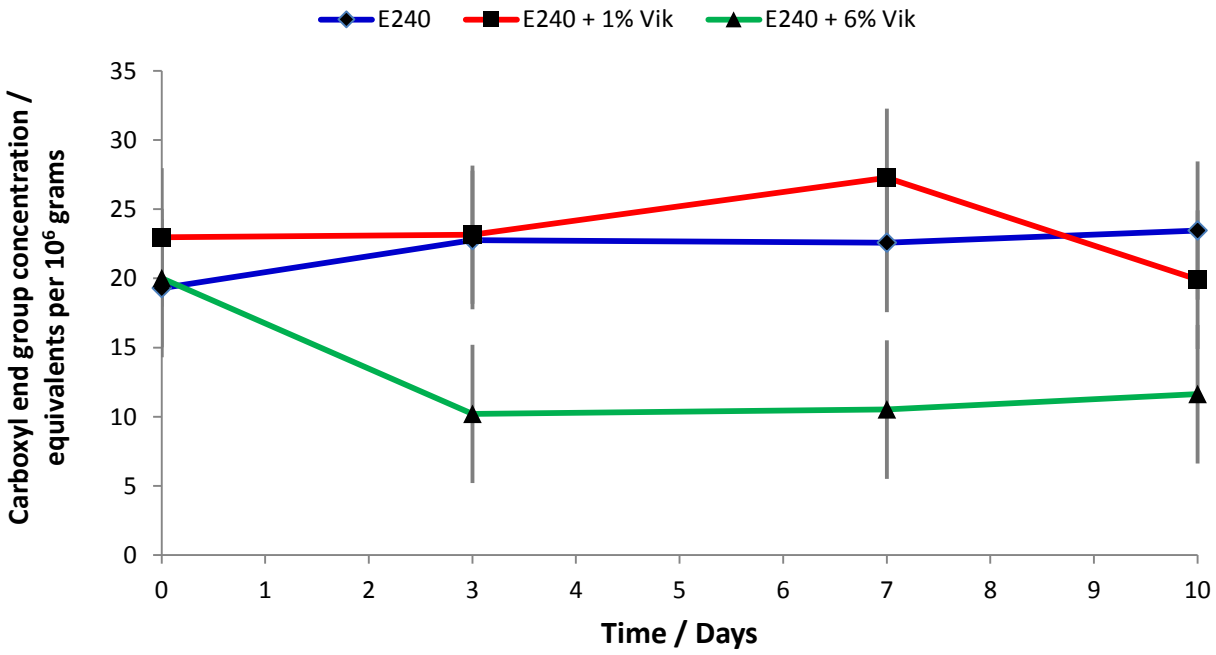

Figure 7.7 – Scatter plot for the average carboxyl end group concentration versus hydrolysis time for the E240 samples with Vikolox aged at room temperature. N=3. The error bar is 5 equivalents per 10^6 grams which is the calculated error in the method.

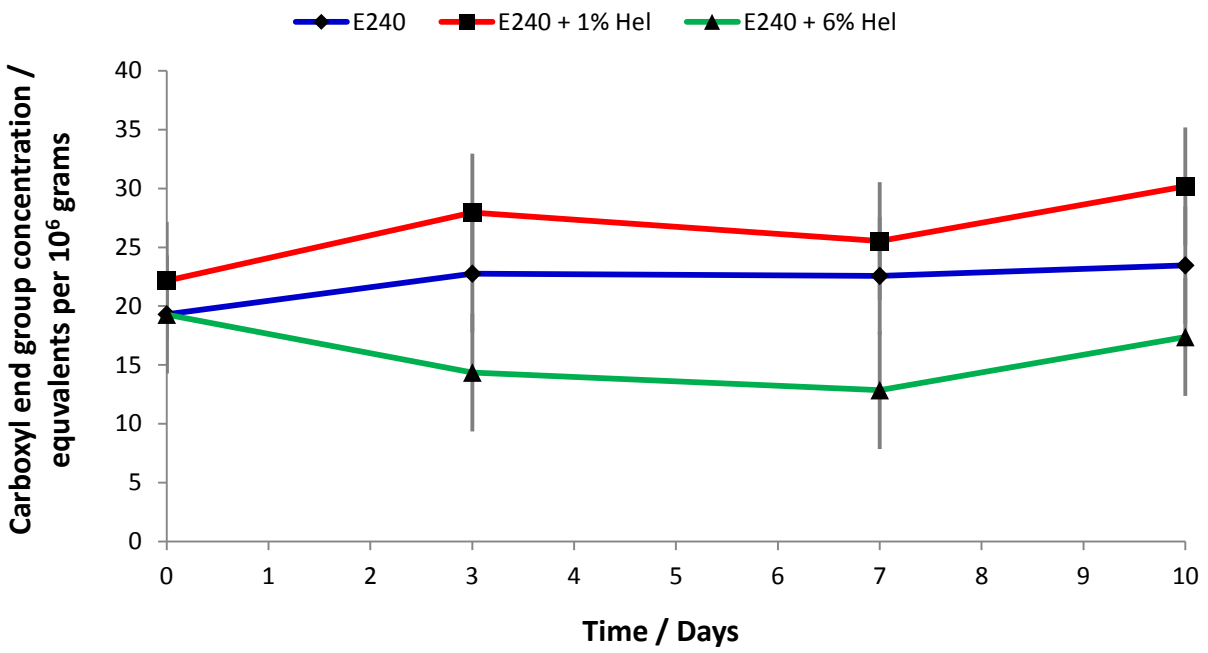

Figure 7.8 – Scatter plot for the average carboxyl end group concentration versus hydrolysis time for the E240 samples with Heloxy aged at room temperature. N=3. The error bar is 5 equivalents per 10^6 grams which is the calculated error in the method. .

There are two regions where the hydrolysis reaction can occur in the semi-crystalline PET. The chain scission reaction occurs in the amorphous regions of PET but not the crystalline fraction. This is because water molecules can diffuse into the amorphous region, but the crystalline region acts a barrier to moisture. The hydrolysis reaction can also occur at the crystalline edges. It is therefore important to know how much moisture is absorbed by PET. The volume of water absorbed by PET depends on a number of factors, including the time exposed to moisture and the degree of PET crystallinity. It is suggested that as the number of end groups increase during degradation there will be an increase in hydrophilicity, and more water will penetrate into the system.

The importance of how much water is absorbed into the PET samples resulted in the water uptake being determined. The surface areas of the extruded samples were calculated to ensure that they were similar by measuring the diameter and length of the rods. Table 7.1 shows the calculated surface area, and that the values obtained for the polymers are all very similar. A

more detailed method for calculating the surface area could be investigated in the future to look for any small changes between the samples. The water uptake was calculated by PET samples being prepared at room temperature using the method described in section 3.15.1. The polymer samples were removed from the water and the surface dried using a paper towel before the samples were reweighed. The difference between the initial and final weights of the polymer samples were normalised and shown as scatter plots versus time. The graph for the water uptake of the E187 sample at room temperature is shown in figure 7.9. There was no significant change noticed in the water uptake over the time investigated due to the low amount of water entering the polymer and the high error of the experiment. The maximum water uptake witnessed was recorded after 3 days, which would be expected as it takes time for the water molecules to penetrate the polymer sample.

The E240 and E239 samples follow a similar trend as witnessed with the E187 polymer, and they have a maximum water uptake after 4 and 5 days respectively. The scatter plot showing the water uptake of the E239 and E240 samples can be seen in figure 7.10. The longer time for water to diffuse into the samples is explained due to these polymers being solid state polymerised, causing them to have a higher crystalline content and a lower end group concentration, which in turn makes them more hydrophobic. The E239 has a very high normalised uptake, which is expected to be a result of excess surface water still being present. Future work should be carried out to obtain more information in this area.

The E187 samples that were prepared with Cardura, Heloxy and Vikolox were also monitored for their water uptake. The scatter plot showing the samples are shown in figure 7.11. The E187 + 6% Cardura also reached a maximum water uptake at 3 days similar to the E187 polymer samples without any epoxide. The samples containing Vikolox and Heloxy take longer than the Cardura samples to reach a maximum. The epoxides Vikolox and Heloxy are more hydrophobic than Cardura, which likely explains the increased length of time to reach the maximum water uptake. To confirm this conclusion further work would be required, as the error in the experiment is high and there are some outlying points expected to be a result of excess surface water.

Table 7.1 – Surface area of the different polymer samples

Sample	Surface area (mm^2 per gram)
E187	7493 ± 2345
E239	6653 ± 1569
E240	7339 ± 1747

.

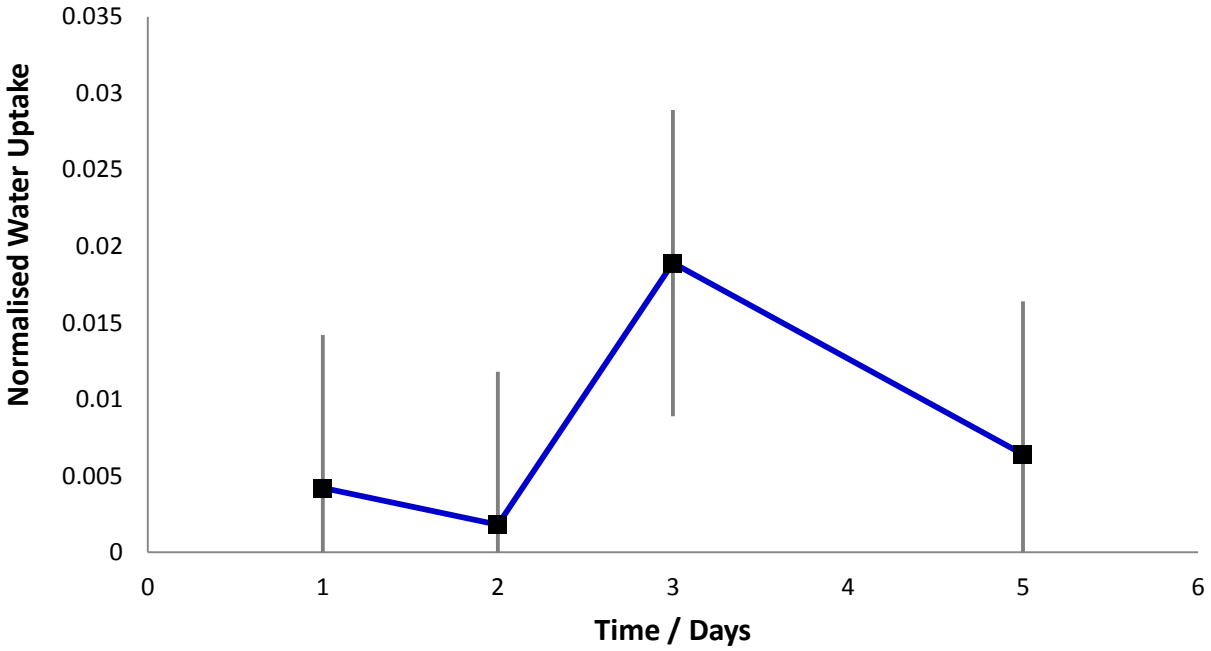

Figure 7.9– Scatter plot showing the average water uptake over time at room temperature for the E187 sample. N=3. Error bars represent the standard deviation of three repeats.

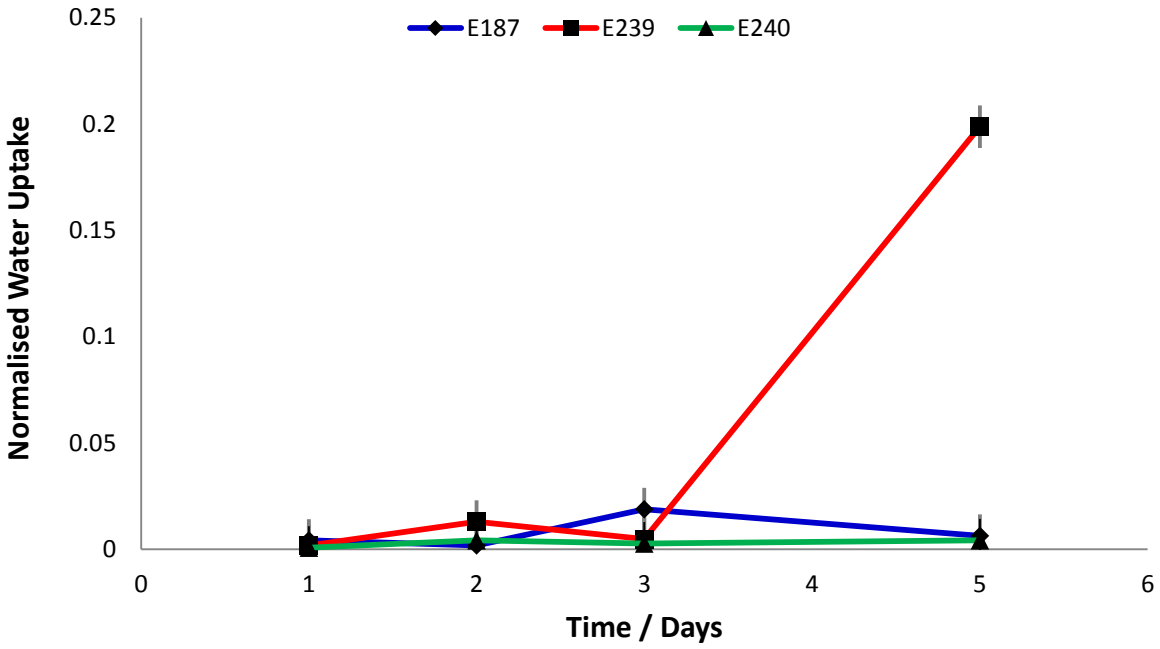

Figure 7.10 – Scatter plot showing the average water uptake over time at room temperature for the E187, E239 and E240 samples. N=3. Error bars represent the standard deviation of three repeats.

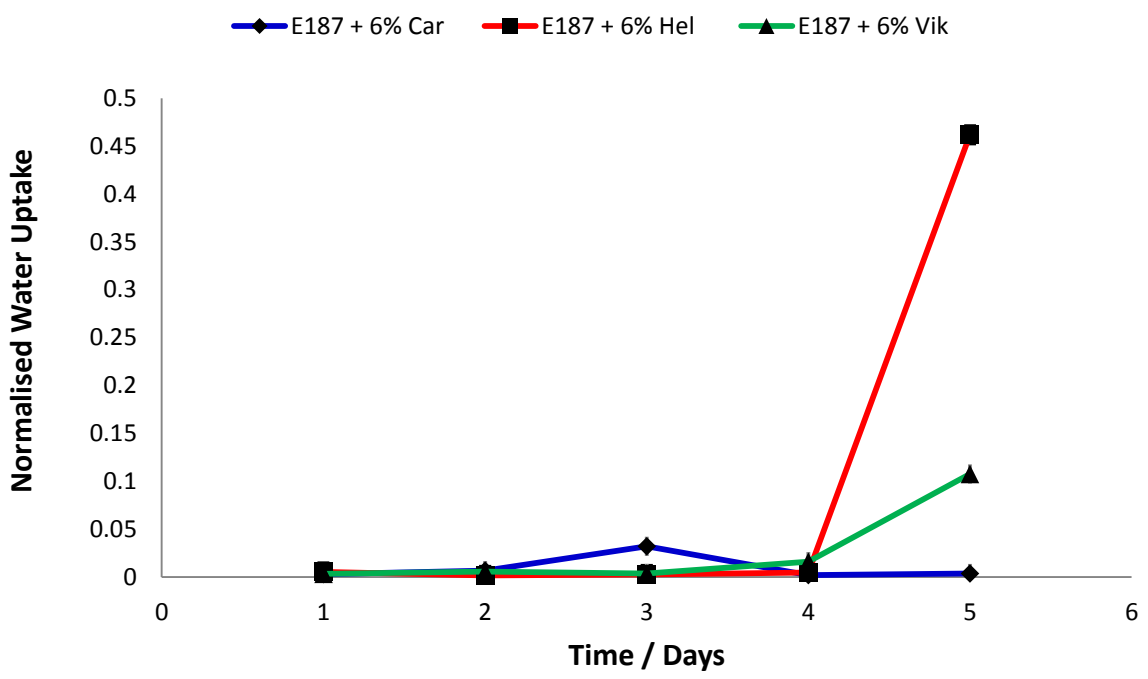

Figure 7.11 – Scatter plot showing the average water uptake over time at room temperature for the E187 + 6% Cardura, E187 + 6% Heloxy and E187 + 6% Vikolox. N = 3. Error bars represent the standard deviation of three repeats.

7.2.2 Hydrolysis at 50 °C

The carboxyl end group concentration was measured for all of the samples aged for up to 14 days at 50 °C. The only significant change in the E187 samples was for the initial E187 sample, which had a carboxyl end group concentration of 41.54 equivalents per 10^6 grams, and after being exposed to the conditions for hydrolysis for 3 days the carboxyl end group concentration decreased to 30.33 equivalents per 10^6 grams. As mentioned previously this reduction in carboxyl end group is expected to be due to the low molecular weight oligomers that are present from the polymerisation process which are water soluble. The lack of any other significant change shows that the hydrolytic degradation is not occurring in the sample under these conditions. These results are shown in the scatter plot in figures 7.12. No hydrolytic degradation was noticed in the E239 and E240 polymer samples that were aged for 14 days, and these scatter plots can be seen in figures 7.13 and 7.14 respectively.

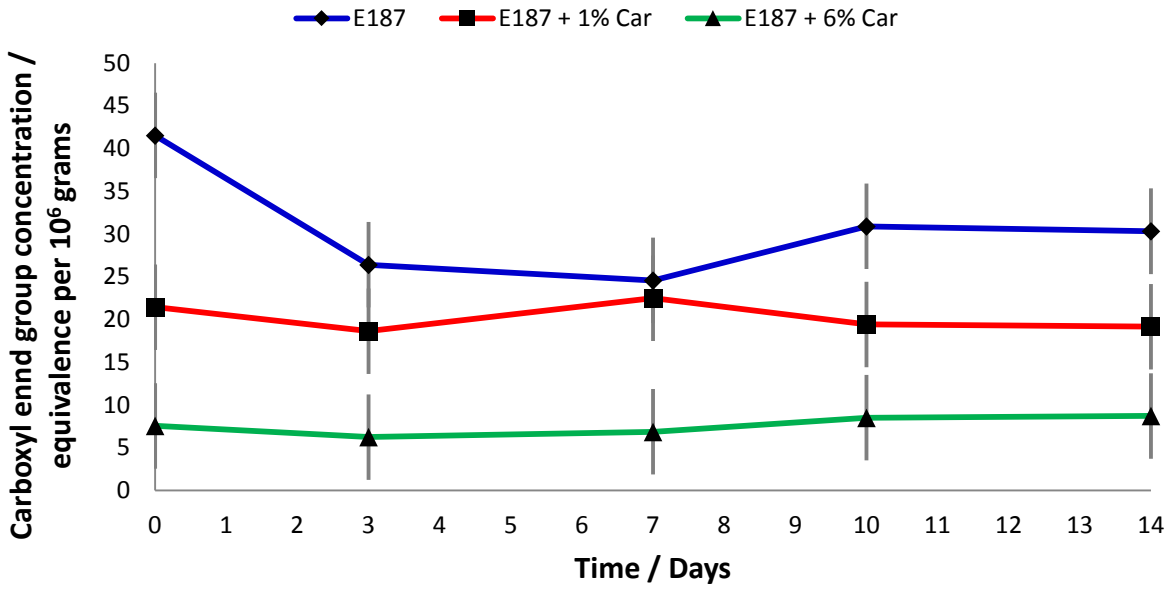

Figure 7.12 - Scatter plot for the average carboxyl end group concentration versus hydrolysis time for the E187 samples with Cardura aged at 50 °C. . N=3. The error bar is 5 equivalents per 10^6 grams which is the calculated error in the method.

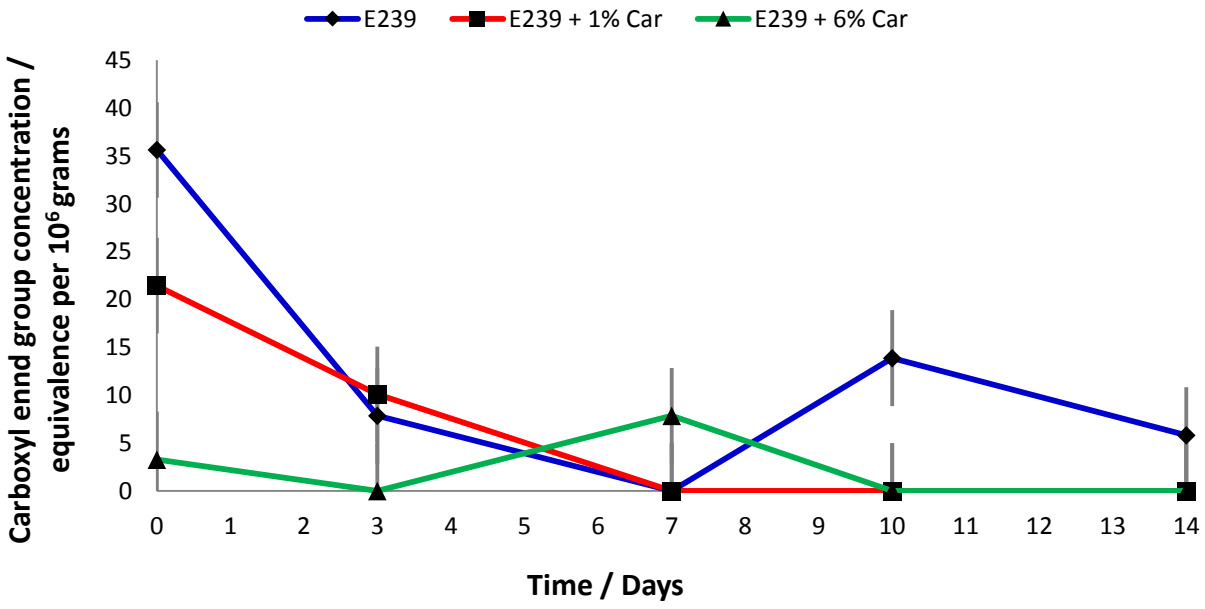

Figure 7.13 – Scatter plot for the average carboxyl end group concentration versus hydrolysis time for the E239 samples with Cardura aged at 50 °C. . N=3. The error bar is 5 equivalents per 10^6 grams which is the calculated error in the method.

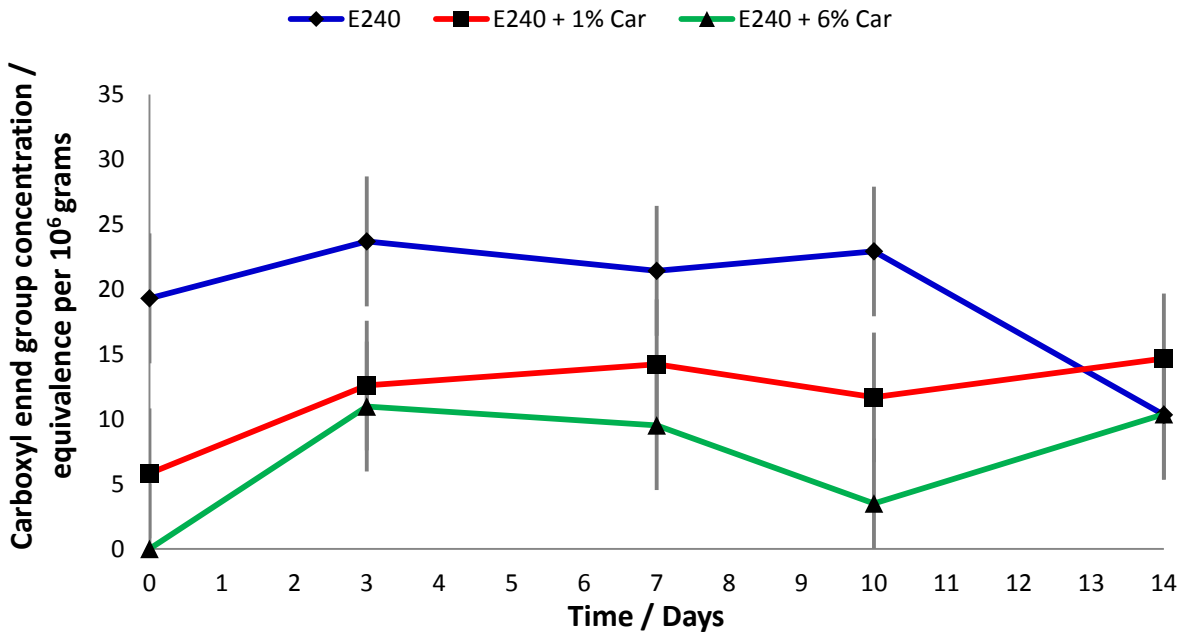

Figure 7.14– Scatter plot for the average carboxyl end group concentration versus hydrolysis time for the E240 samples with Cardura aged at 50 °C. N=3. The error bar is 5 equivalents per 10^6 grams which is the calculated error in the method.

Figures 7.12 to 7.14 show the carboxyl end group concentration for the aged polymer samples with Cardura. There was no significant change in the carboxyl end group concentration of the E187 + 1% Cardura samples aged for 10 days. The initial carboxyl end group concentration was 21.44 equivalents per 10^6 grams, and after being exposed to the conditions for hydrolysis for 10 days the carboxyl end group concentration was 19.17 equivalents per 10^6 grams. A similar conclusion was noticed for the E187 + 6% Cardura samples, which had an initial concentration of 7.56 equivalents per 10^6 grams, and after being exposed to the conditions for hydrolysis for 10 days the carboxyl end group concentration was only 8.71 equivalents per 10^6 grams. There were no significant changes noticed for the E239 and E240 samples that contain Cardura, indicating that hydrolytic degradation is not occurring at the conditions investigated. Hydrolytic degradation was not expected to occur at the conditions investigated because the temperature used was considerably lower than the glass transition temperature. Other research groups have shown that significant hydrolytic degradation only occurs above the glass transition temperature of PET. [42-44]

Samples of E187 + 1% Vikolox and E187 + 6% Vikolox were also aged for up to 10 days. The scatter plots for the E187 + 1% Vikolox and E187 + 6% Vikolox samples are shown in figure 7.15. There were no significant changes in either of the sample sets. The initial sample of the E187 + 6% Vikolox had a carboxyl end group concentration of 18.02 equivalents per 10^6 grams, and after being exposed to the conditions for hydrolysis the carboxyl end group concentration was 21.63 equivalents per 10^6 grams. The polymer E240 samples were also investigated with 1% and 6% Vikolox. The scatter plots for the 1% and 6% Vikolox in E240 samples are shown in figure 7.16. There was no significant difference in the E240 samples, confirming that hydrolytic degradation is not occurring in the samples at the conditions investigated. Figures 7.17 and 7.18 show the scatter plots of the end group concentrations of the E187 and E240 samples with Heloxy. There was no significant hydrolysis witnessed with the samples that were prepared with 1% or 6% Heloxy samples.

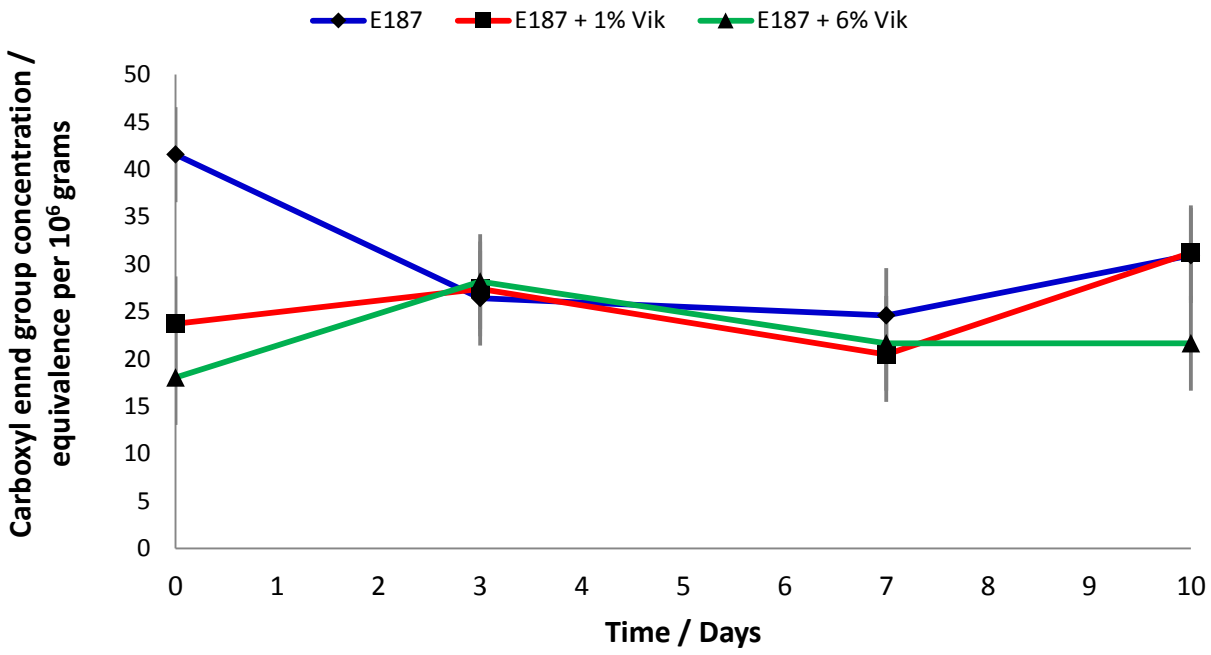

Figure 7.15 - Scatter plot for the average carboxyl end group concentration versus hydrolysis time for the E187 samples with Vikolox aged at 50 °C. N=3. The error bar is 5 equivalents per 10^6 grams which is the calculated error in the method.

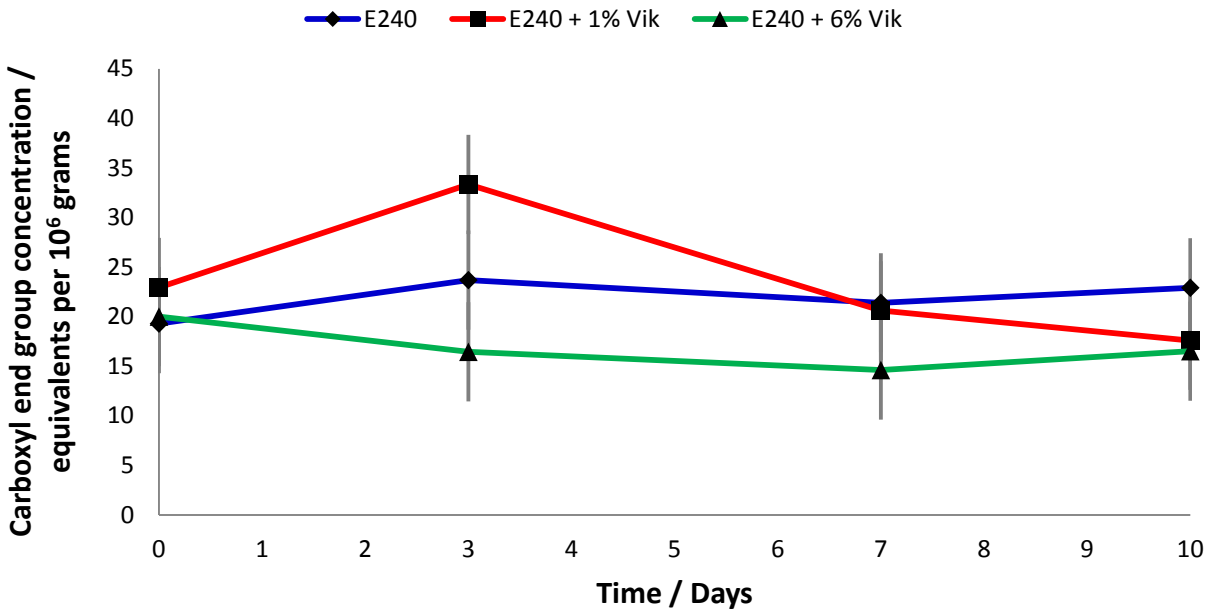

Figure 7.16 – Scatter plot for the average carboxyl end group concentration versus hydrolysis time for the E240 samples with Vikolox aged at 50 °C. N=3. The error bar is 5 equivalents per 10^6 grams which is the calculated error in the method.

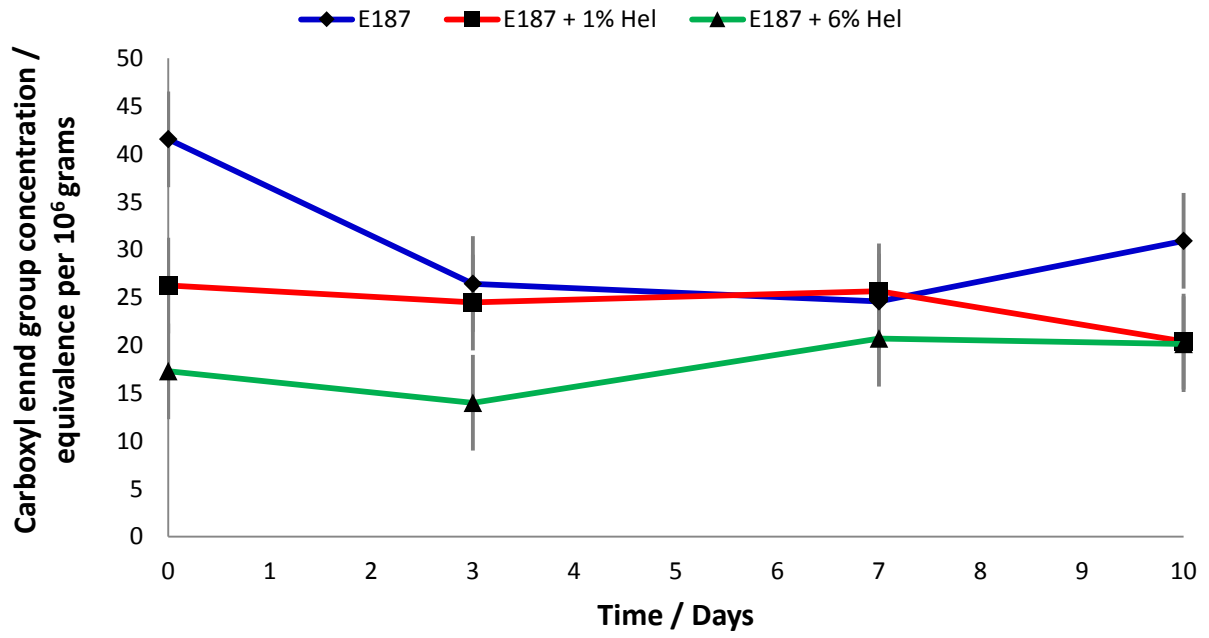

Figure 7.17 - Scatter plot for the average carboxyl end group concentration versus hydrolysis time for the E187 samples with Heloxy aged at 50 °C. N=3. The error bar is 5 equivalents per 10^6 grams which is the calculated error in the method.

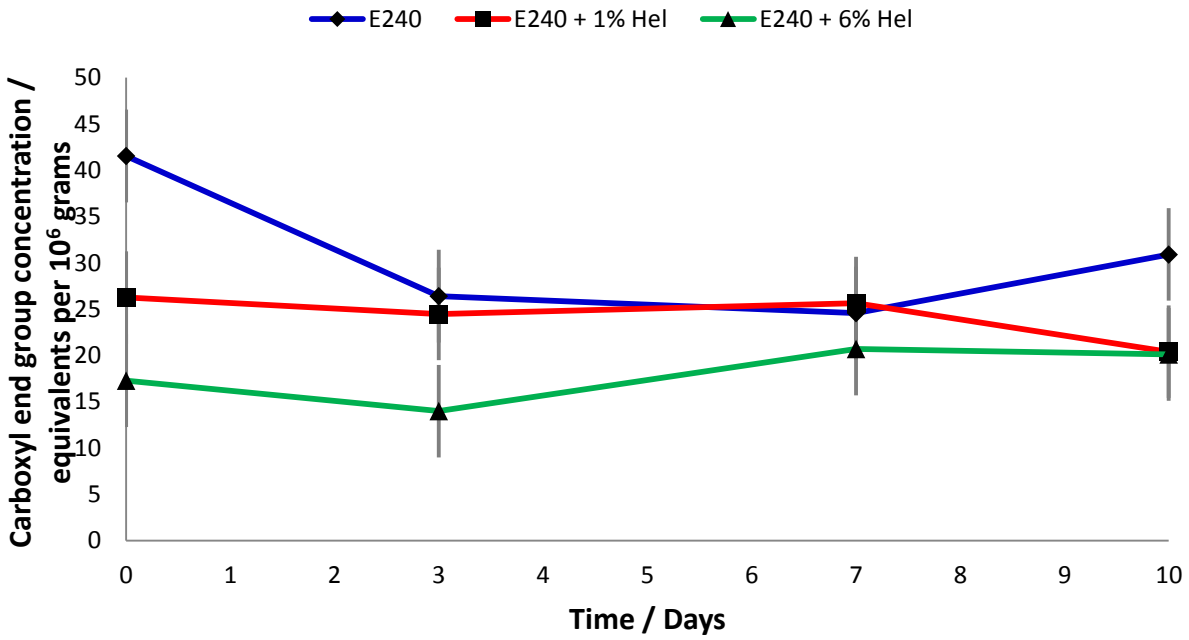

Figure 7.18 – Scatter plot for the average carboxyl end group concentration versus hydrolysis time for the E240 samples with Heloxy aged at 50 °C. N=3. The error bar is 5 equivalents per 10^6 grams which is the calculated error in the method.

The water uptake was also measured at 50 °C for the samples E187, E239 and E240. Figure 7.19 shows the water uptake for the E187, E239 and E240 samples. Similar trends are noticed in these samples compared with the samples measured at room temperature. The E187 sample exposed to the hydrolysis conditions for 4 days had a very high normalised uptake, which is expected to be a result of excess surface water still being present as it does not fit into the trend of the other samples. The concentration of water in the remaining samples was similar to the concentrations obtained for the water uptake of the samples at room temperature. The highest value obtained for the E239 and E240 samples was obtained between 2 and 4 days, which is similar to the results obtained at room temperature. Future work should be carried out to obtain more information in this area.

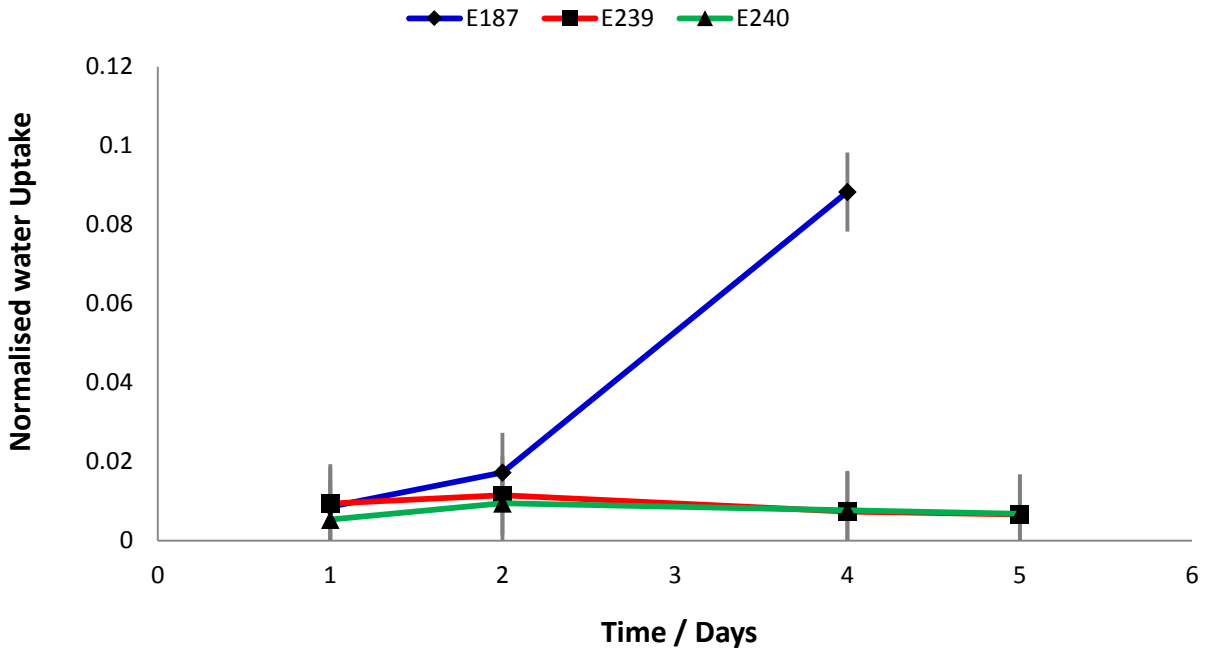

Figure 7.19 – Scatter plot showing the average water uptake at 50 °C over time for the E187, E239 and E240 samples. N=3. Error bars represent the standard deviation of three repeats.

7.2.3 Hydrolysis at 100 °C

The PET samples were aged in boiling water to study the hydrolysis reaction above the glass transition temperature. The PET samples aged were the E187, E239 and E240 samples. Samples of each polymer were prepared without Cardura as well as with 1% and 6% Cardura. The carboxyl end group concentration of the aged samples was measured using the Pohl titration method to monitor the hydrolysis reaction. The polymers E239 and E240 have a significantly lower starting carboxyl end group concentration than the E187 starting material as it has been solid state polymerised. There is a considerable increase in the carboxyl end group concentration as the ageing time increases for all the polymer types - the graphs are shown in figures 7.20 to 7.22. The carboxyl end group concentration increases as the time exposed to the hydrolysis condition increases for all the polymer samples, with an exponential trend always

being produced. The exponential trend that is produced implies an auto-catalysis reaction is occurring. The E187 samples have the largest increase in carboxyl end group concentration, going from 41.54 equivalents per 10^6 grams to 721.21 equivalents per 10^6 grams after they have been aged for 28 days.

It can be seen from figures 7.20 to 7.22 that the presence of Cardura in the samples drastically reduces the carboxyl end group concentration in all cases. It reduces the number of carboxyl end group concentrations in the E187 sample from 41.54 to 21.44 equivalents per 10^6 grams with the addition of only 1% Cardura. Unsurprisingly the addition of 6% Cardura by mass is more effective than 1%, which is not sufficient to fully end cap the PET chains in E187. Similar results are shown for the E239 and E240 samples.

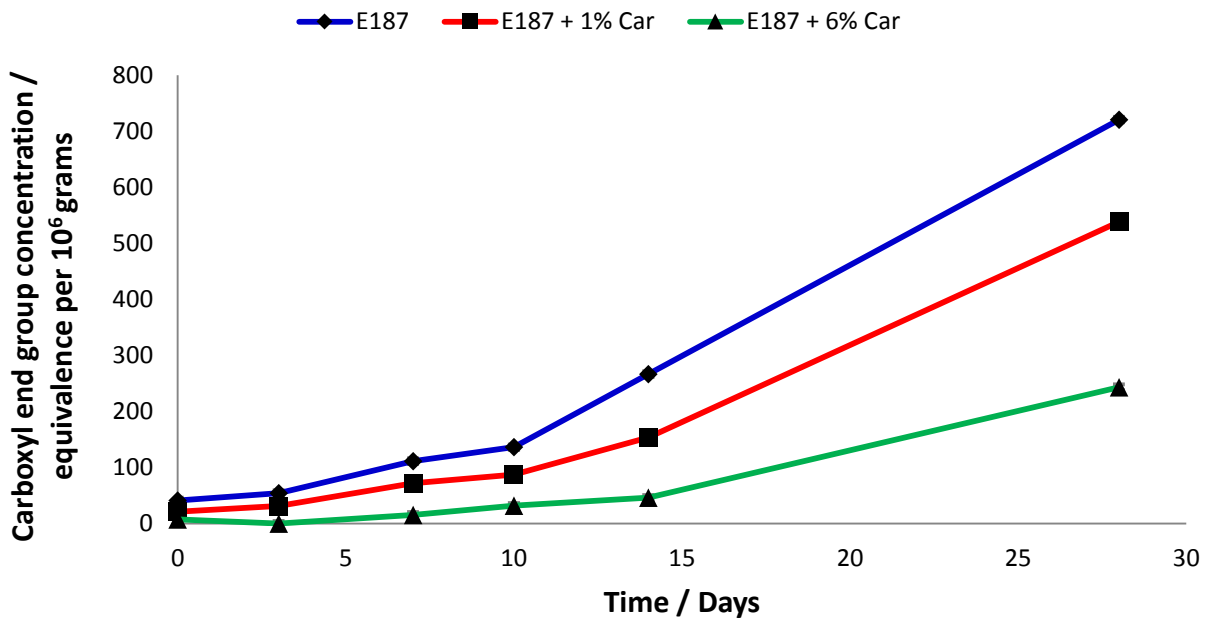

Figure 7.20 - Scatter plot for the average carboxyl end group concentration versus hydrolysis time for the E187 samples with Cardura aged at 100 °C. N=3. The error bar is 5 equivalents per 10^6 grams which is the calculated error in the method.

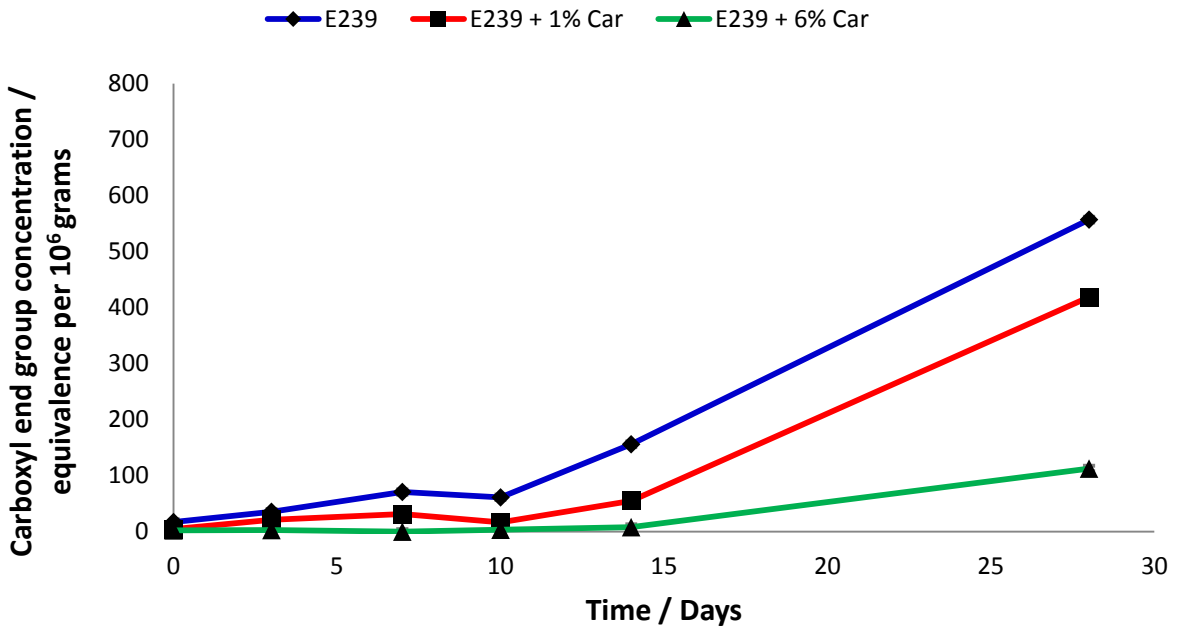

Figure 7.21 - Scatter plot for the average carboxyl end group concentration versus hydrolysis time for the E239 samples with Cardura aged at 100 °C. N=3. The error bar is 5 equivalents per 10^6 grams which is the calculated error in the method.

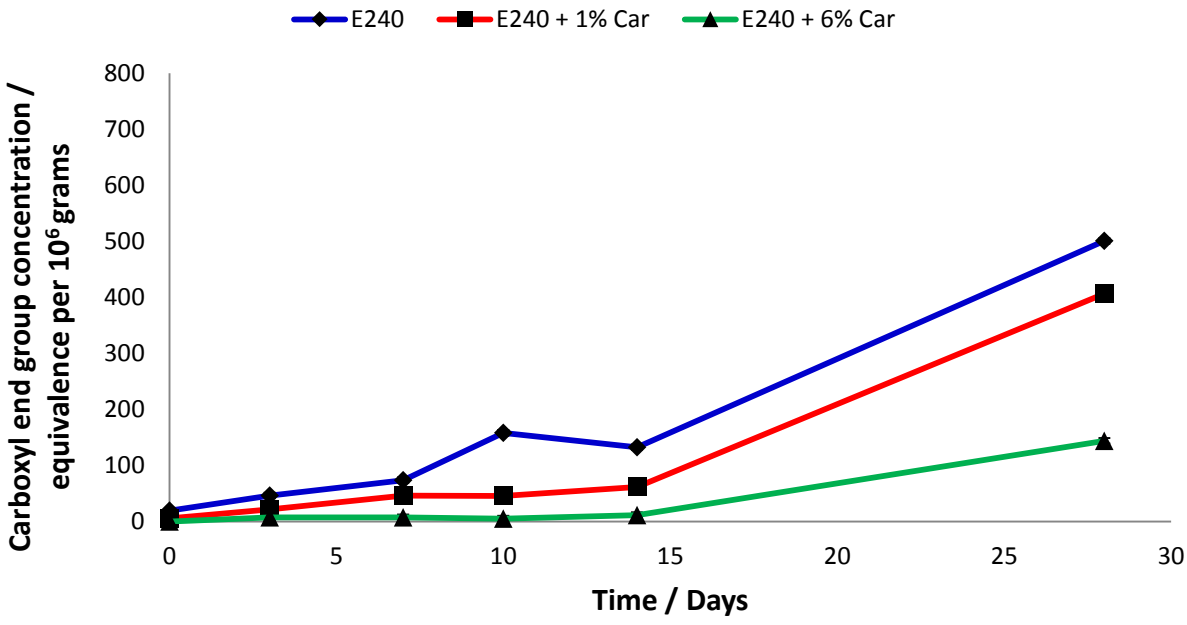

Figure 7.22 - Scatter plot for the average carboxyl end group concentration versus hydrolysis time for the E240 samples with Cardura aged at 100 °C. N=3. The error bar is 5 equivalents per 10^6 grams which is the calculated error in the method.

The large increase in the carboxyl end group concentration as the ageing time increases is expected, as extensive hydrolysis has been reported in the literature to occur above the glass transition temperature by a number of different research groups. [15 - 18] It has been reported that as the polymer chains are able to move more above the glass transition temperature this allows more water and hydrolysis products to diffuse in and out of the polymer easily.

The concentration of water being absorbed by the polymer was measured using the above method; the data can be seen in figure 7.23. Similar trends are noticed in these samples compared with the samples measured at room temperature. The highest value obtained for the E239 and E240 samples was obtained between 2 and 4 days, which is similar to the results obtained from the samples exposed to the hydrolysis conditions at room temperature and 50 ^{o}C. Future work should be carried out to obtain more information in this area. The data gathered for the water uptake supports the literature findings that water is taking time to penetrate the sample. The less crystalline polymer (E187) seems to generate a higher water uptake than the E239 and E240 samples, but further work is required to confirm this.

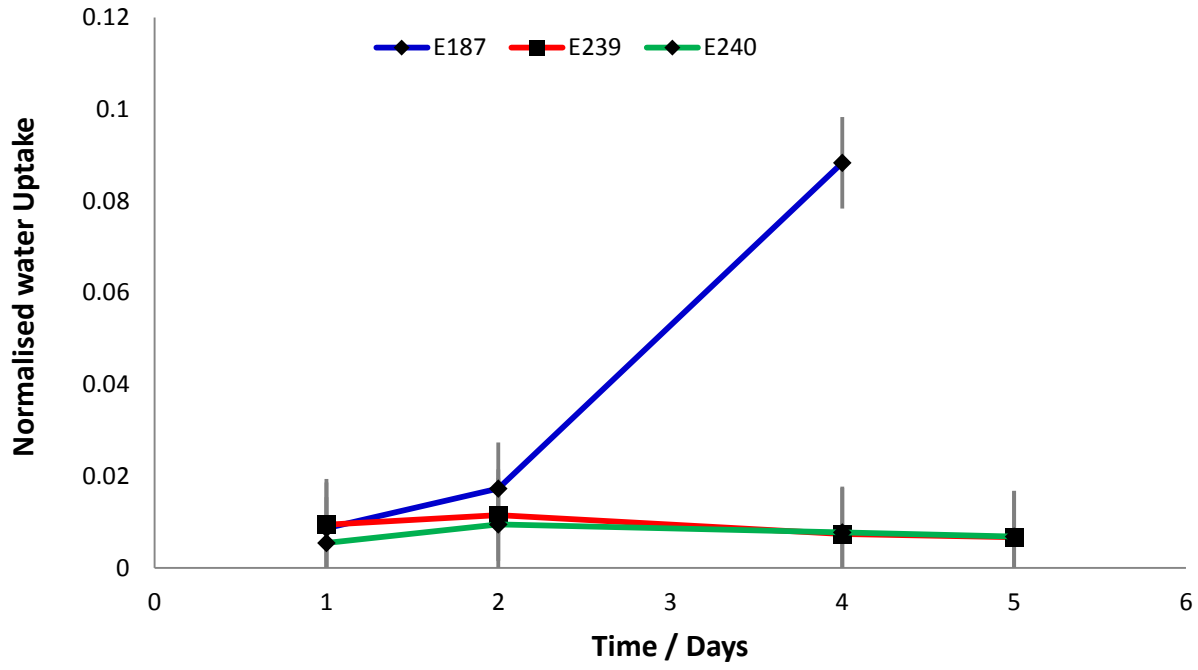

Figure 7.23 – Scatter plot showing the average water uptake at 100 ^{o}C over time for the E187, E239 and E240 samples. N=3. Error bars represent the standard deviation of three repeats.

The carboxyl end group concentration for the samples containing epoxides Vikolox and Heloxy were also monitored. The data for the E187 samples with Vikolox and Heloxy can be seen in figures 7.24 and 7.25 respectively. The scatter plots in figures 7.26 and 7.27 shows the carboxyl end group concentration as a function of hydrolysis time for the E240 samples with Vikolox and Heloxy. It can be seen in all cases that the epoxide addition markedly reduces the rate of hydrolysis. Not surprisingly 6% by mass is more effective in all cases than 1%, which is not sufficient to fully end cap the PET chains.

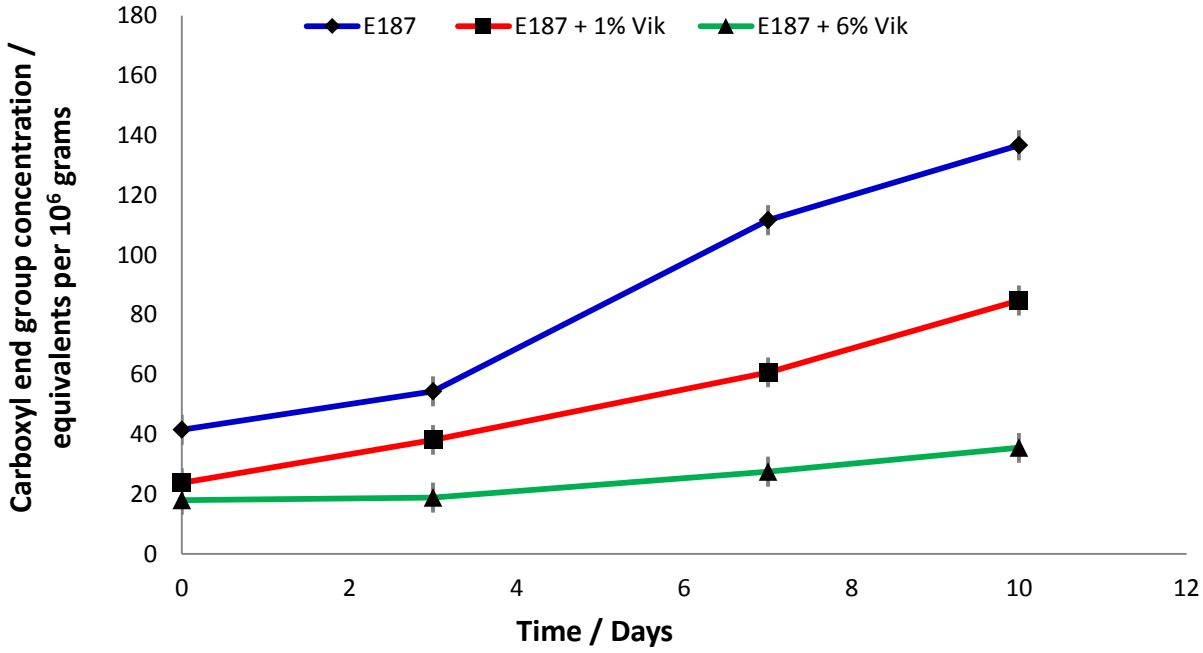

Figure 7.24 - Scatter plot for the average carboxyl end group concentration versus hydrolysis time for the E187 samples with Vikolox aged at 100 °C. N=3. The error bar is 5 equivalents per 10^6 grams which is the calculated error in the method.

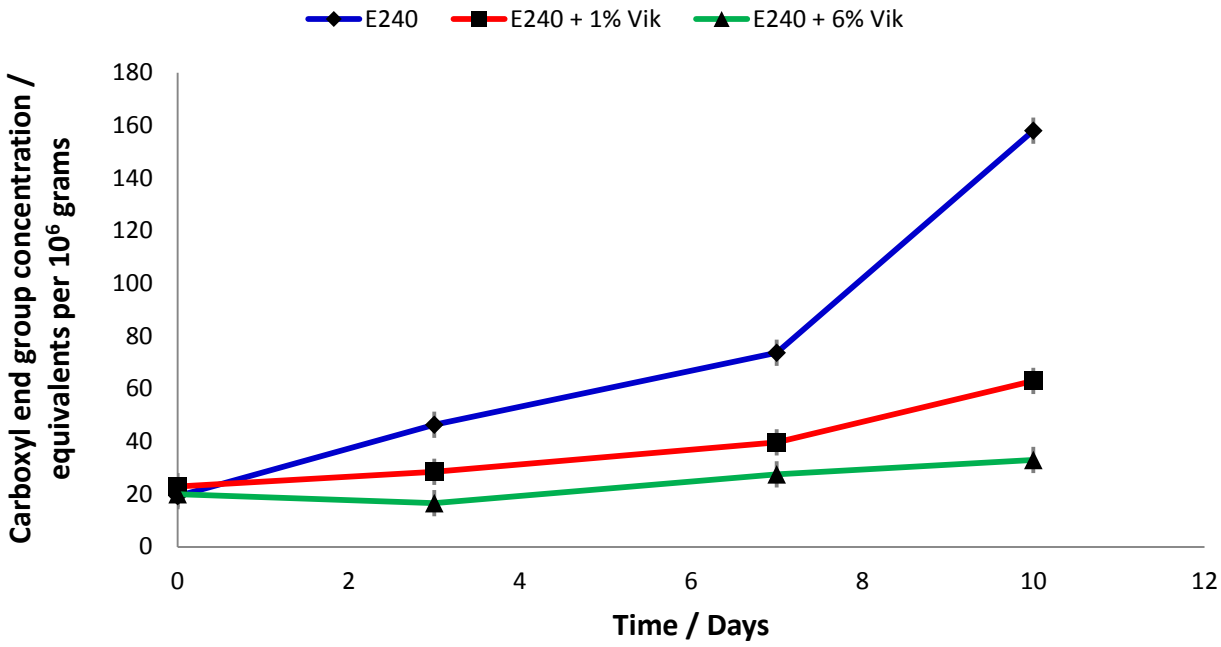

Figure 7.25 – Scatter plot for the average carboxyl end group concentration versus hydrolysis time for the E240 samples with Vikolox aged at 100 °C. N=3. The error bar is 5 equivalents per 10^6 grams which is the calculated error in the method.

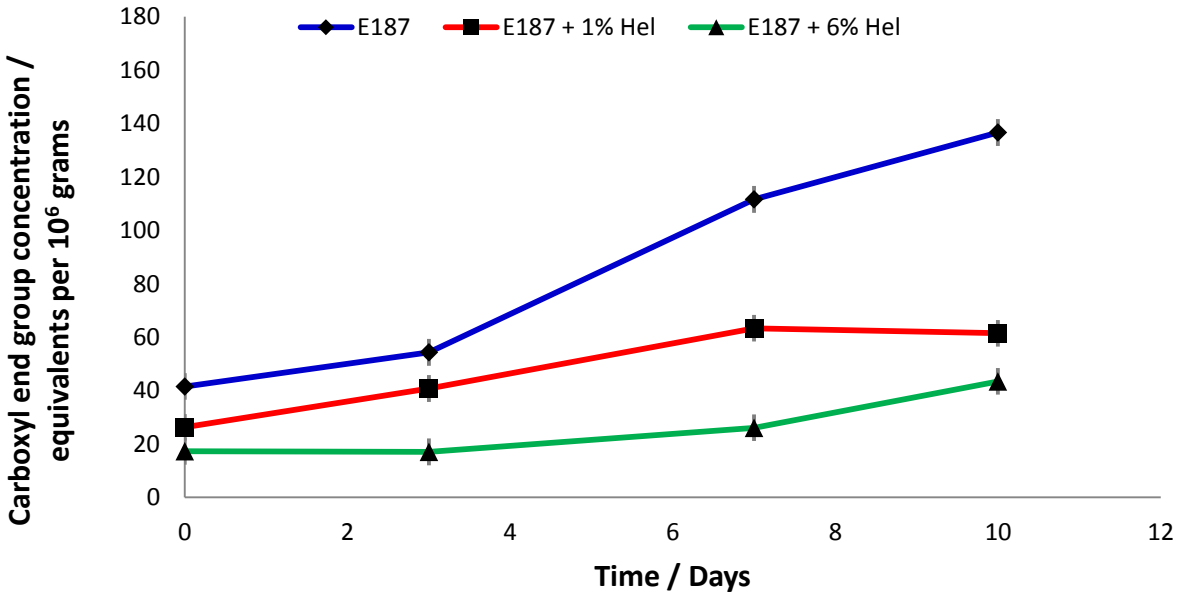

Figure 7.26- Scatter plot for the average carboxyl end group concentration versus hydrolysis time for the E187 samples with Heloxy aged at 100 °C. N=3. The error bar is 5 equivalents per 10^6 grams which is the calculated error in the method.

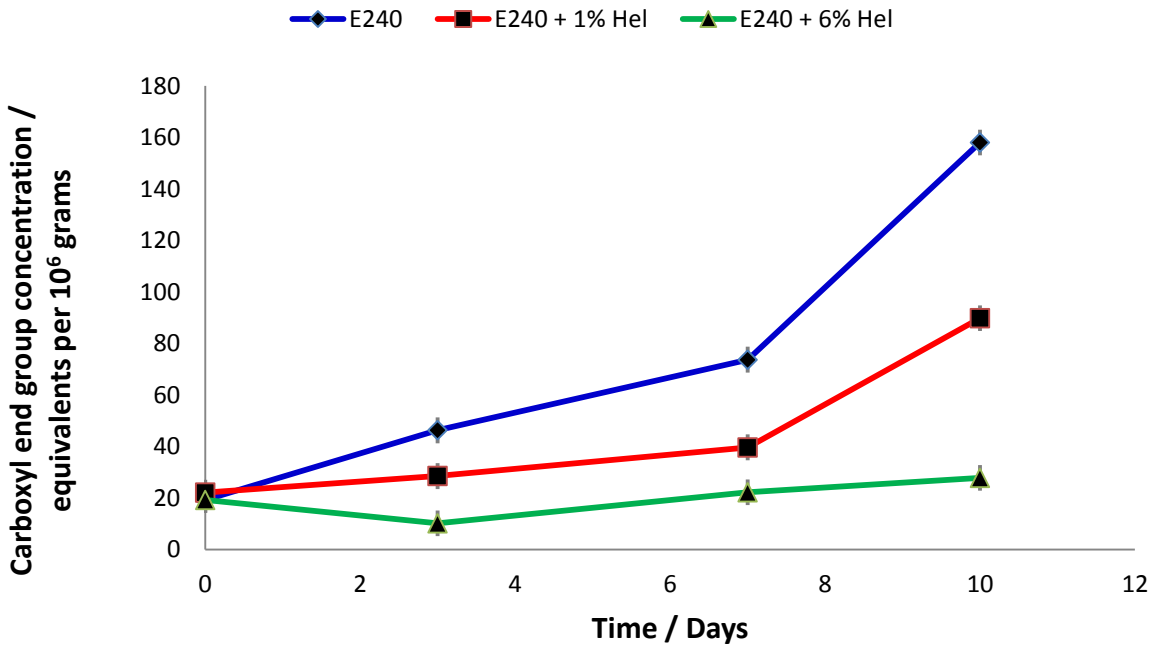

Figure 7.27 – Scatter plot for the average carboxyl end group concentration versus hydrolysis time for the E240 sample with Heloxy aged at 100 °C. N=3. The error bar is 5 equivalents per 10^6 grams which is the calculated error in the method

7.2.4 Hydrolysis at 100 °C Without Water Changes

In all of the samples discussed above the water was changed every two days to ensure that acidic degradation products were not altering the pH of the water. Acidic conditions have been widely reported in the literature to catalyse the hydrolysis reaction. [14 and 42] Such conditions accelerate the hydrolysis process by protonation of an oxygen atom from the ester groups in the backbone of PET, and this is then followed by the reaction with water to produce the carboxyl and hydroxyl end groups. Samples of E187 and E239 samples were aged up to 14 days without the water being changed to study the carboxyl end group concentration in slightly acidic conditions. The scatter plots showing the carboxyl end group concentration versus ageing time for the E187 and E239 samples with and without Cardura are shown in figures 7.28 and 7.29. The data generated shows that there was no significant difference between the samples with the water being changed (see figures 7.20 and 7.21) and the samples where the water was unchanged.

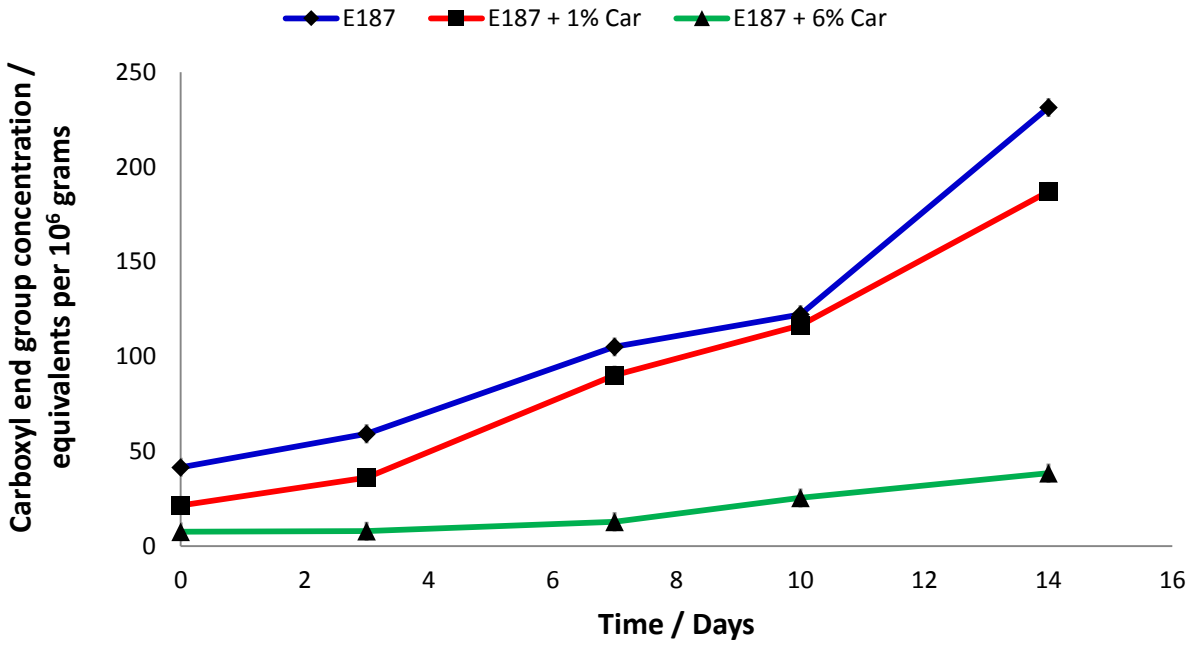

Figure 7.28 - Scatter plot for the average carboxyl end group concentration versus hydrolysis time for the E187 samples with Cardura aged at 100 °C without the water being changed. N=3. The error bar is 5 equivalents per 10^6 grams which is the calculated error in the method.

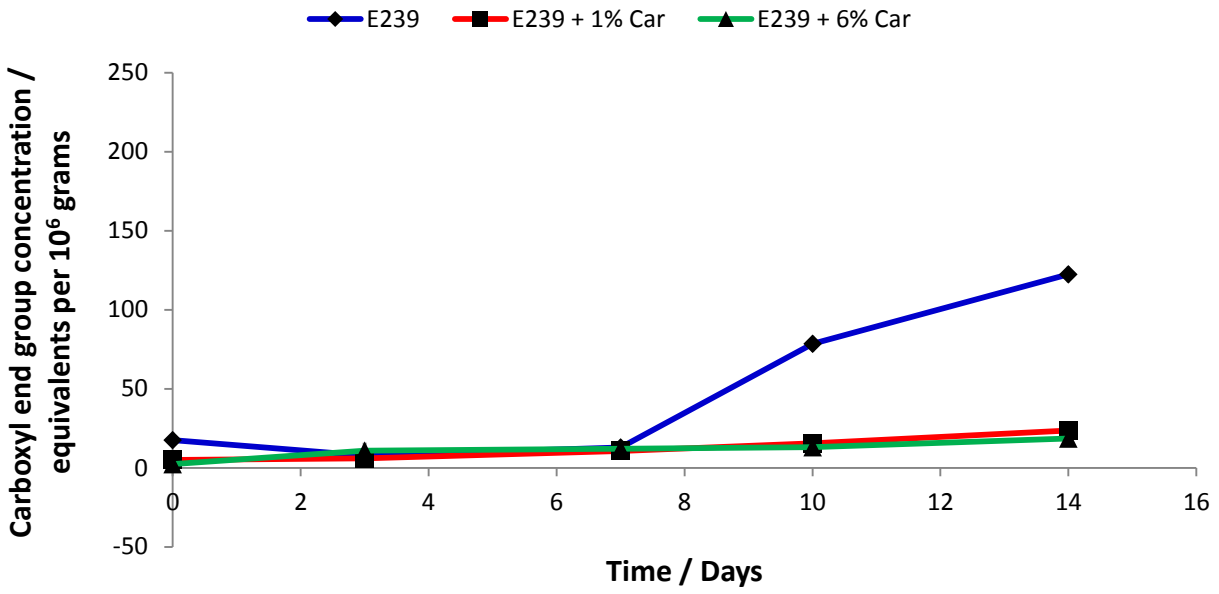

Figure 7.29 – Scatter plot for the average carboxyl end group concentration versus hydrolysis time for the E239 samples with Cardura aged at 100 °C. The water was not changed during this experiment. N=3. The error bar is 5 equivalents per 10^6 grams which is the calculated error in the method.

7.2.5 Kinetics

The apparent rate constant (K) for the hydrolytic degradation reaction for each of the polymer types was calculated using the method outlined in the experimental section. Figures 7.30 to 7.32 show the graphs of $(([COOH]_t)^{0.5} - ([COOH]_0)^{0.5})$ versus time for the E187, E187 + 1% Cardura and E187 + 6% Cardura samples. The data shown is for the samples generated where the water has been changed. The graphs for all other data sets are shown in the appendices (A7.1.1 to A7.1.14).

The plots of $([COOH]_t)^{0.5} - ([COOH]_0)^{0.5})$ versus time for the E187, E187 + 1% Cardura and E187 + 6% Cardura sample sets were linear with coefficients of determinations normally greater than 0.95. These results support that the hydrolysis of PET is a half order reaction with respect to the carboxyl end group concentration. Several research groups have proposed that the hydrolysis of PET is a half order reaction including Zhang *et al.* [90 and 95] The E187 samples where the water has not been changed also generate graphs of $(([COOH]_t)^{0.5} - ([COOH]_0)^{0.5})$ versus time that are straight lines. The R^2 coefficient of the straight lines are greater than 0.98. Similar trends are

noticed with samples prepared from E239 and E240, but the coefficients of determinations are slightly reduced. Further data points would be beneficial to strengthen the data, especially at higher data points between 14 and 28 days.

The apparent reaction rate has been shown to decrease with increasing Cardura content. The apparent reaction rates are shown in table 7.2. The reduction in the reaction rate shows that the epoxide sample is protecting the PET from hydrolysis. As expected the samples containing 6% by mass of Cardura are reducing the reaction rate further. Similar results are obtained for the other polymers investigated (E239 and E240) and for samples where the water in the ageing experiment was not changed.

Table 7.3 shows the initial crystallinity values for the samples as K is linked to the crystallinity of the samples. With an experimental error calculated from repeat samples being 5 J/g there was no significant difference noted in the crystallinity. This eliminates different crystallinity values affecting the results obtained.

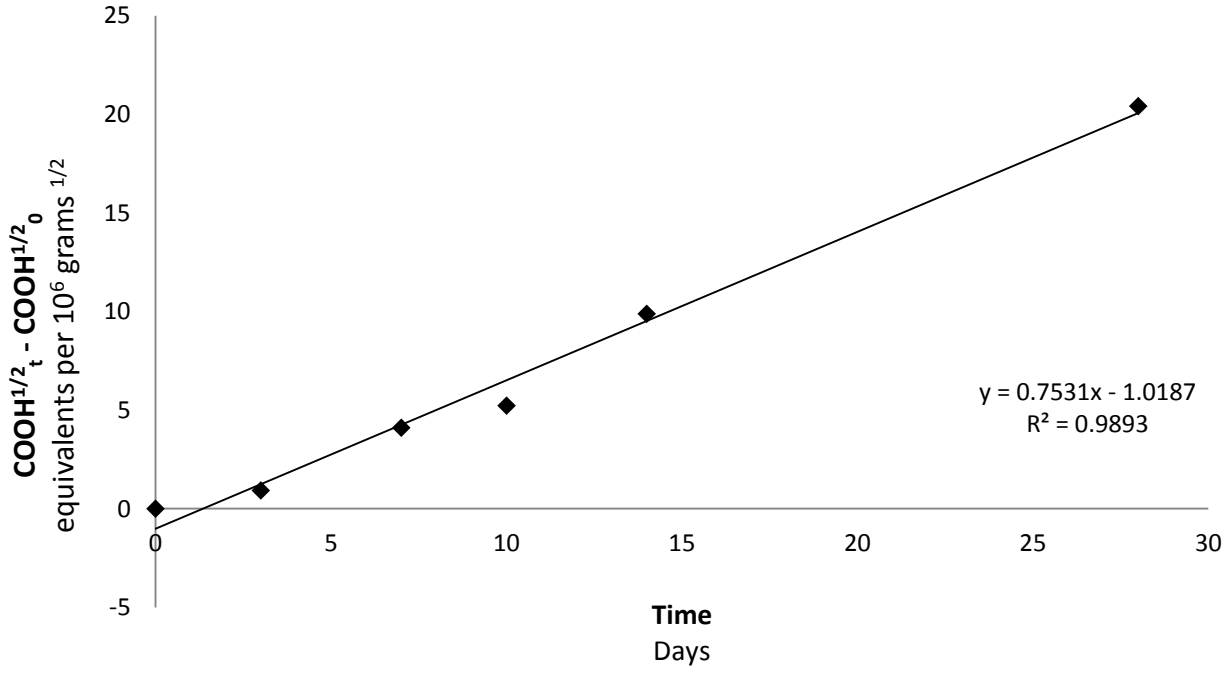

Figure 7.30 – Scatter plot of $(([COOH]_t)^{0.5} - ([COOH]_0)^{0.5})$ versus time for the E187 samples.

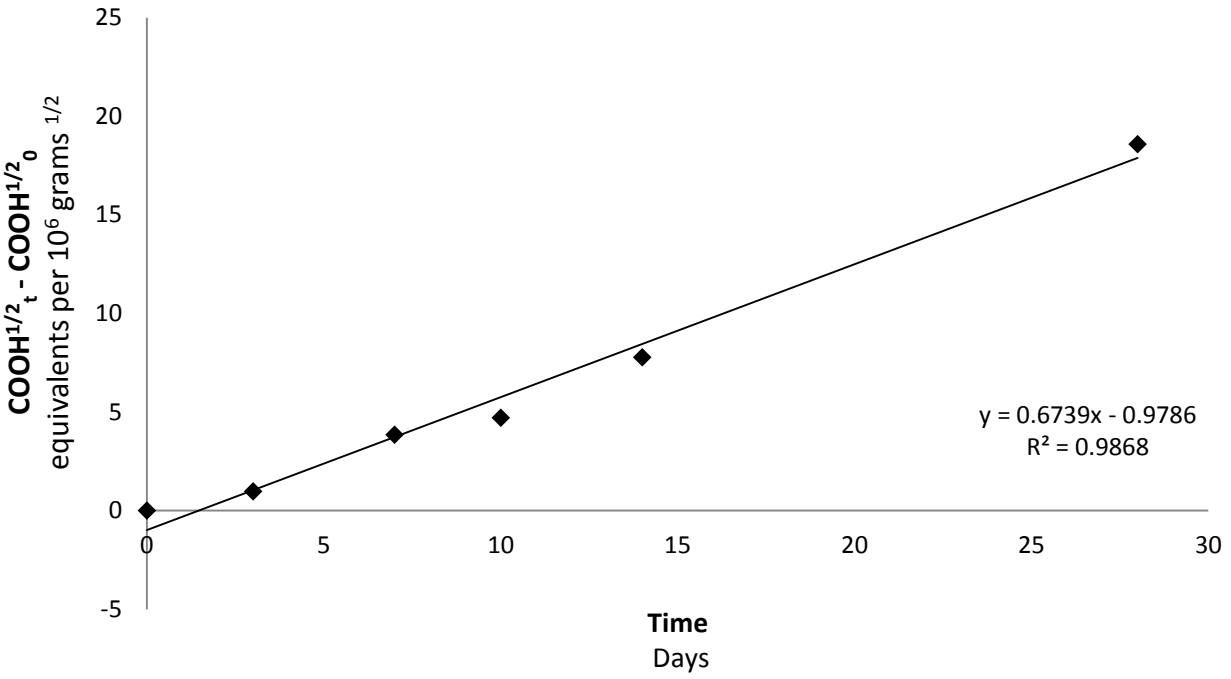

Figure 7.31 – Scatter plot of $(([COOH]_t)^{0.5} - ([COOH]_0)^{0.5})$ versus time for the E187 + 1% Cardura samples.

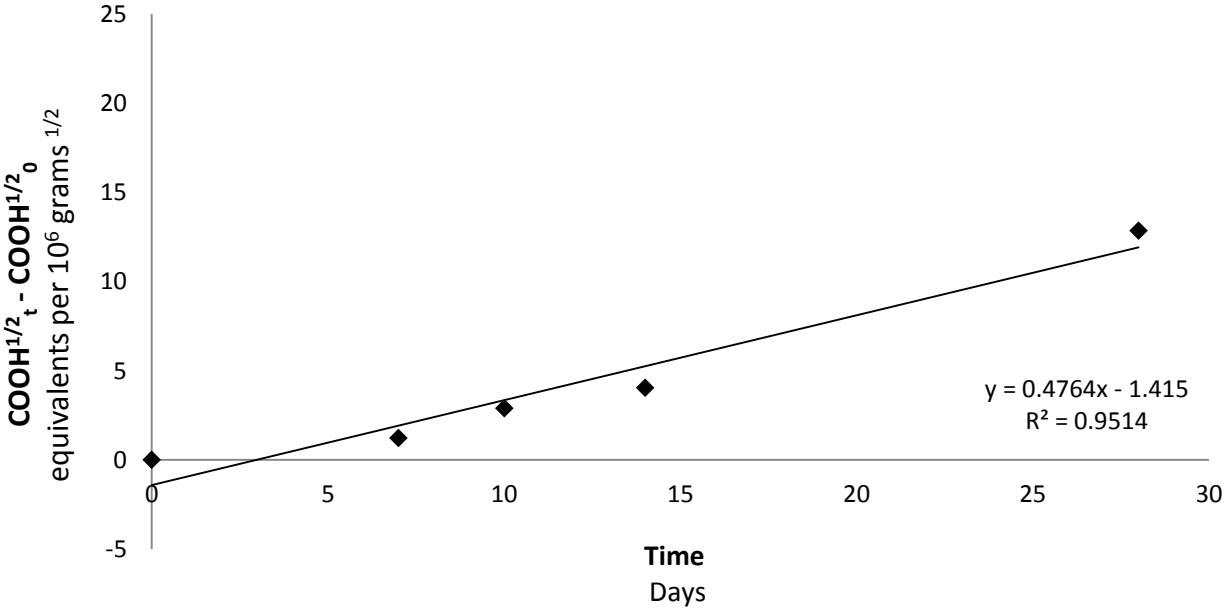

Figure 7.32 – Scatter plot of $(([COOH]_t)^{0.5} - ([COOH]_0)^{0.5})$ versus time for the E187 + 6% Cardura samples.

Table 7.2 - Apparent reaction rate for the polymer samples with and without Cardura.

Sample	K equivalents per 10^6 grams $^{1/2}$
E187	0.38
E187 + 1% Car	0.34
E187 + 6% Car	0.23
E239	0.35
E239 + 1% Car	0.31
E239 + 6% Car	0.16
E240	0.31
E240 + 1% Car	0.30
E240 + 6% Car	0.20

Table 7.3 – Average enthalpy of crystallisation for the polymer samples with and without Cardura. N=3.

Sample	Enthalpy of Crystallisation J/g
E187	38.71
E187 + 1% Car	39.02
E187 + 6% Car	36.64
E239	37.31
E239 + 1% Car	38.98
E239 + 6% Car	45.40
E240	39.30
E240 + 1% Car	41.18
E240 + 6% Car	39.54

Graphs of $(([COOH]_t)^{0.5} - ([COOH]_0)^{0.5})$ versus time were also created for the samples containing Vikolox and Heloxy, and the apparent rate constant (K) for the hydrolytic degradation reaction was calculated. Figures 7.33 to 7.36 show the graphs of $(([COOH]_t)^{0.5} - ([COOH]_0)^{0.5})$ versus time for the E187 samples with Heloxy and Vikolox. The data shown is for samples aged for only 10 days and generated in experiments where the water has been changed every two days. The graphs for the E240 samples with Heloxy and Vikolox samples are shown in the appendices (A7.1.15 to A7.1.18). The plots of $(([COOH]_t)^{0.5} - ([COOH]_0)^{0.5})$ versus time are more variable, and not all the sample sets produced straight lines. This is because the samples have a low average carboxyl end group concentration. Further data points, especially for samples that have been aged for longer periods of time, would allow the apparent rate constant to be accurately determined for the epoxides Heloxy and Vikolox as the data only for 10 days is not sufficient for kinetic analysis.

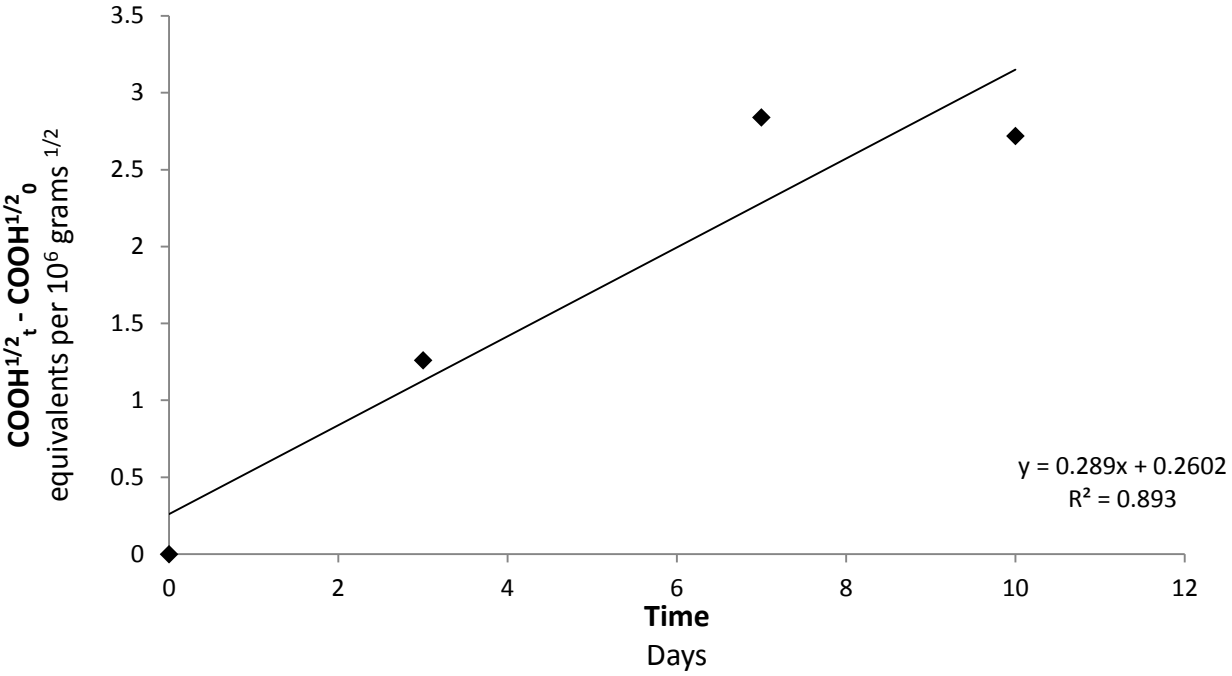

Figure 7.33 – Scatter plot of $(([COOH]_t)^{0.5} - ([COOH]_0)^{0.5})$ versus time for the E187 + 1% Heloxy samples.

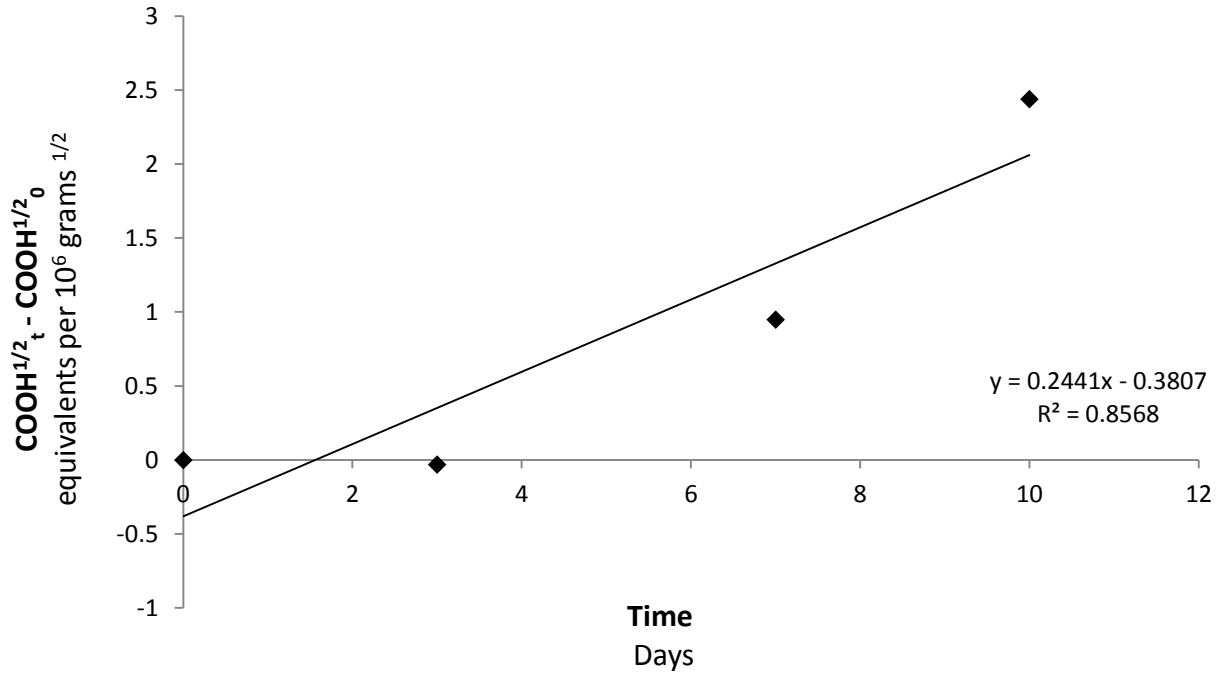

Figure 7.34– Scatter plot of $(([COOH]_t)^{0.5} - ([COOH]_0)^{0.5})$ versus time for the E187 + 6% Heloxy samples.

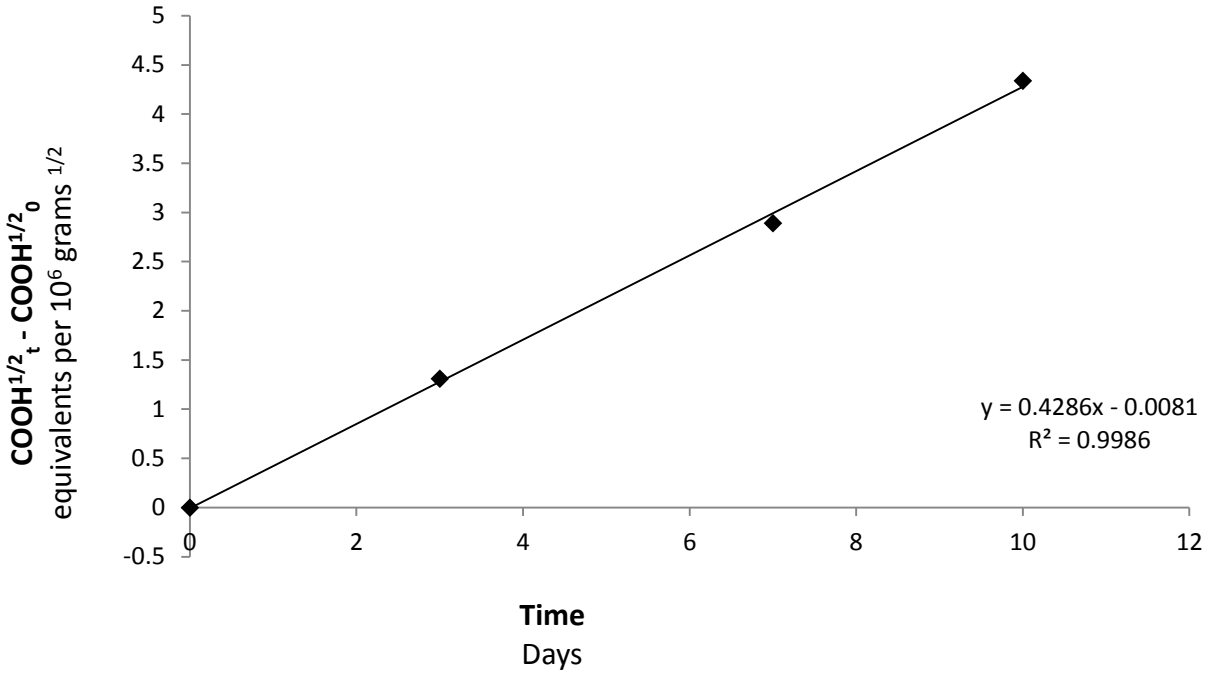

Figure 7.35 – Scatter plot of $(([COOH]_t)^{0.5} - ([COOH]_0)^{0.5})$ versus time for the E187 + 1% Vikolox samples.

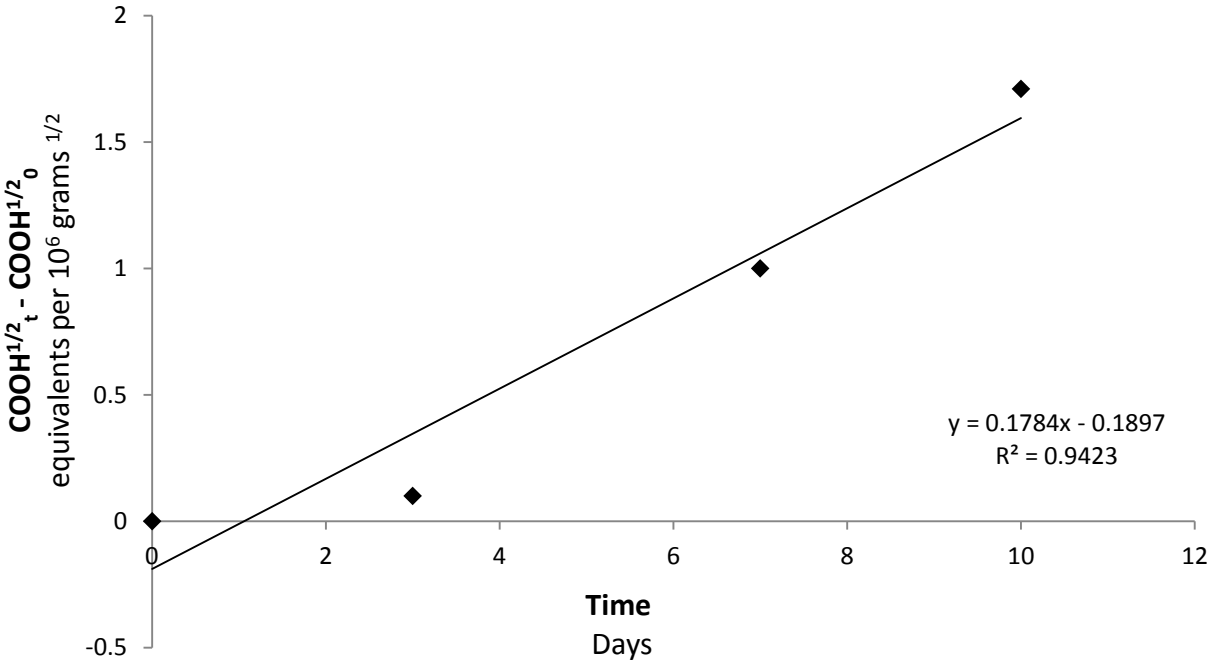

Figure 7.36 – Scatter plot of $(([COOH]_t)^{0.5} - ([COOH]_0)^{0.5})$ versus time for the E187 + 6% Vikolox samples.

7.2.6 Hydrolysis Products at 100 °C

Two products were noticed in the samples that were aged for longer periods of time. These samples were removed from the water that was used to age the E187 and E239 samples for 28 days. The products generated for both samples were a clear film that coated the round bottom flask and a white powder. IR spectra of the two products produced were obtained, shown in figures 7.37 and 7.38. The white powder generated has consistent peaks, such as the peak at 1688 cm^{-1}, which suggests that it is terephthalic acid that is being produced. It is expected that there is a mixture of products (perhaps oligomers) as there are considerably more peaks than would correspond to terephthalic acid. Further analysis would be required to confirm the products that are being released during hydrolysis. There are peaks in the IR spectrum generated for the clear film produced that are consistent with polyethylene, which could be from ethylene glycol polymerising at the conditions investigated. Ethylene glycol is the other expected product from complete hydrolytic degradation.

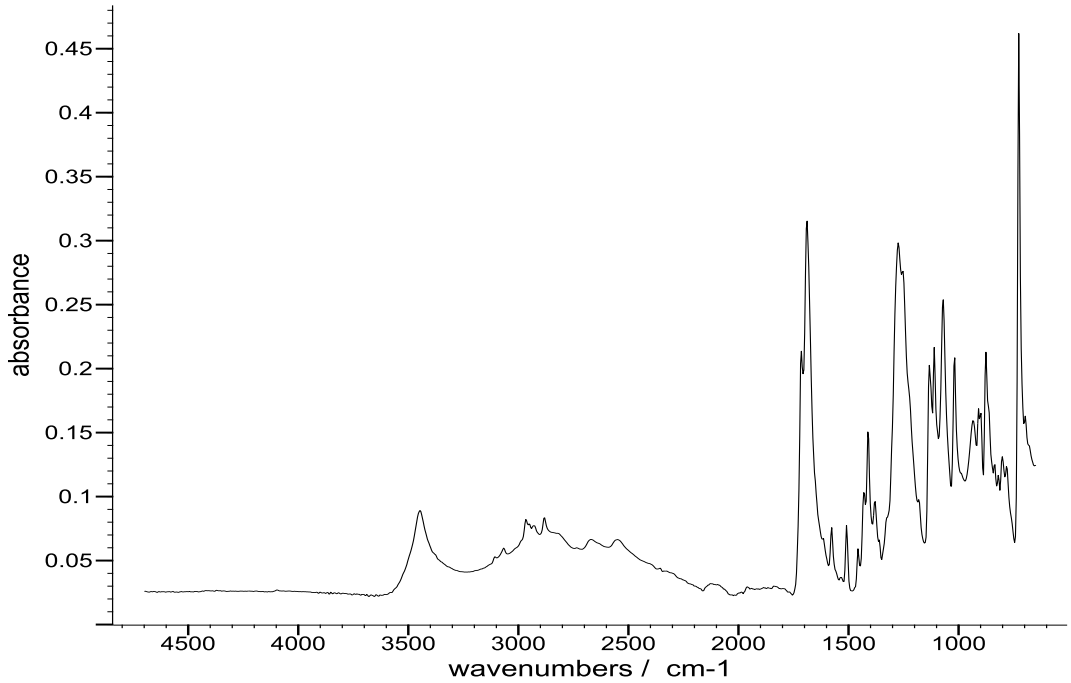

Figure 7.37 – IR spectrum of the white powder formed during the hydrolysis of E187 and E239 samples for 28 days at 100 °C.

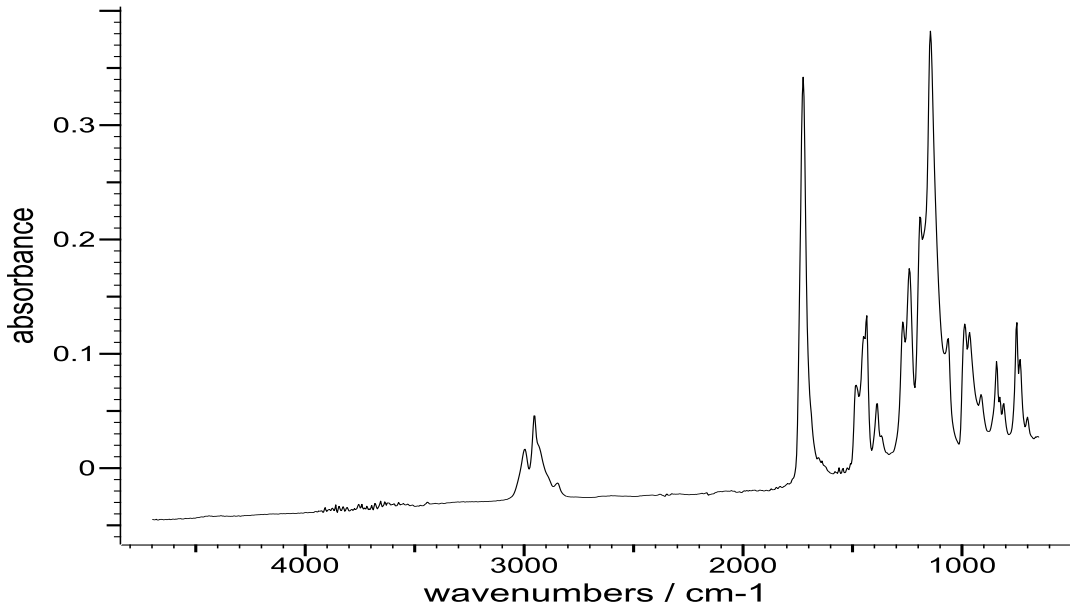

Figure 7.38– IR spectrum of the clear film formed during the hydrolysis of E187 and E239 samples for 28 days at 100 °C.

7.2.7 IV Measurements

The IV of the extruded samples of E187 and E239 were compared with those for the starting materials. IV measurements for all of the samples that were aged in unchanged boiling water were also obtained. The IV of the E187 and E239 samples against ageing time are shown in the scatter plots in figure 7.39 and 7.40. The graphs both show that as the ageing time increases the IV is reduced.

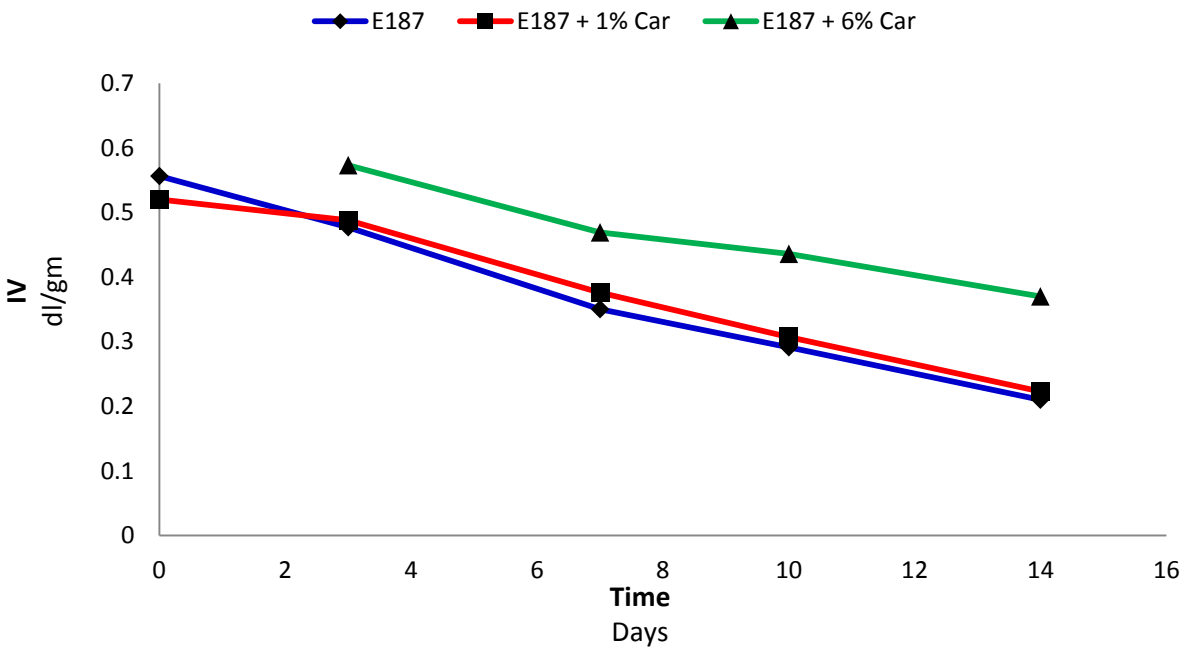

Figure 7.39 – Scatter plot of IV versus time for the E187 samples, with and without Cardura. A single measurement was obtained.

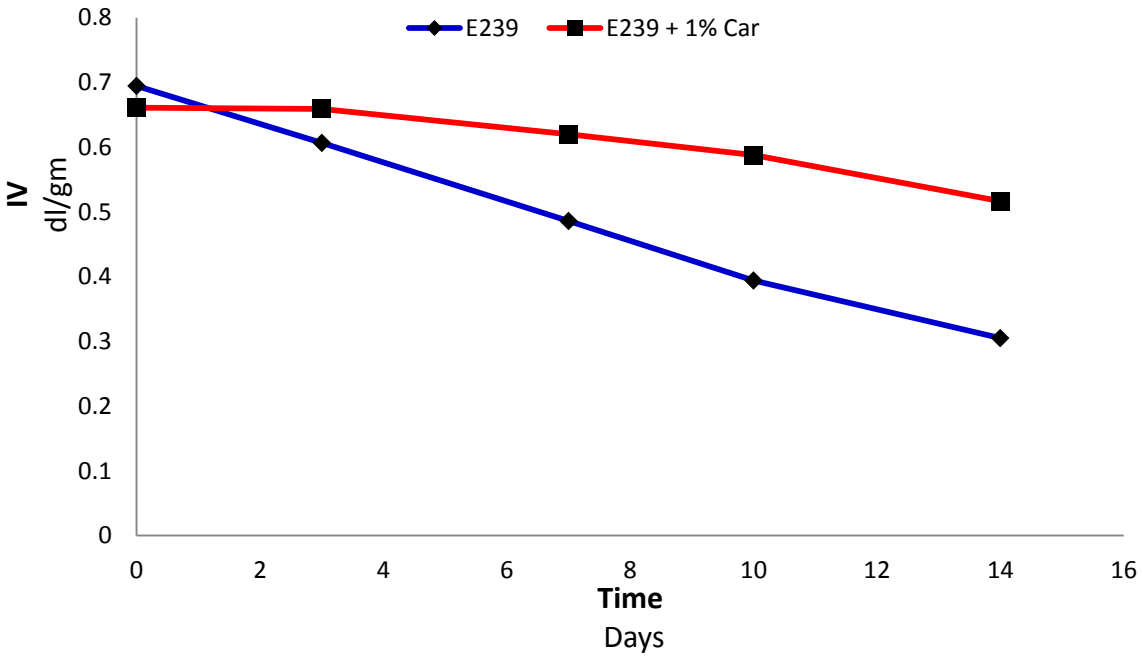

Figure 7.40 – Scatter plot of IV versus time for the E239 samples, with and without Cardura. A single measurement was obtained.

The E187 starting material has an initial IV of 0.57 dl/gm, and the IV of the extruded E187 material was 0.56 dl/gm. These values are very similar despite the fact that the extruded E187 sample has been through another high temperature processing step. The slight reduction is expected to be a result of thermal degradation occurring in the extruder; however the short residence time of the extruder barrel prevents the result of degradation from being more significant. The E239 samples have a similar trend as the E239 starting material has an IV of 0.79 dl/gm, which was reduced to 0.70 dl/gm for the extruded material. There is a slight reduction in the IV of the polymer samples when Cardura is added; this is expected to be a result of the Cardura plasticising the polymer sample.

There was a reduction in the IV as the length of time the samples were aged for was increased. This is a result of the hydrolytic chain scission. Hosseini *et al*. reported a similar reduction in the IV of PET samples that were hydrolysed in distilled water for up to 25 days. [18]

The aged E187 + 1% Cardura samples have a slightly higher IV than the value obtained for the aged E187 samples. This is because the Cardura is end capping some of the carboxyl end groups present in the polymer, which is resulting in it taking longer for the conditions required for an auto-catalytic reaction to be reached. The samples of E187 + 6% Cardura have an even higher IV, showing that the polymer is being protected from hydrolysis. The IV of the aged E239 and E239 + 1% Cardura samples follow a similar trend to the aged E187 samples. The E239 samples have a considerably higher IV after being aged for 14 days compared with the E187 samples. The differences are due to the lower carboxyl end group concentration of E239 preventing the conditions that are required for an auto-catalytic reaction, and the fact that the E239 sample is more crystalline than the E187 polymer samples which prevents water molecules from easily finding the amorphous regions to break down the polymer.

The aged E239 + 1% Cardura samples have a considerable improvement in the IV when compared to the aged E239 samples. The higher IV of the E239 samples at the end of the 14 day ageing period is a result of less hydrolytic degradation occurring in the samples. This is a result of the E239 starting material having a lower starting carboxyl end group concentration. The initially low starting carboxyl end group concentration results in the 1% Cardura that was added reacting with a large percentage of the initial carboxyl end groups. This end capping of the carboxyl end group concentration makes the polymer less hydrophilic.

7.2.8 Relationship between End Group Concentration and IV

The IV of a polymer sample links to the molecular weight by the Mark-Houwink equation which is shown in equation 7.1. [54] This results in a clear relationship between the IV and the carboxyl end group concentration of a polymer, as the ester links in the polymer chains are broken to form carboxyl and hydroxyl end groups. This breaking of the polymer chain during hydrolysis lowers the molecular weight. The IV data was plotted against the carboxyl end group concentrations for all of the polymer types. The graphs for the E187 and E239 samples with and without Cardura are shown in figures 7.41 and 7.42 respectively. All of the graphs show that as the IV decreases the carboxyl end group concentrations increase.

$$[\eta] = KM^{\alpha}$$ **Equation 7.1**

where [η] is intrinsic viscosity and M is the molecular weight. The values of K and α are constants which depend on the nature of the polymer and solvent

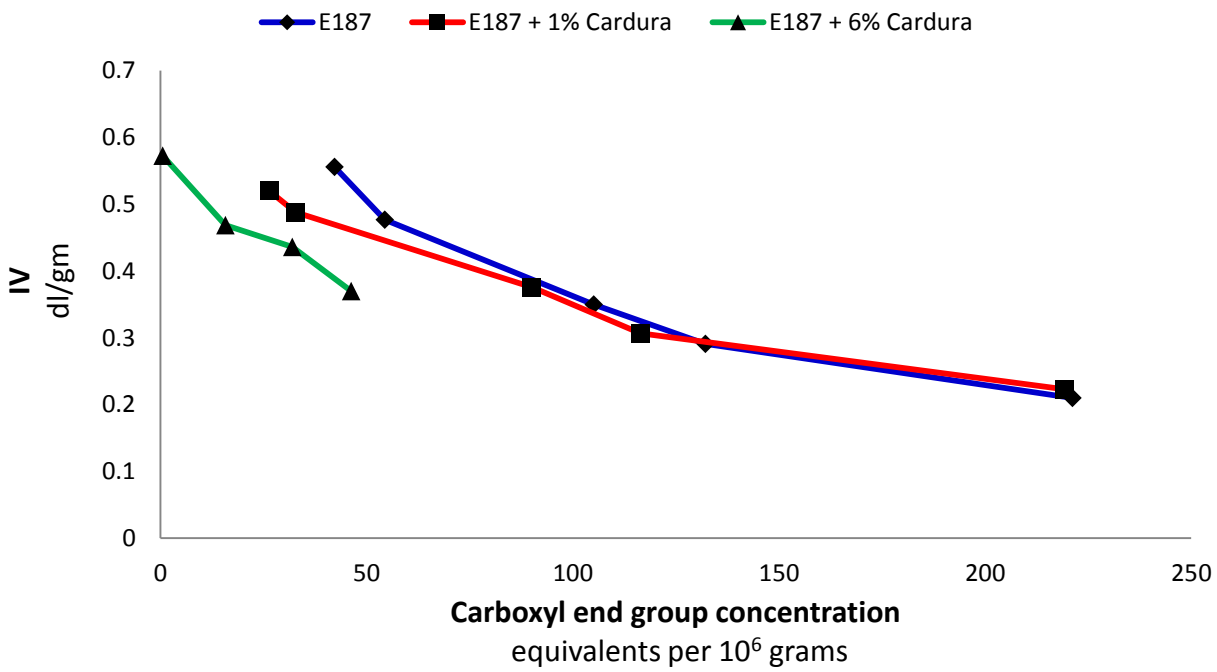

Figure 7.41 – Scatter plot of IV versus the carboxyl end group concentrations of the E187 samples. A single measurement was obtained.

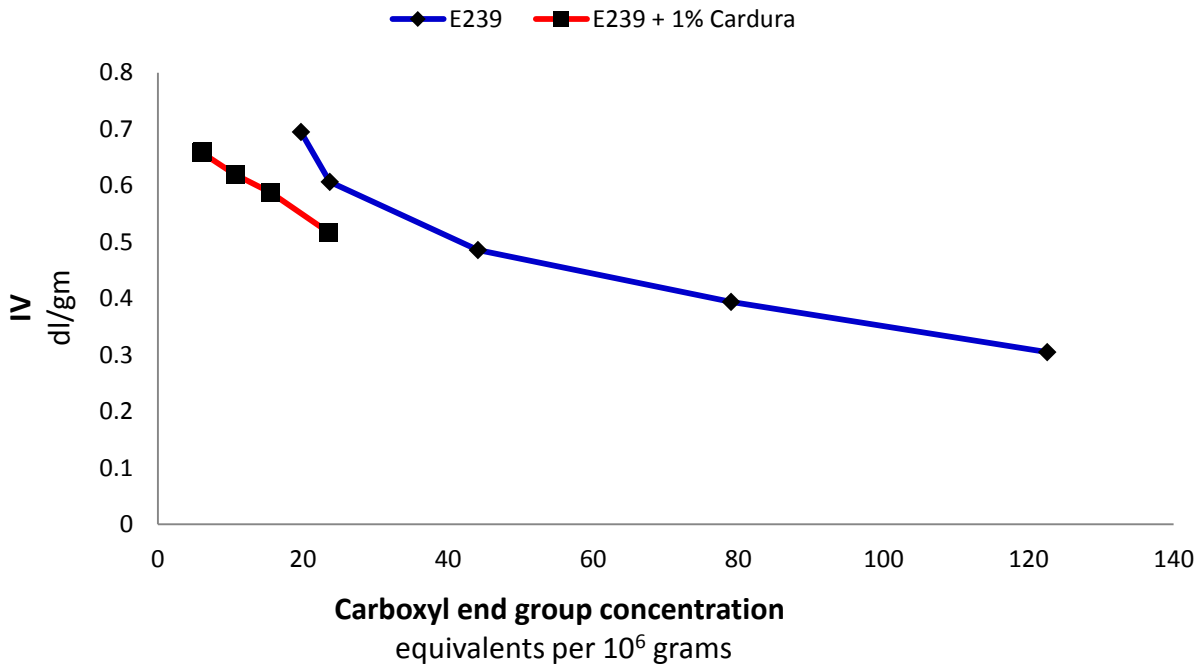

Figure 7.42 – Scatter plot of IV versus the carboxyl end group concentrations of the E239 samples. A single measurement was obtained.

The relationship between the IV and the carboxyl end group concentration for most of the polymer types is exponential. The samples with low carbonyl end group concentrations (E187 + 6% Cardura and E239 + 1% Cardura) appear to be linear. This is expected to be the start of the exponential, and samples that have been aged for longer could be added to support this. All of the IV data for the different polymer types was plotted against the average carboxyl end group concentration (Figure 7.43). The trend produced is similar to the graphs generated for the individual polymer types. The equation of the line produced is $y = 0.606e^{-0.005x}$. More data points could be added to the graph, particularly for samples that have been aged for longer periods of time to strengthen the data.

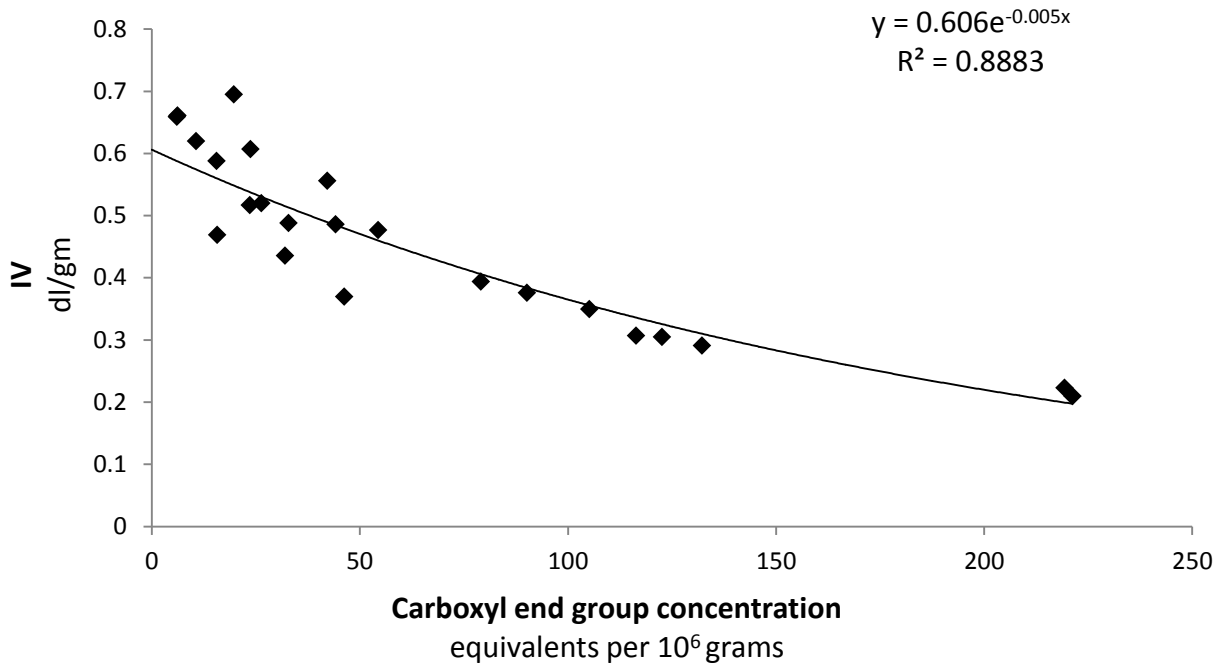

Figure 7.43 – Scatter plot of IV versus the carboxyl end group concentrations.

The carboxylic end group concentration is linearly proportional to molecular weight but a more complicated relationship exists for IV and molecular weight. It would be of interest to carry out a kinetic study of this in the future.

7.2.9 Crystallisation Temperature

All of the aged samples were analysed by DSC to obtain the crystallisation temperature upon cooling from the melt. It is expected that the samples would become more crystalline the longer they were aged, producing an increase in the melting temperature and crystalline content. This increase is due to a phenomenon known as chemi-crystallisation. This is a secondary crystallinity process where entangled polymer chains in the amorphous phase undergo chain scission. The smaller chain segments released can form new crystals or attach to the growth faces of pre-existing crystals, increasing crystallinity. Graphs of the crystallisation temperature versus the carboxyl end group concentration for each of the E187, E239 and E240 sample sets that have been aged where the water has been changed are shown in figures 7.44

to 7.46. The graphs for the polymer samples where the water has not been changed are shown in the appendices (A7.2.1 to A7.2.2).

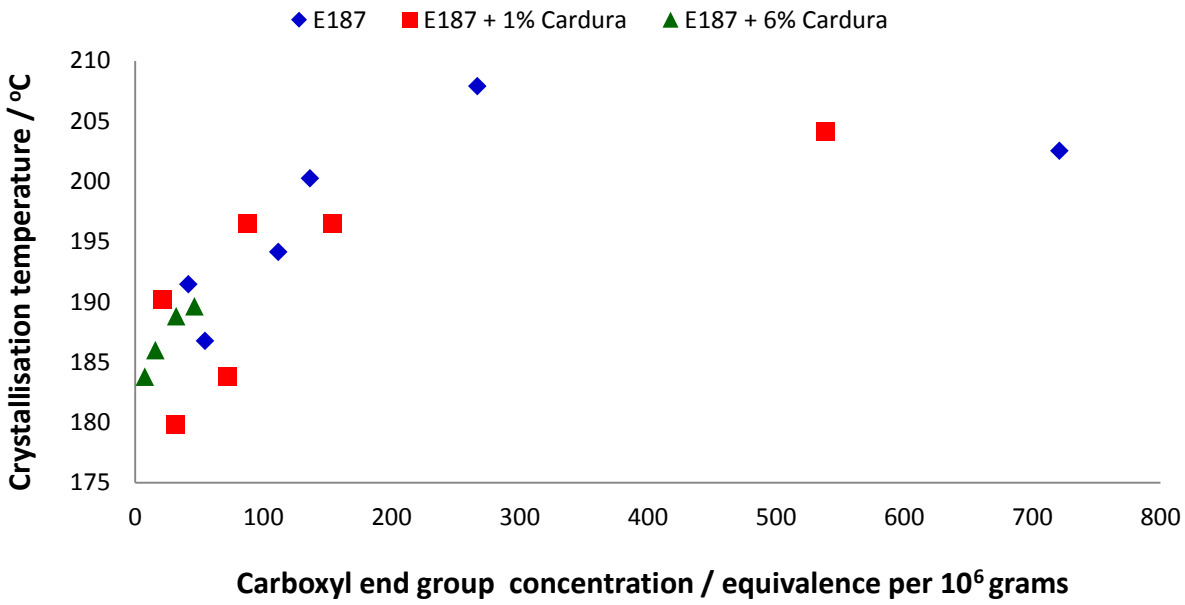

Figure 7.44 - Scatter plot of crystallisation temperature versus the end group concentration for the E187 samples that were prepared with the water being changed. A single sample was analysed.

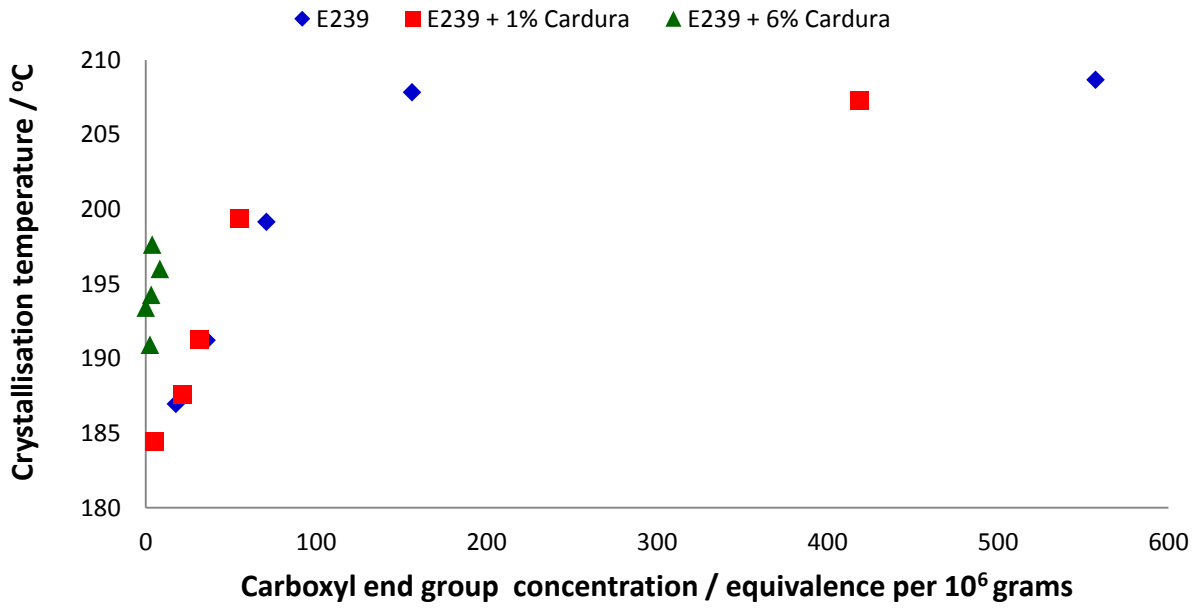

Figure 7.45 - Scatter plot of crystallisation temperature versus the end group concentration for the E239 samples that were prepared with the water being changed. A single sample was analysed.

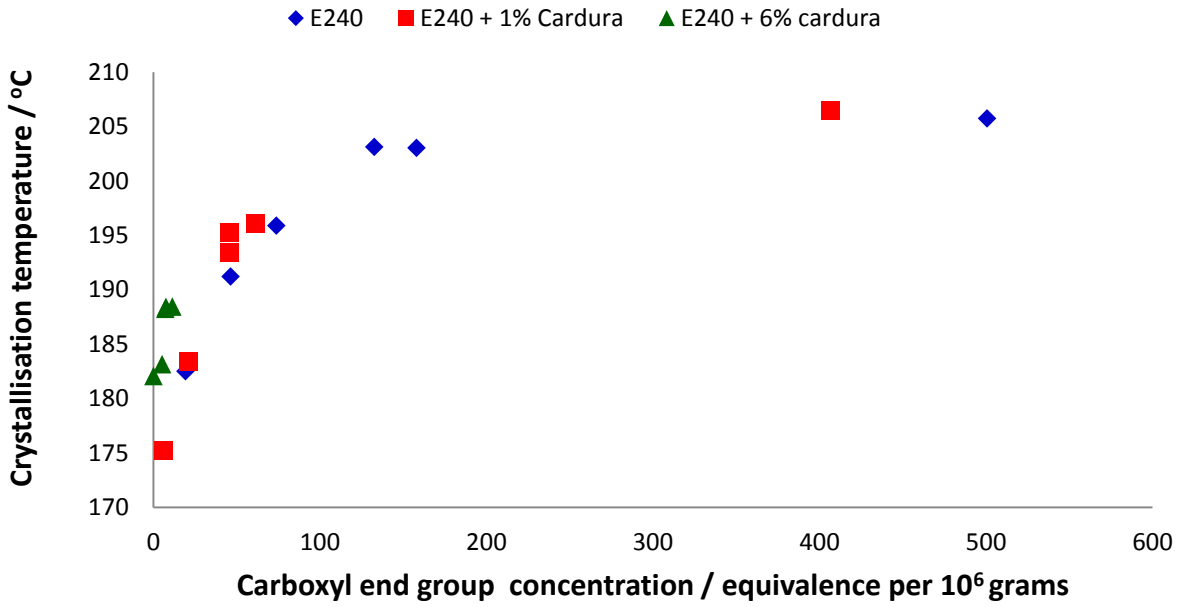

Figure 7.46 - Scatter plot of crystallisation temperature versus the end group concentration for the E240 samples that were prepared with the water being changed. A single sample was analysed.

Based on the data acquired for the hydrolysed samples that contained 1% Cardura, a lower crystallisation temperature was present. This is a result of the polymer not being broken down into smaller chains as much as in the samples without Cardura. A reliable relationship linking the crystalline temperature to the carboxyl end group concentration could not be obtained, as the difference between the values are relatively small and the standard deviations of the crystallisation temperature ranged from 0.19 to 2.44 °C.

7.2.10 Melting Point

The melting points of the aged samples were also investigated to see if any trends were present. Graphs were obtained of the melting point versus the carboxyl end group concentrations for the E187, E239 and E240 sample sets, with and without Cardura. Figures 7.47 and 7.48 show the average melting points obtained of both the initial and reheat scans of the DSC program for the E187 and E187 + 1% Cardura samples that have been hydrolysed for

28 days, with the water in the experiment being changed every two days. The graphs for the other polymer types and for the sample sets where the water was not changed can be found in the appendices section (A7.3.1 to A7.3.13).The initial melting points are normally higher than the reheat scans for all polymer types. There is also normally a slight increase in the initial melting points of the samples as the carboxyl end group concentration increases. These trends apply until the carboxyl end group concentration is too high.

The slight increase in the average melting point obtained from the initial DSC scan as the carboxyl end group concentration increases during hydrolysis is due to the lamellar interface causing lamellar thickening. As the ageing time increases significantly, the melting point decreases sharply, as the molecular weight is decreasing significantly in this environment. The melting point obtained from the initial DSC scan is always higher than the reheat scan because the initial scan's melting point peak is broader. This is due to the distribution in molecular weight, but after the samples have crystallised the peak becomes sharper. There is only a small change in the melting points obtained from the reheat scans of the aged samples, but with a high error value ranging from 0.15 to 1.98 ^{o}C. The values used in the scatter plots are for three repeat experiments.

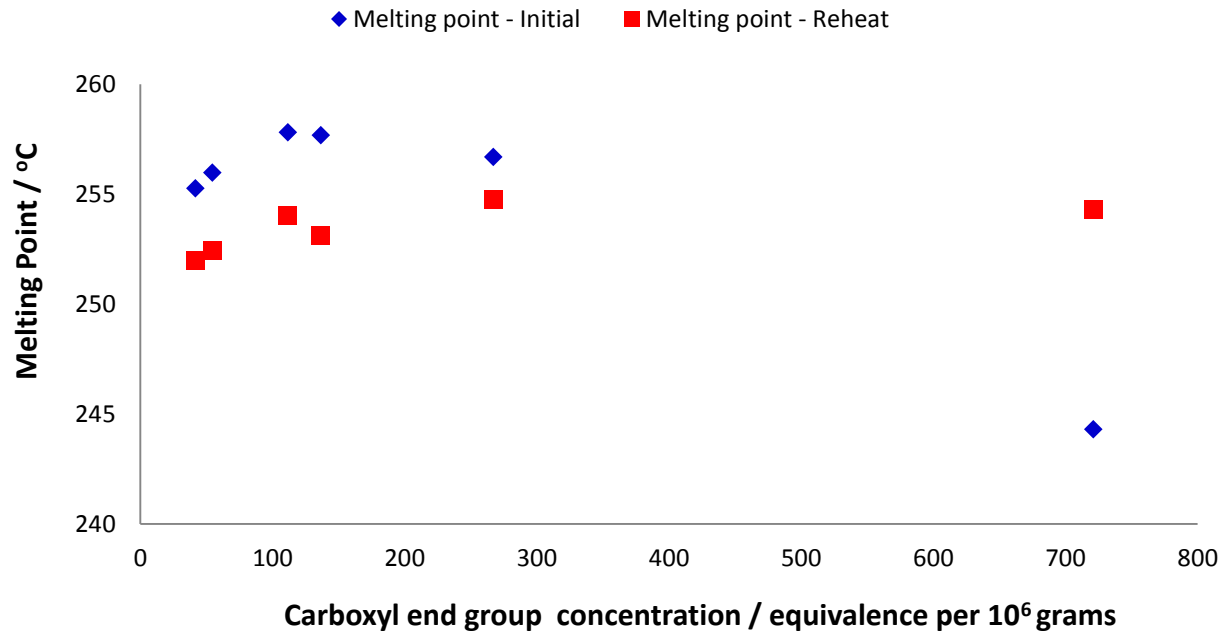

Figure 7.47 – Scatter graph of the melting temperature versus the carboxyl end group concentrations for the E187 samples. A single sample was analysed.

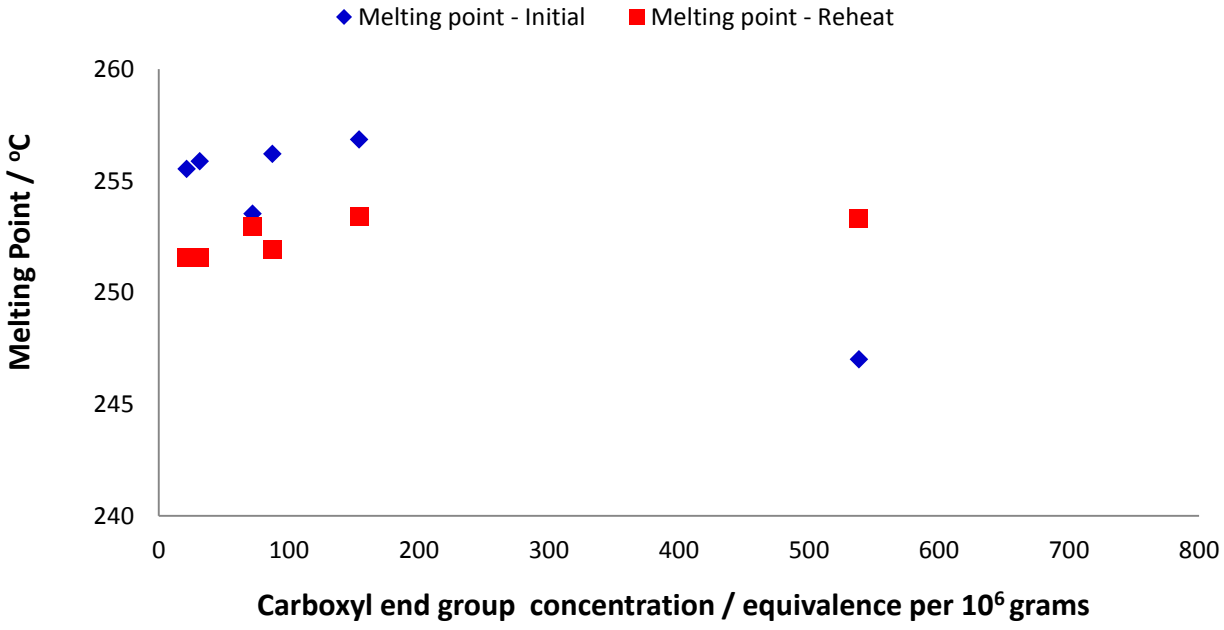

Figure 7.48 – Scatter graph of the melting temperature versus the carboxyl end group concentrations for the E187 + 1% Cardura samples. A single sample was analysed.

An interesting trend is however noticed where the melting point increases for shorter ageing times (between 7 and 10 days). This is due to hydrolysis occurring at the folds in the amorphous region, and as hydrolysis occurs at the folds the chains straighten. [10]This is known as lamellae thickening. At the longer ageing times the melting point drops since the chains have become so degraded. The graphs in figures 7.49 to 7.52 show the trends described above with the E187, E187 + 1% Cardura, E239 and E239 + 1% Cardura samples that have been aged without the water being changed. All other data can be seen on the attached disc in the folder *Chapter 7* under *DSC* and follows the same trend.

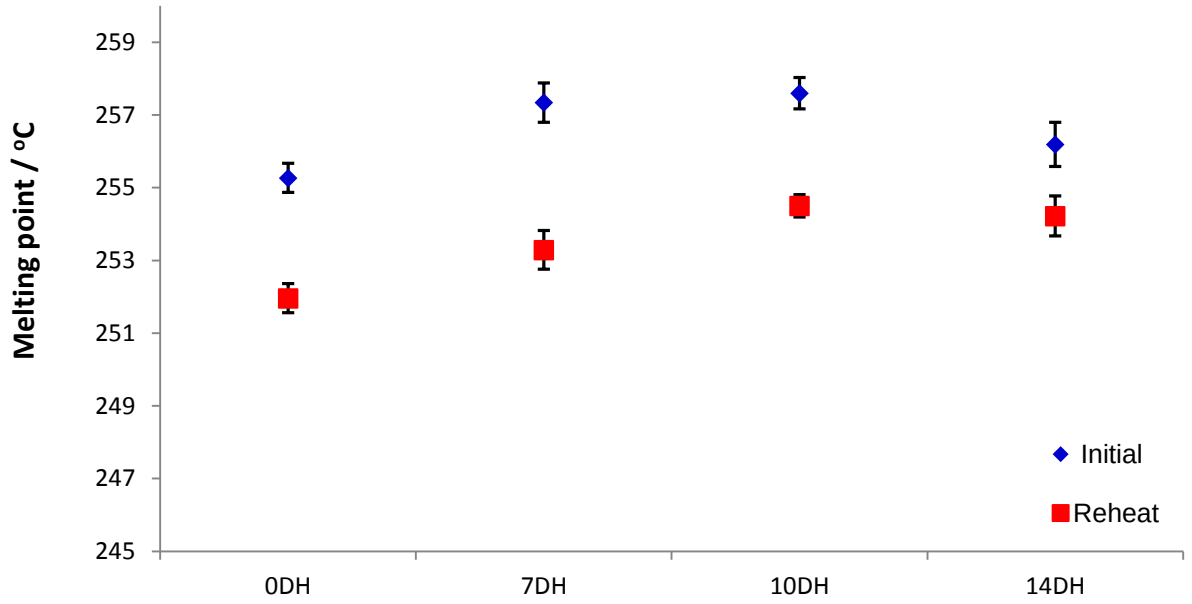

Figure 7.49 – Scatter plot of the melting point versus carboxyl end group concentration for the E187 samples. A single sample was analysed.

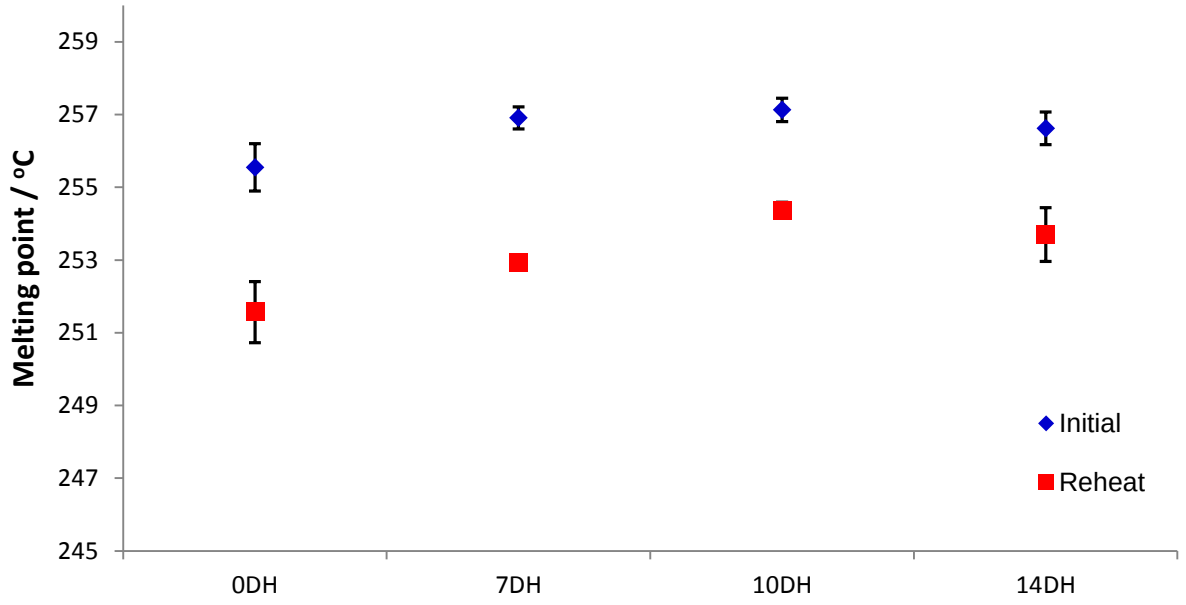

Figure 7.50 – Scatter plot of the melting point versus carboxyl end group concentration for the E187 + 1% Cardura samples. A single sample was analysed.

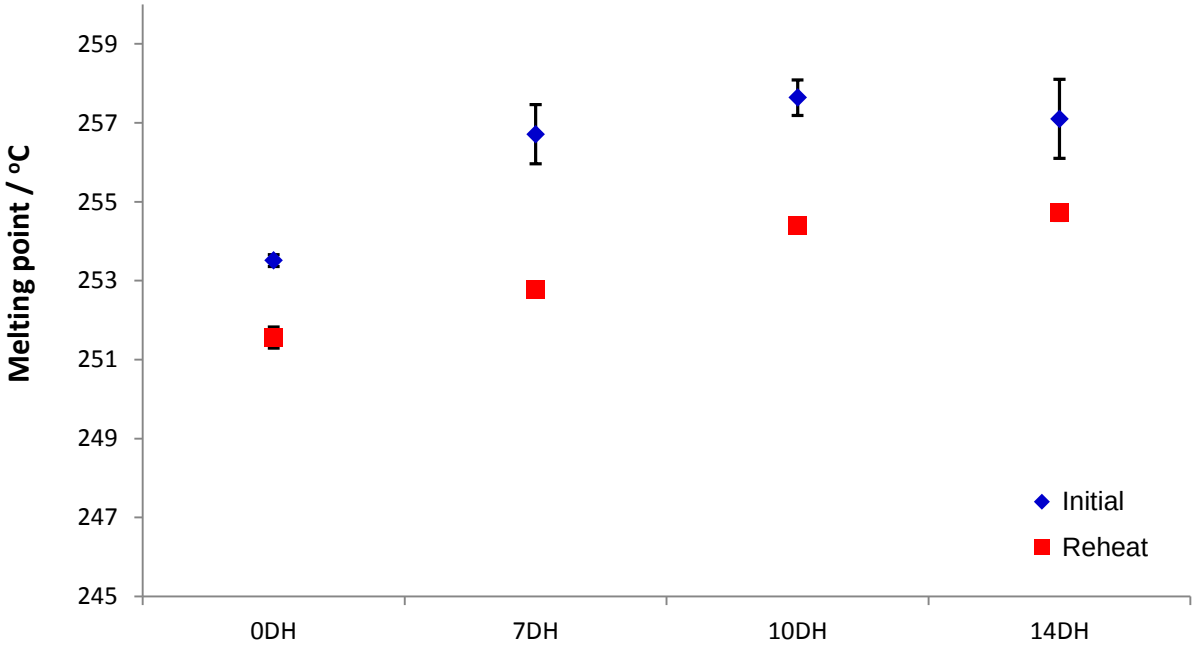

Figure 7.51 – Scatter plot of the melting point versus carboxyl end group concentration for the E239 samples. A single sample was analysed.

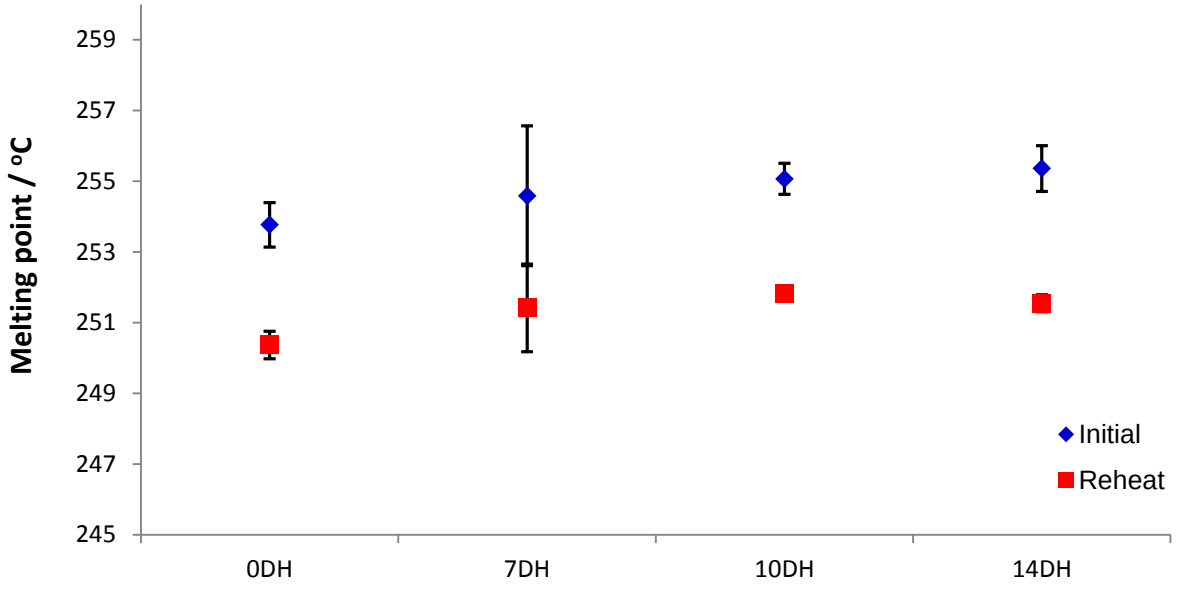

Figure 7.52 – Scatter plot of the melting point versus carboxyl end group concentration for the E239 + 1% Cardura samples. A single sample was analysed.

7.2.11 IR

The IR spectra were obtained using a portable ATR instrument from Agilent Technologies for the E187 samples that were aged at room temperature. Figure 7.53 shows the IR spectra of the E187 samples aged at room temperature for up to 14 days. There were no significant changes between any of the spectra. Changes witnessed in the spectra are due to intensity differences created because of varying clamping pressures between the samples. If hydrolysis was occurring there would be changes witnessed at the peaks 1092, 1237, 1717 and 2960 cm^{-1}. The clamp is used to hold the sample in close contact with the diamond interface. There was no difference noticed in the IR spectra of the E187 + 1% Cardura and E187 + 6% Cardura sample sets aged up to 14 days at room temperature, the spectra for which can be seen in the appendices (A7.4.1. and A7.4.2). The IR spectra were similarly obtained for the E187 samples that were aged up to 14 days at 50 °C. Figure 7.54 shows the IR spectra of the E187 samples aged at 50 °C for up to 14 days. There were no noticeable changes between any of the spectra.

The same trend was noticed in the IR spectra of the E187 + 1% Cardura and E187 + 6% Cardura sample sets aged up to 14 days at room temperature. The IR spectra for the E187 + 1% Cardura and E187 + 6% Cardura samples are seen in the appendices (A7.4.3 and A7.4.4).

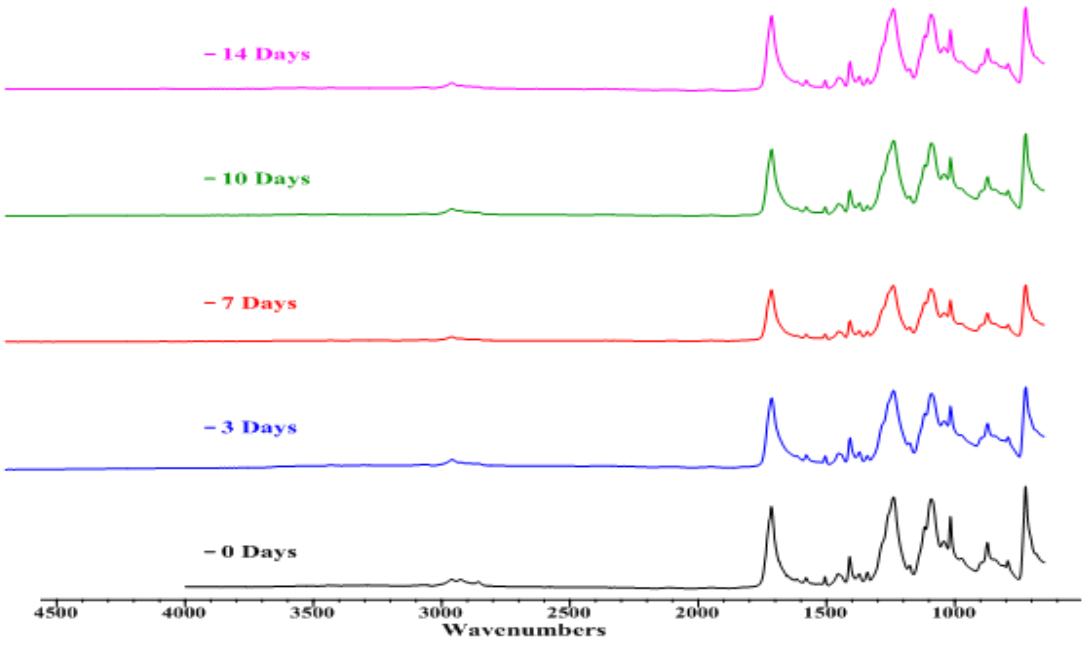

Figure 7.53 - IR spectra of the E187 samples aged at room temperature for up to 14 days. A single spectrum is shown for each time point.

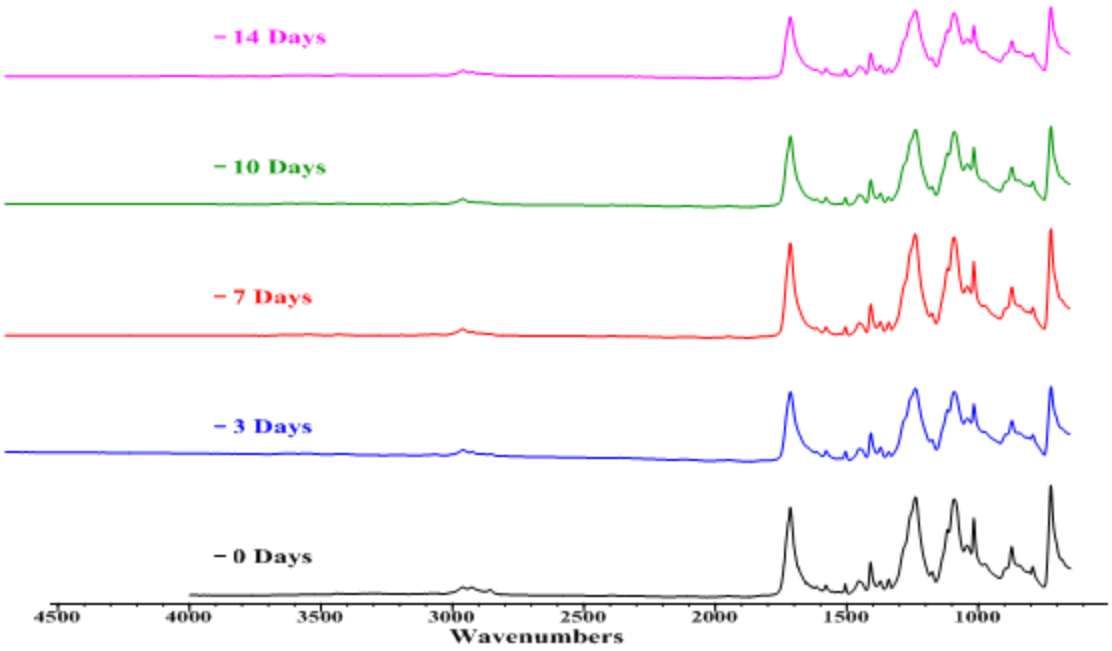

Figure 7.54 - IR spectra of the E187 samples aged at 50 °C for up to 14 days. A single spectrum is shown for each time point.

The samples that were aged for 28 days at 100°C were analysed by IR spectroscopy. The spectra for the E187 samples that were aged at 100 °C for 28 days are shown in figure 7.55. The main peaks in the IR spectra are the same as the samples that were not aged. There are slight changes in the peaks at 1043, 1453, 1091, 1240, 1717 and 2960 cm^{-1}. The peak at 2960 cm^{-1} appears to be reducing significantly, which would indicate that hydrolysis is occurring because the aliphatic backbone of PET is being reduced. This size reducing in the peak could however be due to the pressure of the clamp varying between samples. Similar changes were noticed in the IR spectra of the E187 + 1% Cardura and E187 + 6% Cardura sample sets that have been aged for 28 days at 100 °C. The IR spectra for all aged E187 samples that contain Cardura are shown in the appendices (A7.4.5 and A7.4.6). Further analysis of the IR spectra would be required to determine if hydrolysis was occurring and to indicate how significantly so.

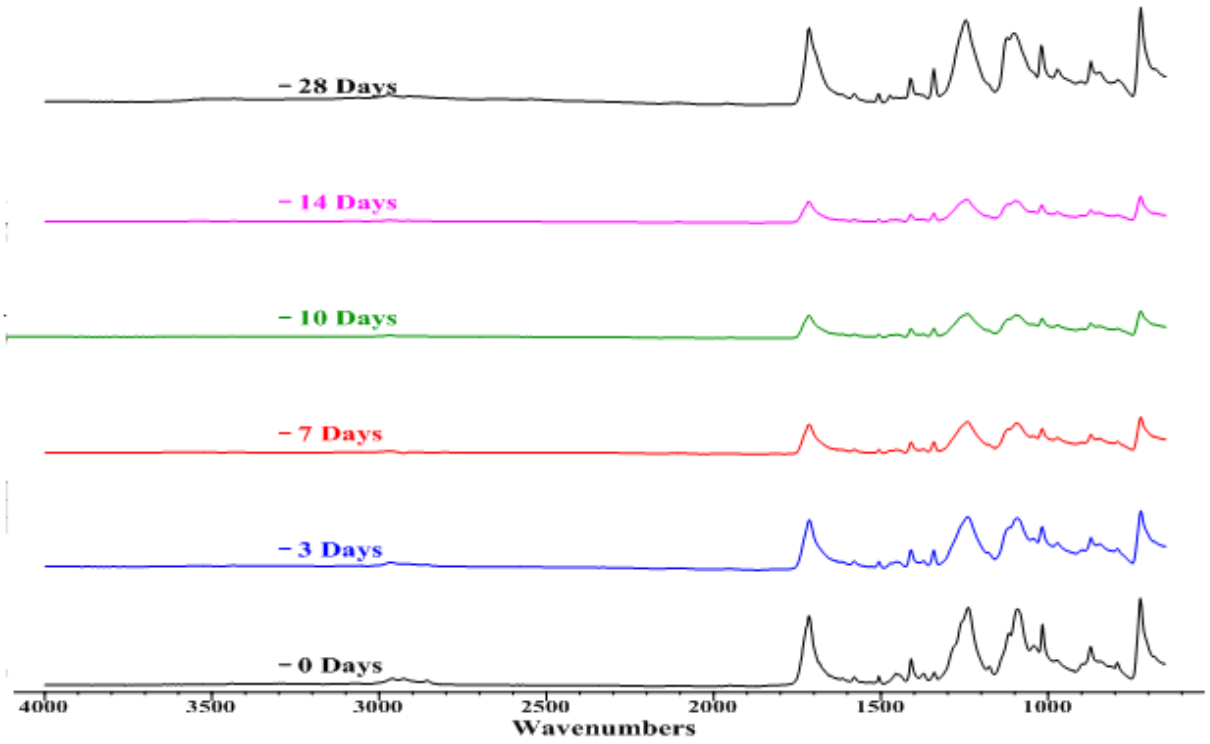

Figure 7.55- IR spectra of the E187 samples aged at 100 °C for up to 28 days. A single spectrum is shown for each time point.

The changes witnessed in the IR spectra are consistent with the hydrolysis reaction occurring, but the changes are very small. The ester peaks change from 1092 and 1237 cm^{-1} in the non-aged PET to 1096 and 1245 cm^{-1} in the PET aged for 10 days. These changes are consistent with the ester hydrolysis. To confirm that hydrolysis is occurring, multiple spectra were normalised and averaged. The area of the peaks at 1092, 1237, 1717 and 2960 cm^{-1} were calculated and then ratioed with a peak in the spectra that corresponds to an aromatic peak from the backbone of PET which does not change. Figure 7.56 shows the IR spectra of the samples that have been hydrolysed for 0, 3 and 7 days, with the peaks at 1092, 1237, 1717 and 2960 cm^{-1} highlighted as these are the points of interest. The data is only analysed up to 10 days because samples that have been aged for longer change physical state. After the samples have been aged for 10 days the sample becomes very brittle and turns to powder under the pressure of the clamp.

The changes due to the ester linkages at 1092 and 1237 cm^{-1} are shown to be increasing slightly as the ageing time increases; these can be seen in figures 7.57 and 7.58, respectively. The peak at 1717 cm^{-1} changes position slightly, and there is an increase in this region due to carbonyls from the acid end group being more intense than the ester groups. The ratioed peak area corresponding to the CH_2CH_2 sections of the PET backbone (2960 cm^{-1}) decreases as the time exposed to the hydrolysis conditions increases. This decrease is due to these units being changed into alcohol and carboxylic acid groups. This graph is shown in figure 7.59. This highlights that these components are being consumed the longer the polymer is exposed to the accelerated ageing conditions. This confirms that these peaks are breaking down into smaller molecules. The literature states that during hydrolysis the PET backbone breaks at the ester linkage to form carboxyl end groups. The ratioed peak area for the carboxyl peak (1717 cm^{-1}) does agree with the literature by showing an increase as the time exposed to the hydrolysis conditions increased. This increase is caused by the more intense carbonyl groups present in the acid end groups instead of the ester groups. The graph for this is seen in figure 7.60. The results obtained from the AT-IR measurements agree with results obtained from the Pohl titration. The two methods show that the carboxyl end group concentration increases the longer the samples are aged.

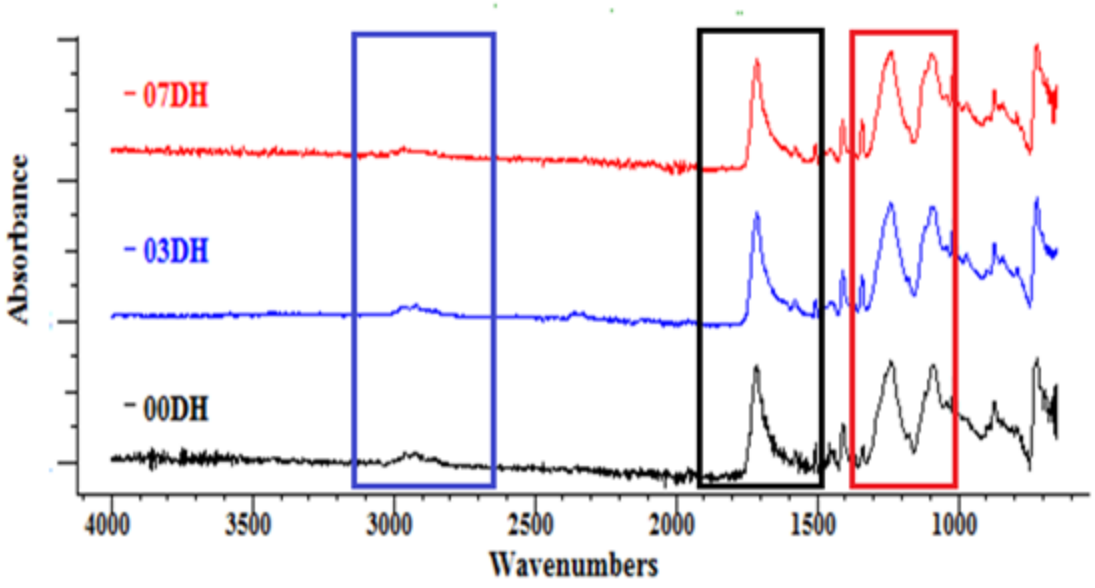

Figure 7.56 – IR spectra of the samples that have been hydrolysed for 0, 3 and 7 days. Highlighted sections show regions of interest namely the peaks at 1092, 1237, 1717 and 2960 cm^{-1}. Average of 10 spectra are shown for each time point.

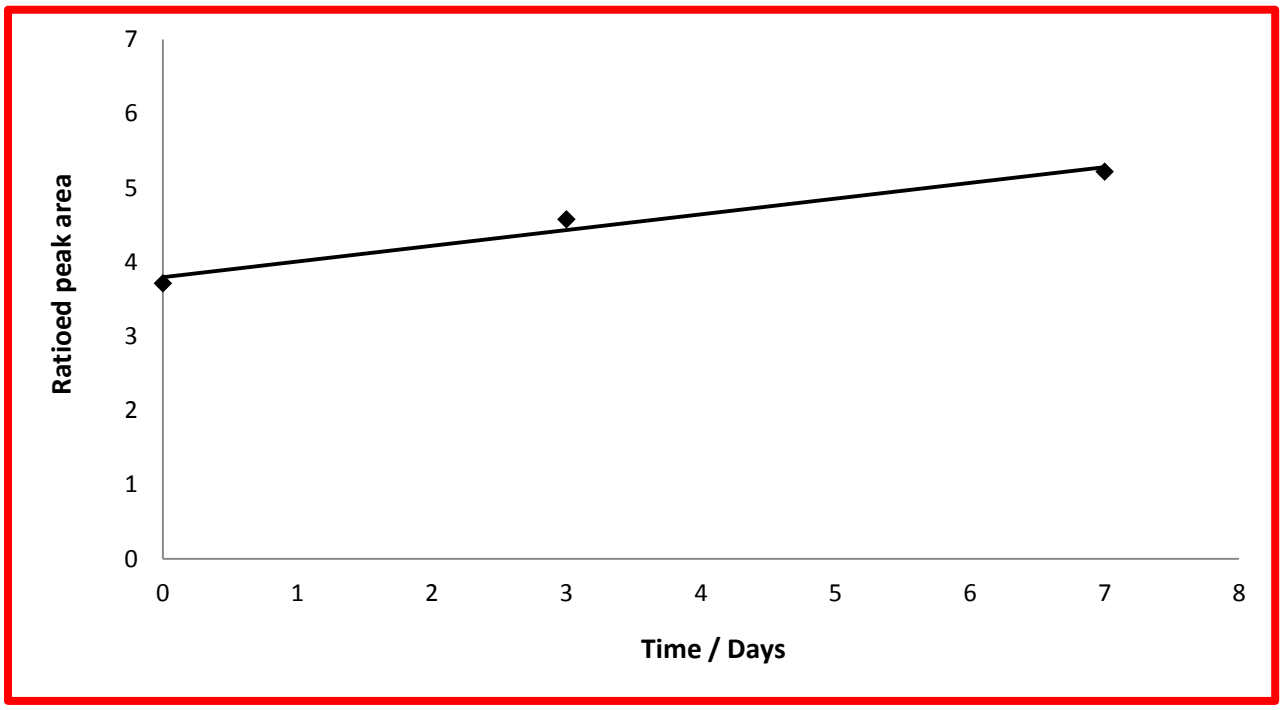

Figure 7.57 - Ratioed peak area vs. ageing time for the peak at 1092 cm^{-1} from the IR spectra of the samples that have been hydrolysed for 0, 3 and 7 days .

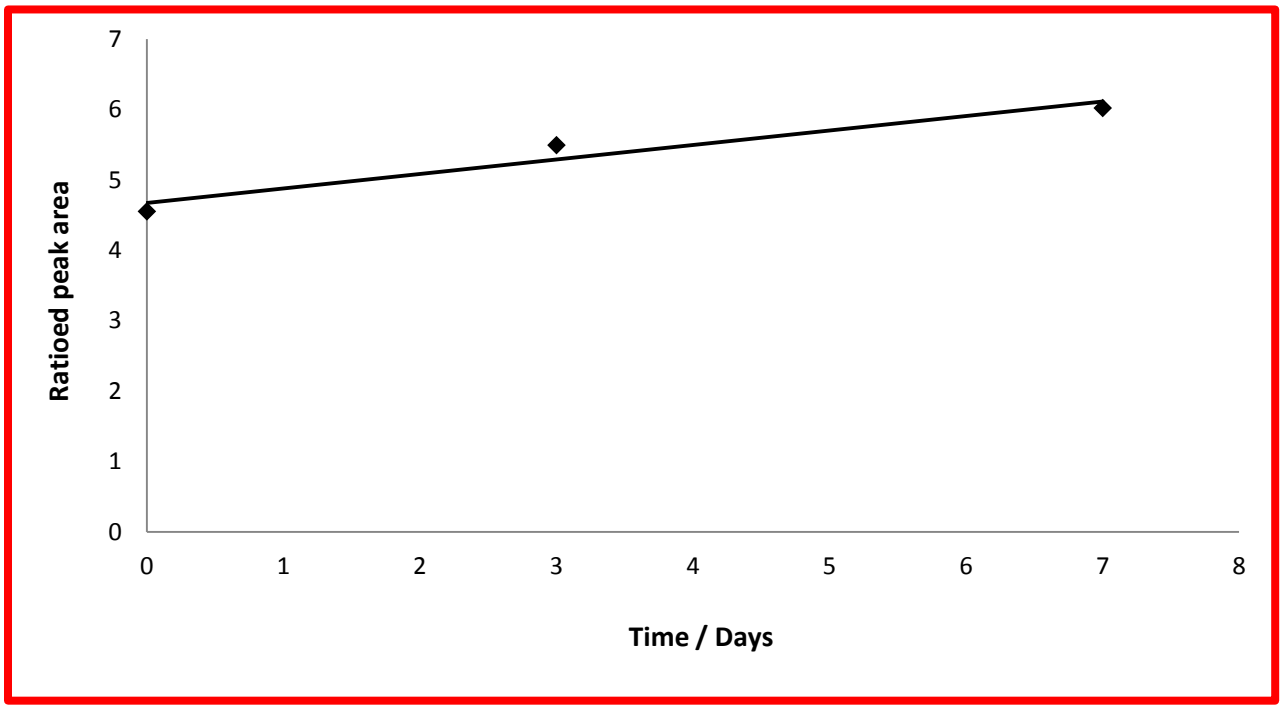

Figure 7.58 - Ratioed peak area vs. ageing time for the peak at 1237 cm^{-1} from the IR spectra of the samples that have been hydrolysed for 0, 3 and 7 days .

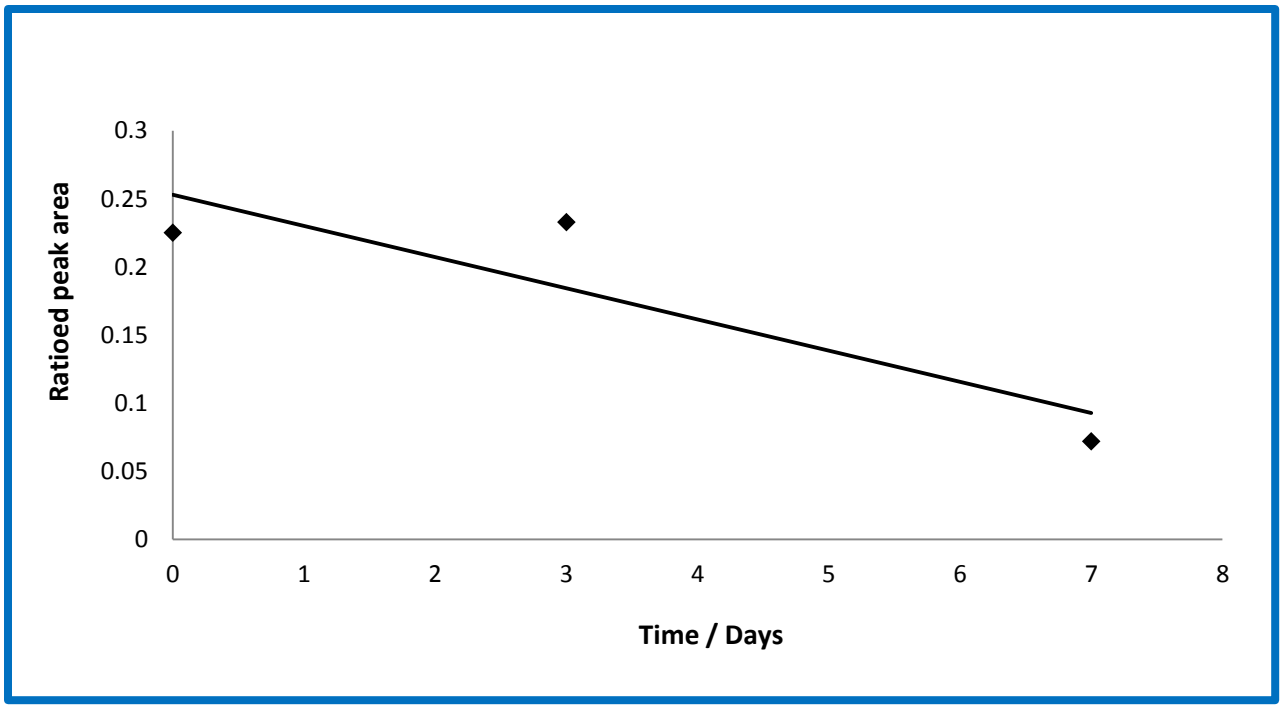

Figure 7.59 - Ratioed peak area vs. ageing time for the peak at 2960 cm^{-1} from the IR spectra of the samples that have been hydrolysed for 0, 3 and 7 days .

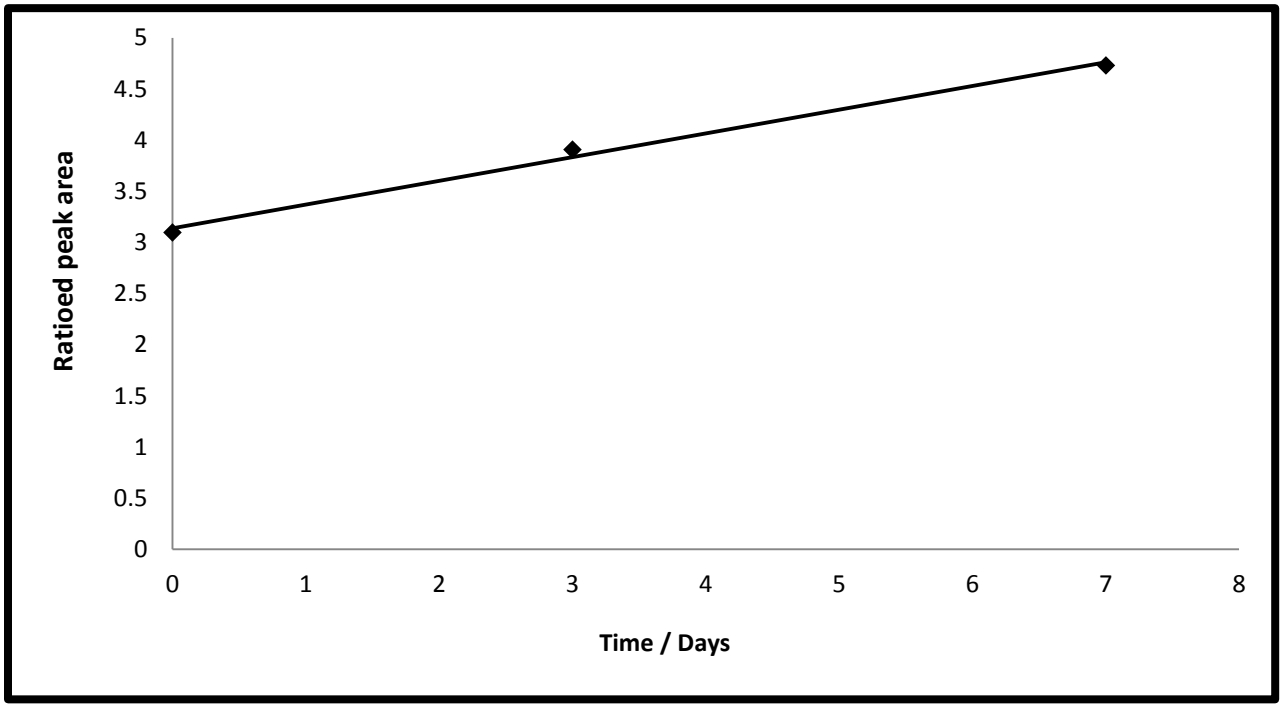

Figure 7.60 - Ratioed peak area vs. ageing time for the peak at 1717 cm^{-1} from the IR spectra of the samples that have been hydrolysed for 0, 3 and 7 days .

7.3 Conclusions

There were no changes measured in any of the polymer samples aged in distilled water at room temperature up to 14 days. The same trend was noticed for the E187 samples prepared with Cardura, Vikolox and Heloxy. There were no noticeable changes between any of the sample sets that were prepared at 50 ^{o}C. The water uptake measured in these samples was shown to be very small, but further experiments would be beneficial to strengthen this data.

It was shown that significant hydrolytic degradation occurs in PET above it's glass transition temperature. Hydrolytic degradation is expected to occur mostly above the glass transition temperature from the literature. [10 and 42] The longer the polymer is exposed to the conditions to promote hydrolytic degradation the more the carboxyl end group concentration increases. An exponential trend is generated for the sample that implies an auto-catalytic reaction is occurring. The end group concentrations of the samples have been investigated under two different conditions and the values obtained are similar.

The monofunctionalised epoxide referred to as Cardura reacts significantly with the carboxyl end groups of PET, causing a significant reduction in the carboxyl end group concentration. A reduction in the carboxyl end group concentration does reduce the effects of hydrolytic degradation as it reduces the parameters required for an auto-catalysis reaction to occur. It has been shown that a higher concentration of Cardura increases the protective effect, as it ensures that all of the carboxyl end groups are end capped. The other two epoxides investigated (Heloxy and Vikolox) also reduce the carboxyl end group concentration of the aged samples. This shows that these epoxides also end cap the end groups, reducing the effects of hydrolytic degradation occurring, which results in it taking longer to reach auto-catalytic conditions. The Heloxy samples had a higher carboxyl end group concentration than Vikolox and Cardura, which suggested it was less efficient as an end capping agent.

The data gathered suggests that Cardura is the most efficient at increasing PET's life span when exposed to the conditions of hydrolytic degradation. Cardura would be the most desirable

epoxide to be selected for reacting with PET in the application of solar cell panels. This epoxide has been shown in Chapters 4 to 6 to be the most reactive and a suitable candidate to be used in reactive extrusion.

The data comparing the solid state polymerised samples (E239 and E240) with E187 suggests there is a slight decrease in the rate of hydrolytic degradation due to the lower initial carboxyl end group concentration. This would allow a lower concentration of the epoxide additive to be used by DTF to achieve a similar result. Having to solid state polymerise the PET adds a process step and as a result a cost. The most economical and cost effective solution will be carefully decided by DTF.

The scatter plots created of $[COOH]_t^{0.5} - [COOH]_0^{0.5}$ against time for all of the polymer samples with and without Cardura produced straight lines with high coefficients of determination. This confirmed that the hydrolysis reaction was a half order reaction. The apparent reaction rate was shown to reduce with the addition of Cardura to the samples. This confirmed that the Cardura was reducing the effects of hydrolytic degradation, allowing it to maintain its properties for longer in the environment studied. This would allow PET to survive longer in an application where it comes into contact with excessive heat and excess water, such as when used as a backsheet for solar cell panels. Similar plots were obtained for the epoxides Vikolox and Heloxy, but these were only aged up to 10 days. The carboxyl end group concentration generated for these samples was very low and with the high error of the Pohl titration method these graphs were not straight lines. Samples would need to be generated at higher ageing temperatures to allow these to be fed into the same model.

Some IR spectra were obtained of the two hydrolysis products generated to give an indication of their nature. The hydrolysis products were suspected to be terephthalic acid and ethylene glycol. There is a possibility some oligomers were also present. Further work would have to be carried out to further identify the hydrolysis products produced.

It has been shown that as the carboxyl end group concentration increases the IV of the sample will decrease. A reliable connection between the carboxyl end group concentration and the IV has been established.

The crystallisation temperature increases as the carboxyl end group concentration increases. Lamellar thickening was witnessed in the initial DSC scan of the PET samples that were hydrolysed. An interesting trend was noticed in the graphs of melting point versus time where the samples aged for a short period of time (less that 10 days) produced an increased melting point but the samples aged over 10 days showed a decrease in melting point due to significant degradation occurring.

There were no significant changes in any of the IR spectra of the samples exposed to the room temperature or 50 ^{o}C conditions, but there were small changes that were consistent with hydrolysis occurring in the samples aged at 100 ^{o}C. To confirm that the esterification reaction could be monitored by AT-IR spectroscopy the samples had to be normalised and averaged to prevent the effects of the pressure clamp causing variations in the intensity. The results were integrated and the changes confirm that the esterification reaction is occurring and can be monitored. It was shown to be limited when monitoring the highly aged samples such as 14 days and 28 days, as they were brittle and broke easily under the pressure of the clamp. This turned the samples into a powder, changing their physical state.

8.0 Characterisation of the Degradation Behaviour of Extruded Materials - Thermal Degradation

8.1 Introduction

As discussed in Chapter 1, thermal degradation can occur during processing of PET. It is therefore important that DTF is aware of any beneficial or adverse effects on the degradation behaviour of the samples that were occurring for successful utilisation of these additives by DTF.

The thermal degradation behaviour was studied for the polymer samples containing Cardura, Vikolox and Heloxy using DSC, TGA, TVA, a custom-built ageing rig and a Hiden CATLAB system.

8.2 Results and Discussion

8.2.1 DSC

The DSC scans showing the degradation behaviour were obtained for the polymer samples. The DSC scans for the E187 and E187 + 6% Cardura samples are shown in figures 8.1 and 8.2 respectively. The DSC scans for the E187 + 6% Heloxy and E187 + 6% Vikolox samples are shown in the appendices (A8.1.1 and A8.1.2). The onset temperature of degradation was determined by observation. The temperature of the degradation peaks was also obtained from the DSC scans. The other transitions shown in the DSC scans are the T_g, crystallisation and melting points. The values for all of the transitions for the samples are summarised in table 8.1.

Table 8.1 – Information obtained from the DSC scans of the E187 samples. Values quoted are from a single measurement.

	E187	E187 + 6% Cardura	E187 + 6% Heloxy	E187 + 6% Vikolox
Glass Transition /^{o}C	75	69	75	63
Crystallisation Temperature /^{o}C	135	137	141	108
Enthalpy of Crystallisation / J/g	34	33	32	31
Melting Point / ^{o}C	254	260	253	253
Enthalpy of Fusion / J/g	47	46	44	57
Onset of Degradation / ^{o}C	368	365	373	357
Degradation Peak / ^{o}C	453	448	448	445

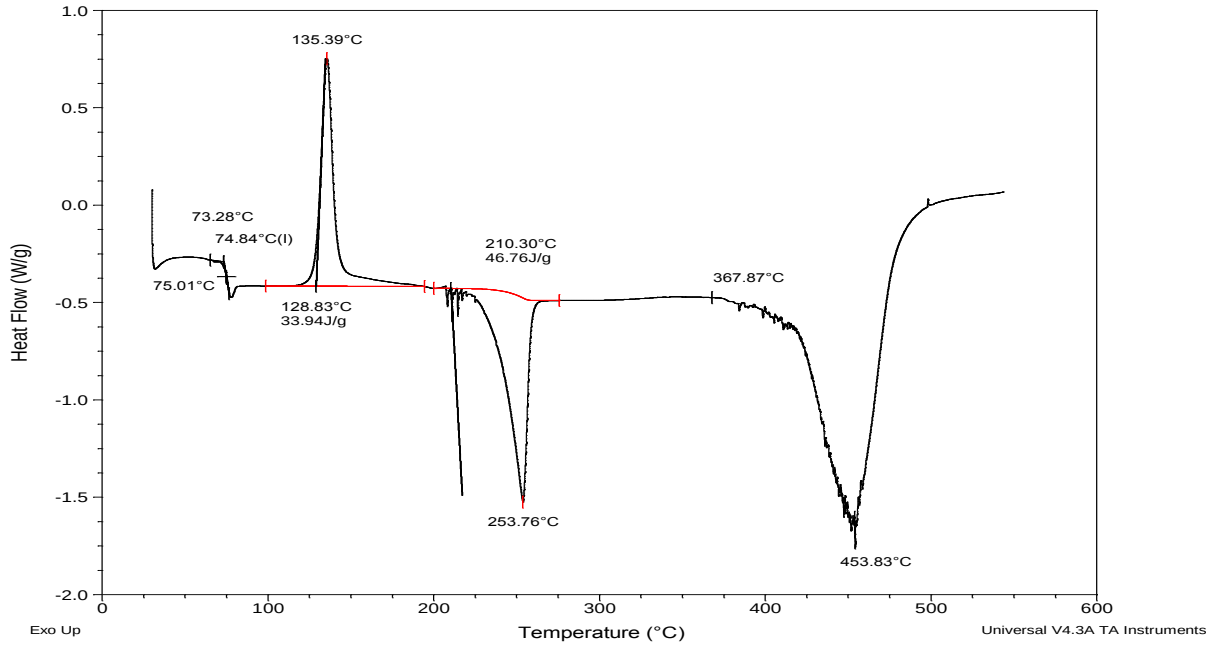

Figure 8.1 – DSC scan of the E187 sample.

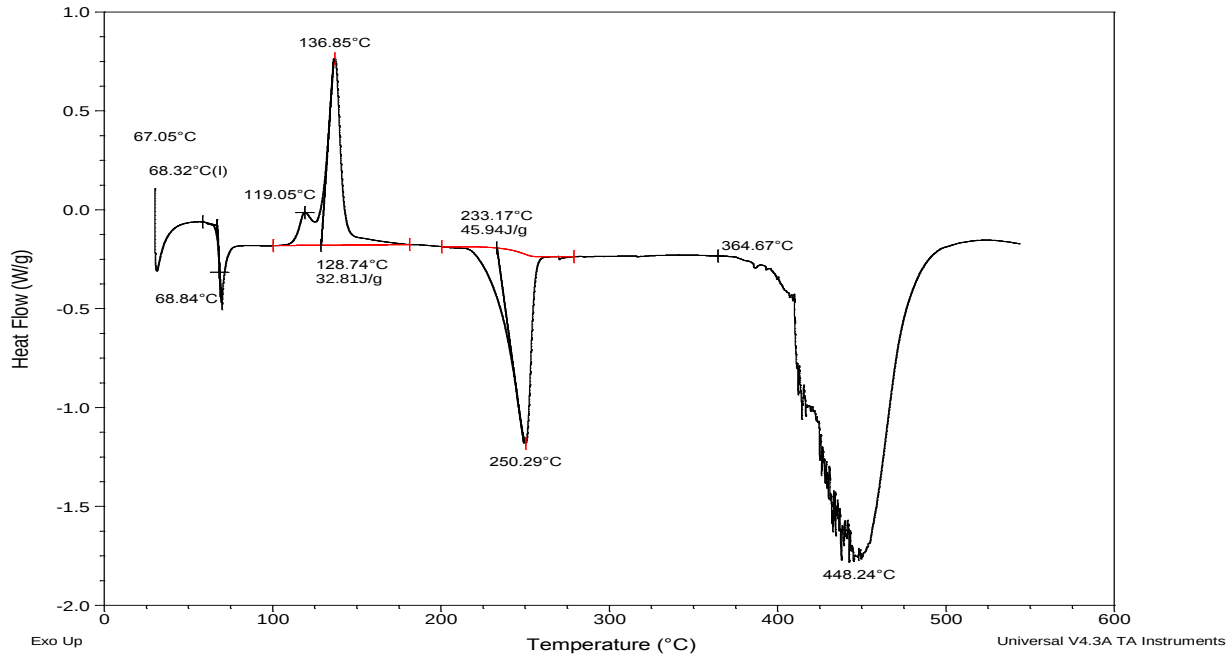

Figure 8.2 – DSC scan of the E187 + 6% Cardura sample.

The onset of degradation for the E187 sample was determined to be 368 ^{o}C. The addition of 6% Cardura made very little difference to the onset of degradation as the value obtained was 365 ^{o}C. A similar reduction was noticed when looking at the degradation peak, which was reduced from 453 ^{o}C for the E187 sample to 448 ^{o}C for the E187 + 6% Cardura sample. The slight reductions are not significant changes for a DSC scan. There were no significant changes noticed in the crystallisation temperature and melting points for the samples with and without Cardura.

The onset of degradation was also determined for the samples that contained E187 + 6% Vikolox and E187 + 6% Heloxy. The onset of degradation for the E187 + 6% Vikolox sample is 373^{o}C, which is only slightly higher than that obtained for the E187 and E187 + 6% Cardura samples. This is expected to be due to the subjective way of determining the onset of thermal degradation. This was confirmed as there is no significant change in the temperature of the degradation peak. The E187 + 6% Vikolox sample had a main crystallisation peak at 108 ^{o}C, which is significantly less than the crystallisation temperature for the E187 samples with and without Cardura.

The onset of degradation was determined to be 357 ^{o}C for the E187 + 6% Heloxy samples which is very similar to the value obtained for the other polymer samples with and without additives. The fact that the changes were not significant was also confirmed by the peak temperature, which was 445 ^{o}C for the sample containing 6% Heloxy and 448 ^{o}C for the samples containing the other epoxides. The crystallisation temperature and melting point are similar to the values obtained for the blank E187.

8.2.2 TGA

The TGA thermograms were obtained for the E187, E239 and E240 samples with and without Cardura. All data from the TGA thermograms is summarised in table 8.2. The onset of degradation was defined as the 0.5% mass loss. The thermograms for the E187 samples with and without Cardura are shown in figures 8.3 and 8.4. The thermograms for the E239 and E240 samples are shown in the appendices (Figures A8.2.1 to A8.2.6). The onset of thermal degradation was calculated to be 332 ^{o}C for the E187 sample. This value is slightly lower than the value of 368 ^{o}C obtained from the DSC scan which is suggested to be the result of a higher than expected experimental error. The error value was calculated to be 9 ^{o}C, which was obtained from the standard deviation of multiple experiments.

The values obtained for the onset of mass loss for the samples that contain Cardura are shown to reduce, as the value obtained for the E187 + 6% Cardura sample was 230 ^{o}C compared with 332 ^{o}C for the E187 sample. This reduction is expected to be due to the excess Cardura in the sample volatilising and not the onset of thermal degradation. The peak temperatures obtained from the derivative of the TGA thermogram show no significant change, which suggests that Cardura is having no effect on the thermal degradation behaviour of PET. Figures 8.3 and 8.4 show no significant changes are occurring in the thermograms. The same trends are shown with the E239 and E240 samples.

Table 8.2 – Table summarising the information from the TGA thermograms. Values quoted are from a single measurement.

	0.5% Mass Loss °C	Peak in DTG °C
E187	332	472
E187 + 1% Cardura	325	459
E187 + 6% Cardura	230	469
E239	344	442
E239 + 1% Cardura	365	463
E239 + 6% Cardura	258	465
E240	389	430
E240 + 1% Cardura	311	463
E240 + 6% Cardura	254	439

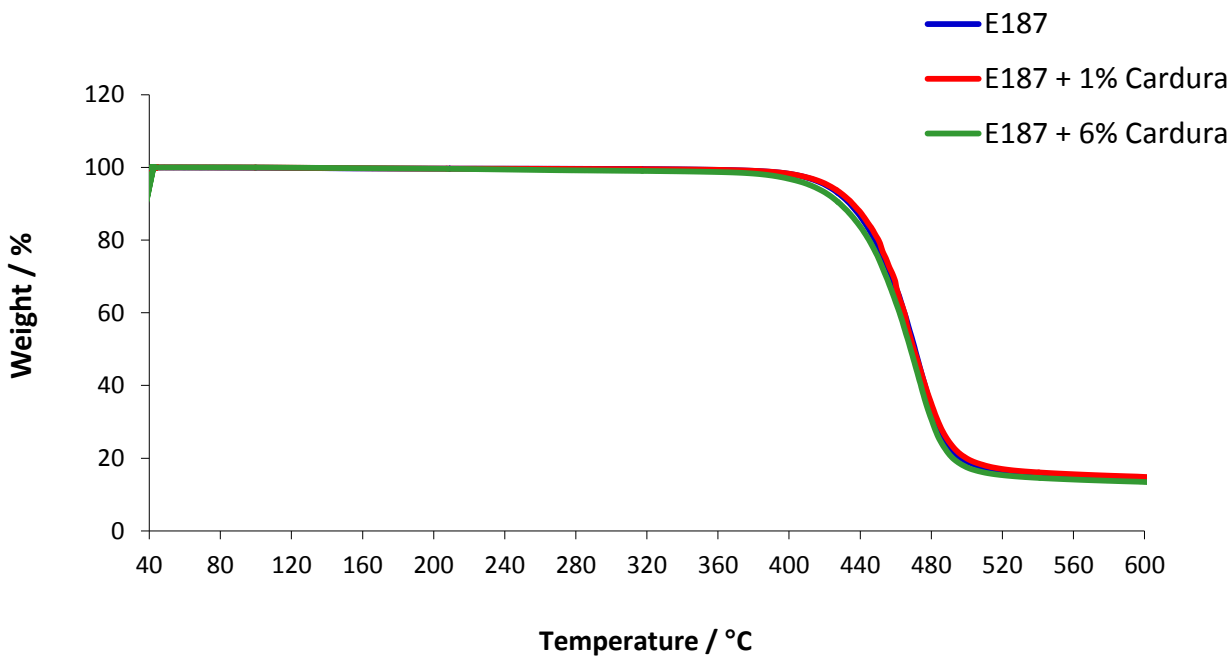

Figure 8.3 – TGA thermogram showing the mass loss of the E187 samples. A single sample was analysed.

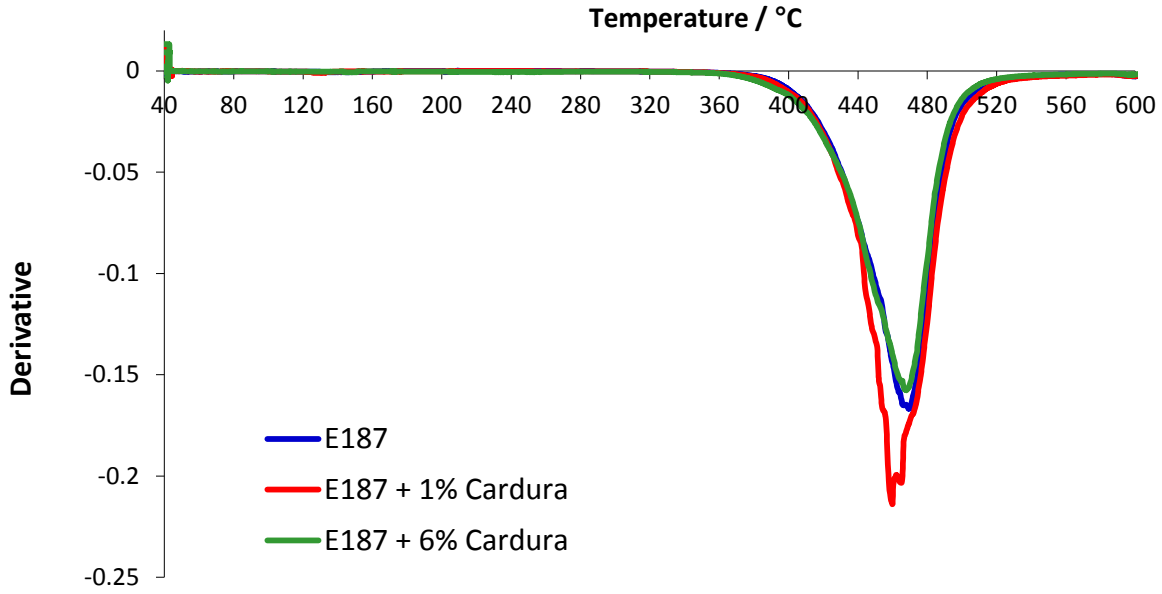

Figure 8.4– Derivative of the TGA thermogram for the E187 samples. A single sample was analysed.

The epoxides Heloxy and Vikolox also show a significant reduction in the onset of mass loss. The E239 + 6% Heloxy sample produced an onset of mass loss of 177 °C, and the E239 + 6% Vikolox sample produced an onset of mass loss value of 209 °C. These reductions are again expected to be due to the excess epoxide boiling off, which was seen in Chapter 4, and not the onset of thermal degradation. No trends were noticed in peak temperature, therefore supporting this conclusion. All epoxides were concluded to have no effect on the thermal degradation behaviour of PET.

Table 8.3 – Table summarising the information from the TGA thermograms. Values quoted are from a single measurement.

	0.5% Mass Loss °C	Peak in DTG °C
E239	344	442
E239 + 6% Cardura	258	465
E239 + 6% Heloxy	177	424
E239 + 6% Vikolox	209	429

8.2.3 TVA

8.2.3.1 Degradation

The thermal degradation of E187 was also investigated using the TVA line. A sample was prepared and analysed for degradation in the TVA line as described in Chapter 3. Figure 8.5 shows the TVA thermogram for the E187 sample. The pressure increase from the Pirani gauges was noticed at 331 ^{o}C. This pressure increase corresponds to the release of gases during thermal degradation, and so provides a reliable temperature value for the onset of thermal degradation. The value that was obtained from the TVA technique is identical to the onset of thermal degradation obtained by TGA, which gave a value of 332 ^{o}C. There was a small peak identified at 98 ^{o}C, which was expected to be a result of moisture being present. This increase is so small that it is not noticed on the thermogram generated for the E187 sample.

The samples containing 1% and 6% w/w of the epoxides, Cardura, Heloxy and Vikolox, all produce a very small peak between 80 and 100 ^{o}C. These peaks are too small to appear on the thermogram and are expected to be a result of moisture present within the sample. The values obtained for the onset of volatile release are shown in table 8.4. The onset of volatile release of the E187 + 1% Cardura sample was determined to be 331 ^{o}C, which is identical to the blank E187 sample. A significant reduction was noticed in the onset of volatile release for the E187 + 6% Cardura, which was 259 ^{o}C compared to the onset of volatile release obtained for the E187 sample, 331 ^{o}C. The reduction in the onset of volatile release was also noticed in the TGA thermogram for the E187 + 6% Cardura. The lower results determined by TGA and TVA is predicted to be a result of excess Cardura volatilising from the sample. The TVA thermograms produced are similar to the sample without Cardura, supporting that the lower onset value witnessed was actually Cardura volatilising, and the additives have little effect on the thermal degradation of PET.

The TVA thermogram of the E187 samples containing Heloxy and Vikolox all generated an onset of volatile release lower than the value of 331 ^{o}C obtained for the E187 sample. This trend is similar to what is noticed in the TGA thermograms. This reduction is due to the excess epoxide volatilising and not degradation products being released.

Table 8.4 – Table summarising the information from the TVA thermograms. Values quoted are from a single measurement.

	Onset of Volatile Release °C
E187	331
E187 + 1% Cardura	331
E187 + 6% Cardura	259
E187 + 1% Heloxy	237
E187 + 6% Heloxy	227
E187 + 1% Vikolox	310
E187 + 6% Vikolox	275

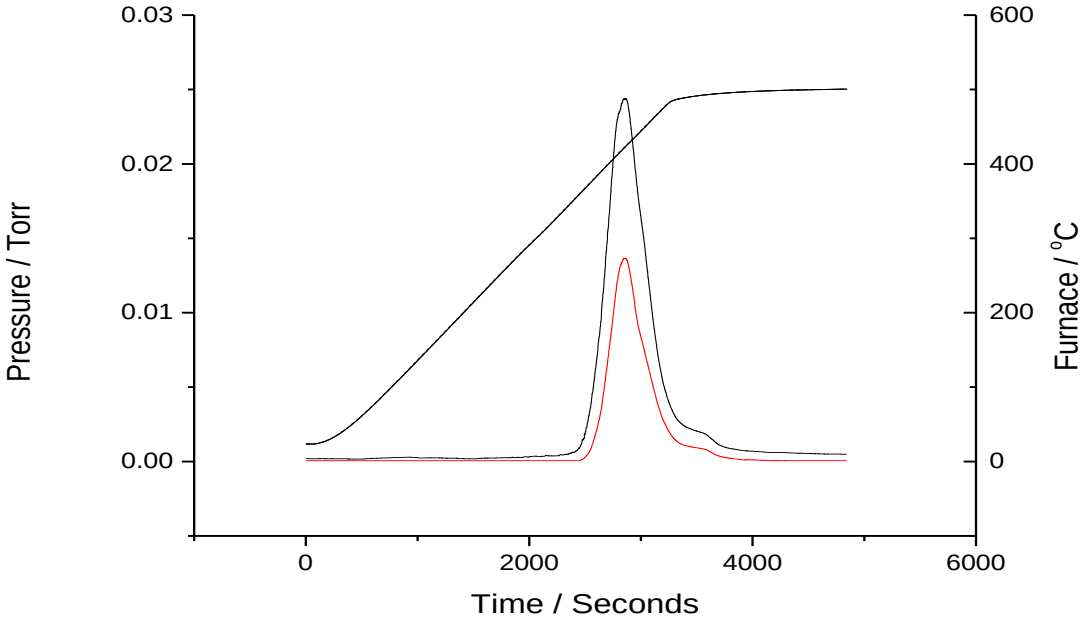

Figure 8.5 – TVA thermogram for the E187 sample. The black solid line shows the total volatiles that are being released and the red solid line shows the volatile gases that do not condense at liquid nitrogen temperatures, these are measured on the pressure y axis. The dotted black line represents the furnace temperature that is measured on the furnace y axis. A single sample was analysed.

The on-line mass spectrometer was used to monitor the non-condensable volatiles being released for all of the samples. The only non-condensable product monitored during the thermal degradation for all of the samples was carbon monoxide, which is an expected thermal degradation product of PET. Carbon monoxide is well documented in the literature as a volatile released during thermal degradation of PET. [42-65] Buxbaum noticed that 8% of the gaseous mixture produced from PET heated at 280 ^{o}C under nitrogen was carbon monoxide. [42] The mass spectra produced can be seen on the accompanying disc in the folder *Chapter 8* under *TVA.*

8.2.3.2 Sub-ambient Distillation

The products of thermal degradation will distil off depending on their boiling point. The SATVA trace produced for the E187 sample is shown in figure 8.6. The temperature that the products volatilise gives an indication of the volatiles that are produced when PET degrades in the absence of oxygen. The SATVA trace can be used for identification as several calibration experiments have been carried out to identify where common volatiles appear. Six peaks can be seen in figure 8.6, indicating that there are six different volatiles being released from E187 as it thermally degrades. These peaks correspond to acetylene, carbon dioxide, acetaldehyde, aromatics, water and higher boiling point aromatics. It was not possible to narrow the aromatics down to any specific volatiles because the peak is broad, and it is difficult to determine if the peak consists of only one or multiple products. All of the peaks that have been identified are indicated in the literature as products produced during the thermal degradation of PET. [42-65]

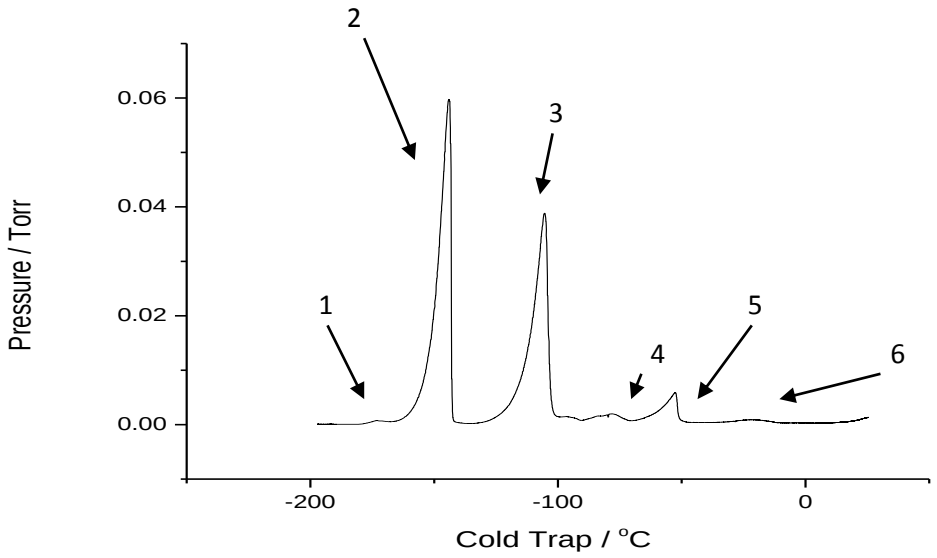

Figure 8.6 – SATVA trace for the E187 sample. A single sample was analysed.

The TVA line used had 4 separate limbs, allowing the volatiles to be trapped in specially made IR spectroscopy gas cells. IR spectroscopy was used to confirm the identity of these volatiles. Figure 8.7 shows the IR spectrum of the volatiles released from the E187 sample. The IR spectrum of the first fraction shows the presence of carbon dioxide, and the second fraction shows the gas phase IR spectrum of acetaldehyde. The IR spectra for fractions three and four showed no compounds due to their low concentration.

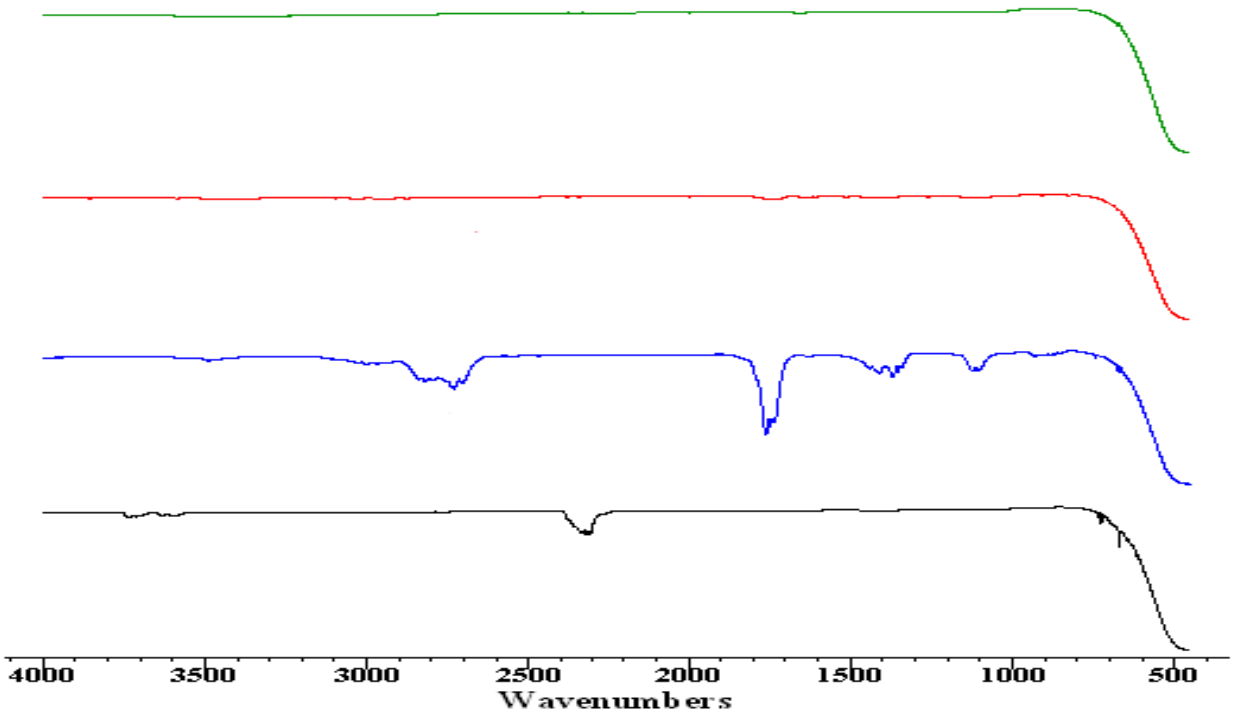

Figure 8.7 – IR spectra of the volatiles generated from a sample of E187. The black line shows the IR spectrum of limb one, the blue line shows the IR spectrum of limb two, the red line shows the IR spectrum of limb three and green line shows the IR spectrum of limb four. A single sample was analysed.

The volatiles trapped in the fourth gas cell were dissolved in spectrometric grade chloroform and analysed by gas chromatography – mass spectrometry using the instrument and parameters outlined in Chapter 3. Figure 8.8 shows the gas chromatogram produced for fraction four and clearly shows one large peak produced with a retention time at 17.90 minutes. The mass spectrum of the compound has a parent ion peak at 167 amu. The mass spectrum is shown in figure 8.9. The Xcalibur software has a library containing the mass spectra of a wide range of compounds. The software compares the mass spectrum of the compounds in the sample of fraction 4 to the mass spectra in the library. The library search has a poor match for any specific compound but does suggest a large aromatic ester compound.

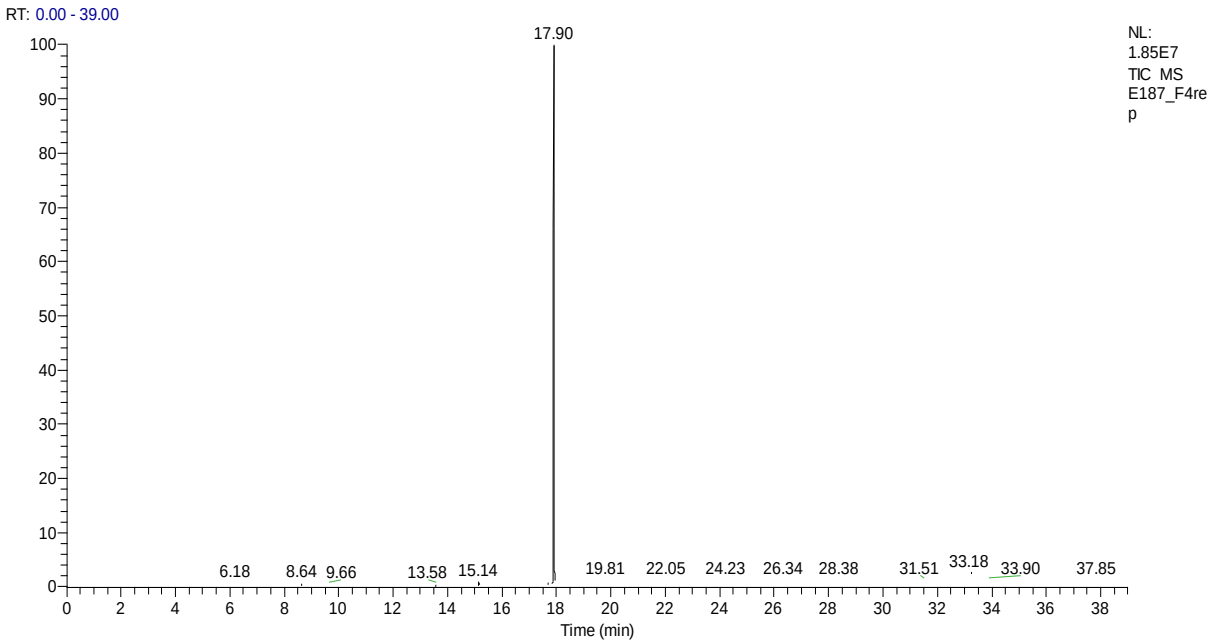

Figure 8.8 – Gas chromatogram generated for the TVA line extract of an E187 sample. Sample was analysed in EI mode.

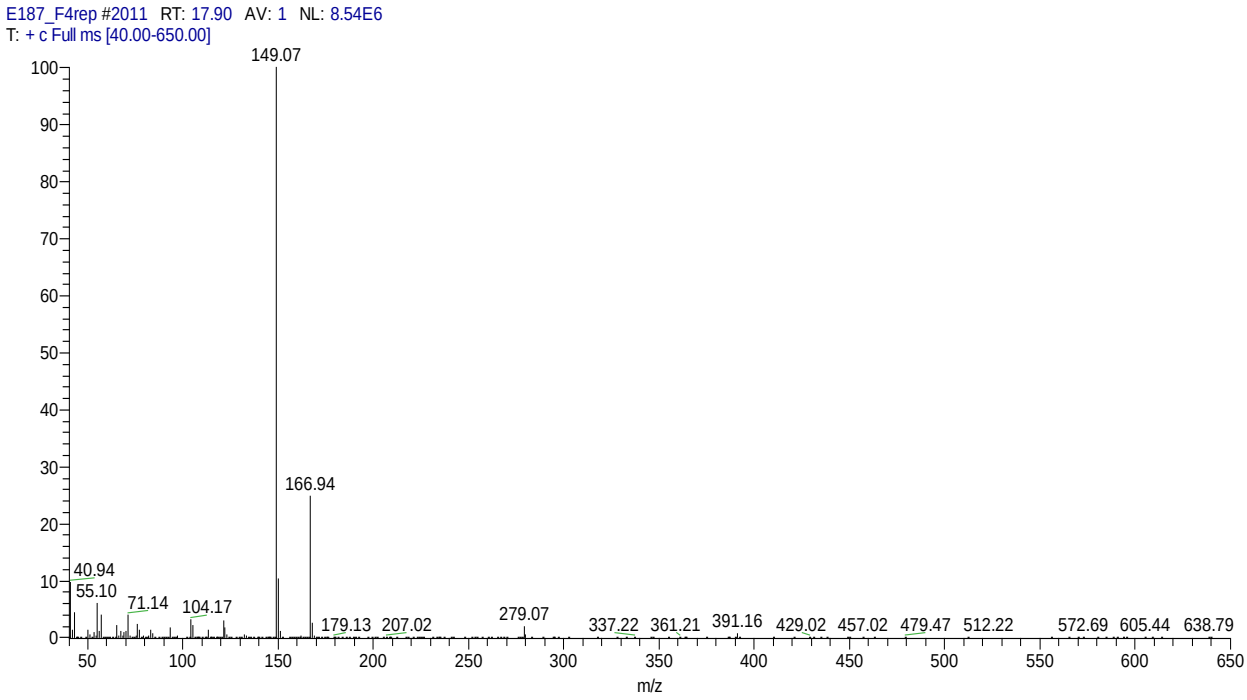

Figure 8.9– Mass spectrum of the peak with a retention time of 17.90 minutes in the gas chromatogram (see figure 8.8) generated for the TVA line extract of an E187 sample.

As the volatiles were being released from the primary trap creating the SATVA trace, an on-line mass spectrometer was used to confirm the identity of the peaks. The mass spectrum that corresponds to the first small peak in the SATVA trace has a parent ion of 26 amu, which is consistent with acetylene. The next peak has a parent ion at 44 amu, which is very commonly seen in the thermal degradation of polymers. This mass spectrum is consistent with carbon dioxide. The third peak shown in the SATVA trace is consistent with acetaldehyde as the parent ion is at 44 amu, with fragments at 15 amu and 29 amu. The fourth peak is small and very broad which made it difficult to identify. A very broad peak around -50 ^{o}C is consistent with water and has been shown in a number of experiments carried out using the TVA lines. The presence of water in the system often causes issues in analysis as it can mask other volatiles that are being generated. The final peak that is seen in the SATVA trace was expected to be a result of higher boiling point aromatic components such as benzoic acid. The aromatic peaks identified were all possible thermal degradation products from PET.

Similarly for the E187 sample, there were six volatile peaks identified for the E187 + 1% Cardura and E187 + 6% Cardura samples. The TGA thermograms were identical to that produced for the E187 sample. This means that acetylene, carbon dioxide, acetaldehyde, aromatics, water and higher boiling point aromatics were being produced as the E187 + 1% Cardura and E187 + 6% Cardura samples degrade. The IR spectra, mass spectra and gas chromatograms generated confirm the identity of these peaks. There were extra peaks in the gas chromatogram for the E187 + 6% Cardura sample when being compared to the E187 and E187 + 1% Cardura. These peaks had retention times of 11 and 13 minutes. One of these extra peaks was suggested to be nonanoic acid by the library search feature on Xcalibur, which is expected to be from the Cardura present. The other extra components identified in the E187 + 6% Cardura sample contained long alkane, ester and aromatic sections in their structure. With the exception of the presence of the nonanoic acid there were no other changes identified in the thermal degradation of the samples containing Cardura compared to the thermal degradation profile for the blank PET sample.

The six volatile peaks corresponding to acetylene, carbon dioxide, acetaldehyde, aromatics, water and higher boiling point aromatics were also identified in the E187 samples that contain Heloxy and Vikolox. These peaks were confirmed by the SATVA trace, IR spectroscopy, mass spectrometry and gas chromatography to be acetylene, carbon dioxide, acetaldehyde, aromatics, water and higher boiling point aromatics. All of the components identified from the mass spectra have aromatic, ester and alkane functionality. There was no evidence of the nonanoic acid in these samples, which is expected as this compound presumably arose as a result of the presence of Cardura. The data gathered proved that the epoxides Heloxy and Vikolox, like Cardura, have no significant effect on the degradation on PET.

8.2.3.3 Cold Ring

The cold ring fraction that was generated was swabbed with spectrometric grade chloroform and was analysed using gas chromatograph – mass spectrometry. The chromatogram produced for the cold ring sample is shown in figure 8.10. The chromatogram produced shows that the sample is very weak but contains many peaks. The mass spectra of the peaks produced were all checked against the library, but the only suggestion was silicone from the column. Figure 8.11 shows an example of a mass spectrum generated for the peak with the retention time of 16.22 minutes. The cold ring fraction was suggested to be too weak to show any components that are present.

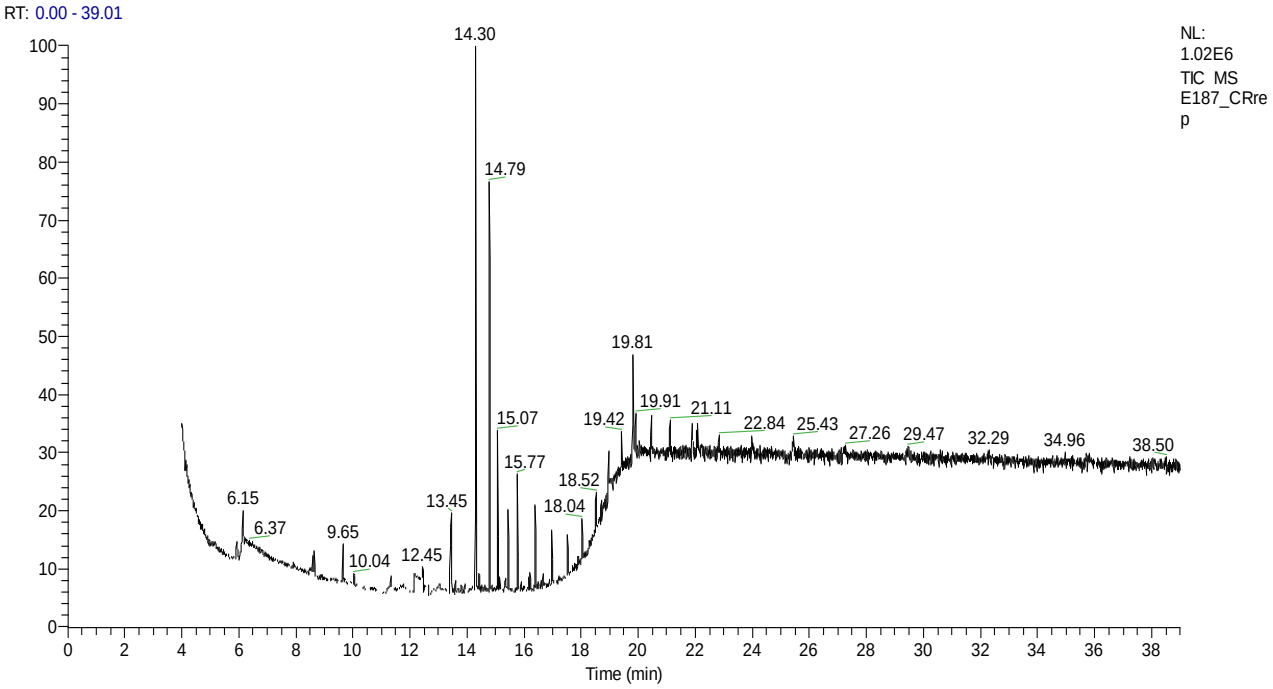

Figure 8.10 – Gas chromatogram generated for the E187 cold ring fraction. Sample was analysed in EI mode. A single sample was analysed.

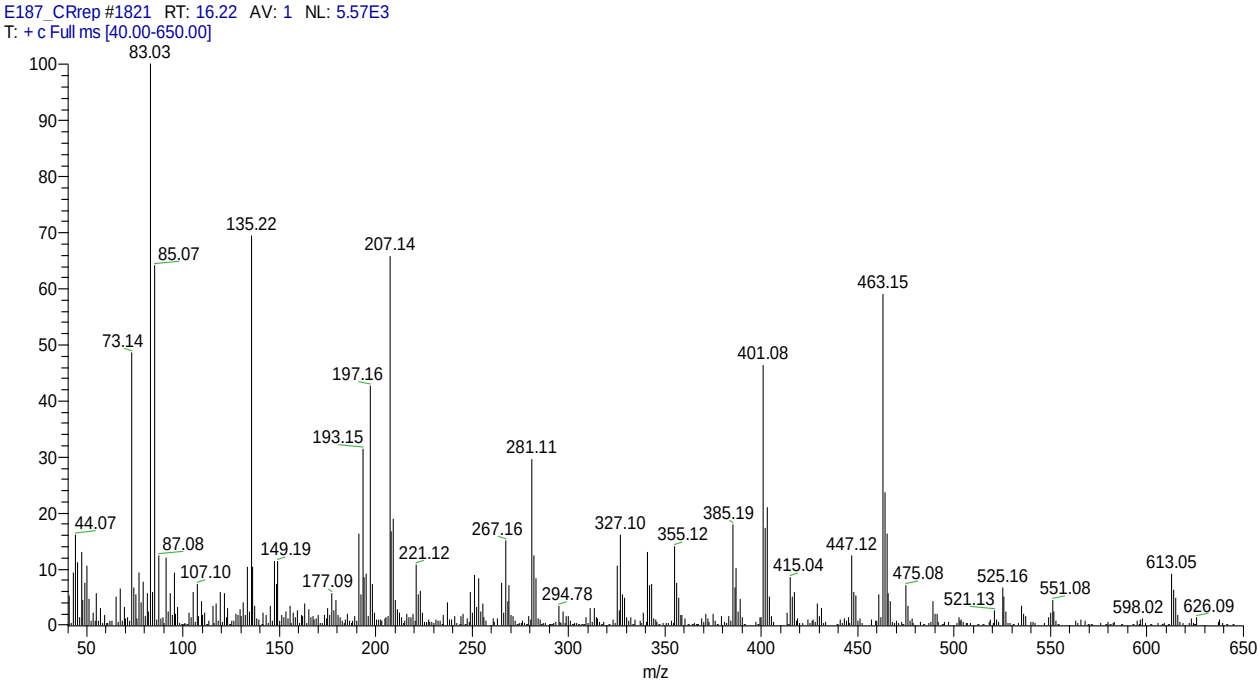

Figure 8.11 – Mass spectrum of the peak with a retention time of 16.22 minutes in the gas chromatogram (see figure 8.10) of the E187 cold ring sample.

The cold ring fractions generated from the E187 samples containing Cardura, Heloxy and Vikolox were also analysed by gas chromatograph – mass spectrometry. The only peaks present in the chromatogram correspond to the silicone from the column. The chromatogram and corresponding mass spectra for all of the samples can be seen on the attached accompanying disc in the folder *Chapter 8* under *TVA.*

8.2.4 Ageing Rig

8.2.4.1 Colour Changes

The E239 polymer samples were prepared using the ageing rig as outlined in Chapter 3. Samples were aged at 290 ^{o}C for 5, 60 and 300 minutes. Figure 8.12 shows an example of the pictures that are generated for the samples prepared at these conditions. The samples aged for 5 minutes had no significant change in colour. The E239 samples contain TiO_2 which caused the initial white appearance of the samples. There was a swirl of light brown present in the E239 polymer sample that was aged for 60 minutes. The samples that were aged for 300 minutes had more sections that are a lighter brown in colour. The light brown streaks in the white polymer samples give the samples the appearance of marble. The brown colour noticed is an indication that thermal degradation is occurring in these samples.

Photographs were also taken of the samples that were prepared in the ageing rig at 305 and 320 ^{o}C. Samples were prepared at each of these temperatures for 5, 60 and 300 minutes. Examples of the photographs obtained for the samples aged at 305 and 320 ^{o}C are shown in figures 8.13 and 8.14 respectively. The samples that were aged at 305 ^{o}C were similar to the samples aged at 290 ^{o}C. The samples that were aged at 320 ^{o}C were slightly darker in colour. Some bubbles can also be seen in the samples that have been aged for a longer period of time, which is a result of gases being released during thermal degradation. The gases being released are expected to be degradation products. Similar trends were noticed for the E187 and E240 samples. All other photographs that were taken of the aged samples can be seen on the disc attached.

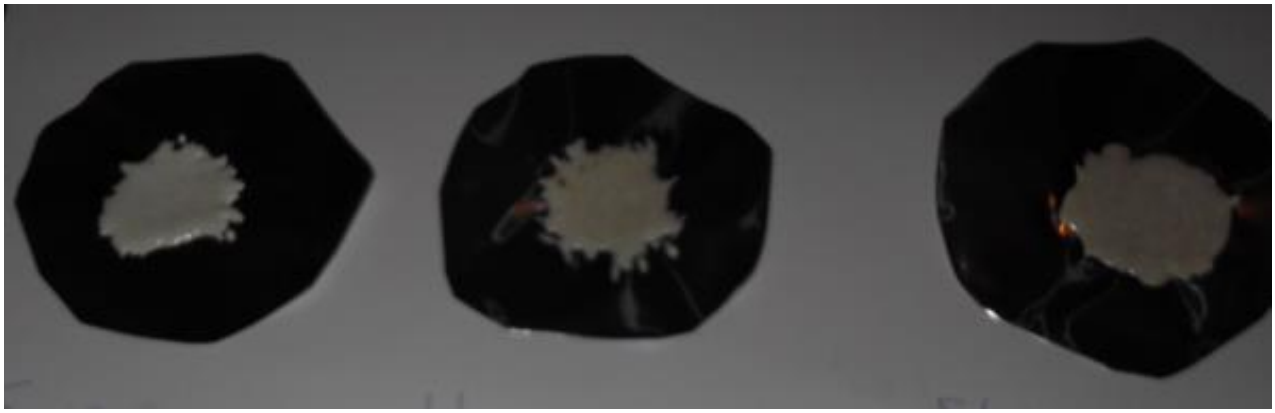

Figure 8.12 – Photographs of the E239 samples created from the ageing rig. The pictures going from left to right show the samples that have been aged for 5, 60and 300 minutes at 290 ^{o}C.

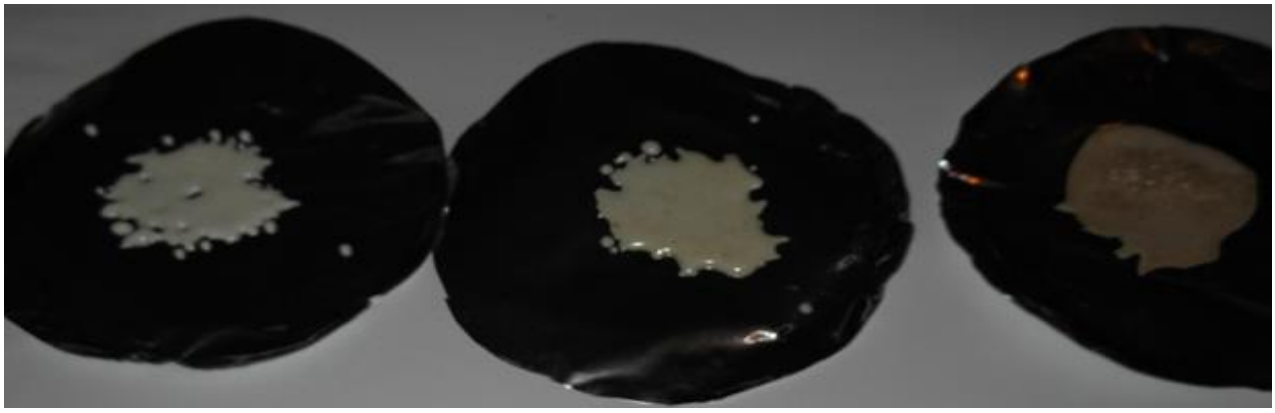

Figure 8.13 – Photographs of the E239 samples created from the ageing rig. The pictures going from left to right show the samples that have been aged for 5, 60 and 300 minutes at 305 ^{o}C.

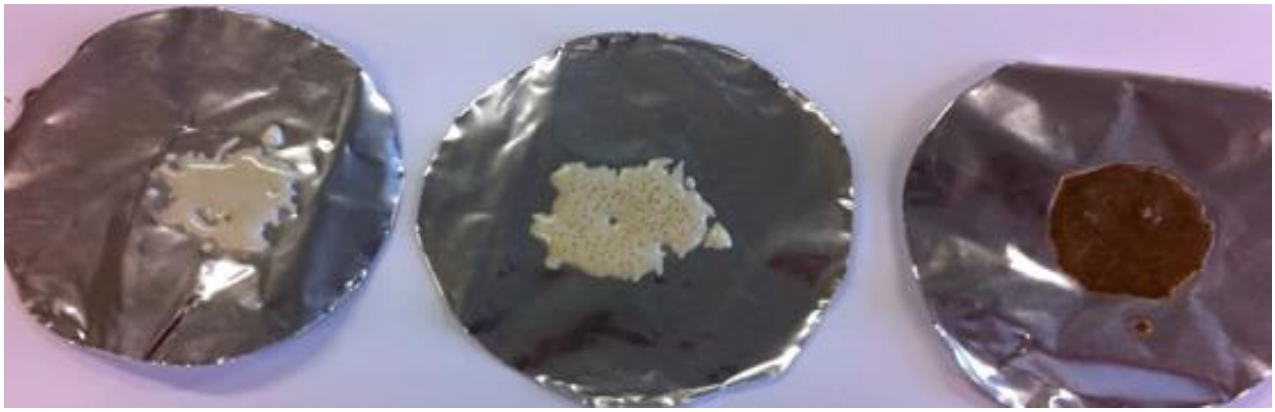

Figure 8.14 – Photographs of the E239 samples created from the ageing rig. The pictures going from left to right show the samples that have been aged for 5, 60 and 300 minutes at 320 ^{o}C.

The ageing rig was also used to investigate the thermal degradation of samples containing the epoxide Cardura. Photos were taken of the samples prepared on the ageing rig after they were weighed. The samples that contain Cardura look similar to the samples without any Cardura. The samples that contain 6% Cardura aged for 300 minutes at 320 ^{o}C have more bubbles present and are perhaps slightly darker in colour. The bubbles in the sample are expected to be a result of excess Cardura boiling off. Figures 8.15 and 8.16 show photos of the samples of E239 + 1% Cardura and E239 + 6% Cardura prepared using the ageing rig at 320 ^{o}C.

Figure 8.15 – Photographs of the E239 samples created from the ageing rig. The pictures going from left to right show the samples that have been aged for 5 , 60 and 300 minutes at 320 ^{o}C.

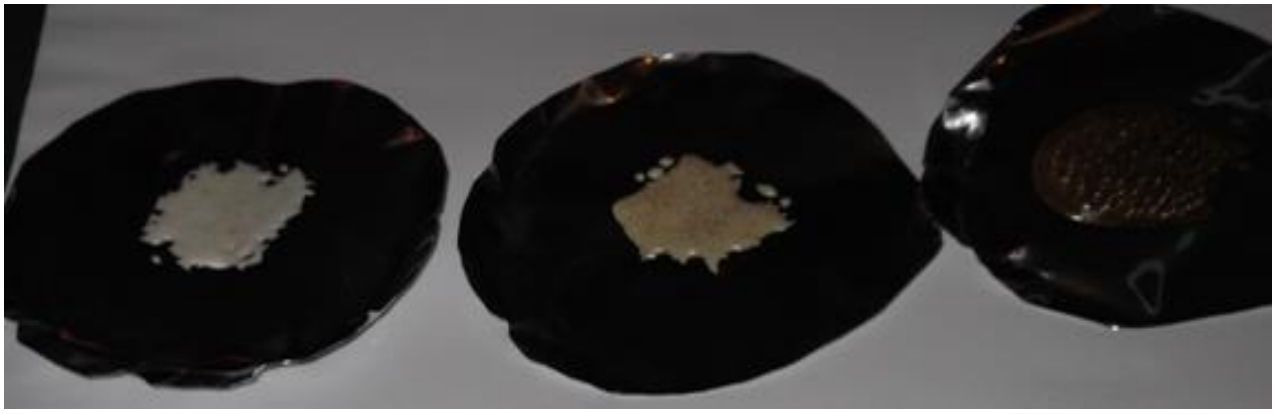

Figure 8.16 – Photographs of the E239 samples created from the ageing rig. The pictures going from left to right show the samples that have been aged for 5, 60 and 300 minutes at 320 ^{o}C.

8.2.4.2 % Volatilisation

The % volatilisation for all of the samples prepared in the ageing rig at 290, 305 and 320 ^{o}C are mostly similar within experimental error. The % volatilisation is starting to increase slightly for some of the samples with high concentration of the epoxides added. Examples include the E239 + 6% Cardura sample, which had a % volatilisation of 6.25%, and the E239 + 6% Vikolox which has a % volatilisation of 12.94%. The E239 + 6% Vikolox sample aged for 300 minutes at 320 ^{o}C gave the only significantly higher % volatilisation value. This increase was expected to be due to the epoxide boiling off. The experimental error was calculated to be 4.20% and was obtained from the standard deviation from three repeat experiments. The bar charts in figures 8.17 to 8.19 show the similarities of all of the samples. The three epoxides are suggested to have no significant effect on the % volatilisation at the temperature range studied. These temperatures were studied as they are the high range of processing temperatures that the samples could be exposed to when DTF is processing PET into films for the solar cells.

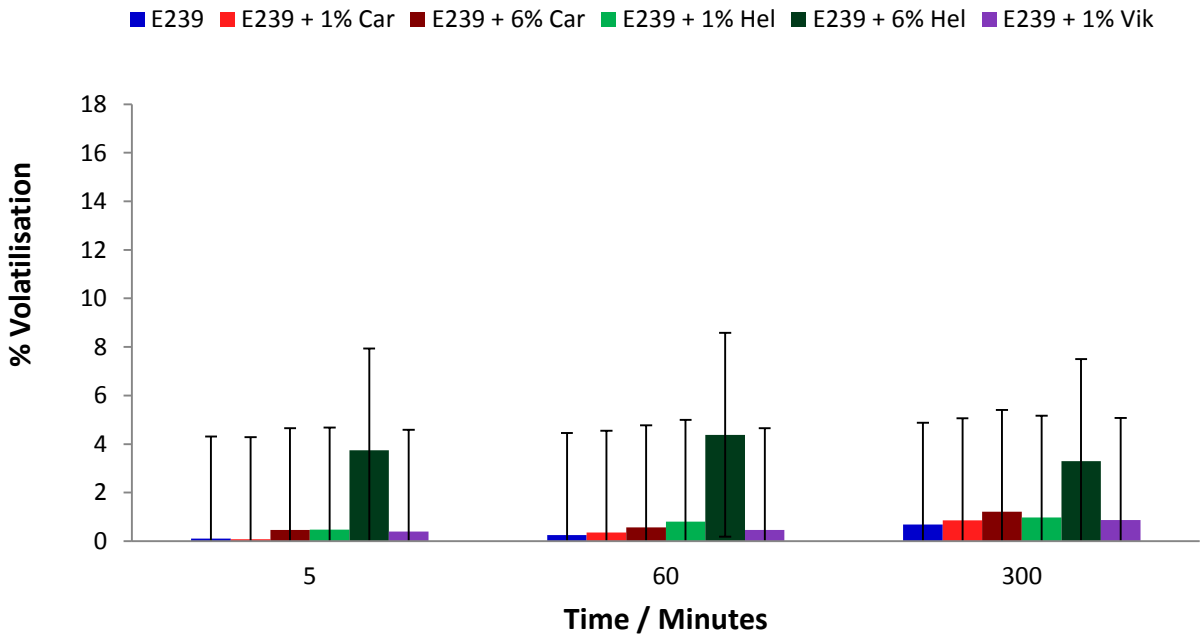

Figure 8.17 – Bar chart showing the % volatilisations for the E239 samples aged for 5, 60 and 300 minutes in nitrogen on the ageing rig at 290 ^{o}C. N=1. The error bar is 4.20% which is the calculated error in the method.

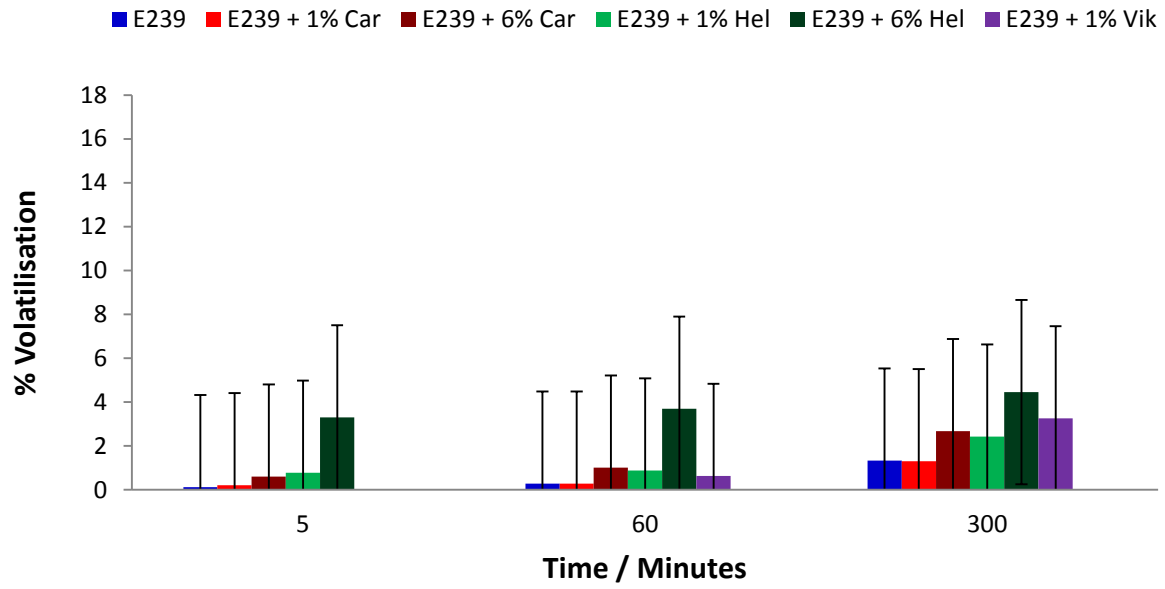

Figure 8.18 – Bar chart showing the % volatilisations for the E239 samples aged for 5, 60 and 300 minutes in nitrogen on the ageing rig at 305 °C. N=1. The error bar is 4.20% which is the calculated error in the method.

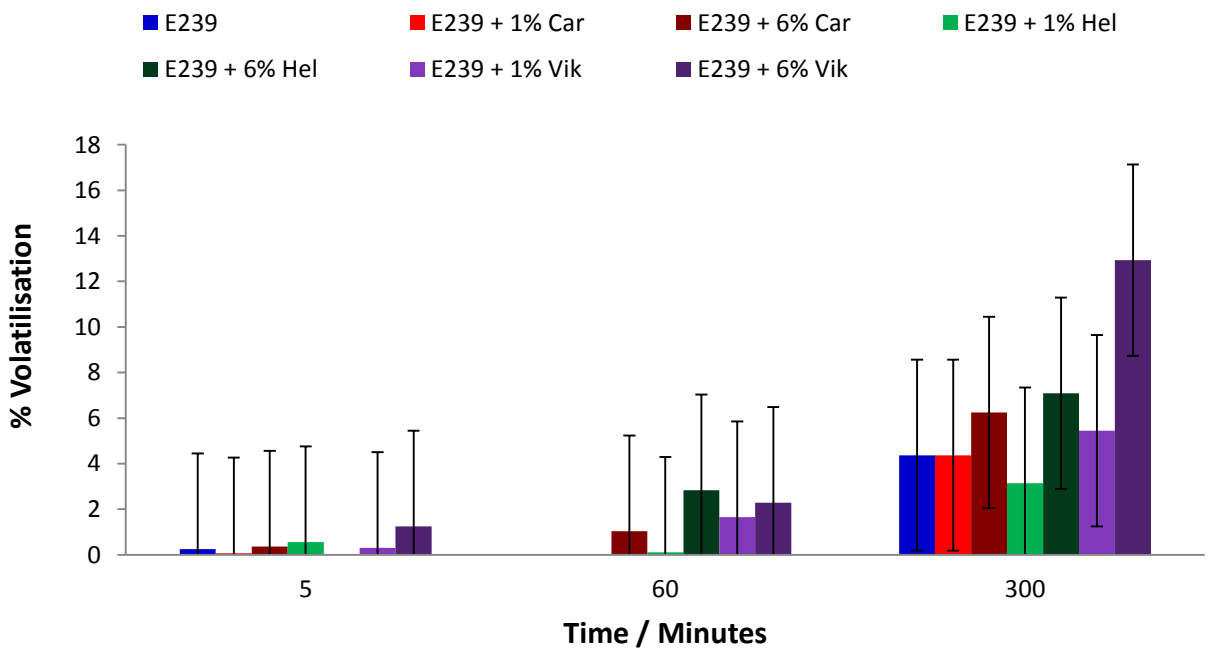

Figure 8.19 – Bar chart showing the % volatilisations for the E239 samples aged for 5, 60 and 300 minutes in nitrogen on the ageing rig at 320 °C. N=1. The error bar is 4.20% which is the calculated error in the method.

8.2.4.3 Gel Content

The residual gel content was calculated for the samples prepared on the ageing rig with E239, E239 + 1% Cardura and E239 + 6% Cardura. The epoxide Cardura was focused on for the post ageing analysis of the ageing samples, as it is the samples which contain Cardura that show the most potential to be used as the backsheet for solar cell panels. The bar charts for the E239, E239 + 1% Cardura and E239 + 6% Cardura samples are shown in figures 8.20 to 8.22. As can be seen in the figures there were no significant changes in any of the samples. This is expected to be a result of the high error and the very low gel content produced. The original value was also calculated for the samples. There was no significant change in any of the samples analysed. The data for the original percentage gel content can be seen in the appendices (A8.5.1 to A8.5.3).

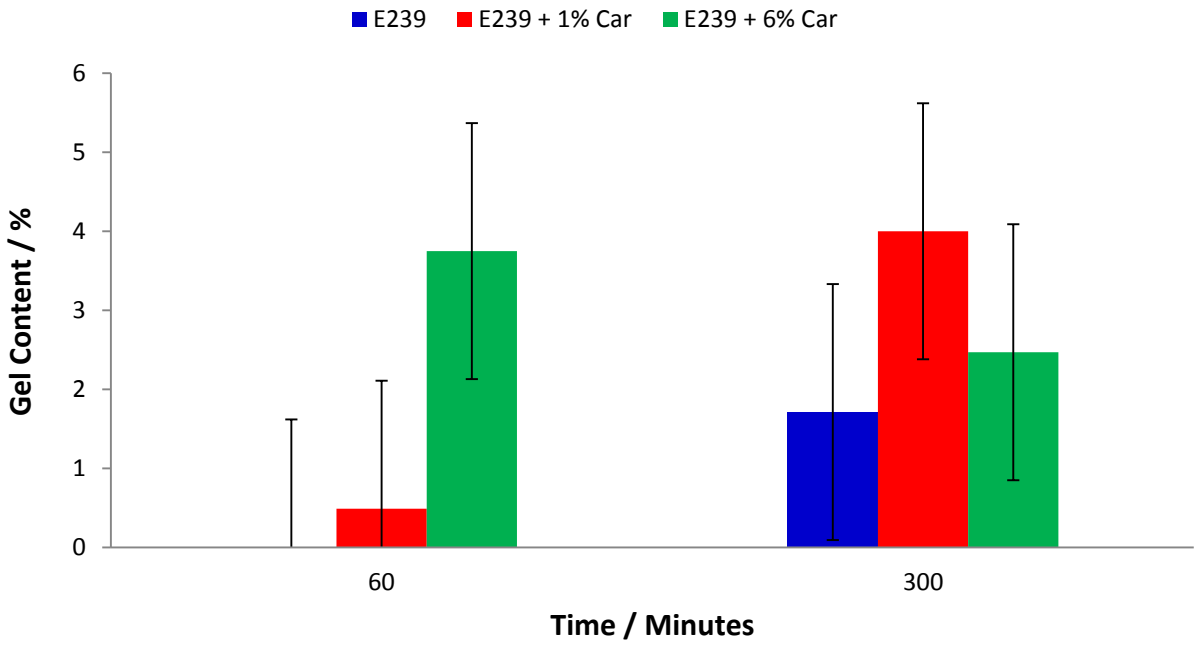

Figure 8.20 – Bar chart showing the residual gel content (Residual) for the E239 samples aged for 5, 60 and 300 minutes on the ageing rig at 290 °C. N=3. The error bar is 1.81% which is the calculated error in the method.

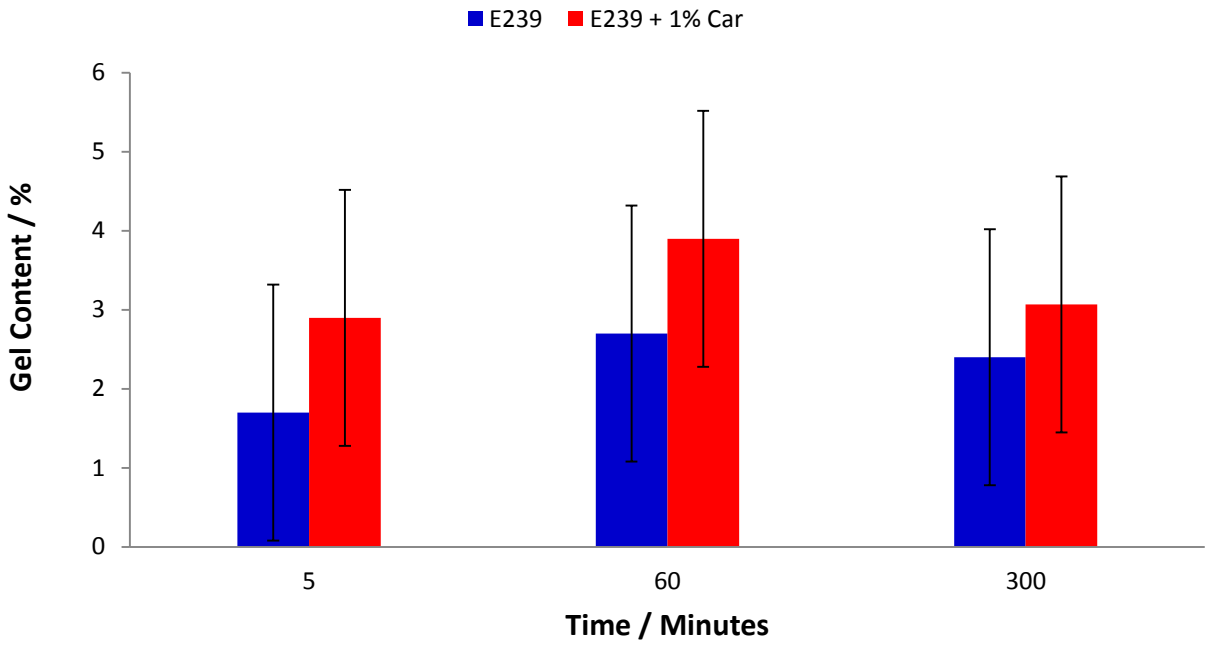

Figure 8.21 – Bar chart showing the gel content (Residual) for the E239 samples aged for 5, 60 and 300 minutes in nitrogen on the ageing rig at 305 °C. N=3. The error bar is 1.81% which is the calculated error in the method.

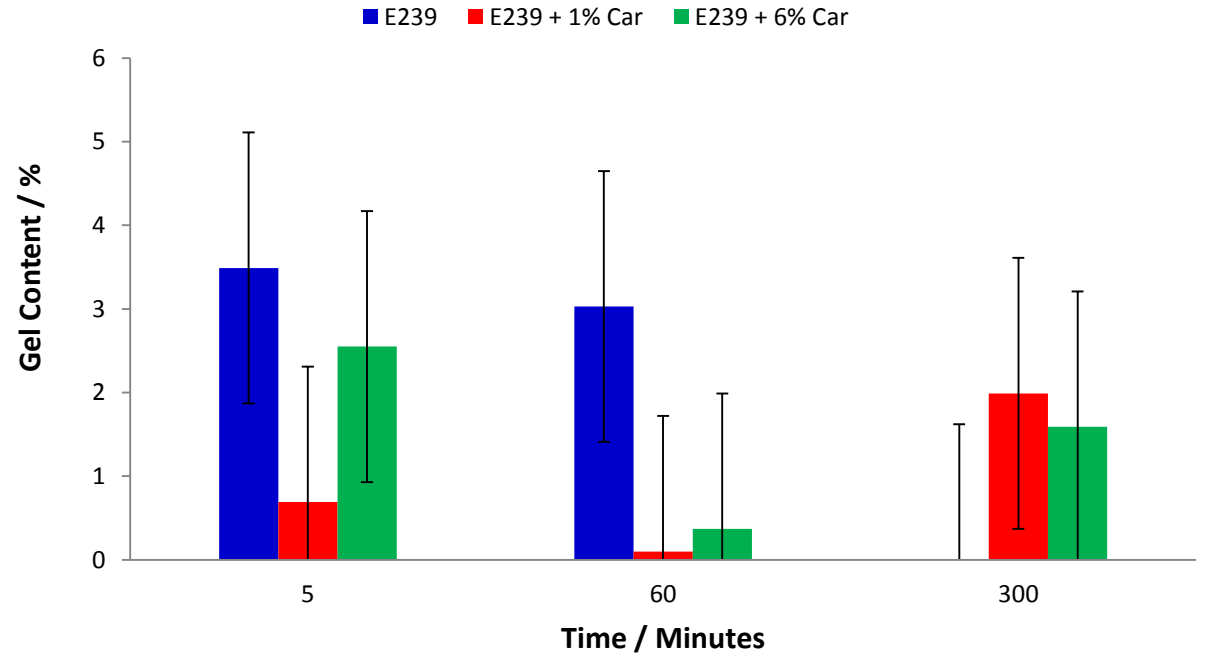

Figure 8.22 – Bar chart showing the gel content (Original) for the E239 samples aged for 5, 60 and 300 minutes on the ageing rig at 320 °C. N=3. The error bar is 1.81% which is the calculated error in the method.

8.2.4.4 IR

The IR spectra for all of the aged E239, E239 +1% Cardura and E239 + 6% Cardura samples were obtained. The spectra for the E239 sample and the E239 sample that were aged at 320 ^{o}C for 300 minutes is shown in figure 8.23. Small changes were noticed in the spectra, including the disappearance/reduction of peaks at 1175, 1410 and 1454 cm^{-1}. There were also new peaks identified at 846, 872, 1472, 1796 and 2348 cm^{-1}. The peak at 2348 cm^{-1} is due to carbon dioxide in the atmosphere. These changes are consistent with the backbone of PET being broken down into smaller components, which can be seen by the presence of the new carbonyl peak at 1796 cm^{-1}. The other peaks are consistent with changes in saturated and unsaturated aliphatic chains. These changes are expected for the thermal ageing of PET. Figure 8.24 shows the IR spectra of the E239 + 6% Cardura samples aged at 320 ^{o}C for 5, 60 and 300 minutes. The changes are similar to the sample without any Cardura present. All other IR spectra can be seen on the disc attached.

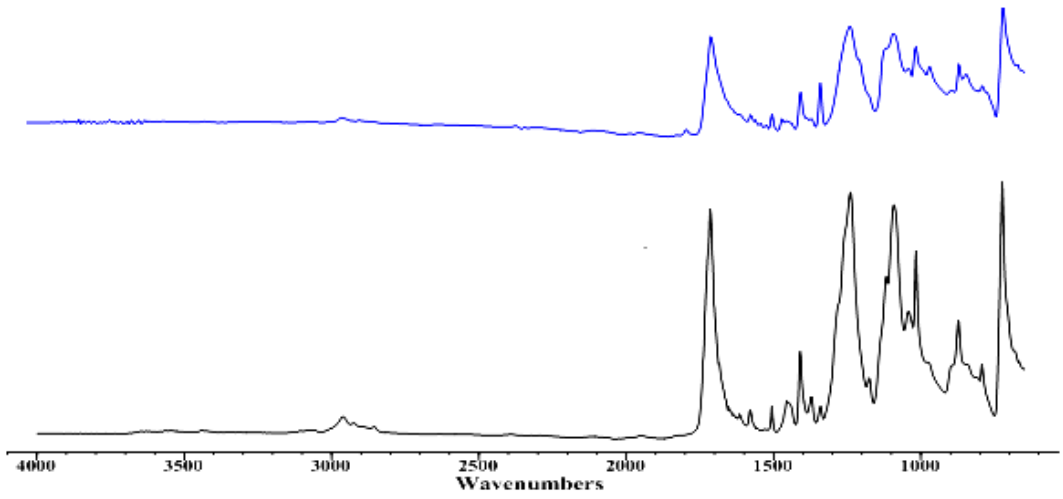

Figure 8.23– Comparison of the IR spectra of the E239 samples that were not aged (Black Spectrum) with the E239 sample aged in the ageing rig under nitrogen for 300 minutes at 320 ^{o}C (Blue Spectrum).

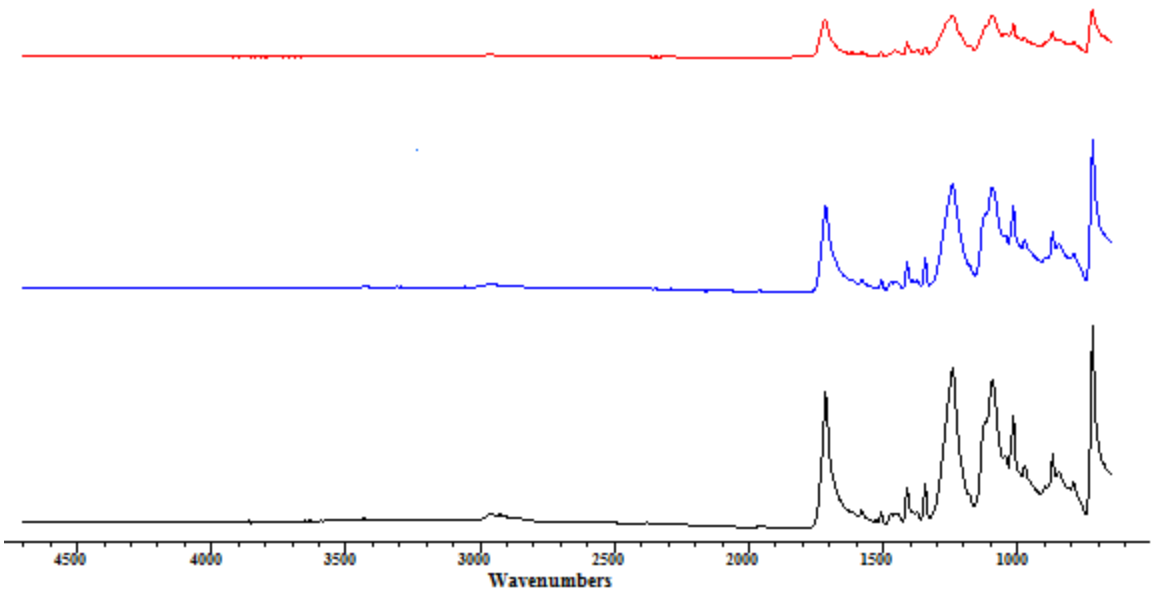

Figure 8.24 – Comparison of the IR spectra of the E239 + 6% Cardura samples that were generated on the ageing rig at 320 °C. The black line is for the spectrum aged for 5 minutes, the blue line is for the spectrum aged for 60 minutes and the red line is for the spectrum aged for 300 minutes.

8.2.5 CATLAB

The E187, E239 and E240 samples were analysed using the CATLAB microreactor. Several volatiles were identified including carbon monoxide, carbon dioxide and water. The components identified were also found to be released during thermal degradation from the TVA technique. These volatiles are degradation products that are commonly seen in the literature. [42-65]

The emission of carbon dioxide was closely studied to determine the onset of thermal degradation. The plot showing the evolution of carbon dioxide is shown in figure 8.25. All of the samples produce a similar trace and the data can be seen on the accompanying disc in the folder *Chapter 8* under *CATLAB*. The onsets of thermal degradation calculated for the samples are shown in tables 8.5 to 8.7. No trends were identified in the samples and conditions investigated. The error obtained from the standard deviation of three repeat experiments was

14 ^{o}C. The values obtained are all similar within experimental error, again confirming that the epoxide Cardura has no adverse effects on the thermal degradation behaviour of PET.

Table 8.5 – Table showing the onset of thermal degradation based on the release of carbon dioxide for the E187 samples. N=1.

Sample	Rate ^{o}C min^{-1}	Onset Temperature ^{o}C
E187	5	296
	10	323
	20	343
E187 + 1% Cardura	5	336
	10	326
	20	299
E187 + 6% Cardura	5	292
	10	307
	20	307

Table 8.6 – Table showing the onset of thermal degradation based on the release of carbon dioxide for the E239 samples. N=1

Sample	Rate ^{o}C min^{-1}	Onset Temperature ^{o}C
E239	5	307
	10	322
	20	318
E239 + 1% Cardura	5	306
	10	322
	20	318
E239 + 6% Cardura	5	291
	10	293
	20	343

Table 8.7 – Table showing the onset of thermal degradation based on the release of carbon dioxide for the E240 samples. N=1

Sample	Rate $^{o}C\ min^{-1}$	Onset Temperature ^{o}C
E240	5	312
	10	326
	20	329
E240 + 1% Cardura	10	319
	20	335
E240 + 6% Cardura	10	349
	20	335

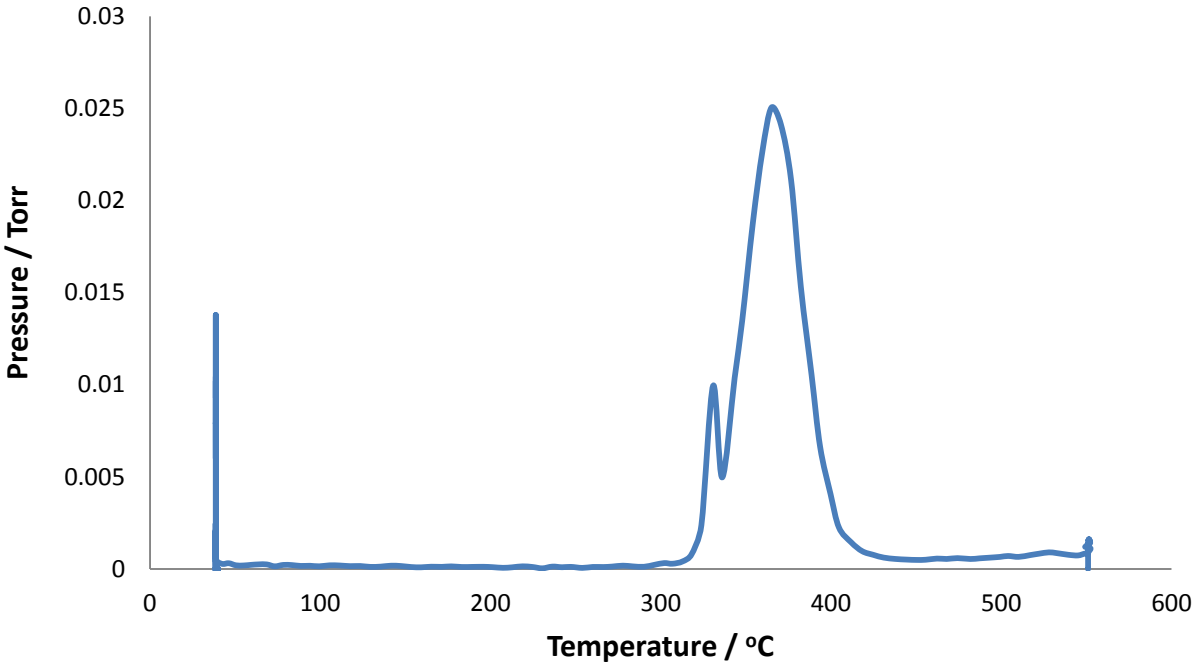

Figure 8.25 –Mass spectrum obtained from the CATLAB instrument showing the evolution of carbon dioxide (m/z 44) versus temperature for the E239 sample heated at a rate of 5 $^{o}C\ min^{-1}$.

8.3 Conclusions

The DSC scans and TGA thermograms show no significant changes in the thermal degradation behaviour of PET with the addition of the epoxides Cardura, Heloxy and Vikolox. The onsets of mass loss for the samples containing epoxides were lower than the blank PET samples, which was due to the excess epoxide boiling.

The onset of thermal degradation obtained from the TVA technique is similar to the values obtained by the TGA thermograms. The volatiles being released from all of the PET samples during thermal degradation were identified as acetaldehyde, carbon monoxide, carbon dioxide, acetylene, water and higher boiling point aromatics. . The peaks identified using GC-MS were shown to contain compounds with aromatic, ester and alkane functionality. Nonanoic acid was also detected for the E239 + 6% Cardura sample, which is due to the presence of Cardura. With the exception of nonanic acid all of the components were identified in the literature as being possible thermal degradation products of PET. [42-65]

The onset of thermal degradation calculated using the CATLAB system was similar to the values obtained from the TGA and TVA techniques. Further work would be required to identify any trends, and for kinetic studies to be carried out as the error value was too high.

Photos taken of the samples prepared on the ageing rig suggest that thermal degradation is occurring more predominantly in samples that have been aged for longer and/or using a higher ageing temperature. This is supported by the results from IR spectroscopy. There were no significant changes in the % volatilisations of the E239 samples prepared with any of the epoxides at 290, 305 or 320 ^{o}C in the ageing rig. The only sample that had a significant increase was the E239 + 6% Vikolox sample, which was expected to be down to a higher error than expected in the samples or excess Vikolox volatilising. The data from the ageing supports the conclusion that the epoxides do no not have a significant effect on the thermal degradation behaviour of PET at the temperatures studied. The temperatures were chosen as they are the temperatures the extruder barrel would be set to when processing PET. This information gives confidence that the additives could be utilised in DTF's current manufacturing process without complications.

There are no significant changes noticed in the gel content of the samples studied, which is expected to be a result of the high error in the method and the very low gel content in the samples. The percentage of gel was expected to be low from thermal degradation based on the literature. [42] This is good for DTF as an increase in the gel formation could contaminate the film being produced for solar cell panels or build up on the extruder. The data shows that all three epoxides could be used without an increase in gel concentration causing processing issues.

9.0 Characterisation of the Degradation Behaviour of Extruded Materials – Thermo-oxidative Degradation

9.1 Introduction

As discussed in Chapter 1, thermo-oxidative degradation can occur during processing of PET. It is therefore important that DTF is aware of any beneficial or adverse effects on the degradation behaviour of the samples that were occurring for successful utilisation of these additives.

The thermo-oxidative degradation behaviour was studied for the polymer samples containing Cardura, Vikolox and Heloxy using DSC, TGA, TVA, a custom-built ageing rig and Hiden CATLAB system.

9.2 Results and Discussion

9.2.1 DSC

The DSC scan obtained for the E187 sample is shown in figure 9.1. The onset temperature of degradation was carried out by observation. From this the onset of degradation was determined to be 306 ^{o}C. This is considerably lower than the value obtained for the onset of thermal degradation, which was 368^{o}C. It has been shown in the literature that thermal-oxidative degradation occurs at a lower temperature than thermal degradation. [10, 31 and 42] Thermo-oxidative degradation, unlike thermal degradation, has been shown to occur significantly in the solid state. [10 and 31] This has been shown to be most significant in injection moulding processes and moulding of the molten polymer using extrusion. During this time to solidify the polymer can react with air, causing a decrease in molecular weight and undesirable products to be formed. The mechanism for thermo-oxidative degradation is shown in Chapter 1.

The onset of degradation was 309 ^{o}C for the E187 + 6% Cardura sample which is similar to the onset obtained for the E187 sample. Figure 9.2 shows the DSC scan for the E187 + 6% Cardura sample. The DSC scan produced for the E187 + 6% Cardura sample looks slightly different from

the E187 sample and the samples prepared with the other epoxides. This is likely due to the presence of the Cardura affecting the properties of the polymer, which is likely to result in an increase in crystallinity and/or gel content formation. Factors such as crystallinity and cross-linking occurring in the polymer chain have been shown to affect thermo-oxidative degradation. [10, 31 and 42] The values for enthalpy of crystallisation and enthalpy of fusion are very small, supporting the premise that the crystallinity of the sample has been disrupted. The values are very low and some further DSC experiments would confirm if the values obtained were real. The thermo-oxidative degradation behaviour for the Cardura-containing samples were studied closely using TGA, ageing rig and CATLAB analysis to determine if significant changes were occurring.

The onset of thermo-oxidative degradation was also determined for the sample that contained E187 + 6% Vikolox and E187 + 6% Heloxy. The DSC scans for the E187 + 6%Vikolox and E187 + 6% Heloxy samples are shown in the appendices (A9.1.1 and A9.1.2). The onset of degradation for the E187 + 6% Vikolox sample is 298 ^{o}C, which is similar to the values obtained for the E187 and E187 + 6% Cardura. The onset of thermal-oxidative degradation was calculated to be 335 ^{o}C for the E187 + 6% Heloxy. This value was slightly higher than the value obtained for E187, E187 + 6% Cardura and E187 + 6% Vikolox. The determination of the onset of the thermo-oxidative degradation by DSC was subjective, therefore the onset of thermo-oxidative degradation for the E187 + 6% Heloxy samples was confirmed by TGA and CATLAB analysis.

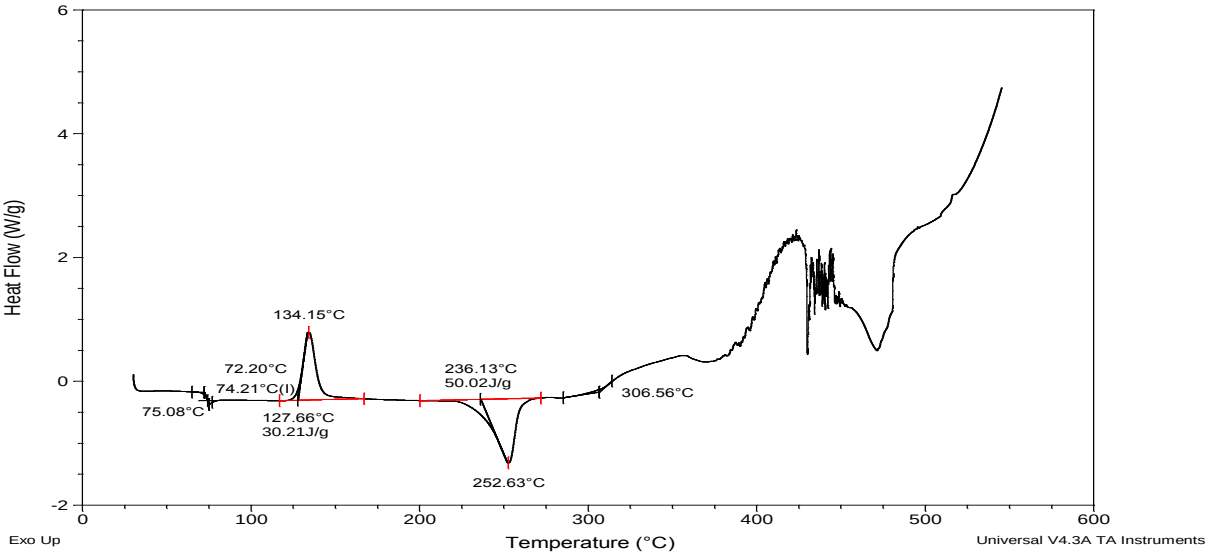

Figure 9.1 – DSC scan of the E187 sample.

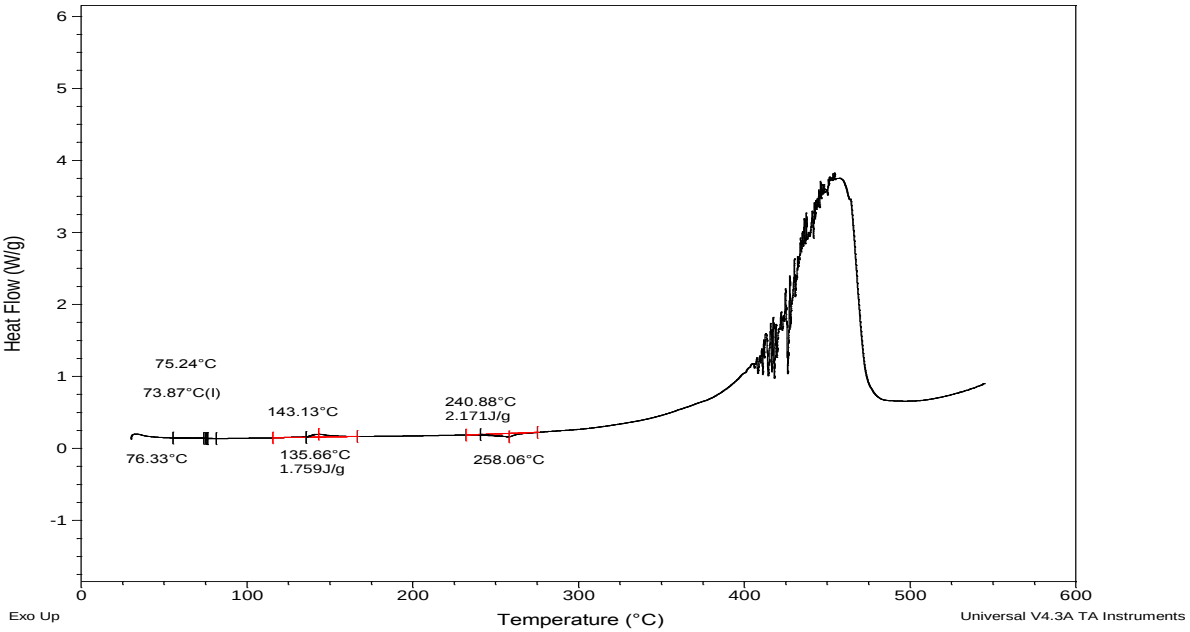

Figure 9.2 – DSC scan of the E187 + 6% Cardura sample.

.

Table 9.1 – Information obtained from the DSC scans of the E187 samples. Values quoted are from a single measurement.

	E187	E187 + 6% Cardura	E187 + 6% Heloxy	E187 + 6% Vikolox
Glass Transition / °C	76	76	75	63
Crystallisation Temperature / °C	134	143	141	109
Enthalpy of Crystallisation / J/g	30	2	30	27
Melting Point / °C	253	258	254	254
Enthalpy of Fusion/ J/g	50	2	49	60
Onset of Degradation/ °C	306	309	335	298

9.2.2 TGA

The TGA thermograms were obtained for samples of E187, E239 and E240. Figure 9.3 shows the thermogram for the E187 samples and the data is summarised in table 9.2. Data for the other polymer samples can be seen in the appendices (A9.2.1 and A9.2.6). The onset of thermal-oxidative degradation was calculated at 0.5% mass loss. The value obtained for the E187 sample was determined to be 302°C. The onset is similar to the value obtained from the DSC scan, which was 306 °C. The value obtained for the E187 + 1% Cardura sample was very similar to the E187 sample without Cardura when considering the experimental error. The error value was calculated to be 9 °C, which was obtained from the standard deviation of three repeat experiments. The E187 + 6% Cardura sample had an onset of mass loss at 232 °C. This value is very low when compared to the literature and the values obtained for the DSC scans. This is expected to be excess Cardura boiling off. This is supported by the fact that all of the TGA thermograms are very similar. The peak temperatures for thermo-oxidative degradation are very similar; the values obtained are 444, 444 and 443 °C for the E187, E187 + 1% Cardura and E187 + 6% Cardura samples respectively.

The values obtained for the onset of mass loss for the E239 and E240 show similar trends. The onset of mass loss for the E239 and E240 samples was 294 and 414 °C, respectively. The values

obtained for the TGA thermograms are shown in table 9.2. The E240 samples produced a higher onset of mass loss compared to the E187 and E239 samples. The onset of themo-oxidative degradation is suggested to be delayed in the E240 samples since it has a lower initial carboxyl end group concentration. Bikiaris *et al.* discovered that the higher initial carboxylic acid concentration in polyesters from the beginning of the degradation potentially contributes to it's lower stability. [31] The E239 samples are also solid state but these samples contain titanium dioxide. It has been shown in the literature that metal catalysts have a large impact on thermo-oxidative stability. [10, 31 and 42]

The addition of the epoxides is shown to reduce the onset of thermo-oxidative degradation, which is expected to be mass loss due to the excess epoxide volatilising and not thermo-oxidative degradation. This is noticed with all of the epoxides and was shown to occur in Chapter 4. The values obtained from the TGA thermograms can be seen in table 9.3. The peak temperature for the E239 samples fall in the range 407 to 408 ^{o}C, therefore the Heloxy and Vikolox samples are similar to the blank.

It has been concluded that the additives have little effect on the thermo-oxidative degradation behaviour, and the significant differences noticed are due to volatilisation of unreacted additive. The lack of significant changes makes the use of these additives by DTF very attractive. The extruder line is carried out in an inert atmosphere so that the exposure to thermo-oxidative conditions would be minimal.

Table 9.2 – Table summarising the information from the TGA thermograms. Values quoted are from a single measurement.

Sample	0.5% Mass Loss °C	Peak in DTG °C
E187	302	444
E187 + 1% Cardura	313	444
E187 + 6% Cardura	232	443
E239	294	416
E239 + 1% Cardura	320	458
E239 + 6% Cardura	304	445
E240	414	466
E240 + 1% Cardura	316	450
E240 + 6% Cardura	229	480

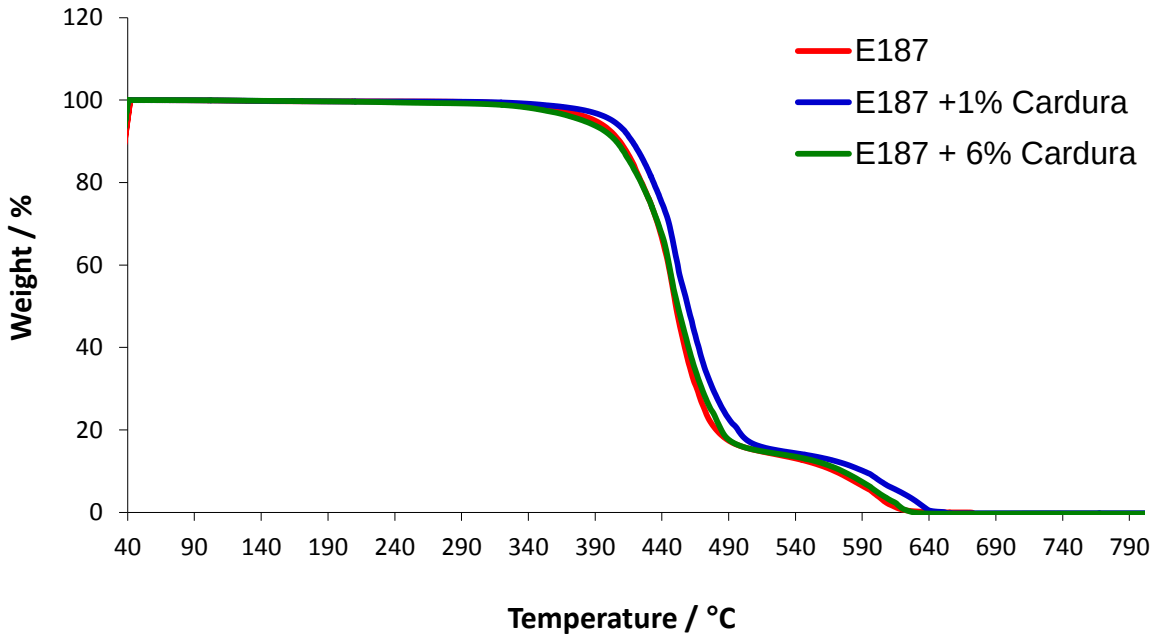

Figure 9.3 – TGA thermogram showing the mass loss of the E187 samples.

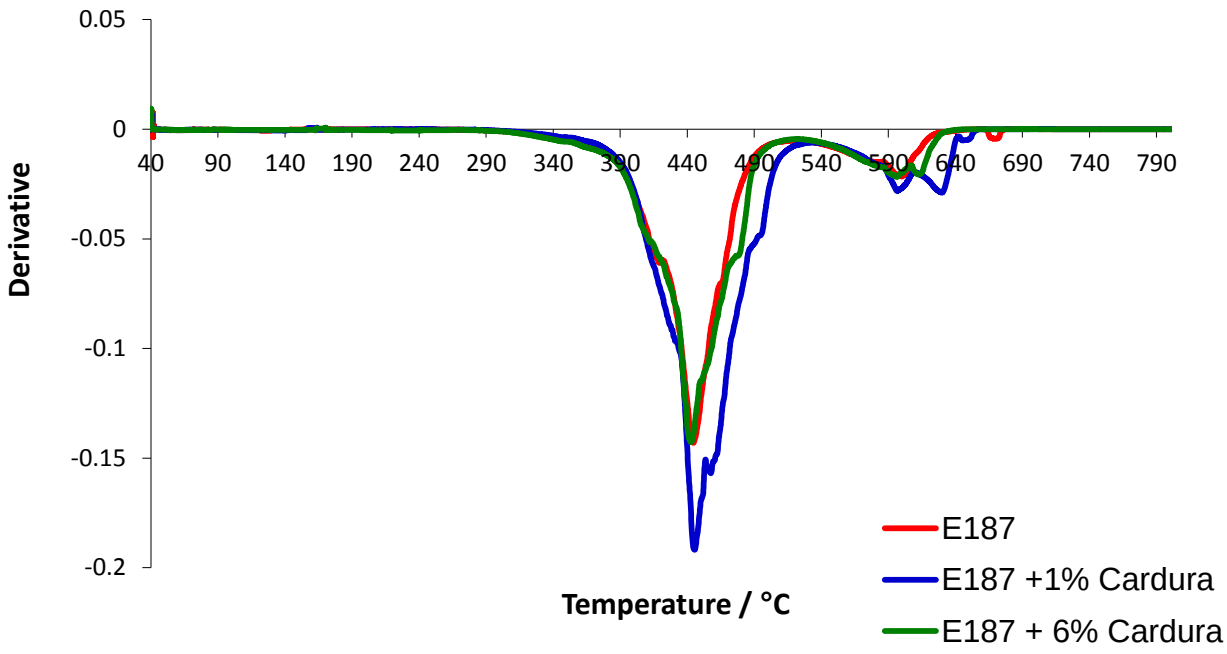

Figure 9.4 – Derivative of the TGA thermogram showing the mass loss of the E187 samples.

Table 9.3 – Table summarising the information from the TGA thermograms. Values quoted are from a single measurement.

Sample	Temperature 1% mass loss °C	Peak in DTG °C
E239	294	416
E239 + 6% Cardura	304	458
E239 + 6% Heloxy	222	408
E239 + 6% Vikolox	209	407

9.2.3 Ageing Rig

9.2.3.1 Colour Changes

Photographs were taken of the E239 polymer samples that were prepared using the ageing rig. Samples were aged at 290 °C for 5 minutes, 60 minutes and 300 minutes. Figure 9.5 shows an example of the pictures that were generated for the samples prepared under these conditions. Unlike the samples aged for 5 minutes at 290 °C under nitrogen, which showed no changes, the

sample aged with the same conditions under air exhibited changes. The changes had swirls of light brown present in the E239 polymer sample. The samples that were aged for 60 minutes changed to be completely light brown in colour. The sample aged at 290 ^{o}C for 300 minutes changed from white to dark brown in colour. The discolouration of all of the samples is an indication that degradation is occurring in these samples. Photographs were also taken of the samples that were prepared in the ageing rig at 305 and 320 ^{o}C, and are shown in figures 9.6 and 9.7 respectively. The samples prepared at the higher temperature for 5 minutes at 305 and 320 ^{o}C looked similar to the samples generated at 290 ^{o}C.

Similar trends were also noticed for the E187 and E240 samples. All other photographs that were taken of the aged samples can be seen on the accompanying disc in the folder *Chapter 9* under *Ageing Rig.* The discolouration was expected when thermo-oxidative degradation occurs because the polymer chain is breaking down to the acidic and colour forming species mentioned in Chapter 1.

Figure 9.5 – Photographs of the E239 samples created from the ageing rig. The pictures going from left to right show the samples that have been aged for 5 , 60 and 300 minutes at 290 ^{o}C.

Figure 9.6 – Photographs of the E239 samples created from the ageing rig. The pictures going from left to right show the samples that have been aged for 5, 60 and 300 minutes at 305 ^{o}C.

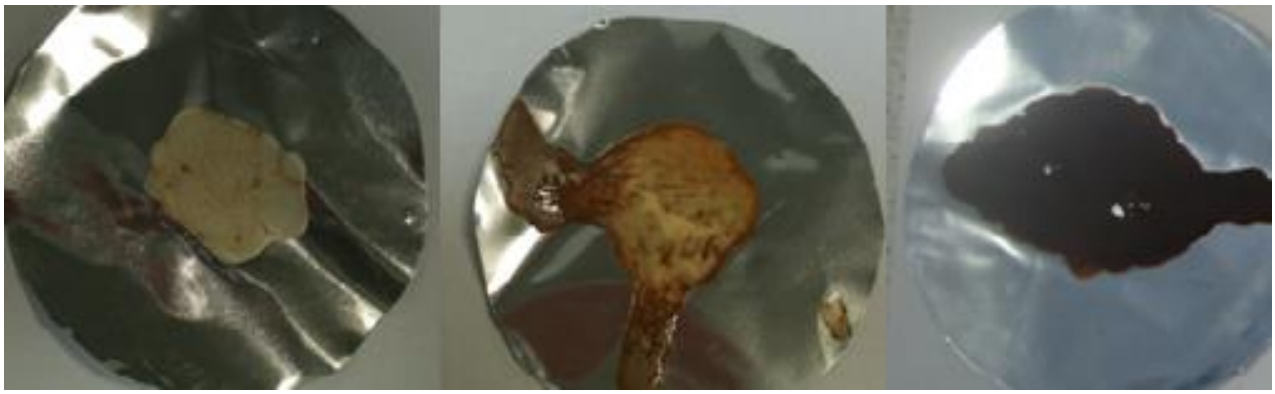

Figure 9.7 – Photographs of the E239 samples created from the ageing rig. The pictures going from left to right show the samples that have been aged for 5, 60 and 300 minutes at 320 ^{o}C.

The thermo-oxidative degradation behaviour was also investigated using the ageing rig for the samples containing Cardura, Heloxy and Vikolox. The aged samples containing Heloxy and Vikolox resemble the respective blank polymer samples. The presence of Cardura in the sample, especially at higher concentrations, is suggested to discolour more significantly during the conditions used to promote thermo-oxidative degradation. Figure 9.8 shows photos of the samples of E239 + 6% Cardura prepared using the ageing rig at 320 ^{o}C. The other photos obtained for samples containing Cardura are shown on the accompanying disc in the folder *Chapter 9* under *Ageing Rig*.

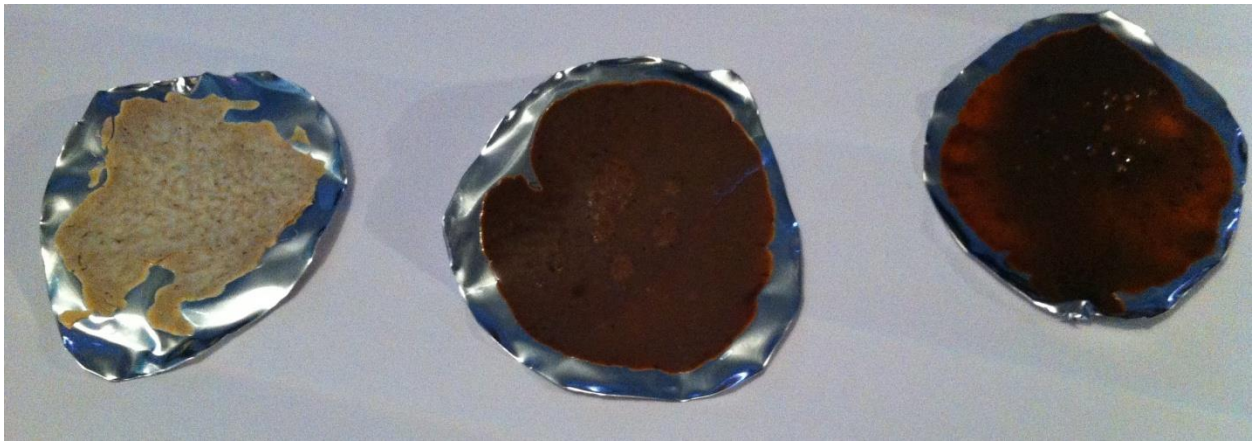

Figure 9.8 – Photographs of the E239 + 6% Cardura samples created from the ageing rig. The pictures going from left to right show the samples that have been aged for 5, 60 and 300 minutes at 320 °C.

9.2.3.2 % Volatilisation

The % volatilisation for all of the samples prepared in the ageing rig at 290 and 305 °C for 5 minutes were similar within experimental error. The values obtained for the % volatilsation ranged from 0.00 and 3.45%. The experimental error was calculated to be 4.20% and was obtained from the standard deviation from three repeat experiments. The additives are suggested to have no effect on the % volatilisation; the bar charts in figures 9.8 and 9.9 clearly show there is no difference in any of the samples. The bar charts also show no significant changes in the samples prepared in the ageing rig at 290 and 305 °C for 60 minutes. The % volatilisation values for the samples prepared at 320 °C for 5, 60 and 300 minutes are also all similar, suggesting the impact of the temperatures studied is very minimal. The bar charts shown in figures 9.9 to 9.11 highlight the similarity of the values obtained.

These temperatures were studied since they are the high range of processing temperatures that the samples could be exposed to when DTF is processing PET into films for the solar cells. This again confirms that DTF could successfully use these additives in their current processing line. The values obtained for the % volatilisation were higher than the values prepared using nitrogen, for example the average % volatilisation for the sample heated to 320 °C for 300

minutes under air gave a % volatilisation of 25.80%, which is considerably higher than the 4.37% created for the sample prepared under nitrogen at the same conditions. The fact that the % volatilisation under air is higher than those obtained in nitrogen is expected given the information obtained from the available literature. [10, 31 and 42]

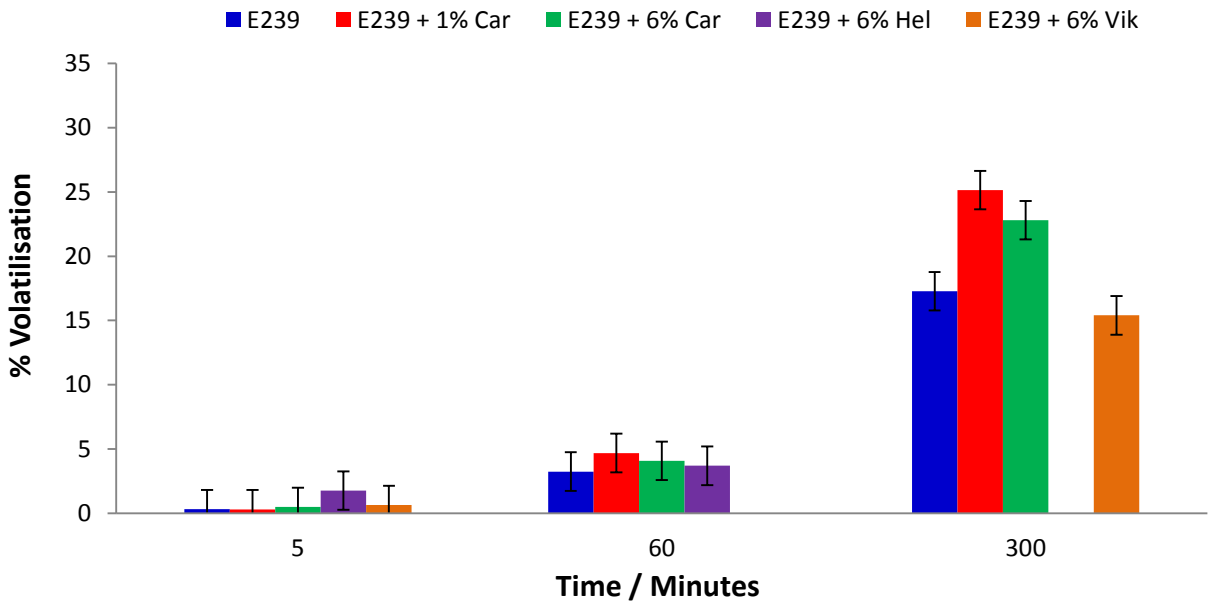

Figure 9.9– Bar chart showing the % volatilisations for the E239 samples aged for 5, 60 and 300 minutes in air in the ageing rig at 290 °C. . N=1. The error bar is 4.20% which is the calculated error in the method.

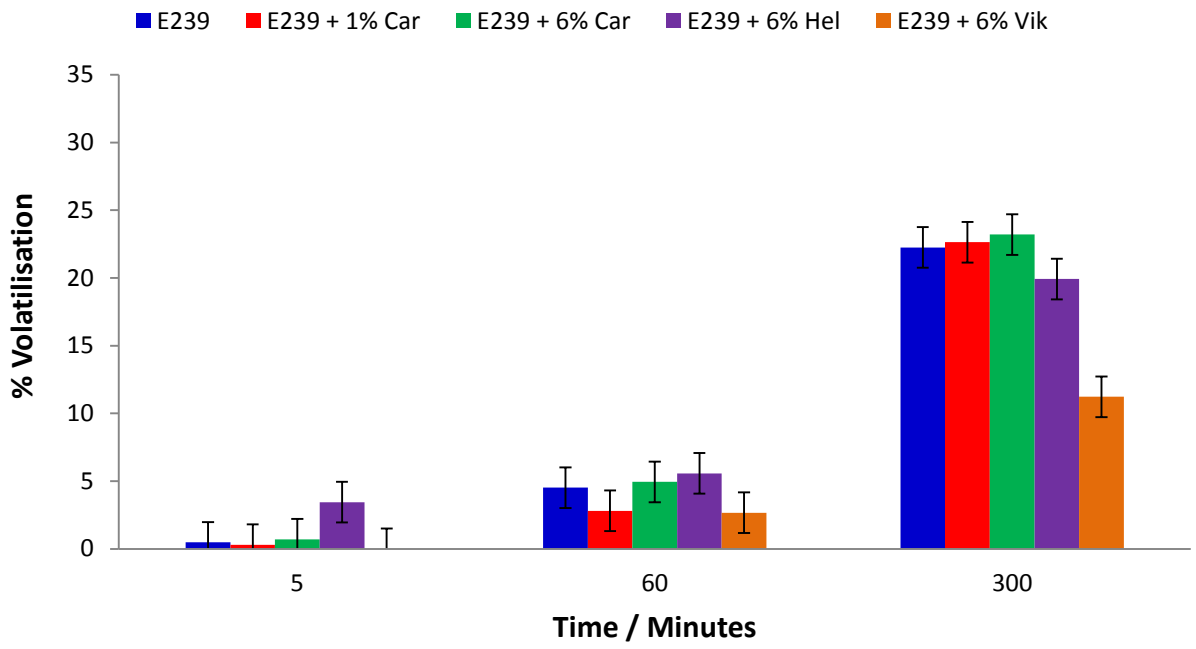

Figure 9.10– Bar chart showing the % volatilisations for the E239 samples aged for 5, 60 and 300 minutes in air in the ageing rig at 305 °C. N=1. The error bar is 4.20% which is the calculated error in the method.

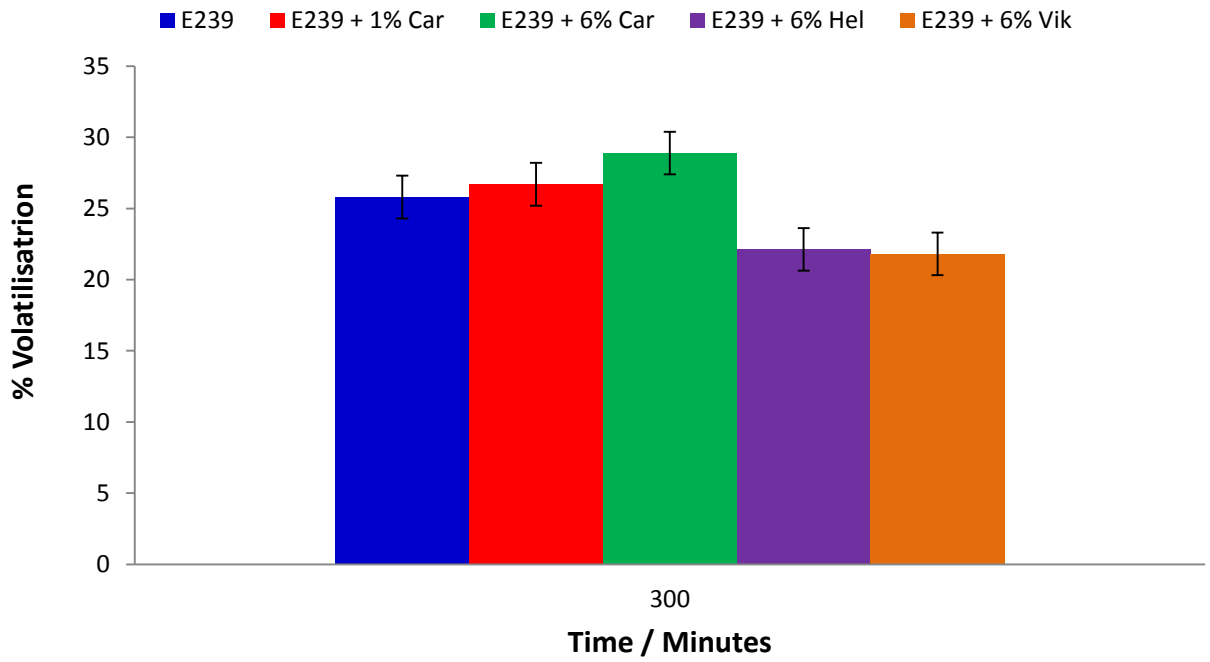

Figure 9.11– Bar chart showing the % volatilisations for the E239 samples aged for 300 minutes in air in the ageing rig at 320 °C. N=1. The error bar is 4.20% which is the calculated error in the method.

9.2.3.3 Gel Content

In the samples prepared using the ageing rig under air, gel was visible in the samples that were dissolved in a mixture of HFIP and chloroform. Figure 9.12 shows an example of the gel that is produced during the ageing process on the ageing rig. The residual and original gel content were calculated for the samples prepared on the ageing rig with E239, E239 + 1% Cardura and E239 + 6% Cardura. The bar charts for the percentage gel content (Residual) for the E239, E239 + 1% Cardura and E239 + 6% Cardura samples are shown in figures 9.13 to 9.15. The values for the percentage gel content (Original) are shown in the appendicles (A9.3.1 to A9.3.3).

The samples that were aged at 290 ^{o}C for 5, 60 and 300 minutes are all similar. The % volatilsation for the E239 + 6% Cardura samples aged at 290 ^{o}C for 300 minutes is slightly higher than the values obtained for the E239 and E239 + 1% Cardura samples because of a higher than expected error; or the excess Cardura is reacting with carboxyl and hydroxyl groups making complicated gel structures. All samples prepared at 305 ^{o}C for 5 and 60 minutes are similar, suggesting that the Cardura additive is not having a large impact. This is supported by the fact that the samples held at 305 ^{o}C for 300 minutes also show no significant differences.

The samples that were aged at 320 ^{o}C for 5 and 60 minutes are all similar except for the E239 + 6% Cardura. This suggests that Cardura can cause an increase in the production of gel particles under oxidative conditions. This has to be carefully considered by DTF as it could result in a buildup of material on their process line. This has the possibility of causing contamination in future samples and could increase down time of the processing line in order to remove this material.

The gel contents produced for the samples aged under air are all higher than those under the same conditions aged in an inert atmosphere. There were no significant changes noticed in the gel content for the samples prepared at 290 and 320 ^{o}C under air for 5 minutes and 60 minutes. A similar level of gel was also obtained for the sample prepared at 290 ^{o}C for 300

minutes as the other samples. The presence of an inert atmosphere could reduce a buildup of gel on the extruder.

Figure 9.12 – Picture of the gel produced from the E239 sample prepared at 320 °C under air for 300 minutes.

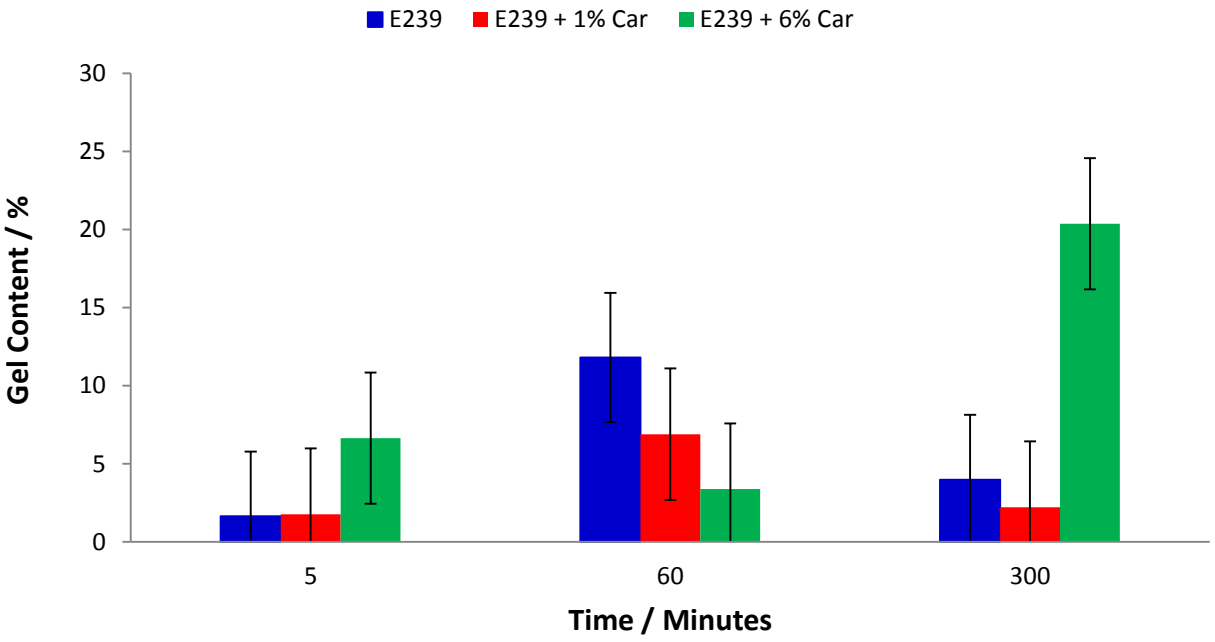

Figure 9.13– Bar chart showing the gel content (Residual) for the E239 samples aged for 5, 60 and 300 minutes in air at 290 °C. N=3. The error bar is 1.81% which is the calculated error in the method.

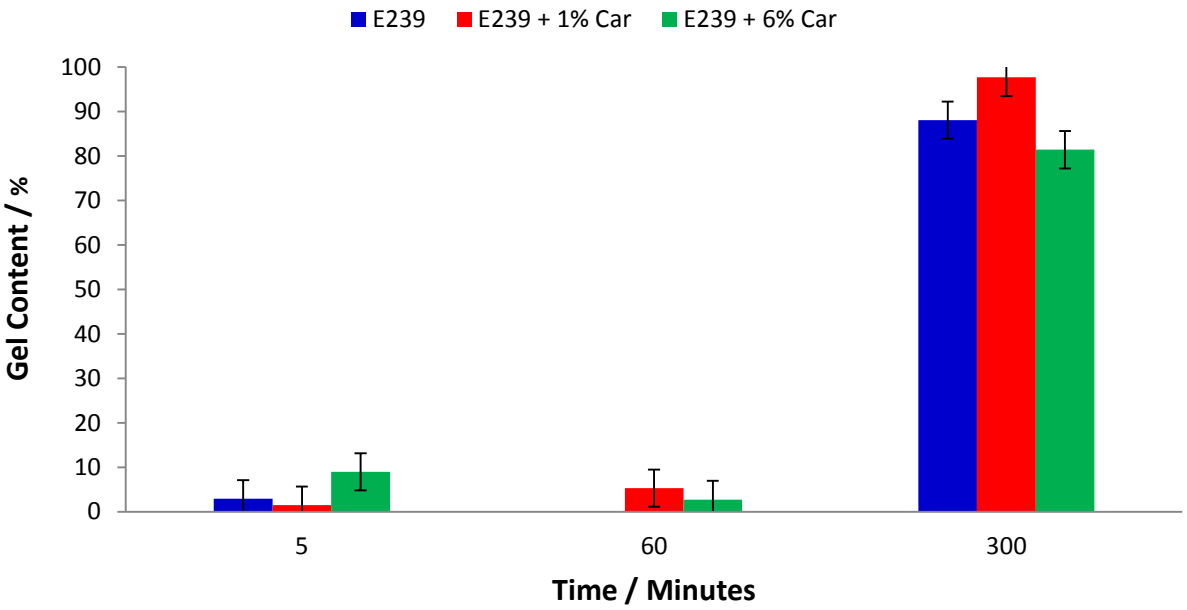

Figure 9.14– Bar chart showing the gel content (Residual) for the E239 samples aged for 5, 60 and 300 minutes in air at 305°C. N=3. The error bar is 1.81% which is the calculated error in the method.

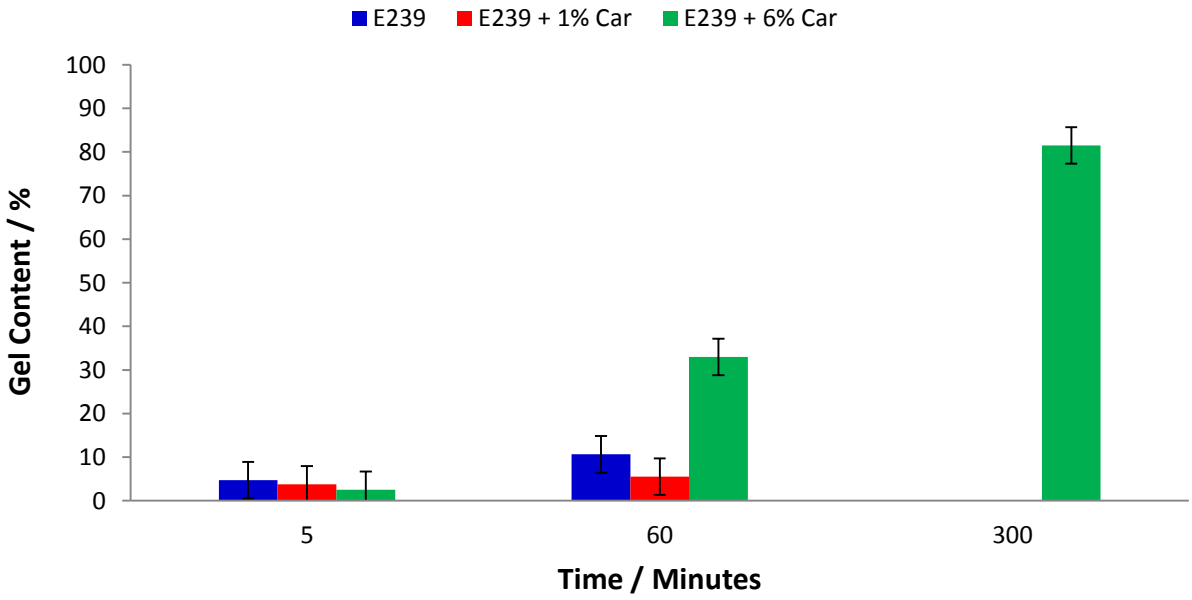

Figure 9.15– Bar chart showing the gel content (Residual) for the E239 samples aged for 5, 60 and 300 minutes in air at 320 °C. N=3. The error bar is 1.81% which is the calculated error in the method.

9.2.4 IR

The IR spectra were also obtained for all of the samples aged in air. Figure 9.16 shows the IR spectra of the E239 samples aged at 320 ^{o}C for 5 , 60 and 300 minutes, and figure 9.17 shows the IR spectra of the E239 samples aged at 320 ^{o}C for 5 , 60 and 300 minutes. All other IR spectra obtained for the E239, E239 +1% Cardura and E239 + 6% Cardura samples can be seen on the accompanying disc in the folder *Chapter 9* under *Ageing Rig*.

Small changes can be seen in the IR spectra, including the disappearance/reduction of peaks at 1175 and 1410 cm^{-1}. There were also new peaks identified at 846, 872, 1472, 1796 and 2348 cm^{-1}. These changes are consistent with the backbone of PET being broken down into smaller components. The new carbonyl peak at 1796 cm^{-1} is consistent with the formation of carboxyl end groups. The other peaks are consistent with changes in the aliphatic section of PET.

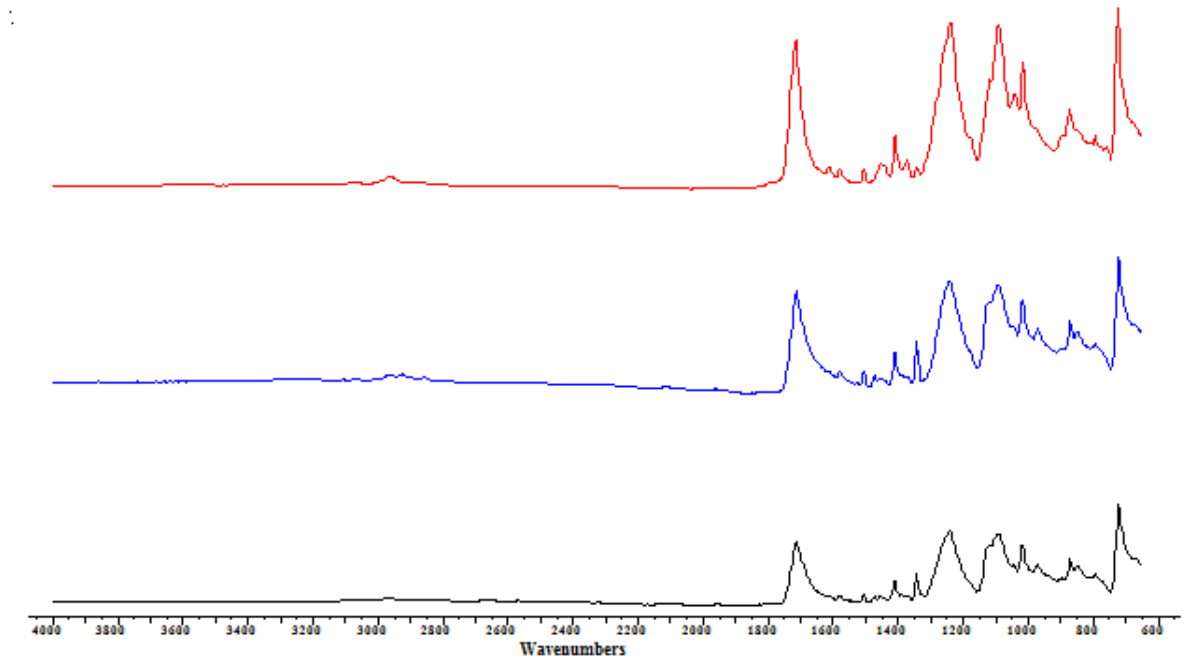

Figure 9.16 – Comparison of the IR spectra of the E239 samples that were generated on the ageing rig at 320 ^{o}C. The black line shows the spectra of the sample aged for 5 minutes, the blue line shows the spectra of the sample aged for 60 minutes and the red line shows the spectra for the sample aged for 300 minutes.

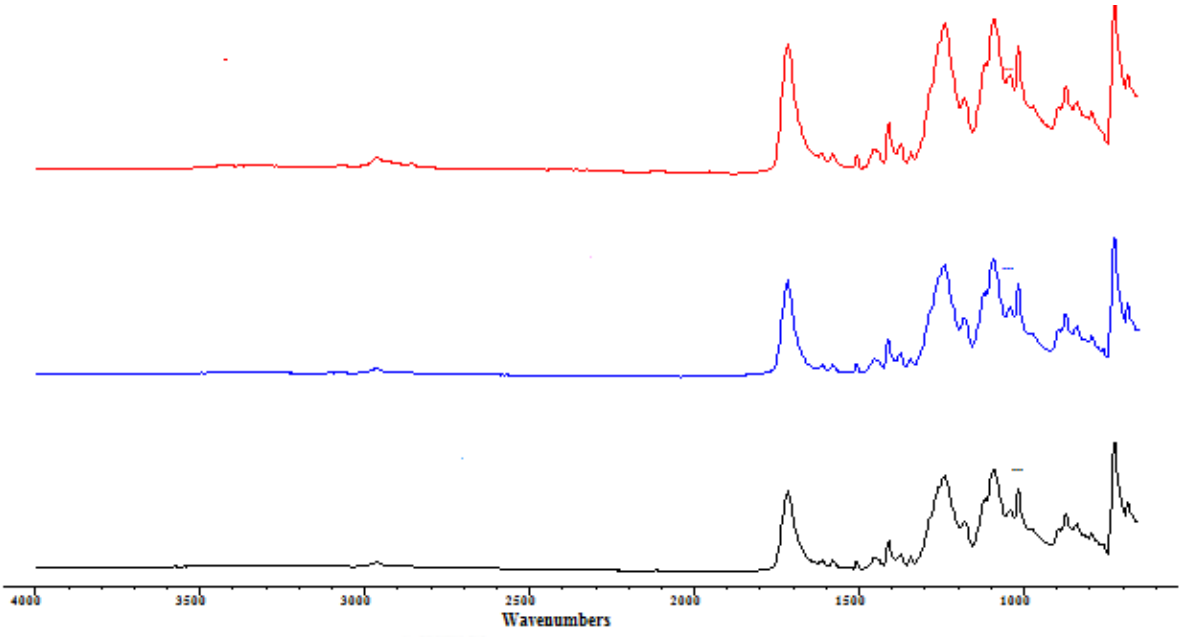

Figure 9.17 – Comparison of the IR spectra of the gel created for the E239 + 6% Cardura samples that were generated on the ageing rig at 320 °C. The black line shows the spectra of the sample aged for 5 minutes, the blue line shows the spectra of the sample aged for 60 minutes and the red line shows the spectra for the sample aged for 300 minutes.

9.2.5 CATLAB

The E239, E239 + 1% Cardura and E239 + 6% Cardura sample were all analysed using the CATLAB microreactor. Similar to the study on the onset of thermal degradation, the emission of carbon dioxide was closely studied to determine the onset of thermal-oxidative degradation. The plot showing the evolution of carbon dioxide is shown in figure 9.18 for the sample of E239 heated at 5 °C min^{-1}. The trace shows a two stage degradation mechanism for the thermo-oxidative degradation process of PET. A two stage mechanism for thermo-oxidative degradation has been discussed in the literature for PET. [10, 31 and 42] The mechanism is discussed in detail in Chapter 1. All of the samples produce a similar trace, suggesting that Cardura had no major impact on the mechanism for thermal degradation. All traces can be seen on the accompanying disc in the folder *Chapter 9* under *CATLAB*.

The values obtained for the onset of thermo-oxidative degradation are shown in tables 9.4 to 9.6. The onsets were similar to the values obtained for the DSC and TGA techniques. The error

obtained from the standard deviation of three repeat experiments was 40 °C. This is too high to draw reliable conclusions regarding trends indentified in the data. Further work would need to be carried out to reduce the error value obtained in this method to identify reliable trends. Once this has been achieved it should be possible to use the data for kinetic studies.

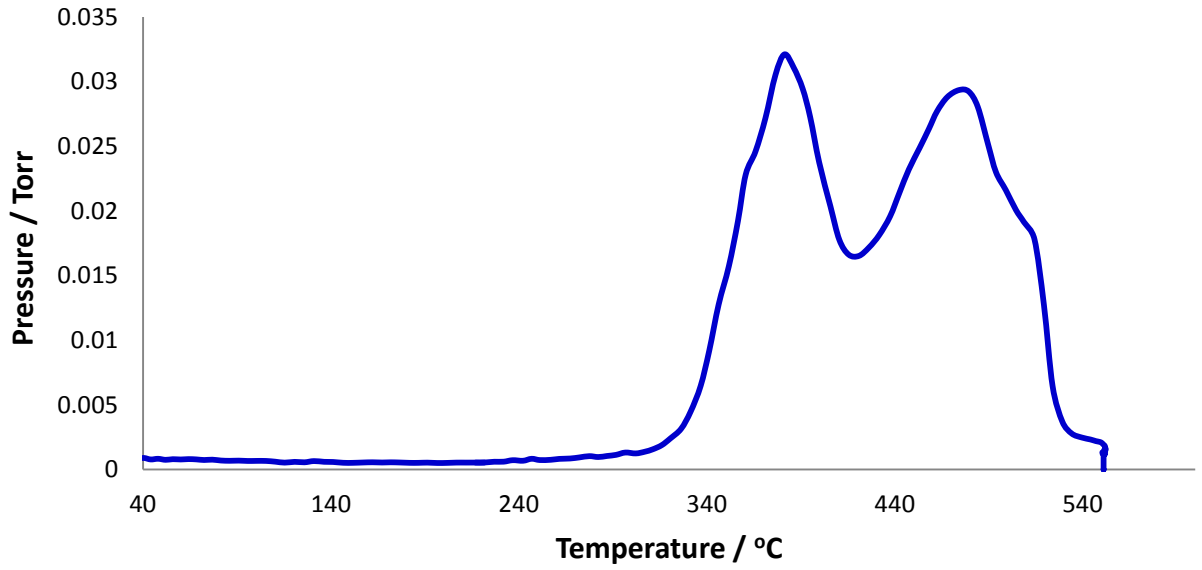

Figure 9.18 – Mass spectrum obtained from the CATLAB instrument showing the evolution of carbon dioxide (m/z 44) versus temperature for the E239 sample heated at a rate of 5 °C min^{-1}.

Table 9.4 – Table showing the onset of thermal-oxidative degradation based on the release of carbon dioxide for the E187 samples. N=1.

Sample	Rate °C min^{-1}	Onset temperature °C
E187	5	318
	10	296
	20	274
E187 + 1% Cardura	5	228
	10	289
	20	248
E187 + 6% Cardura	5	252
	10	262
	20	294

Table 9.5 – Table showing the onset of thermal-oxidative degradation based on the release of carbon dioxide for the E239 samples. N=1.

Sample	Rate $^{o}C\ min^{-1}$	Onset temperature ^{o}C
E239	5	227
	20	324
E239 + 1% Cardura	5	290
	10	294
	20	311
E239 + 6% Cardura	5	227
	10	271
	20	276

Table 9.6 – Table showing the onset of thermal-oxidative degradation based on the release of carbon dioxide for the E240 samples. N=1.

Sample	Rate $^{o}C\ min^{-1}$	Onset temperature ^{o}C
E240	5	223
	10	273
	20	324
E240 + 1% Cardura	5	213
	10	261
	20	298
E240 + 6% Cardura	5	208
	10	260

9.3 Conclusions

Using the DSC, the onset of thermo-oxidative degradation was shown to be considerably lower than the onset of thermal degradation. For example, the E187 sample has an onset of thermal degradation of 368 ^{o}C, but the same sample has an onset of thermo-oxidative degradation of 306 ^{o}C. This trend was also noticed in the TGA and CATLAB results. A lower onset of degradation shown in the samples containing epoxides has been proposed to be in fact the excess epoxides volatilising.

Small changes were noticed in the data obtained, such as the crystallinity being altered in the DSC scans and the Cardura-containing samples having increased gel content after being aged under certain conditions. The photographs from the ageing rig show changes that can be seen visually in the all of the samples prepared on the ageing rig under air, even the sample prepared at 290 ^{o}C for 5 minutes. There are traces of discolouration of the sample as there was a light brown presence on the sample, showing that degradation is occurring even at low temperatures in air. No changes were noticed in the samples held in an inert atmosphere for 5 minutes at 290 ^{o}C.

There were no significant changes to the thermo-oxidative degradation behaviour. The process is still shown to occur as a two step mechanism as mentioned in Chapter 1 and all of the products were identified from CATLAB analysis that were expected for thermo-oxidative behaviour, such as the formation of carbon dioxide.

As the epoxides were concluded to have little effect on the thermo-oxidative degradation they could successfully be trialed at DTF on their current processing line. The current extrusion system is sealed and the only exposure that the system would have to thermo-oxidative degradation is during the cooling of the molten polymer from the extruder die. The system being under an inert atmosphere has been shown in Chapter 8 to prevent Cardura containing samples from building up a gel. The limited effect of the epoxides on thermo-oxidative behaviour resulted in the approval of the epoxides by DTF to be trialed further for applications, such as the backsheet in solar cell panels.

10.0 Conclusions and Future Work

DTF required an additive that could be reacted with the end groups of PET to lower the carboxyl end group concentration, allowing the manufacture of a polymer that could be used as the backsheet for solar cell panels. The esterification reaction was shown to occur between the three epoxides and the model compounds benzoic acid and PEI. The analysis of the ^{1}H NMR spectra and the more detailed kinetic samples showed that the higher the reaction temperature the faster the esterification reaction occurs. It was shown that the most reactive monofunctionalised epoxide was Cardura followed by Vikolox, with Heloxy being the least reactive.

The data from the model compounds suggested that the epoxide Cardura could successfully be utilised in a reactive extrusion process as the reaction occurs in minutes, which is similar to the extruder residence times. It is essential that the additive can be used in reactive extrusion processes as the processing lines can be easily set up for addition of the liquid epoxide, which would make the manufacture of the modified PET commercially viable. Cardura was shown to significantly lower the carboxyl end group concentration of PET when added to an extruder. Very little to no significant esterification reaction was noticed to occur inside the extruder barrel with the epoxides Vikolox and Heloxy.

It was concluded that Cardura was the most suitable additive to be used for application in solar cell panels, as the reduction in the carboxyl end group concentration caused by the reaction of PET and Cardura does reduce the effects of hydrolytic degradation. This is because it reduces the parameters required for an auto-catalysis reaction to occur. It has been shown that a higher concentration of Cardura increases the protective effect as it ensures that all of the carboxyl end groups are end capped. The other two epoxides investigated (Heloxy and Vikolox) also reduce the carboxyl end group concentration, but are not as efficient as Cardura as they do not react as well with the carboxyl end groups of PET.

Analysis of the data gathered regarding the epoxides' extrusion stability suggests that Cardura does not promote thermal degradation inside the extruder barrel. There were no significant differences detected in the carboxyl end group concentration for the samples containing Cardura that were prepared at different temperature profiles, increased residence times and exposed to different levels of shear. This provides DTF with the confidence that the material will not cause adverse effects if the extrusion process is interrupted. The other requirements of the additive were to have no adverse effects on the polymer properties, for example the molecular weight or crystallinity. The experiments carried out show that the Cardura has no significant effect on the polymer. The gel content was not shown to increase, which could affect clarity. This is an important property in the manufacture of films.

The next stage would be to scale up the process from the lab scale extruder at Strathclyde University to the processing lines at DTF, where the film can go through final trials before being manufactured for customers. If successful trials are carried out on the extruder lines at DTF the samples would go through their current processes to determine suitability for manufacture. These processes include autoclave and weatherometer tests.

Interesting further work for the project would be to investigate the carboxyl end group concentration of samples autoclaved and treated on the weatherometer at DTF, as this would provide a detailed picture of what carboxyl end group concentration is required to pass or fail quality checks and allow an indication as to how long the sample can be used before it will fail. This would strengthen the use of the Pohl titration method developed as a simple screening method for DTF's polymer samples.

The data comparing some of the different polymers show that the solid state polymerised samples (E239 and E240) have a slight decrease in the rate of hydrolytic degradation due to the lower initial carboxyl end group concentration when compared to E187, which is not solid state polymerised. This allowed for a lower concentration of the epoxide additive to be used to achieve a similar result. However, having a solid state polymerised PET adds a process step and as a result, a cost. Further work would be required to prepare the process flow diagrams for the reactive extrusion process outlining the costs for the various materials and processes required.

These process flow diagrams will highlight the most economical and cost effective solution to create the Cardura end-capped PET to be used in the application of solar cell panels.

The kinetic study confirmed that the hydrolysis reaction was a half order reaction. The apparent reaction rate was shown to reduce with the addition of Cardura to the samples. This confirmed that the Cardura was reducing the effects of hydrolytic degradation, allowing the PET to maintain its properties for longer in the environment studied. A similar study was obtained for the epoxides Vikolox and Heloxy, but these were only aged up to 10 days. The carboxyl end group concentration generated for these samples was very low, and with the high error of the Pohl titration method these graphs were not straight lines. Further work would be required to generate samples aged for longer to ensure the model is an adequate fit.

Another area that could benefit from further work is confirming the nature of the hydrolysis products. There is a possibility some oligomers were also present. The concentration of excess epoxide remaining in the polymer and its impact should be studied, as the polymer is intended for use in the environment parameters. One area that should be investigated is the ability for excess epoxide to leach from the polymer.

11.0 References

1. A. Labouret and M. Villoz "*Solar Photovoltaic Energy*" Published by the Institution of Engineering and Technology; London; 2010

2. J. Mazer "*Solar Cells: An Introduction to Crystalline Photovoltaic Technology*" Published by Kluwer Academic Publishers; Massachusetts; 1997

3. L. Frass and L. Partain "*Solar Cells and Their Applications*" Published by John Wiley & Sons, Inc; New Jersey; 2010

4. S. Wenham, M. Green, M. Watt, R. Corkish and A. Sproul "*Applied Photovoltaics*" Published by Earthscan; New York; 2011

5. http://www.allaboutcircuits.com; Accessed 22-04-2012

6. A. M^{c}Evoy, L. Castaner and T. Markvart "Solar *Cells – Materials, Manufacture and Operation*" Published by Elservier; London; 2013

7. M. Poliskie "*Solar Module Packaging-Polymeric Requirements and Selection*" Published by CRC Press; Boca Raton; 2011

8. P. Pointer and M. Coleman "*Essentials of Polymer Science and Engineering*" Published by DEStech Publications; Pennsylvania; 2009

9. J. Cowie and V. Arrighi "*Polymers: Chemistry and Physics of Modern Materials*" Published by CRC Press; Boca Raton; 2008

10. J. Scheirs and T. Long "*Modern Polyesters – Chemistry and Technology of Polyesters and Copolyesters*" Published by John Wiley & Sons, Inc; West Sussex; 2003

11. J. Otton and S. Ratton "*Investigations of the Formation of Poly(ethylene terephthalate) with Model Compounds: Kinetics and Mechanisms of the Catalytic Esterification and Alcoholysis Reaction. 1. Carboxylic Acid Catalysis (Mono-functional Reactants)*" Journal of Polymer Science: Part A – Polymer Chemistry; 26; 1988; 2187-2197

12. G. Karayannidis, C. Roupakias, D. Bikiaris and D. Achilias "*Study of Various Catalysts in the Synthesis of Poly(propylene terephthalate) and Mathematical Modeling of the Esterification Reaction*" Polymer; 44; 2003; 931-942

13. B. Duh "*Effect of Antimony Catalyst on Solid-State Polycondensation of Poly(ethylene terephthalate)*" Polymer; 43; 2002; 3147-3154

14. T. Kushimoto, Y. Ozawa, A. Baba and H. Matsuda "*Niobium Compound Catalyst for Polycondensation Reaction to Form Poly(ethylene terephthalate) (PET)*" Catalysis Today; 16; 1993; 571-578

15. J. Otton and S. Ratton "*Investigations of the Formation of Poly(ethylene terephthalate) with Model Compounds: Kinetics and Mechanisms of the Catalytic Esterification and Alcoholysis Reactions . 2. Catalysis by Metallic Derivatives (Mono-functional Reactants)*" Journal of Polymer Science: Part A – Polymer Chemistry; 26; 1988; 2199-2224

16. DTF Internal Reports & Communications

17. M. O'Donnell "*The Development of D243PV*" 4th year Industrial Report; University of Strathclyde; 2011

18. R. Brückner *"Reaktionsmechanismen. Organische Reaktionen, Stereochemie, moderne Synthesemethoden"* Spektum Akademischer Verlag; Heidelberg; Germany, 1996

19. G. Hovenkamp and P. Munting "*Formation of Diethylene Glycol as A Side Reaction During Production of Poly(ethylene terephthalate*)" Journal of Polymer Science: Part A – Polymer Chemistry; 8; 1970; 679-682

20. H. Peebles, W. Huffmann and T. Ablett "*Isolation and Identification of the Linear and Cyclic Oligomers of Poly(ethylene terephthalate) and the Mechanism of Cyclic Oligomer Formation*" Journal of Polymer Science: Part A – Polymer Chemistry; 7; 1969; 479-496

21. O. Kadkin, K. Osajda, P. Kaszynski and T. Barber "*Polyester Polyols: Synthesis and Characterization of Diethylene Glycol Terephthalate Oligomers*" Journal of Polymer Science: Part A – Polymer Chemistry; 41; 2003; 1114-1123

22. W. Hergenrother "*Influence of Copolymeric Poly(diethylene glycol) Terephthalate on the Thermal Stability of Poly(ethylene terephthalate)*" Journal of Polymer Science: Polymer Chemistry Edition; 12; 1974; 875-883

23. H. Lecomte and J. Liggat "*Degradation Mechanism of Diethylene Glycol Units in a Terephthalate Polymer*" Polymer Degradation and Stability; 91; 2006; 681-689

24. B. Holland and J. Hay "*The Thermal Degradation of PET and Analogous Polyesters Measured by Thermal Analysis – Fourier Transform Infrared Spectroscopy*" Polymer; 43; 2002; 1835-1847

25. S. Lee, M. Ree, C. Park, Y. Jung, C. Park, Y. Jin and D. Bae "*Synthesis and Non-isothermal Crystallization Behaviors of Poly(ethylene isophthalate-co-terephthalate)*" Polymer; 40; 1999; 7137-7146

26. R. Kotek, K. Pang, B. Schmidt and A. Tonelli "*Synthesis of Gas Barrier Characterization of Poly(ethylene isophthalate)"* Journal of Polymer Science: Part B – Polymer Physics; 42; 2004; 4247-4254

27. B. Li, J. Yu, S. Lee and M. Ree "*Crystallizations of Poly(ethylene terephthalate co ethylene isophthalate)*" Polymer; 40; 1999; 5371-5375

28. J. Ubach, A. Martínez De Ilarduya, R. Quintana, A. Alla, E. Rudé and S. Muñoz-Guerra "*Poly(ethylene terephthalate-co-isophthalate) Copolyesters Obtained from Ethylene Terephthalate and Isophthalate Oligomers*" Applied Polymer Science; 115; 2010; 1823-1830

29. B. Li, J. Yu, S. Lee and M. Ree "*Poly(ethylene terephthalate co ethylene isophthalate) Relationship Between Physical Properties and Chemical Structure*" European Polymer Journal; 35; 1999; 1607-1610

30. http://composite.about.com/od/Plastics/a/What-Are-Pbt-Plastics.htm; Accessed 08-06-2016

31. D. Bikiaris and G. Karayannidis "*Effect of Carboxylic End Groups on Thermooxidative Stability of PET and PBT*" Polymer Degradation and Stability; 63; 1999; 213-218

32. C. Wang and C. Lin "*Synthesis and Properties of Phosphorous – Containing PEN and PBN Copolyesters*" Polymer; 40; 1999; 747-757

33. L. Lillwitz "*Production of Dimethyl-2,6-naphthalenedicarboxylate: Precursor to Polyethylene naphthalate*" Applied Catalysis A: General; 221; 2001; 337-358

34. https://www.dupontteijinfilms.com/; Accessed 11-06-2016

35. I. Campbell "*Introduction to Synthetic Polymers*" Oxford University Press Inc; New York; 2000

36. D. Bower "*An Introduction to Polymer Physics*" Published by Cambridge University Press, Cambridge; 2002

37. V. Ratta "*Crystallization, Morphology, Thermal Stability and Adhesive Properties of Novel High Performance Semicrystalline Polyimides*" PhD Thesis; Virginia Tech; 2011

38. G. Lamberti "*Flow Induced Crystallisation of Polymers*" Chemical Society Reviews; 43; 2014; 2240-2252

39. http://nvlpubs.nist.gov; Accessed 24-04-12

40. http://www.doitpoms.ac.uk/tlplib/polymers/spherulites.php; Accessed 12-06-16

41. http://faculty.uscupstate.edu; Accessed 12-06-16

42. L. H Buxbaum "*The Degradation of Poly(ethylene terephthalate)*" Angewandte Chemie International edition; 7; 1968; 182-190

43. E. Pirzadeh, A. Zadhoush and M. Haghighat "*Hydrolytic and Thermal Degradation of PET Fibres and PET Granule: The Effects Of Crystallization, Temperature And Humidity*" Journal of Applied Polymer Science; 106; 2007; 1544-1549

44. C. Sammon, J. Yarwood and N. Everall "*An FT-IR Study of the Effects of Hydrolytic Degradation on the Structure of PET Films*" Polymer Degradation and Stability; 67; 2000; 149-158

45. J. Campanelli, M. Kamal and D. Cooper "*A Kinetic Study of the Hydrolytic Degradation of Poly(ethylene terephthalate) at High Temperature*" Journal of Applied Polymer Science; 48; 1993; 443-451

47. S. Hosseini, S. Taheri, A. Zadhoush and A. Mehrabani-Zeinabad "*Hydrolytic Degradation of Poly(ethylene terephthalate*" Journal of Applied Polymer Science; 103; 2007; 2304-2309

48. S. Ruetsch, X. Huang, D. Salem and H. Weigmann "*UV Stabilization of PET Fibres: Microscopy Study*" Textile Research Journal; 66; 1996; 185-195

49. B. Holland and J. Hay "*The Thermal Degradation of PET and Analogous Polyesters Measured by Thermal Analysis – Fourier Transform Infrared Spectroscopy*" Polymer; 43; 2002; 1835-1847

50. F. Samperi, C. Puglisi, R. Alicata and G. Montaudo "*Thermal Degradation of Poly(ethylene terephthalate) at the Processing Temperatures*" Polymer Degradation and Stability; 83; 2004; 2-10

51. M. Edge, N. Allen, R. Wiles, W. McDonald and S. Mortlock "*Identification Of Luminescent Species Contributing To The Yellowing Of Poly(ethylene terephthalate) On Degradation*" Polymer; 36; 1995; 227-234

52. F. Viillain, J. Coudane and M. Vert "*Thermal Degradation of Poly(ethylene terephthalate): Study of Polymer Stabilization*" Polymer Degradation and Stability; 49; 1995; 393-397

53. Y. Sakata, M. Uddin, K. Koizumi and K. Murata "*Thermal Degradation Of Poly(ethylene) Mixed With Poly(vinyl chloride) And Poly(ethylene terephthalate*)" Polymer Degradation and Stability; 53; 1996; 111-117

54. M. Day and D. Wiles "*Photochemical Degradation of Poly(ethylene terephthalate). I. Irradiation Experiments with the Xenon and Carbon Arc*" Journal of Applied Polymer Science; 16; 1972; 175-189

55. M. Day and D. Wiles "*Photochemical Degradation of Poly(ethylene terephthalate). II. Effects of Wavelength and Environment on the Decomposition Process*" Journal of Applied Polymer Science; 16; 1972; 191-202

56. M. Day and D. Wiles "*Photochemical Degradation of Poly(ethylene terephthalate). III. Determination of Decomposition Products and Reaction Mechanism*" Journal of Applied Polymer Science; 16; 1972; 203-215

57. P. Blais, M. Day and D. Wiles "*Photochemical Degradation of Poly(ethylene terephthalate). IV. Surface Changes*" Journal of Applied Polymer Science; 17; 1973; 1895-1907

58. G. Fechine, M. Rabello, R. Souto Maior and L. Catalani "*Surface Characterization of Photodegraded Poly(ethylene terephthalate). The Effect of Ultraviolet Absorbers*" Polymer; 45; 2004; 2303-2308

59. M. Mohammadian, N. Allen, M. Edge and K. Jones "*Environmental Degradation of Poly(ethylene terephthalate)*" Textile Research Journal; 61; 1991; 690-696

60. W. Wang, A. Taniguchi, M. Fukuhara and T. Okada "*Two-step Photodegradation Process of Poly(ethylene terephthalate)*" Journal of Applied Polymer Science; 74; 1999; 306-310

61. S. Fernando, P. Christensen, T. Egerton, R. Eveson, S. Martins-Franchetti, D. Voisin and J. White "*Carbon Dioxide Formation During Initial Stages of Photodegradation of Poly(ethylene terephthalate) (PET) Films*" Material Science and Technology; 25; 2009; 549-555

62. Z. Zhu and M. Kelley "*IR Spectroscopic Investigation of the Effects of Deep UV Irradiation on PET Films*" Polymer; 46; 2005; 8883-8891

63. G. Fechine, M. Rabello and R. Souto-Maior "*The Effects of Ultraviolet Stabilizers on the Photodegradation of Poly(ethylene terephthalate)*" Polymer Degradation and Stability; 75; 2002; 153-159

64. G. Fechine and R. Souto-Maior "*Structural Changes During Photodegradation of Poly(ethylene terephthalate)*" Journal of Material Science; 37; 2002; 4979-4984

65. Y. Nakayama, K. Takahashi and T. Sasamoto "*ESCA Analysis of Photodegraded Poly(ethylene terephthalate) Film Utilizing Gas Chemical Modification*" Surface and Interface Analysis; 24; 1996; 711-717

66. M. Xanthos, C. Wan, R. Dhavalikar, G. Karayannidis and D. Bikiaris "*Identification of Rheological and Structural Characteristics of Foamable Poly(ethylene terephthalate) by Reactive Extrusion*" Polymer International; 53; 2004; 1161-1168

67. J. Forsythe, K. Cheah, D. Nisbet, R. Gupta, A. Lau, A. Donovan and M. O'Shea "*Rheological Properties of High Melt Strength Poly(ethylene terephthalate) formed by Reactive Extrusion*" Journal of Applied Polymer Science; 100; 2006; 3646-3652

68. N. Torres, J. Robin and B. Boutevin "*Chemical Modification of Virgin and Recycled Poly(ethylene terephthalate) by Adding Chain Extenders During Processing*" Journal of Applied Polymer Science; 79; 2001; 1816-1824

69. E. Taylan and H. Küsefoğlu "*Chain Extension Reactions of Unsaturated Polyesters with Epoxy Compounds*" Journal of Applied Polymer Science 112; 2009; 1184-1191

70. Y. Zhang, C. Zhang, H. Li, Z. Du and C. Li " *Chain Extension of Poly(ethylene terephthalate) with Bisphenol-A Dicyanate*" Journal of Applied Polymer Science; 117; 2010; 2003-2008

71. T. Loontjens "*Modular Approach for Novel Nanostructured Polycondensates Enabled by the Unique Selectivity of Carbonyl Biscaprolactam*" Journal of Polymer Science: Part A- Polymer Chemistry; 41; 2003; 3198-3205

72. G. Karayannidis and E. Psalida "*Chain Extension of Recycled Poly(ethylene terephthalate) with 2,2'-(1,4-phenylene)bis(2-oxazoline)*" Journal of Applied Polymer Science; 77; 2000; 2206-2211

73. Z. Qian, X. Chen, J. Xu and B. Guo "*Chain Extension of PA1010 by Reactive Extrusion by Diepoxide 711 and Diepoxide TDE85 as Chain Extenders*" Journal of Applied Polymer Science; 94; 2004; 2347-2355

74. B. Jacques, J. Devaux, R. Legras and E. Nield " *Reactions Influenced by Triphenyl Phosphite Addition During Melt Mixing of PET/PBT blends: Chromatographic Evidence of a Molecular Weight Increase due to the Different Creation of Bonds of Two Different Natures*" Polymer; 38; 1997; 5367-5777

75. L. Incarnato, P. Scarfato, L. Di Maio and D. Acierno "*Structure and Rheology of Recycled PET Modified by Reactive Extrusion*" Polymer; 41; 2000; 6825-6831

76. X. Xu, Y. Ding, Z. Qjan, F. Wang, B. Wen, H. Zhou, S. Zhang and M. Yang " *Degradation of Poly(ethylene terephthalate)/Clay Nancomposities During Melt Extrusion: Effect of Clay Catalysis and Chain Extension*" Polymer Degradation and Stability; 94; 2009; 113-123

77. P. Raffa, M. Coltellia, S. Savi, S. Bianchi and V. Castelvetro "*Chain Extension and Branching of Poly(ethylene terephthalate) (PET) with Di- and Multifunctional Epoxy or Isocyanate Additives: An Experimental and Model Study*" Reactive and Functional polymers; 72. 2012; 50-60

78. M. Xanthos, U. Yilmazer, S. Key and J. Quintans "*Melt Viscosity of Poly(ethylene terephthalate) Resins For Low Density Extrusion Foaming*" Polymer Engineering and Science, 40; 2003; 554-566

79. D. Bikiaris and G. Karayannidis "*Chain Extension of Polyesters PET and PBT with Two New Diimidodiepoxides. II*" Journal of Polymer Science: Part A - Polymer Chemistry; 34; 1996; 1337-1342

80. A. Haralabakopoulos, D. Tsiourvas and C. Paleos "*Chain Extension of Poly(ethylene terephthalate) by Reactive Blending Using Diepoxides*" Journal of Applied Polymer Science; 71; 1999; 2121-2127

81. S. Japon, L. Boogh, Y. Leterrier and J. Månson "*Reactive Processing of Poly(ethylene terephthalate) Modified with Multifunctional Epoxy-based Additives*" Polymer; 41; 2000; 5809-5818

82. J. Lacoste, V. Boounor-Legaré, M. Llauro, C. Monnet, P. Cassagnau and A. Michel "*Functionalization of Poly(ethylene terephthalate) in the Melt State: Chemical and Rheological Aspects*" Journal of Polymer Science: Part A - Polymer Chemistry; 43; 2005; 2207-2223

83. M. Xanthos and M. W. Young "*Reactive Modification of Poly(ethylene terephthalate) with Polyepoxides*" Polymer Engineering and Science; 41; 2001; 643-655

84. R. Dhavalikar, M. Yamaguchi and M. Xanthos "*Molecular and Structural Analysis of a Triepoxide - Modified Poly(ethylene terephthalate) from Rheological Data*" Journal of Polymer Science: Part A – Polymer Science; 41; 2003; 958-969

85. R. Dhavalikar and M. Xanthos "*Parameters Affecting the Chain Extension and Branching of PET in the Melt State by Polyepoxides*" Journal of Applied Polymer Science; 87; 2003; 643-652

86. H. Pohl "*Determination of Carboxyl End Group in Polyesters, Poly(ethylene terephthalate)*" Analytical Chemistry; 26; 1954; 1614-1616

87. M. Maurice and F. Huizinga "*The Determination of Carboxyl Groups in Poly(ethylene terephthalate)*" Analytica Chemica Acta; 22; 1960; 363-368

88. S. Burow and D. Turner "*γ-Irradiation of Poly(ethylene terephthalate*). 1. Yields of Gas and Carboxyl groups" Journal of Polymer Science: Part A-1; 4; 1966; 613-622

89. D. Nissen, V. Rossbach and H. Zahn "*Determination of Carboxyl Endgroups and Comonomers in Poly(ethylene terephthalate) with Hydrazine*" Journal of Applied Polymer Science; 18; 1974; 1953-1968

90. I. Ward "*The Measurement of Hydroxyl and Carboxyl End Groups in Poly(ethylene terephthalate*)" Transactions of the Faraday Society; 53; 1975; 1406-1412

91. R. Addleman and V. Zichy "*Accurate Measurement of Carboxyl and Hydroxyl End-group Concentrations in Poly(ethylene terephthalate) Film by Infra-red Spectroscopy*" Polymer; 13; 1972; 391-398

92. A. Kenwright, S. Peace, R. Richards, A. Bunn and W. MacDonald "*End Group Modification in PET*" Polymer; 40; 1999; 2035-2040

93. B. Fox, G. Moad, G. Diepen and I. Wiling "*Characterization of Poly(ethylene terephthalate) and Poly(ethylene terephthalate) Blends*" Polymer; 38; 1997; 3035-3043

94. S. Al-Abdulrazzak, E. Lofgren and S. Jabarin "*End-group Determination in Poly(ethylene terephthalate) By Infrared Spectroscopy*" Polymer International; 51; 2002; 174-182

95. R. Pétiaud, H. Waton and Q. Pham "*A ^{1}H and ^{13}C NMR Study of the Products from Direct Polyesterification of Ethylene Glycol and Terephthalic Acid*" Polymer; 33; 1992; 3155-3161

96. Y. Ma, U. Agarwal, J. Vekemans and D. Sikkema "*NMR Based Determination of a Minute Acid Functionality: End-groups in PET*" Polymer; 44; 2003; 4429-4434

97. A. Donovan and G. Moad "*A Novel Method for Determination of Polyester End-Groups by NMR Spectroscopy*" Polymer; 46; 2005; 5005-5011

98. R. Macomber "*A Complete Introduction to Modern NMR Spectroscopy*" Published by John Wiley & Sons, Inc; USA; 1998

99. R. Abraham, J. Fisher and P. Loftus "*Introduction to NMR Spectroscopy*" Published by John Wiley & Sons, Inc; Essex; 1988

100. J. Keeler "*Understanding NMR Spectroscopy*" Published by John Wiley & Sons, Inc; Singapore; 2010

101. J. Akitt "*NMR And Chemistry - An Introduction to Modern NMR Spectroscopy*" Published by Chapman & Hall; London; 1992

102. C. Campbell, R. Pethrick and J. White "*Polymer Characterization - Physical Techniques*" Published by Stanley Thornes Ltd; Cheltenham; 2000

103. G. Gale "*Rapra Review Reports – Current Developments in Materials Technology and Engineering - Report 17 Extrusion*" Published by Pergamon Press Plc; Oxford; 1991

104. J. Benbow and J. Bridgewater "*Paste Flow and Extrusion*" Published by Oxford University Press; United Kingdom; 1993

105. L. Janssen "*Twin Screw Extrusion*" Published by Elsevier Scientific; The Netherlands; 1978

106. J. Brydson and D. Peacock "*Principles of Plastic Extrusion*" Published by Applied Science Publishers Ltd; Norfolk; 1973

107. P. Haines *"Principles of Thermal Analysis and Calorimetry"* Published by the Royal Society of Chemistry; Cornwall; 2002

108. T. Hatakeyama and F. Quinn *"Thermal Analysis: Fundamentals and Applications to Polymer Science"* Published by Wiley; Michigan; 1999

109. S. Duckett and B. Gilbert "*Foundations of Spectroscopy*" Published by Oxford Science; New York; 1999

110. W. Dudley and I. Fleming "*Spectroscopic Methods in Organic Chemistry*" Published by McGraw-Hill; Glasgow; 1995

111. W. Kemp "*Organic Spectroscopy – Second Edition*" Published by MacMillan; Hong Kong; 1975

112. http://www.utsc.utoronto.ca/~traceslab/ATR_FTIR.pdf ; Accessed 10-12-14

113. W. Kulicke and C. Clasen "*Viscosity of Polymers and Polyelectrolytes*" Published by Springer Laboratories; Hamburg; 2009

114. http://www.ias.ac.ininitiatsci_edresourceschemistryViscosity.pdf ; Accessed 10-12-14

115. I. McNeill *"Thermal Volatilisation Analysis of High Polymers"* European Polymer Journal; 3; 1967; 409-421

116. N. Grassie and H. Meville "*The Thermal Degradation of Polyvinyl Compounds"* Proceedings of the Royal Society of London A; I – *IV*; 1949

117. I.C. McNeill "*Thermal Volatilisation Analysis, A New Method for the Characterisation of Polymers and the Study of Polymer Degradation*" Journal of Polymer Science A1; 4; 1966; 2479

118. I.C. McNeill "*Thermal Volatilisation Analysis of High Polymers"* European Polymer Journal; 3; 1967; 409

119. I.C. McNeill "*Polymer Degradation and Characterisation by Thermal Volatilisation Analysis with Differential Condensation of Products*" European Polymer Journal; 6; 1970; 373-395

120. Michael O'Donnell "*The Hydrolysis of Polyethylene Terephthalate Film as Relevant in Photovoltaic Applications*" Report; University of Strathclyde; 2011

121. D. Gardner and I. McNeill "*The Thermal Degradation of Polychloroprene parts I – III"* European Polymer Journal; 7; 1971; 569-592

122. http://www.hidenanalytical.com; Accessed 12-12-14

123. E. Hoffmann and V. Strooband "*Mass Spectroscopy – Principles and Application*" Published by John Wiley and Son Ltd; West Sussex; 2007

124. R. Golike and S. Lasoski Jr "*Kinetics of Hydrolysis of Poly(ethylene terephthalate) Films*" The Journal of Physical Chemistry; 64; 1960; 895-898

125. S. Zumdahl and S. Zumdahl "*Chemistry*" Published by Books/Cole Cengage Learning; USA; 2010

126. T. Engel and P. Reid "*Physical Chemistry*" Published by Pearson Education; San Francisco; 2006

127. C. Kao, B. Wan and W. Cheng "*Kinetics of Hydrolytic Depolymerization of Melt Poly(ethylene terephthalate)*" Industrial and Engineering Chemical Research; 37; 1998; 1228-1234

128. S. Mishra, V. Zope and A. Goje "*Kinetics and Thermodynamics of Hydrolytic Depolmerization of Poly(ethylene terephthalate) at High Pressure and Temperature*" Journal of Applied Polymer Science; 90; 2003; 3305-3309

129. H. Zhang and I. Ward "*Kinetics of Hydrolytic Degradation of Poly(ethylene naphthalene-26-dicarboxylate)*" Macromolecules; 28; 1995; 7622-7629

130. L. Turnbull "*Thermal, Oxidative and Hydrolytic Degradation Studies of Poly(ethylene naphthalate*" PhD Thesis; University of Strathclyde; 2013

131. J. Clayden, N. Greeves, S. Warren and P. Wothers "*Organic Chemistry*" Oxford University Press Inc; New York; 2001

132. G. Botelho, A. Queirós and P. Gilsman "*Thermooxidative Studies of Poly(ether-esters) 1. Copolymer of Poly(butylene terephthalate) and Poly(ethylene oxide)"* Polymer Degradation and Stability; 67; 2000; 13-20

133. T. Kushimoto, Y. Ozawa, A. Baba and H. Matsuda "*Niobium Compound Catalyst for Polycondensation Reaction to Form Polyethylene Terephthalate (PET)*" Catalysis Today; 16; 1993; 571-578

134. M. Tasaki, H. Yamamoto, T. Yoshioka, M. Hanesaka, T. Nihh, K. Tashiro, H. Jeon, K. Choi, H. Jeong, H. Song and M. Ree "*Crystal Structure Analyses of Arylate Polyesters with Long Methylene Segments and their Model Compounds on the Basis of 2-D X-ray Diffractions and Infrared Progression Bands*" Polymer; 55; 2014; 1228-1248

135. R. Dhavalikar *"Reactive Melt Modification of Polyethylene Terephthalate"* PhD Thesis; Faculty of New Jersey Institute of Technology' 2003

136. R. Parker and N Isaacs "*Mechanisms of Epoxide Reactions*" Chemical Review; 59; 1959; 737-799

137. B. Bimestre and C. Saron "*Chain Extension of Poly (Ethylene Terephthalate) by Reactive Extrusion with Secondary Stabilizer*" Materials Research; 15; 2012; 467-472

138. S. Makkam and W. Harnnarongchai "*Rheological and Mechanical Properties of Recycled PET Modified by Reactive Extrusion*" Energy Procedia; 57; 2014; 547-553

139. F. Awaja and D. Pavel "*Recycling of PET*" European Polymer Journal; 41; 2005; 1253-1477

140. J. Fink "*Reactive Polymers Fundamentals and Applications*" Published by William Andrew Publishing; New York; 2005

141. N Takeuchi, H. Komentani, T. Miki, S. Ando and Y. Tamura "*Prevention of Polymer Degradation during the Extrusion Process*" Mitsubishi Heavy Industries, Ltd Technical Review; 34; 1997; 120-124

12.0 Appendices

Key

When referring to all graphs and tables within this section, the letter A refers to it being in Chapter 12 (A for appendices), the first digit corresponds to the chapter that the graph/table is relevant to, the second digit refers to the relevant section within that particular chapter, and the third digit acts as the unique designation for that particular graph/table.

A3 – Chapter 3 – Experimental

Table A3.1.1 – Carboxyl end group concentration of the 10 repeats for the E187 samples obtained by Titration.

Sample	Carboxyl end group concentration / equivalents per 10^6 grams
E187 - 1	32.67
E187 - 2	32.43
E187 - 3	30.21
E187 - 4	31.59
E187 -5	31.05
E187 -6	30.28
E187 - 7	32.45
E187 -8	29.99
E187 - 9	28.92
E187 -10	30.95

Table A3.1.2 – Average carboxyl end group concentration of two batches of SJ1 and SJ3 samples obtained by Titration. Each batch contains three repeats.

Sample	Batch One / equivalents per 10^6 grams	Batch Two / equivalents per 10^6 grams
SJ1	27.14	17.12
SJ3	0.00	2.13

Table A3.1.3 – Average carboxyl end group concentration for the film samples supplied by DTF measured by the Pohl titration method. All values are measured in equivalents per 10^6 grams. The titration method is the average of three repeats and the value from DTF is from a single sample.

Sample	Titration	DTF
DAD 1	23.00	24.80
DAD 3	4.00	4.00
DAD 4	11.00	7.70
DAD 6	7.00	9.00
DAD 10	11.00	12.00
BM4	5.00	2.00
SJ1	20.25	21.70
SJ3	2.77	3.40

Table A3.1.4 – Carboxyl end group concentration of the 10 repeats for the E187 samples obtained by the Ma ^{1}H NMR methods.

Sample	Carboxyl end group obtained by Ma ^{1}H NMR / equivalents per 10^{6} grams
E187 - 1	35.47
E187 - 2	32.65
E187 - 3	32.81
E187 - 4	31.02
E187 -5	35.80
E187 -6	34.33
E187 - 7	31.94
E187 -8	33.94
E187 - 9	31.91
E187 -10	29.33

Table A3.1.5 – The integer values obtained for the Ma ^{1}H NMR spectra of the E187 samples. A single spectrum was analysed.

Sample	Integral of TFT	Integral of ester
E187 - 1	1.0000	0.8853
E187 - 2	1.0000	0.9119
E187 - 3	1.0000	0.8347
E187 - 4	1.0000	0.8116
E187 -5	1.0000	0.9283
E187 -6	1.0000	0.9069
E187 - 7	1.0000	0.8428
E187 -8	1.0000	0.5377
E187 - 9	1.0000	0.8401
E187 -10	1.0000	0.7967

Table A3.1.6 –Carboxyl end group concentration, obtained by Ma ^{1}H NMR method, for three repeats of a sample of E239

Sample	Carboxyl end group obtained by Ma ^{1}H NMR / equivalents per 10^{6} grams
E239 1	17.55
E239 2	16.97
E239 3	16.96

Table A3.1.7 – The integer values obtained for the Ma ^{1}H NMR spectra of the repeats of a E239 sample. A single spectrum was analysed.

Sample	Integral of TFT	Integral of ester
E239 1	1.0000	0.4224
E239 2	1.0000	0.4115
E239 3	1.0000	0.4113

.

Table A3.1.8 – Average carboxyl end group concentration of the three repeats of DAD and BM4 film samples obtained by the Ma ^{1}H NMR method.

Sample	Carboxyl end group obtained by Ma ^{1}H NMR / equivalents per 10^{6} grams
DAD 1	12.03
DAD 3	4.12
DAD 4	7.50
DAD 6	4.17
DAD 10	6.47
BM4	0.81

Table A3.1.9– The integer values obtained for the Ma ^{1}H NMR spectra of the DAD and BM4 film samples. A single spectrum was analysed.

Sample	Integral of TFT	Integral of ester
DAD 1	1.0000	0.2694
DAD 3	1.0000	0.0862
DAD 4	1.0000	0.1604
DAD 6	1.0000	0.0849
DAD 10	1.0000	0.1320
BM4	1.0000	0.0162

Table A3.1.10 – Carboxyl end group concentration of the three repeats of SJ1 and SJ3 obtained by Ma ^{1}H NMR method.

Sample	Repeat 1 / equivalents per 10^6 grams	Repeat 2 / equivalents per 10^6 grams	Repeat 3 / equivalents per 10^6 grams
SJ1	19.84	17.11	20.32
SJ3	4.18	4.76	4.62

Table A3.1.11 – The integer values obtained for the Ma ^{1}H NMR spectra of the SJ1 and SJ3 samples. A single spectrum was analysed each time.

Sample	Integral of TFT	Integral of ester
SJ1 – S1	1.0000	0.5343
SJ1 – S2	1.0000	0.4433
SJ1 – S3	1.0000	0.5023
SJ3 – S1	1.0000	0.1121
SJ3 – S2	1.0000	0.1146
SJ3 – S3	1.0000	0.0992

Table A3.1.12 – Table showing the average feed rates of the polymer chips into the extruder barrel. Feed rate was measured every minute for 20 minutes.

Sample	Small Screw Feed Rate / grams per minute	Large Screw Feed Rate / grams per minute
E333	14.80	9.66
E187	18.38	12.36
E238	20.96	14.54
E239	20.56	16.32

Table A3.1.13 – The carboxyl end group concentrations for the samples obtained using the liquid feed. The titration value is an average of three repeats and a single sample was analysed for the NMR method.

Sample		Repeat 1 / equivalents per 10^6 grams	Repeat 2 / equivalents per 10^6 grams	Repeat 3 / equivalents per 10^6 grams
E187	Titration Ma ^{1}H NMR	32.67 35.47	30.28 32.65	32.43 32.81
E187 + 1% Cardura	Titration Ma ^{1}H NMR	19.63 23.33	15.21 29.65	25.20 34.40

Table A3.1.14 – The integrals from the Ma ^{1}H NMR spectra for the samples that were prepared using the liquid feed. A single spectrum was analysed each time.

Sample	Integral of TFT	Integral of ester
E187 – S1	1.0000	0.8853
E187 – S2	1.0000	0.9119
E187 – S3	1.0000	0.8347
E187 + 1% Cardura – S1	1.0000	0.6315
E187 + 1% Cardura – S2	1.0000	0.8185
E187 + 1% Cardura – S3	1.0000	0.9100

Table A3.1.15 – Average carboxyl end group concentration for the E239 + 1% Cardura sample taken over time. Three samples were analysed to obtain the average.

Time	End group concentration / Equivalents per 10^6 grams
0 min	3.99
5 min	14.45
10 min	11.51
15 min	18.50
20 min	5.94

Table A3.1.16 –Average carboxyl end group concentration for the E239 + 4% Cardura sample taken over time. Three samples were analysed to obtain the average.

Time	End group concentration / Equivalents per 10^6 grams
0 min	0.00
5 min	8.60
10 min	13.16
15 min	6.72
20 min	1.34

A4 – Chapter 4 - Benzoic Acid and Epoxides – Starting Material

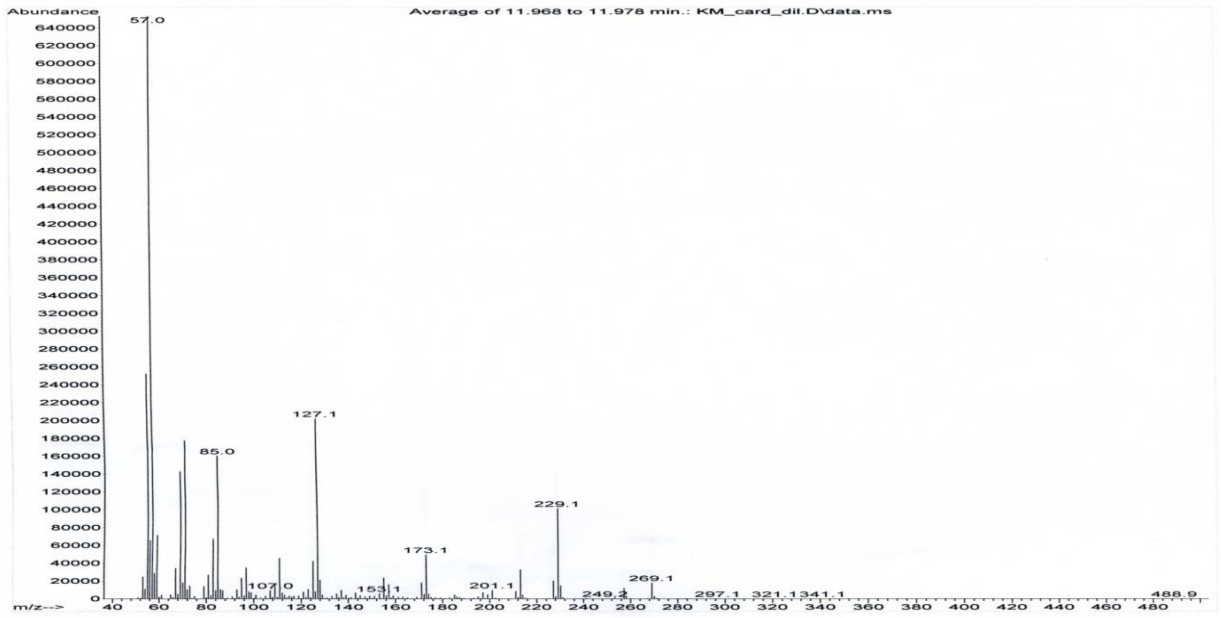

Figure A4.1.1 - Mass spectrum of one of the peaks from the GC chromatogram of Cardura.

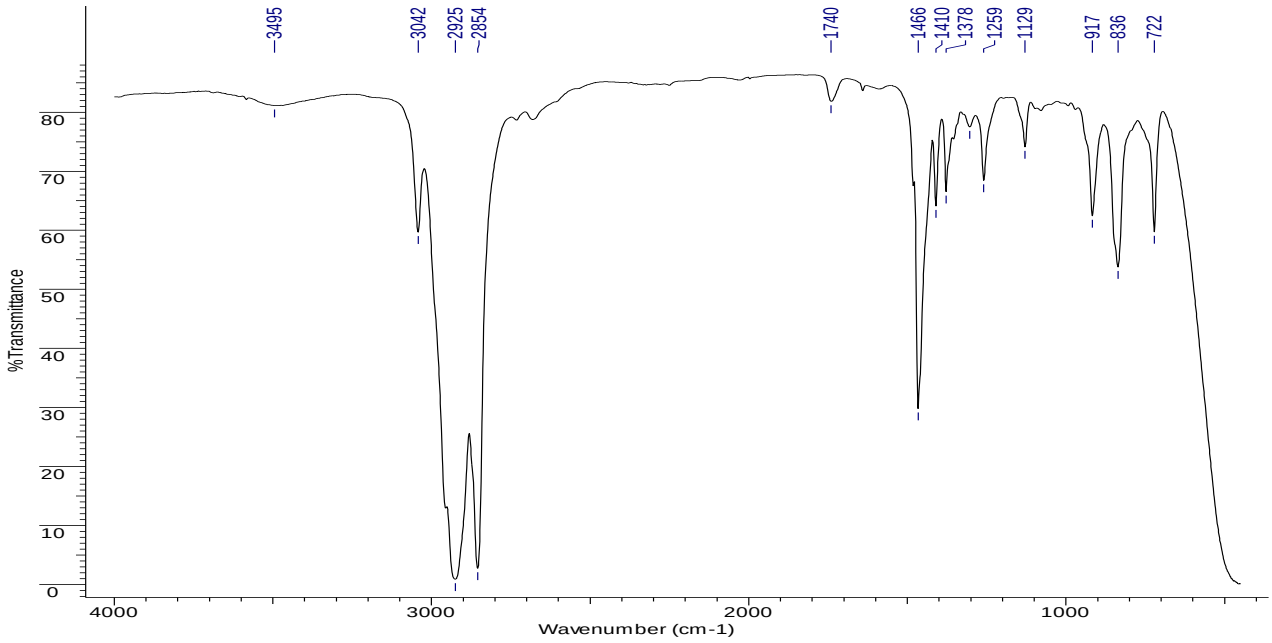

Figure A4.1.2 – IR spectrum of Vikolox.

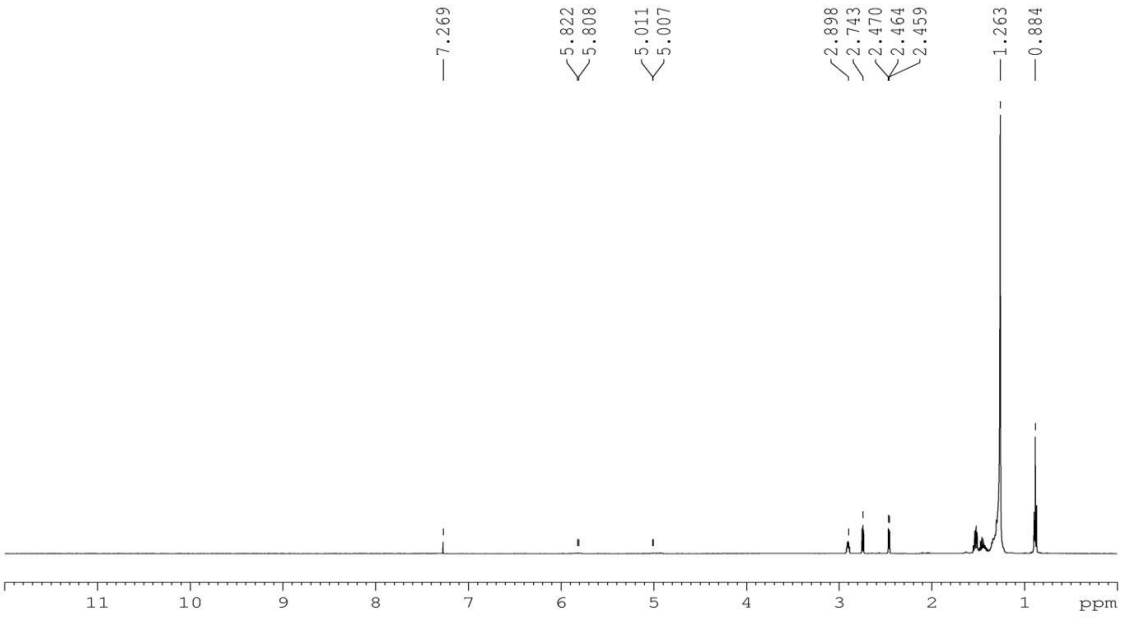

Figure A4.1.3– ^{1}H NMR spectra for Vikolox.

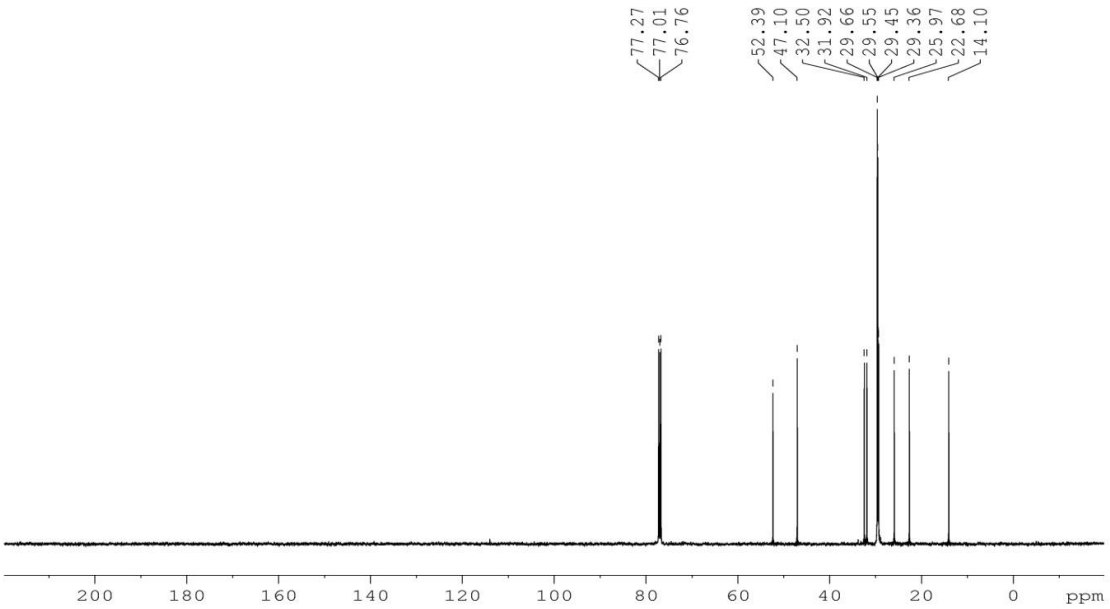

Figure A4.1.4 – ^{13}C NMR spectra of Vikolox.

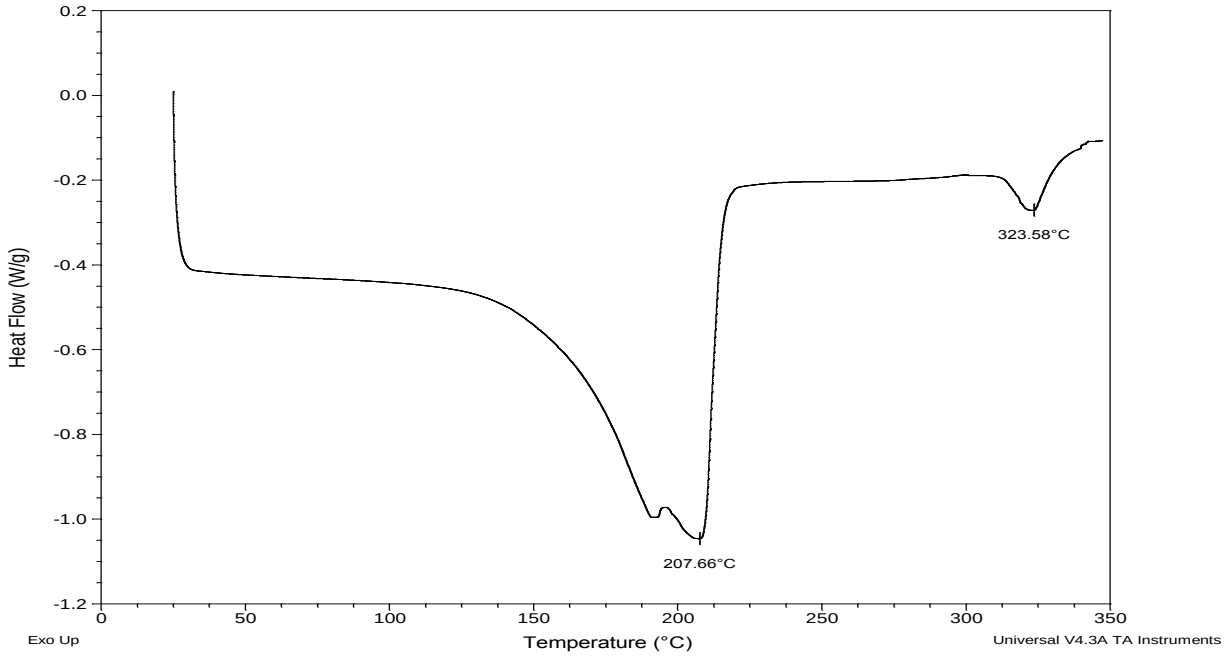

Figure A4.1.5 – DSC scan of Vikolox.

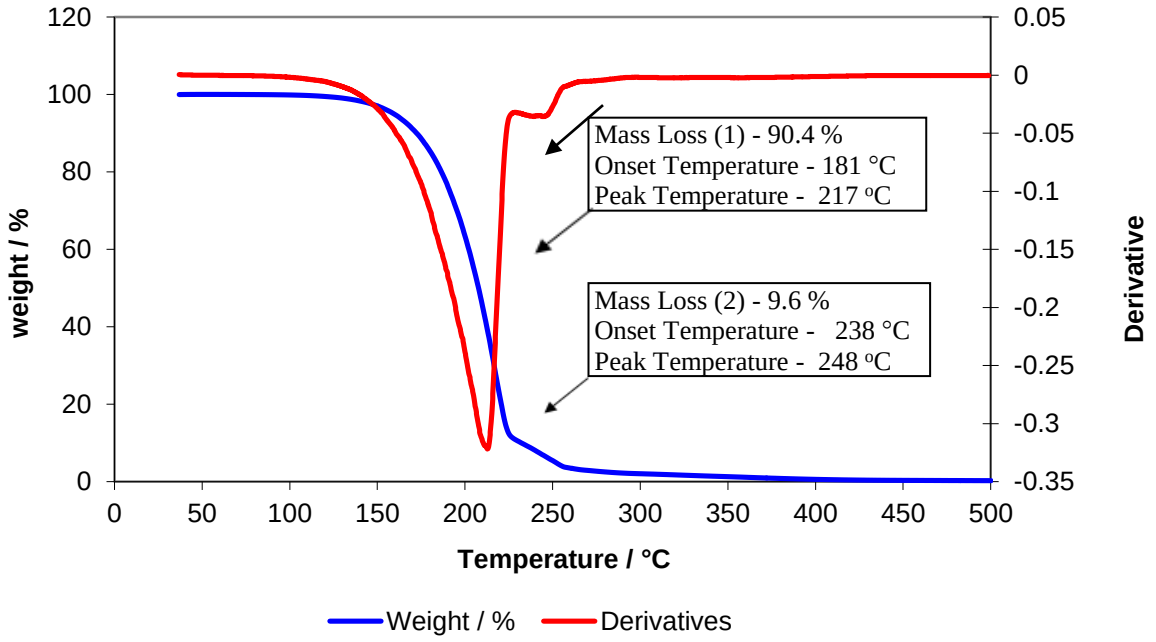

Figure A4.1.6 – TGA thermogram of Vikolox.

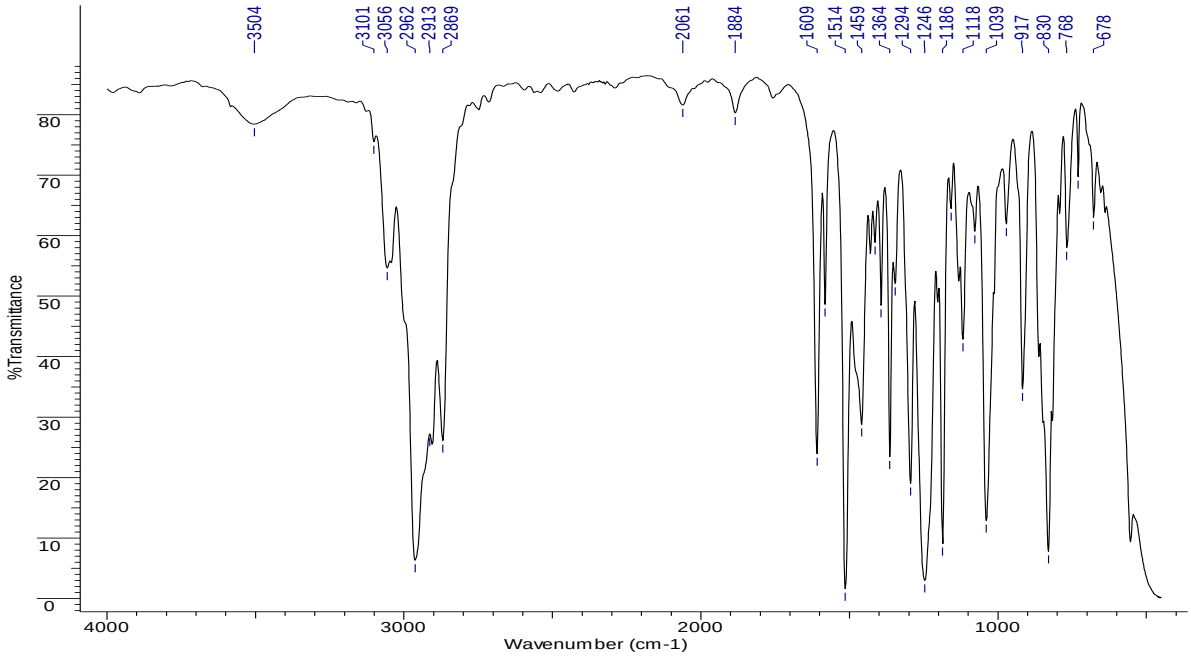

Figure A4.1.7 – IR spectrum of Heloxy.

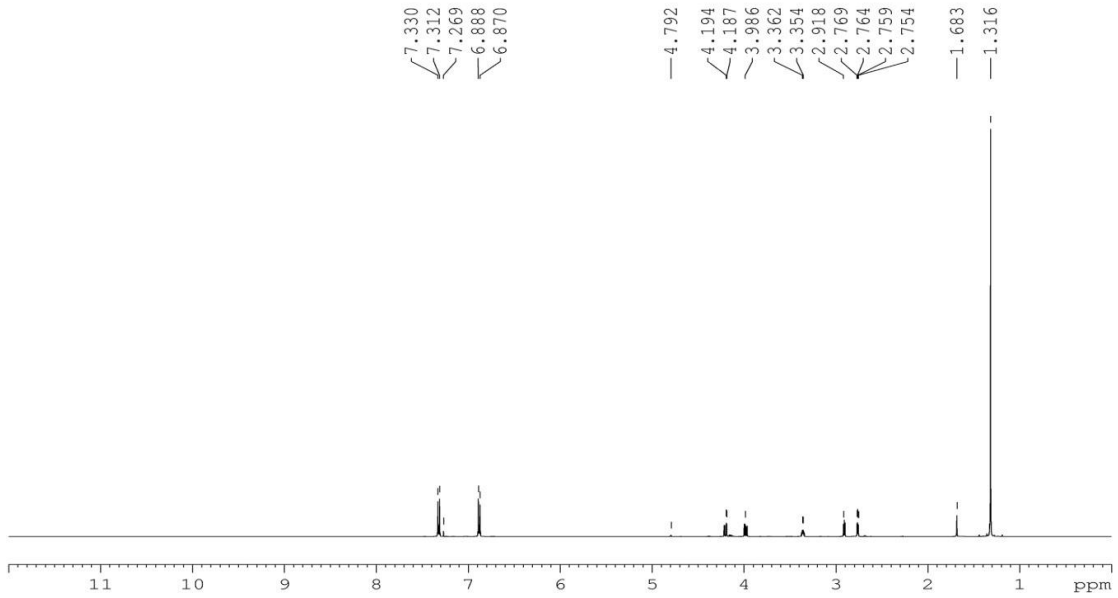

Figure A4.1.8 – ^{1}H NMR spectrum of Heloxy.

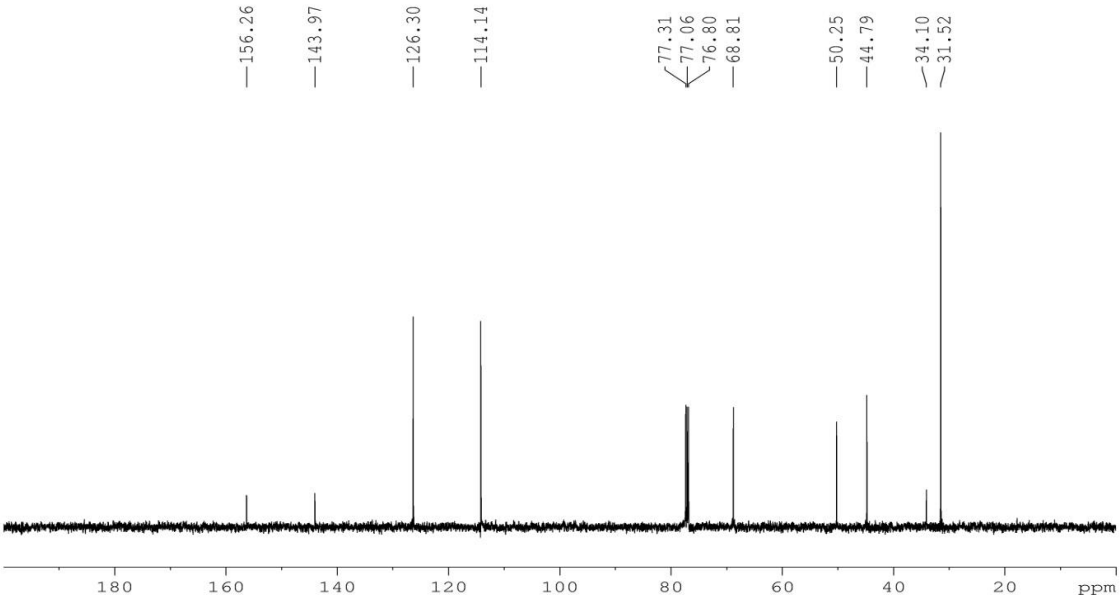

Figure A4.1.9 – ^{13}C NMR spectrum of Heloxy.

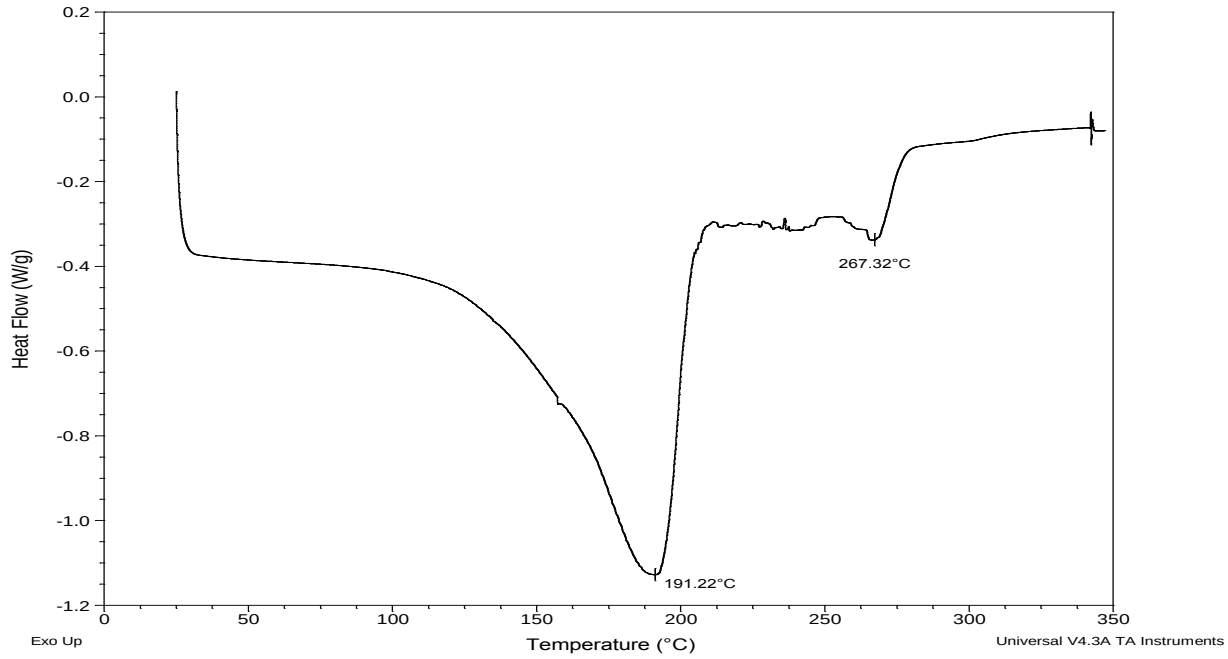

Figure A4.1.10 - DSC scan of Heloxy.

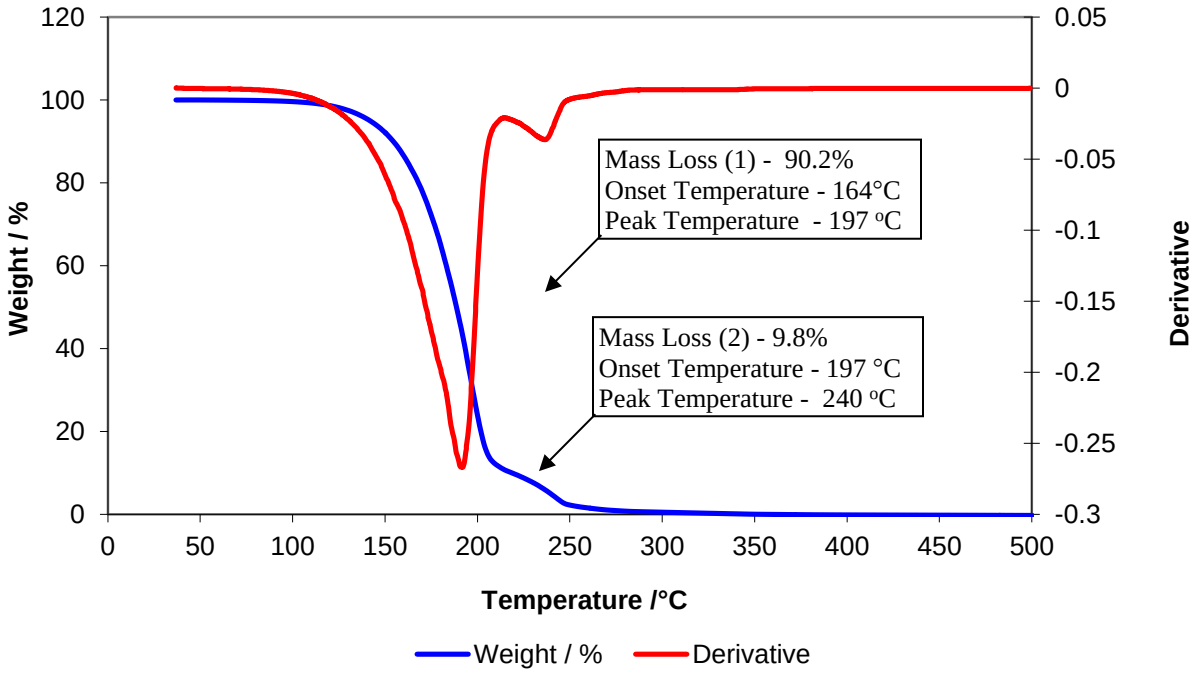

Figure A4.1.11 – TGA thermogram of Heloxy.

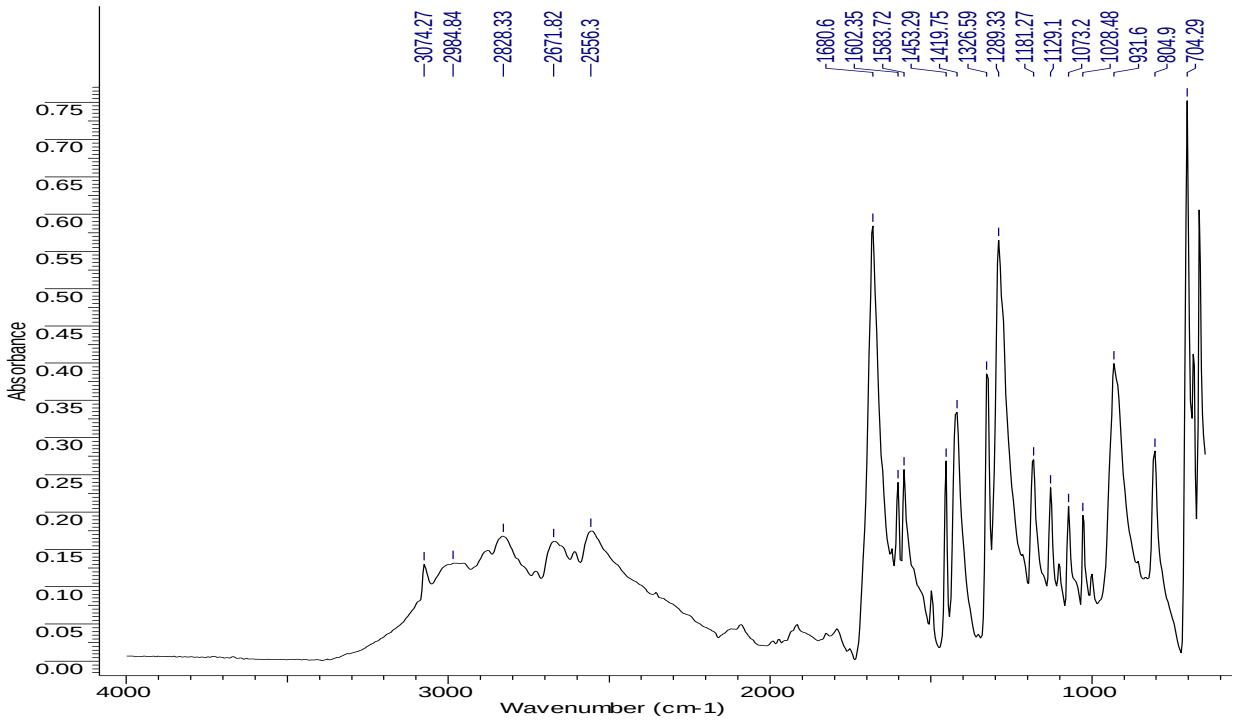

Figure A4.1.12 – IR Spectrum of Benzoic Acid.

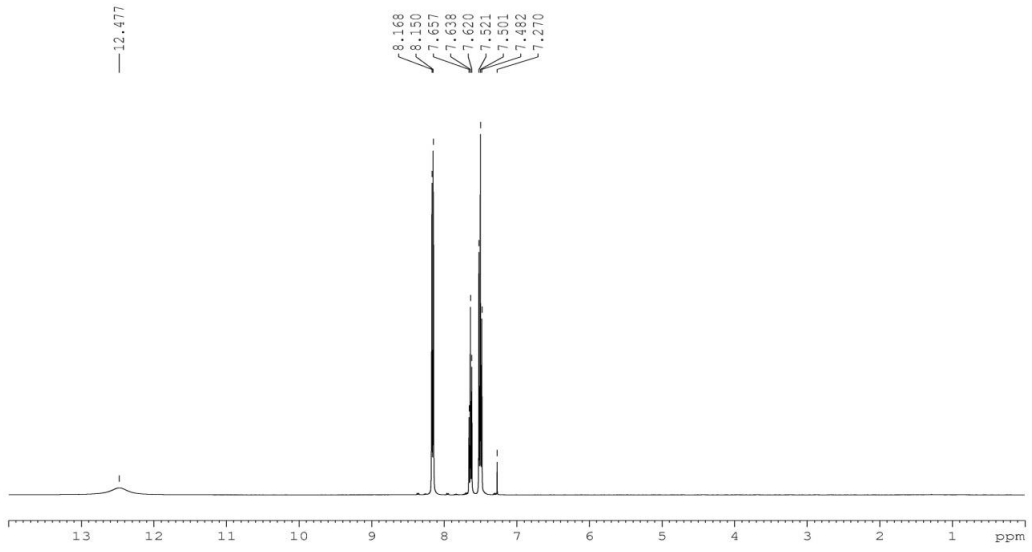

Figure A4.1.13 – ^{1}H NMR spectrum of Benzoic Acid.

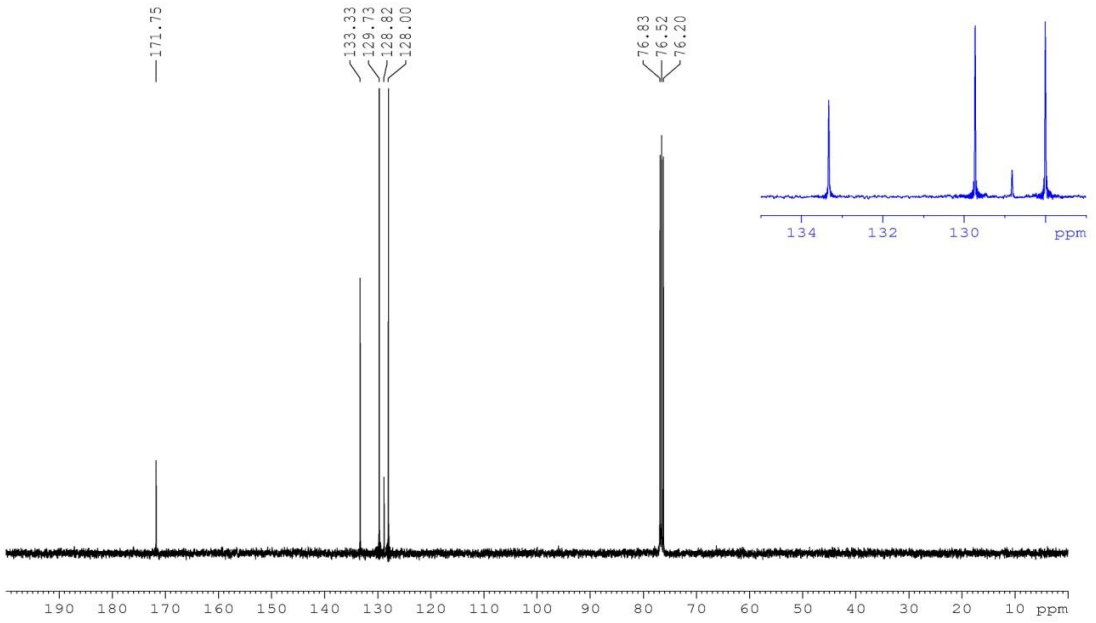

Figure A4.1.14 – ^{13}C NMR spectrum of Benzoic Acid.

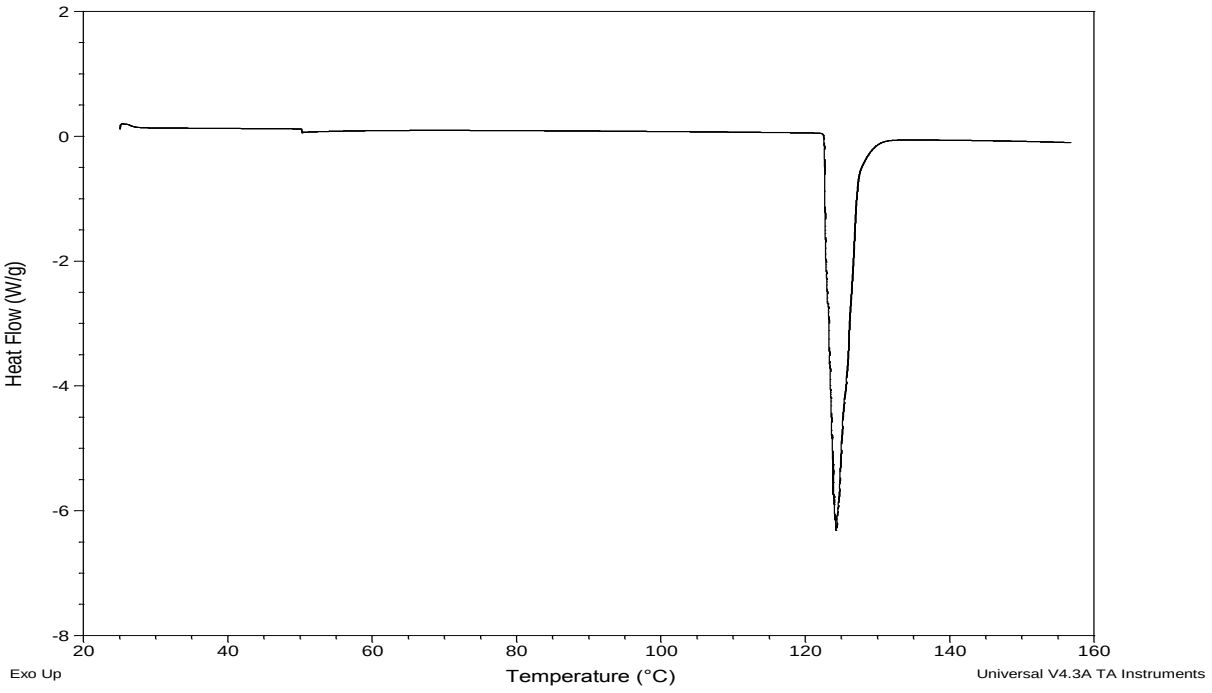

Figure A4.1.15 - DSC scan of Benzoic Acid.

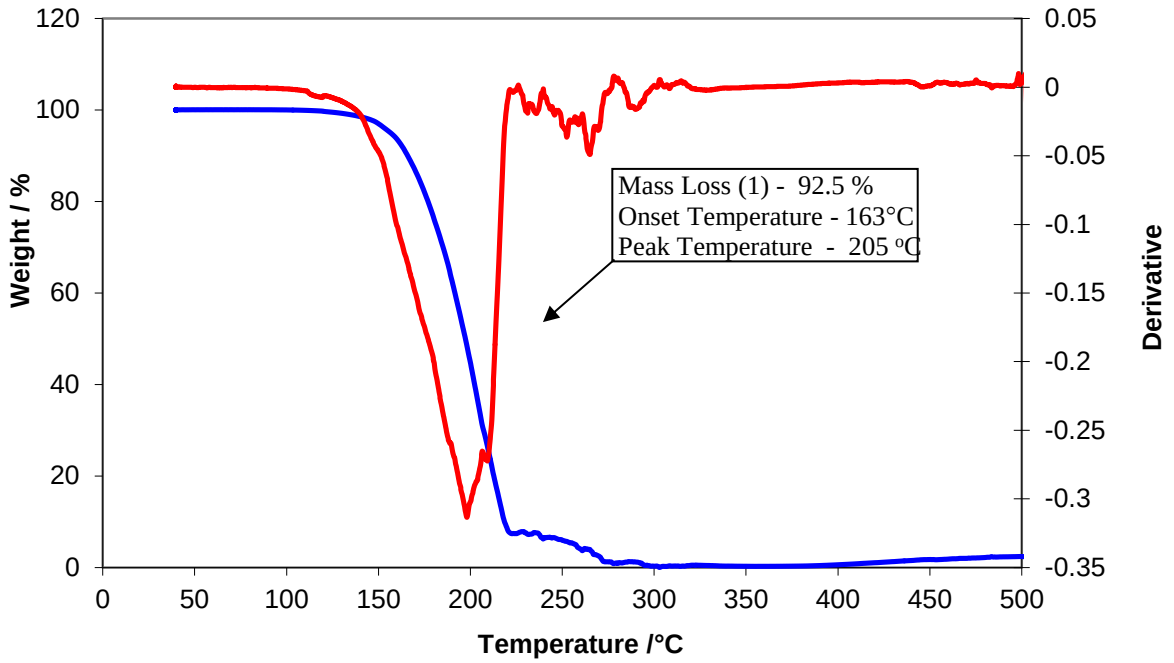

Figure A4.1.16 – TGA thermogram of Benzoic Acid.

A4 - Chapter 4 – Benzoic Acid and Epoxides – Epoxide Reactions

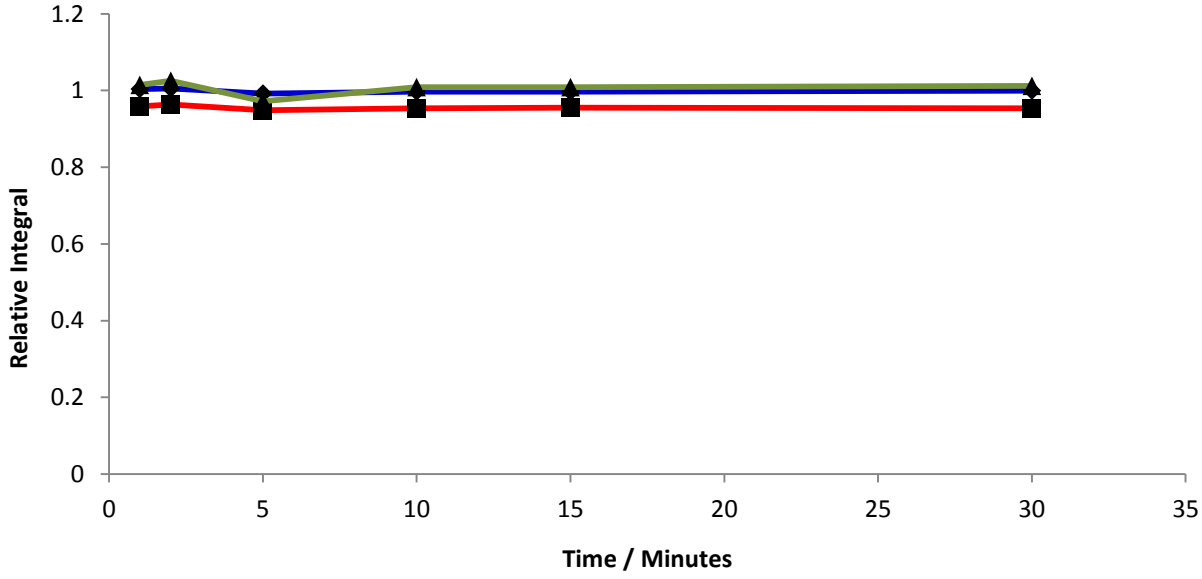

Figure A4.2.1 – Relative integrals from the NMR spectra of the Cardura samples heated under nitrogen at 110 °C. The blue is for the peak at 2.62, the red is for the peak at 2.80 and the green is for the peak at 3.17ppm.

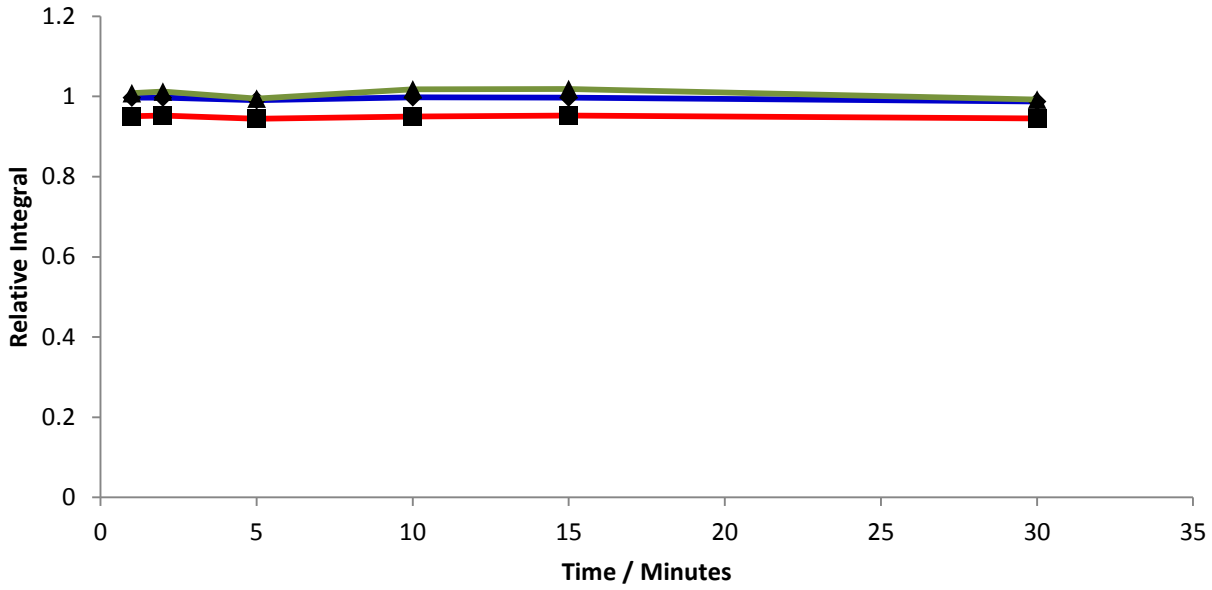

Figure A4.2.2 – Relative integrals from the NMR spectra of the Cardura samples heated under nitrogen at 130 °C. The blue is for the peak at 2.62, the red is for the peak at 2.80 and the green is for the peak at 3.17ppm.

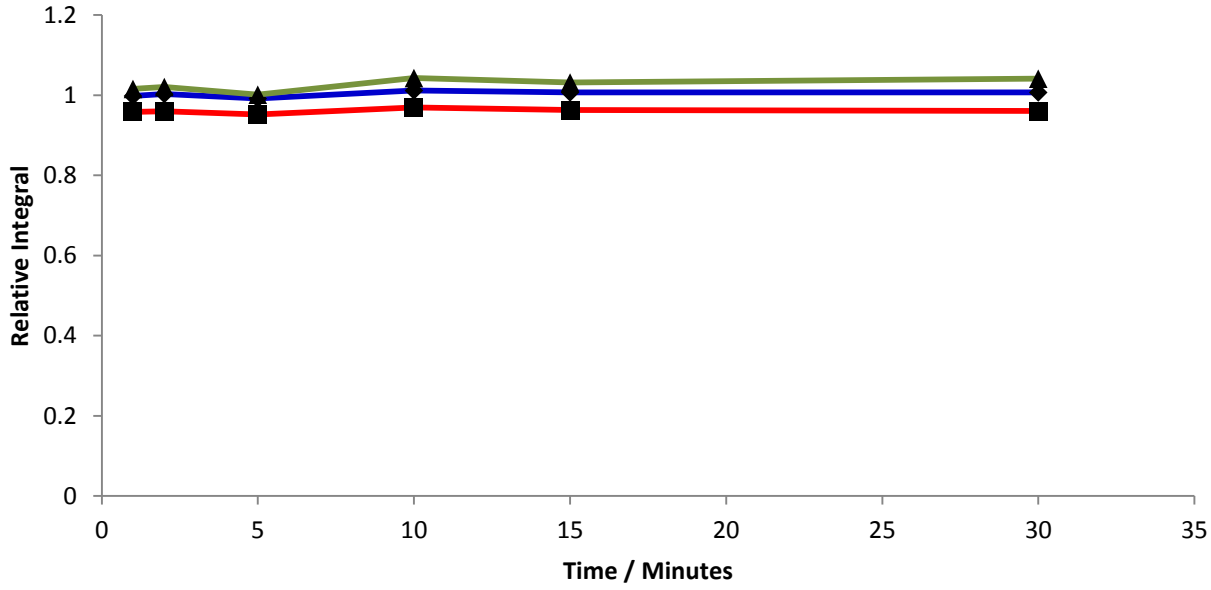

Figure A4.2.3 – Relative integrals from the NMR spectra of the Cardura samples heated under nitrogen at 150 °C. The blue is for the peak at 2.62, the red is for the peak at 2.80 and the green is for the peak at 3.17ppm.

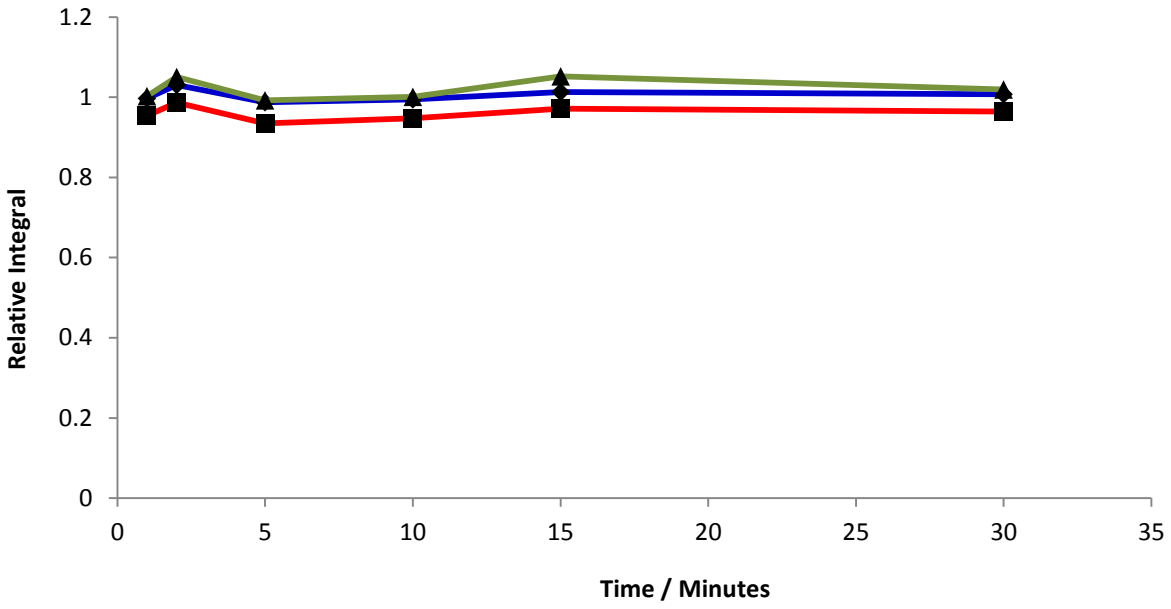

Figure A4.2.4 – Relative integrals from the NMR spectra of the Cardura samples heated under air at 90 °C. The blue is for the peak at 2.62, the red is for the peak at 2.80 and the green is for the peak at 3.17ppm.

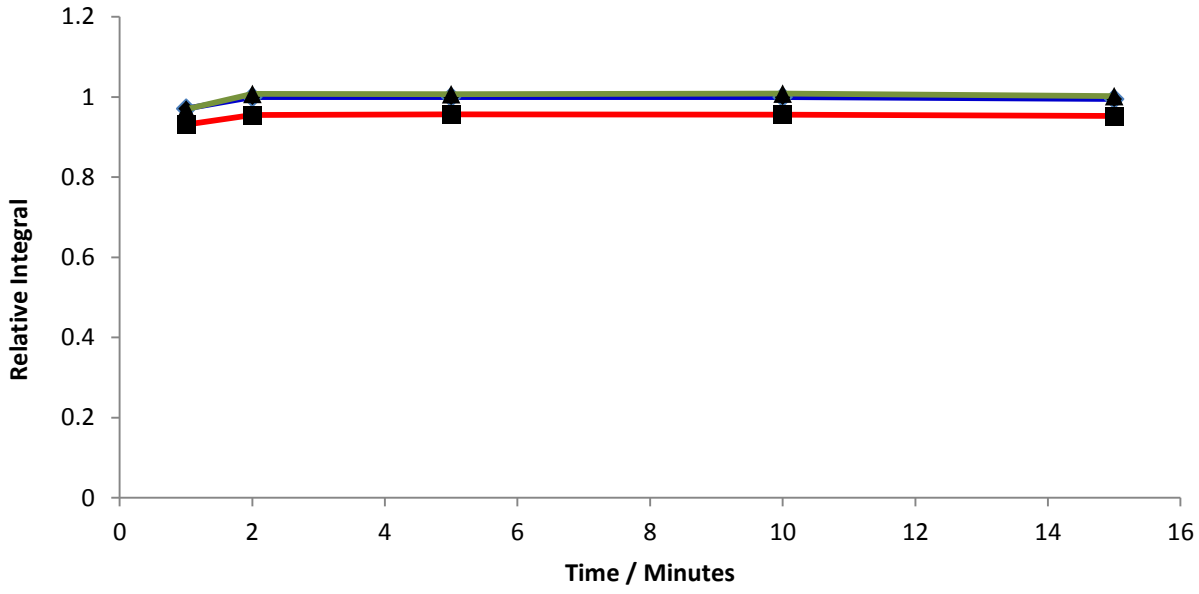

Figure A4.2.5 – Relative integrals from the NMR spectra of the Cardura samples heated under air at 110 °C. The blue is for the peak at 2.62, the red is for the peak at 2.80 and the green is for the peak at 3.17ppm.

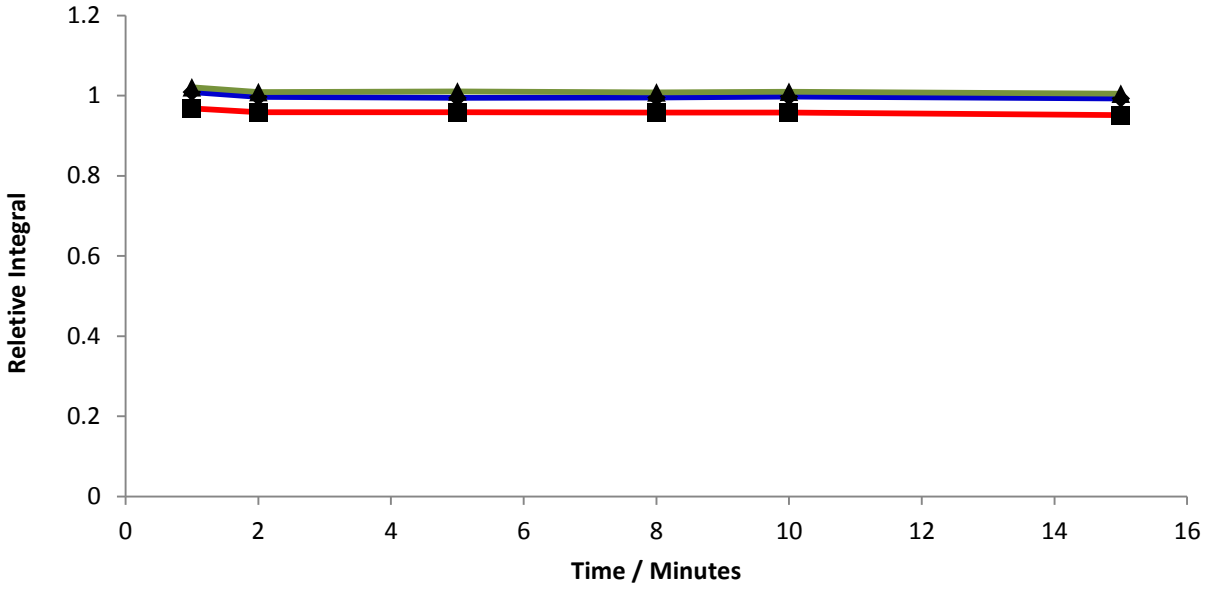

Figure A4.2.6 – Relative integrals from the NMR spectra of the Cardura samples heated under air at 130 °C. The blue is for the peak at 2.62, the red is for the peak at 2.80 and the green is for the peak at 3.17ppm.

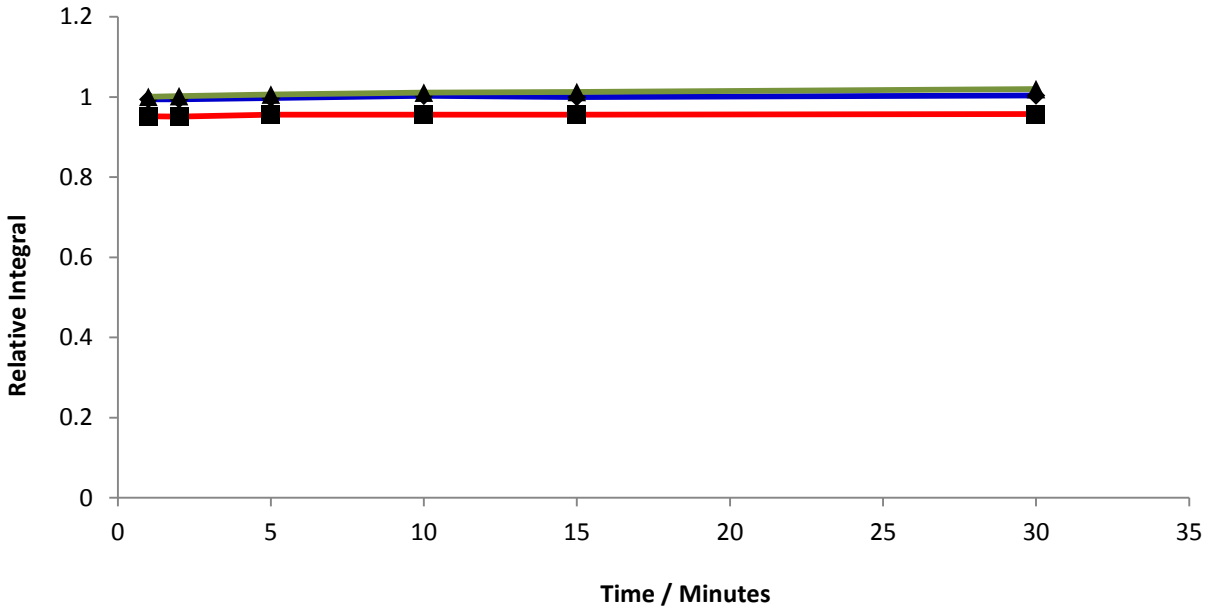

Figure A4.2.7 –Relative integrals from the NMR spectra of the Cardura samples heated under air at 150 °C. The blue is for the peak at 2.62, the red is for the peak at 2.80 and the green is for the peak at 3.17ppm.

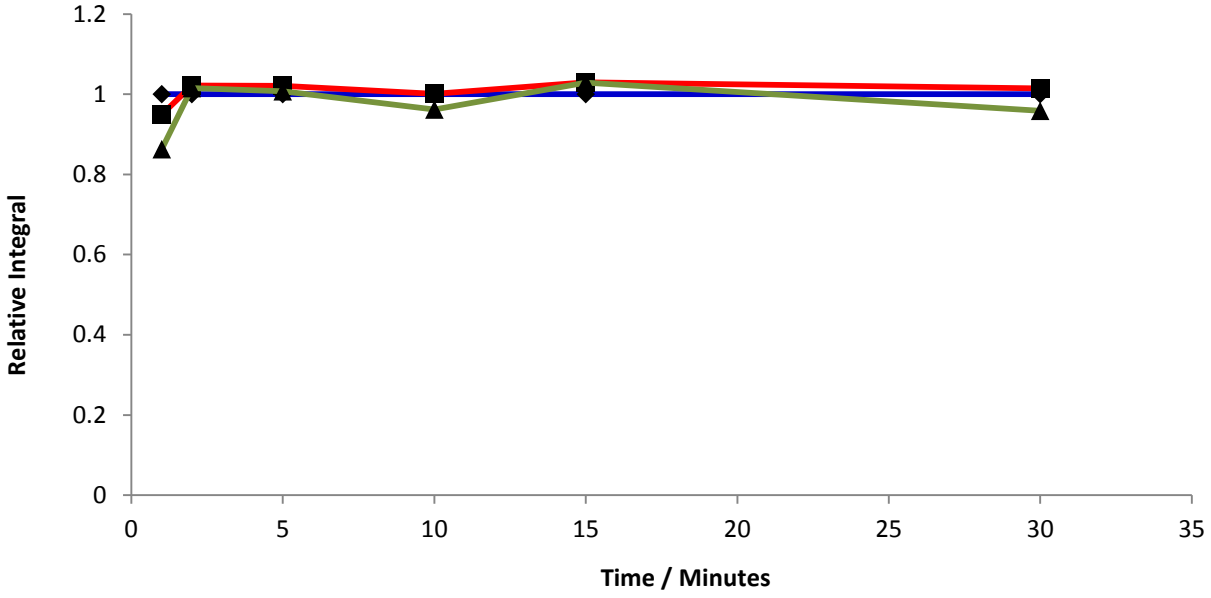

Figure A4.2.8 – Relative integrals from the NMR spectra of the Vikolox samples heated under nitrogen at 90 °C. The blue is for the peak at 2.46, the red is for the peak at 2.74 and the green is for the peak at 2.90ppm.

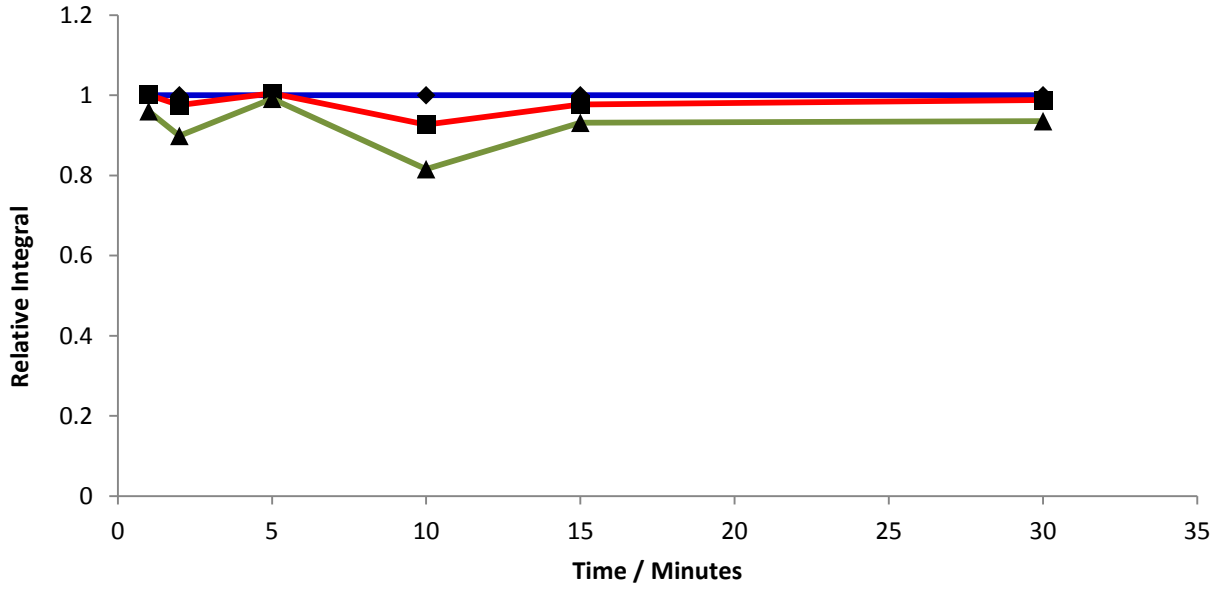

Figure A4.2.9 - Relative integrals from the NMR spectra of the Vikolox samples heated under nitrogen at 110 °C. The blue is for the peak at 2.46, the red is for the peak at 2.74 and the green is for the peak at 2.90ppm.

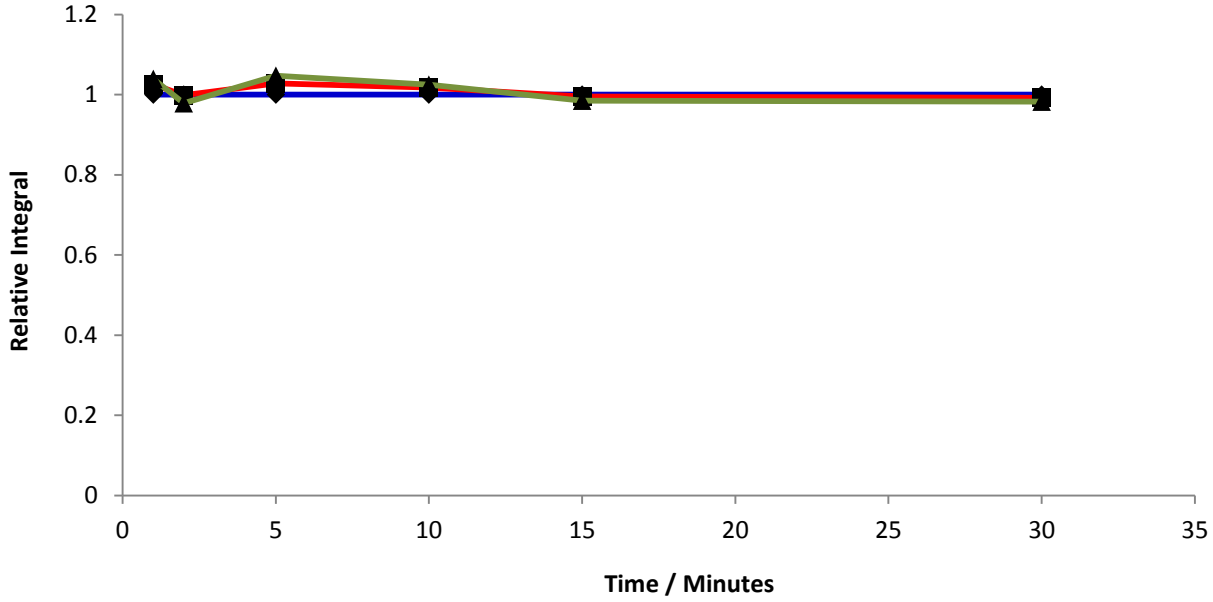

Figure A4.2.10 - Relative integrals from the NMR spectra of the Vikolox samples heated under nitrogen at 130 °C. The blue is for the peak at 2.46, the red is for the peak at 2.74 and the green is for the peak at 2.90ppm.

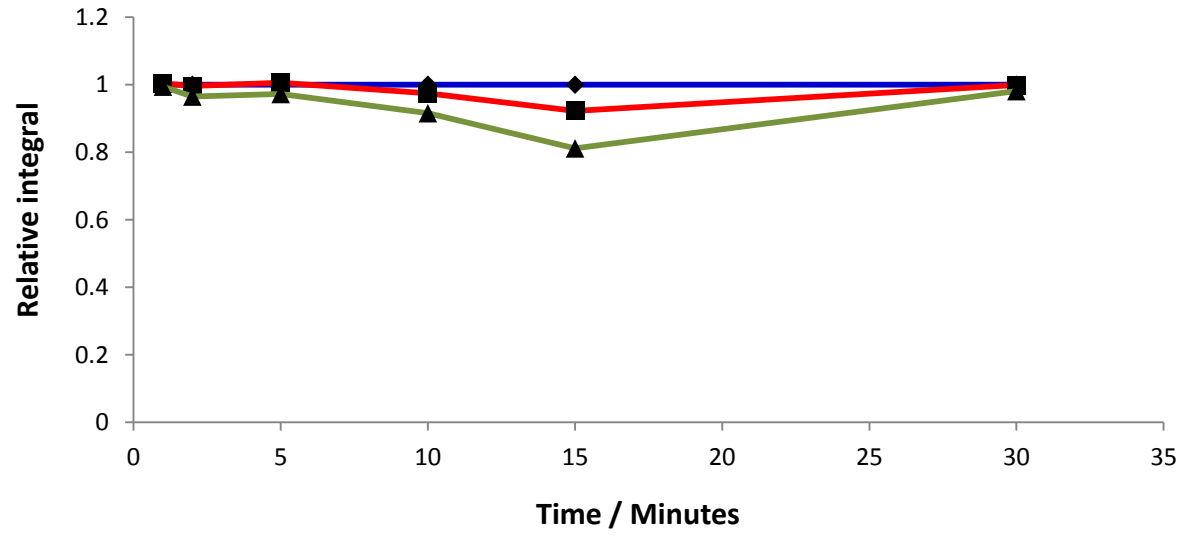

Figure A4.2.11 – Relative integrals from the NMR spectra of the Vikolox samples heated under nitrogen at 130 °C. The blue is for the peak at 2.46, the red is for the peak at 2.74 and the green is for the peak at 2.90ppm.

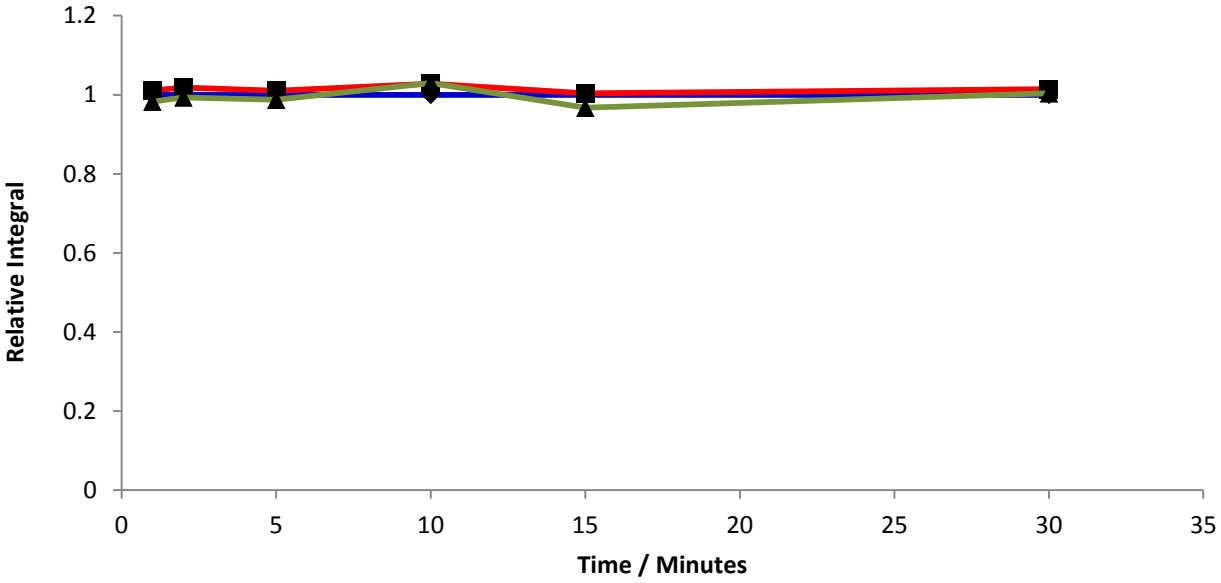

Figure A4.2.12 - Relative integrals from the NMR spectra of the Vikolox samples heated under air at 90 °C. The blue is for the peak at 2.46, the red is for the peak at 2.74 and the green is for the peak at 2.90ppm.

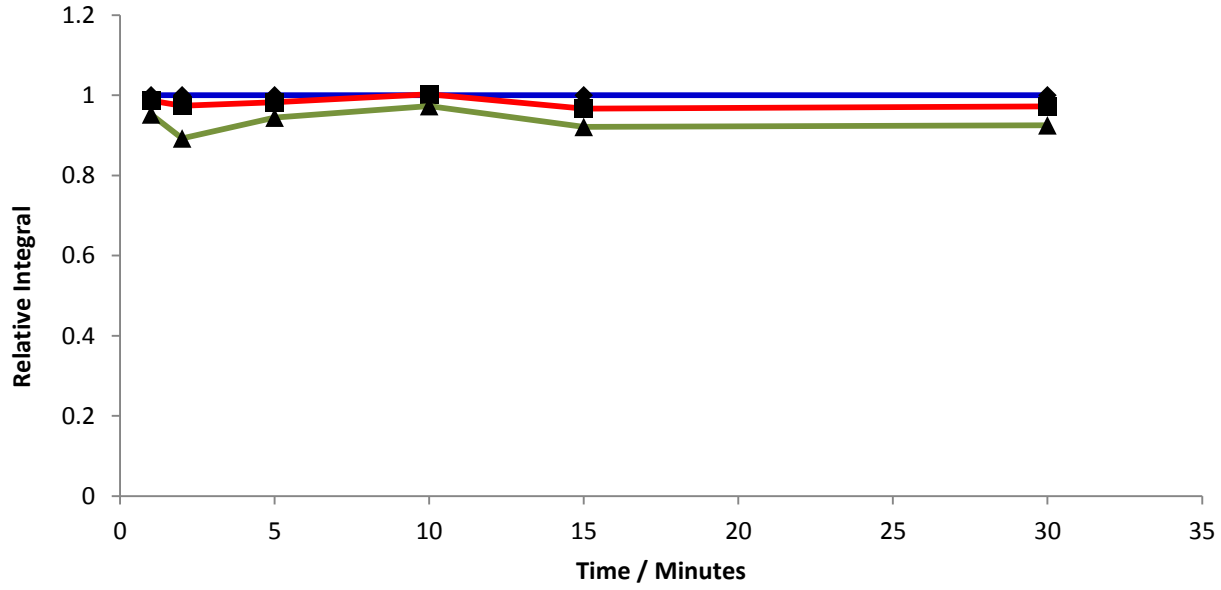

Figure A4.2.13 - Relative integrals from the NMR spectra of the Vikolox samples heated under air at 110 °C. The blue is for the peak at 2.46, the red is for the peak at 2.74 and the green is for the peak at 2.90ppm.

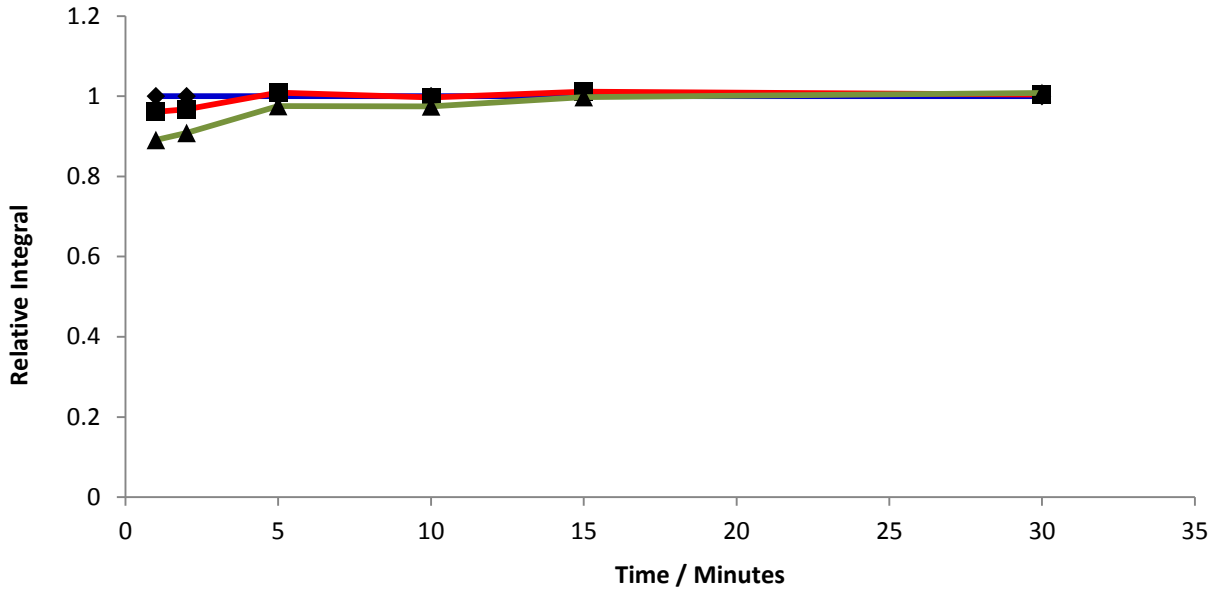

Figure A4.2.14 - Relative integrals from the NMR spectra of the Vikolox samples heated under air at 130 °C. The blue is for the peak at 2.46, the red is for the peak at 2.74 and the green is for the peak at 2.90ppm.

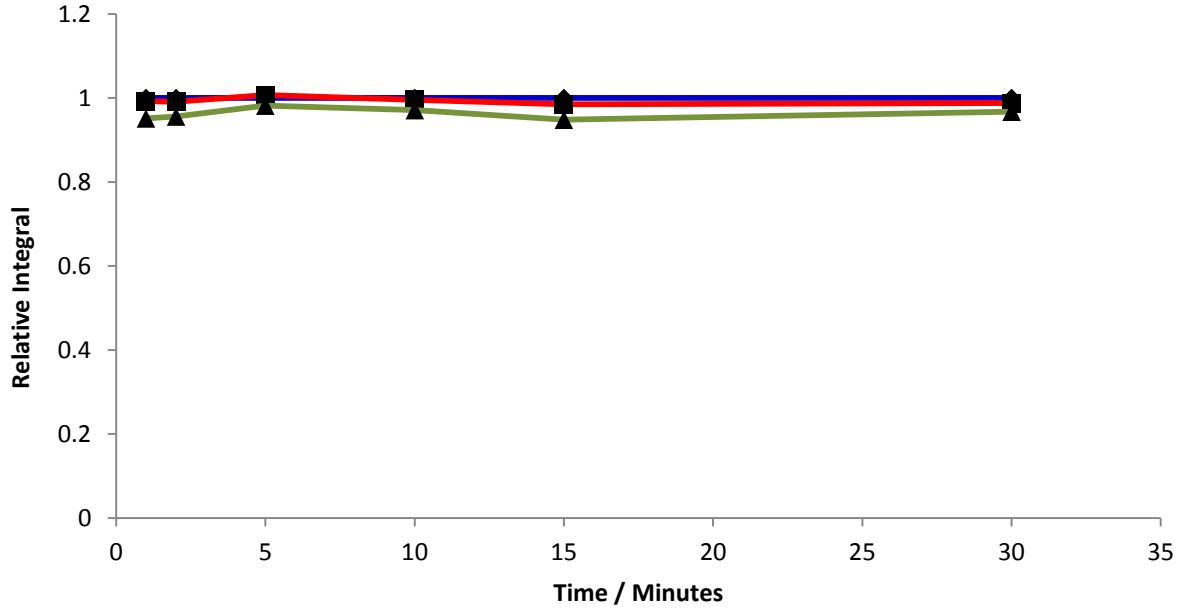

Figure A4.2.15 - Relative integrals s from the NMR spectra of the Vikolox samples heated under air at 150 °C. The blue is for the peak at 2.46, the red is for the peak at 2.74 and the green is for the peak at 2.90ppm.

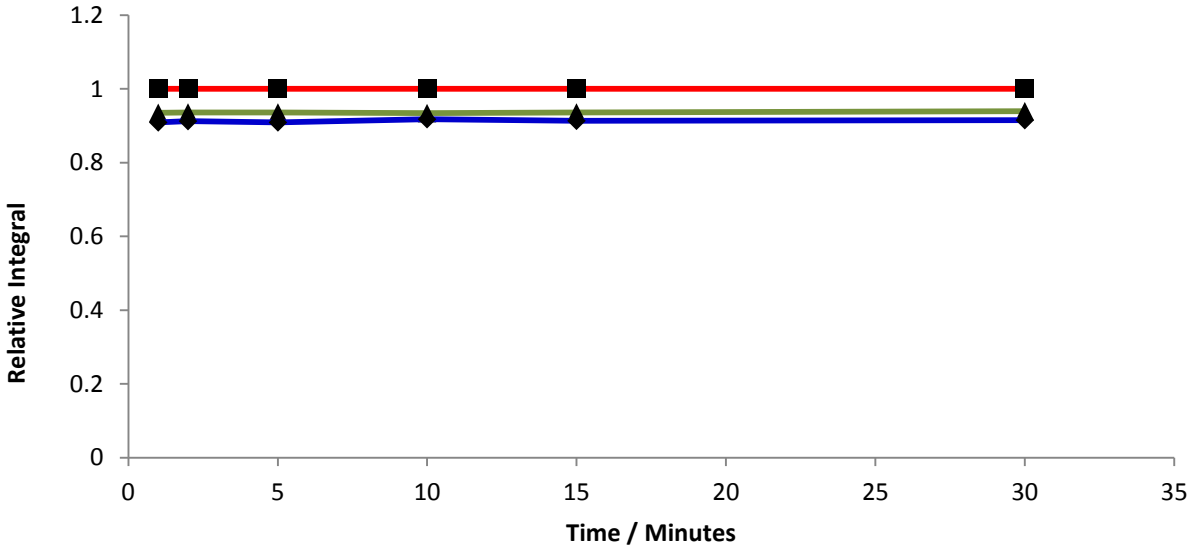

Figure A4.2.16 - Relative integrals from the NMR spectra of the Heloxy samples heated under nitrogen at 90 ºC. The blue is for the peak at 2.80, the red is for the peak at 2.90 and the green is for the peak at 3.40ppm

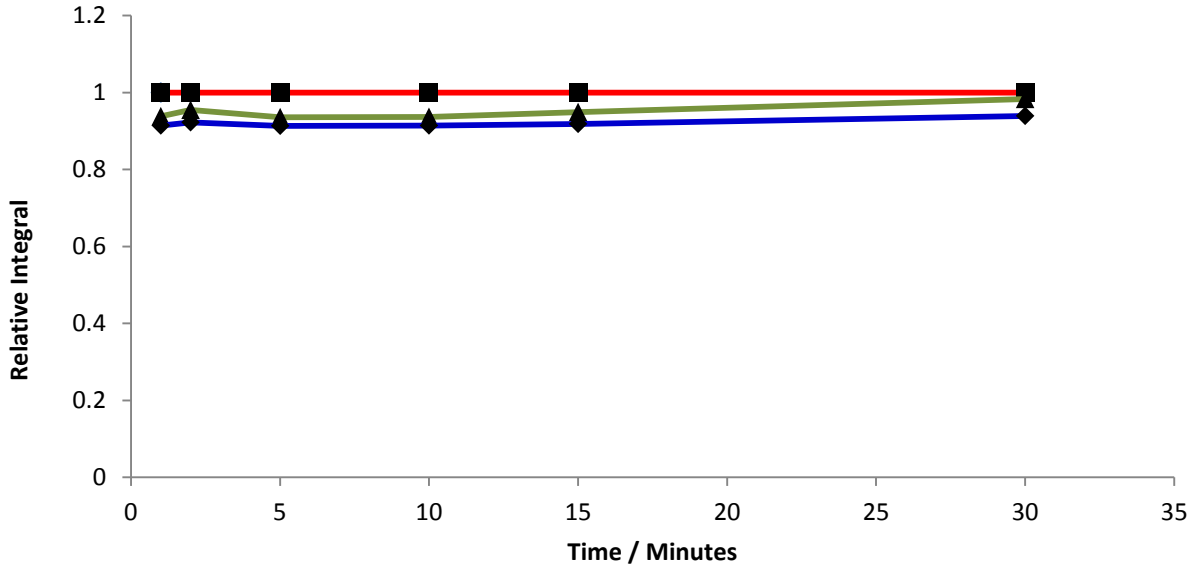

Figure A4.2.17 - Relative integrals from the NMR spectra of the Heloxy samples heated under nitrogen at 110 ºC. The blue is for the peak at 2.80, the red is for the peak at 2.90 and the green is for the peak at 3.40ppm.

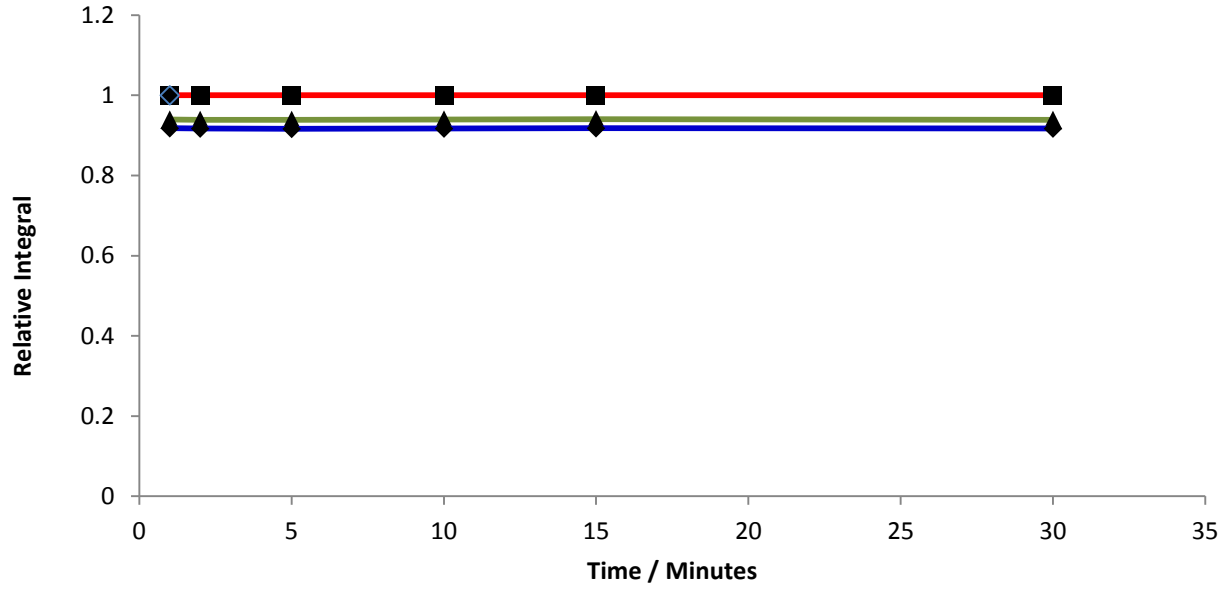

Figure A4.2.18 - Relative integrals from the NMR spectra of the Heloxy samples heated under nitrogen at 130 ºC. The blue is for the peak at 2.80, the red is for the peak at 2.90 and the green is for the peak at 3.40ppm

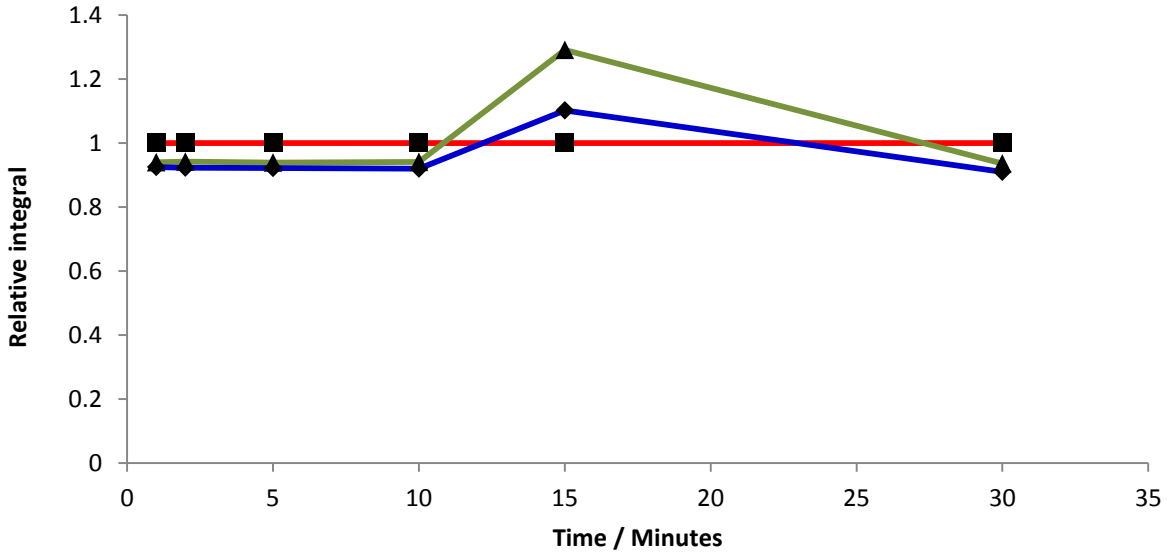

Figure A4.2.19 – Relative integrals from the NMR spectra of the Heloxy samples heated under nitrogen at 130 ºC. The blue is for the peak at 2.80, the red is for the peak at 2.90 and the green is for the peak at 3.40ppm.

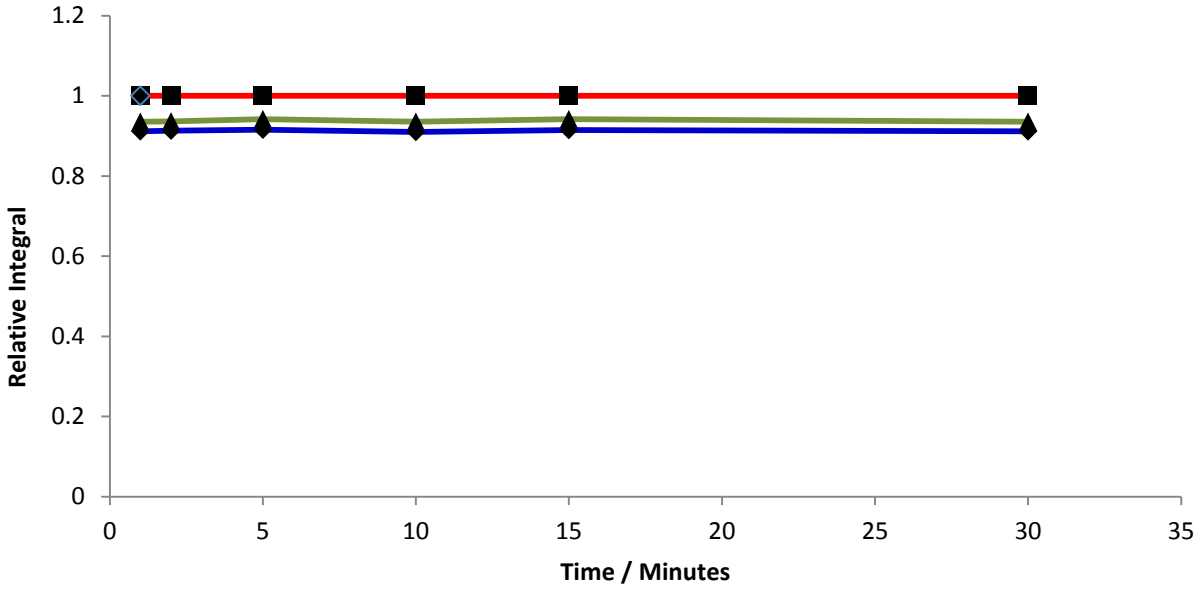

Figure A4.2.20 - Relative integrals from the NMR spectra of the Heloxy samples heated under air at 90 ºC. The blue is for the peak at 2.80, the red is for the peak at 2.90 and the green is for the peak at 3.40ppm

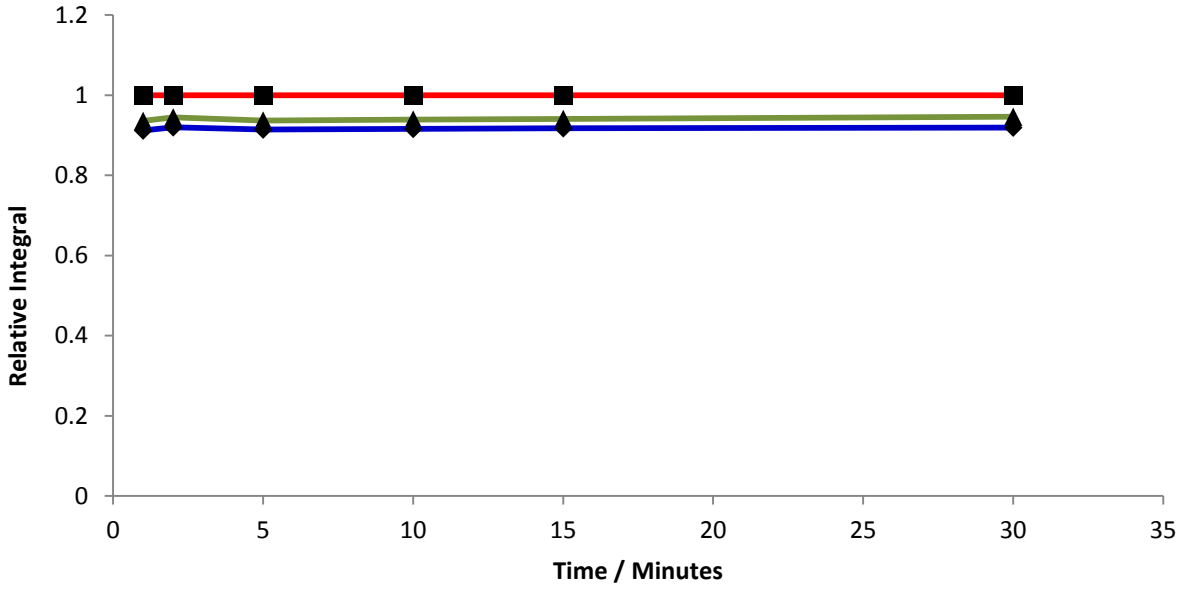

Figure A4.2.21 - Relative integrals from the NMR spectra of the Heloxy samples heated under air at 110 ºC. The blue is for the peak at 2.80, the red is for the peak at 2.90 and the green is for the peak at 3.40ppm

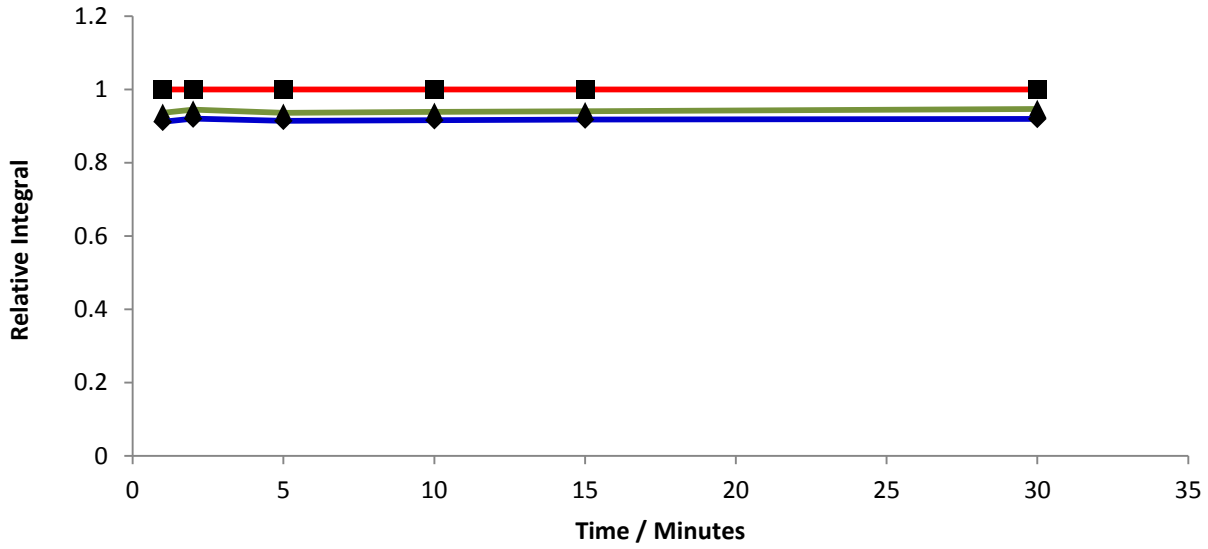

Figure A4.2.22 - Relative integrals from the NMR spectra of the Heloxy samples heated under air at 130 ºC. The blue is for the peak at 2.80, the red is for the peak at 2.90 and the green is for the peak at 3.40ppm

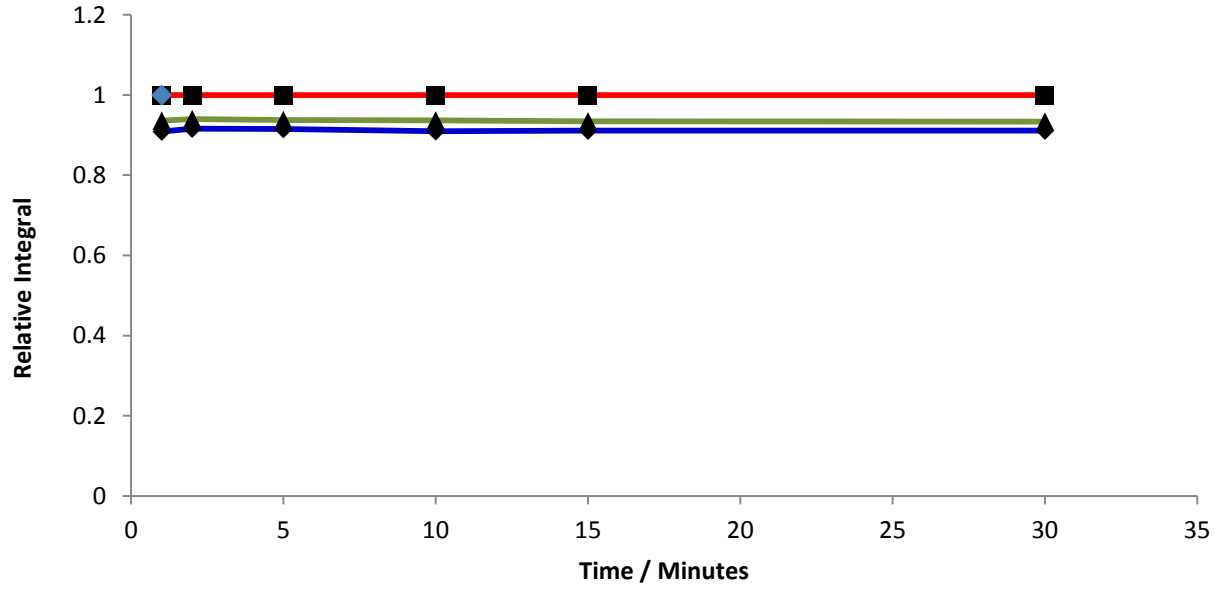

Figure A4.2.23 - Relative integrals from the NMR spectra of the Heloxy samples heated under air at 150 ºC. The blue is for the peak at 2.80, the red is for the peak at 2.90 and the green is for the peak at 3.40ppm.

A4 - Chapter 4 – Benzoic Acid and Epoxides – Benzoic and Epoxide Reactions

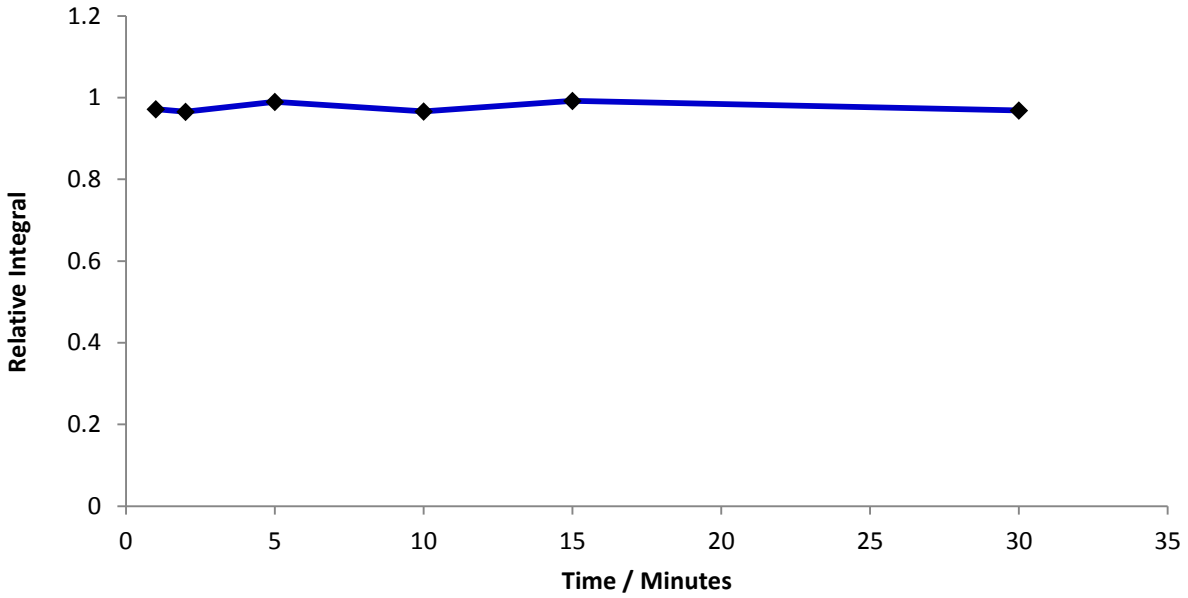

Figure A4.3.1 - Relative integrals of the benzoic acid sample heated under nitrogen at 90 °C (11.99 ppm peak).

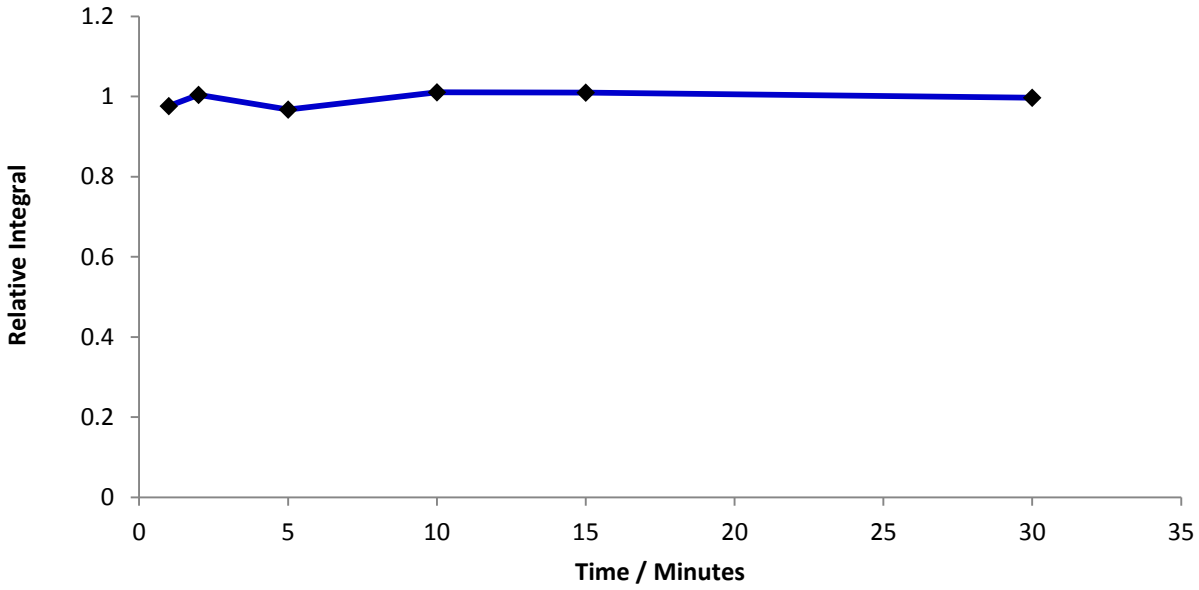

Figure A4.3.2 - Relative integrals of the benzoic acid sample heated under nitrogen at 110 °C (11.99 ppm peak).

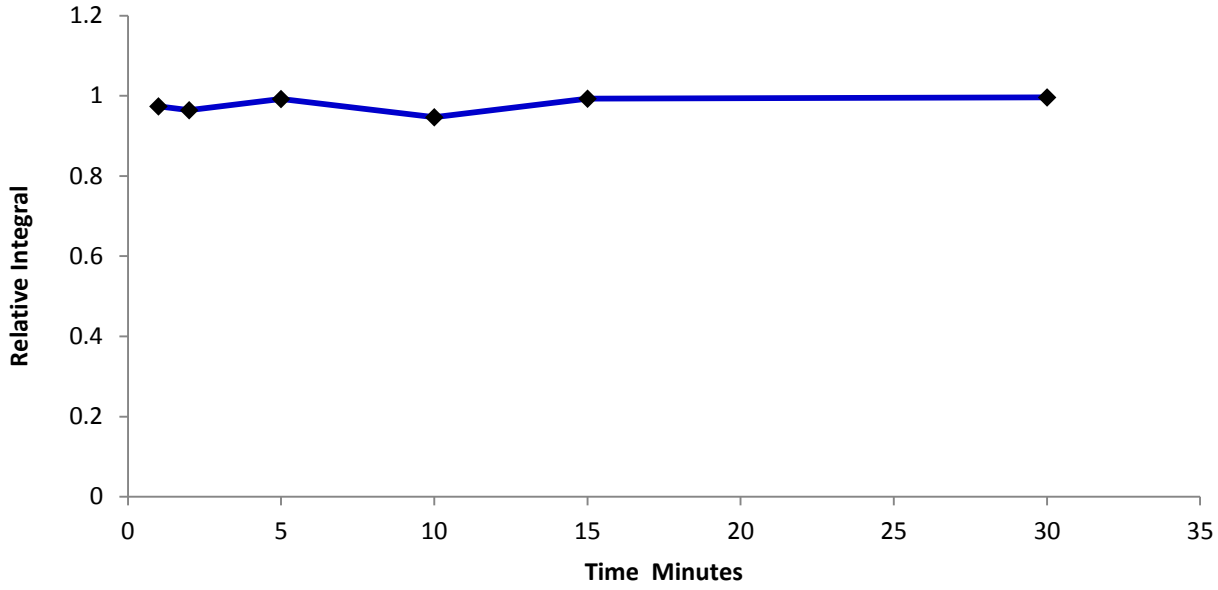

Figure A4.3.3 - Relative integrals of the benzoic acid sample heated under nitrogen at 130 °C (11.99 ppm peak).

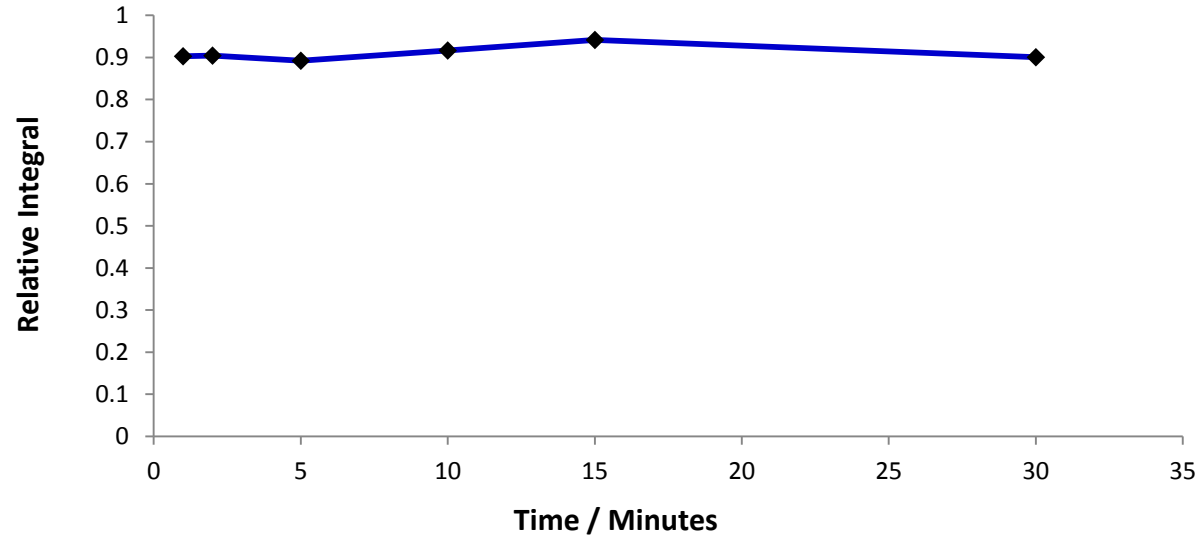

Figure A4.3.4 - Relative integrals of the benzoic acid sample heated under nitrogen at 150 °C (11.99 ppm peak).

A6 – Chapter 6 – PET and Epoxides - Starting Materials

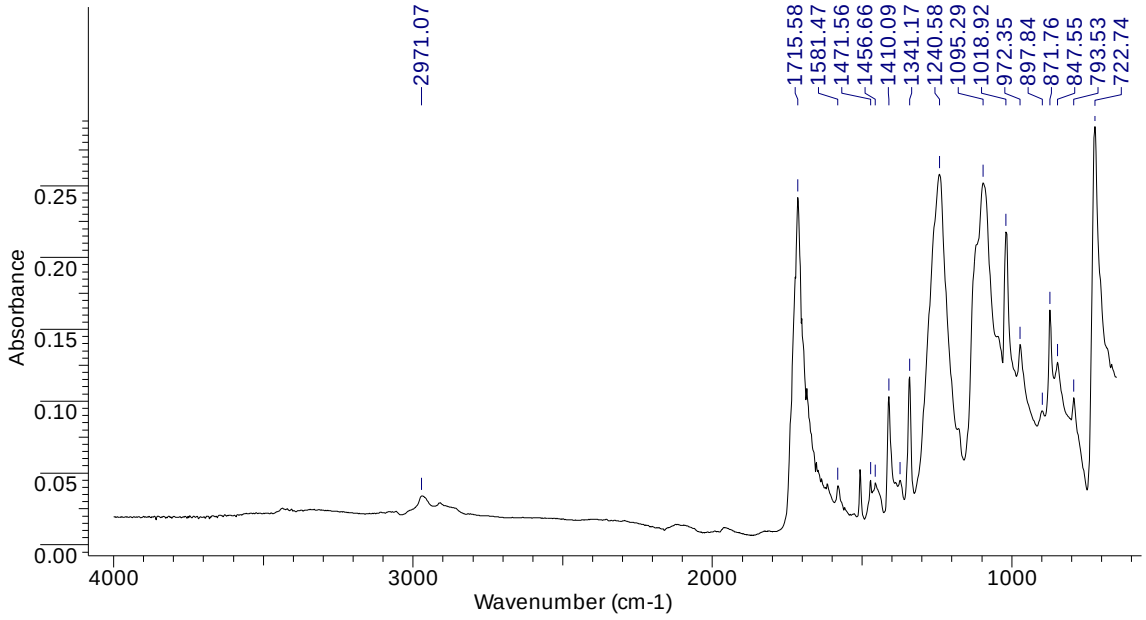

Figure A6.1.1 – IR spectrum of E239 sample.

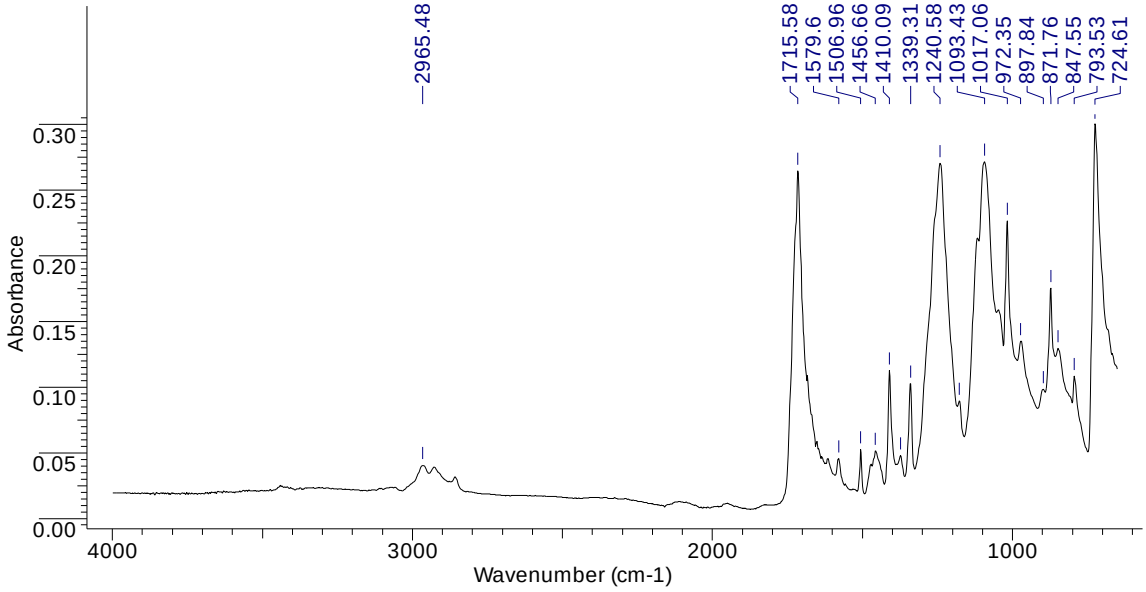

Figure A6.1.2 - IR spectrum of E240 sample.

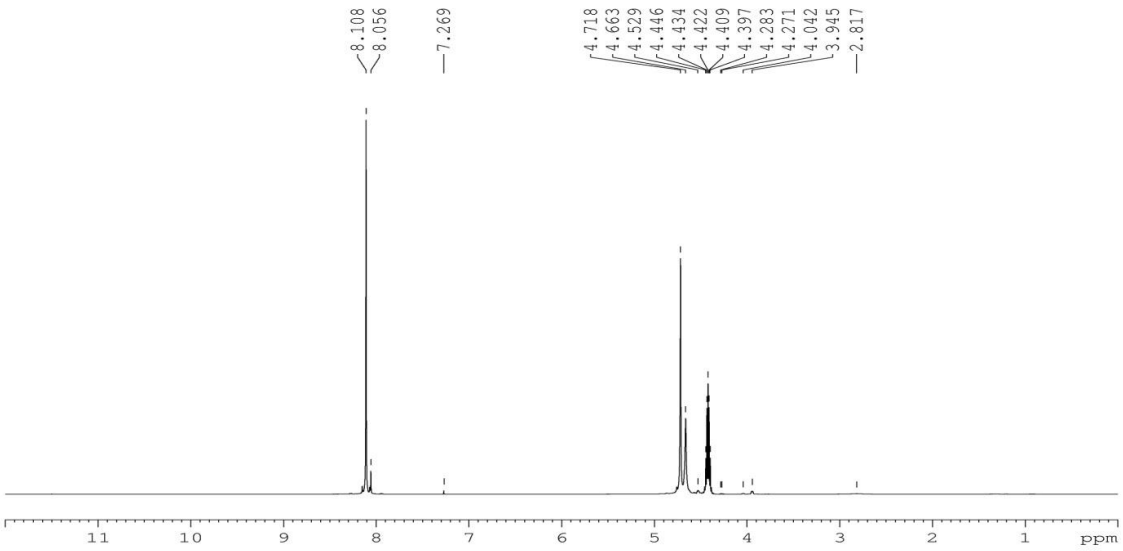

Figure A6.1.3 – ^{1}H NMR spectra of E239.

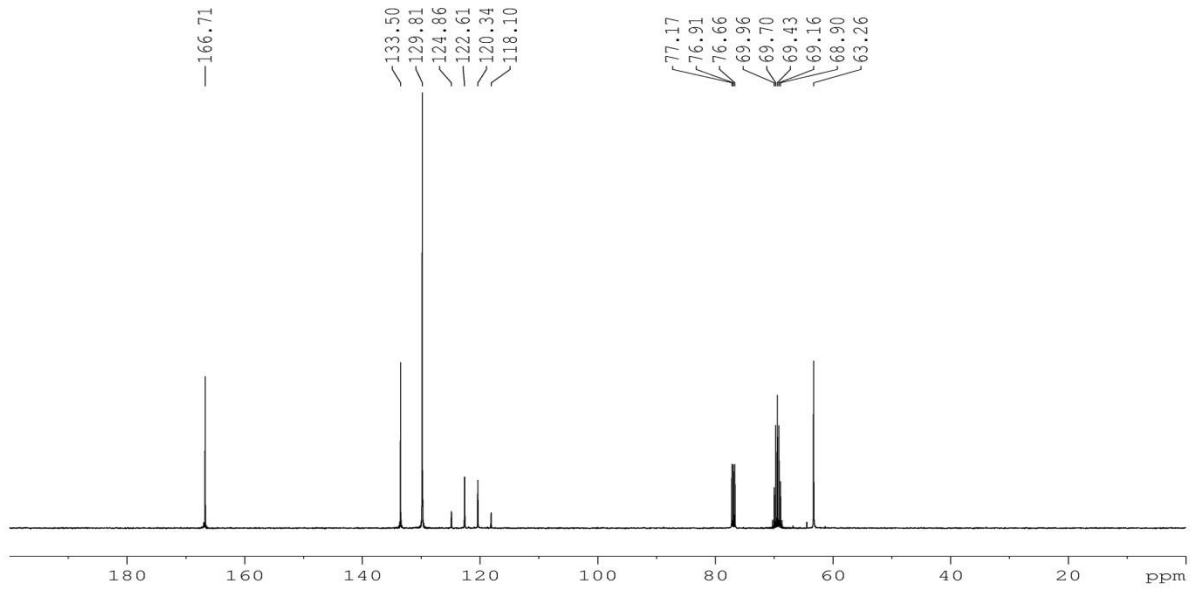

Figure A6.1.4 – ^{13}C NMR spectra of E239.

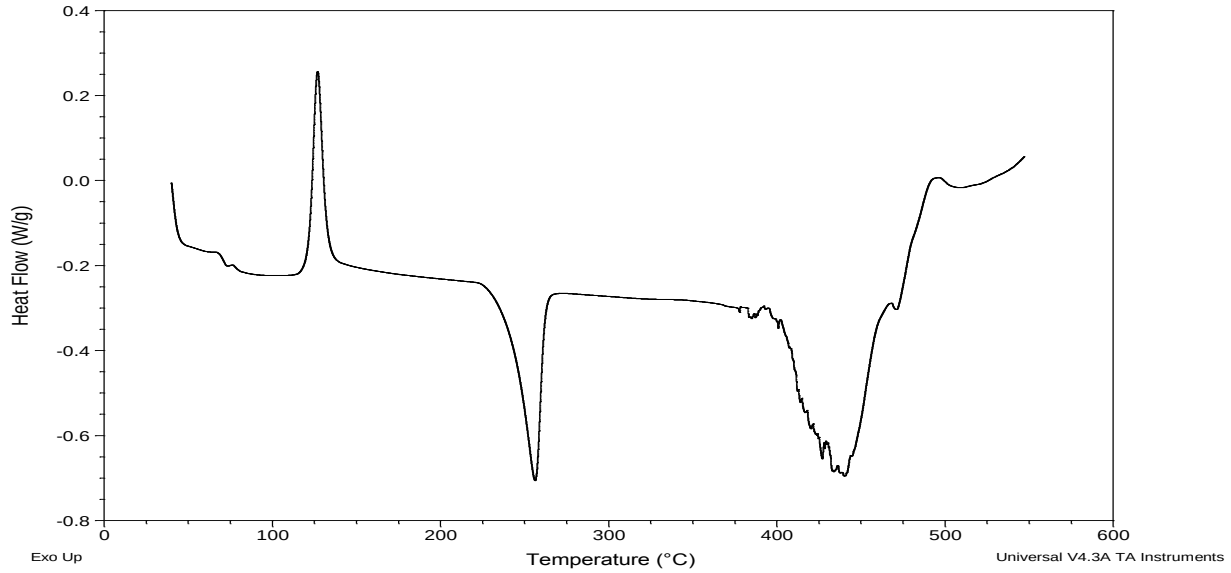

Figure A6.1.5 - DSC scan showing the degradation behaviour of E239.

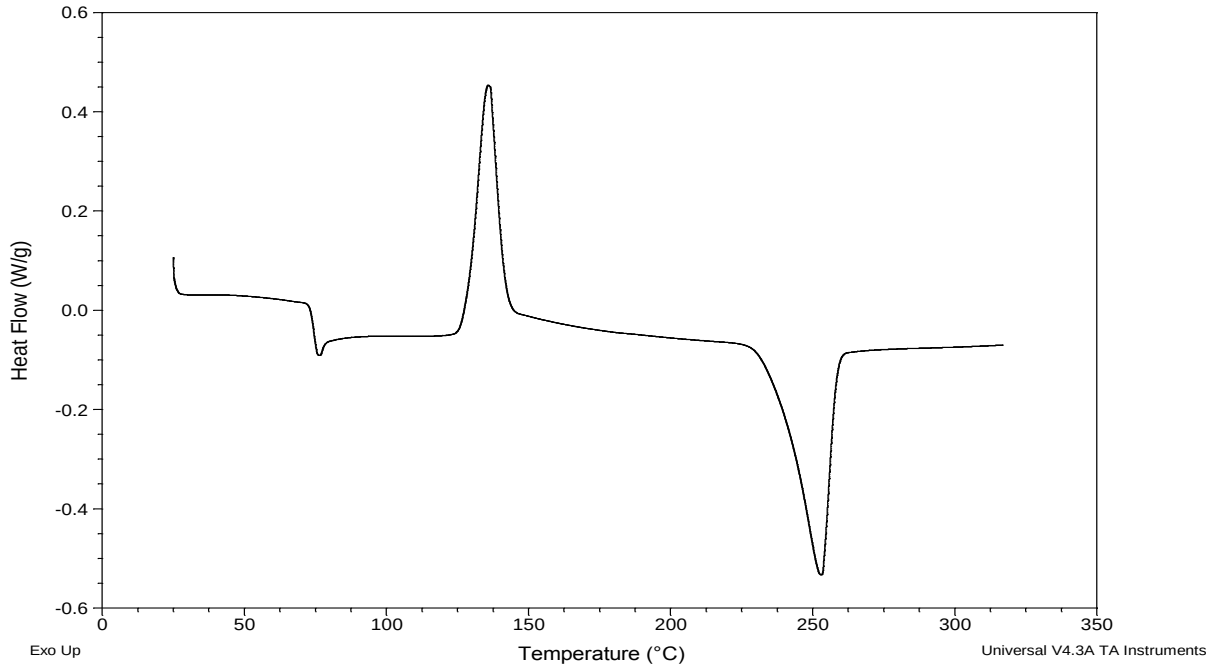

Figure A6.1.6 - DSC scan showing the degradation behaviour of E240.

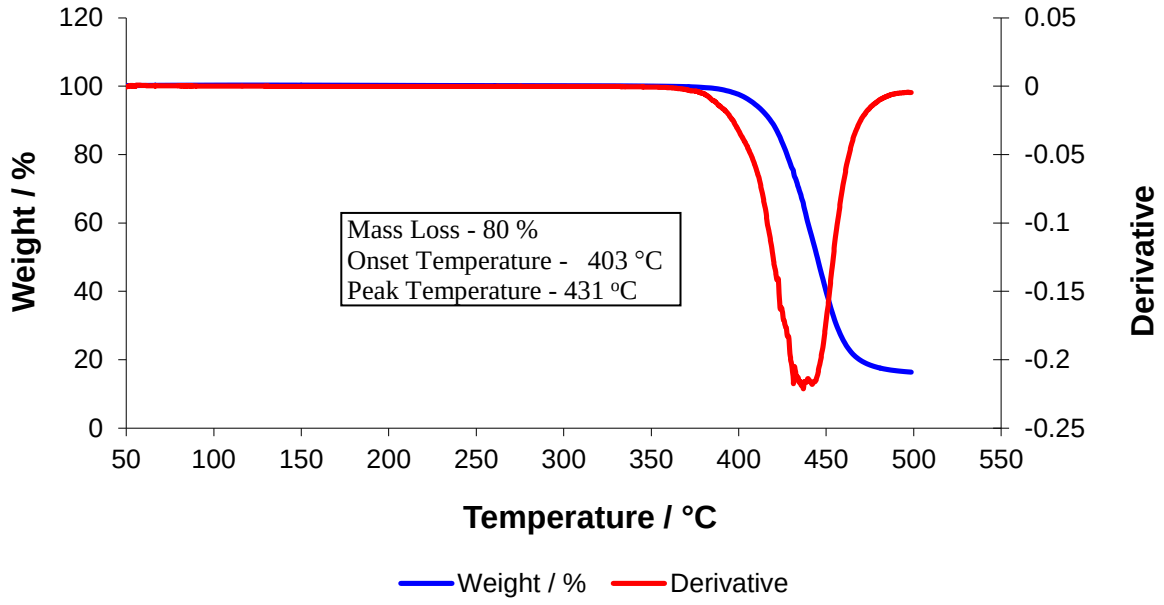

Figure A6.1.7 – TGA thermogram of E239 sample.

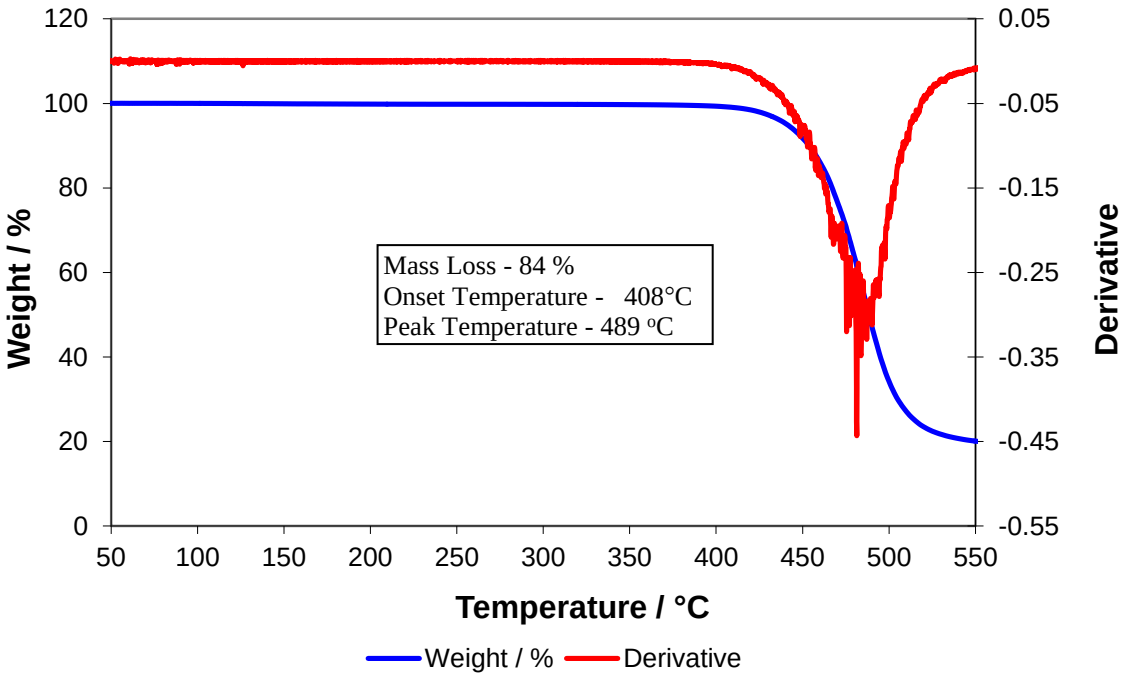

Figure A6.1.8 – TGA thermogram of E240 sample.

A7 – Chapter 7 – Characterisation of the Degradation Behaviour, Hydrolytic Degradation - Kinetics

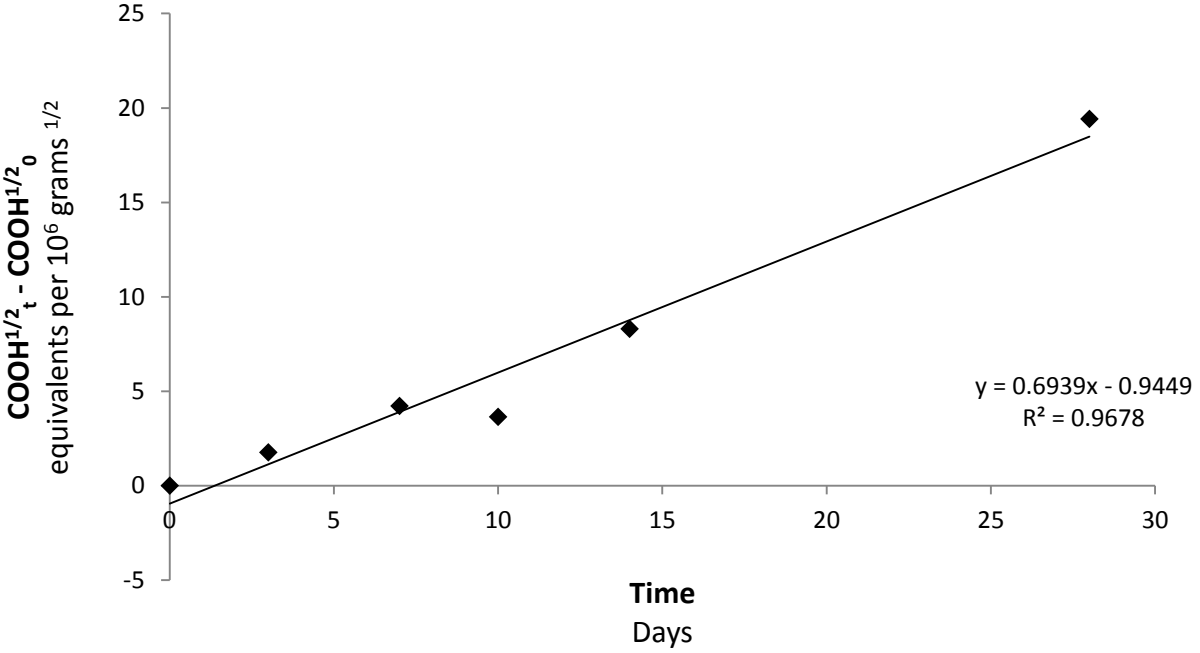

Figure A7.1.1 – Scatter plot of $(([COOH]_t)^{0.5} - ([COOH]_0)^{0.5})$ versus time for the E239 samples, with the water for hydrolysis being changed every two days.

.

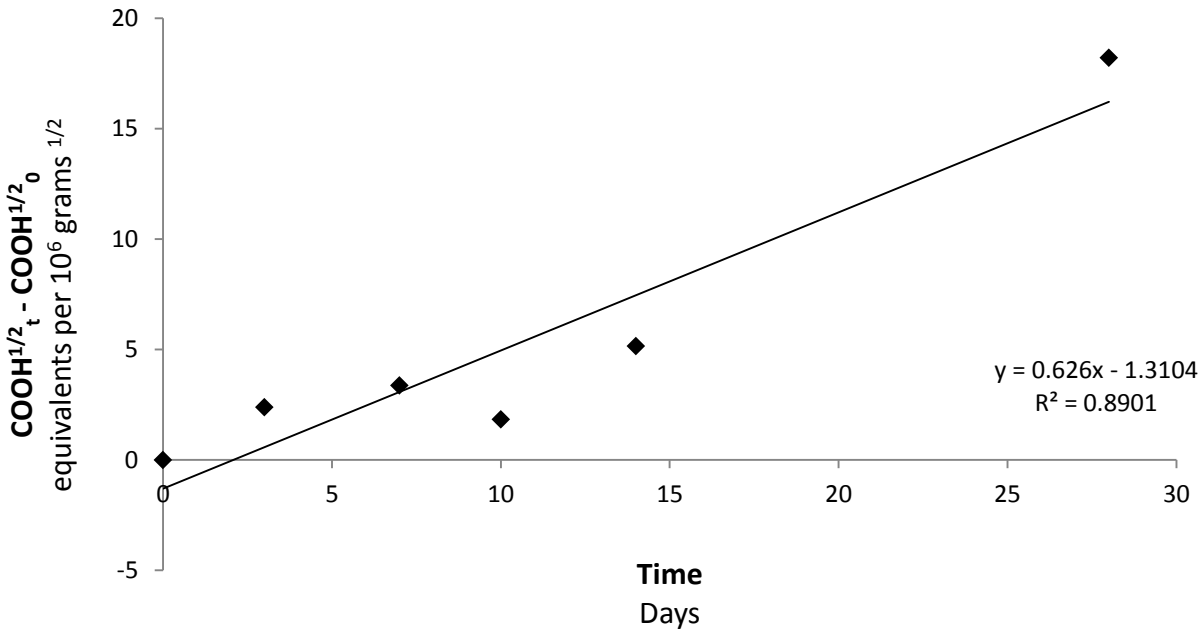

Figure A7.1.2 – Scatter plot of $(([COOH]_t)^{0.5} - ([COOH]_0)^{0.5})$ versus time for the E239 + 1% Cardura samples, with the water for hydrolysis being changed every two days.

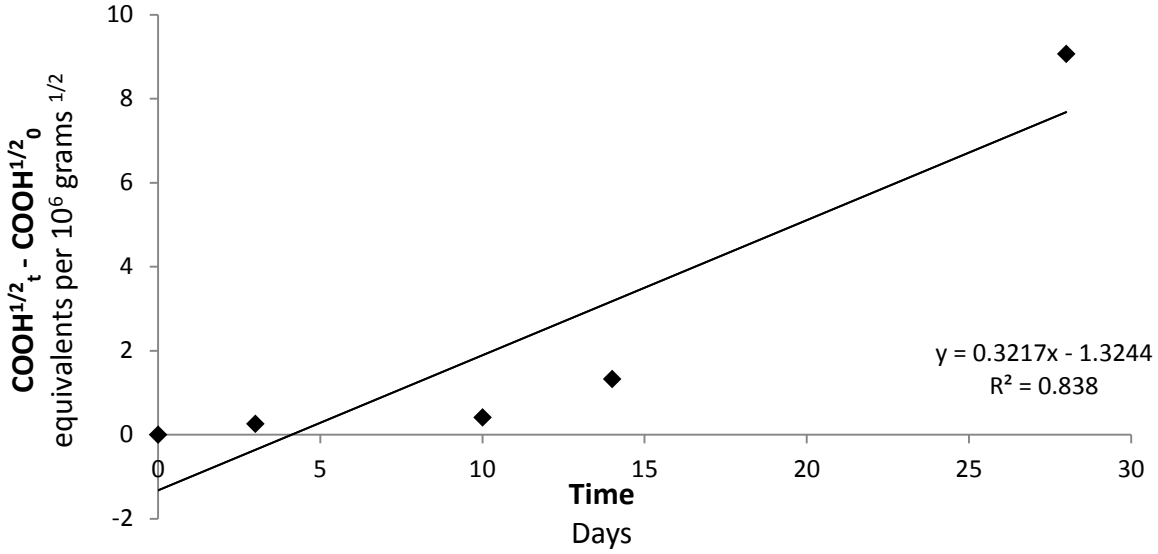

Figure A7.1.3 – Scatter plot of $(([COOH]_t)^{0.5} - ([COOH]_0)^{0.5})$ versus time for the E239 + 6% Cardura samples, with the water for hydrolysis being changed every two days.

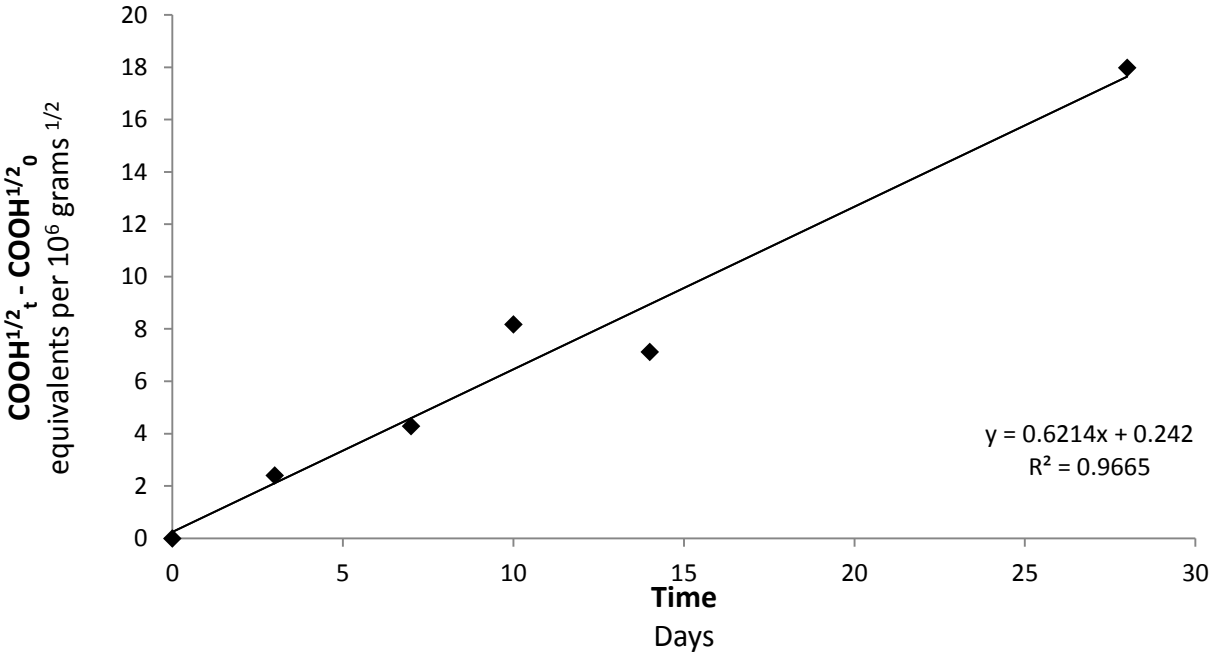

Figure A7.1.4– Scatter plot of $(([COOH]_t)^{0.5} - ([COOH]_0)^{0.5})$ versus time for the E240 samples, with the water for hydrolysis being changed every two days.

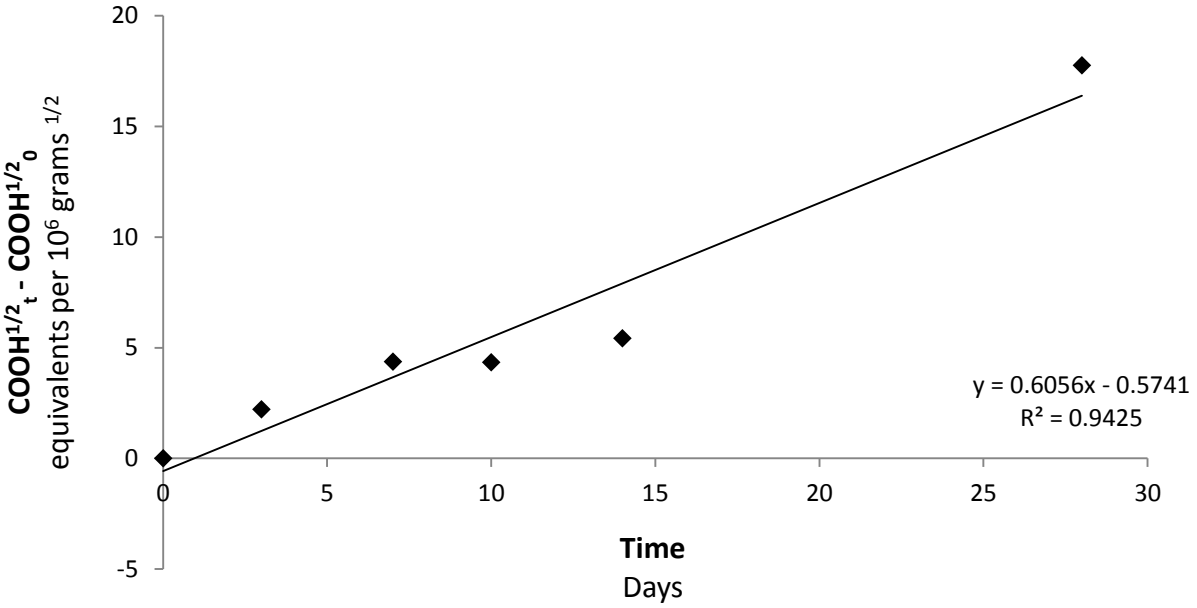

Figure A7.1.5 – Scatter plot of $(([COOH]_t)^{0.5} - ([COOH]_0)^{0.5})$ versus time for the E240 + 1% Cardura samples, with the water for hydrolysis being changed every two days.

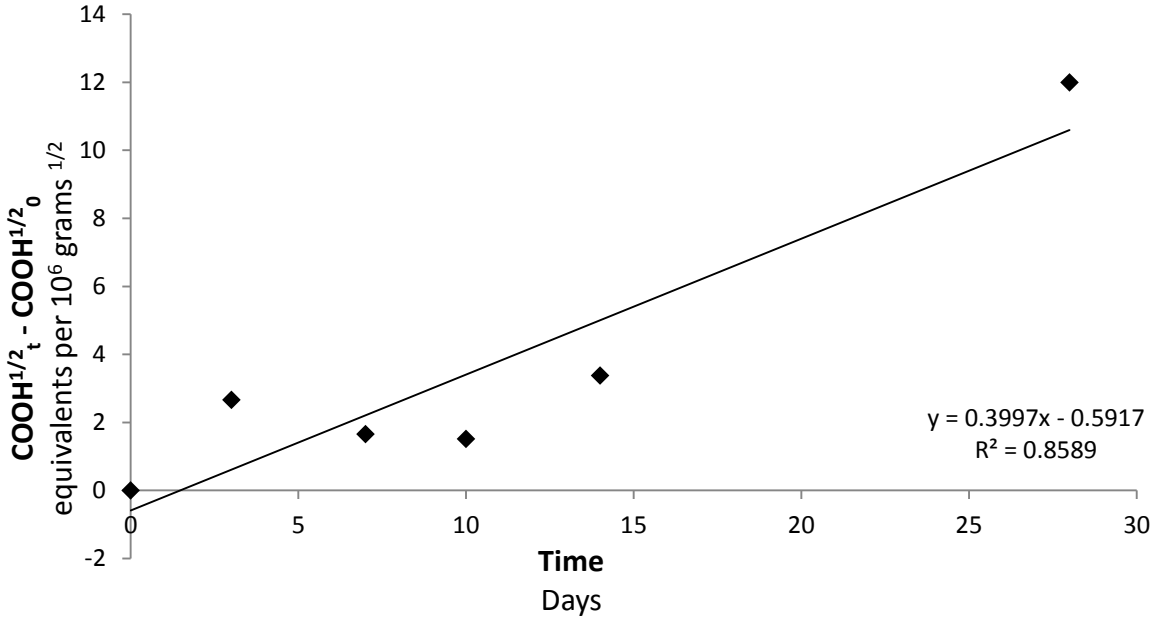

Figure A7.1.6 – Scatter plot of $(([COOH]_t)^{0.5} - ([COOH]_0)^{0.5})$ versus time for the E240 + 6% Cardura samples, with the water for hydrolysis being changed every two days.

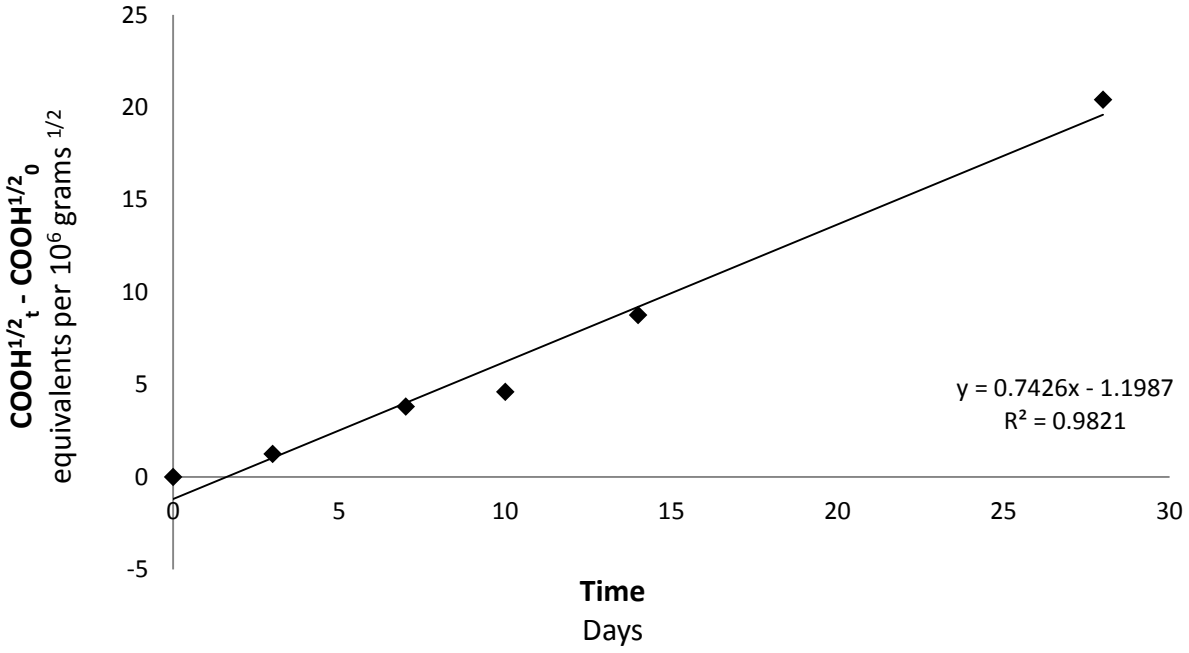

Figure A7.1.7 - Scatter plot of $(([COOH]_t)^{0.5} - ([COOH]_0)^{0.5})$ versus time for the E187 samples, with the water for hydrolysis not being changed.

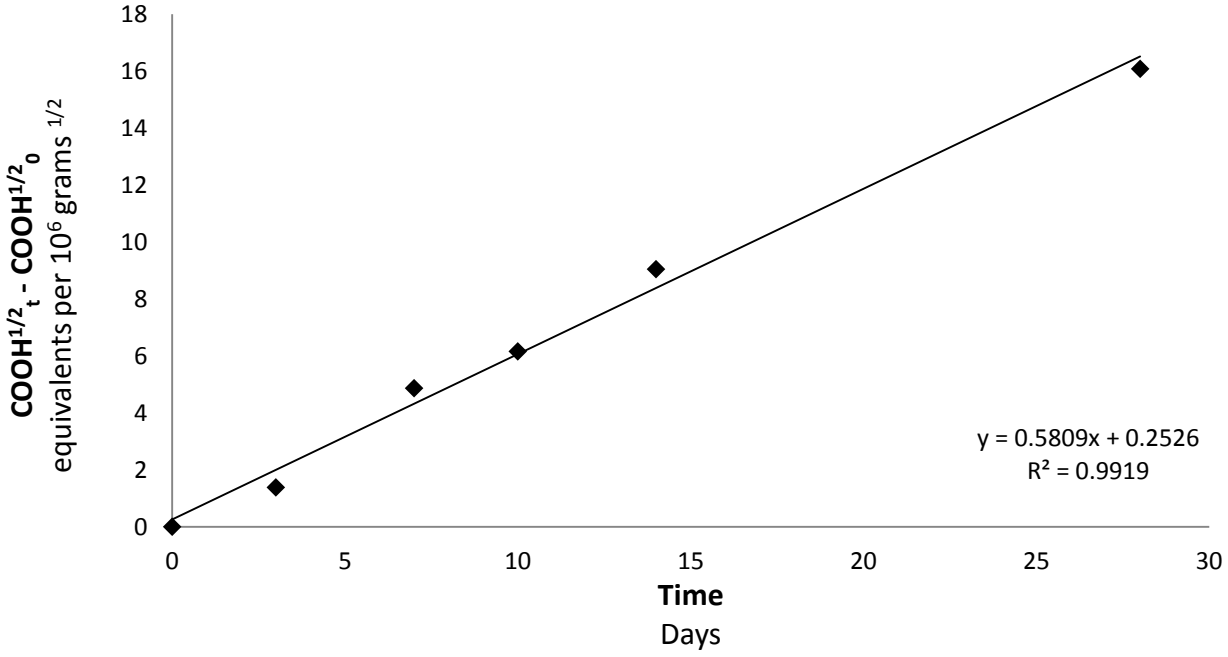

Figure A7.1.8 - Scatter plot of $(([COOH]_t)^{0.5} - ([COOH]_0)^{0.5})$ versus time for the E187 + 1% Cardura samples, with the water for hydrolysis not being changed.

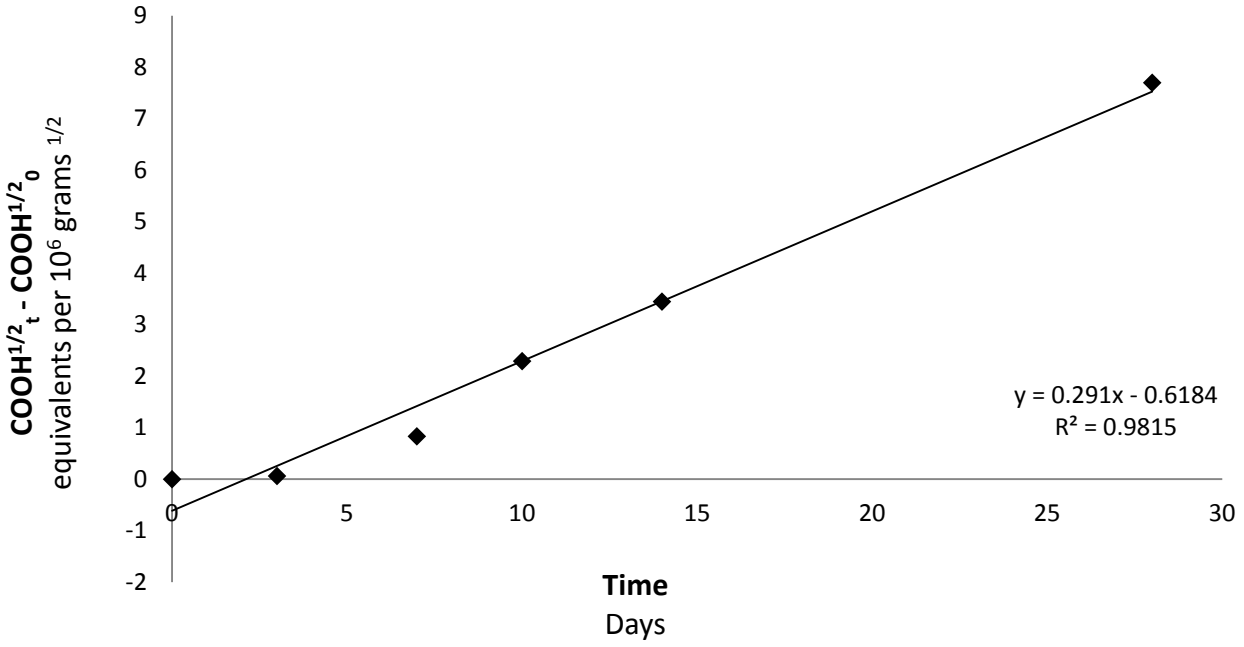

Figure A7.1.9 - Scatter plot of $(([COOH]_t)^{0.5} - ([COOH]_0)^{0.5})$ versus time for the E187 + 6% Cardura samples, with the water for hydrolysis not being changed.

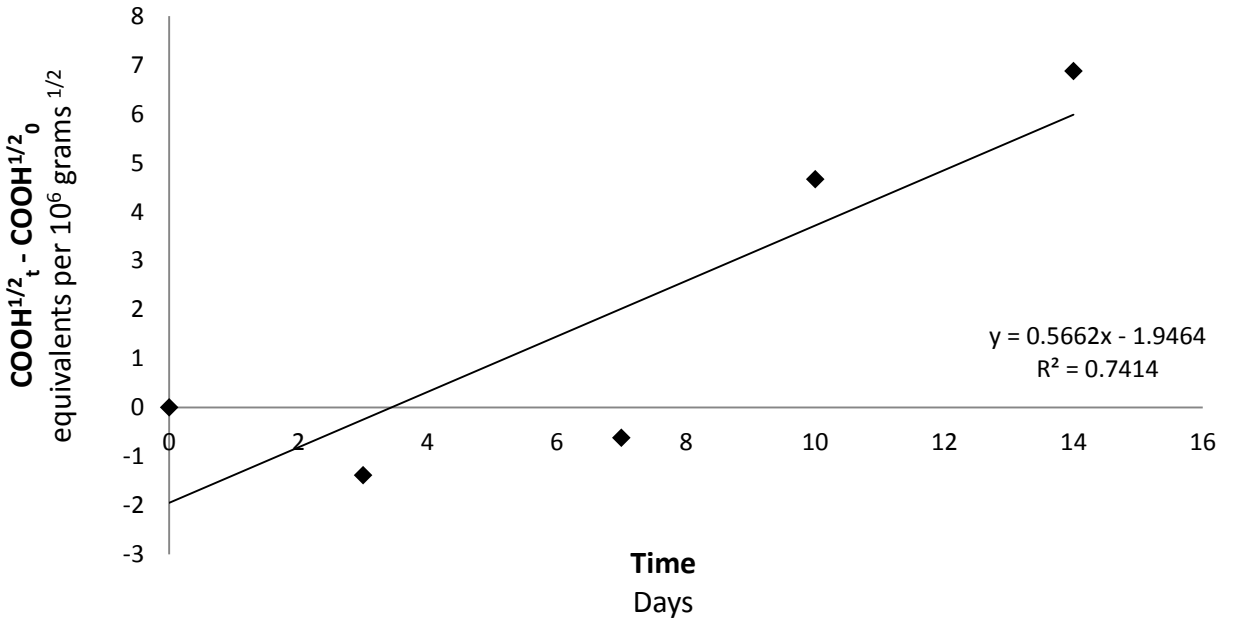

Figure A7.1.10 - Scatter plot of $(([COOH]_t)^{0.5} - ([COOH]_0)^{0.5})$ versus time for the E239 samples, with the water for hydrolysis not being changed.

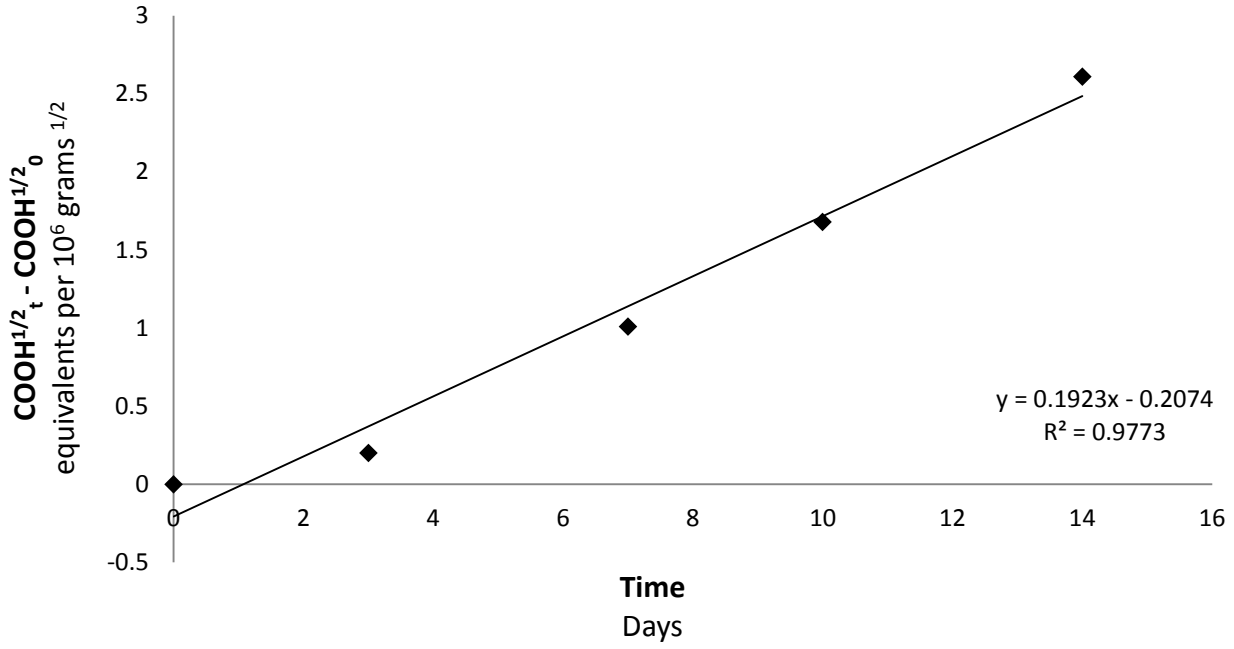

Figure A7.1.11 - Scatter plot of $(([COOH]_t)^{0.5} - ([COOH]_0)^{0.5})$ versus time for the E239 + 1% Cardura samples, with the water for hydrolysis not being changed.

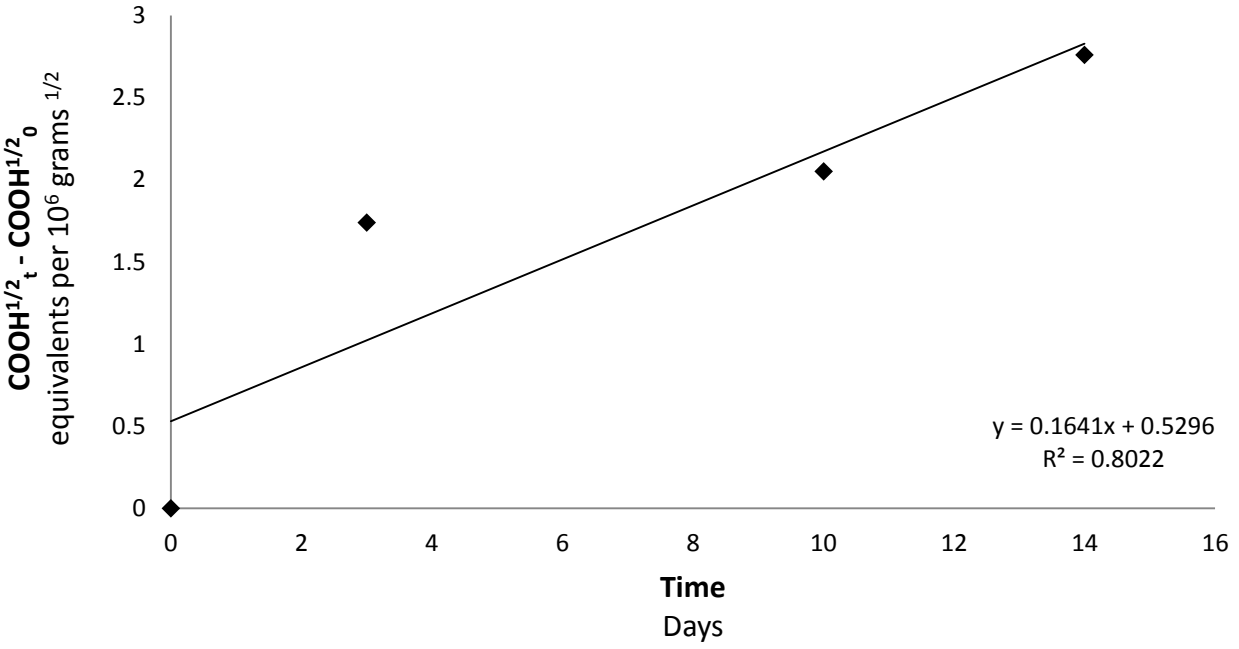

Figure A7.1.12 - Scatter plot of $(([COOH]_t)^{0.5} - ([COOH]_0)^{0.5})$ versus time for the E239 + 6% Cardura samples, with the water for hydrolysis not being changed.

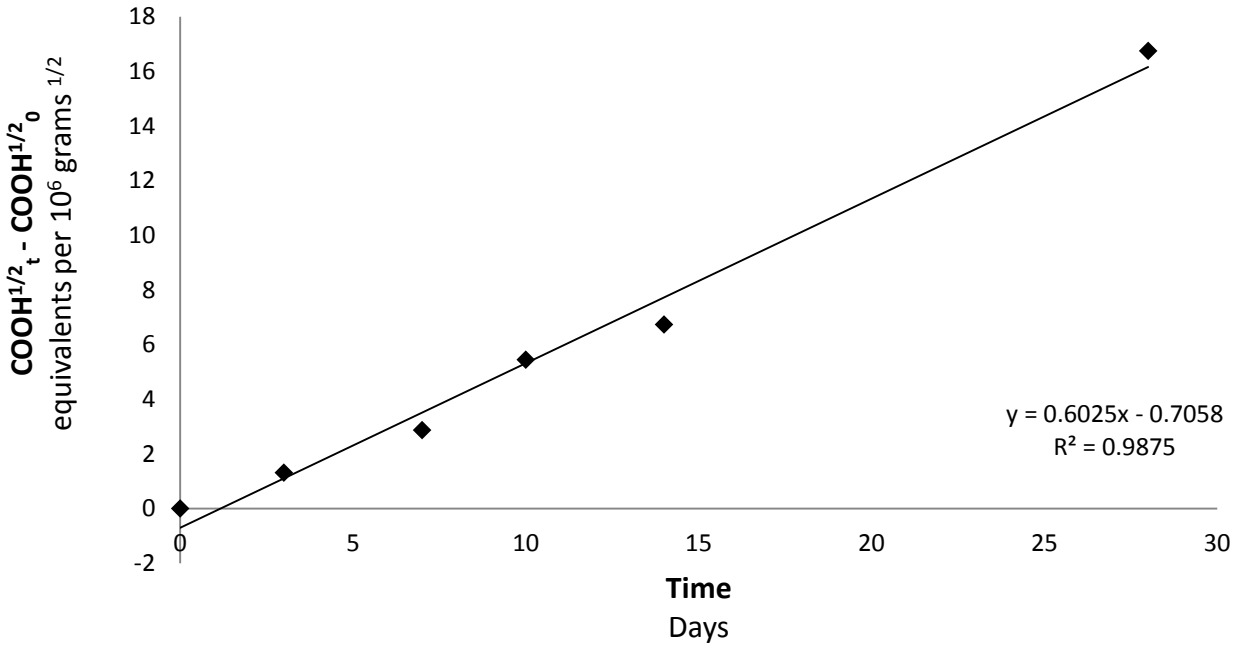

Figure A7.1.13 - Scatter plot of $(([COOH]_t)^{0.5} - ([COOH]_0)^{0.5})$ versus time for the E240 samples, with the water for hydrolysis not being changed.

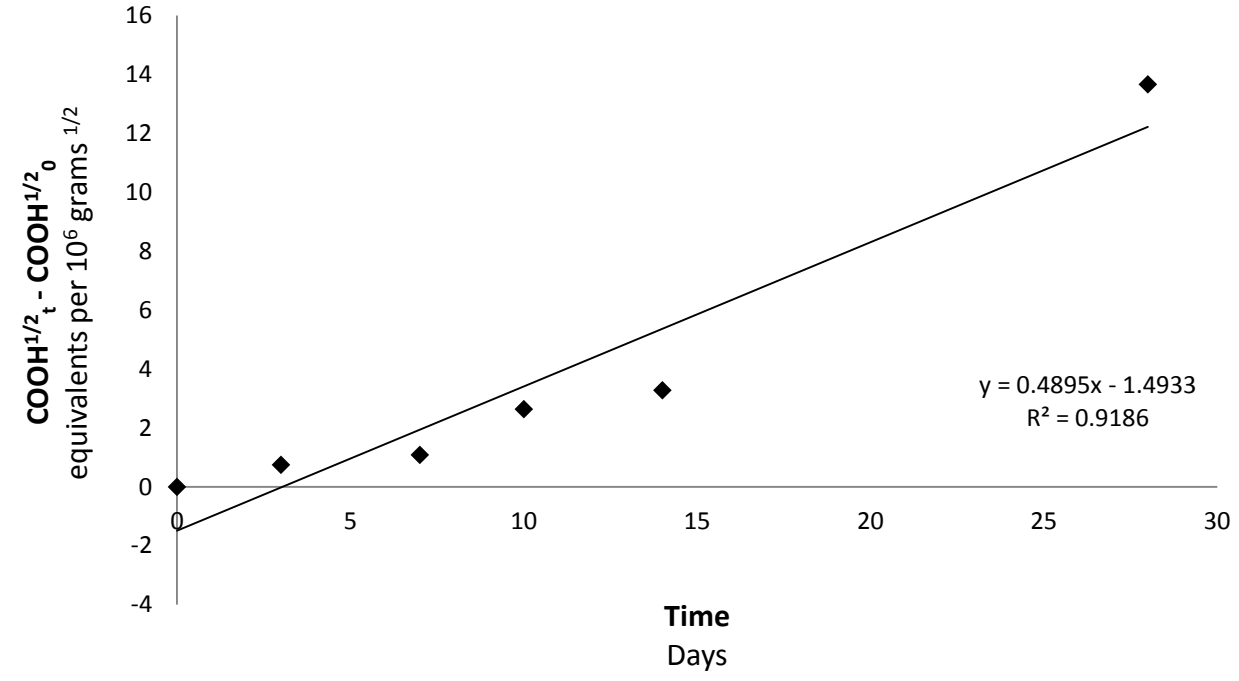

Figure A7.1.14 - Scatter plot of $(([COOH]_t)^{0.5} - ([COOH]_0)^{0.5})$ versus time for the E240 + 1% Cardura samples, with the water for hydrolysis not being changed.

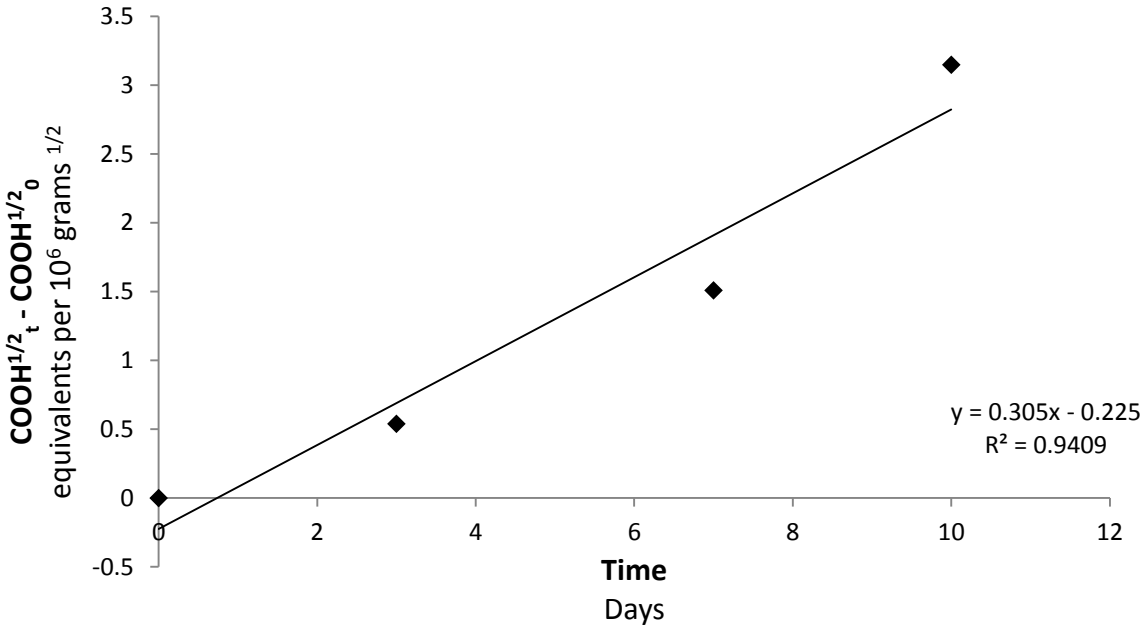

Figure A7.1.15 – Scatter plot of $(([COOH]_t)^{0.5} - ([COOH]_0)^{0.5})$ versus time for the E240 + 1% Vikolox samples, with the water for hydrolysis being changed every two days.

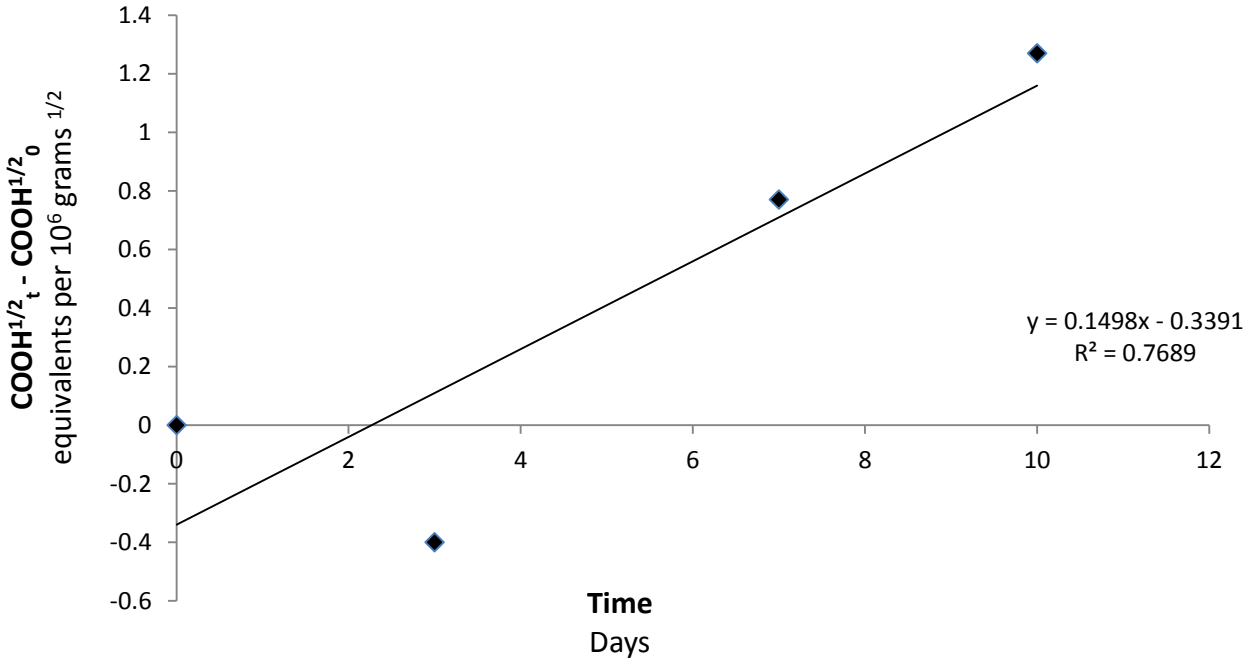

Figure A7.1.16 – Scatter plot of $(([COOH]_t)^{0.5} - ([COOH]_0)^{0.5})$ versus time for the E240 + 6% Vikolox samples, with the water for hydrolysis being changed every two days.

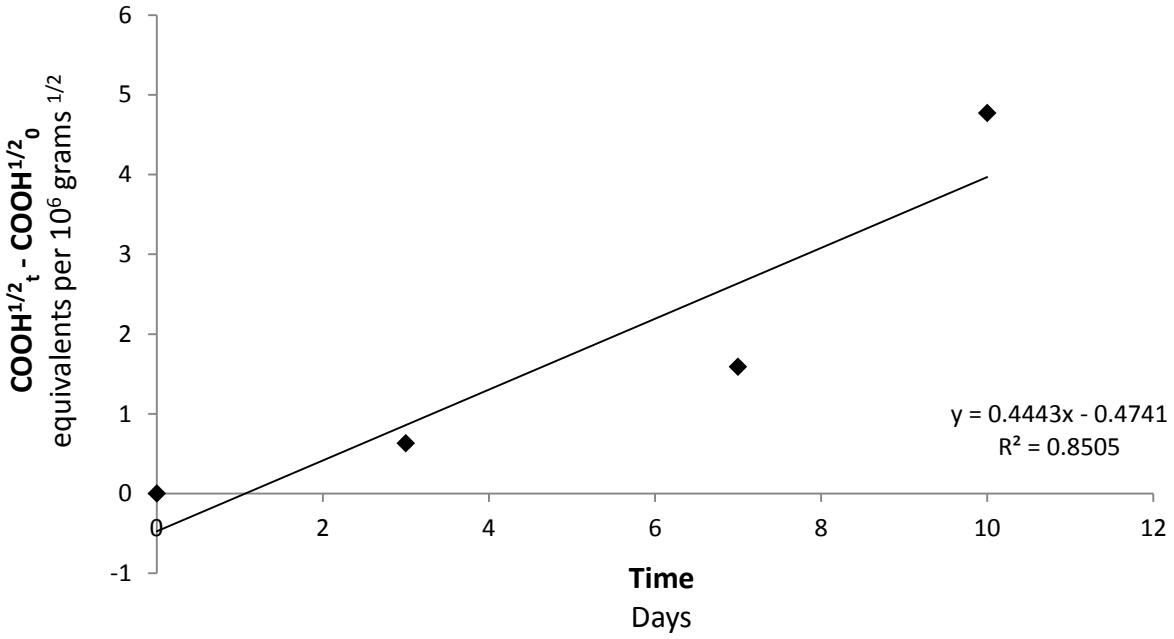

Figure A7.1.17 – Scatter plot of $(([COOH]_t)^{0.5} - ([COOH]_0)^{0.5})$ versus time for the E240 + 1% Heloxy samples, with the water for hydrolysis being changed every two days.

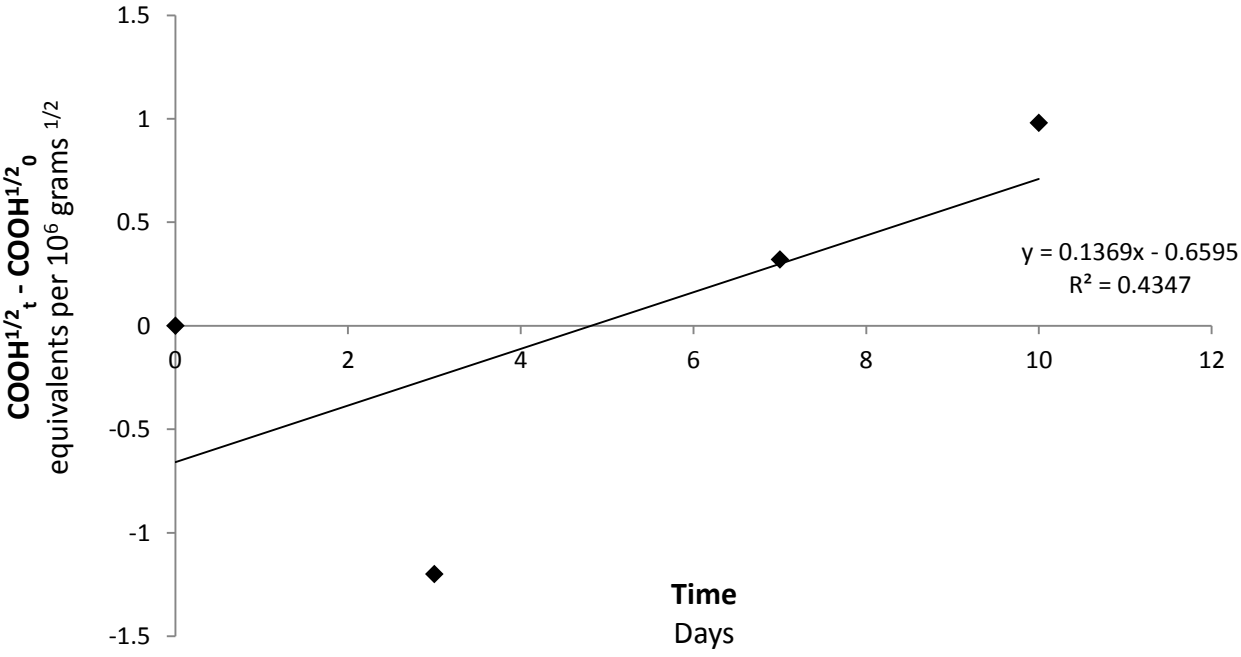

Figure A7.1.18 – Scatter plot of $(([COOH]_t)^{0.5} - ([COOH]_0)^{0.5})$ versus time for the E240 + 6% Heloxy samples, with the water for hydrolysis being changed every two days.

A7 – Chapter 7 – Characterisation of the Degradation Behaviour, Hydrolytic Degradation – Crystallisation Temperature

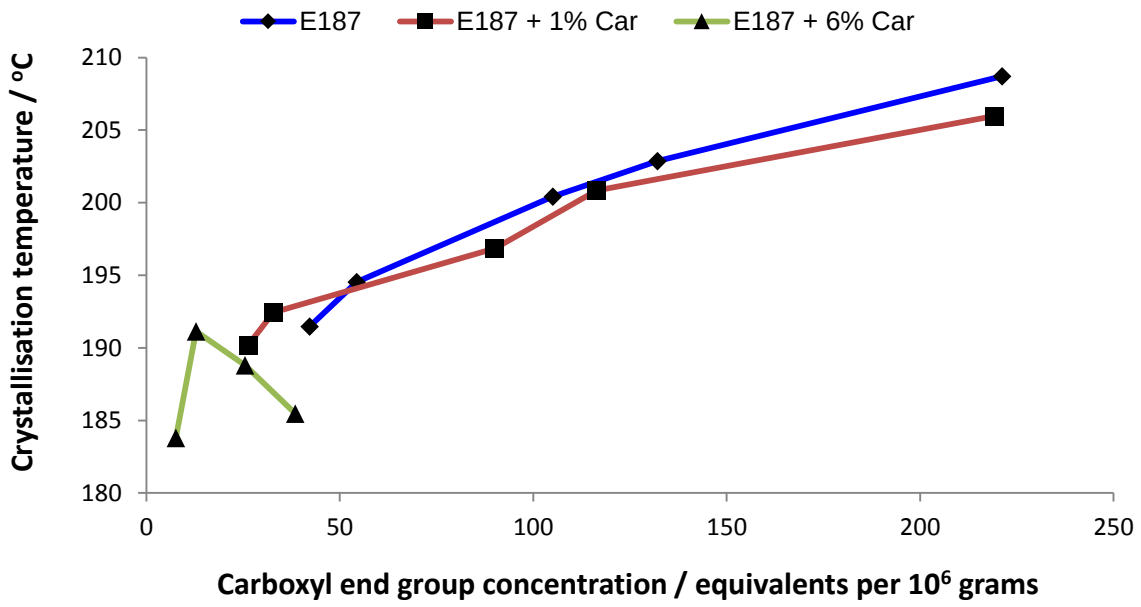

Figure A7.2.1 - Scatter plot of crystallisation temperature versus the end group concentration for the E187 samples that were prepared without changing the water. A single sample was analysed.

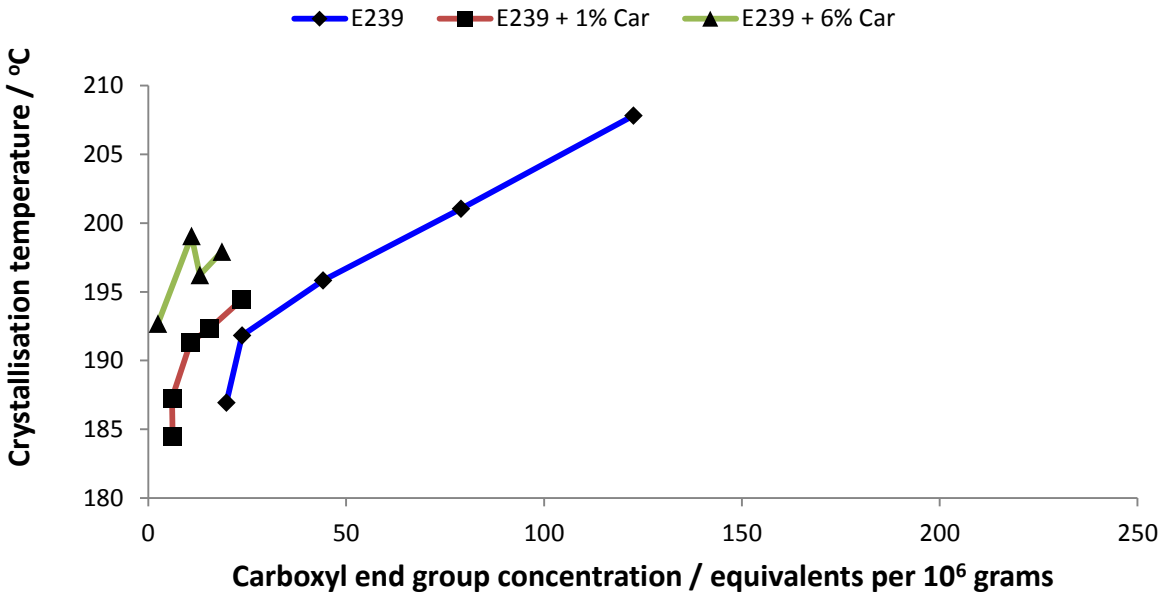

Figure A7.2.2 - Scatter plot of crystallisation temperature versus the end group concentration for the E239 samples that were prepared without changing the water. A single sample was analysed.

A7 – Chapter 7 – Characterisation of the Degradation Behaviour, Hydrolytic Degradation – Melting Point

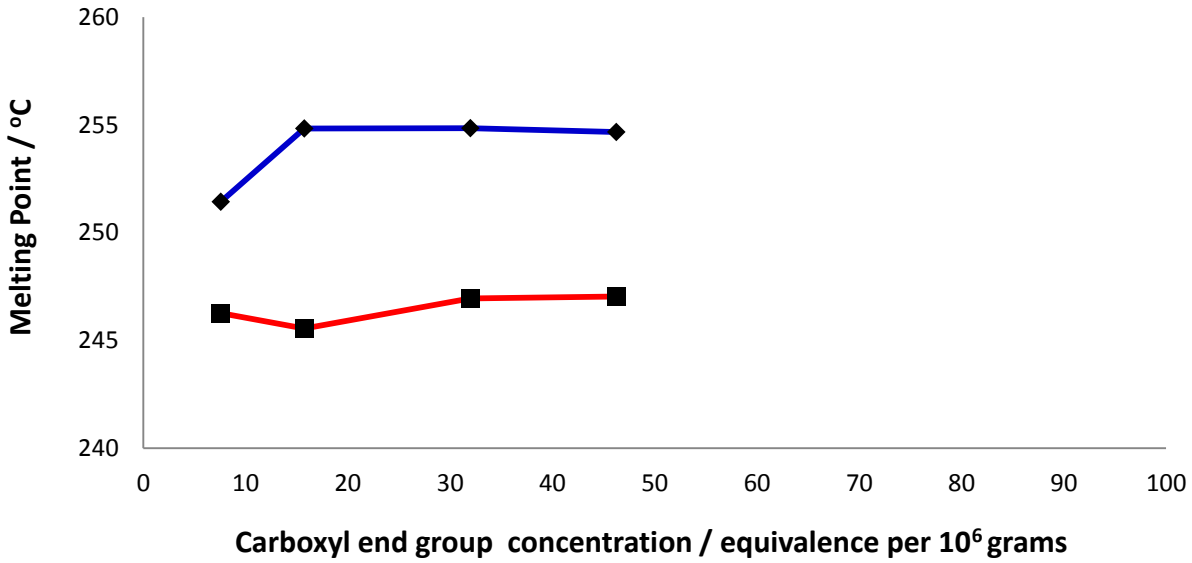

Figure A7.3.1 – Scatter graph of the melting temperature versus the carboxyl end group concentrations for the E187 + 6% Cardura samples. The blue line represents the initial melting point and the red line represents the reheat melting point. A single sample was analysed.

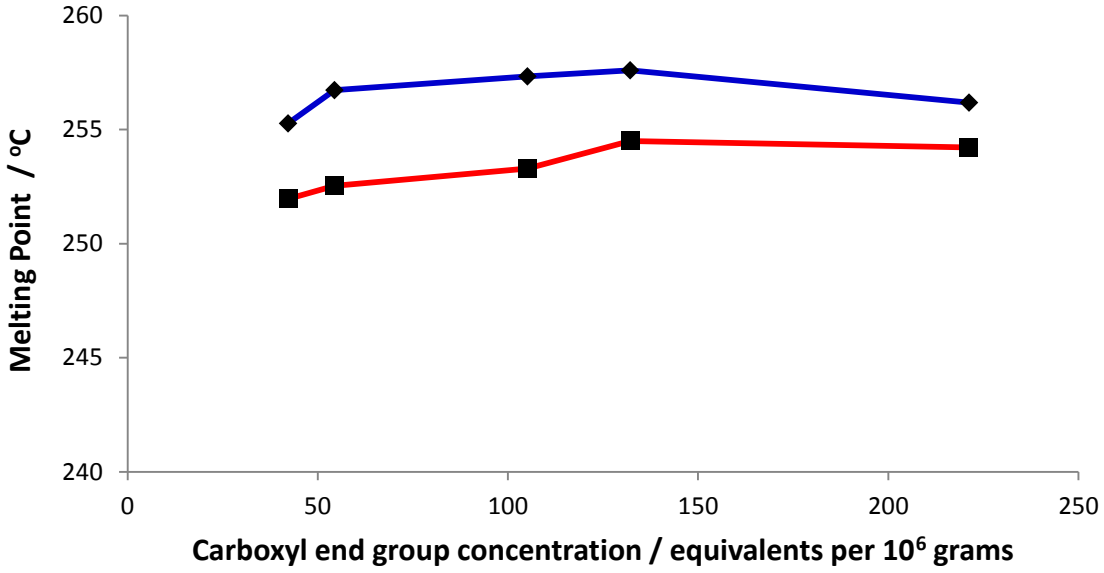

Figure A7.3.2 – Scatter plot of the melting point versus the end group concentration for the E187 samples that were prepared without the water being changed. The blue line represents the initial melting point and the red line represents the reheat melting point. A single sample was analysed.

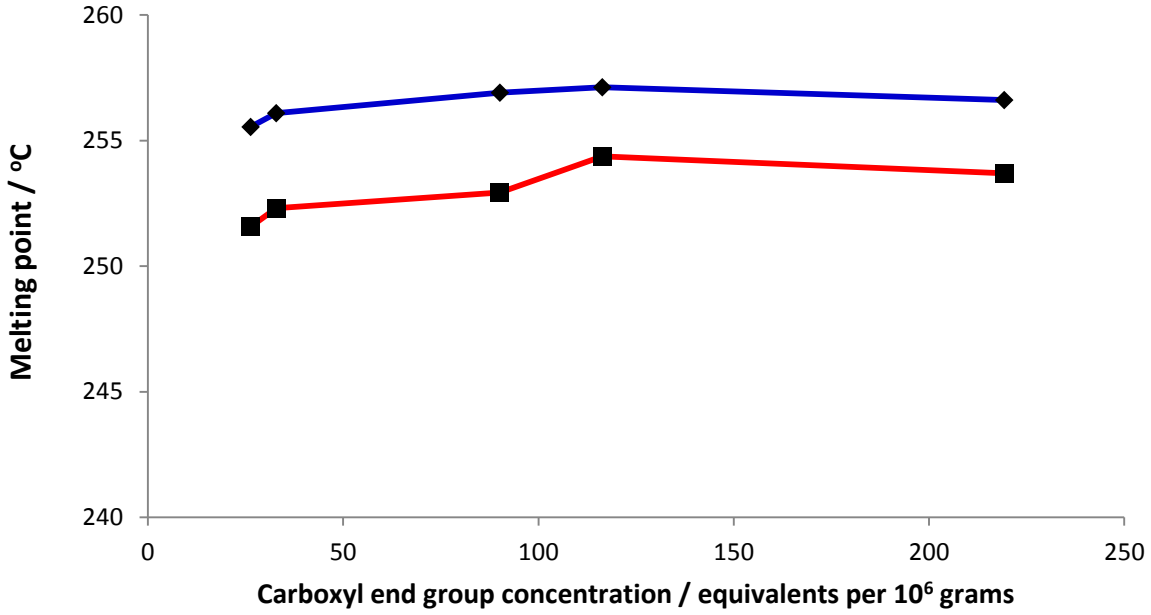

Figure A7.3.3 – Scatter plot of the melting point versus the end group concentration for the E187 + 1% Cardura samples that were prepared without the water being changed. The blue line represents the initial melting point and the red line represents the reheat melting point. A single sample was analysed.

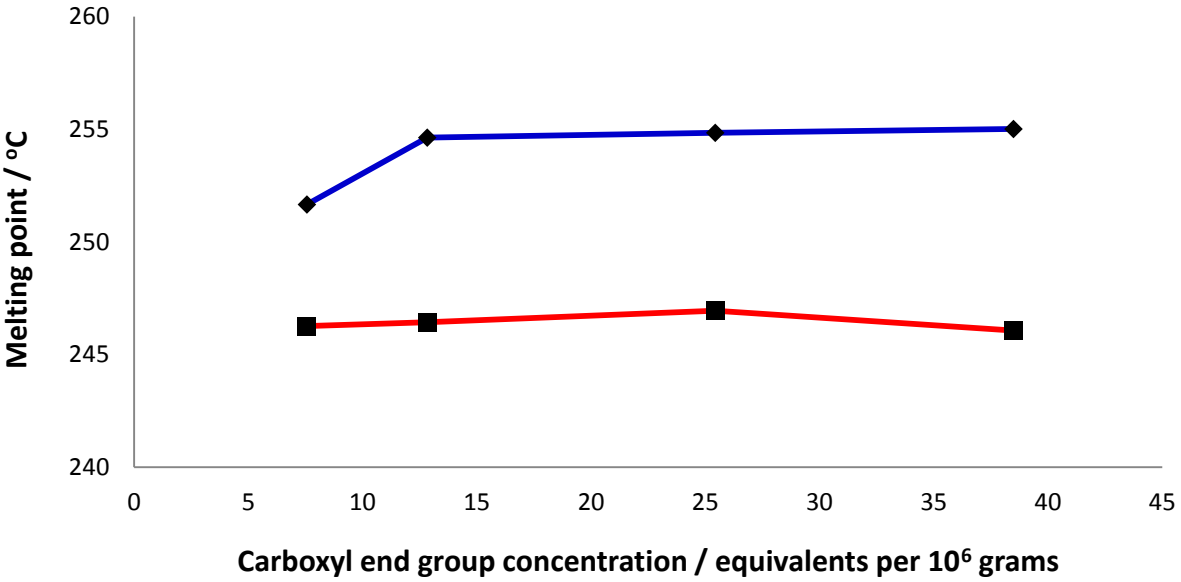

Figure A7.3.4 – Scatter plot of the melting point versus the end group concentration for the E187 samples + 6% cardura that were prepared without the water being changed. The blue line represents the initial melting point and the red line represents the reheat melting point. A single sample was analysed.

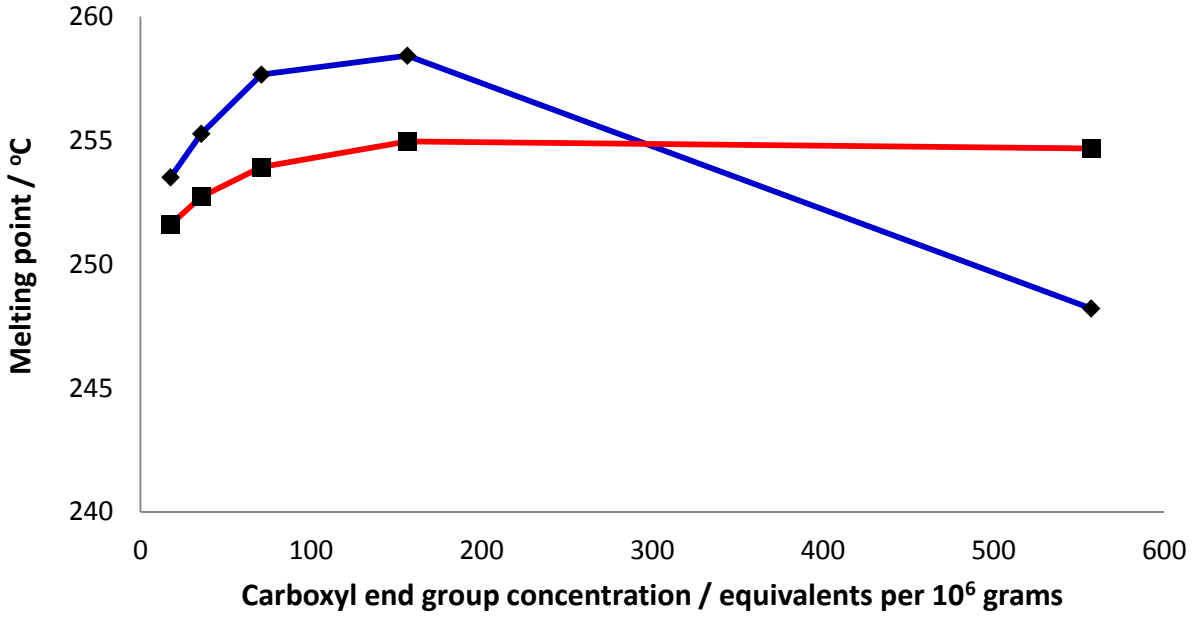

Figure A7.3.5 – Scatter plot of the melting point versus the end group concentration for the E239 samples that were prepared with the water being changed. The blue line represents the initial melting point and the red line represents the reheat melting point. A single sample was analysed.

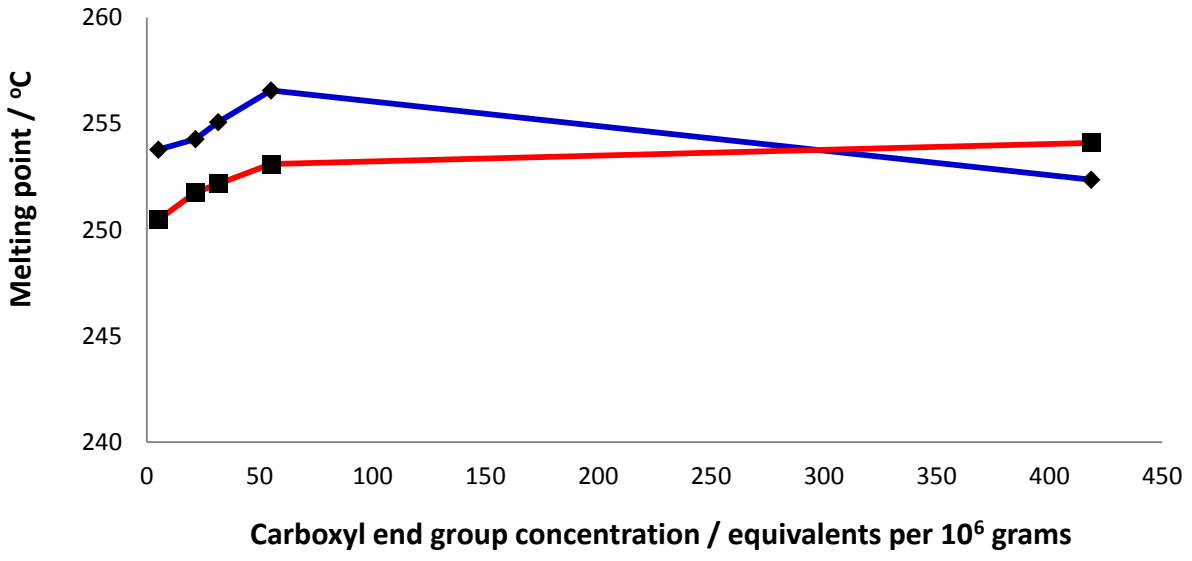

Figure A7.3.6 – Scatter plot of the melting point versus the end group concentration for the E239 + 1% Cardura samples that were prepared with the water being changed. The blue line represents the initial melting point and the red line represents the reheat melting point. A single sample was analysed.

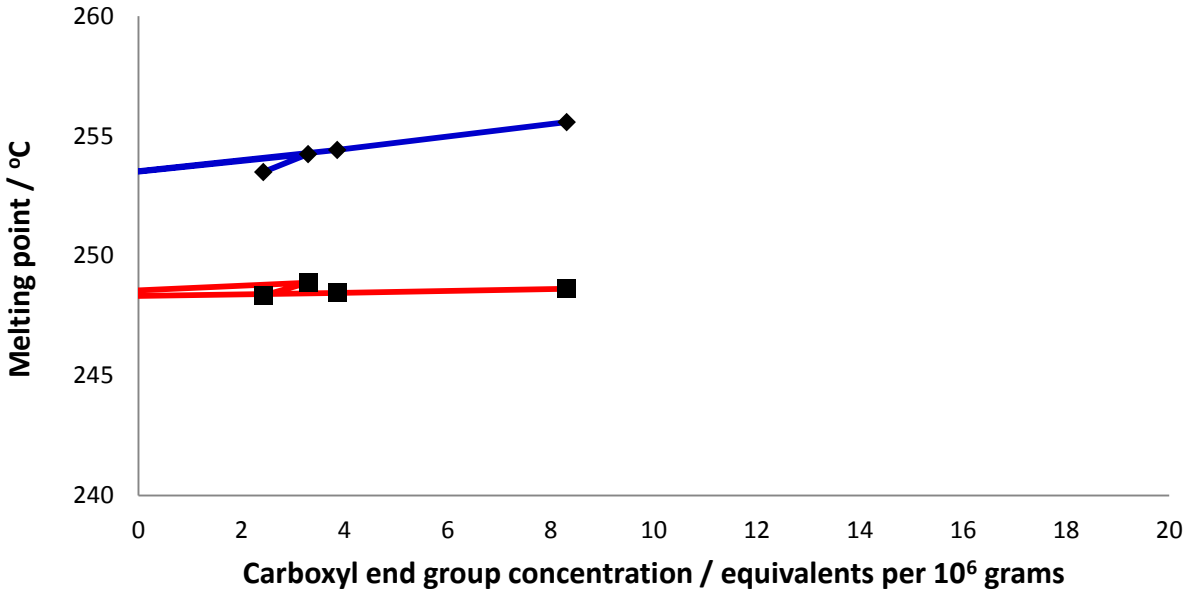

Figure A7.3.7 – Scatter plot of the melting point versus the end group concentration for the E239 + 6% Cardura samples that were prepared without the water being changed. The blue line represents the initial melting point and the red line represents the reheat melting point. A single sample was analysed.

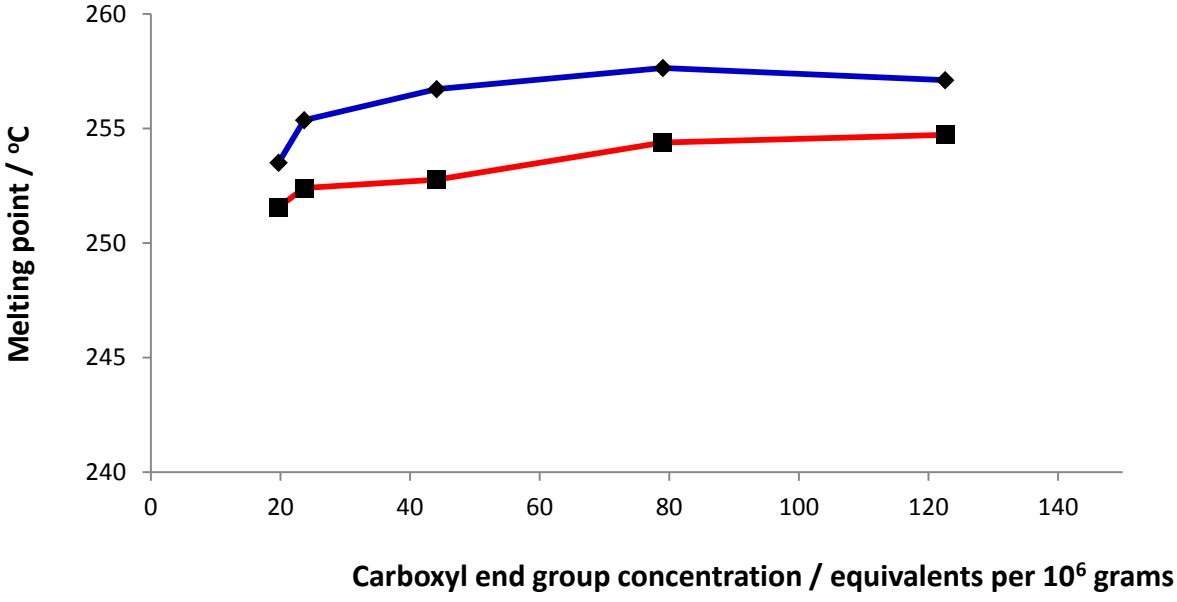

Figure A7.3.8 – Scatter plot of the melting point versus the end group concentration for the E239 samples that were prepared without the water being changed. The blue line represents the initial melting point and the red line represents the reheat melting point. A single sample was analysed.

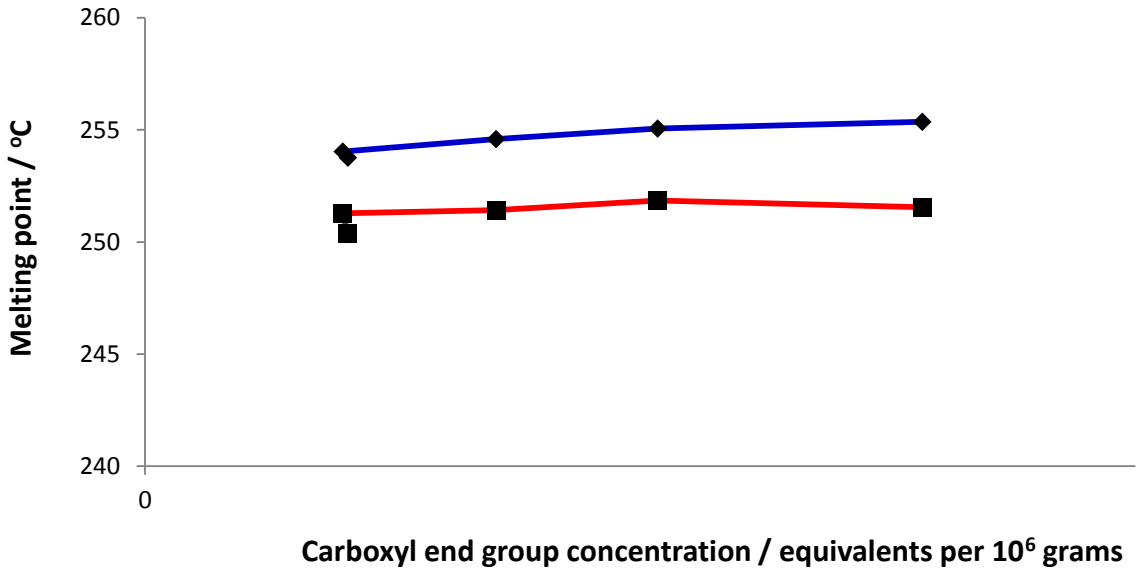

Figure A7.3.9 – Scatter plot of the melting point versus the end group concentration for the E239 + 1% Cardura samples that were prepared without the water being changed. The blue line represents the initial melting point and the red line represents the reheat melting point. A single sample was analysed.

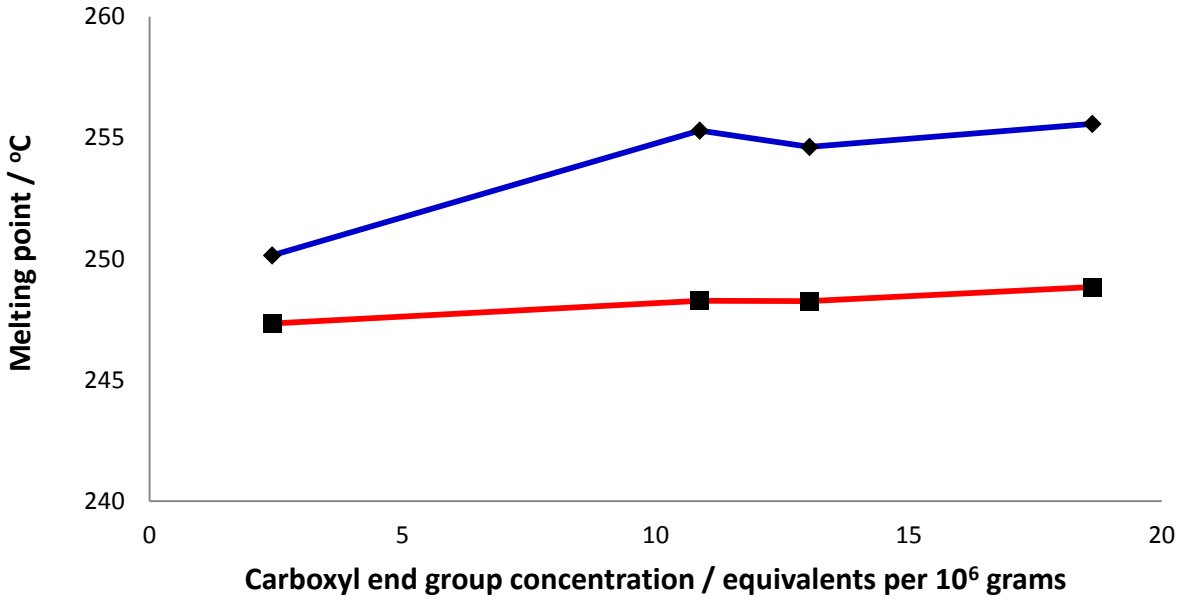

Figure A7.3.10 – Scatter plot of the melting point versus the end group concentration for the E239 + 6% Cardura samples that were prepared without the water being changed. The blue line represents the initial melting point and the red line represents the reheat melting point. A single sample was analysed.

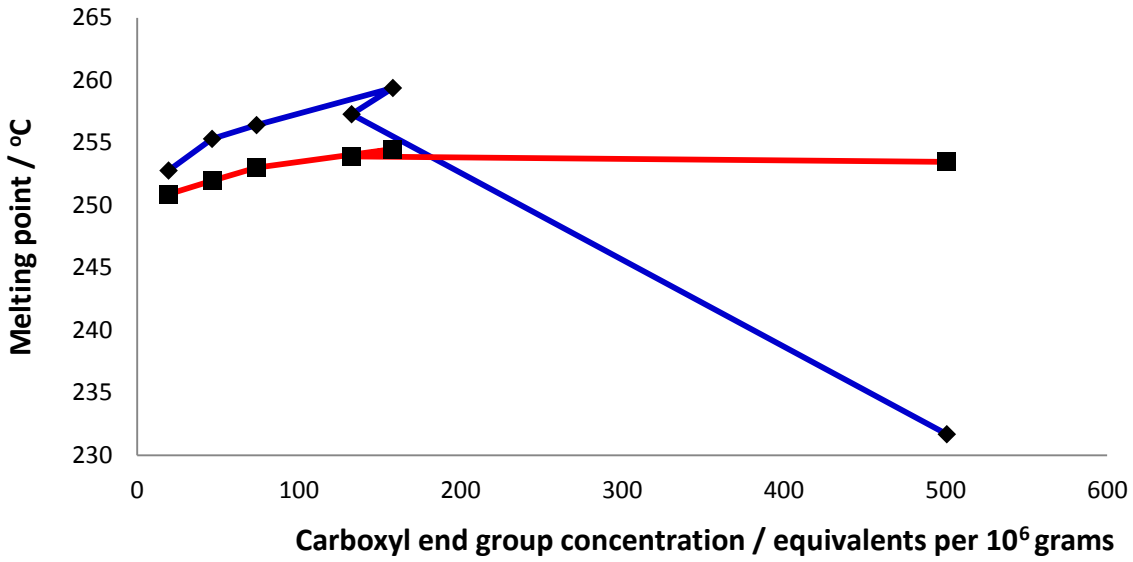

Figure A7.3.11 – Scatter plot of the melting point versus the end group concentration for the E240 samples that were prepared with the water being changed. The blue line represents the initial melting point and the red line represents the reheat melting point. A single sample was analysed.

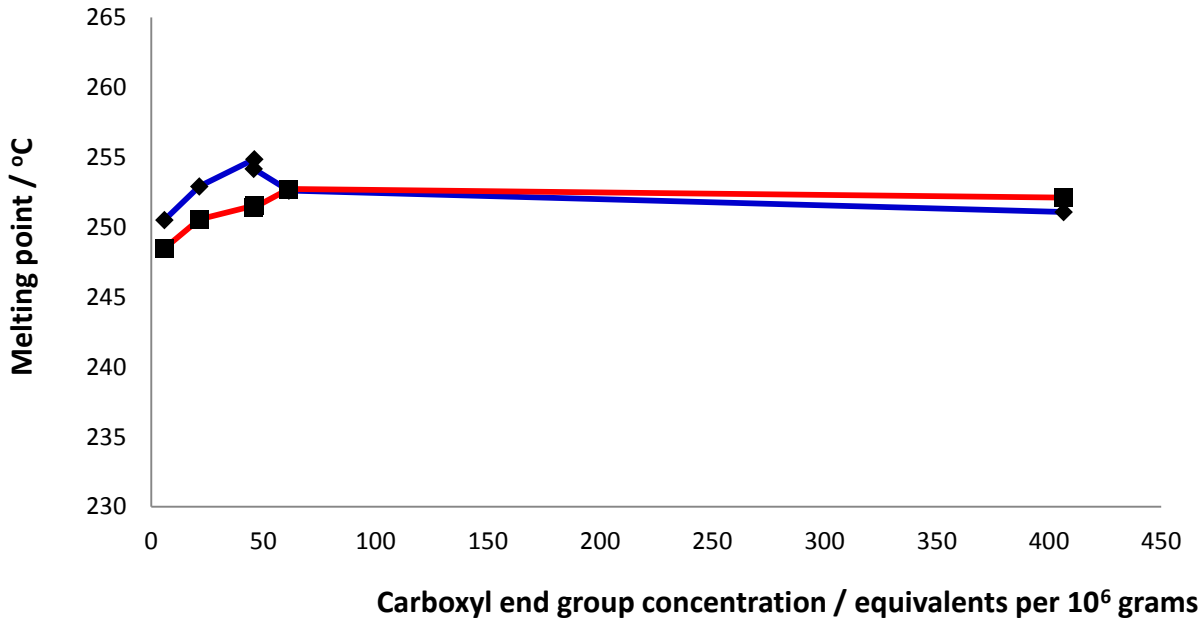

Figure A7.3.12 – Scatter plot of the melting point versus the end group concentration for the E240 + 1% Cardura samples that were prepared with the water being changed. The blue line represents the initial melting point and the red line represents the reheat melting point. A single sample was analysed.

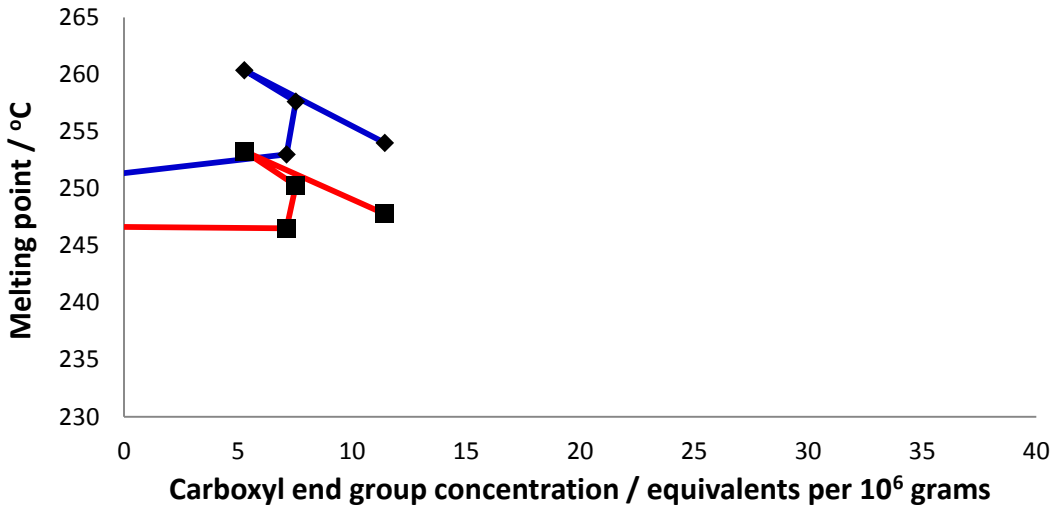

Figure A7.3.13 – Scatter plot of the melting point versus the end group concentration for the E240 + 6% Cardura samples that were prepared with the water being changed. The blue line represents the initial melting point and the red line represents the reheat melting point. A single sample was analysed.

A7 – Chapter 7 –Characterisation of the Degradation Behaviour, Hydrolytic Degradation – IR

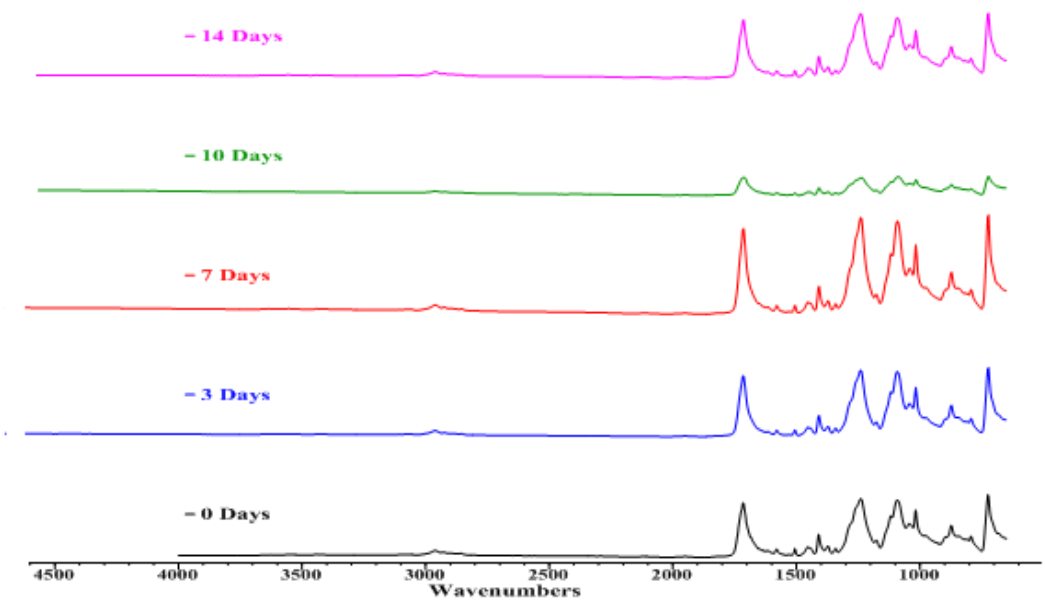

Figure A7.4.1 – IR spectra of the E187 + 1% Cardura samples aged at room temperature for up to 14 days. A single spectra is shown for each time point.

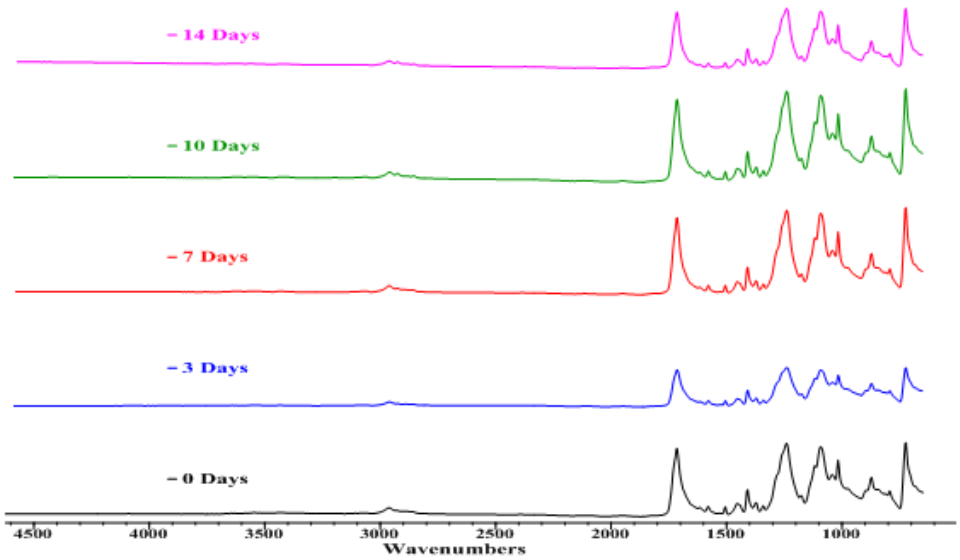

Figure A7.4.2 – IR spectra of the E187 + 6% Cardura samples aged at room temperature for up to 14 days. A single spectra is shown for each time point.

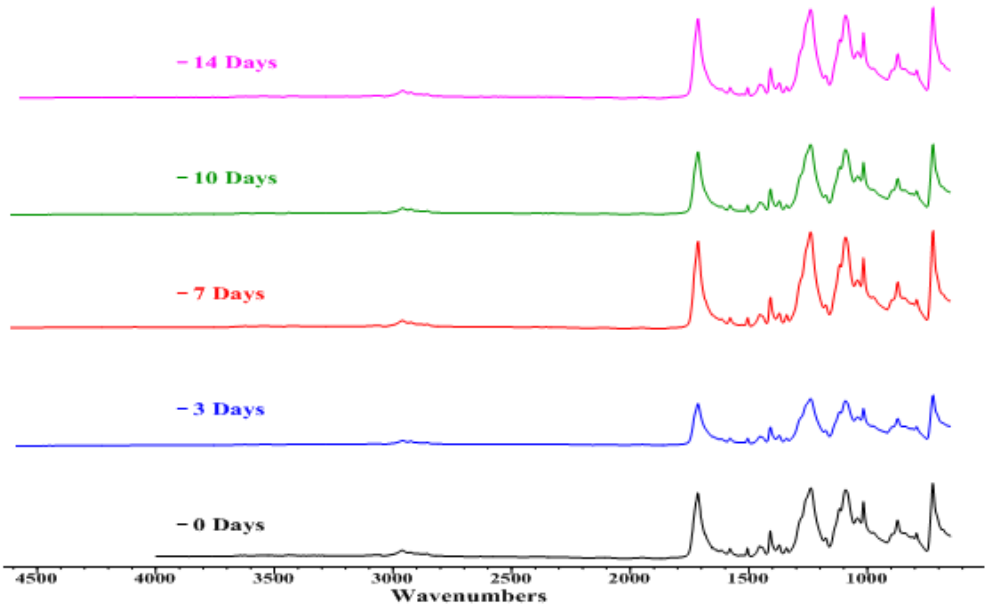

Figure A7.4.3 – IR spectra of the E187 + 1% Cardura samples aged at 50 °C for up to 14 days. A single spectra is shown for each time point.

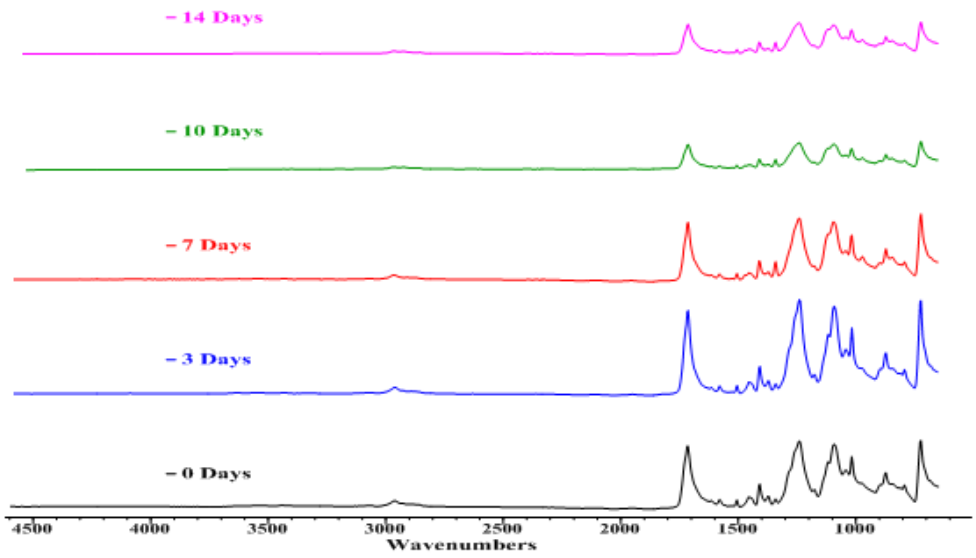

Figure A7.4.4 – IR spectra of the E187 + 6% Cardura samples aged at 50 °C for up to 14 days. A single spectra is shown for each time point.

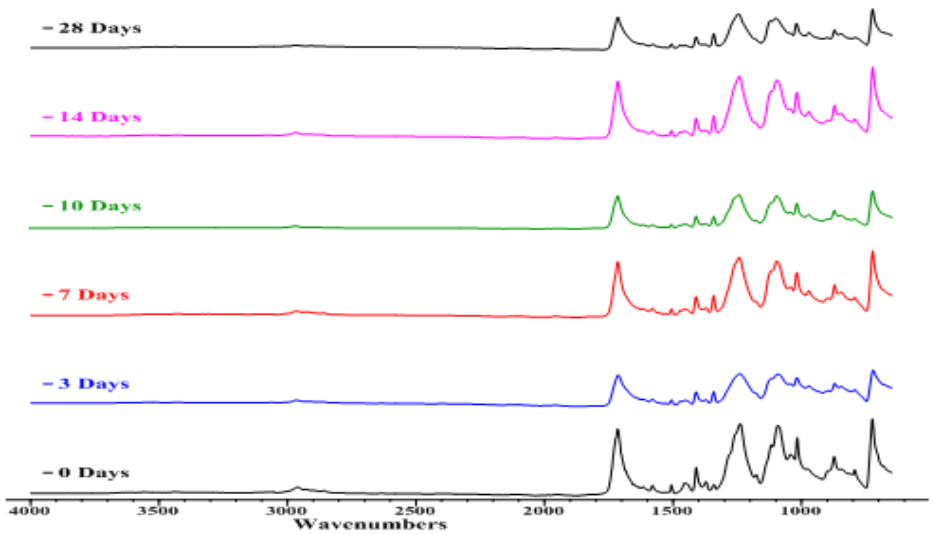

Figure A7.4.5 – IR spectra of the E187 + 1% Cardura samples aged at 100 °C for up to 28 days. A single spectra is shown for each time point.

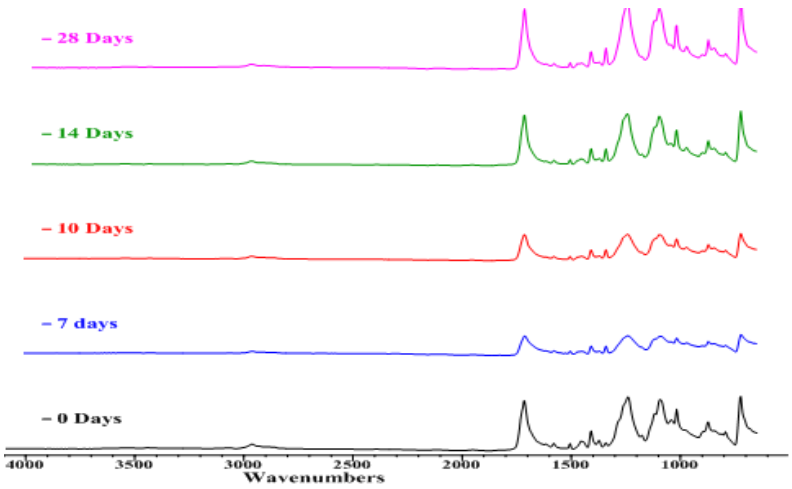

Figure A7.4.6 – IR spectra of the E187 + 1% Cardura samples aged at 100 °C for up to 28 days. A single spectra is shown for each time point.

A8 – Chapter 8 –Characterisation of the Degradation Behaviour, Thermal Degradation – DSC

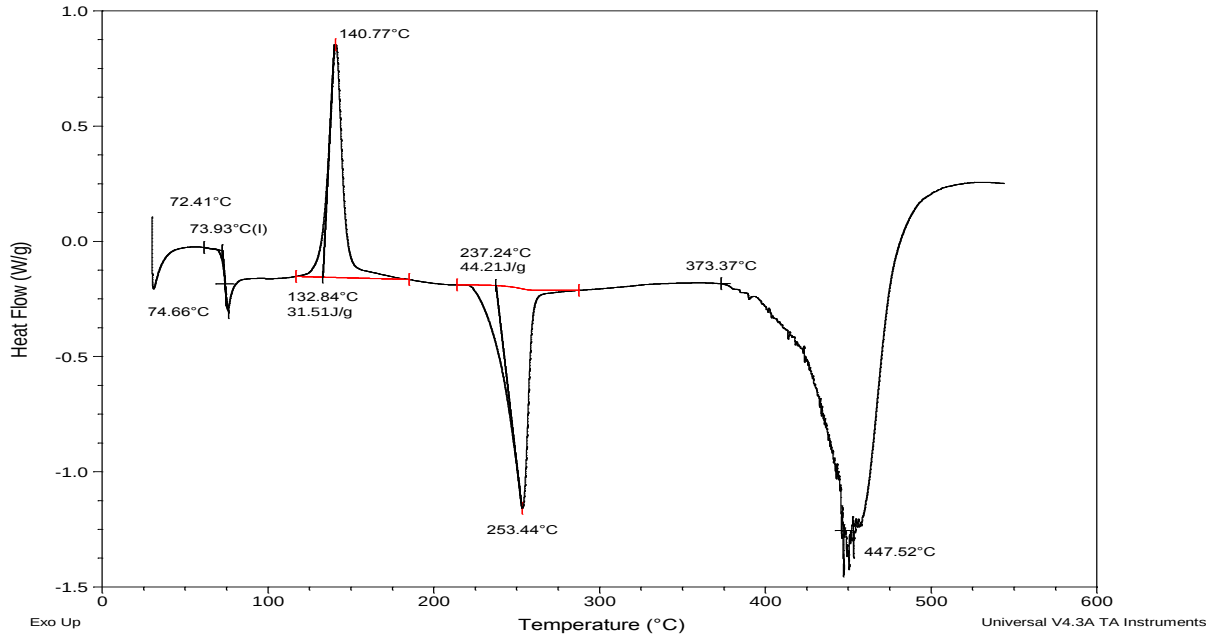

Figure A8.1.1 – DSC scan of the E187 + 6% Heloxy sample. A single sample was analysed.

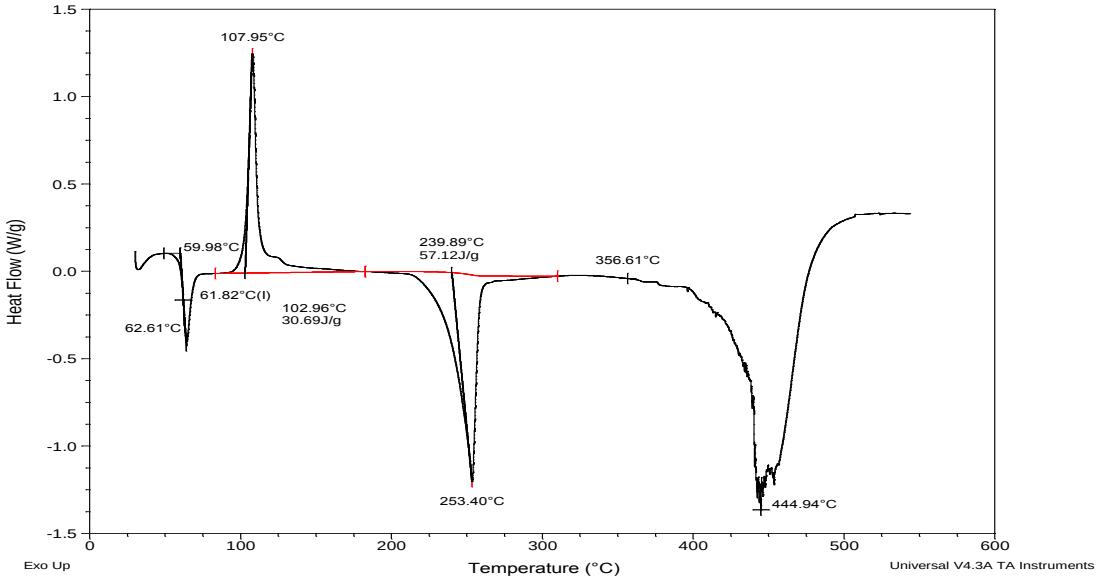

Figure A8.1.2 – DSC scan of the E187 + 6% Vikolox sample. A single sample was analysed.

A8 – Chapter 8 –Characterisation of the Degradation Behaviour, Thermal Degradation – TGA

.

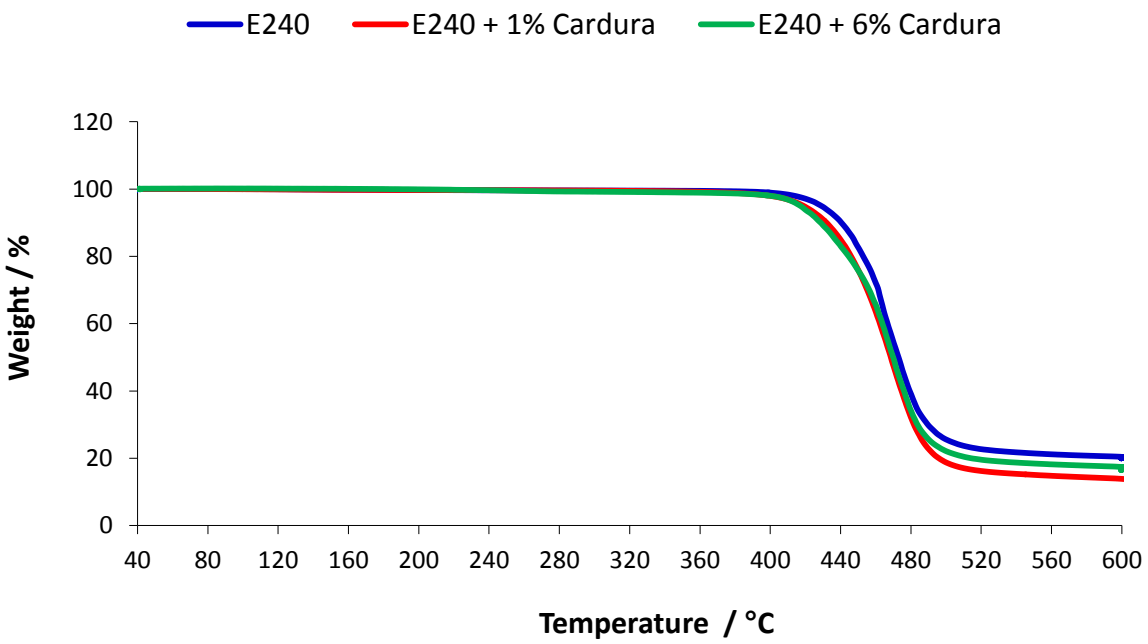

Figure A8.2.1 – TGA thermogram showing the mass loss of the E240 samples. A single sample was analysed.

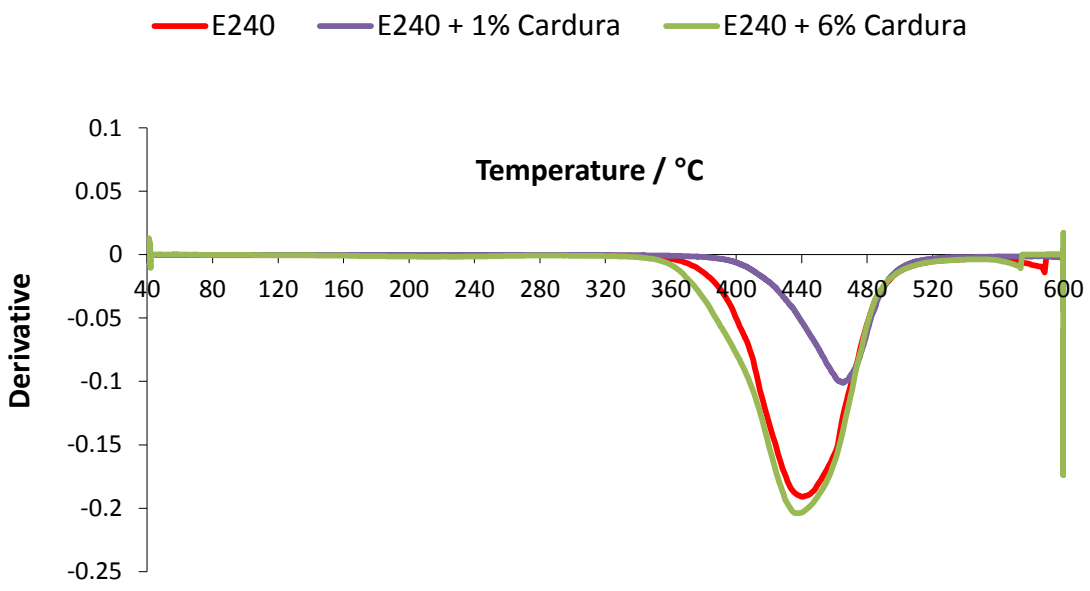

Figure A8.2.2– TGA thermogram showing the derivative of the E240 samples. A single sample was analysed.

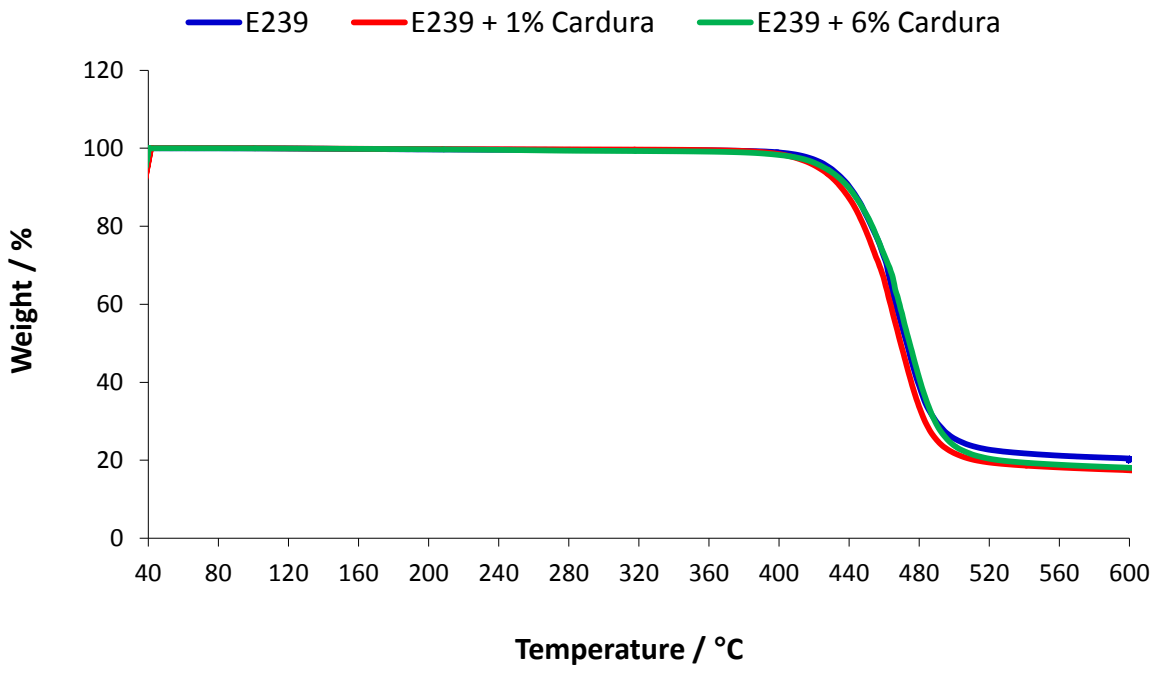

Figure A8.2.3 – TGA thermogram showing the mass loss of the E239 samples. A single sample was analysed.

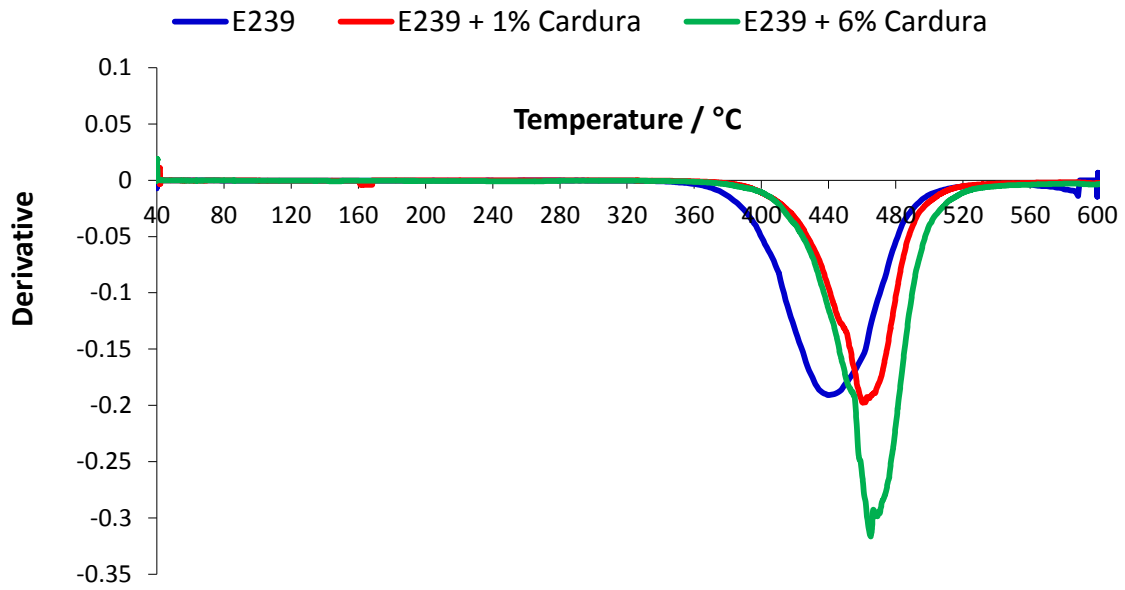

Figure A8.2.4 – TGA thermogram showing the mass loss of the E239 samples. A single sample was analysed.

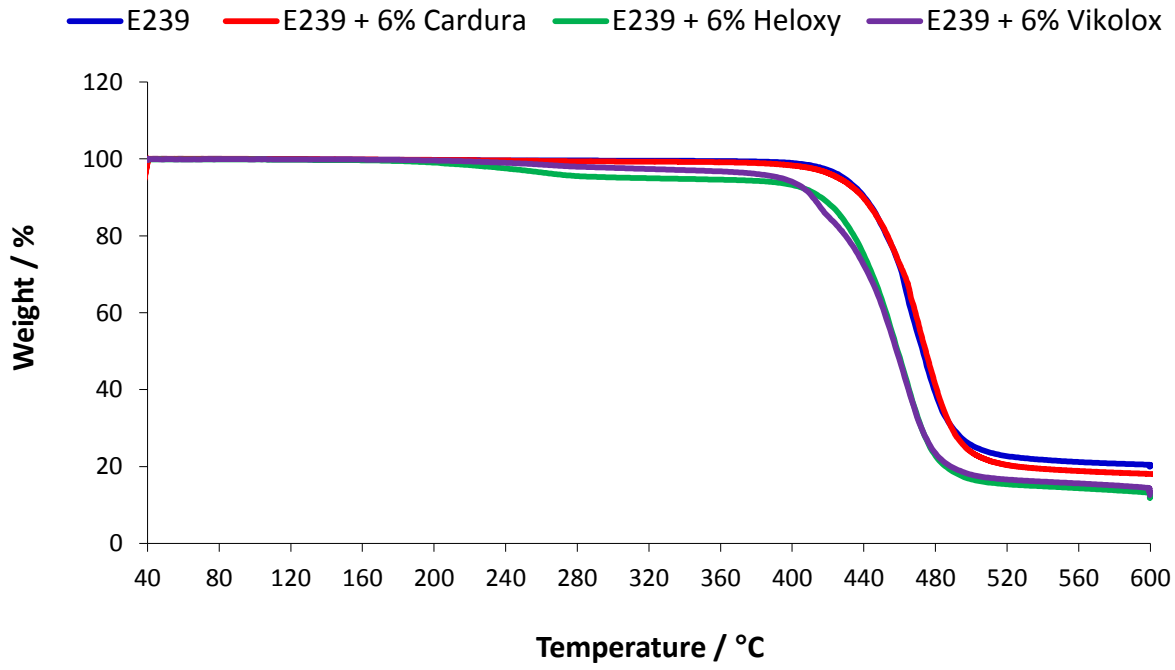

Figure A8.2.5 – TGA thermogram showing the mass loss of the E239 samples with different epoxides. A single sample was analysed

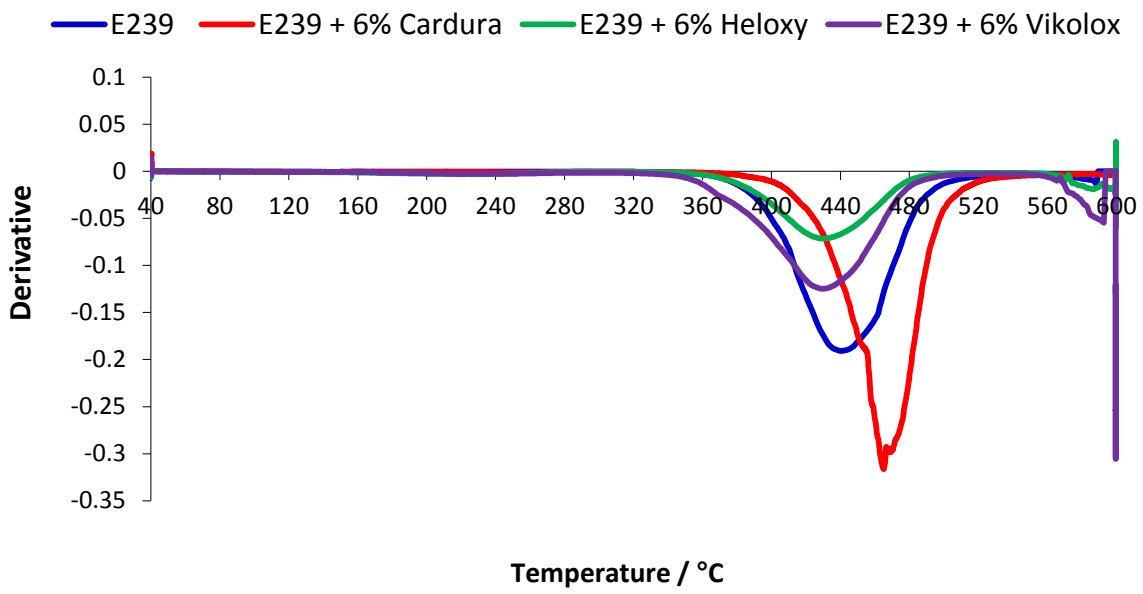

Figure A8.2.6 – TGA thermogram showing the derivative of the E239 samples with different epoxides. A single sample was analysed.

A8 – Chapter 8 –Characterisation of the Degradation Behaviour, Thermal Degradation – TVA

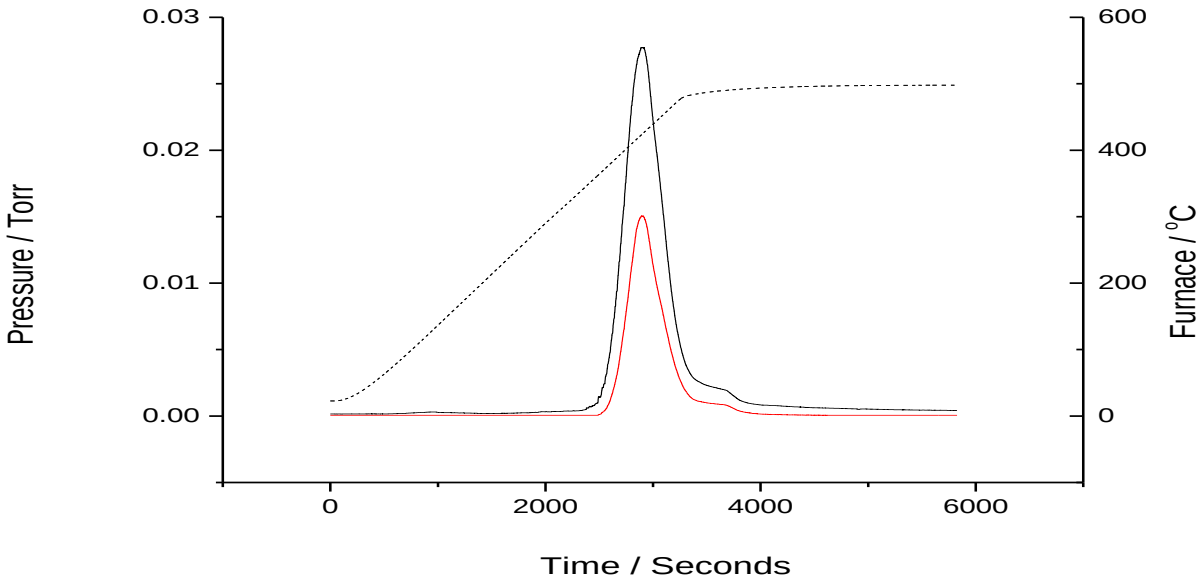

Figure A8.3.1 – TVA thermogram for the E187 + 1% sample. A single sample was analysed.

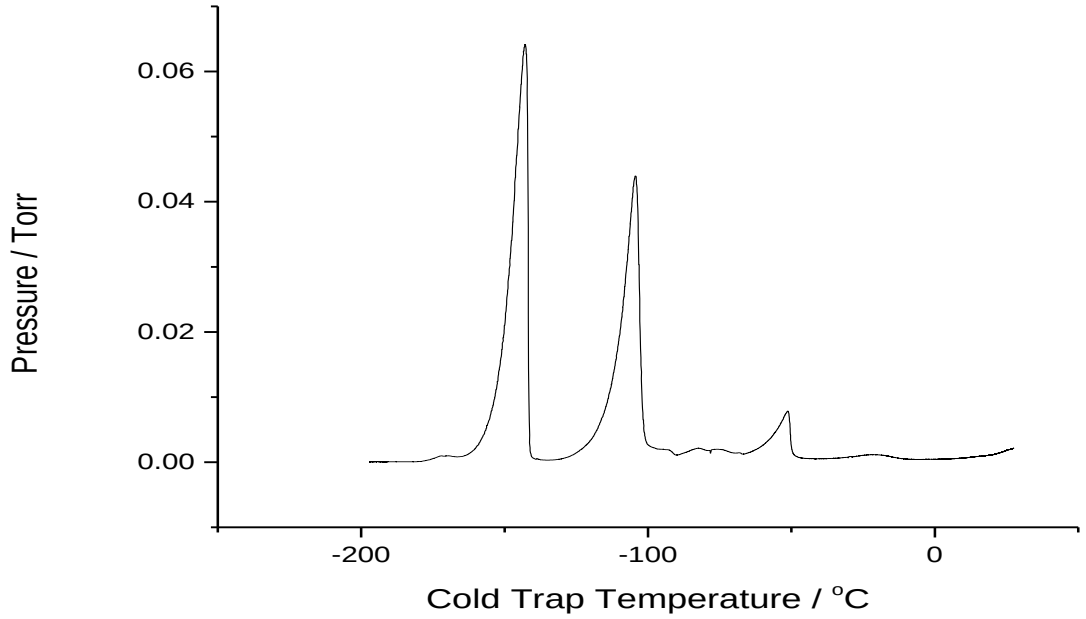

Figure A8.3.2 – SATVA trace for the E187 + 1% Cardura sample. A single sample was analysed.

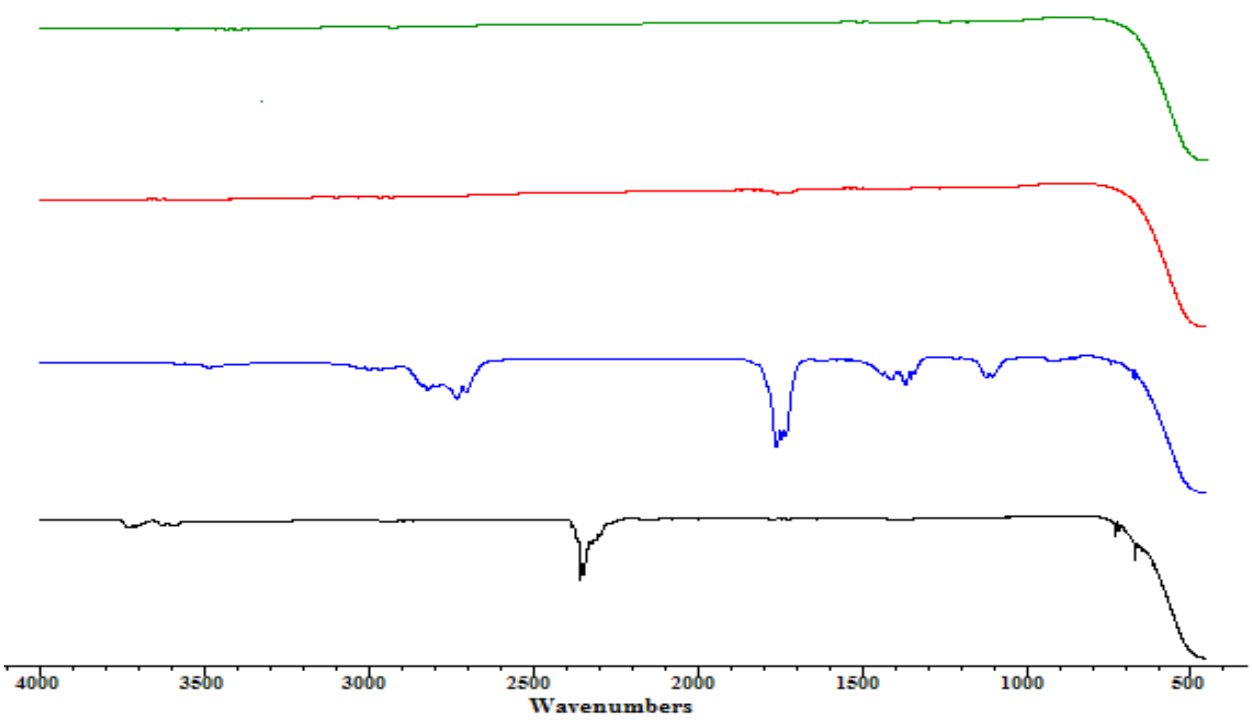

Figure A8.3.3 – IR spectra of the volatiles released from the E187 + 1% Cardura sample. The black IR spectra of limb one, the blue IR spectra of limb two, the red IR spectra of limb three and green IR spectra of limb four are shown. A single sample was analysed

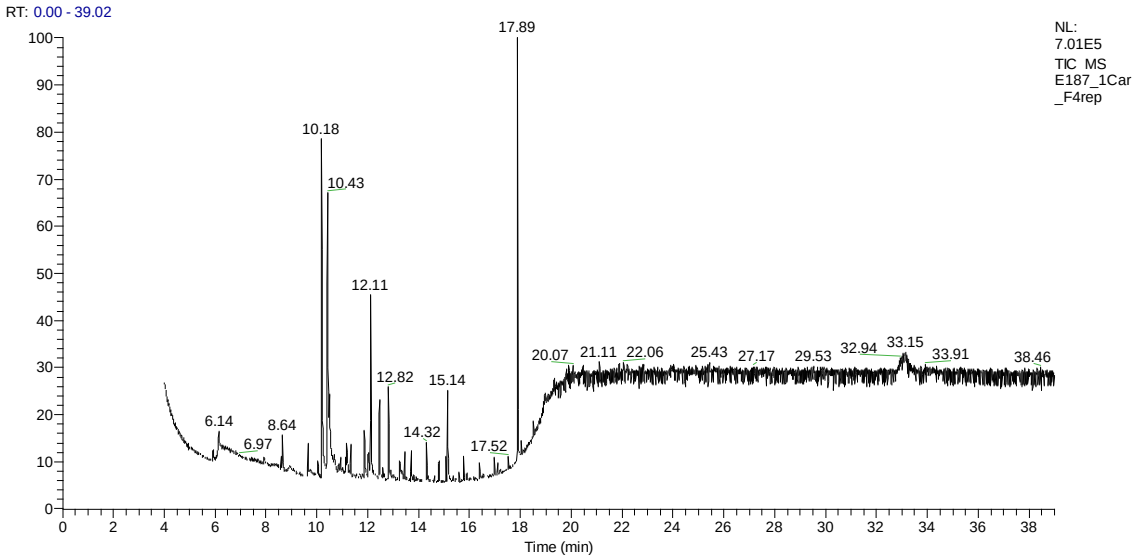

Figure A8.3.4 – Chromatogram generated for the fourth fraction of the E187 + 1% Cardura. Sample was analysed in EI mode. A single sample was analysed.

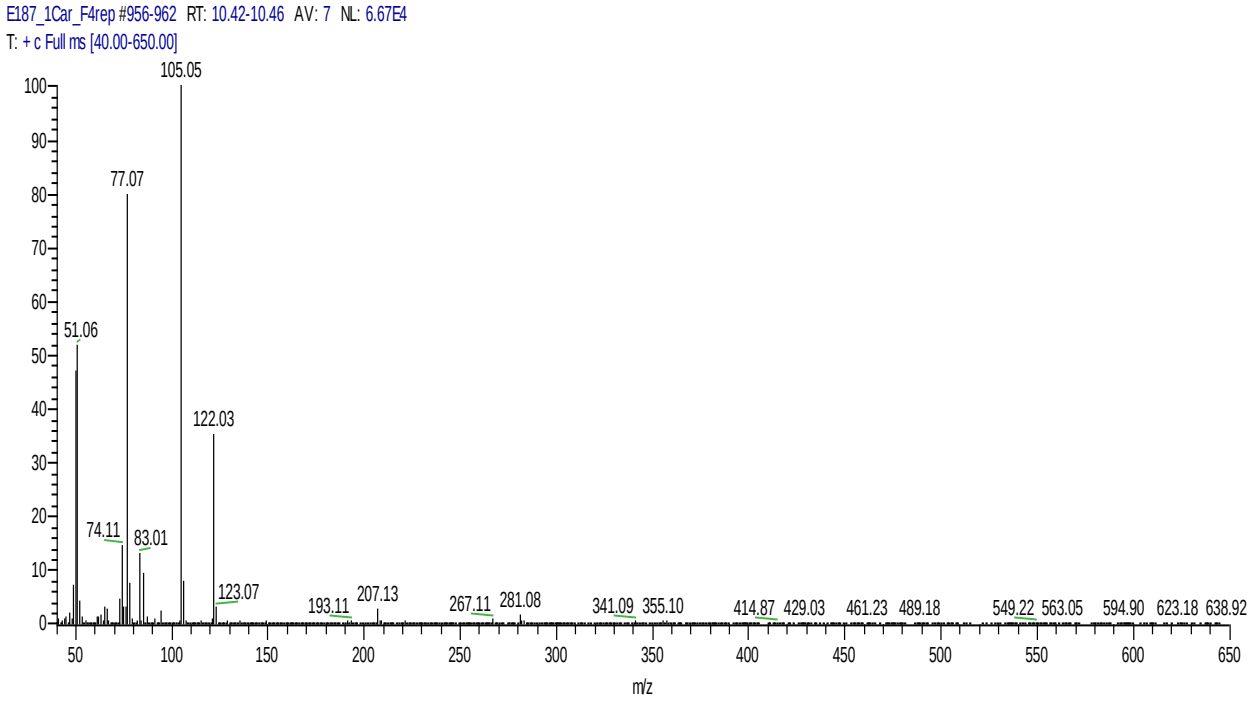

Figure A8.3.5 – Mass spectrum of the peak with a retention time of 10.42-10.46 minutes in the gas chromatogram generated for the TVA line extract of an E187 + 1% Cardura sample. A single sample was analysed.

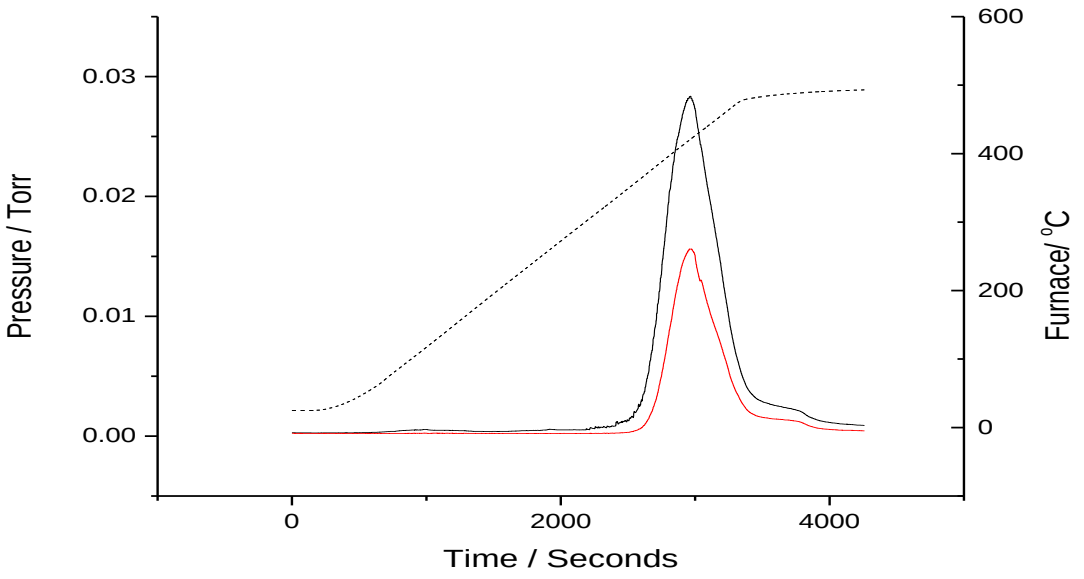

Figure A8.3.6– TVA thermogram for the E187 + 6% Cardura sample. A single sample was analysed.

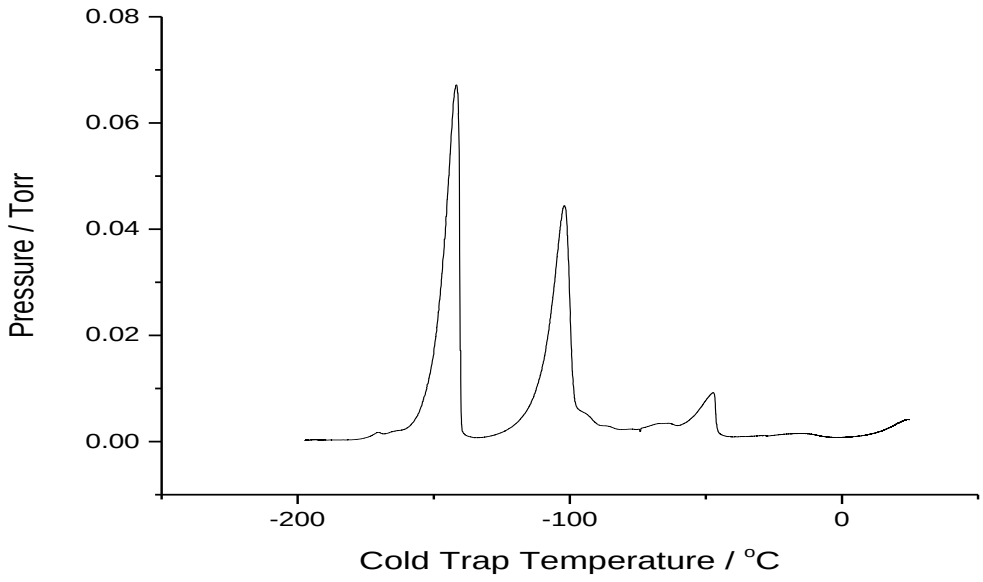

Figure A8.3.7 – SATVA trace for the E187 + 6% Cardura sample. A single sample was analysed.

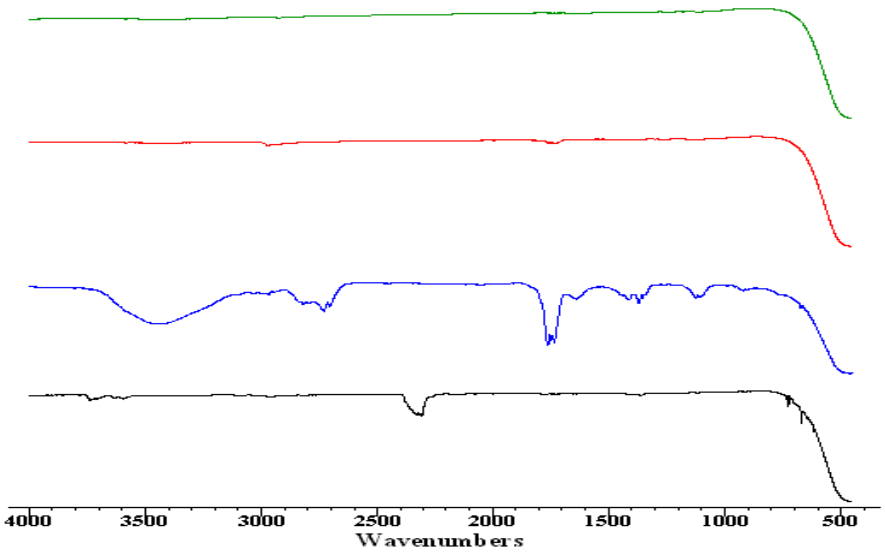

Figure A8.3.8 – IR spectra of the volatiles released from the E187 + 6% Cardura sample. The black IR spectra of limb one, the blue IR spectra of limb two, the red IR spectra of limb three and green IR spectra of limb four are shown. A single sample was analysed.

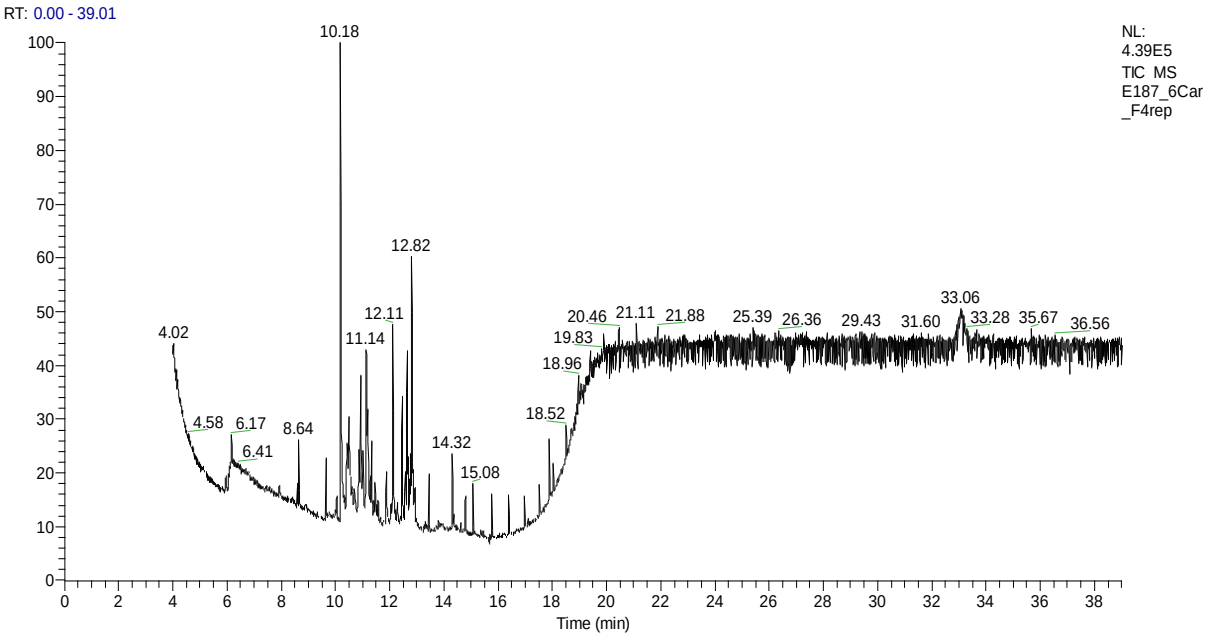

Figure A8.3.9 – Chromatogram generated for the fourth fraction of the E187 + 6% Cardura. A single sample was analysed.

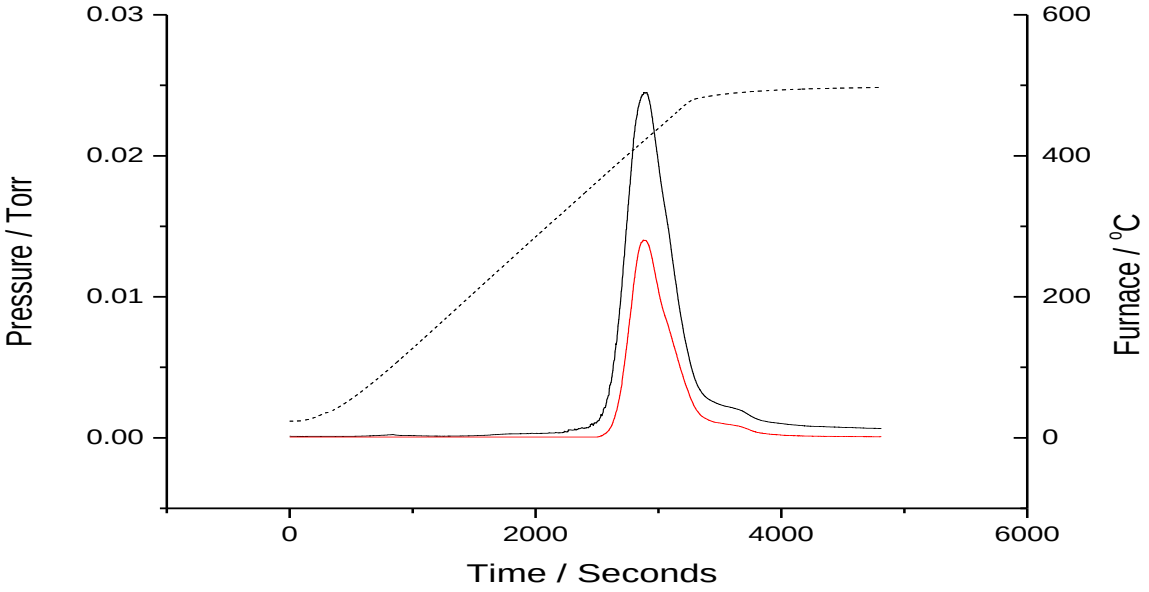

Figure A8.3.10 – TVA thermogram for the E187 + 1% Heloxy sample. A single sample was analysed.

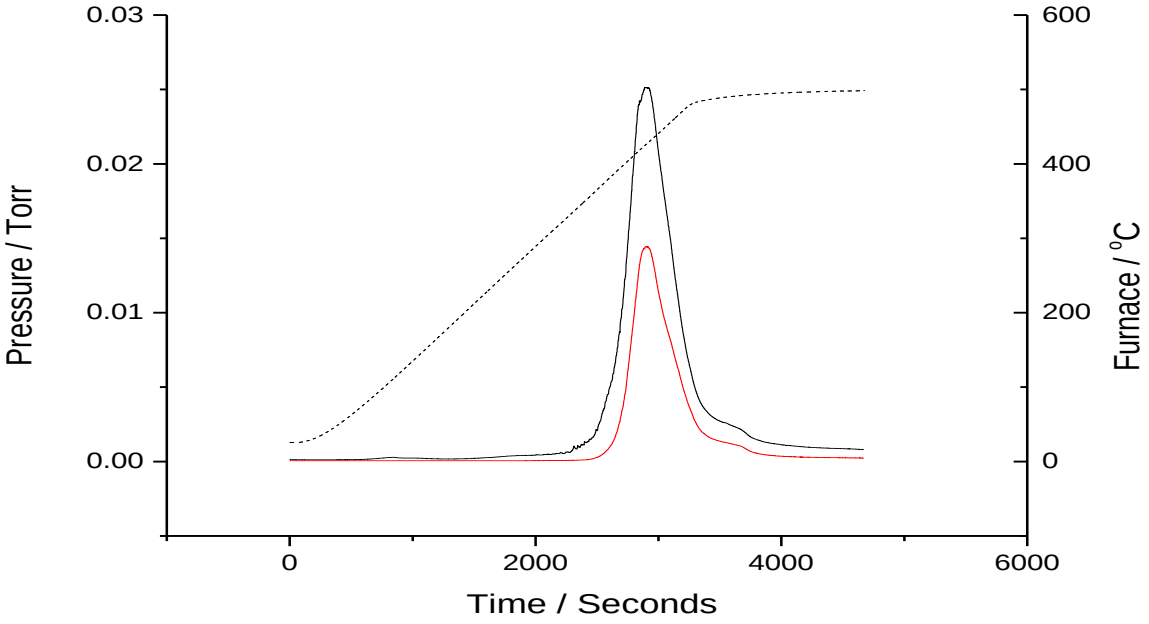

Figure A8.3.11 – TVA thermogram for the E187 + 6% Heloxy sample. A single sample was analysed.

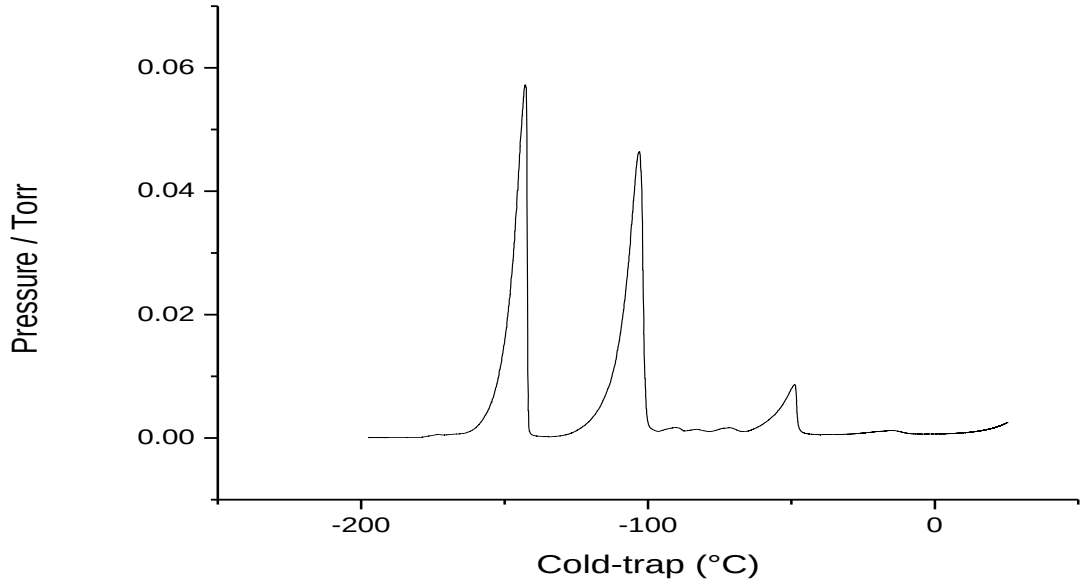

Figure A8.3.12 – SATVA trace for the E187 + 1% Heloxy sample. A single sample was analysed.

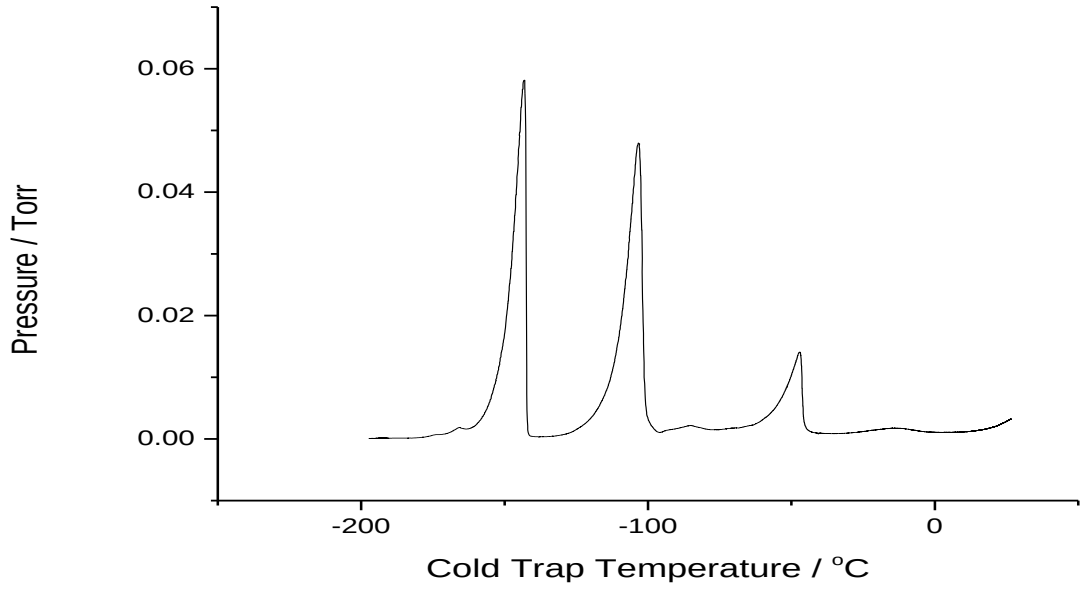

Figure A8.3.13 – SATVA trace for the E187 + 6% Heloxy sample. A single sample was analysed.

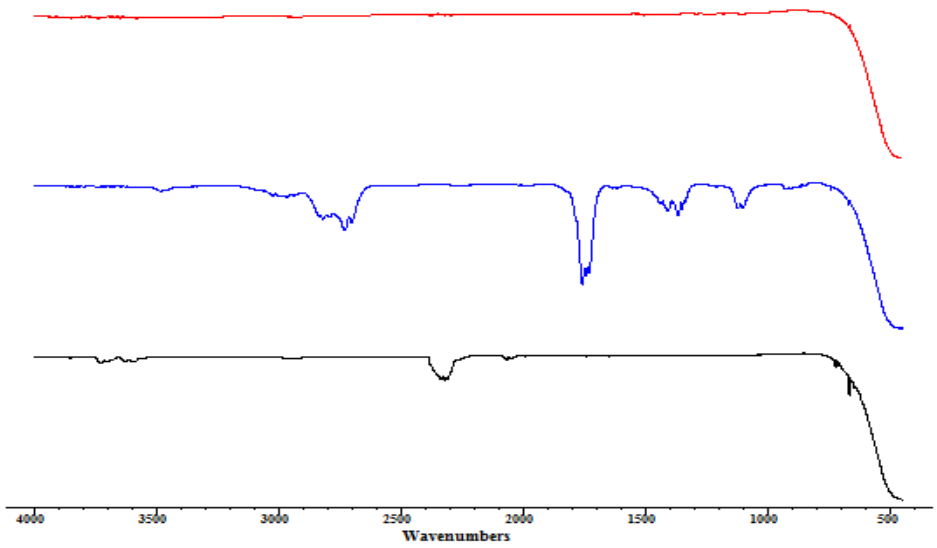

Figure A8.3.14 – IR spectra of the volatiles released from the E187 + 6% Heloxy sample. The black IR spectra of limb one, the blue IR spectra of limb two and the red IR spectra of limb three are shown. A single sample was analysed.

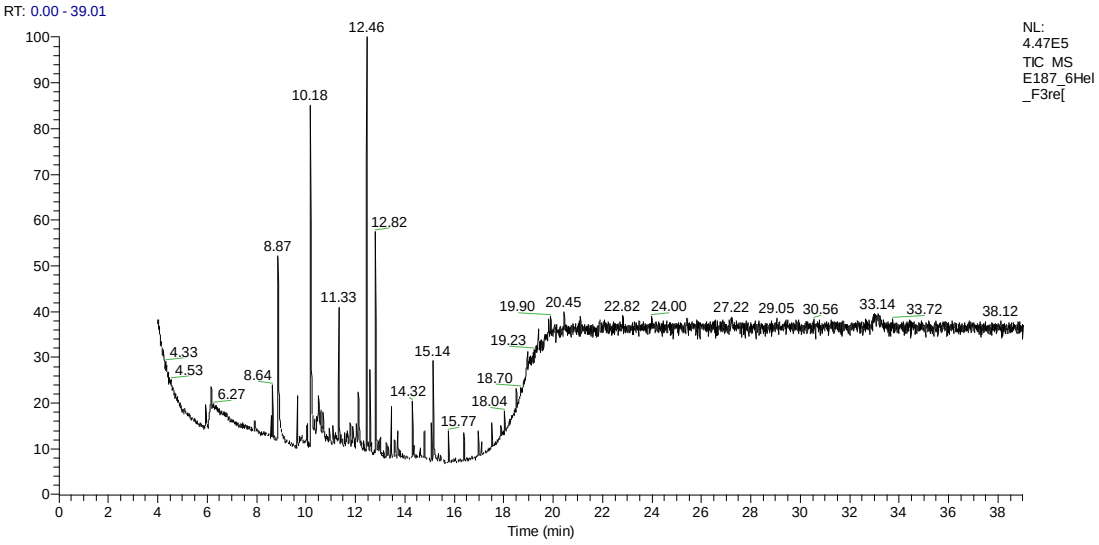

Figure A8.3.15 – Chromatogram generated for the third fraction of the E187 + 6% Heloxy. Sample was analysed in EI mode. A single sample was analysed.

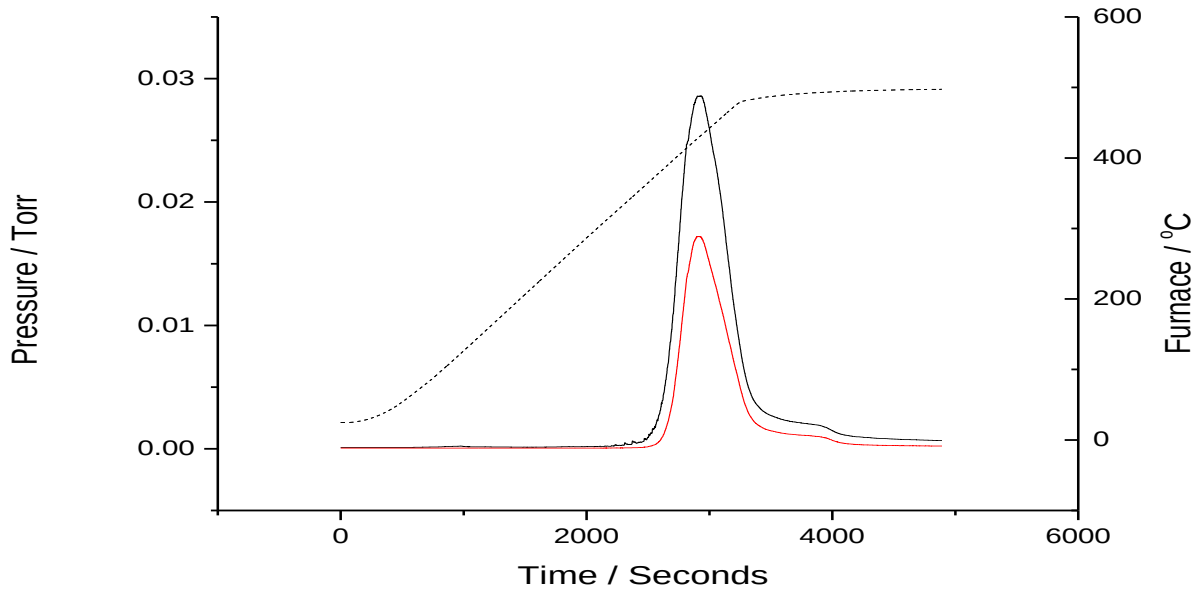

Figure A8.3.16 – TVA thermogram for the E187 + 1% Vikolox sample. A single sample was analysed.

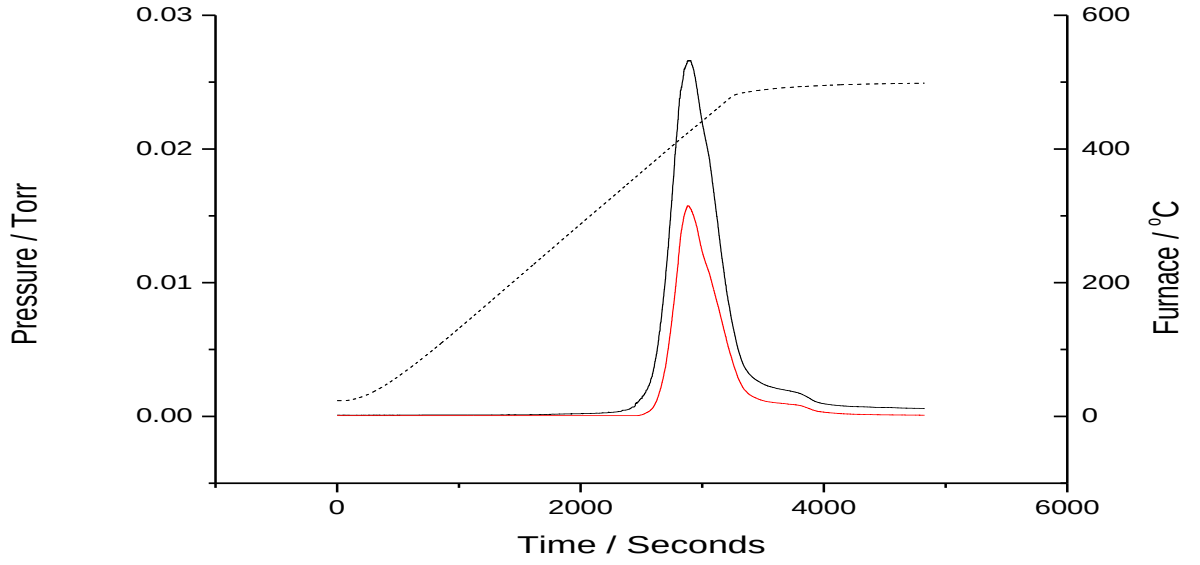

Figure A8.8.17– TVA thermogram for the E187 + 6% Vikolox sample. A single sample was analysed.

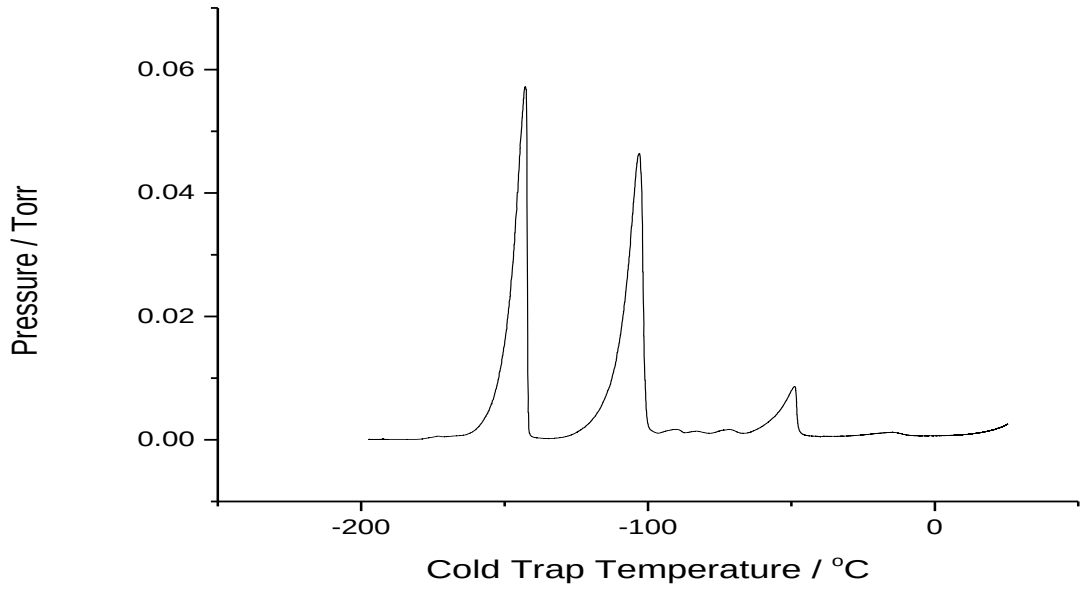

Figure A8.3.18 – SATVA trace for the E187 + 1% Vikolox sample. A single sample was analysed.

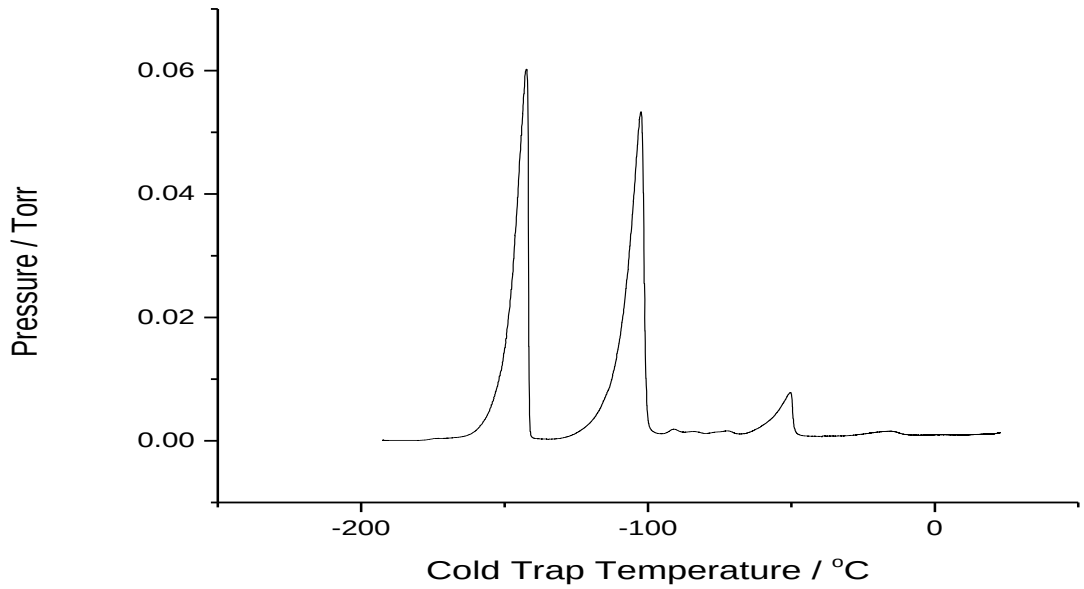

Figure A8.3.19 – SATVA trace for the E187 + 6% Vikolox sample. A single sample was analysed.

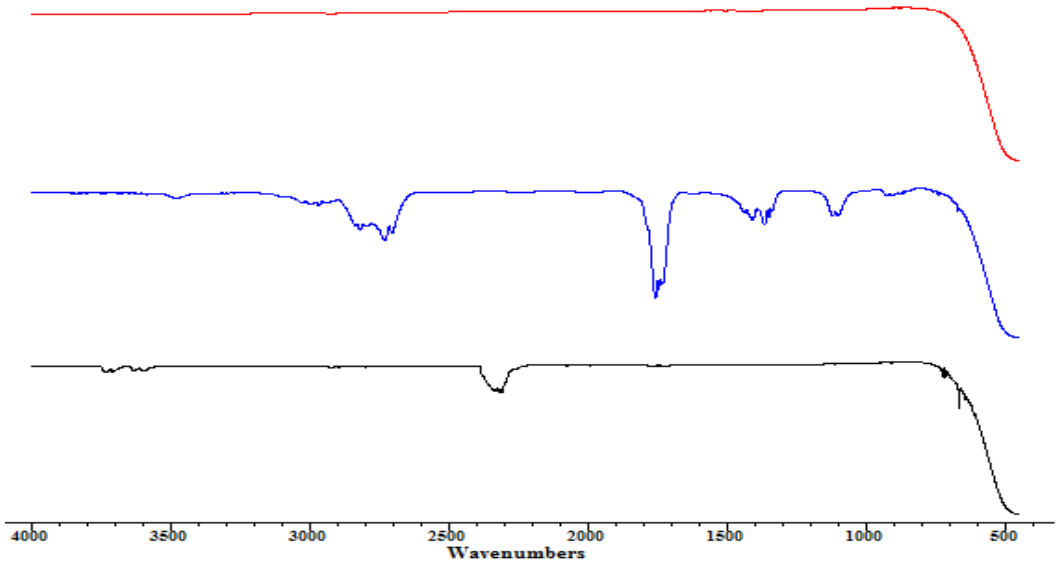

Figure A8.3.20– IR spectra of the volatiles released from the E187 + 6% Vikolox sample. The black IR spectra of limb one, the blue IR spectra of limb two and the red IR spectra of limb three are shown. A single sample was analysed.

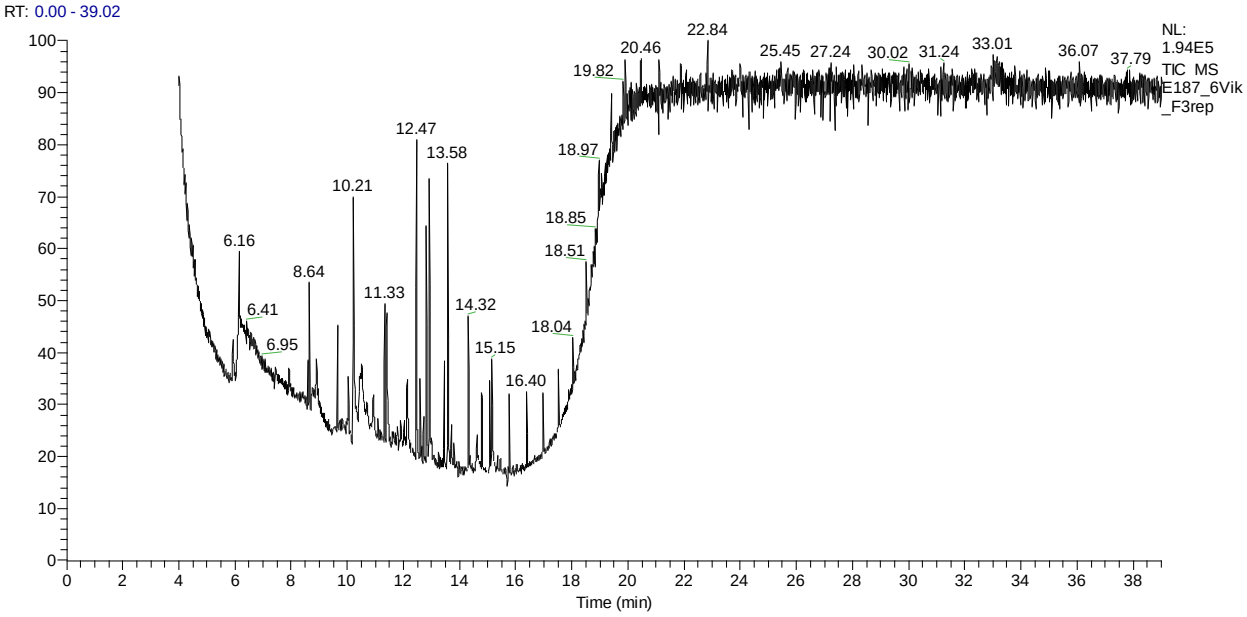

Figure A8.3.21 – Chromatogram generated for the third fraction of the E187 + 6% Vikolox. Sample was analysed in EI mode. A single sample was analysed.

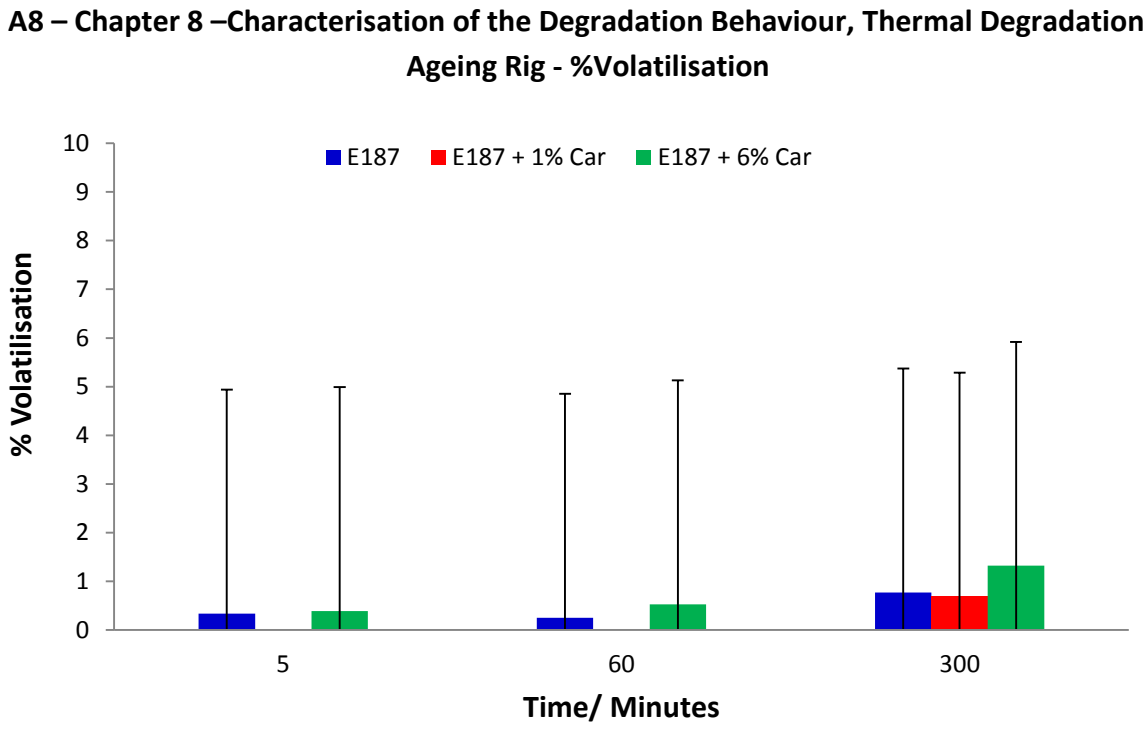

Figure A8.4.1 – Bar chart showing the % volatilisations for the E187 samples aged for 5, 60 and 300 minutes in nitrogen on the ageing rig at 290 °C. N=1. The error bar is 4.20% which is the calculated error in the method.

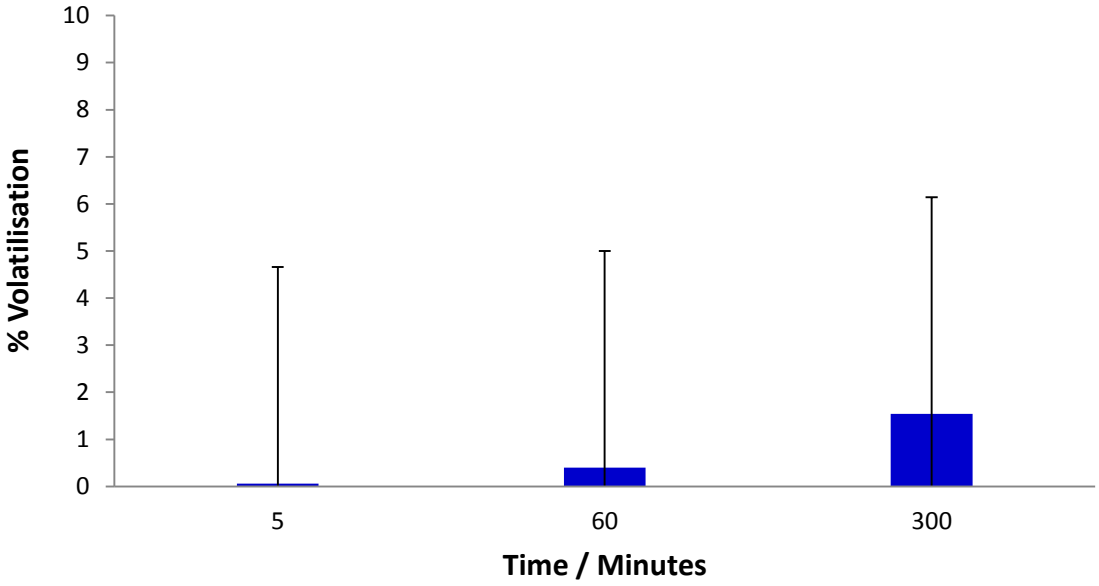

Figure A8.4.2 – Bar chart showing the % volatilisations for the E187 samples aged for 5, 60 and 300 minutes in nitrogen on the ageing rig at 305 °C. N=1. The error bar is 4.20% which is the calculated error in the method.

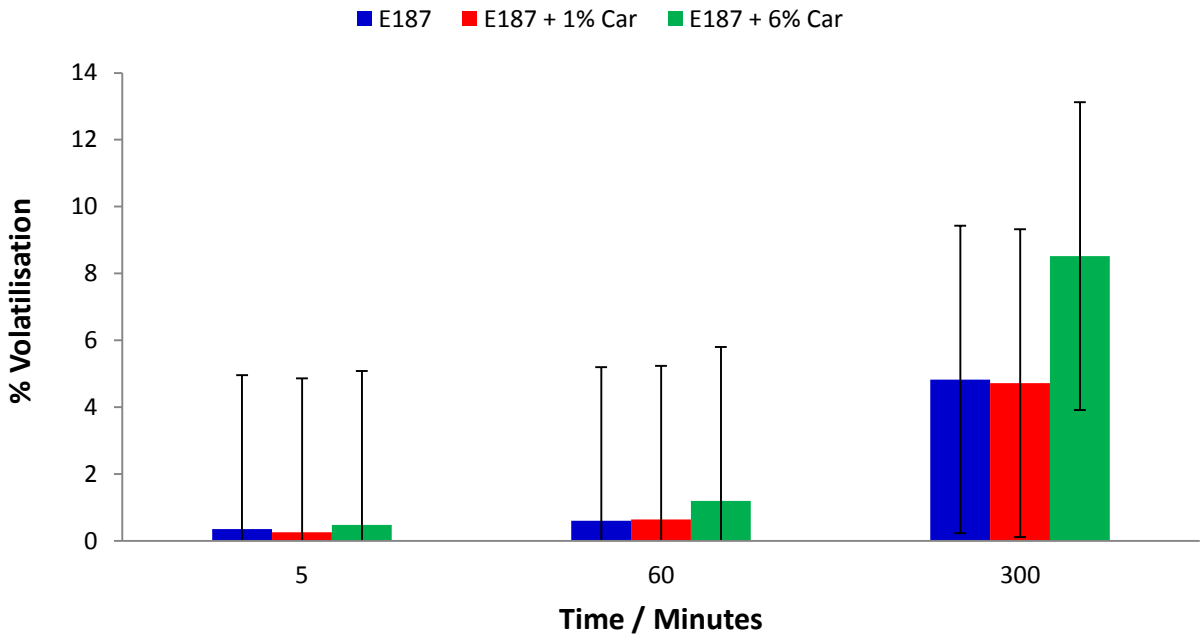

Figure A8.4.3 – Bar chart showing the % volatilisations for the E187 samples aged for 5, 60 and 300 minutes in nitrogen on the ageing rig at 320 °C. N=1. The error bar is 4.20% which is the calculated error in the method.

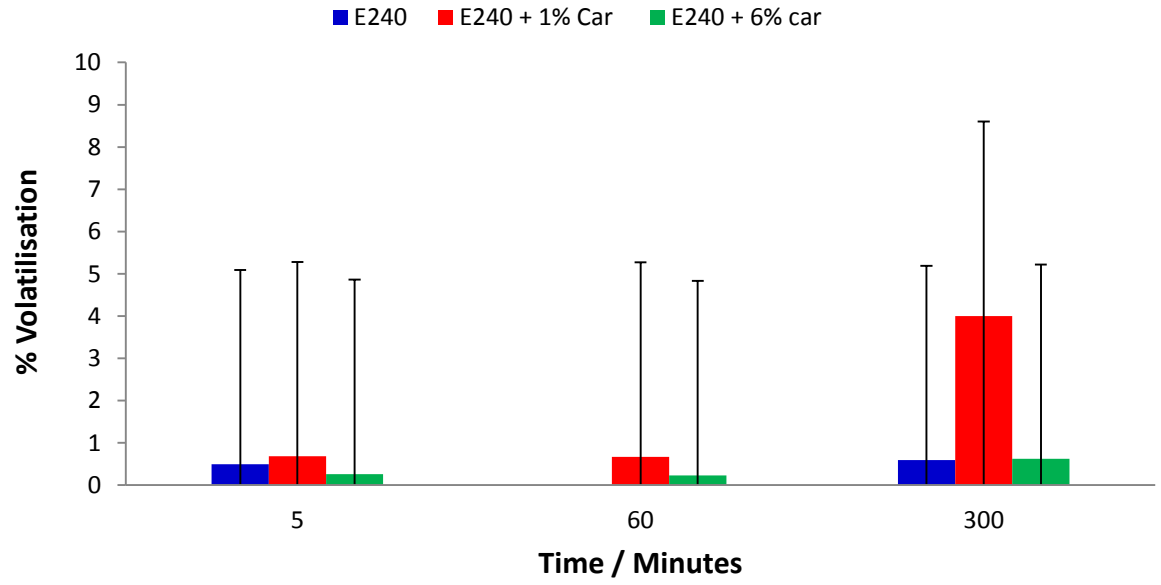

Figure A8.4.4 – Bar chart showing the % volatilisations for the E240 samples aged for 5, 60 and 300 minutes in nitrogen on the ageing rig at 290 °C. N=1. The error bar is 4.20% which is the calculated error in the method.

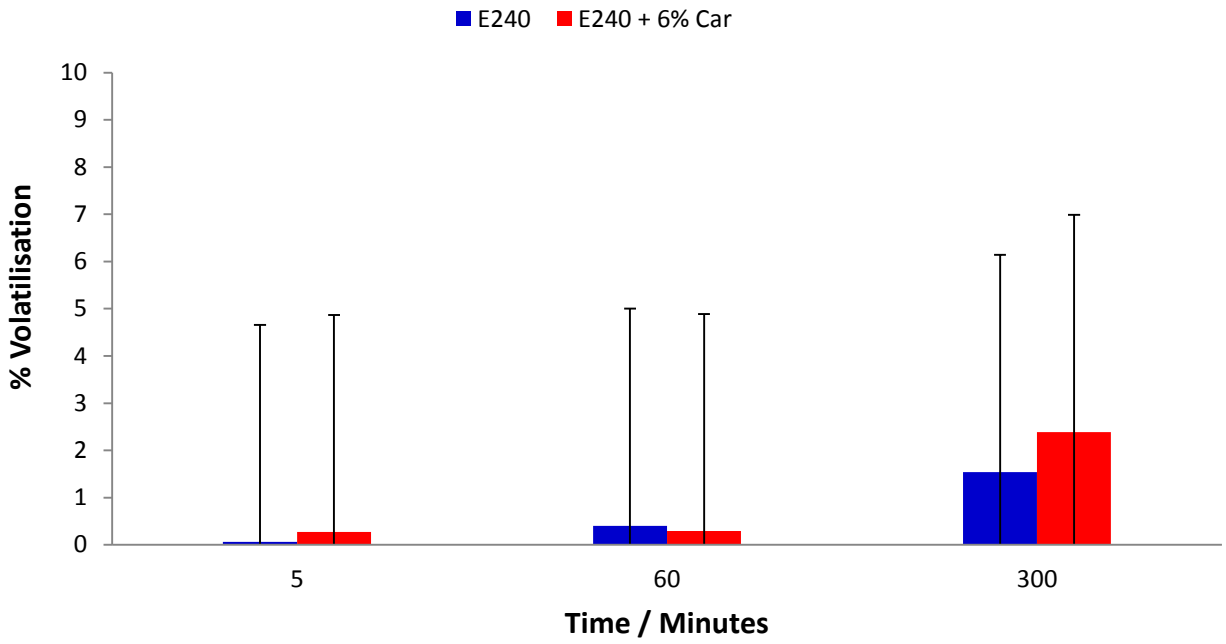

Figure A8.4.5 – Bar chart showing the % volatilisations for the E239 samples aged for 5, 60 and 300 minutes in nitrogen on the ageing rig at 305 °C. N=1. The error bar is 4.20% which is the calculated error in the method.

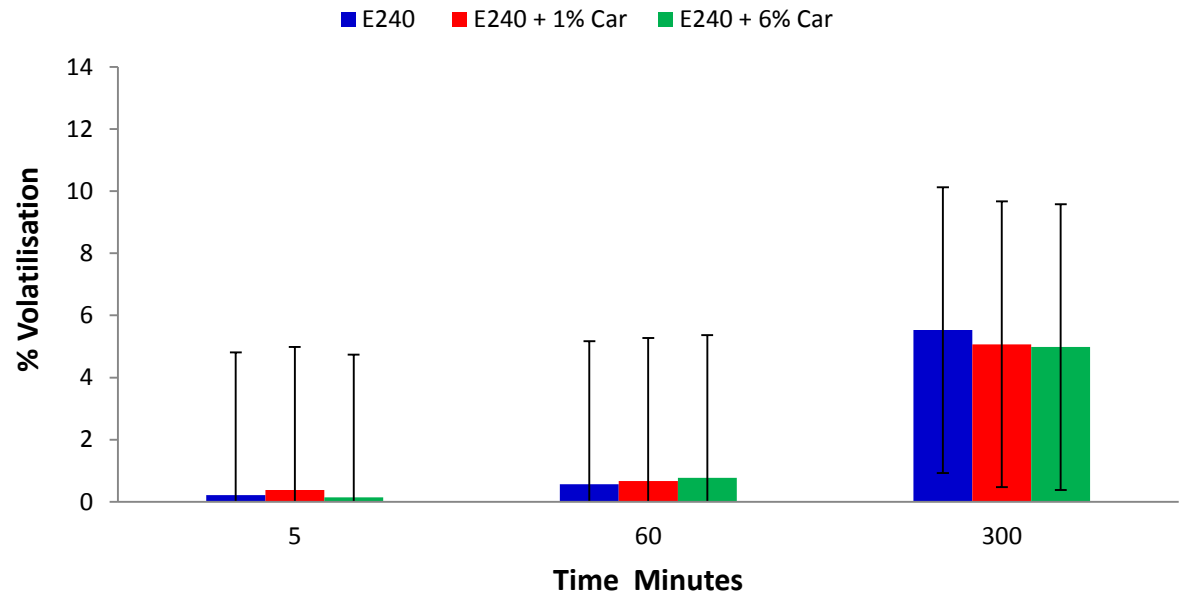

Figure A8.4.6 – Bar chart showing the % volatilisations for the E239 samples aged for 5, 60 and 300 minutes in nitrogen on the ageing rig at 320 °C. N=1. The error bar is 4.20% which is the calculated error in the method.

A8 – Chapter 8 –Characterisation of the Degradation Behaviour, Thermal Degradation – Ageing Rig – Gel Content

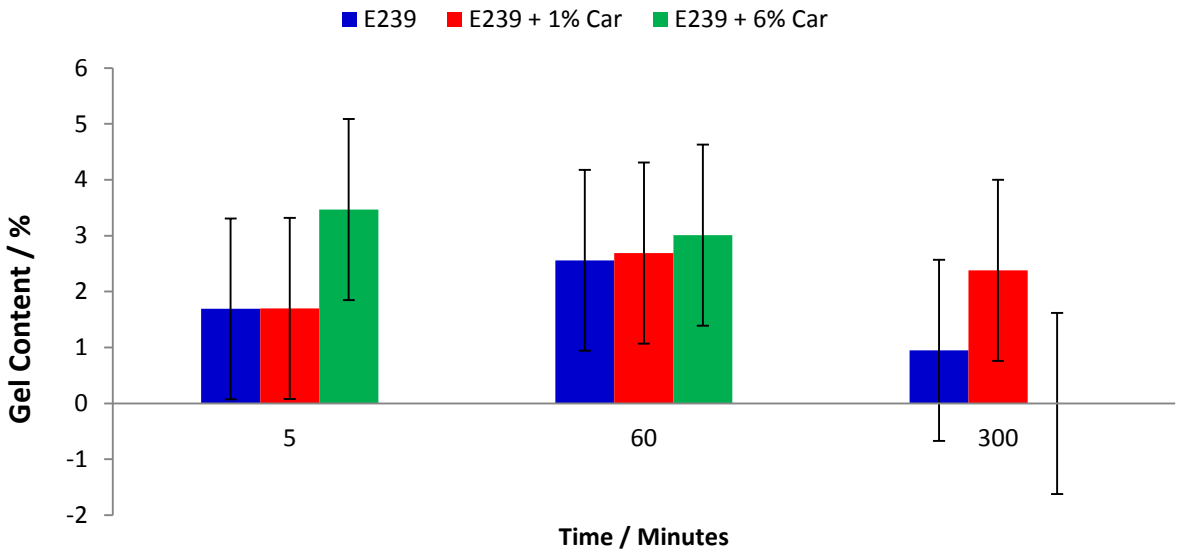

Figure A8.5.1 - Bar chart showing the residual gel content (Original) for the E239 samples aged for 5, 60 and 300 minutes on the ageing rig at 290 °C. N=3. The error bar is 1.81% which is the calculated error in the method.

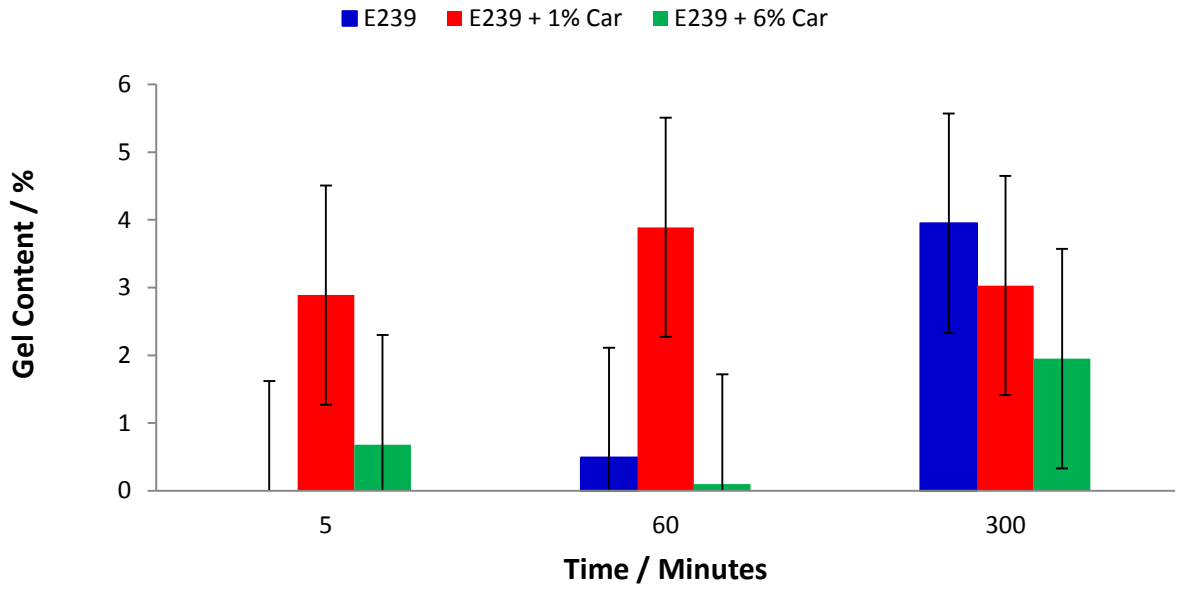

Figure A8.5.2 - Bar chart showing the residual gel content (Original) for the E239 samples aged for 5, 60 and 300 minutes on the ageing rig at 305 °C. N=3. The error bar is 1.81% which is the calculated error in the method.

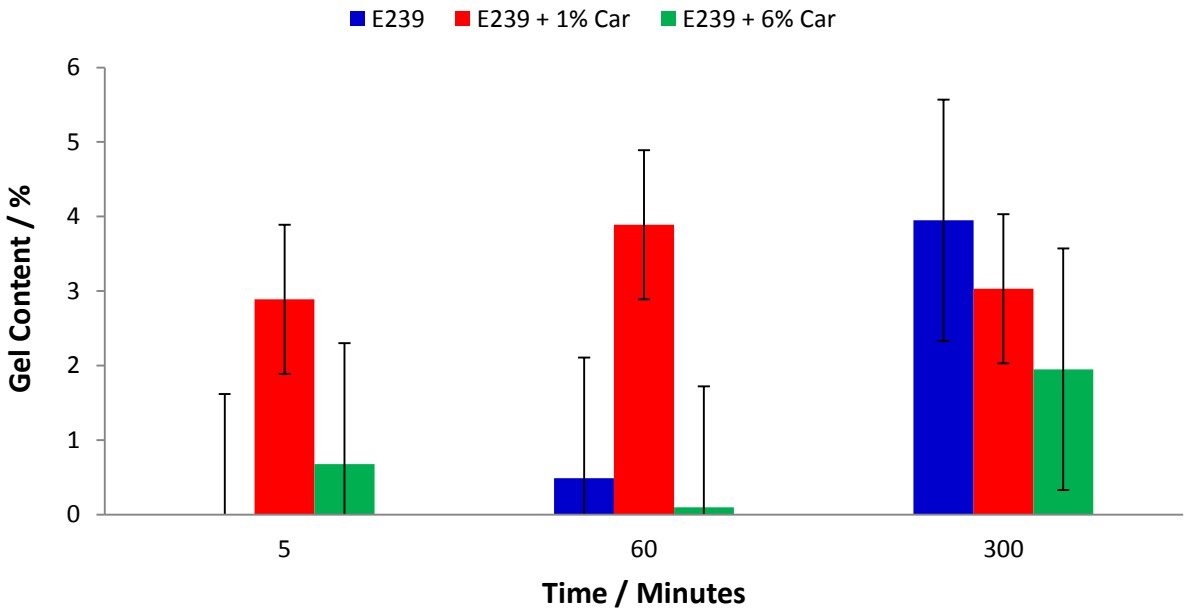

Figure A8.5.3 - Bar chart showing the residual gel content (Original) for the E239 samples aged for 5, 60 and 300 minutes on the ageing rig at 320 ºC. N=3. The error bar is 1.81% which is the calculated error in the method.

A9 – Chapter 9 –Characterisation of the Degradation Behaviour, Thermo-oxidative Degradation – DSC

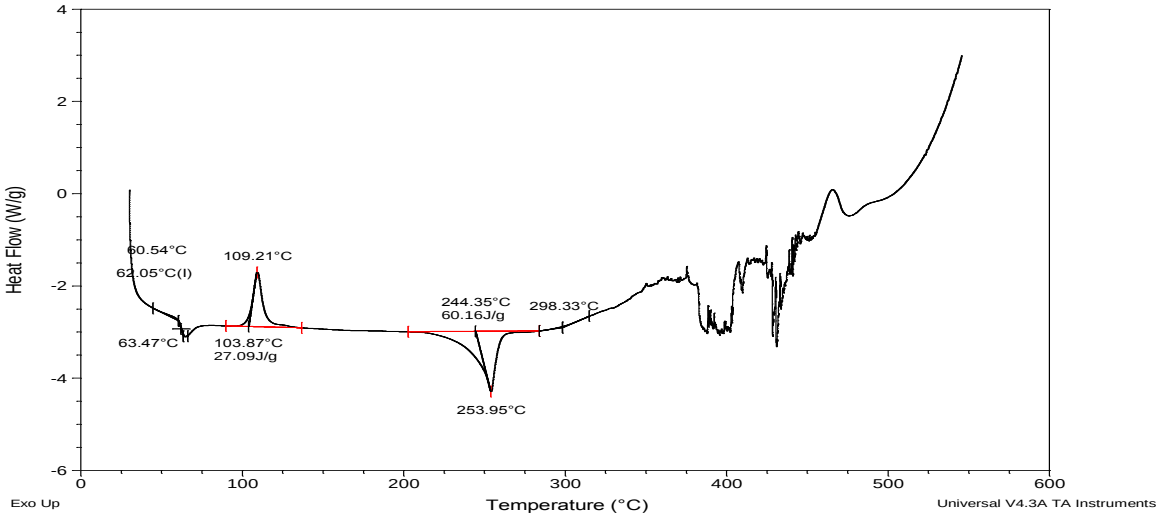

Figure A9.1.1 – DSC scan of the E187 + 6% Vikolox sample. A single sample was analysed.

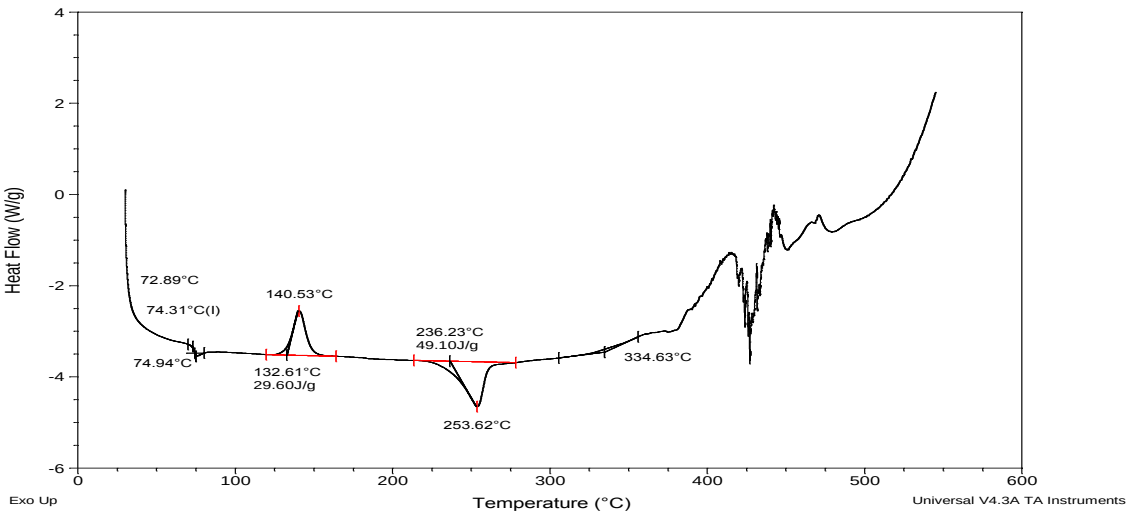

Figure A9.1.2 – DSC scan of the E187 + 6% Vikolox sample. A single sample was analysed.

A9 – Chapter 9 –Characterisation of the Degradation Behaviour, Thermo-oxidative Degradation – TGA

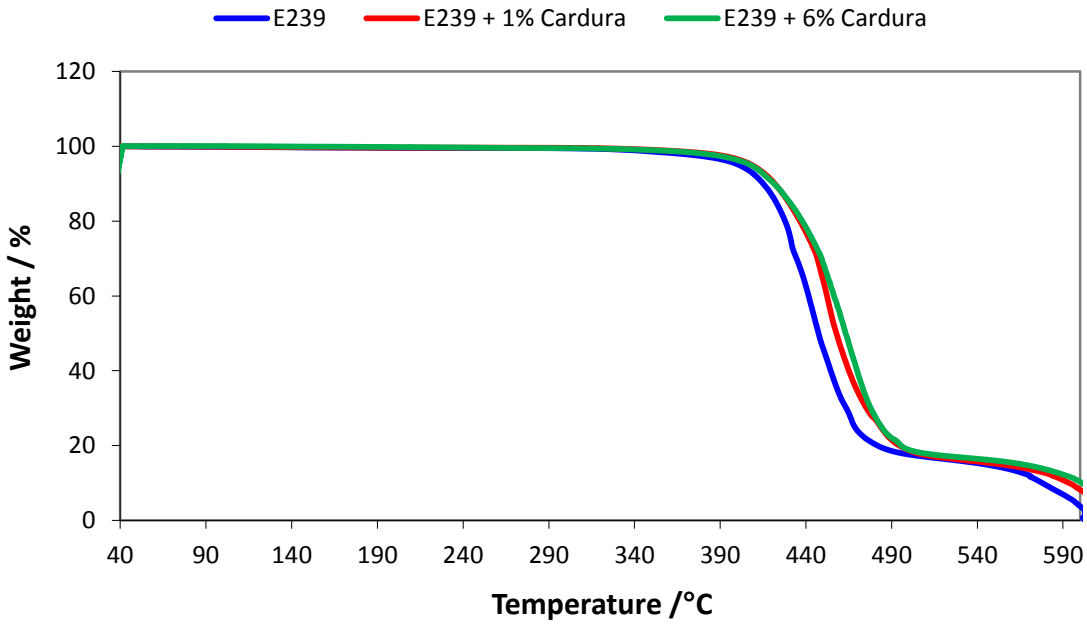

Figure A9.2.1 – TGA thermogram showing the mass loss of the E239 samples. A single sample was analysed.

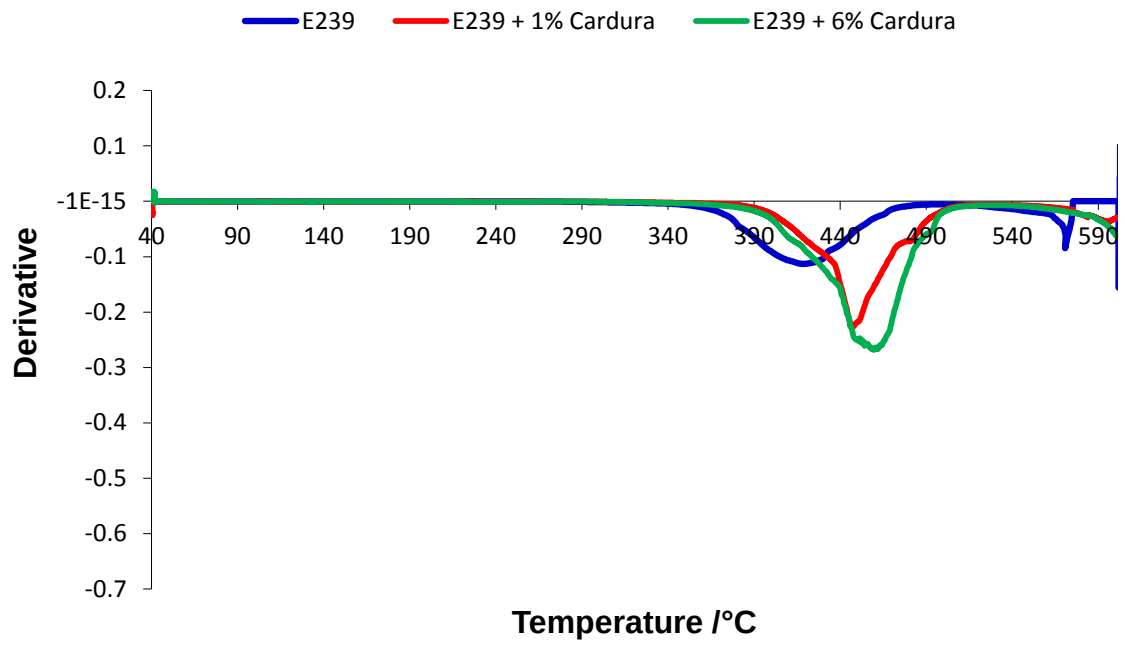

Figure A9.2.2 – TGA thermogram showing the mass loss of the E239 samples. A single sample was analysed.

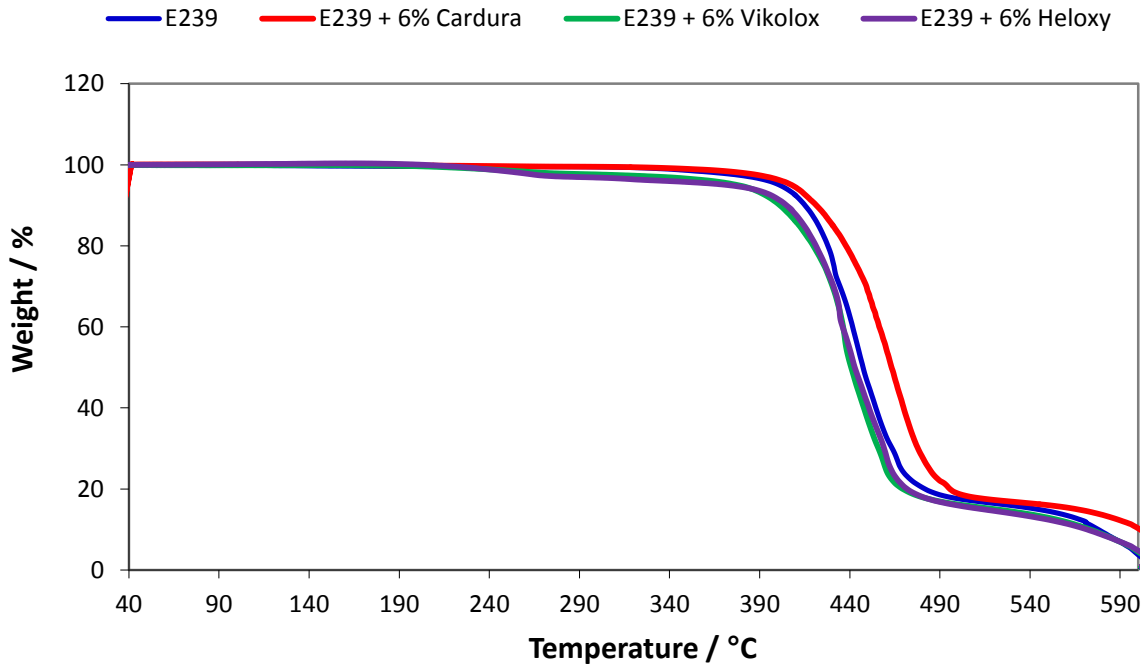

Figure A9.2.3 – TGA thermogram showing the mass loss of the E239 samples with the different epoxides. A single sample was analysed.

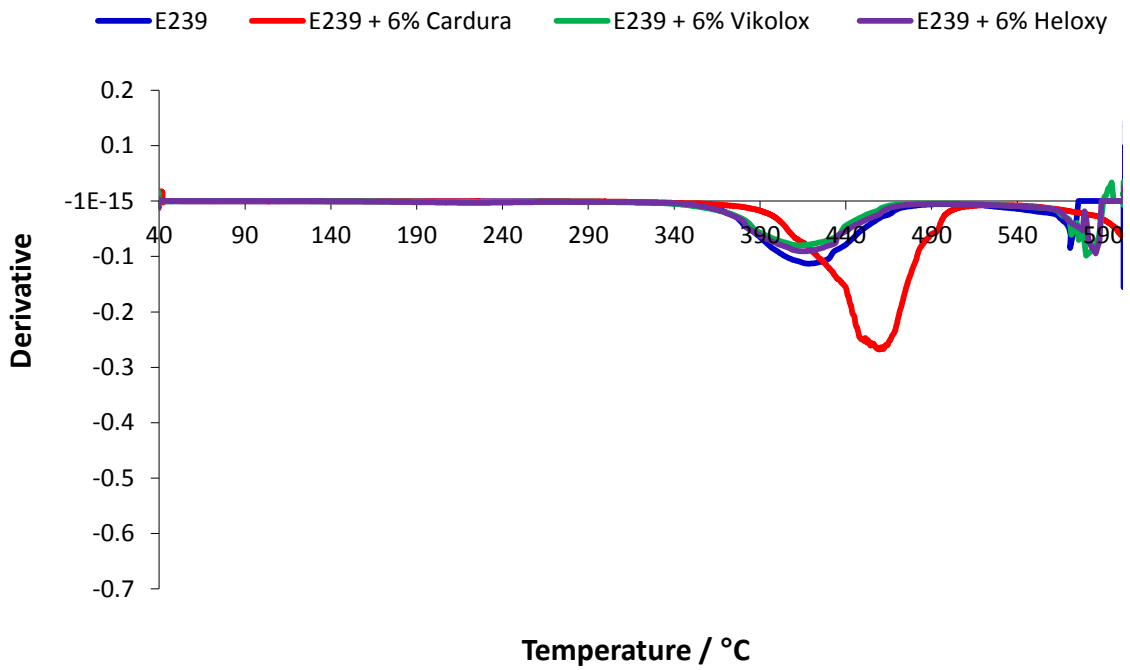

Figure A9.2.4 – TGA thermogram showing the mass loss of the E239 samples with the different epoxides. A single sample was analysed.

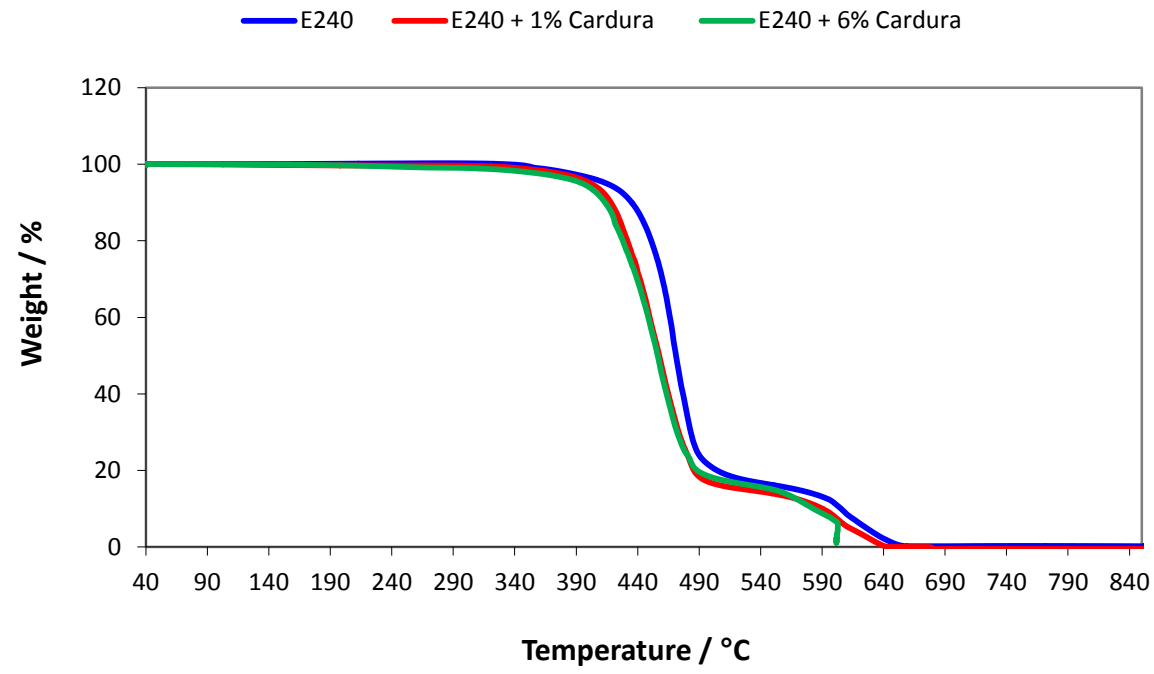

Figure A9.2.5 – TGA thermogram showing the mass loss of the E240 samples. A single sample was analysed.

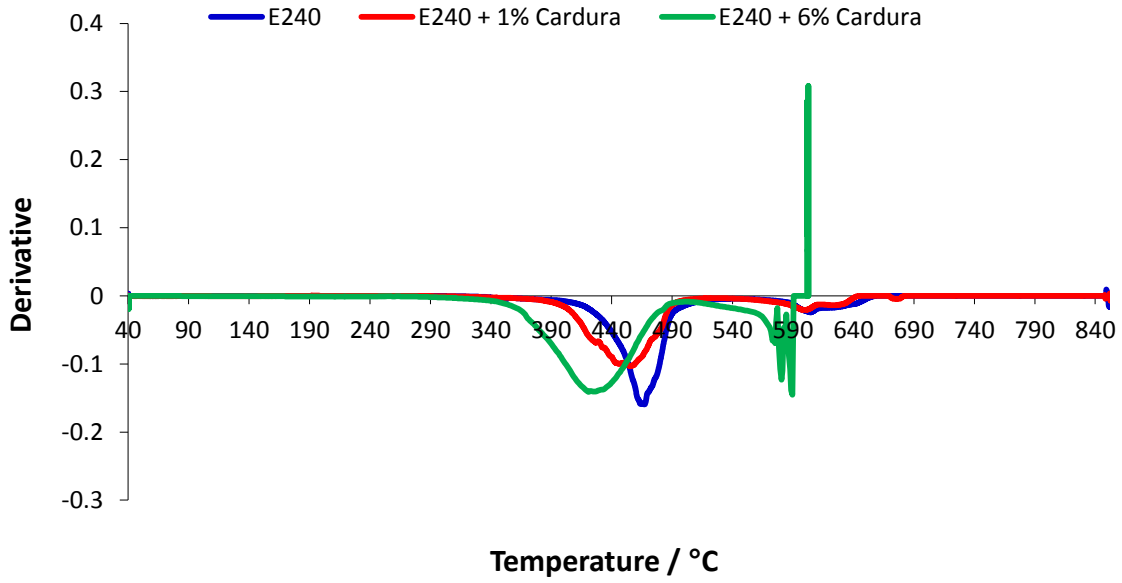

Figure A9.2.6 – TGA thermogram showing the mass loss of the E240 samples. A single sample was analysed.

A9 – Chapter 9 –Characterisation of the Degradation Behaviour, Thermo-oxidative Degradation – Ageing Rig - % Volatilisation

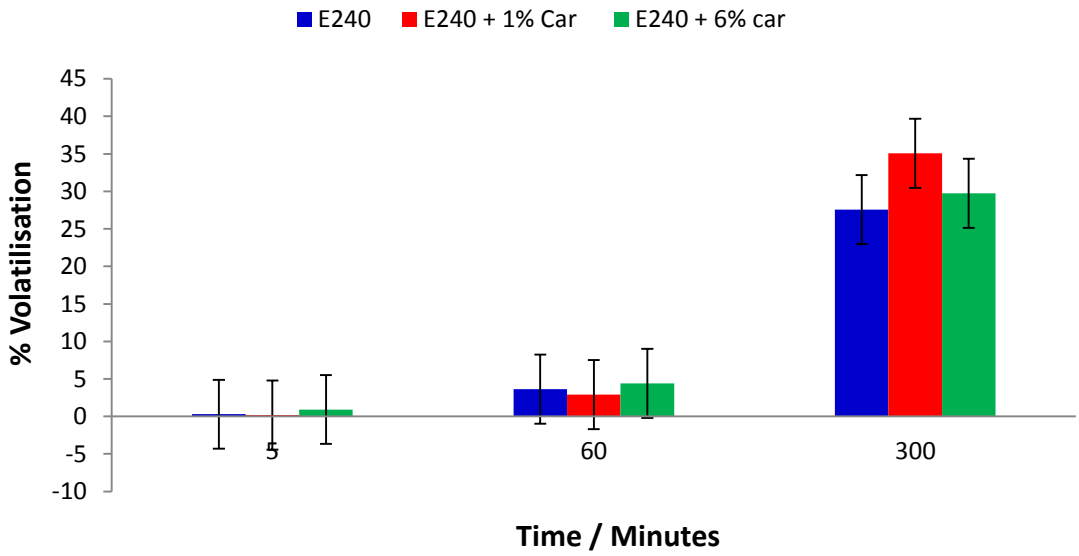

Figure A9.3.1 – Bar chart showing the % volatilisations for the E187 samples aged for 5, 60 and 300 minutes in nitrogen on the ageing rig at 290 °C. N=1. The error bar is 4.20% which is the calculated error in the method.

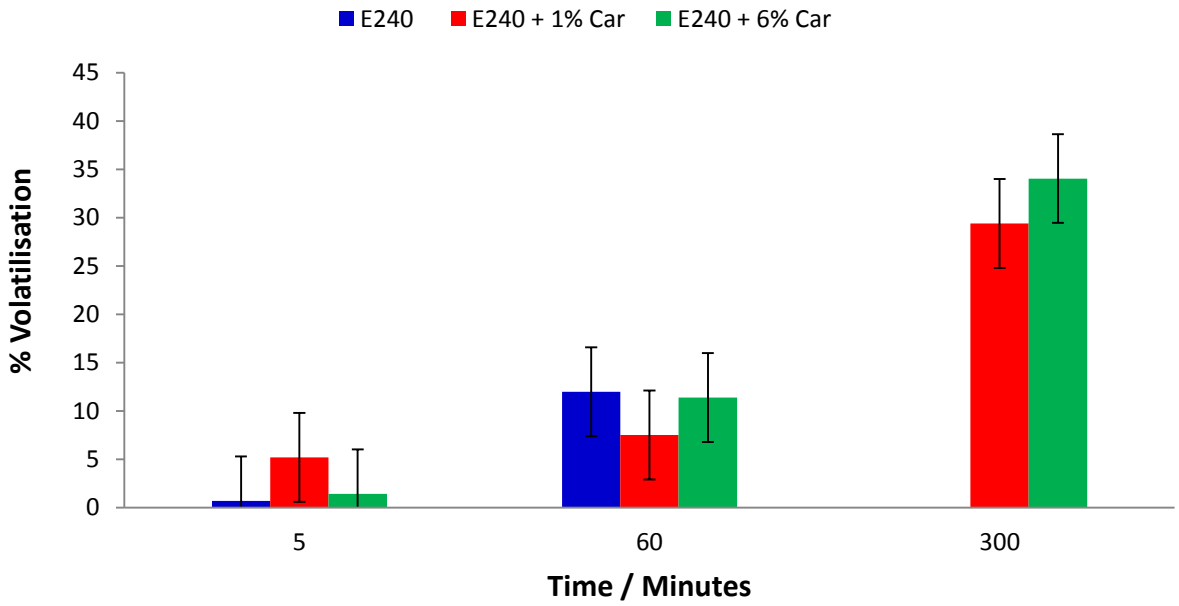

Figure A9.3.2 – Bar chart showing the % volatilisations for the E187 samples aged for 5, 60 and 300 minutes in nitrogen on the ageing rig at 320 °C. N=1. The error bar is 4.20% which is the calculated error in the method.

A9 – Chapter 9 –Characterisation of the Degradation Behaviour, Thermo-oxidative Degradation – Ageing Rig – Gel Content

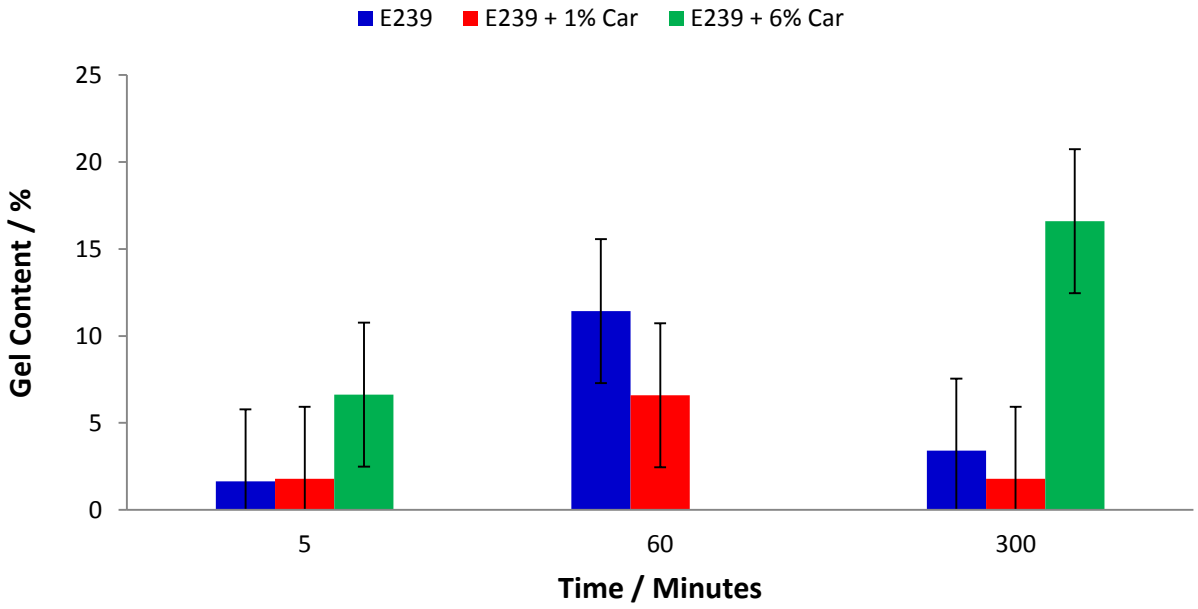

Figure A9.4.1 - Bar chart showing the residual gel content (Original) for the E239 samples aged for 5, 60 and 300 minutes on the ageing rig at 290 °C. N=3. The error bar is 1.81% which is the calculated error in the method.

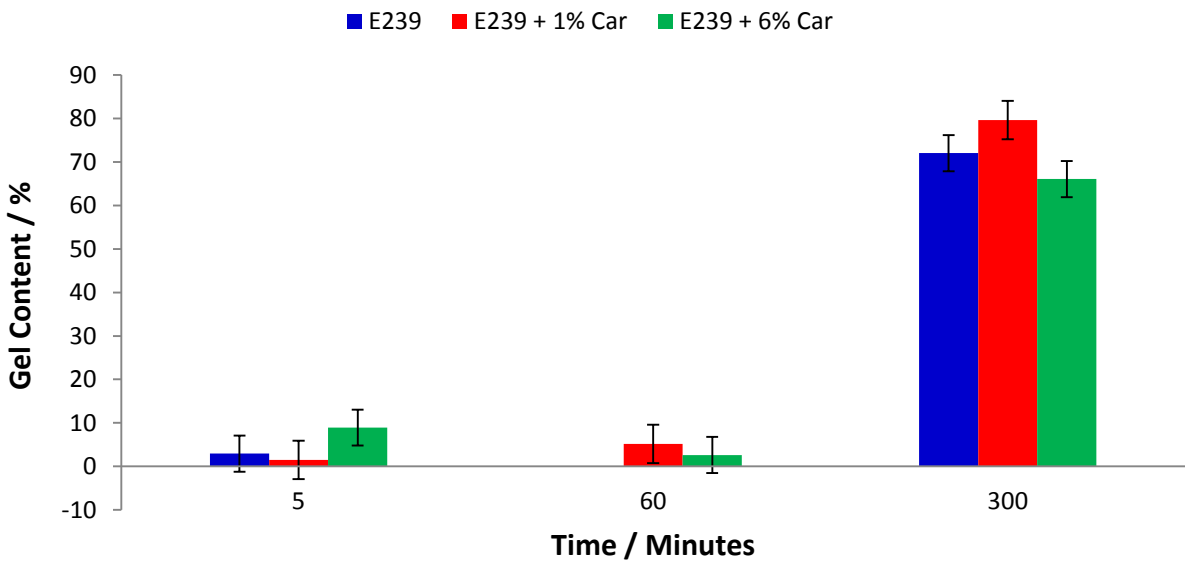

Figure A9.4.2 - Bar chart showing the residual gel content (Original) for the E239 samples aged for 5, 60 and 300 minutes on the ageing rig at 305 °C. N=3. The error bar is 1.81% which is the calculated error in the method.

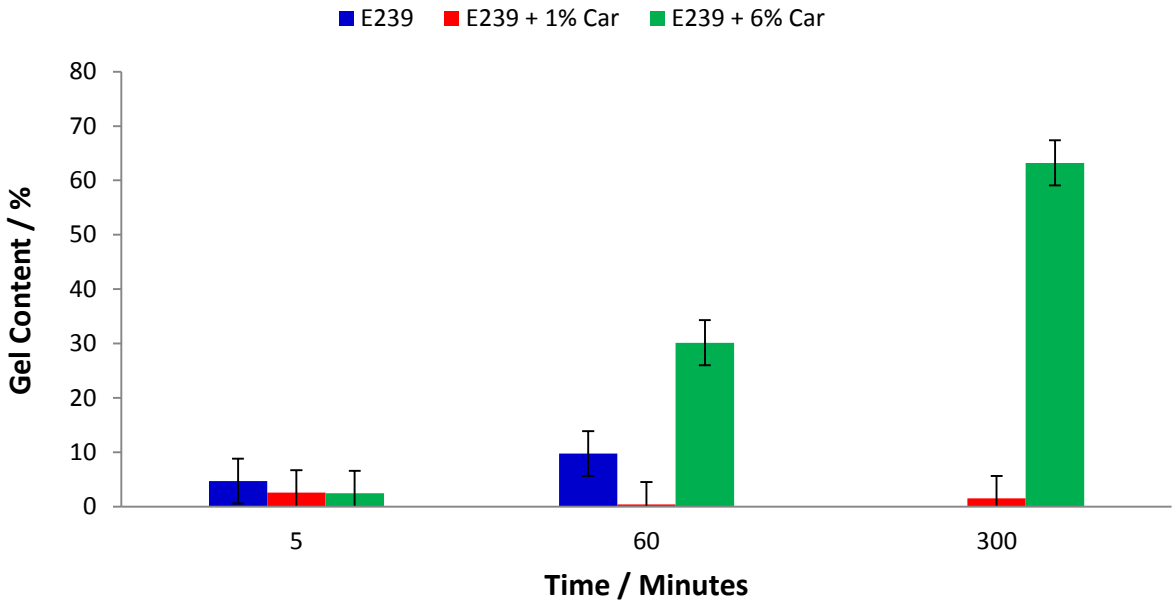

Figure A9.4.3 - Bar chart showing the residual gel content (Original) for the E239 samples aged for 5, 60 and 300 minutes on the ageing rig at 320 °C. N=3. The error bar is 1.81% which is the calculated error in the method.